LEABHARLANN CHOLÁISTE NA TRÍONÓIDE, BAILE ÁTHA CLIATH | TRINITY COLLEGE LIBRARY DUBLIN
Ollscoil Átha Cliath | The University of Dublin

Terms and Conditions of Use of Digitised Theses from Trinity College Library Dublin

Copyright statement

All material supplied by Trinity College Library is protected by copyright (under the Copyright and Related Rights Act, 2000 as amended) and other relevant Intellectual Property Rights. By accessing and using a Digitised Thesis from Trinity College Library you acknowledge that all Intellectual Property Rights in any Works supplied are the sole and exclusive property of the copyright and/or other IPR holder. Specific copyright holders may not be explicitly identified. Use of materials from other sources within a thesis should not be construed as a claim over them.

A non-exclusive, non-transferable licence is hereby granted to those using or reproducing, in whole or in part, the material for valid purposes, providing the copyright owners are acknowledged using the normal conventions. Where specific permission to use material is required, this is identified and such permission must be sought from the copyright holder or agency cited.

Liability statement

By using a Digitised Thesis, I accept that Trinity College Dublin bears no legal responsibility for the accuracy, legality or comprehensiveness of materials contained within the thesis, and that Trinity College Dublin accepts no liability for indirect, consequential, or incidental, damages or losses arising from use of the thesis for whatever reason. Information located in a thesis may be subject to specific use constraints, details of which may not be explicitly described. It is the responsibility of potential and actual users to be aware of such constraints and to abide by them. By making use of material from a digitised thesis, you accept these copyright and disclaimer provisions. Where it is brought to the attention of Trinity College Library that there may be a breach of copyright or other restraint, it is the policy to withdraw or take down access to a thesis while the issue is being resolved.

Access Agreement

By using a Digitised Thesis from Trinity College Library you are bound by the following Terms & Conditions. Please read them carefully.

I have read and I understand the following statement: All material supplied via a Digitised Thesis from Trinity College Library is protected by copyright and other intellectual property rights, and duplication or sale of all or part of any of a thesis is not permitted, except that material may be duplicated by you for your research use or for educational purposes in electronic or print form providing the copyright owners are acknowledged using the normal conventions. You must obtain permission for any other use. Electronic or print copies may not be offered, whether for sale or otherwise to anyone. This copy has been supplied on the understanding that it is copyright material and that no quotation from the thesis may be published without proper acknowledgement.

Towards a Gene Therapy for RP10 Retinitis Pigmentosa

A Thesis Submitted to the University of Dublin for the Degree of Doctor for Philosophy

by

Lawrence Chi Shing Tam

Department of Genetics

University of Dublin

Trinity College

March 2008

TRINITY COLLEGE
0 5 AUG 2008
LIBRARY DUBLIN
THESIS
8587

Declaration

This thesis has not been previously submitted to this or any other university for examination for a high degree. The work presented here is entirely my own except where noted. This thesis may be made available for consultation within the university library. It may be photocopied or lent to other libraries for the purpose of consultation.

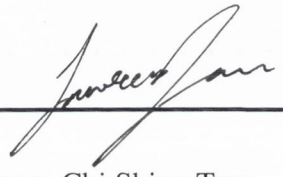

Lawrence Chi Shing Tam

March 2008

Acknowledgements

I would like to take this opportunity to thank all those who have helped and inspired me throughout the course of my PhD study. First, I would like to thank Prof. Pete Humphries for giving me this wonderful opportunity to embark on such an interesting and challenging project. A huge thank you goes to Dr. Sophie Kiang, who has taught me so much and has always been there to answer my questions. In particular, thanks Sophie for reading my thesis, for your guidance, and most of all, for being such a great friend. Special thanks to Dr. Avril Kennan, Dr. Paul F. Kenna, Dr. Naomi Chadderton and Dr. Marius Ader for their enormous contributions to the project. In particular, special thanks to Dr. Paul Kenna for all the animal work and Dr. Naomi Chadderton for helping me with the AAV work. A big thank you also goes to everyone in the Ocular Genetics Unit who have made this lab such a fabulous place to work in: Dr. Marian Humphries, Dr. Jane Farrar, Dr Mary O'Reilly, Dr. Alison Reynolds, Dr. Sophia Millington-Ward, Dr. Matthew Campbell, Dr. Danny Allen, Dr. Arpad Palfi, Dr. Niamh McNally, Dr. Mandy Tivnan, Dr. Helena McMahon, Fiona Cassidy, Alex McKee, Sarah Cannon, Sylvie Mehigan, Caroline Woods, and past; Dr Aileen Aherne and Dr. Fiona Kiernan. I would also like to thank all our collaborators who have contributed to the work described in this study. Thanks to Dr. Sara Bowne in Texas for providing all the IMPDH1 antibodies. Special thanks to Dr. Alfonso Blanco for the help with FACS analyses in UCD. In addition, I would like to thank The Irish Research Council for Science, Engineering and Technology (IRCSET) for providing me with a three-year scholarship.

On a personal note, I would like to thank my brother, Joseph, for his continuous support. Special thanks to Sally, who has stood by me always and for being the main source of motivation (I couldn't have done it without you!). Lastly, I would like to dedicate this thesis to my parents, Monica and Steven, who have provided me with endless support and encouragement. Thank you Mom and Dad for being there for me always. THANK YOU ALL!

Summary

The main focus of this thesis is on the development of a gene therapy strategy using RNAi-mediated suppression for the RP10 form of retinitis pigmentosa (RP), which accounts for approximately 2% of all autosomal dominant RP cases. Comparative analysis of the transcriptional profiles within the retinas of mice carrying a targeted disruption of the rhodopsin gene resulted in the identification of the gene encoding inosine 5'-monophosphate dehydrogenase 1 (IMPDH1) as a candidate for RP10 (Kennan *et al.,* 2002). IMPDH1 is the rate-limiting enzyme in the *de novo* biosynthesis pathway for guanine nucleotides, which are important prerequisites for many cellular functions and play crucial regulatory roles in the phototransduction cascade. Several studies have revealed that specific mutations within the IMPDH1 gene segregate with RP-affected families (Bowne *et al.*, 2002). Furthermore, structural protein analyses have indicated that mutant IMPDH1 protein misfolding and aggregation are the likely cause of severe retinopathy in humans (Aherne *et al.,* 2004). In contrast, IMPDH1$^{-/-}$ mice at four months of age, show little structural or functional degeneration of the retina (Aherne *et al.*, 2004). This observation suggests that the dominant segregation pattern associated with RP10 is not caused by haploinsufficiency of the normal IMPDH1 gene, but that the disease pathology is caused by a dominant negative phenotypic effect exerted by mutant protein. The mild phenotype observed in IMPDH1 knockout mice has presented the human form of RP10 as a potential therapeutic target, whereby, simultaneous ablation of wild type and mutant IMPDH1 transcripts by RNA interference (RNAi), may be sufficient to abolish the dominant negative effect exerted by mutant IMPDH1 protein.

In this study, two synthetic siRNAs targeting distinct regions of human and mouse IMPDH1 have shown effective and sequence-specific suppression of endogenous IMPDH1 transcripts and exogenous IMPDH1 protein expression in mammalian cell cultures. The silencing efficiency of the two synthetic IMPDH1-siRNAs was also retained in human H1-promoter driven short hairpin RNA (shRNA) vectors. In particular, both IMPDH1-specific shRNAs provided effective mutation-independent suppression of wild type and mutant IMPDH1 harbouring the Arg224Pro and Asp226Asn mutations at the mRNA and protein level in mammalian cells. Furthermore, use of a dual expression vector system directing the synthesis of IMPDH1-specific shRNA and enhanced green

fluorescent protein (EGFP) resulted in the demonstration of efficient knockdown of endogenous IMPDH1 transcripts following *in-vitro* electroporation of murine retinal explants from 1-day-old mouse pups. Recombinant AAV vectors encoding an IMPDH1-specific shRNA and EGFP within an AAV serotype 2 (AAV2) genome contained in an AAV5 capsid (AAV-2/5) exclusively transduced the retinal pigment epithelium (RPE) and photoreceptors of wild type C57B6/CBA mice following subretinal injection. Transgene expression was observed as early as two weeks post injection, and vector-mediated fluorescence continued to be detected in animals four months post injection, the longest time point in the present study. In addition, AAV-shRNA delivery into the subretinal space of wild type mice resulted in ~70% reduction of endogenous IMPDH1 transcripts and also caused significant downregulation of IMPDH1 protein *in-vivo*. However, prolonged suppression of IMPDH1 for up to four months in one mouse resulted in pronounced reduction of photoreceptor structure and function. Therefore, long-term therapy for RP10 may require the replacement of endogenous IMPDH1 mRNA with shRNA-resistant mRNA encoding wild type IMPDH1, or the use of alternative multiple shRNAs, which in combination may have a less toxic effect. AAV-mediated over-expression of mutant IMPDH1 harbouring the Arg224Pro mutation (but not wild-type IMPDH1) in the photoreceptor cells of wild type 129 S2/SvHsd mice has produced some of the hallmarks found in other autosomal dominant RP (adRP) animal models (e.g. P23H mouse model; Olsson *et al.*, 1992), including rapid deterioration of photoreceptor outer nuclear layer and diminished ERG response. Importantly, despite the negative observations associated with long-term shRNA expression alone mentioned above, simultaneous delivery of AAV-mutant IMPDH1 with AAV-IMPDH1-specific shRNA by subretinal injection in wild-type 129 S2/SvHsd mice, as compared to control virus, provided therapeutic protection of photoreceptor function and structure.

In summary, expression of wild type and mutant IMPDH1 genes *in-vitro*, *ex-vivo* and *in-vivo* has been markedly downregulated by shRNA. Furthermore, application of an AAV-mediated suppression strategy to a mutant IMPDH1-induced RP10 mouse model showed effective protection of retinal structure and function. These observations have demonstrated *in-vivo* the potential use of AAV-mediated RNAi as a therapy for the RP10 form of retinitis pigmentosa.

Table of Contents

	Page Number
Declaration	I
Acknowledgements	II
Summary	III
Table of contents	V
Figures and Tables	XVI
Abbreviations	XXII

Chapter 1: General Introduction

1. General Introduction	1
1.1 The Human Eye	1
1.2 The vascular supply of the eye	3
1.3 Anatomy of the retina and photoreceptor cells	4
1.3.1 Retinal pigment epithelium	5
1.3.2 Photoreceptor layer of rods and cones	5
1.3.3 External limiting membrane	8
1.3.4 Outer nuclear layer	8
1.3.5 Outer plexiform layer	8
1.3.6 Inner nuclear layer	9
1.3.7 Inner plexiform layer	11
1.3.8 Ganglion cell layer	11
1.3.9 The nerve fibre layer	12
1.3.10 Internal limiting membrane	13
1.4 The phototransduction pathway	14
1.5 Retinitis Pigmentosa (RP)	17
1.5.1 Genetic defects in Retinitis Pigmentosa	19
1.5.2 Clinical assessment of Retinitis Pigmentosa	22
1.6 Mouse models of ocular diseases	24
1.6.1 Mouse models of Retinitis Pigmentosa	25
1.6.2 Mutant mouse models with a combined phenotype of RP and other photoreceptor dystrophies	26

1.6.3 Mutant mouse models of Macular degeneration 27
1.6.4 Mouse models of Leber Congenital Amaurosis (LCA) 28
1.6.5 Combined retinal and neuronal degeneration phenotype 29
1.6.6 Retinal degeneration as part of a multisyndromic defect 30
1.6.7 Other retinopathy models 31
1.7 Mutations in rhodopsin associated with Retinitis Pigmentosa 33
1.8 Conventional treatments for RP 42
1.8.1 Vitamin A supplementation 42
1.8.2 Dietary modification and nutrition supplementation 44
1.8.3 Trophic factors 44
1.8.4 Calcium blockers 45
1.8.5 Stem cells and precursor cells 45
1.8.6 Inhibitors of apoptosis 46
1.8.7 Implanted electrical devices 46
1.9 RNA interference (RNAi): Discovery and mechanistic description 47
1.9.1 Introduction 47
1.9.2 Mechanism of RNAi 49
1.9.3 Thermodynamic properties of siRNAs 50
1.9.4 Induction of interferon response by double-stranded RNA 52
1.9.5 The design of effective siRNAs 52
1.9.6 Off-target effects 54
1.9.7 Chemical modification of siRNAs 55
1.9.8 Vector and viral delivery systems *in-vivo* 58
1.9.8.1 siRNA expression vectors 58
1.9.8.2 Viral delivery of siRNA *in-vivo* 60
1.9.8.3 Retroviral vectors 61
1.9.8.4 Lentiviral vectors 61
1.9.8.5 Adenoviral vectors 62
1.9.8.6 Adeno-associated virus (AAV) 62
1.9.8.7 Herpes simplex virus type 1 (HSV-1) 63
1.9.9 The use of siRNA *in-vivo* 64

1.9.10 Systemic delivery 65
1.9.10.1 Intravenous administration using hydrodynamic delivery 65
1.9.10.2 Intraperitoneal administration 66
1.9.11 Direct injections 66
1.9.11.1 Intraocular 66
1.9.11.2 Intramuscular 67
1.9.11.3 Direct injection in central nervous system (CNS) 68
1.9.11.4 Intratumoural 69
1.9.12 Experimental controls for RNAi 69
1.9.13 Saturation of the RNAi pathway is lethal to cell survival 71
1.10 MicroRNAs (miRNAs) 73
1.10.1 A mechanistic view of miRNAs 74
1.10.2 MicroRNA target recognition and RNA accessibility 76
1.10.3 The similarities between miRNAs and other regulatory pathways 76
1.10.4 The role of miRNA in animal development 77
1.10.5 Identification and characterisation of miRNAs in the mouse eye 79
1.10.6 The use of miRNAs as suppressive reagents 80
1.11 P-bodies 82
1.11.1 Introduction 82
1.11.2 The formation of GWBs/P-bodies in mammalian cells 84
1.11.3 RNAi in P-bodies 85
1.11.4 Alternative quality control mechanisms targeted by GWBs/P-bodies 86
1.11.5 The interaction of GWBs/P-bodies with stress granules 87
1.11.6 Functional interactions between GWBs and miRNAs 88
1.12 Aptamers 90
1.13 Gene therapy for ocular diseases 93
1.13.1 Introduction 93
1.13.2 Gene replacement therapies 94
1.13.3 RNAi in the treatment of autosomal dominant RP (adRP) 96
1.13.4 RNAi in the treatment of ocular neovascularisation 98
1.13.5 RNAi-mediated downregulation of apoptosis mediators in ganglion cells 99

1.13.6 RNAi in the treatment of oxidative damage in the retina 100
1.13.7 RNAi as a therapeutic approach for ocular fibrosis 101
1.13.8 Genetic tests for RP 101
1.14 Mutations in inosine 5'-monophosphate dehydrogenase type I (IMPDH1) cause the RP10 form of adRP 104
1.14.1 Introduction 104
1.14.2 Characterisation of inosine 5'-monophosphate dehydrogenase 106
1.14.3 Gene regulation of IMPDH type I and II 108
1.14.4 Localisation of IMPDH type I and II in the retina 110
1.14.5 IMPDH inhibitors 111
1.14.6 Mutations in IMPDH1 cause the RP10 form of adRP 113
1.15 Objectives of study 120

Chapter 2: Materials and Methods

2.1 General materials and reagents 121
2.1.1 Materials and reagents used for general molecular cloning procedures 121
2.1.2 Materials and reagents for tissue culture 123
2.1.3 Materials and reagents for RNA study 123
2.1.4 Materials and reagents for protein study 124
2.1.5 Materials and reagents for immunohistochemistry 127
2.1.6 Animals 128
2.2 General molecular methods 129
2.2.1 Determination of DNA and RNA concentration using UV spectrometer 129
2.2.2 Agarose Gel Electrophoresis 129
2.2.3 Phenol-chloroform extraction and ethanol precipitation of nucleic acids 129
2.2.4 XL-1 Blue *E.coli* competent cells preparation 130
2.2.5 Transformation of XL-1 Blue competent cells 130
2.2.6 Plasmid Mini-prep Boiling Method 130
2.2.7 DNA ligations 131
2.2.8 Design of oligonucleotides 131
2.2.9 Polymerase Chain Reaction (PCR) 132

2.2.10 Restriction enzyme digestions 132
2.2.11 Qiaquick (Qiagen) PCR purification 132
2.2.12 Qiaquick maxi-preps 133
2.2.13 DNA sequencing 133
2.3 Tissue culture methods 135
2.3.1 Cell culture maintenance 135
2.3.2 Cell passaging 135
2.3.3 Haemocytometer cell counting 135
2.3.4 Cryopreservation of cells 135
2.3.5 Poly-L-lysine coating of coverslips 136
2.3.6 General transfection protocol using Lipofectamine 2000® 136
2.3.7 RNA extraction from cultured cells 137
2.3.8 DNase treatment of RNA samples 137
2.4 Real Time RT-PCR analysis using SYBR Green I dye on a Light Cycler 138
2.5 Western blot analysis 141
2.5.1 SDS-PAGE electrophoresis 141
2.5.2 Determination of protein concentration with BCA protein assay 141
2.5.3 Gel cassette assembly 142
2.5.4 Mini-protean 3 electrophoresis module assembly and sample loading 142
2.5.5 Coomassie Blue staining 142
2.5.6 Electrophoretic transfer of protein onto nitrocellulose membrane 143
2.5.7 Blocking of immunoblots 143
2.5.8 Antibody probing of immunoblots 143
2.5.9 Stripping of immunoblots 144
2.5.10 Densitometry 144
2.6 Retinal explants 145
2.6.1 *In-vitro* electroporation and retinal explants culture 145
2.6.2 Fluorescent activated cell sorting (FACS) analysis of cultured retinal explants 145
2.6.3 RNA extraction from retinal explant tissues using Qiagne RNeasy Kit 146
2.7 Adeno-associated virus (AAV) 147

2.7.1 Adeno-associated virus production 147
2.7.2 Caesium chloride purification method 147
2.7.3 Determination of genomic viral titre 148
2.8 Statistical analysis 149

Chapter 3: Evaluation of IMPDH1-specific siRNAs and shRNAs in mammalian cell cultures

3.1 Introduction 150
3.2 Methods 155
3.2.1 Construction of small hairpin RNAs targeting IMPDH1 using pSuper DNA vector based approach 155
3.2.1.1 Design of short hairpin RNAs 155
3.2.1.2 Annealing of oligonucleotides 155
3.2.1.3 Linearisation of pSuper vectors 156
3.2.1.4 Ligation of annealed oligonucleotide inserts into linearised pSuper vectors 156
3.2.1.5 Transformation of Sure® 2 Supercompetent cells 156
3.2.1.6 Detection of positive recombinant clones 157
3.2.2 An 8-criterion algorithm method for the design of chemically synthesised siRNA 157
3.2.3 Construction of wild type and mutant IMPDH1 expression vectors 159
3.2.4 Determination of transfection efficiency 160
3.2.4.1 β-galactosidase method 160
3.2.4.2 Determination of vector-based RNAi transfection efficiency by transfection of EGFP expression plasmids in HeLa cells 160
3.2.5 Transfection protocols 161
3.2.5.1 Transfection of chemically synthesised siRNAs and pBluescriptH1-driven shRNAs in HEK293T and HeLa cells for RNA analysis 161
3.2.5.2 Co-transfection of pWtIMPDH1 and chemically synthesised siRNA in HeLa cells 161

3.2.5.3 Inhibition of wild-type and mutant IMPDH1-EGFP fusion proteins by siRNAs in HeLa cells 162
3.2.5.4 Western blot analyses of wild type and mutant protein suppression by IMPDH1-specific si/shRNAs in HeLa cells 163
3.2.5.5 Time-dependent protein expression profile 163
3.2.5.6 Suppression of mutant IMPDH2 transcripts in mouse neuronal N2a cells 164
3.2.6 Detection of apoptosis 164
3.2.7 Statistical analysis 165
3.3 Results 166
3.3.1 Initial design of short hairpin RNAs targeting human and mouse IMPDH1 166
3.3.2 Determination of transfection efficiency 167
3.3.3 Suppression of endogenous IMPDH1 transcripts by short hairpin RNAs in HEK293T cells 168
3.3.4 Downregulation of endogenous IMPDH1 mRNA by chemically synthesised siRNAs in HeLa cells 169
3.3.5 Dose-dependent downregulation of IMPDH1 mRNA expression by synthetic siRNA duplexes 171
3.3.6 Co-transfection of synthetic siRNA duplexes and wild type IMPDH1 expression vectors in HeLa cells 171
3.3.7 siRNA-mediated downregulation of wild-type and mutant IMPDH1 tagged with enhanced green fluorescent protein (EGFP) 172
3.3.8 Downregulation of mutant IMPDH1 transcripts harbouring the Arg224Pro missense mutation in N2a mouse neuronal cells 173
3.3.9 Downregulation of IMPDH1 protein expression following IMPDH1 RNAi-mediated suppression 174
3.3.10 Subcloning of si1224/si2048 into pBluescriptH1 vector system and analysis of suppression activity 175
3.3.11 Induction of apoptosis by over-expression of wild type and mutant IMPDH1 177
3.4 Discussion 179
3.5 Summary of current findings 193

Chapter 4: Suppression of IMPDH1 *ex-vivo* in mouse retinal explants

4.1 Introduction 194

4.1.1 Background 194

4.1.2 Gene delivery by chemical approaches 195

4.1.3 Gene transfer by physical approaches 196

4.1.3.1 Enhanced gene transfer by particle bombardments 196

4.1.3.2 Enhancement of gene transfer using ultrasound 197

4.1.3.3 Hydrodynamic gene delivery 198

4.1.3.4 Enhanced gene transfer by electroporation 199

4.1.4 The application of electroporation and iontophoresis to ocular gene therapy 200

4.1.4.1 Electroporation-assisted gene transfer in ocular gene therapy 202

4.1.4.2 Iontophoresis –assisted gene transfer in ocular gene therapy 203

4.1.5 Fluorescence-activated cell sorting (FACS) 204

4.1.6 Objectives 206

4.2 Methods 207

4.2.1 Construction of pshLuc.EGFP and psh2048.EGFP 207

4.2.2 Suppression of IMPDH1 mRNA expression in N2a cells 207

4.2.3 Electroporation of murine retinal explants and fluorescence activated cell sorting (FACS) 208

4.2.4 Real Time RT-PCR analysis of endogenous mouse IMPDH1 transcript levels in retinal explants 208

4.2.5 Vibratome sectioning of retinal explant tissues 209

4.2.6 Statistical Analysis 209

4.3 Results 210

4.3.1 Construction of dual expression RNAi-vector systems 210

4.3.2 Suppression of endogenous IMPDH1 mRNA by psh2048.EGFP in N2a cells 210

4.3.3 RNAi-mediated suppression of IMPDH1 mRNA in retinal explants following *in-vitro* electroporation 211

4.4 Discussion 213

4.5 Summary of current findings 217

Chapter 5: *In-vivo* suppression of IMPDH1 in mouse retinas

5.1 Introduction 218

5.1.1 Adeno-associated viruses (AAVs) 219

5.1.2 Vectors based on adeno-associated viruses 220

5.1.3 Adeno-associated viral vectors for retinal gene transfer 223

5.1.4 Important aspects in the use of AAV-mediated gene transfer for retinal gene therapy 226

5.1.4.1 Expression level of transgene is critical for gene therapy 226

5.1.4.2 Time of delivery 227

5.1.4.3 Safety and Biodistribution 228

5.1.5 AAV-based therapy for diseases due to loss-of-function mutations 229

5.1.6 AAV-based therapy for diseases due to gain-of-function mutations 232

5.1.7 AAV-based therapy for ocular neovascular diseases 233

5.1.8 Electroretinography (ERG) 235

5.1.9 Objectives of this study 236

5.2 Methods 237

5.2.1 AAV vector production and purification 237

5.2.2 Animals and subretinal AAV injections 238

5.2.3 Electroretinographic analysis (ERG) 238

5.2.4 AAV-mediated gene transfer in retinal explant cultures 239

5.2.5 Isolation of FACS sorted retinal RNA for quantitative analysis of IMPDH1 mRNA 240

5.2.6 Retinal protein extraction and western blot analysis of IMPDH1 protein levels 240

5.2.7 Histological analysis and quantification of outer nuclear layer (ONL) thickness 241

5.2.8 Immunohistochemistry 241

5.2.9 Statistical analysis 242

5.3 Results 243

5.3.1 Construction of AAV-2/5 vectors expressing IMPDH1-specific shRNA and evaluation of transduction efficiency 243

5.3.2 Immunolocalisation of IMPDH1 in mouse retina 244
5.3.3 AAV RNAi-mediated suppression of IMPDH1 transcripts *in-vivo* 244
5.3.4 AAV shRNA-mediated suppression of IMPDH1 protein *in-vivo* 248
5.3.5 Detection of AAV-mediated RNAi suppression of IMPDH1 *in-vivo* by immunohistochemistry 249
5.3.6 Time-dependent analysis of the effect elicited by AAV shRNA-mediated suppression of IMPDH1 on retinal histology 250
5.3.7 Induction of retinopathy by AAV-mediated over-expression of mutant IMPDH1 252
5.4 Discussion 256
5.5 Conclusions 264

Chapter 6: Evaluation of off-target effects against IMPDH2

6.1 Introduction 266
6.2 Methods 273
6.2.1 Construction of IMPDH2 expression vectors 273
6.2.2 Transfections and quantitative Real Time RT-PCR analysis 273
6.2.3 Inhibition of wild type IMPDH2 and EGFP fusion proteins by siRNAs in HeLa cells 274
6.2.4 Western blot analysis of IMPDH2 protein levels *in-vitro* and *in-vivo* 274
6.2.4.1 *In-vitro* analysis of IMPDH2 protein levels 274
6.2.4.2 *In-vivo* analysis of IMPDH2 protein levels 275
6.2.5 Statistical analysis 275
6.3 Results 277
6.3.1 Alignment of IMPDH1-specific siRNAs against human and mouse IMPDH2 transcripts 277
6.3.2 siRNA-mediated suppression of IMPDH2 mRNA in HeLa cells 277
6.3.3 siRNA-mediated suppression of IMPDH2–tagged enhanced green fluorescent protein (EGFP) protein in HeLa cells 277
6.3.4 shRNA-mediated suppression of IMPDH2 protein in HeLa cells 278
6.3.5 AAV-mediated shRNA inhibition of IMPDH2 *in-vivo* 278

6.4 Discussion 280
6.5 Conclusions 285

Chapter 7: Concluding remarks and future studies 287

Appendix: si/shRNA and primer sequences

References

Figures and Tables

Figure 1.1: Anatomy of the human eye

Figure 1.2: Fundus photograph of the human eye

Figure 1.3: Structural compositions of the retina

Figure 1.4: Light micrograph of a plastic-embedded retinal section

Figure 1.5: Anatomy of human photoreceptor cells

Figure 1.6: Structural model of rhodopsin

Figure 1.7: The phototransduction cascade

Figure 1.8: Comparison of a normal retina to a RP retina

Figure 1.9: Schematic illustration of rhodopsin-mediated cell death pathways

Figure 1.10: Mechanism of RNA interference

Figure 1.11: The DNA-vector based RNAi system

Figure 1.12: The routes of *in-vivo* siRNA delivery into animal models

Figure 1.13: Genomic organisation of miRNAs

Figure 1.14: Gene silencing by miRNAs

Figure 1.15: Model of miRNA target accessibility

Figure 1.16: The mRNA cycle

Figure 1.17: The reversal of aptamer activity by classical antisense oligonucleotide antidote and aptamer-caged antidote

Figure 1.18: The *de novo* guanine nucleotide synthesis pathway

Figure 1.19: The use of alternative promoters for the expression of three different IMPDH type I transcripts.

Figure 1.20: Schematic representation of the IMPDH1 gene exon structure and the human IMPDH1 crystal structure

Figure 1.21: Light micrographs and ERG responses from IMPDH1 knockout mice

Figure 1.22: Novel human IMPDH1 transcripts and proteins identified through alternative splicing

Figure 1.23: Novel mouse IMPDH1 transcripts and proteins identified through alternative splicing

Table 1.1: Identified genes responsible for retinitis pigmentosa and functions of their protein products

Table 1.2: A classification of known mutations in rhodopsin

Table 1.3: P-bodies compositional components

Table 1.4: Aptamers currently in the clinical pipeline

Figure 2.1: Analyses of amplification, regression and melting curves for Real Time RT-PCR quantification

Figure 2.2: Vector map of pBluescript-H1

Figure 2.3: Vector map of CMV-promoter driven pcDNA3.1(+)

Figure 2.4: Restriction map and multiple cloning sites of pEGFP-1

Figure 2.5: Vector map and multiple cloning sites of pUb6/V5-His A, B, C

Figure 2.6: Vector map and multiple cloning sites of pAAV-MCS

Figure 3.1: Vector maps and sequencing of wild type and mutant IMPDH1 expressing vectors

Figure 3.2: Alignment of IMPDH1-specific shRNAs with human and mouse IMPDH1 cDNAs

Figure 3.3: Secondary structure of human IMPDH1 mRNA

Figure 3.4: Sub-cloning of shRNA oligonucleotides into pBluescriptH1 vector to construct the human H1 polymerase III promoter driven vector for short hairpin RNA

Figure 3.5: Determination of transfection efficiency by β-galactosidase staining

Figure 3.6: Effect of dose on the transfection efficiency of plasmid vectors in mammalian cells

Figure 3.7: Suppression of endogenous IMPDH1 transcripts in HEK293T cells

Figure 3.8: siRNA-mediated suppression of endogenous IMPDH1 mRNA expression in HeLa cells

Figure 3.9: Dose-dependent suppression of IMPDH1 transcripts in HeLa cells

Figure 3.10: Comparisons of the levels of endogenous and exogenous IMPDH1 transcripts in HeLa cells by quantitative Real Time RT-PCR analysis

Figure 3.11: Efficiency of IMPDH1-specific siRNAs in targeting total IMPDH1 (exogenous and endogenous transcripts) in HeLa cells

Figure 3.12: Analyses of EGFP expression by fluorescence microscopy

Figure 3.13: siRNA-mediated knockdown of mutant IMPDH1 transcripts in N2a cells

Figure 3.14: siRNA-mediated suppression of wild type IMPDH1 protein in HeLa cells

Figure 3.15: Time-dependent expression of wild type IMPDH1 protein in HeLa cells

Figure 3.16: siRNA-mediated suppression of mutant IMPDH1 protein harbouring the Arg224Pro mutation in HeLa cells

Figure 3.17: Suppression of endogenous IMPDH1 mRNA in HeLa cells by polymerase III H1-promoter driven shRNAs

Figure 3.18: Suppression of wild type IMPDH1 protein in HeLa cells by IMPDH1-specific shRNAs

Figure 3.19: Suppression of mutant IMPDH1 protein harbouring the Arg224Pro mutation in HeLa cells by IMPDH1-specific shRNAs

Figure 3.20: Suppression of mutant IMPDH1 protein harbouring the Asp226Asn mutation in HeLa cells by IMPDH1-specific shRNAs

Figure 3.21: Cleaved-caspase 3 staining in HeLa cells

Figure 3.22: Induction of apoptosis by over-expression of mutant IMPDH1 harbouring the Arg 224Pro mutation in HeLa cells

Figure 4.1: Schematic illustration of Fluorescent activated cell sorting (FACS) analysis

Figure 4.2: Schematic representation of a dual expression vector system

Figure 4.3: Schematic diagram of *in-vitro* electroporation

Figure 4.4: Vibratome sectioning of retinal explants

Figure 4.5: Suppression of endogenous mouse IMPDH1 transcripts in N2a cells by sh2048

Figure 4.6: FACS analysis of retinal explants electroporated with non-targeting shRNA (Experiment 1)

Figure 4.7: FACS analysis of retinal explants electroporated with IMPDH1-specific shRNA (Experiment 1)

Figure 4.8: FACS analysis of retinal explants electroporated with non-targeting shRNA (Experiment 2)
Figure 4.9: FACS analysis of retinal explants electroporated with IMPDH1-specific shRNA (Experiment 2)
Figure 4.10: Suppression of IMPDH1 transcripts in mouse retinal explants
Figure 4.11: Vibratome sections of *in-vitro* electroporated mouse retinal explants

Figure 5.1: The wild type genome of adeno-associated virus (AAV)
Figure 5.2: Life cycles of wild type AAVs and recombinant AAVs
Figure 5.3: Schematic illustration of pseudotyped AAV production and target tissues
Figure 5.4: The biphasic waveforms of electroretinography (ERG) and schematic illustration of subretinal injection
Figure 5.5: Schematic illustration of AAV-2/5 shRNA vectors
Figure 5.6: Schematic overview of the production of recombinant AAV particles expressing IMPDH1-specific shRNAs
Figure 5.7: rAAV transduction of mouse retinal explants and *in-vivo* mouse retinas
Figure 5.8: Immunolocalisation of IMPDH1 in wild type C57B6/CBA mouse retina
Figure 5.9; **Injection #1**: FACS analysis of eight 2-weeks old wild type C57B6/CBA
Figure 5.10; **Injection #1***:* AAV-mediated shRNA suppression of IMPDH1 in wild type C57B6/CBA retinas
Figure 5.11: **Injection #2;** FACS analysis of six 3 month-old wild type C57B6/CBA mice
Figure 5.12: **Injection #2**; AAV-mediated suppression of IMPDH1 in six 3-month-old wild type C57B6/CBA mice
Figure 5.13: **Injection #3;** FACS analysis of six 2 week-old wild type C57B6/CBA mice
Figure 5.14: **Injection #3;** AAV-mediated suppression of IMPDH1 in six 2-weeks old wild type C57B6/CBA mice
Figure 5.15: **Injection #4:** *In-vivo* suppression of IMPDH1 transcripts (Part A)
Figure 5.16: **Injection #4**: *In-vivo* suppression of IMPDH1 transcripts (Part B)

Table 5.17: A summary of FACS analyses data and corresponding % IMPDH1 mRNA suppression obtained from four separate injection experiments

Figure 5.18: Detection of endogenous mouse IMPDH1 and IMPDH2 proteins in wild type C57CBA/B6 mouse retinas

Figure 5.19: Western blot analysis of AAV-mediated shRNA suppression of IMPDH1 protein in wild type C57CBA/B6 mouse retinas

Figure 5.20: Immunohistochemical analysis of AAV-mediated shRNA suppression of IMPDH1 in wild type C57B6/CBA mouse retinas

Figure 5.21: Time-course analysis of the effect of AAV-mediated suppression of IMPDH1 on retinal histology

Table 5.22: A table illustrating b-wave amplitudes of rod-isolated response from wild type 129 S2/SvHsd mice co-injected with AAV-IMPDH1 and AAV-shRNAs

Figure 5.23: The effect of AAV-mediated co-expression of IMPDH1 and shRNA on b-wave amplitudes of rod-isolated response in wild type 129 S2/SvHsd mice.

Figure 5.24: Pathohistological analysis of wild type 129 S2/SvHsd retinas co-injected with AAV vectors expressing wild type IMPDH1 and shRNAs.

Figure 5.25: Pathohistological analysis of wild type 129 S2/SvHsd retinas co-injected with AAV vectors expressing mutant IMPDH1 harbouring the Arg224Pro mutation and IMPDH1-specific shRNAs

Figure 5.26: Poor AAV transduction observed in mouse retinal sections

Figure 5.27: AAV-mediated shRNA suppression of mutant IMPDH1 protects retinal histology

Appendix

Table 1: Sequences of IMPDH1-specific shRNAs and synthetic siRNAs, and non-targeting control si/shRNAs

Table 2: Sequences of HPLC-purified primers for Real-Time RT-PCR amplification

Table 3: Sequences of primers for template-DNA amplification

Table 4: Sequences of primers used for sequencing of shRNAs subcloned into pBluescript-H1 and IMPDH2 cDNA subcloned into pcDNA3.1(+)

Table 5: Primers used for sequencing pWtIMPDH1, pMutIMPDH1(224), pWtIMPDH1.EGFP, pMutIMPDH1(224).EGFP and pMutIMPDH1(226).EGFP.

Table 6: Primers used for PCR amplification of human Ubc intron from pUB6/V5-His

Table 7: Primers for sequencing pshLuc.EGFP and psh2048.EGFP

Abbreviations

AAV	Adeno-associated virus
AdRP	Autosomal dominant retinitis pigmentosa
AD	Alzheimer's disease
AGTPBP1	ATP/GTP binding protein 1
ALS	Amylotrophic lateral sclerosis
AMD	Age-related macular degeneration
ArRP	Autosomal recessive retinitis pigmentosa
ARE	AU-rich element
Arg	Arginine
Asn	Asparagine
Asp	Aspartic acid
ATCC	American Tissue Culture Collection
ATP	Adenosine tri-phosphate
BCP	Blue cone pigment
BBS	Bardet-Biedl Syndrome
CBS	Cystathionine β-synthase
cDNA	Complementary DNA
cGMP	Cyclic guanosine monophosphate
CLN	Ceroid lipofuscinosis
CMV	Cytomegalovirus
CNS	Central nervous system
CNTF	Ciliary neurotrophic factor
CNV	Choroidal neovascularisation
CRX	Cone-rod homeobox
CSBN	Congenital stationary night blindness
DAT	Dopamine transporter
DHA	Docosahexaenoic acid
DMEM	Dulbecco's modified eagle medium
dNTP	Di-nucleotide triphosphate
DPR	Diabetic proliferative retinopathy

DTT	Dithiothreitol
EDTA	Ethylenediamine tetra acetic acid
EIF	Eukaryotic initiation factor
ER	Endoplasmic reticulum
ERG	Electroretinography
FIV	Feline immunodeficiency virus
GAPDH	Glyceraldehyde 3-phosphatedehydrogenase
GCL	Ganglion cell layer
GDP	Guanosine diphosphate
GFAP	Glial fibrillary acid protein
Glu	Glutamic acid
GMP	Guanosine monophosphate
GNDF	Glial cell derived neurotrophic factor
GPCR	G-protein coupled receptor
GTP	Guanosine triphosphate
HCL	Hydrochloric acid
HEK	Human embryonic kidney
His	Histidine
HPRT	Hypoxanthine phosphoribosyl transferase
HSV	Herpes simplex virus
IBRP	Interphotoreceptor retinoid binding protein
Ile	Isoleucine
ILM	Internal limiting membrane
IMP	Inosine 5'-monophosphate
IMPDH	Inosine 5'-monophosphate dehydrogenase
IMPDH1	Inosine 5'-monophosphate dehydrogenase type 1
IMPDH2	Inosine 5'-monophosphate dehydrogenase type 2
INL	Inner nuclear layer
IPL	Inner plexiform layer
ISH	In-situ hybridisation
LB	Luria- Bertani

LCA	Leber Congenital Amaurosis
Leu	Leucine
LRAT	Lecithin retinol acetyltransferse
Lys	Lysine
mRNA	Messenger RNA
miRNA	Micro RNA
NAD	Nicotinamide adenine dinucleotide
NADH	Nicotinamide adenine dinucleotide, reduced
NFL	Nerve fibre layer
NRL	Neural retina leucine zipper
OCT	Optical coherence tomography
ONL	Outer nuclear layer
OPL	Outer plexiform layer
PBS	Phosphate buffer saline
PCR	Polymerase chain reaction
PDE	Phosphodiesterase
PEDF	Pigment epithelium derived factor
Pro	Proline
PRPF	Pre-mRNA processing factors
PRPS	Phosphoribosyl pyrophosphate synthetase
RCS	Royal College of Surgeons
RD	Retinal degeneration
RDRP	RNA dependent RNA polymerase
RDS	Retinal degeneration slow
RHO	Rhodopsin
RISC	RNA-inducing silencing complex
RLBP	Retinaldehyde binding protein
ROM	Rod-cell outer membrane protein
ROS	Reactive oxygen species
RP	Retinitis pigmentosa
RPA	Retinitis punctata albescens

RPE	Retinal pigment epithelium
RT-PCR	Reverse transcriptase-PCR
SCA	Spinocerebellar ataxia
SDS	Sodium dodecyl sulphate
SDS-PAGE	SDS-polyacrylamide gel electrophoresis
shRNA	Short hairpin RNA
siRNA	Small interfering RNA
SNALP	Stable nucleic acid-lipid particles
SNP	Single nucleotide polymorphism
SOD	Superoxide dismutase
STGD	Stargardt disease
TAE	Tris-acetate-EDTA
TFD	Transcription factor decoys
TNF	Tumour necrosis factor
UPR	Unfolded protein response
UPS	Ubiquitin proteasome system
UTR	Untranslated retgion
Val	Valine
VEGF	Vascular endothelial growth factor
XMP	Xanthosine 5'-monophosphate

" O admirable necessity!

O powerful action!

What mind can penetrate your nature?
What language can express this marvel?
None, to be sure.

This is where human discourse turns
toward the contemplation of the divine."

-*Leonardo da Vinci* on the miracle of the
human eye

"The desire to know is natural to good men"

-*Leonardo da Vinci*

Chapter 1
General Introduction

1 General introduction

Approximately 7,000 people are on the Register of Blind persons maintained by the National Council for the Blind of Ireland, although at least twice that number are believed to be visually handicapped to the extent that they would be classifiable as legally blind (visual acuity 6/60 and field loss to 10%). The most prevalent cause of blind registration among people of working age is the hereditary degenerative retinopathy, retinitis pigmentosa (RP). While the condition is currently incurable, relentless progress has been made in the identification of genes responsible for this hereditary condition. RNA interference (RNAi)-mediated suppression of mutations within one of these genes, encoding inosine 5'-monophosphate dehydrogenase type I (IMPDH1) has been the subject of the research reported in this thesis. Hence, in this introductory chapter, an outline of the structure of the mammalian eye and retina is provided, together with the process of visual transduction. This will be followed by a detailed account of the symptoms associated with RP and its hereditary patterns. Use of animal models is central to the development of gene therapies and hence coverage will also be provided by available animal models of RP and related diseases. RNAi has been used extensively in the work-up of methodologies for the suppression of IMPDH1 transcripts, and hence background information is provided to this immensely powerful technology. The final section focuses on the identification of mutations in the IMPDH1 gene that cause the RP10 form of autosomal dominant RP, and also recent progress made in understanding the underlying disease mechanism associated with RP10.

1.1 The Human Eye

The human eye is a receptor organ of the visual system that imports information from the environment in the form of light, and transforms it into the world we see. A physicist, Richard Feynman, once described the extraordinary nature of visual perception as follows: "we are immersed in a sea of electromagnetic waves whose lengths vary over a wide range. These waves interact with each other and also with objects around us to present a cacophony of electromagnetic signals to our eyes. Through a tiny aperture of ~2mm in diameter, the eye selects a small fraction of these

wavelengths and together with the brain, reconstructs the position, colour, shape and even motion of each object we see around us."

The eye is a unique and delicate sense organ that is enwrapped in a framework of connective tissues situated in the anterior part of the orbital cavity. The anatomy of the eye may be divided into three distinctive coats: (1) the outer fibrous layer of connective tissue forms the cornea and sclera; (2) the middle vascular layer is composed of the iris, ciliary body, and choroids; (3) and the inner neural layer is the retina (*Figure 1.1*; Remington, Clinical anatomy of the visual system).

Furthermore, the eye is also divided into three segmented chambers: (1) the anterior chamber; (2) the posterior chamber in which the crystalline lens is located; (3) the vitreous chamber (*Figure 1.1*). The sclera is a tough outer coat that is fibrous and the cornea is continuous with the sclera and provides the first component of the refractive media that bend the light to form an image on the retina. The biconvex lens that is supported by suspensory ligaments lies behind the iris, and directly behind the lens is the vitreous humor, which makes up the greater part of the globe. Aqueous humor fills both the posterior and the anterior chamber, where both chambers are continuous through the pupil. The retina is a multilayered neural structure that makes up the lining at the back of the eye, and can be visualised in the living eye with an ophthalmoscope. Axons radiate from the retina through the optic disc or optic papilla and enter the optic nerve to reach the brain. At the posterior post of the eye, the retina thins to form the fovea, which is a specialised area dedicated for high-visual acuity. Posterior to the retina is the pigment epithelium, which is separated from the sclera by the vascular choroids. The vascular choroids coat is continuous with fibrovascular components of the ciliary body and the iris, and collectively, these three components constitute the uvea (*Figure 1.1*; Remington, Clinical anatomy of the visual system; McIlwain, An introduction to the biology of vision).

1.2 The vascular supply of the eye

Arterial blood reaches the eye principally through the ophthalmic artery, which is the primary intracranial branch of the internal carotid artery. A family of ciliary arteries that are branches of the ophthalmic artery supplies the uveal vasculature, and some of these may enter the eye around the margins of the optic disc, or via the anterior segment of the eye before penetrating the sclera. The central retinal artery enters the eye through the optic disc and branches out across the retina. After the blood passes through the retinal capillaries, it leaves the retina through the central retinal vein passing the jugular vein and eventually back to the heart. The human retina depends on both the choroid and the retinal vessels for its blood supply. These two supply systems serve different parts of the retina and are also regulated in different ways. First the choroid blood vessels supply the nearby photoreceptor cells, which have a high blood flow rate that is determined by the arterial pressure. Since the photoreceptor layer is one of the most metabolically demanding areas of the body, the choroid is always swamped with blood to ensure a constant supply.

The retinal vessels in contrast supply blood to the inner layers of the retina (retinal layers closest to the vitreous humor), and the blood flow rate is independent of arterial pressure as the arterioles change their diameters in response to the metabolic needs of the local tissue. For example, an increased need for oxygen and removal of wastes products result in dilation of the vessels and increased blood flow. This 'autoregulation' of blood flow in the retinal vessels is a unique property of the vascular smooth muscle, which are not innervated by the autonomic nervous system. Blood circulation does not merely supply oxygen and nutrients to the eye, but also removes waste products of metabolism and aqueous humor. Furthermore, blood circulation also controls the temperature of the eye within normal limits. Because the lens and aqueous vitreous are devoid of vessels, heat generated by metabolism or by external light sources can only be removed by blood flowing through the choroidal and retinal circulations.

Blood carried to the eye may contain cellular elements and other substances that would interfere with retinal function if allowed access to the neural tissues. Therefore, tight junctions between the cells of the retinal capillary walls have formed a barrier that only permits the entry of certain constituents of plasma to cross to the retina. This system is essentially similar to that of the blood-brain barrier. The large amount of fluids leaving the choroid is filtered by the pigment epithelium that regulates the composition of materials before reaching the retina. Similarly, large amount of fluids must be supplied through the ciliary processes to form the aqueous humor, but the double-layered epithelium of the ciliary processes operates as a barrier to the passage of unwanted substances (McIlwain, An introduction to the biology of vision).

1.3 Anatomy of the retina and photoreceptor cells

The innermost lining of the eye is a neural layer called the retina, which is located between the choroid and the vitreous humor. The neural retina appears as a thin transparent layer of nervous tissue that has a surface area of ~0.266 mm^2, and is thickest near the optic disc measuring 0.56 mm, and becomes thinner towards the periphery reducing to 0.18mm. The centre of the retina is the optic nerve head, which is an oval-shaped white area measuring 2 x 1.5 mm in diameter where major blood vessels radiate out. The circular shaped reddish spot which is free of blood vessels is the fovea, representing the centre of the macular (*Figure 1.2*). The retina is the site of transformation of light energy into neural signals where this information is transmitted to the central nervous system for interpretation. In general, the retina has a laminar appearance that is composed of a single layer of pigmented epithelium and three layers of neuronal sensory cells bodies (photoreceptors, bipolar cells and ganglion cells) connected by a network of synapses. However, upon closer examination of retinal cross-section under the light microscope, ten distinct layers of retinal neurons are found to be arranged in a remarkable framework of interacting cell bodies. The ten layers of the retina are illustrated in *Figures 1.3* and *1.4* and are discussed in detail below (Bron *et al.*, Wolff's anatomy of the eye and orbit; Remington, Clinical anatomy of the visual system).

1) Retinal pigment epithelium (RPE)
2) Photoreceptor layer of rods and cones
3) External limiting membrane
4) Outer nuclear layer (ONL)
5) Outer plexiform layer (OPL)
6) Inner nuclear layer (INL)
7) Inner plexiform layer (IPL)
8) Ganglion cell layer (GCL)
9) Nerve fiber layer (NFL)
10) Internal limiting membrane (ILM)

1.3.1 Retinal pigment epithelium

The RPE is the outermost retinal layer consisting of a single layer of approximately five million pigmented cells attached firmly to its basal lamina. The apical portion of the RPE cells consists of microvilli that are extended into the photoreceptor layer. However, there is no intercellular junctions connecting the two layers, and a potential space separates the pigmented epithelial cells and the outer segments of photoreceptors forming the subretinal space. The RPE is an active area that has several protective functions; a) the zonulae occludens of RPE are an important component of the blood-ocular barrier that selectively removes unwanted substances from the choriocapillaries before entry into the retina; b) the cellular lysosomes within the interphotoreceptor matrix enable phagocytosis of disposed fragments from the continual shedding of the photoreceptor outer segment discs; c) the RPE metabolizes and stores vitamin A which is needed for the formation of photopigment molecules; d) melanin, the pigment granules within RPE cells can also absorb scattered light, thereby reducing excess scattering (*Figure 1.3 and 1.4*)

1.3.2 Photoreceptor layer of rods and cones

The basic components of vertebrate photoreceptors consist of six different compartments; i) the outer segment, which contains the photopigment responsible for the conversion of light into neural signals; ii) a connecting cilium stalk; iii) the inner

segment that contains the metabolic apparatus; iv) the outer fiber, cell body and the inner fiber which ends in a synaptic terminal (*Figures 1.3, 1.4 and 1.5*).

i) The outer segment is a specialised cilium that is made up of a stack of membranous discs enclosed within the plasmalemma of the cell. Each disc is a flattened membrane sac with a narrow intradisc space, and the photopigments that absorb light and initiate the phototransduction cascade are part of the major structural element in these membranous discs.

ii) The ciliary stalk or cilium extends from the innermost disc and connects the outer segment to the inner segment, acting as a guiding tunnel for transferring incident photons to the light-sensitive pigments. The cilium is made up of nine pairs of tubules from which the central pair is absent, and the plasmalemma around the outer segment is continuous across the cilium with that of the inner segment.

iii) The structure of the inner segment can be divided into two parts: the *ellipsoid* is closer to the outer segment and possesses a number of mitochondria that provides the metabolic needs of the photoreceptor, the *myoid* is located nearer to the cell body contains other cellular organelles (endoplasmic reticulum, golgi apparatus) where protein synthesis is concentrated.

iv) The outer fiber extends from the inner segment to the cell body, which contains the photoreceptor nucleus. The inner fiber is an axonal structure composing of numerous microtubules that connects the cell body to a specialised synaptic terminal ending, where synaptic vesicles are situated.

Vertebrate retinas have two types of photoreceptor cells, termed rods and cones, which are named after the morphological shapes of their outer segments. On average, there are approximately 92 million rods and 4.6 million cones in the human eye. The density of the cones is maximal at the fovea, but their numbers decrease rapidly with increasing eccentricity from the fovea. In contrast, the rods are highly concentrated along the center of the optic nerve extending towards the nasal and superior retina, but decreases gradually from this area to the far periphery.

The differences between rods and cones lie mainly in the morphology of their outer segments. The outer segments of rods are cylindrical in shape and contain uniform stacks of flattened double lamella membrane in the form of discs. There are approximately 800 discs per rod, and individual discs are not attached to each other or to the surface plasma membrane. Rod photoreceptor cells are highly sensitive and are used to perceive the environment under low illumination. The discs contain 90% of the photosensitive pigment rhodopsin, which has a maximum absorption at 495nm. Studies have also shown that the components of disc membranes are produced within the inner segment, and transported to the discs at the outer segment base via the cilium. The old discs are gradually displaced outward by the formation of new discs, and once the discarded discs reach the tip of the outer segment, they are taken up to the retinal pigment epithelium and become phagocytosed. The shedding of disc occurs on a regular basis with the most predominant time being in the early morning.

The morphology of cone outer segments differs greatly depending on their location in the retina. Typically the cones have a long outer segment similar to that of the rods near the center of the fovea, but become shortened and conical near the periphery region. The outer segments of cones have approximately 1100 discs and the intra- and inter- disc spaces are much wider than that of rods. In contrast to rods, cone discs are attached to each other and also to the surrounding plasma membrane over short segments of their circumference, thus they do not detach easily. Cone photoreceptor cells provide high visual acuity that allows for colour perception and fine details. The primary function of cones is to perceive the environment in good illumination (day light vision), and absorb light at three different wavelengths (λ) known as trichromatic vision (long λ-red at 560nm, medium λ-green 530nm and short λ-blue at 420nm). Electron-microscopic studies have shown that cone discs formation occur at the base of the outer segment similar to the rods, and are too shed periodically often at the end of the day, and phagocytosed by the retinal pigment epithelium (Bron *et al.*, Wolff's anatomy of the eye and orbit; Remington, Clinical anatomy of the visual system).

1.3.3 External limiting membrane

Under the light microscope, the external limiting membrane separates the layer of rods and cones from the overlying outer nuclear layer (*Figure 1.3 and 1.4*). However, the external limiting membrane is not a true membrane, but instead it consists of intercellular junctions among photoreceptor cells, and also between the photoreceptors and Muller cells at the inner segment level. The main functional implications of these junctional complexes are to provide a selective barrier for the passage of nutrients between adjacent Muller cells and to stabilise the transducing portion of the photoreceptors.

1.3.4 Outer Nuclear Layer (ONL)

The outer nuclear layer (ONL) lies internal to the external limiting membrane and contains the cell bodies and nuclei of the photoreceptor cells. The nuclei of cones are located internal to the external limiting membrane and are slightly larger than those of the rods. The outer fibres of cones are usually short, and are organised in a single layer because of the close proximity of their nuclei to their inner segment and the external limiting membrane. However, the outer fibres of rods are much longer, and are organised in several rows further away from the external limiting membrane, therefore the inner fibres of the rods pass over a shorter distance to reach their second-order neurons in the outer nuclear layer than do the cone inner fibres. The outer fibres of both rods and cones contain mitochondria, smooth endoplasmic reticulum and perinuclear neurotubules (*Figures 1.3 and 1.4*).

1.3.5 Outer Plexiform Layer (OPL)

The outer plexiform layer (OPL) possesses two different cell layers, a wider external band consisting of inner fibres of rods and cones, and a narrower band that is made up of dendrites of the bipolar and horizontal cells. The OPL is thickest near the macula and predominantly consists of oblique fibres that have deviated from the fovea. The rods synapse with bipolar and horizontal cells through round cytoplasmic expansions known as spherules, whereas cone synapses through larger cytoplasmic expansions called pedicles. The spherule of rods contains numerous presynaptic

vesicles filled with acetylcholine, mitochondria and neurotubules. The axons of horizontal cells are buried deeply inside the spherule, whereas the penetration is not as deep in axons of bipolar cells. A horizontal cell can only contact a rod spherule once, but each spherule may be contacted by numerous horizontal cells. In addition, up to four bipolar cells may contact an individual spherule at different points.

The cone pedicle has a pyramidal shape with the axon forming its apex. The synaptic indentations on the pedicles receive three different neurons arranged in a specific structural order called the 'triad'. The central axon of the triad originates from a midget bipolar cell and may contact the same cone at up to 25 different points. The other two dendrites on either side of the triad belong to different horizontal cells, and only come into contact with the cone pedicle at one point (*Figures 1.3, 1.4 and 1.5*).

1.3.6 Inner Nuclear Layer (INL)

The inner nuclear layer (INL) is probably the most complex layer of the retina, because it is made up of 8-12 rows of closely packed nuclei of five different cell types; bipolar cells, horizontal cells, amarcine cells, interplexiform cells and supportive Muller cells. Under the light microscope, the inner nuclear layer itself can be distinguished into four parts: i) the outermost layer containing the horizontal cell nuclei, ii) the outer intermediate layer with bipolar cell nuclei, iii) the inner intermediate layer with Muller cell nuclei, iv) the innermost layer with amacrine and interplexiform cell nuclei (*Figures 1.3 and 1.4*).

i) Horizontal cells function in the modulation and transformation of visual information received from the photoreceptors. Unlike bipolar cells, from which the information is transferred radially through the retina, horizontal cells form a network of fibres that activate the activity of photoreceptor cells horizontally. Each horizontal cell has a long axon and several short dendrites with branching terminals. Depending on the size and the synapses made by the dendrites and axons, three types of horizontal cells have been identified to date: H1, HII and HIII. The H1 cell is characterised by its long, stout dendrites that synapse with seven to nine cone pedicles and has a large thick axon in a fan-shaped terminal

contacting rod spherules. Most of the HII cells have slim overlapping dendrites and a short curved axon that contact cones and might be particularly sensitive to blue cones. The HIII cells have a broad dendritic tree that synapses with a large number of cones, and might be selective for red and green cones.

ii) The bipolar cells are the second-order neurons in the visual circuitry. The dendrites of bipolar cells synapse with photoreceptors and horizontal cells, while the axons synapse with ganglion and amacrine cells. The main function of bipolar cells is to relay information from photoreceptors to horizontal and ganglion cells, and also to receive synaptic feedback from amacrine cells. Nine different types of bipolar cells have been identified based on the morphology and synaptic relationships with photoreceptor cells: 1) Rod (mop) bipolar cells make up 20% of the total population and synapse with rod spherules only; 2) Flat midget bipolar cells synapse with cone pedicles; 3) Invaginating midget bipolar cells contain dendrites that make contact with cone pedicles as the central tuft of the 'triad'; 4, 5) Both flat diffuse and invaginating diffuse bipolar cells contain a broad expanse of dendritic processes that terminate at the pedicles of many cones; 6, 7) The on-centre blue cones and off-centre blue cones both innervate more than one cone pedicle; 8, 9) Giant bi-stratified and giant diffuse bipolar cells both have a major dendrite that branches into three long sinuous trees, and clusters of processes branch from these to cone pedicles., and only differ in the location of their axon termination.

iii) Muller cells are large neuroglial cells that make up most of the inner intermediate layer of the inner nuclear layer. Muller cells appear like columnar epithelial cells and they are also the largest of all cells in the retina, with its cell mass extending from the external to the internal limiting membrane. As the major glial cells of the retina, they play a supportive role in conserving the structural alignment of its neuronal elements. During the development of a retina, Muller cells play an important role in orientation, displacement and positioning of developing

neurons. The Muller cell is also involved in glycogen metabolism and has high glycogen content, which contributes to retinal nutrition.

iv) The amacrine cell has a large cell body, a lobulated nucleus and a single process that branches extensively throughout the inner plexiform layer. The amacrine process, which possesses characteristics of both dendrites and axons, mainly function in carrying information horizontally by forming synapses with axons of bipolar cells, dendrites of ganglion cells and processes of interplexiform neurons. Three groups of amacrine cells have been described based on the area covered by their intertwined branching process: small-field, medium-field and large-field amacrine cells. To add to this complexity, these groups can be further divided into eight different subgroups based on their dendritic tree size, branching pattern and stratification level of nerve endings.

The nuclei of interplexiform neurons occupy the innermost part of the inner nuclear layer. The processes of interplexiform neurons extend into both inner and outer plexiform layers conveying information between these layers, and may provide feedback from inner retinal layers to the photoreceptors (Bron *et al.*, Wolff's anatomy of the eye and orbit; Remington, Clinical anatomy of the visual system).

1.3.7 Inner Plexiform Layer (IPL)

The inner plexiform layer (IPL) marks the junction between bipolar cells and ganglion cells, and also hosts a series of synaptic connections between the axons and dendrites of bipolar, ganglion, amacrine and interplexiform cells. The bipolar cell terminals provide input into the IPL and the ganglion cells carry the output. In addition, amacrine cells also mediate interactions among this layer using two distinct synapses; reciprocal and serial synapses. In a reciprocal synapse, the process of amacrine cells contacts a nearby bipolar cell terminal, thus allowing for feedback of amacrine and bipolar cells. The serial synapses contain two consecutive synaptic connections between two amacrine cells and a third connection with either a ganglion, bipolar or another amacrine cell. This network of connections enables local

interactions among neighboring amacrine cells. The interplexiform cells receive input from the amacrine cells through conventional synapses. The inner plexiform layer is thicker and has a greater variety of synapses than the outer plexiform layer *(Figures 1.3 and 1.4)*.

1.3.8 Ganglion Cell Layer (GCL)

The ganglion cell layer (GCL) is mainly composed of large ganglion cell bodies, although other elements such as displaced amacrine or Muller cells, other astroglial cells and branches of retinal vessels are also present. The ganglion cell layer generally forms a single layer near the peripheral retina, and two layers are formed at the temporal side of the optic disc. However, the thickness may extend eight to ten layers near the macular region of the retina. Ganglion cells have a large nucleus and abundant cytoplasm that contains rough endoplasmic reticulum. The ganglion cell cytoplasm appears dense as numerous microfilaments exist and make them easily distinguishable from that of Muller cells. Approximately 1.2 million ganglion cells are present in the retina and each of these produces a single axon that converges and exits through the eye as the optic nerve. In general, the ganglion cells are multipolar, with dendrites extending horizontally and radially into the inner plexiform layer. Almost 18 different types of ganglion cells have been identified across different species based on variations in both morphology and physiology, and two major types of ganglion cells, designated as P and M ganglion cells, have been identified in the human retina. The P ganglion cells are specialised cells in primates for colour vision and M cells resemble the α-ganglion cells of the cat retina (*Figures 1.3 and 1.4*).

1.3.9 The Nerve Fibre Layer

The nerve fibre layer (NFL) consists of the ganglion cell axons (called afferent fibres), glial cells, a rich capillary bed and centrifugal (efferent) fibres. The ganglion cell axons/afferent fibres run in a delinearised pathway parallel to the retina surface, and proceed towards the optic disc, where it takes a right angle turn to exit the eye through the lamina cribrosa as the optic nerve. The ganglion cell axons/afferent fibres are generally unmyelinated until they reach the optic nerve. Within the NFL, afferent

fibres have a regulatory bidirectional axoplasmic flow that function at two flow rates; a slow flow rate (0.5-5mm per day) is responsible for the transportation of high molecular weight proteins for axonal growth and maintenance of the axons; the fast rate (10-2000mm per day) caters the molecules involved in synaptic function. The NFL is the thickest along the margins of the optic disc, where all the fibres accumulate together. The area in which the group of afferent fibres radiates out to the optic disc from the macular region is called the papillomacular bundle. This grouping of fibres is of utmost importance because it carries the information that determines visual acuity. The retinal vessels, including the superficial capillary network serve primarily in the NFL layer, and Muller cells may also be present in the NFL to provide protective covering for vessels and nerve fibres (*Figures 1.3 and 1.4*).

1.3.10 Internal Limiting Membrane (ILM)

The internal limiting membrane (ILM) forms the inner most layer of the retina, and the outermost boundary of the vitreous body. The retina and the vitreous body both contribute evenly to the structural formation of the ILM; a smooth inner vitreous surface is made up of the collagen fibres and proteoglycans of the vitreous body, and an uneven outer retinal surface is composed of expanded terminations of the Muller cells (footplates) covered by a basement membrane. The ILM is a region of occluding junctions and serve as a tight barrier for sealing off the retinal components from potentially harmful materials present in the vitreous body (*Figures 1.3 and 1.4*) (Bron *et al.*, Wolff's anatomy of the eye and orbit; Remington, Clinical anatomy of the visual system).

1.4 The Phototransduction Pathway

The phototransduction pathway is responsible for the conversion of photons (elementary particles of light) into electrical signals, and is initiated by the visual pigment rhodopsin. Rhodopsin is a prototypic member of G-protein coupled receptor (GPCR) superfamily, and it is the main protein component of the stacked discs found in the outer segments of rod cells (Bockaert and Pin, 1999; Ji *et al.*, 1998). The members of this family share a basic seven-transmembrane helical design and their basic function involves binding and activating a G-protein, which is transducin in the case of the visual system (Hamm, 2001; Meng and Bourne, 2001). Each visual pigment rhodopsin is composed of the apoprotein opsin (348 amino acid residues organised into three distinct domains: cytoplasmic, transmembrane and intradiscal) and the 11-cis retinal chromophore (a small molecule derived from vitamin A) bound to Lys-296 in the seventh transmembrane helix, through a protonated Schiff base linkage (*Figure 1.6*) (Hargrave, 2001; Pepe, 2001; Palczewski *et al.*, 2000). In general, the phototransduction cascade can be divided into three main biochemical events (*Figure 1.7*) (Ridge *et al.*, 2003; McIlwain, An introduction to the biology of vision).

1) ***The activation of opsin molecules in the photoreceptors***:

When light enters the eye, the photons are absorbed by 11-*cis* retinal, which causes it to undergo isomerisation to its all-*trans* retinal form. This in turn changes the shape and receptors bound to rhodopsin, and converts it into its activated form called metarhodopsin II (R*).

2) ***Activated rhodopsin causes a decrease in cGMP intracellular levels***:

In photoreceptor cells, the cytoplasmic levels of cGMP are controlled by the membrane-bound cGMP phosphodiesterase, and the activity of this enzyme is relatively low in the dark state. However, upon activation of rhodopsin (R*) via photon absorption, the resulting conformational change activates transducin (a member of G-protein family that functions solely in visual signal transduction), causing its alpha subunit to dissociate from the trimer and exchange bound GDP

for GTP. GTP-bound active transducin then increases the activity of cyclic-GMP phosphodiesterase in hydrolysing cGMP to GMP. In resting rod cells, high levels of cGMP keeps the cyclic-GMP gated sodium channel open in the plasma membrane, and the membrane of the resting rod cells depolarised. However, the hydrolysis of cGMP to GMP causes a reduction in cGMP levels, resulting in the closure of cGMP-gated cation channels and decreases the inward flow of both sodium and calcium positive ions. The blockade of positive ion intake causes the plasma membrane to hyperpolarise, and initiates the electrochemical impulse responsible for conveying the signal from the sensory neuron to the CNS. Furthermore, resting rod cells release high levels of the inhibitory neurotransmitter, glutamate, and upon hyperpolarisation of the membrane, the release of glutamate is repressed to trigger a downstream action potential by ganglion cells that convey signals to the brain. Interestingly, a single photoactivated rhodopsin can catalyze the activation of 500 transducin molecules. While each transducin can stimulate one cGMP phosphodiesterase molecule, every cGMP phosphodiesterase molecule can hydrolyse 10^3 cGMP molecules per second. Therefore, a single activated rhodopsin can cause the hydrolysis of more than 10^5 cGMP molecules per second.

3) ***Termination of the phototransduction cascade:***

The photoreceptors must reliably signal the occurrence of different photic events over time; therefore the effects of a single exposure to light must be short-lived. This is achieved by limiting the lifetimes of the activated forms of rhodopsin (R*), transducin and phosphodiesterase (PDE), and also by restoring intracellular levels of cGMP. First, activated rhodopsin is returned to its pre-activated form by phosphorylation mediated by recoverin and rhodopsin kinase Grk1. Phosphorylated rhodopsin undergoes further internal transformations by binding to arrestin, and dissociates into the opsin and the chromophore, which returns to the all-*trans* form. The opsin remains in the disc membrane, while the all-*trans* retinal is converted back into its alcohol form (retinol), and transported to the pigment epithelium where it is re-isomerised to 11-*cis* retinol. The 11-*cis* retinal

is then returned to the photoreceptor outer segment, and oxidised to recombine with opsin. Inactivation of transducin occurs through the hydrolysis of bound GTP to GDP via an intrinsic GTPase activity that is accelerated by the GTPase activating protein RGS9 (regulator of G-protein signaling). The inactivation of phosphodiesterase is closely associated with the inactivation of transducin, where inactivated transducin dissociates from PDE, resulting in a cessation of PDE-mediated cGMP hydrolysis. Finally the activation of guanylate cyclase (GC-1 and GC-2) by guanylate cyclase activating protein (GCAP) restores cGMP levels and promotes the reopening of cGMP-gated channels.

1.5 Retinitis Pigmentosa (RP)

Retinitis pigmentosa (RP) is a heterogeneous group of inherited retinopathies that affects 1 in 4,000 people worldwide and leaving more than 1.5 million people visually handicapped (Hartong *et al.*, 2006; Mordes *et al.*, 2006). Initially described in the 18th century, RP encompasses a variety of retinal dystrophies, including both sporadic and familial forms. Familial RP displays all three modes of Mendelian inheritance, where the disease can be inherited as an autosomal dominant (30-40% of all cases), autosomal recessive (50-60% of all cases) or X-linked (5-15%) trait (Bunker *et al.*, 1984; Grondahl, 1987; Novak-Laus *et al.*, 2002). When the segregation pattern cannot be deciphered due to absence of family history, it is denoted as simplex RP. Although the majority of RP forms are monogenic, studies have reported digenic-diallelic, digenic-triallelic and maternal (mitochondrial) inheritance patterns, but only account for a small proportion of cases (Mansergh *et al.*, 1999; Kajiwara *et al.*, 1994; Katsanis *et al.*, 2001; Lestienne and Ponsot, 1988; Zeviani *et al.*, 1988). Digenic-diallelic inheritance was first reported in patients with double heterozygosity for mutations in the ROM1 and RDS gene (Kajiwara *et al.*, 1994). An example of digenic-triallelic inheritance was described in Bardet-Biedl syndrome (BBS) in which families required two mutant alleles on one gene, and a mutant allele on another for disease development (Katsanis *et al.*, 2001).

In most forms of typical RP, also called rod-cone dystrophy, mutations affect rods exclusively causing them to die by apoptosis, whereas cones are rarely affected by identified mutations, but degenerate secondarily almost invariably after rod depletion. A possible explanation for this phenomenon is that the breakdown of rod cells could adversely affect neighboring cones through non-specific environmental influences. The progressive disintegration of the surrounding rods might leave the cone outer segment more vulnerable to toxic insults. The accumulation of toxicity could possibly cause cone outer segment shortening, cytoplasmic densification, axonal elongation and ultimately, cone cell death (Li *et al.*, 1996). Although rod cells die by apoptosis which avoids the release of toxic cellular metabolites, and hence prevents the extension of cellular breakdown of adjacent cells, it seems nevertheless possible that

degeneration of abundant rods (20 fold greater than cones in mammalian species) could exert detrimental effects on neighboring cones (Li *et al.*, 1996).

Interphotoreceptor retinoid binding protein (IBRP) is a primary product of the rods, with less of a contribution from the cones (Porello *et al.*, 1991). IBRP is a major component of the inner plexiform layer and is thought to transport retinoids between retinal pigment epithelium and photoreceptors in the visual cycle (Saari, 1990). Evidence has shown that IRBP immunoreactivity is decreased in RP retinal regions where rod cells have been lost (Li *et al.*, 1994). A decrease in IBRP due to rod cell death and a loss of the RPE-recycled products of rod outer segment shedding may contribute to the observed cone outer segment shortening. A decrease in retinoid transportation may also lead to cone cell death found in RP retinas due to local deficiency in vitamin A, as it is known that vitamin A deficiency causes photoreceptor outer segment cell death (Carter-Dawson *et al.*, 1979). Excitotoxicity could also be implicated in the degenerative process of cone cells, possibly in the early stages of the disease. Biochemical analysis of *rd* mouse retina showed high levels of glutamate in Muller glial cells prior to onset of photoreceptor degeneration (Fletcher and Kalloniatis, 1997).

The mechanism of cone cell death should not continue once all rods have disappeared. Each cone is individually surrounded by an insoluble glycocalyx that forms a privileged structural microdomain linking each cone to a retinal pigment epithelium cell. Death may therefore act as an early limited event. Changes in the structural and biochemical microenvironment might also induce cone cell degeneration e.g. loss of structural support by neighboring rods, alterations of the interphotoreceptor matrix which contains factors promoting cone survival (Hewitt *et al.*, 1990). Failure to form appropriate synaptic connections is a well known mechanism of neuronal degeneration (Jacobson *et al.*, 1997). Secondary changes at the level of the RPE and of glial cells including microglia have been described and could impede proper retinal development, differentiation and survival. In some atypical forms of RP called cone-rod dystrohy, cones reduction may exceed that of

rods, causing prominent early symptoms such as loss of visual acuity and defective color vision (Birch *et al.*, 1999).

RP is a highly variable disorder where patients may develop symptomatic visual loss in early childhood, while others may remain asymptomatic until mid-adulthood (Hartong *et al.*, 2006). Normally, initial symptoms of RP begin in young adulthood where patients may experience impaired adaptation, inability to see in dark-dim conditions (night blindness) and weakening of peripheral vision (tunnel vision). As the disease progresses, further reduction in visual acuity and impairments in color vision occur due to the loss of cone cells, and subsequently total blindness ensue by the sixth decade of life with complete loss of central vision. The most prominent pathological finding of RP is the progressive loss of photoreceptor cells, which is followed by retinal pigment epithelium (RPE) thinning and atrophy in the peripheral retina, accompanied by attenuation of retinal arterioles. The degeneration of RPE releases melanin pigment that accumulates in the walls of retinal vessels. These perivascular deposits are responsible for the bone-spicule like pigment deposition pattern as detected by fundoscopic examination (*Figure 1.8*) (Mordes *et al.*, 2006; Seiving, 2004).

1.5.1 Genetic defects in Retinitis Pigmentosa

Genetic studies on retinitis pigmentosa in the past 20 years have greatly advanced our knowledge of retinal degeneration. The first locus for inherited photoreceptor was identified in 1989 (McWilliam *et al.*, 1989), and in 1990, rhodopsin was recognised as the first autosomal dominant gene to harbour mutations in RP patients (Dryja *et al.*, 2000). Mutations in virtually every identified gene involved in the photoreceptor outer segment and phototransduction cascade have been found associated with RP phenotypes (*Table 1.1*). These genes include the visual pigment rhodopsin (Dryja *et al.*, 2000), the α-subunit of transducin (Dryja *et al.*, 1996), guanylate cyclase (Perrault *et al.*, 1996), cGMP-dependent phosphodiesterases (McLaughlin *et al.*, 1993), the α-subunit of rod cyclic nucleotide gated channel (CNGA1) (Dhallan *et al.*, 1992) and arrestin (SAG) (Fuchs *et al.*, 1995). Mutations in genes essential for visual cycles that are associated with photoreceptor degeneration include RPE 65 (Moiseyev *et al.*,

2005), retinaldehyde binding protein (RLBP1) (Saari *et al.*, 2001) and RPE G-protein coupled receptor (RGR) (Chen *et al.*, 2001). These genes are mainly expressed in RPE cells and are responsible for the recycling of rhodopsin chromophore 11-*cis* retinaldehyde. Another group of defective genes that encode for photoreceptor structural proteins include peripherin/RDS, rod cell outer membrane protein 1 (ROM1) (Kajiwara *et al.*, 1994; Dryja *et al.*, 1997), and retinal actin-binding protein fascin (FSCN2) (Tubb *et al.*, 2000). A further category of genes that encode proteins involved in transcriptional and post-transcriptional gene regulation have also been associated with retinal degeneration. Mutations found in the nuclear receptor (NR2E3), neural retina leucine zipper (NRL) (Bessant *et al.*, 1999) and cone rod homeobox (CRX) (van Lith-Verhoeven *et al.*, 2002); all encode transcription factors and posttranscriptional RNA processing factors that are specific to the photoreceptor. In contrast, a novel group of adRP genes that are expressed ubiquitously in different tissues have also been found to be associated with retinal degeneration. These genes encode proteins required for pre-mRNA splicing and pre-mRNA processing factors (PRPF), including PRPF31 (RP11) (Vithana *et al.*, 2001), PRPF 8 (RP13) (McKie *et al.*, 2001), PRPF3 (RP18) (Chakarova *et al.*, 2002), and PAP1 (RP9) (Maita *et al.*, 2004). Furthermore, mutations found in genes that are not exclusively expressed in the retina have been associated with retinal degeneration. These include the genes encoding critical metabolic enzymes such as inosine 5'-monophosphate dehydrogenase type 1 (IMPDH1) (Bowne *et al.*, 2002; Kennan *et al.*, 2002) and lecithin retinol acetyltransferse (LRAT) (Xue *et al.*, 2004), both of which are ubiquitously expressed and are important for retinal function.

To date, 16 autosomal dominant, 16 autosomal recessive and 6 X-linked forms have been mapped through linkage studies and candidate gene screening, and many of these RP defective genes have been cloned. In addition, many other syndromic, systemic and complex forms of RP have been identified (RetNet; http//:www.sph.uth.tmc.edu/RetNet/ provided in the public domain by the University of Texas Houston Health Science Center, Houston, TX). For each set of segregation pattern, multiple genes have been identified, but many unidentified RP loci still

exists. In Drosophila, over 70 loci responsible for photoreceptor degeneration have been discovered, suggesting more may still to be discovered in humans (Dryja and Li, 1995). RP is extremely heterogeneous both genetically and phenotypically. RP can either be locus heterogeneous, where mutations at different loci can cause the same disease, or phenotypically heterogeneous, such that a single mutation is associated with different phenotypes even within members of the same family. To add to this complexity, some 20-30% of RP patients also have associated non-ocular diseases. Usher's syndrome is a complex disease where RP is associated with hearing impairment, and it is the most frequent syndromic form accounting for 20-40% of individuals with autosomal recessive disease. Patients with Usher syndrome type I have severe to profound congenital hearing impairment, vestibular dysfunction, and retinal degeneration beginning in early childhood. While those suffering from Usher syndrome type II have moderate to severe hearing impairment, normal vestibular function, and later onset of retinal degeneration. Usher syndrome type III is characterised by progressive hearing loss and variable age onset of retinal degeneration (Keats and Corey, 1999). Alterations in at least eleven different genes can cause Usher's syndrome with different mutations leading to type I, II and III disease (Pennings *et al.*, 2003). Another major form of syndromic RP is Bardet-Biedl syndrome (BBS); in this case RP is associated with obesity, cognitive impairment, polydactyly, hypogenitalism, and renal disease. BBS accounts for 5-6% of all RP cases (Tieder *et al.*, 1982; Beales *et al.*, 1999), and ten related genes have been identified. BBS can be inherited in an autosomal recessive manner, however mutations at two unlinked BBS genes have been recorded in some families (Katsanis *et al.*, 2001), with compound heterozygosity at one locus and a mutation at the second (Beales *et al.*, 2003). The determination of different mutations and the range of phenotypes associated with each RP gene is one of the first steps to understanding the pathophysical mechanisms that lead to photoreceptor death, a crucial step in the development of treatment.

1.5.2 Clinical assessment of Retinitis Pigmentosa

Today, our electrically illuminated night-time environment can pose a serious threat to people who are unaware of a severe loss of rod function because night-time activities are typically carried out with sufficient lighting for cone function. Sadly, by the time an individual recognises the symptom of night blindness, a reduction in cone sensitivity may have occurred in addition to the loss of rods. RP patients can lose 90% of cones in the fovea before having a reduction in visual acuity (Grover *et al.*, 1999). In addition, visual acuity can remain normal in individuals with advanced RP with a small island of central vision remaining. Therefore objective measurements of photoreceptor sensitivity are more accurate and reliable than symptoms for diagnosis of retinitis pigmentosa, and also for grading the severity of the disease. Various standard clinical tests are used nowadays to stage and monitor different aspects of vision throughout the disease progression of RP.

1. ***Visual fields*** are measured with a Goldmann perimeter or a Humphrey analyser (Carl Zeiss, Dublin, CA, USA). In moderate to advanced RP, only small islands of vision remain in the far peripheral field and in the visual axis, subsequently these areas of vision disappear over time.
2. ***Colour vision*** is assessed by Ishihara plates, the Farnsworth D15 panel (Munsell Colour Laboratory, MacBeth, New Windsor, NY, USA), or other tests that might show a deficiency in blue cone function (acquired tritanopia), which is a characteristic of advanced RP.
3. ***Contrast sensitivity*** is measured with a contrast chart (Peli-Robson chart) (Pelli *et al.*, 1988), where a decline in contrast sensitivity is a common finding in RP patients (Lindberg *et al.*, 1981).
4. ***Still-lamp biomicroscopy*** and ***ophthalmoscopy*** show posterior subcapular cataracts in ~50% of retinitis pigmentosa individuals (Berson *et al.*, 1980). Attenuation of retinal vessels is an universal trademark, and the fundus regularly shows intraretinal pigmentation referred to as bone-spicule deposits (*Figure 1.8*). The optic nerve head can also exhibit a waxy pale colour.

5. ***Optical coherence tomography (OCT)*** is a non-invasive technique for assessing the morphology of the retina and the macula. It is useful for measuring retinal thickness, assessment of the status of the photoreceptor layer and determining the presence of macular oedema in RP patients (van Hooser *et al.*, 2000; Sandberg *et al.*, 2005).
6. ***Electroretinograms (ERGs)*** are used to measure the electrical response of the retina to visual stimuli and are recorded either with a contact-lens electrode placed on the topically anaesthetized cornea, or an electrode applied to the eyelid. The scoptopic (dark-adapted condition) examines the activity of rods and the photopic (light-adapted condition) investigates the activity of cones. Clinically, ERGs are useful in distinguishing rod-cone dystrophy from cone-rod dystrophy, and also in determining the severity of photoreceptor cell loss (Holopigian *et al.*, 1996).
7. ***Fundus autofluorescence imaging*** shows that RP patients have increased concentrations of lipofuscin in the retinal pigment epithelium (RPE). Regions of the retina with the highest levels of autofluorescence indicate those producing the lowest ERG amplitudes, as measured by mulitfocal ERGs (Robson *et al.*, 2006).

The age of onset of retinitis pigmentosa is normally referred to the age at which a patient first reports visual symptoms, and this can range from early childhood to adulthood. In some cases, the age of onset of symptoms is an imprecise measurement of disease severity because it is dependent on individual's awareness of vision loss, and provides little information of when photoreceptor degeneration actually begins. For example, ERG data shows that photoreceptor degeneration already persists at the age of 6 years, even in patients who remain asymptomatic until young adulthood (Berson, 1993). Therefore clinical examinations using objective quantitative measurements of retinal function are crucial to describe accurately the degree of visual deterioration and the rate of decline. This information may be possible to provide a prognosis for vision customised to every patient.

1.6 Mouse models of ocular diseases

Ocular diseases, apart from those originating following trauma or infection, are genetic in origin or have strong genetic components (McKusick, 1998). However, clinical research and genetic manipulation studies have been impeded by the lack of human ocular tissues due to the risk of damaging the patient's vision while obtaining tissue samples. Therefore, mice suffering from hereditary eye defects prove to be a better alternative for the study of molecular and histological development of retinal degenerations, and for the characterisation of the genetic basis underlying retinal dysfunction. Although human family studies have been used to identify genes of hereditary retinal disorders, genetic studies on mice have yielded disease models which have enabled the detailed study of RP-causing mutations, including those caused by multiple genes and those influenced by modifying genes (Chang *et al.*, 2005). In addition, many transgenic and knockout animal models have been created using techniques such as gene trapping to investigate the role of specific genes in retinal function (Skarnes *et al.*, 2004).

From a clinical standpoint, mouse mutants with ocular disorders provide excellent models for human eye diseases because the mouse eye is remarkably similar in structure to human, and both species have many similar ocular disorders. Not only are developmental and invasive studies possible in mice, but the mouse's accelerated life span and generation time (1 mouse year equals ~30 human years) allow evaluation of the natural progression of eye diseases in a relatively brief length of time (Chang *et al.*, 2005). Mouse mutations can be maintained on controlled genetic backgrounds, making it possible to analyse the effects of a mutant gene in same-sex and same-age littermates. Furthermore, it is estimated that there is ~95% sequence homology between essential coding regions in the human and mouse genomes (Chang *et al.*, 2005). This means that human homologs of the mutant genes that cause inherited disorders in the mouse are likely to be involved in similar human disorders. In addition, homologous genes are usually linked in conserved chromosomal segments in the mouse and human genomes, mapping a gene in the mouse can quickly identify the location of the same gene in the human genome.

Despite all of these advantages, the mouse retina is somehow different from a human retina, particularly in regard to the number and distribution of photoreceptor cells. The mouse as a nocturnal animal has a retina dominated by rods, in contrast the cones are small in size and represent only 3-5% of the photoreceptors (Dalke and Graw, 2005). In addition, mice do not form cone-rich areas like the human fovea, and only possess two distinct pigments with absorption maxima near 350-510 nm, as opposed to three cone pigments present in the human retina (Lyubarsky *et al.*, 1999).

The Jackson Laboratory (Bar Harbor, USA) possesses the world's largest collection of mouse mutant stocks and genetically diverse inbred strains. In particular, the facility holds up to 109 different mouse models of human hereditary ocular diseases, where 69 of these have been genetically mapped and clinically characterised. Some of the mouse models bearing different ocular diseases are discussed below and more thorough reviews can be found at (Chang *et al.*, 2005; Dalke and Graw, 2005).

1.6.1 Mouse models of Retinitis Pigmentosa

Mutations in the rhodopsin (RHO) gene account for ~15% of all inherited retinal degenerations in humans. The rhodopsin knockout mouse fails to develop rod outer segments and lose their photoreceptor cells within 3 months, indicating that rhodopsin has an important role in stablising the outer segment. At the age of 8 weeks, the visual function is solely mediated by cones only (Humphries *et al.*, 1997). In addition, transgenic mice harbouring the P23H mutation in the rhodopsin gene have shown marked photoreceptor degeneration by postnatal day 20, and reduction of the outer nuclear layer to a single row of sparse photoreceptor nuclei (Olsson *et al.*, 1992). Interestingly, it is not only the loss of rhodopsin function that leads to retinal degeneration, but the addition of rhodopsin activity also has a detrimental effect. Transgenic mice expressing different levels of opsin were generated to study the consequence of opsin over-expression. Opsin expression level at 123% higher than that of normal level leads to a reduction in *a-wave* amplitudes in ERG. The over-expression of normal opsin induces photoreceptor degeneration that is similar to that seen in many mouse models of RP (Tan *et al.*, 2001).

The retinal degeneration (*rd*) mouse is a naturally occurring mutant strain exhibiting mutations in the gene encoding for the β-subunit of rod cGMP phosphodiesterase as seen in some forms of human RP (McLaughlin *et al.*, 1993). In this animal model, rod degeneration is aggressive and usually completes within one month of postnatal age, which is then followed by more gradual progressive cone deterioration.

Nrl, a basic neural retina motif-leucine zipper transcription factor of the *Maf* subfamily, synergistically interacts with the homeodomain protein *CRX* to regulate rhodopsin transcription. Missense mutations in the NRL gene cause RP in humans, and a similar phenotype is observed in $Nrl^{-/-}$ mice, exhibiting the complete loss of rod function and supernormal cone function. Functional transformation of rods into S-cones was demonstrated in the $Nrl^{-/-}$ retina, suggesting that Nrl acts as a molecular switch during rod cell development (Mears *et al.*, 2001).

A late onset of photoreceptor cell degeneration is observed in mice with a mutant Nr2e3 gene, a member of the nuclear receptor transcription factor family. After one year of relatively stable *a*- and *b*- wave ERG responses, a progressive loss of amplitudes follows. The retinal fundus of one month old Nr2e3 mutant mice display discrete white spots, whorls and rosettes due to retinal waves in the outer nuclear layer (ONL) (Cheng *et al.*, 2004).

1.6.2 Mutant mouse models with a combined phenotype of RP and other photoreceptor dystrophies

Two mouse models have been reported with mutation in Crb1 gene encoding for the crumbs homolog 1. The human mutations in the CRB1 gene lead to various forms of hereditable retinal disorders like progressive retinitis pigmentosa and Leber Congential Amaurosis (LCA). Similarly the spontaneous mutant ($Crb1^{rd8}$) shows irregular white spots from the age of three weeks, which are caused by retinal folds and pseudorosettes. Shortened photoreceptor inner and outer segments are also observed as early as two weeks after birth suggesting a developmental defect (Mehalow *et al.*, 2003). The recently described $Crb^{-/-}$ knockout mice initially develop

normal retinas, but by three to nine months the $Crb^{-/-}$ retinas developed lesions where the integrity of the outer limiting membrane (OLM) is lost and giant half rosettes are formed (van de Pavert *et al.*, 2004).

The retinal degeneration slow (*rds*) mouse strain exhibits defects in the gene encoding for the photoreceptor specific membrane glycoprotein (peripherin), and are associated with multiple retinal diseases like macular dystrophy and autosomal dominant RP. Peripherin is essential for outer segment disc morphogenesis. Mice homozygous for the spontaneous mutations $Rds^{Prph2\text{-}rd2}$ fails to develop photoreceptor outer segments, and all photoreceptor cells are completely deteriorated by the age of 12 months. Another *Rds* allele (Rds^{tm1Nmc}) with a targeted single base deletion at codon 307 is identical to a human mutation associated with an autosomal dominant form of RP. The Rds^{tm1Nmc} mutation leads to a more rapid development of the retinopathy than observed in the naturally occurring null mutant, suggesting a dominant negative phenotype in combination with haploinsufficiency (McNally *et al.*, 2002).

1.6.3 Mutant mouse models of Macular degeneration

Macular degeneration is a complex form of retinitis pigmentosa characterised by photoreceptor degeneration and atrophy of the retinal pigment epithelium in the central retina. An example of congenital macular degeneration is Stargardt's macular dystrophy (STGD). One of the genes that have been found to be mutated in patients suffering from STGD is *ABCA4*, encoding for an ATP-binding cassette transporter, and is expressed along the rim of rod outer segment discs. Mice lacking both alleles of ABCA4 gene accumulate toxic lipofuscin pigments in ocular tissues that lead to progressive photoreceptor degeneration and an enhanced delay in dark adaptation with increasing age (Radu *et al.*, 2004). A dominant form of human congenital STGD is caused by mutations in the ELOVL4 gene (elongation of very long fatty acids-like 4). Transgenic mice expressing a mutant form of human ELOVL4 show photoreceptor degeneration in the central retina with a pattern closely resembling that

of human Stargardt's macular dystrophy and age-related macular degeneration (AMD), therefore these mice provide a model for both disorders (Karan *et al.*, 2005).

A common form of macular degeneration in males is X-linked juvenile retinoschisis (RS), which is caused by mutations in the RS1 gene. A corresponding mouse model, *Rs1h* (homolog to human RS1 gene) deficient mice were generated. The pathologic changes in hemizygous mice are evenly distributed across the retina, contrasting the macular dominated features in human. However similar functional anomalies were observed in both man and mouse, suggesting both conditions are a disease of the entire retina, which affected the organisation of the retinal cell layers as well as structural properties of the retinal synapse (Weber *et al.*, 2002).

1.6.4 Mouse models of Leber Congenital Amaurosis (LCA)

Leber Congential Amaurosis (LCA) is a group of autosomal recessive retinal dystrophies with a disease onset in early childhood. This congential blindness has a worldwide prevalence of three in 100,000 newborns and possesses the following clinical features such as severely reduced electroretinogram near birth, amaurotic pupils and wandering nystagmus (Koenekoop, 2004). To date, several different genes have been identified whose mutations cause LCA (i.e. *Crb1* (zonula adherens formation), *Crx* (outer segment development), *AIPL1* (cell cycle progression), *RPE65* (retinoid metabolism) and *Rpgrip1* (disc morphogenesis) (Hanein *et al.*, 2004; Perrault *et al.*, 2004). These genes are predominantly expressed in the photoreceptor cells or retinal pigment epithelium (RPE). In photoreceptor cells, these genes encode enzymes that are involved in the phototransduction cascade or photoreceptor-specific structural proteins, whereas in the RPE, LCA-associated genes encode proteins involved in vitamin A metabolism. The conductive gene for LCA is the *RPE65* gene, which is an abundant protein in the RPE and is associated with the microsomal membrane (Hamel *et al.*, 1993). It plays an important role in vitamin A metabolism and is necessary for the synthesis of the visual pigment chromophore 11-*cis* retinal (Thompson and Gal, 2003). *RPE65* knockout mice ($RPE65^{-/-}$) show disorganisation of outer segment discs in rod photoreceptors. Residual ERG responses of $RPE65^{-/-}$

mice were attributed to rods, which enabled them to mimic cone function by responding under cone-isolating lighting conditions (Seeliger *et al.*, 2001). Studies with RPE65$^{-/-}$ mice clearly showed that activation of sensory transduction by unliganded opsin induces light-independent retinal degeneration in Leber Congential Amaurosis, and that the accumulation of retinal esters was not the cause of disease (Woodruff *et al.*, 2003). Furthermore, a new spontaneous *RPE65* mutant mouse (Rpe65^{rd12}) was reported. Homozygous Rpe65^{rd12} mice exhibit small punctuate white spots in the fundus at the age of 5 months. The first sign of retinal degeneration was seen at 3 weeks of age, when occasional small lipid like droplets were detected in the retinal pigment epithelium. At three months of age, voids were detected in the outer nuclear layer, and ERG phenotype was similar to that reported in the RPE65$^{-/-}$ mice where ERG responses were profoundly diminished except for the brightest stimuli (Pang *et al.*, 2005).

Mutations in the *AIPL1* gene encoding for aryl-hydrocarbon receptor-interacting protein like 1, in humans also lead to Leber Congenital Amaurosis. Rapid retinal degeneration and lack of both rod and cone ERG responses were observed in Aipl1$^{-/-}$ mice. However no gross abnormalities of proliferation during retinal development were detected (Dyer *et al.*, 2004). Another model of LCA was created where cone-rod homeobox containing gene (Crx) was disrupted by homologous recombination. Crx$^{-/-}$ mice display abnormal development of photoreceptors followed by progressive degeneration with increasing age (Pignatelli *et al.*, 2004). The Crx$^{-/-}$ outer segment morphogenesis was found to be blocked in development, leading to a failure in the production of the phototransduction apparatus and highly disorganised synapses were observed in the outer plexiform layer (Morrow *et al.*, 2005).

1.6.5 Combined retinal and neuronal degeneration phenotype

Some mouse models contain a combined phenotype of retinal and neuronal degenerations. Retinal degeneration combined with the loss of cerebellar Purkinje cells was observed in both, *nervous* (nr) and *Agtpbp1* (ATP/GTP binding protein 1) mutant mice. The recessive *nervous* (nr) mutation was associated with hyperactivity

at the age of 3 weeks, retinal disorganisation of the outer segment membranes and thinning of the inner nuclear and inner plexiform layers were also observed. In *Agtpbp1* mutant mice, the outer nuclear layer and the mitral neurons of the olfactory bulb degenerated, and the loss of photoreceptor cells started at 2 weeks of age which proceeded slowly for 1 year (Fernandez-Gonzalez *et al.*, 2002).

Two spontaneous mouse mutants for neuronal ceroid lipofuscinosis, *Cln6* and *Cln 8*, are associated with progressive retinal degeneration, ataxia and neurodegeneration. Mutations in the human orthologues have been shown to underlie neurological syndromes including retinal disorders, seizures and mental retardation. Homozygous mice for both lines died around 9 months and progressive photoreceptor cell loss begins early in life, and by six to nine months the entire retina was atrophied (Bronson *et al.*, 1998). In *Cln8* mice, oxidation and apoptotic processes were involved in the retinopathy (Guarneri *et al.*, 2004).

1.6.6 Retinal degeneration as part of a multisyndromic defect

The Bardet-Biedl syndrome (BBS) is characterised by retinitis pigmentosa as the major defect, but obesity, polydactyly, renal and cardiac malformations, learning disabilities and hypogenitalism have also been reported in affected patients. Two knockout mouse models, lacking the expression of Bbs2 or Bbs4, respectively, displayed major components of the human phenotype including retinal degeneration and other defects associated with cilia dysfunction. Retinal degeneration in $Bbs2^{-/-}$ mice started after normal retinal development by apoptotic death of photoreceptors. Interestingly, photoreceptor cell death was preceded by mislocalisation of rhodopsin, indicating a defect in transport (Mykytyn *et al.*, 2004).

A syndrome including congenital blindness, sensorineural deafness and mental retardation is displayed in X-linked Norrie disease. Hemizygous *Ndph* (Norrie disease homolog) knockout mice developed retrolental structures in the vitreous body and disorganisation of the ganglion cell layer with focal absence of the outer plexiform layer. These ocular findings were consistent with observations in human

patients (Berger *et al.*, 1996). Mice deficient in *norrin*, the gene product of *Ndph*, also indicated a distinct failure in retinal angiogenesis, where the mice lacked the deep capillary layers of the retina.

Usher syndrome is an autosomal recessive disorder that is characterised by congenital hearing loss and the development of progressive retinitis pigmentosa. The mouse model for type I of Usher syndrome, *rd5*, whose linkage on mouse chromosome 7 to *Hbb* and *tub* has homology to human Usher syndrome I was reported by Heckenlively *et al.*, (1995). ERG amplitudes were completely extinguished in homozygous *rd5* mice by six months of age, and auditory-evoked response showed similar results.

1.6.7 Other Retinopathy models

The Chx10 homeobox (*C. elegans* ceh-10 homeodomain containing homolog) is expressed in neural progenitor cells during retinal development. The absence of Chx10 in spontaneously occurring mutant mice causes mutant ocular retardation and microphthalmia (abnormally small eyeball). In $Chx10^{or\text{-}J/or\text{-}J}$ mutants, the rod and cone outer segments are not correctly formed (Rutherford *et al.*, 2004), and retinal cells transdifferentiate into pigmented cells (Rowan *et al.*, 2004). This deflection of the retina towards a retinal pigment epithelium-like identity is caused by the ectopic expression of *Mitf* (a microophthalmia associated transcription factor) in $Chx10^{or\text{-}J/or\text{-}J}$, which is expressed by Chx10 in wild-type mice. The *Vsx1* is a visual system homeobox 1 gene that is expressed in differentiating and mature cone bipolar cells in mice. *Vsx1* deficient mice showed altered ERG responses, demonstrating defects in their cone visual pathway but not in the rods (Chow *et al.*, 2004).

Disabling retinal diseases in humans affects millions each year. Yet research into these diseases is often limited by the various restrictions on studying pathophysiological processes in the human eye. Firstly, many human ocular diseases are genetic in origin, and the appropriate families are not always available for genetic studies. Secondly, the retina is relatively difficult to access and thirdly, the delicate nature of the retina means that invasive investigation into pathophysiology in a

diseased eye is likely to cause further deterioration. Therefore mouse models of inherited ocular disease are invaluable tools for efficient genetic analysis, and are central to the development of treatments for blinding diseases.

1.7 Mutations in Rhodopsin associated with Retinitis Pigmentosa

The first point mutation found to cause a pathological hereditary condition in the retina was identified in the gene encoding the visual protein, rhodopsin. This mutation in the opsin gene produced a Pro23His substitution situated in the intradiscal domain, and was a founder mutation in the North American population (Farrar *et al.*, 1990; Berson *et al.*, 1991) that constituted ~12% of RP patients in USA, but less in other populations (Wada and Tamai, 2003). It has a relatively mild clinical phenotype of RP, and the expression of Pro23His impairs the ubiquitin proteasome pathway, suggesting a mechanism for photoreceptor degeneration (Illing *et al.*, 2002; Heckenlively *et al.*, 1991).To date, more than 120 point mutations have been identified in the rhodopsin gene, and although some mutations cause autosomal recessive RP and congential stationary night blindness (CSNB), the vast majority cause autosomal dominant RP (Mendes *et al.*, 2005). In 1984, Nathan and Hogness assigned the human rhodopsin gene, which consists of five exons, to chromosome 3q21. Virtually all mutations in rhodopsin lead to the production of aberrant protein with one or more amino acid either deleted or altered, and are distributed along the three domains of the protein: the intradiscal, transmembrane and cytoplasmic domains (Dryja and Li, 1995; Cideciyan *et al.*, 1998). It is likely that the discovery of a large number of mutations at different locations throughout the opsin gene is indicative of a highly complex arrangement of physiochemical interactions in the three-dimensional structure of the native rhodopsin molecule. Shortly after the identification of pathogenic mutations in rhodopsin, protein misfolding was first proposed to be one of the main biochemical causes of RP, and subsequent studies have led to the classification of two major classes of autosomal dominant retinitis pigmentosa linked rhodopsin mutations (Garriga *et al.*, 1996; Liu *et al.*, 1996). However, recent studies of other rhodopsin mutations have raised the suggestion that different biochemical and cellular defects may also arise, and up to six major classes of mutations have now been established in rhodopsin (*Table 1.2*) (Mendes *et al.*, 2005).

1. ***Class I*** mutations predominantly occurred in C-terminus of protein and fold normally but are not correctly transported to outer segment and are exclusive to rod-opsin mutations. They resemble wild type rhodopsin in their translocation to the plasma membrane and could form a functional chromophore with 11-*cis*-retinal (Sung *et al.,* 1993a; Kaushal and Khorana, 1994; Sung *et al.*, 1993b).
2. ***Class II*** mutants are most common adRP mutations characterised by mutations in intradiscal, transmembrane, cytoplasmic domains of rhodopsin that results in misfolded protein, causing inability to form functional chromophore with 11-*cis* retinal. These mutations are retained within the ER and cannot easily reconstitute with 11-*cis*-retinal (Sung *et al.*, 1993b; Kaushal and Khorana., 1994).
3. ***Class III*** mutants correspond to mutations that affect endocytosis (R135L) (Chuang *et al.*, 2004).
4. ***Class IV*** mutations do not affect folding, but affect rod-opsin stability and post-transcriptional modification (e.g. T4R mutation causes adRP in dogs) (Zhu *et al.,* 2004).
5. ***Class V*** mutants show no obvious initial folding defect but show an increase in the activation rate of transducin (Andres *et al.*, 2003).
6. ***Class VI*** mutants appear to fold correctly but may lead to the constitutive activation of opsin in the absence of chromophore and in the dark.

However these classes might not be mutually exclusive. For example, the K296E (class II mutant) mutation can re-constitute with 11-*cis* retinal (Robinson *et al.*, 1992) and can also cause protein misfolding (Saliba *et al.*, 2002), but the misfolding phenotype dictates its classification as a class II mutant. Dominance in adRP patients could be due to loss of function, gain of function and dominant negative mutations, or even a combination of the above (Wilson and Wensel, 2003). However loss-of-function mutations alone are not likely to cause adRP as suggested by a line of evidence. First, none of the dominant rhodopsin alleles investigated appears to be a null mutation. Secondly, heterozygous rhodopsin knockout mice showed little

photoreceptor degeneration (Humphries *et al.*, 1997; Lem *et al.*, 1999). These observations suggest that haploinsufficiency may not be the main cause of adRP, rather the disease pathology is possibly due to a gain-of function or dominant negative disease mechanism. Therefore, a clear assessment of the consequences of rhodopsin mutations is vital to establish the underlying disease mechanisms in adRP for design of potential therapeutic strategies. Recently, Mendes *et al.*, (2005) have deciphered twelve different pathways in which pathological mutations in rhodopsin can cause photoreceptor cell death through either gain-of-function or dominant negative mechanisms (*Figure 1.9*).

Pathway 1: Gain-of-function mechanisms, the unfolded protein response:

Heterologous expression systems indicate that wild type rhodopsin translocates to the plasma membrane, whereas the class II mutant opsins, such as P23H, are retained within the endoplasmic reticulum (ER) (Saliba *et al.*, 2002; Frederick *et al.*, 2001; Chapple and Cheetham, 2003). In addition to the folding and maturation of proteins, the endoplasmic reticulum is also responsible for lipid synthesis and Ca^{2+} storage. The tight regulation and maintenance of ER homeostasis is vital, and disturbance of Ca^{2+} homeostasis during hypoxia, and imbalance between the demand and capacity of the protein-folding apparatus, initiates an adaptive response called the unfolded protein response (UPR or ER-stress response) (Rutkowski and Kaufman, 2004). Accumulation of misfolded opsin within ER causes ER stress and subsequently induces UPR. The UPR alleviates ER stress by decreasing the accumulation of misfolded protein by induction of ER-localised chaperones, which leads to the cessation of protein synthesis and an enhancement in protein degradation. If the ER stress persists, the UPR can culminate in cell death by apoptosis (pathway 1 of *Figure 1.9*).

Pathway 2: Aggregation and inclusion formation

Following the retention of class II mutant opsins in ER by cellular quality control machinery, the mutant opsins are retro-translocated from the ER to the ubiquitin-proteasome system (UPS) for degradation. If the ubiquitin-proteasome system fails to

degrade all mutant opsins, these mutants will aggregate in the cytosol and then coalesce into ubiquitinated proteinacious inclusions, as has been demonstrated for the P23H mutation in cell culture (Illing *et al.*, 2002; Kopito, 2000). The pathology of many other neurodegenerative diseases also includes the intracellular aggregation of ubiquitinated proteins and the formation of inclusion bodies. Although most of these protein aggregates are cytosolic, occasionally, ubiquitinated inclusions are found in endosomes/lysosomes such as in Alzheimer's disease and prion encephalopathies. In addition, aggregates are found in nuclei in disorders associated with CAG/polyglutamine repeats such as Huntington's disease and spinocerebella ataxias (Alves-Rodrigues *et al.*, 1998; Forman *et al.*, 2004). Indeed, transient expression of aggregation–prone proteins associated with neurodegenerative diseases such as, Huntington fragment containing pathogenic polyglutamine repeat or folding mutant of cystic fibrosis transmembrane conductance regulator, has also been shown to impair the function of the ubiquitin-proteasome system (Bence *et al.*, 2001). Thus, ubiquitin-dependent proteolysis has a central role in regulating fundamental cellular events (cell division), and such an inhibition by, for example, mutant opsin could stimulate further aggregation and subsequently disrupt cellular homeostasis, causing degeneration of the photoreceptor cells through apoptosis (pathway 2 of *Figure 1.9*).

Pathway 3: Opsin aggregation

Opsin aggregates may have other gain-of–function properties that affect photoreceptor viability. For instance, fibrillar protein aggregates might have inherent and common pathways for cytotoxicity involving Ca^{2+} and reactive oxygen species (ROS) (pathway 3 of *Figure 1.9*) (Bucciantini *et al.*, 2004).

Pathway 4: Recruitment of chaperones

Opsin aggregates and inclusions can recruit other cellular proteins (chaperones) or wild type opsins (Saliba *et al.*, 2002; Chapple and Cheetham, 2003), where such molecules may be part of a cellular response involved to rescue other proteins from these inclusions (Kim *et al.*, 2002), so avoiding the deleterious effects that sequestration of these proteins could have on photoreceptor viability (pathway 4 of

Figure 1.9). The depletion of essential components by sequestration in protein aggregates has also been proposed as a disease mechanism for neurodegenerative diseases and might also be relevant to retinal degeneration. For example, spinocerebellar ataxia type 7 (SCA7) is a neurodegenerative disease that is caused by polyglutamine tract expansion in the ataxin protein. Interestingly, SCA7 is also associated with cone-rod dystrophy through alteration of photoreceptor gene expression due to *Crx* (a homeodomain transcription factor) interference. It was found that both ataxin 7 and Crx engage each other functionally through significant interaction by co-occupying the promoter and enhancer regions of *Crx*-regulated genes *in-vivo*. Therefore the predominant factor in SCA7 mediated cone-rod dystrophy is *Crx* transcription interference (Chen *et al.*, 2004a).

Pathway 5: The deterioration of microtubules in photoreceptor cells

Electron-dense inclusions of rhodopsin have been observed in human and animal adRP models (Bunt-Milam *et al.*, 1983; Li *et al.*, 1998a), but the presence of inclusions tends to appear at later stages of diseases. The formation of inclusions requires intact microtubule network that interferes with normal cytoskeleton within photoreceptors (pathway 5 of *Figure 1.9*) (Saliba *et al.*, 2002; Illing *et al.*, 2002). Microtubules in photoreceptors are organised around the basal bodies within the specialised non-motile connecting cilia at junctions between the outer segment and inner segment, and function in processing concentrated aggregated proteins into pericentriolar inclusion bodies (Kopito, 2000). Without this sequesterisation of toxic opsin aggregates into inclusion bodies, the photoreceptors may be exposed to increasing levels of aggregate related toxicity which could lead to photoreceptor cell death prior to the formation of visible inclusions.

Pathway 6: Gain-of function mechanisms affecting post-golgi traffic and outer-segment targeting

Class I mutant opsins were shown to be incorrectly targeted to the outer segment and that this mis-sorting has correlated to retinal cell death, leading to the conclusion that abnormal rhodopsin sorting was responsible for retinal degeneration (Green *et al.*,

2000). Three distinctive mechanisms have been proposed for class I mutant induction of apoptosis: (a) Mislocalised rhodopsin molecules might overwhelm normal vascular traffic machinery to the outer segment and plasma membrane, thus interfering with the legitimate cargo (Pathway 6 of *Figure 1.9*).

Pathway 7: (b) A large amount of mutant rhodopsin protein in the plasma membrane could interfere with cellular processes, including synaptic transmission (Pathway 7 of *Figure 1.9*) (Green *et al.*, 2000).

Pathway 8: (c) A metabolic burden might be placed on photoreceptors by continuous degradation of large amounts of mis-sorted mutant protein (Pathway 8 of *Figure 1.9*) (Green *et al.*, 2000).

Pathway 9: Gain-of-function mechanisms affecting endocytosis and arrestin binding Mutation at position Arg135 in rhodopsin (Class III mutation) causes a particularly aggressive form of RP characterised by rapid disease progression (Ponjavic *et al.*, 1997). In particular, mutant proteins derived from mutations such as R135K, R135A and R135L, could bind to arrestin in the absence of 11-*cis*-retinal (Shi *et al.*, 1998). These class III mutants might cause disease through abnormal complexing with arrestin, disrupting the dynamic interplay between different endocytic compartments rendering them dysfunctional, and resulting in an imbalance of iron and nutrient levels. Impaired endocytic activity leading to the failure of rhodopsin removal from the rod inner segment could also be another gain-of-function mechanism in the Arg135 mutants (Pathway 9 of *Figure 1.9*) (Chuang *et al.*, 2004).

Pathway 10: Gain-of-function mechanisms cause constitutive or dysregulated activation

The constitutive activation of the phototransduction cascade has been suggested as a potential mechanism of cell death in adRP. However, there is a contradiction to this hypothesis because most rhodopsin mutations assembled around the chromophore binding pocket which can stimulate constitutive activation cause congential stationary

night blindness (CSNB), rather than the autosomal dominant form of RP. Lem and Fain, (2004) suggested a possible explanation for this paradox: mutations in rhodopsin that cause constitutive activation may lead to retinal degeneration, but those that can terminate signaling partially or intermittently, could very well decrease the rate of degeneration sufficiently to give rise to CSNB. Recently, class V mutations have been shown to accelerate the rate of transducin activation in the presence of light (Andres *et al.*, 2003), suggesting that they disrupt the balance of phototransduction cascade. Light is not the only way to activate opsin signaling: opsin in the absence of bound 11-*cis*-retinal can also stimulate the phototransduction pathway (Fain and Lisman, 1993). In such a case, mislocalised class I mutants could fail to insert 11-*cis*-retinal and still be active, whereas class II mutants could remain active even when trapped in the endoplasmic reticulum (Pathway 10 of *Figure 1.9*).

Pathway 11: Inability to terminate the phototransduction cascade

The correct folding of rhodopsin is extremely sensitive to minor changes in the primary amino acid sequence, and misfolded mutant rhodopsin protein is constantly being monitored by the endoplasmic reticulum quality control. It is possible that some of these mutant proteins could escape from the endoplasmic reticulum and migrate to other cellular compartments such as the outer segments. Within the outer segments, mutant rhodopsin proteins appeared to have normal absorbance spectra and photic sensitivity, and the ability of 11-*cis*-retinal to regenerate mutant visual pigment after photolysis was comparable to that of the wild types (Wu *et al.*, 1998a). Nonetheless, there was evidence of an abnormally slow recovery of visual sensitivity, suggesting that the misfolded rhodopsin protein targeted the regeneration process of the rhodopsin in the visual cycle. The potential role of mutant rhodopsin in the outer segment was further highlighted by studies carried out on the T4R class IV mutation. This mutation introduced a positive charge at Arg4, coupled with the failure of glycosylation at Asn2 (Zhu *et al.*, 2004). The lack of glycosylation did not appear to affect folding or transport of the mutant protein, but the protein appeared to have a lower thermal stability than the wild-type protein. The T4R mutation also affected chromophore binding with accelerated release of chromophore and inhibition of *in-*

vitro regeneration with 11-*cis*-retinal (Zhu *et al.*, 2004). The T4R mutation was also structurally unstable in the absence of chromophore which could have led to photoreceptor degeneration (Pathway 11 of *Figure 1.9*).

Pathway 12: Dominant negative mechanisms

Although most of the above mechanisms point towards autosomal dominant RP being caused by gain-of-function mutations in rhodopsin, other studies have suggested that a dominant-negative pathogenesis is also feasible. The co-expression of both wild type and mutant rhodopsin in mammalian cells led to the formation of intracellular proteinacious inclusions that contained wild type protein (Saliba *et al.*, 2002). Therefore in the presence of both wild type and mutant rhodopsin, as in patients heterozygous for adRP, the mutant rhodopsin could affect the processing of wild type protein. Furthermore, the mutant and wild type rhodopsins appeared to form higher molecular weight, detergent like insoluble complexes, in which the two proteins were in close proximity (<70Å). The co-expression of class II mutants also resulted in enhanced proteasome-mediated degradation and steady-state ubiquitination of the wild type protein (Rajan and Kopito, 2005). The misfolded mutant rhodopsin could also exert an effect on the biosynthesis and maturation of the wild type protein, reducing the amount of newly synthesised wild type rhodopsin that matures beyond the ER in photoreceptors. The result would be a reduction in the amount of rhodopsin reaching the outer segments, possibly leading to outer segment shortening and instability (Pathway 12 of *Figure 1.9*) (Frederick *et al.*, 2001).

The important observation from these studies is that these potential disease-causing mechanisms are not exclusive, and that some of them may act in combination to cause photoreceptor cell death. Therefore, different mechanisms are likely to be involved with different classes of mutations, and perhaps it is this complex relationship that explains why similar mutations in rhodopsin cause different clinical phenotypes, and also why the same mutations can have different consequences, different onset and severity on individuals of the same family. This highlights the

urgency of accurate molecular diagnosis, a better understanding of the outcome of each mutation, and application of a suitable therapy for each patient.

1.8 Conventional treatments for Retinitis Pigmentosa

Pharmacological studies have demonstrated the ability of neuroprotective molecules to slow down the progression of photoreceptor degeneration in different models. Nutritional and neuroprotective treatments that affect secondary biochemical pathways share the advantage of being less dependent on the disease causing mutations, and could therefore be widely applicable for different diseases. To date, many mechanistically diverse approaches for the treatment of retinitis pigmentosa are being investigated. These include vitamin A supplementation, dietary modification, introduction of trophic factors/calcium blockers, the potential of stem cells, inhibitors of apoptosis and implanted electrical devices. The concepts of these treatments are that by altering the micro-environment of photoreceptor cells, these neuroprotective strategies can stabilise the disease before rod degeneration. This may allow further understanding of the cellular and molecular interactions between photoreceptors and their environment during cell death, which may help identify the cause of death in neighboring cone cells. The main drawback of these approaches is that treatments can only provide medium term alleviation for the disease as they tackle the symptoms rather than the primary defect; however, they do circumvent the extreme heterogeneity of RP.

1.8.1 Vitamin A supplementation

An initial study carried out in the early 1990's showed that patients taking vitamin A, vitamin E or both were recorded to have slower declines in ERG amplitudes than those not taking the supplements (Berson *et al.*, 1993a). This observation then prompted a randomized clinical trial of oral vitamin A and E supplements in 601 patients with dominant, recessive and X-linked non-syndromic RP and Usher syndrome type II. Each patient was assigned with a daily supplement of vitamin A as retinyl palmitate (15,000 IU), vitamin E (400 IU) as dl-α-tocopherol, or the combination of both vitamins, and was followed up for 4-6 years. Patient's assigned with vitamin A showed significantly slower decline in cone ERG amplitudes than did other groups. Furthermore in a subsequent analysis of 125 patients, it was shown that those assigned vitamin A showed a significantly slower loss of visual field than those

not taking vitamin A (Berson, 1998; Berson *et al.*, 1993b). Based on these results, many clinicians recommend adults with early or middle stages of RP to take 15000 IU of oral vitamin A palmitate daily and avoid high dose vitamin E supplements. β-carotene was found to be unsuitable as a substitute for vitamin A because it is not reliably converted to vitamin A. Older individuals should be monitored for bone health because a slight increased risk for hip fractures from osteoporosis has been reported in postmenopausal women and men older than 49 years taking vitamin A supplements (Feskanich *et al.*, 2002). Also since high doses of vitamin A supplements enhance risk of birth defects, therefore, it is not recommended for pregnant women or those planning to conceive (Lammer *et al.*, 1985). Li *et al.*, (1998b) also studied the effect of vitamin A supplementation on transgenic mice including those bearing class II dominant rhodopsin mutations. Class II mutation is characterised by thermal instability and a fall in the regeneration of chromophores. Long term supplementation of vitamin A was observed to have a stabilising effect on mutant opsins through increasing the availability of chromophores.

Patients with rare syndromic forms of RP such as abetalipoproteinaemia (Bassen-Kornzweig disease) have low concentrations of alipoprotein B in plasma and have fat malabsorption, which results in low amounts of fat-soluble vitamins in plasma. Besides RP, patients also develop ataxia, peripheral neuropathy and steatorrhea. These patients receiving high oral doses of vitamin A resulted in acute restoration of retinal function in the early stages of disease (Gouras *et al.*, 1971). Phytanic acid oxidase deficiency (Refsum's disease) is often associated with cardiac conduction defects, ataxia, polyneuropahty, deafness, anosmia, dry skin, and RP. Dietary modification to severely reduce the intake of phytanic acid while maintaining bodyweight can slow progression of this form of RP (Hungerbuhler *et al.*, 1985). Familial isolated vitamin E deficiency (α-tocopherol transport protein deficiency) can cause adult onset ataxia, dysarthria, reduced touch and positional sense, and also retinitis pigmentosa. Treatment with vitamin E has been reported to halt progression of this disease (Yokota *et al.*, 1997).

1.8.2 Dietary modification and nutrition supplementation

Another nutritional treatment assessed for patients of RP is docosahexaenoic acid (DHA), an omega-3 fatty acid that is found in high concentrations in oily fish. DHA is important for photoreceptor function, since membranes containing rod-opsin and cone opsins in photoreceptor cells have very high concentrations of this fatty acid (Fliesler and Anderson, 1983), and amounts of DHA in red-blood cells are on average lower in patients with RP than in unaffected people, but whether this is due to metabolic variation or changes in diet is unknown (Hoffman *et al.*, 2004). Analysis of 110 participants receiving a combination of vitamin A and omega-3 fatty acid, or vitamin A and placebo, showed that those with a diet containing at least 1.4 g of omega 3 fatty acids per week had a slower rate of visual field degeneration of up to 40-50% compared to those eating less omega-3 fatty acids, thus the combined benefit of vitamin A and oily fish could provide an additional 20 years of visual preservation for the average patients who starts this regimen late in adulthood (Berson *et al.*, 2004).

1.8.3 Trophic factors

The most commonly used trophic factor is ciliary neurotrophic factor (CNTF). Bok *et al.*, (2002) reported a delay in photoreceptor degeneration by inducing morphological rescue in CNTF-treated retinas, but evaluation by electroretinographic responses (ERG) has shown a paradoxical decrease in scoptopic and photopic responses. Similarly, Frasson *et al.*, (1999) shown the use of glial cell derived neurotrophic factors (GDNF) for delaying rod degeneration and preserving visual function in rd mouse. In addition, the expression of both CNTF and GDNF by adenoviral and lentiviral-mediated deliveries has been reported to prolong retinal ganglion cell survival following axonal injury (van Adel *et al.*, 2003). Furthermore, adeno-associated viral over-expression of pigment epithelium derived factor (PEDF) has been shown to inhibit retinal and choroidal neovascularisation by inducing the regression of new blood vessel establishment. The success following this experimental study has led to the development of a phase I clinical trial of adenovirus-mediated PEDF expression by intravitreal delivery in patients with

neovascular age-related macular degeneration (Gehlbach *et al.*, 2003; Saishin *et al.*, 2005).

1.8.4 Calcium blockers

Intracellular Ca^{2+} levels are directly linked to cGMP level where an increase in calcium ions will lead to the activation of apoptotic cascade. cGMP-gated channels are responsible for light sensitive currents. A mutation in the PDE6 gene has been reported to cause an over-expression in cGMP leading to photoreceptor cell death. Frasson *et al.*, (1999) have shown the use of D-cis-diltiazem that acts on cGMP-gated channels to slow down photoreceptor degeneration in rd_1 mouse model. However, diltiazem has been restricted to certain mutations and is dependent on the model used.

1.8.5 Stem cells and precursor cells

Stem cells provide a wide application in therapy for neurodegenerative disorders, such as the activation of progenitors to promote self-repair mechanisms and transplantation to replace lost cells. Neurogenesis in mature retina is presently studied in different models. In adult mouse models, retinal stem cells have been isolated from peripheral ciliary margins, and *in-vitro* isolated progenitors have displayed differentiation into retinal specific cell types such as rods (Ahmad *et al.*, 2000). The teleost fish retina also shows great regenerative capacity latter to damage allowing total visual function restoration. In addition, continual growth associated retinal neurogenesis is observed throughout postnatal development and into adulthood where new retinal cells derived from retinal progenitors are continuously added to the peripheral ciliary margin (Otteson and Hitchcock, 2003). Transplantation of stem cells to replace damaged cells represents a main application of stem-cell based treatment in neurodegenerative disorder. Young *et al.*, (2000) transplanted neural precursor cells into rodent adult retina demonstrating the ability of mature retina to incorporate into grafted neural stem cells. In addition, a phase II clinical trial is ongoing where stem cells have shown to differentiate into cells that express retina specific markers (Sun *et al.*, 2006). Embryonic stem cells transplanted in rats and mice have been observed to integrate into the host retina and protect the host retinal

neurons (Meyer *et al.*, 2006). Maclaren *et al.*, (2006) demonstrated that transplantation of rod photoreceptor precursor cells into the ONL of adult wild-type or degenerating retinas ($RHO^{-/-}$ or *rds*) successfully integrated and differentiated into rod photoreceptors to provide visual function enhancement.

1.8.6 Inhibitors of apoptosis

Apoptosis related to growth factor deprivation and disorganisation of cell cycles is the final pathway in photoreceptor cell death. Several anti-apoptotic therapies have been developed to target secondary mechanisms involved in the apoptotic cascade. In rodent models, anti-apoptotic proto-oncogene *bcl-2* has been reported to delay photoreceptor degeneration (Nir *et al.*, 2000), and intraocular administration of peptide inhibitor of caspase 3 has shown to inhibit pro-apoptotic genes preventing photoreceptor cell deaths (Liu *et al.*, 1999a).

1.8.7 Implanted electrical devices

Electrical devices that stimulate the retina optic nerve and visual cortex are currently being developed in both animal models and human patients (Pardue *et al.*, 2005; Brelen *et al.*, 2005). Patients that have been tested with the first version of this device have reported visualising phosphenes (flashes of light) in response to direct retinal stimulation (Kamei *et al.*, 2006).

1.9 RNAi Discovery and Mechanistic Description

1.9.1 Introduction

The study of gene function has benefited enormously from functional genomic approaches such as low molecular weight pharmacological drugs and gene-targeting techniques. The latter technique exploits the phenomenon of nucleic acid hybridisation, which is extremely specific and theoretically has universal application for any target sequence of interest. The first antisense experiments were performed over 29 years ago where antisense oligodeoxynucleotides (ODN) were employed to inhibit the translation of Rous sarcoma virus RNA (Zamecnik and Stephenson, 1978; Stephenson and Zamecnik, 1978). Subsequently, backbone modifications and packaging techniques were established to increase both the activity and stability of antisense oligonucleotides. Antisense experiments using single-stranded DNA and RNA to inhibit gene expression based on RNase H-mediated downregulation of the target mRNA or steric blockade of translation then followed (Melton, 1985; Graessmann *et al.*, 1991; Crooke, 1999). In the early 1980s, the discovery of catalytically active RNAs called ribozymes, showed for the first time that RNA molecules, apart from their traditional role in the transfer of genetic information, can act as enzymes to break covalent bonds in RNA molecules with high sequence specificity (Cech *et al.*, 1981; Kruger *et al.*, 1982). The development of *trans-acting* ribozymes, such as hammerhead ribozymes, which were derived from the structure introduced by Haseloff and Gerlach (1998) with simplified catalytic motifs, was an important step forward in nucleic-acid based gene silencing. However, the therapeutic use of ribozymes has been hampered by problems including poor delivery into target tissues and major instability. Although methods such as extensive chemical backbone modifications and viral vector mediated delivery of ribozymes have been attempted to circumvent these problems, the use of ribozymes for *in-vivo* and therapeutic applications still remains very limited.

The molecular phenomenon of RNA interference (RNAi) was first demonstrated in petunia plants by two independent groups 15 years ago (Napoli *et al.*, 1990; van der

Krol *et al.*, 1990). The original experiments were designed to increase the colour intensity of petunia petals by introducing extra copies of chalcone synthase gene, which was responsible for the synthesis of red pigment. However, the outcome of these experiments was most unexpected, with many of the genetically engineered flowers losing their natural pigmentation while patterned flowers with white non-clonal sectors on wild-type pigmented background were produced. This ambiguous effect was later termed as co-suppression. Seven years onward, the major explosion in the field of RNAi occurred when Fire and Mello (1998) discovered that intracellular exposure of double-stranded RNA (dsRNA) resulted in specific post-transcriptional gene silencing (PTGS) of homologous cellular RNA. This astonishing natural process was illustrated by the introduction of double-stranded RNA into the invertebrate nematode *Caenorhabditis elegans,* which caused selective downregulation of a corresponding gene product. Subsequently, other studies have shown that RNAi is not restricted to specific organisms, but rather it is a common process encountered in unicellular protozoans, insects, fungi, invertebrates and plants (Prawitt *et al.*, 2004). The degradative pathway of RNAi is thought to have evolved as a defence mechanism against viral pathogens and uncontrolled transposable elements that include a double-stranded RNA step in their replications (Bahasra and Prilliman, 2004), and has also been linked to developmental processes in multicellular organisms and chromatin structure regulation (Rao and Sockanathan, 2005). Although the discovery of RNAi seemed to have offered an additional way to inhibit the expression of every gene in living cells, the introduction of long double stranded RNAs (>30bp) into mammalian cells has been shown to activate protein kinase PKR, which phosphorylates the α-subunit of protein synthesis initiation factor eIF-2α, leading to global inhibition of protein synthesis (Der *et al.*, 1997). As a result, the use of ds-RNA for gene function analysis was discouraged by the unwanted effects encountered in mammalian cells in response to the presence of ds-RNA longer than approximately 30bp. However, Elbashir and Tuschl subsequently showed that short RNA duplexes of 19 base pair with 3'TT overhangs, designed to mimic the products of the DICER enzyme, could promote efficient RNA interference *in-vitro* in *Drosophila* embryo extracts (Tuschl *et al.*, 1999; Elbashir *et al.*, 2001b). This

observation was extended to mammalian somatic cells by Elbashir and Caplen (Elbashir *et al.*, 2001a; Caplen *et al.*, 2001), who showed that chemically synthesised siRNAs could induce gene silencing in a wide range of human and mouse cell lines. In contrast to long dsRNA, siRNAs of 21-23bp can evade the activation of PKR, which has unlocked the potential of RNAi as an effective strategy to selectively silence gene expression in mammalian cells and animals. Today, small interfering RNA (siRNA) has emerged as a valuable tool for studying gene function and serves as a potential new basis for the treatment of human disease. The rapid progress and great acceptance of RNAi within a relatively short period stems from the versatility of siRNA in addition to the application of solid foundations based on the last 30 years of antisense oligonucleotides research during which many important therapeutic hurdles such as cellular uptake and toxicity problems were elucidated.

1.9.2 Mechanism of RNAi

Elucidation of the RNAi mechanism has demonstrated that many steps involved in the process are well-conserved among different species. Upon the production of double stranded RNAs (dsRNA), a host ribonuclease enzyme called Dicer, recognises these molecules and cleaves the long dsRNAs into small interfering RNAs (siRNAs) i.e. 21-25 nucleotide duplexes containing symmetric 2 nucleotide 3' overhangs, and a 5'-phosphate and 3'-hydroxyl group. These double stranded RNAs may also be introduced into any cell by transient transfection to elicit the RNAi response. Dicer is a member of the RNase III family of enzymes. It includes an N-terminal helicase domain known as PAZ domain (Piwi/ Argronaute/ Zwille), a dsRNA binding domain and two RNase III motifs at the C-terminus. The presence of a helicase domain suggests that unwinding of dsRNA is required in subsequent steps (Bernstein *et al.*, 2001). The Dicer-derived siRNA duplexes then act as functional intermediates and are incorporated into a nuclease containing multi-protein complex called RNA-inducing silencing complex (RISC). RISC is a multi-component protein complex involving an endoribonuclease required for cleaving mRNA, and other proteins including eIF2C1, eIF2C2, RNA helicase, Gemin 3 and 4 (Hammond *et al.*, 2000). Upon incorporation, the RISC complex is remodeled to its activated form RISC*

through an ATP-dependent pathway, and carries out unwinding and strand separation of the siRNA duplex. The activated RISC* complex then uses the unwound antisense strand as a guide to locate target mRNA by Watson-Crick base-pairing. Upon binding, the target mRNA is degraded by the RISC endonuclease subunits (near the centre of the regions covered by antisense strand), and the cleaved mRNA is then further digested by cellular exonuclease activity (Elbashir *et al.*, 2001a). Following cleavage, the RISC* complex is dissociated to target additional mRNA molecules (*Figure 1.10*).

In addition to this linear mechanism, a different RNAi pathway has been observed in plants, *C. elegans* and *Drosophila*, though is absent in mammals. This transitive RNAi pathway has developed an amplification cycle with an additional enzyme complex called RNA-dependent RNA polymerase (RDRP) (Argrawal *et al.*, 2003). The RDRP complex uses siRNA as sequence specific primers and the target transcript as templates to produce large quantities of double stranded RNAs which are then processed into siRNAs to elicit RNA silencing. This process effectively eliminates a transcript by targeting multiple sites in its sequence.

1.9.3 Thermodynamic properties of siRNAs

For an effective siRNA, the guide strand (antisense strand) of the duplex is required to be incorporated into RISC, in preference to the passenger strand (sense strand). Thermodynamic profiling of siRNAs and biochemical experiments have revealed that the strand with the lower 5' terminus thermodynamic stability in the siRNA duplex is more functional (Khovorova *et al.*, 2003). The idea of thermodynamic instability for strand selection was tested in SOD1 (hereditary amyotrophic lateral sclerosis) and Huntington's disease (Schwarz *et al.*, 2003). In both scenarios, inactive siRNAs were made functional by introducing mismatches (asymmetry) in the 5' end of the siRNA guide strand. Conversely, thermodynamically stable siRNAs were not uniformly active, despite full complementarity to target mRNA. siRNAs which exhibited thermodynamic instability at the 5' end of guide strand were favoured for entry into RISC. Therefore strand selection can be predetermined by deliberate mismatch of

nucleotides between guide strand and passenger strand. In addition, the mechanism involved in the incorporation of the selected siRNA strand into the RISC complex is also important in mRNA silencing (Hammond *et al.*, 2001). Upon unwinding of the siRNA duplex, RISC proteins position the guide strand into a favourable position to bind to the target mRNA and juxtapose the catalytic subunit of Ago 2 to a vulnerable phosphate bond across from nucleotides 10-11 of the guide strand. 5' phosphorylation of the guide strand is essential to the function of siRNA, which is one of the ATP-dependent steps in RNAi (Nykanen *et al.*, 2001). The 5' initial nucleotide determines the position of the critical endonuclease cleavage of the phosphate between nucleotides 10-11 (Elbashir *et al.*, 2001b and c), and the same site is cleaved independent of the length of the guide strand at 3' end.

In contrast, the 3' end of the guide strand has a lesser role in RNAi, if not negligible, in recognising target mRNA to be cleaved (Doench and Sharp, 2004). A detailed analysis of the 5' end revealed that target recognition requires nucleotide complementarity at bases 2-5 of the guide strand, known as the seed sequence (Doench and Sharp, 2004). However, the 3' end is required to orientate RISC and stabilises the newly formed helix between guide strand and target mRNA. Mismatches at the 3' end of the guide strand to the target mRNA will ultimately decrease the rate of cleavage, but up to 9 mismatches at the 3' terminus are tolerated and will continue to cleave mRNA albeit very slowly (Haley and Zamore, 2004).

The catalytic component of RISC in mammals is Ago2, which is a member of the Argonaute protein family that is capable of assembling with siRNA. Ago2 contains two main structural domains: PIWI/Argonaute/Zwille (PAZ) and Piwi, where the Piwi domain functions in structural stabilisation and shares structural similarity to RNaseH endonuclease (Liu *et al.*, 2004). The strand with relative thermodynamic instability is selected to insert into Ago2 for the RISC loading complex by R2D2. However, if thermodynamic equality pertains throughout, then the passenger strand can also enter RISC which significantly reduces RNAi activity (Tomari *et al.*, 2004). Nevertheless, under normal conditions, the guide strand is selected for incorporation

and the passenger strand becomes the first target of the Ago2 endonuclease activity, where blockade of passenger cleavage by either phosphorothioate or 2'-O'-methyl modification has been shown to dampen RISC activity (Rand *et al.*, 2005). After cleavage, passenger strand remnants leave the RISC and the guide strand is secured and is no longer exchanged with free siRNAs (Martinez *et al.*, 2002).

1.9.4 Induction of interferon response by double-stranded RNAs

Effective silencing of genes in *C. elegans* and *Drosophila* can be achieved using long dsRNA (>500bp). However, exposure of mammalian cells to long dsRNA can lead to the activation of Type-1-interferon response and STAT-mediated expression of protein kinase (PKR). The binding of dsRNA to PKR leads to the phosphorylation of the small sub-unit of the eukaryotic initiation factor 2 (eIF2α) resulting in global translational shutdown. In addition, dsRNA promotes the synthesis of 2'-5' oligoadenylate synthetase (2-5AS) which activates the non-specific RNaseL to cleave single-stranded RNA randomly, leading to cellular metabolism alteration and induction of the apoptotic pathways. Therefore the direct transfection of large dsRNA seems to be limited as a gene-silencing tool in higher organisms (Armant and Fenton, 2002; Tosi, 2005).

1.9.5 The design of effective siRNAs

Tuschl and Elbashir have both demonstrated the ability to evoke RNAi type silencing activity by exogenously introducing short 19-21bp siRNA molecules to selectively suppress target mRNA in a diverse range of cell types without inducing the PKR activated translational arrests (Tuschl *et al.*, 1999; Elbashir *et al.*, 2001a). By mimicking Dicer-processed products, siRNA duplexes of 21-nucleotides with 2-nucleotide 3' overhangs are long enough to mediate gene silencing in mammalian cells but short enough to evade host interferon response.

Most *in vivo* experiments reported to date used chemically synthesised siRNAs that are designed to be 21-23mer duplexes containing a central 19-base central double stranded domain with a preference of uridine residues in the 2 nucleotide 3'

overhangs. Uridine can be replaced by 2' deoxythymidine to confer enhanced nuclease resistance of the duplex. A critical step for effective siRNA is the choice of target sequence within the gene of interest. Therefore many algorithm-based siRNA-design criteria (Reynolds *et al.*, 2004) and automated search engines (www.dharmacon.com) have been generated to assist the selection of optimal target sites for siRNA suppression. In addition, siRNAs are designed to target 50-100 nucleotides downstream of the start codon. The GC content is maintained at approx 50% and strings of 3 or more G/C residues are avoided within the siRNA region (Reynolds *et al.*, 2004). Elbashir *et al.*, (2001c) shown that target recognition process is highly sequence specific but not all positions on the siRNA contribute to target recognition. This has been shown to be particular crucial at the centre of the siRNA, and any mismatch with the target RNA may prevent binding or cleavage. The accessibility and secondary structure of the target RNA is also an important factor in determining the silencing efficiency *in-vivo* (Far and Sczakiel, 2003).

The length of the siRNA strands itself also represents a critical factor for efficient RNAi. Recently Kim *et al.*, (2005) shown that siRNAs of length 25-27 appear to have greater potency than synthetic 21mer siRNAs directed to the same target site in HeLa cells. siRNA duplexes with 3' overhangs and 5' overhangs or blunt ends were also tested for their potency. By using siRNAs at various concentrations, it was observed that duplexes with increased lengths up to 27 base pair showed significantly increased potency, which was also observed for siRNAs with 5' overhangs or blunt ends. In contrast, reduced efficacy was seen in siRNAs with greater than 27 base pair stems. Importantly, 27mers siRNAs did not induce the interferon response or activate PKR. Similarly, Siolas *et al.*, (2005) have reported that synthetic shRNAs with 29 base pair stems and 2-nucleotide 3' overhangs are more potent inducers of RNAi than shorter hairpins. Despite enormous efforts in deciphering the criteria needed for the design of effective siRNAs, the guidelines outlined above are not absolute, and siRNAs still have to be experimentally assessed by trial and error to optimise the knockdown of an individual transcript, since not all siRNA duplexes matching the design criteria work efficiently.

1.9.6 Off-target effects

In traditional antisense oligonucleotide experiments, a genome wide homology search is carried out to eliminate any sites with significant cross-hybridisation potential that would cause non-specific gene targeting. Indeed a single mismatch between siRNA and intended target has been shown to abolish suppression activity (Amarzguioui *et al.*, 2003), and systematic analysis of the functional impact caused by base changes at all positions in the target site has been reported (Du *et al.*, 2005). However, traditional homology and cross hybridisation analysis can no longer accommodate for the complexity involved in off-target effects and transfection of siRNAs in mammals has been shown to cause widespread changes in expression levels of unrelated genes (Jackson *et al.*, 2003; Persengiev *et al.*, 2004).

Degradative RNAi leads to sequence-specific cleavage of a target mRNA as directed by RISC using Ago2 (Meister *et al.*, 2004), and initiation of this event requires perfect to near-perfect base paring between guide strand and target transcript. Conversely, the microRNA pathway results in translational repression and is directed by imperfect base pairing between target and guide strand (He and Hannon, 2004; Kim, 2005). This pathway is theorised to be mediated by a variant of RISC using Ago1. Functionally the siRNA degradative pathway and microRNA (miRNA) translational repression pathway overlap. Therefore, exogenously supplied siRNA duplexes can function as miRNAs (Saxena *et al.*, 2003), and vice versa: miRNAs can direct cleavage events. It seems like many of the off target effects attributed to siRNAs are derived from miRNA-like target interactions, which can be triggered by extremely limited homology. Target specificity for miRNAs is largely directed by a 7-nucleotide seed region at the 5' end of the antisense strand of the miRNA (Doench and Sharp, 2004). Lin *et al.*, (2005) have reported a similar finding where off-target effects resulted from only a 7 basepair complementation between the siRNA and the off target mRNA. Given the high frequency of finding 7-base matches between a given siRNA and non-targeted genes within the entire transcriptome of a mammal, simple homology screening alone is insufficient to predict off-target events. However, when using siRNAs as research tools, a simple strategy to ensure that

results are not misinterpreted because of unsuspected off-target effects is to require that two independent siRNAs against the same target produce the same biological results (Behlke, 2006). To assess off-target effects *in-vivo*, microarray analysis studying documented changes in gene expression profiles that result from siRNA treatment on a genome-wide scale *in-vitro* and *in-vivo* are extremely valuable, and these are discussed in further detail in Chapter 6.

MicroRNAs are important for cellular gene regulation networks and anything that disrupts miRNA processing could potentially have broad effects on gene expression in a cell. It is possible that high doses of exogenous siRNA administered as therapeutics could saturate the RNAi machinery and thereby alter miRNA levels, further complicating the spectrum of off-target effects. Hong *et al.*, (2005) described that high doses of a siRNA can induce expression of some genes involved in siRNA degradation and processing (meri-1 and adar-1). Stimulation of IFN pathways, off-target effects, and desired gene knockdown are all dose dependent events. The precise dose needed to trigger each response can be different and it may be possible to influence the relative magnitude of undesired side effects by careful attention to dosing. Dose response profiles should be performed *in-vivo* and administration of siRNA should be at the lowest levels required to achieve desired knockdown.

1.9.7 Chemical modification of siRNAs

Although siRNA duplexes are more resistant to nuclease attack than single stranded DNA, unmodified siRNAs are nevertheless rapidly degraded when administered intravenously in mammals. However, degradation can be delayed or avoided by chemical modification of the oligonucleotide backbone or complex with a carrier delivery particle. Morrissey *et al.*, (2005a) reported that the plasma half life of an unmodified siRNA duplex in mice was 0.03 hour, and the half-life of a modified duplex packaged via stable nucleic acid-lipid particles (SNALP) was 6.5 hours. Soutschek *et al.*, (2004) reported studies using modified siRNAs in rats in which an unconjugated duplex had an elimination half life of 0.1 hour, while a cholesterol conjugated duplex had a half life of 1.5 hours. A number of chemical modifications

that confer nuclease resistance have already been successfully employed in single stranded antisense oligonucleotides and ribozymes. These modifications can be imported directly into siRNA and have already provided similar benefits as listed below.

1) **Phosphorothioate and bornaophosphate modification of the internucleotide linkage improve nuclease stability**
   - Phosphorothioate (PS) modifications can be easily placed in the RNA duplex at any desired position and will prolong the life of the duplex when exposed to serum or other nuclease sources. Limited PS modification preserves potency of the siRNA, however, extensively modified duplexes show reduced potency and increased toxicity (Harborth *et al.*, 2003; Chiu and Rana, 2003; Braasch *et al.*, 2003; Amarzguioui *et al.*, 2003). Extensive PS modification can also lead to artifacts due to nonspecific protein binding (Krieg and Stein, 1995), so it may be preferable to limit the use of this modification to terminal positions (or 3' overhangs) where additional nuclease resistance is probably important.
   - Boranophosphate-modified RNAs have substantially nuclease resistance, unfortunately boranophosphate modified RNAs cannot be manufactured using standard chemical synthesis methods. However, the bases can be incorporated into RNA by enzymatic synthesis using *in-vitro* transcription (Hall *et al.*, 2004), which makes site selective placement of this modification difficult.

2) **Modification of the 2' position of the ribose can increase duplex stability (T_M) and confer varying degrees of nuclease resistance**
   - 2'-O-methyl RNA is a naturally occurring base that is present in mammalian ribosomal RNA. A number of reports have described patterns of 2'-O-methyl incorporation that retain full potency of the siRNA compared with unmodified RNA and are stable in serum (Czauderna *et al.*, 2003; Chiu and Rana 2003; Amarzguioui *et al.*,

2003). The precise pattern of incorporation is important and RNAs that are entirely substituted with 2'-O-methyl are inactive as triggers of RNAi. Alternating the 2'-O-methyl bases retains potency and confers nuclease resistance (Czauderna *et al.*, 2003).

- The 2'-fluoro (2'-F) modification is incorporated selectively at pyrimidines bases in the siRNA duplex due to reagent issues and has been used with good results (Harborth *et al.*, 2003; Chiu and Rana, 2003; Braasch *et al.*, 2003). This modification is either used alone or in combination with 2' O-methyl purines to stablise RNA duplexes, and all the nucleotides within the duplexes can be modified (Allerson *et al.*, 2005). Morrissey *et al.*, (2005b) compared the activity of an unmodified siRNA targeting hepatitis B virus to that of a highly modified duplex that included DNA bases, 2'-O-methyl purines, 2'-F-pyrimidines, terminal inverted-dT bases, and PS linkage modification at selected positions, leaving no unmodified RNA. A hepatitis B virus (HBV) expression plasmid was co-injected with the modified and unmodified duplexes into the tail vein of mice using hydrodynamic delivery method. The production of HBV DNA and HBV surface antigen was assayed 72 hrs post-injection, and as expected, the modified duplexes outperformed the unmodified showing greater suppression of hepatitis B virus for 72 hrs after initial administration.

3) **Locked nucleic acids (LNAs)** are a different class of 2' modification in which a methylene bridge connects the 2'-O with the 4'-C of the ribose. This modification locks the ribose in the 3'-endo conformation and improves both duplex stability and nuclease resistance. LNAs can be incorporated into siRNAs, but the placement of modification to achieve best effect is more stringent than for 2'-O-methyl or 2'-F bases (Braasch *et al.*, 2003; Grunweller *et al.*, 2003; Elmen *et al.*, 2005).

Various chemical groups can be placed at the ends of oligonucleotides that may facilitate entry into cells to improve biodistribution. For example, conjugation of cholesterol to a siRNA can improve serum protein binding, pharmacokinetics, and increase delivery to hepatocytes (Lorenz *et al.*, 2004; Soutschek *et al.*, 2004). In particular, systemic administration of cholesterol conjugated siRNA targeting apoB, a constituent of low density lipoproteins, downregulated hepatic apoB and reduced serum concentrations of low-density lipoproteins (Soutschek *et al.*, 2004). Additionally, a dinitrophenol end modification has also been shown to improve transfection and increase intracellular stability in tissue culture (Liao and Wang, 2005), while peptide-oligonucleotide conjugates can improve cell permeation properties as well as nuclear targeting (Juliano, 2005).

1.9.8 Vectors and viral delivery systems *in-vivo*

1.9.8.1 siRNA expression vectors

In *C. elegans*, the RNAi effect is observed to be stable and long lasting due to the presence of the RNA dependent RNA polymerase (RdRp) that amplifies siRNA activity (Wadhwa *et al.*, 2004). However, since mammalian cells lack RdRp, the RNAi effect is transient and limited to four to eight cell-doublings only. In order to circumvent the temporally limited activity of exogenously transfected siRNAs, polymerase III promoters such as the human ribonuclease P RNA component H1, human U6 or mouse U6 small nuclear RNA promoters (Taxman *et al.*, 2006) have been used to express short hairpin RNAs (shRNA) intracellularly to maintain stable suppression in mammalian cells. The advantages of expression cassettes containing the polymerase III promoter are that: (i) transcripts from these promoters end in a run of 4-5 thymidines allowing for specific determination of transcript length; (ii) polymerase transcripts terminate in the second thymidine resulting in two nucleotide 3'-overhangs which are similar to the most effective siRNA incorporated into the RISC complex; (iii) generation of siRNAs from expression vectors are more cost-effective than chemically synthesised siRNAs; (iv) polymerase III initiates transcription at either a G or A, so that the transcription start site for shRNA can be

predetermined offering a system in which any sequence can be inserted downstream of the start site.

DNA-vector based expression of siRNA *in-vivo* is based on two specific designs: (i) Brummelkamp *et al.*, (2002) developed a vector system containing a H1-polymerase III promoter directing the synthesis of small complementary inverted repeats separated by a non-complementary spacer region of varying lengths that cause the resulting RNA transcript to fold back upon itself forming a hairpin structure called short hairpin RNA (shRNA), which is analogous to naturally occurring microRNAs. The short hairpin RNA is then recognised by processing bodies of RNAi and is processed by DICER to 21-23 nucleotide siRNAs *in-vivo.* In general, shRNAs contain stems that have specific targets sequences, a loop sequence of 3-9 nucleotides and 3' uridine overhangs (*Figure1.11A*). In another system, two U6/H1 promoters are placed in tandem or in two separate expression vectors to direct the synthesis of sense and antisense strand of siRNA with 19 nucleotide specific target sequence and 3'-UU overhangs. The sense and antisense strands then anneal to form duplexes *in-vivo* and function similarly to chemically synthesised siRNAs (Chen *et al.*, 2005) (*Figure 1.11B*). These vectors are more robust for cloning because of the lack of secondary structure and incur low level of DNA synthesis error due to shorter sequence. Upon comparison of the two systems, Miyagishi and Taira (2002a) have shown that the hairpin type siRNA expression vector elicited higher suppressive activity than the tandem type siRNA-expression vector at low concentrations.

Although constitutive expression of shRNAs by polymerase III promoters often result in stable and efficient suppression of target genes, the inability to adjust the levels of suppression has imposed limitations in the analysis of genes essential for cell survival, cell development and cell cycle regulation. This problem can be resolved by generating inducible regulatory siRNA strategies including tetracycline, doxycycline and ecdysone-response transcriptional elements. For example, a doxycycline inducible form of the RNA polymerase III H1 promoter has been developed to drive siRNA expression to inducibly downregulate β-caterin/TCF activity in colorectal

cancer cells (van de Watering *et al.*, 2003). In addition, Gupta *et al.*, (2004) have developed an ecdysone-inducible polymerase III specific U6 promoter for the synthesis of shRNAs targeting p53 in human and murine cells. Cells containing the stably integrated shRNA expression construct demonstrated stringent dosage and time dependent kinetics of induction with undetectable background of expression in the absence of the inducer ecdysone, with induction of the shRNA causing cell cycle arrests. In addition, the induction is reversed after the removal of the inducers.

Vector-based shRNA libraries and chemically synthesised oligonucleotide libraries have been developed for high-throughput genome wide screening in mammalian cells. Berns *et al.*, (2004) used their library to search for genes that affect the function of p53 (tumour suppressor gene). Paddison *et al.*, (2004a) constructed and applied an shRNA library targeting 9610 human and 5563 mouse genes, and subsequently used the library as a genetic screen to detect defects in human proteasome function.

1.9.8.2 Viral delivery of siRNA *in-vivo*

The use of siRNA for target validation *in-vivo* has been confronted with many obstacles such as poor stability, non-specificity of gene silencing and limitation in size due to induction of interferon response by long dsRNAs. In addition, stable transfection and accurate tissue specificity delivery remain a significant *in-vivo* challenge. Although mammalian cell based DNA constructs has been successful in alleviating some of these problems, delivery of siRNA into primary neural and hemopoietic cells still remains difficult. Viral-based vectors have been developed as an alternate strategy that can provide higher transfection efficiencies, and a number of viruses including retroviruses, lentiviruses, adenoviruses, adeno-associated virus (AAV) and herpes simplex virus type 1 (HSV-1) have been used extensively to deliver stable knockdown *in-vivo* by integration into the genome or by extrachromosomal existence.

1.9.8.3 Retroviral vectors

Retroviruses are a class of enveloped viruses in which the genome is made up of a single stranded RNA molecule of 10 kb. Following infection this genome is reverse transcribed into double stranded DNA and integrated into the host genome. Retroviral vectors are derived from the Moloney murine leukemia virus (Mo-MLV) which is an amphotrophic virus capable of infecting both mouse and human cells, thus enabling vector development in cells of both species. The viral proto-oncogene is routinely replaced by the gene of interest and transgene expression can either be driven by the promoter enhancer region in the 5' LTR or alternative viral or cellular promoters. A requirement for retroviral integration and expression of viral genes is that the target cells should be dividing. This is particularly useful for targeting proliferating cells *in-vivo*, especially in cancer therapy where the tumour cells are preferentially targeted. Roth *et al.*, (1996) used a retroviral vector to successfully transfer wild type p53 into human non-small lung cells, and many retroviral-based shRNA vectors have been used for functional genome analysis (Sliva and Schnierle, 2006). Unfortunately, the use of retroviral vectors in transgenic animals has been reported to induce inflammatory interferons (Ghazizadeh *et al.*, 1997). Retroviruses are also inactivated in human sera *in-vivo* by *cl* complement proteins and anti-alpha galactosyl epitope antibodies (Rother *et al.*, 1995). However, this may be overcome by development of complement resistant retroviral vectors.

1.9.8.4 Lentiviral vectors

Lentiviruses are a type of retrovirus that can infect both dividing and non dividing cells because their virus capsid can pass through the intact membrane of the nucleus (Rubinson *et al.*, 2003), enabling them to target terminally differentiated cells such as neurons, macrophages, haematopoietic stem cells, liver or muscle cells. A major advantage of lentiviral gene delivery is that transgenes expressed from lentiviruses are not silenced during development and can be used to generate transgenic animals through infection of embryonic stem cells or embryos. Rubinson *et al.*, (2003) have used a lentiviral system for delivery of shRNAs into cycling and non-cycling mammalian cells, stem cells, zygotes and their differentiated progenies in transgenic

mice. Given this host of advantages, lentiviral vectors have been widely used to clone and express many shRNAs for stable knockdown of gene expression (Janas *et al.*, 2006; Morris and Rossi, 2006).

1.9.8.5 Adenoviral vectors

Adenoviruses (Ads) are encapsidated viruses that contain a linear 35kb double-stranded DNA genome which do not integrate into the host genome, but exist as episomal elements within the nucleus of the host cells. For vector generation, up to 30kb of viral genome can be replaced (Smith, 1995; Verma and Somia, 1997), and 'gutless' adenoviruses, which refers to recombinant Ad cassettes with all native viral genes being deleted, have been used for long term expression in liver and brain tissues (Thomas *et al.*, 2000). Ads have shown high transduction efficiencies in both dormant and dividing cell types and a total of 43 different human Ad serotypes have been characterised (Horwitz, 1990). They also deliver high levels of short term expression that carries significant benefit for siRNA technology. An adenoviral vector expressing p53 siRNA has been used to target breast cancer MCF 7 and lung carcinoma A549 cells, suggesting adenoviral vectors may have *in-vivo* clinical applications in cancer therapy (Shen *et al.*, 2003). Similarly, treatment of subcutaneous tumour xenografted with adenoviral vector expressing human telomerase RNA (hTR) siRNA decreased the rate of tumour growth *in-vivo* (Li *et al.*, 2007). Furthermore, Sabbioni *et al.*, (2007a) demonstrated that adenoviral vectors expressing anti-T-antigen siRNA were able to stably suppress the T-antigen oncogene expression *in-vivo* to inhibit the malignant phenotype of human polyomavirus BK transformed mouse cells.

1.9.8.6 Adeno-associated virus (AAV)

Adeno-associated viruses (AAVs) are small encapsidated viruses with a single-stranded DNA genome, and are one of the most successful delivery systems for siRNA because of several unique features that distinguish them from other therapeutic vectors (Stilwell and Samulski, 2003). Adeno-associated virus possesses the ability to infect a broad host range including both dividing and non-dividing cells;

secondly, wild-type AAV has never been implicated in any disease pathology. Also, while wild-type AAV2 can integrate into a specific site (AAVS1 region) in chromosome 19, removal of *rep* genes reduces integration site specificity as well as the propensity to integrate in infected cells (Duan *et al.*, 1997; Wu *et al.*, 1998b). Thus, the lack of cell-mediated immune response against the vector and the ability to persist episomally without integration into the host genome have made AAV a much safer choice of delivery. Moreover, recent DNA microarray studies have shown that infection with AAV vectors has no impact on the overall pattern of cellular gene expression (Stilwell and Samulski, 2003). Currently, there are at least eight serotypes of AAV being under study, with demonstrable differences in tropism of cell types transduced (Davidson *et al.*, 2000). Machida *et al.*, (2006) have demonstrated recombinant adeno-associated virus (rAAV)-mediated delivery of RNAi into the Huntington disease (HD) model mouse striatum after the onset of disease. Neuropathological abnormalities associated with HD, such as insoluble protein accumulation, neuronal aggregates in the striatum and down-regulation of DARPP-32 expression, were successfully ameliorated by the RNAi transduction. Similarly, Miller *et al.*, (2005) have used an adeno-associated virus carrying siRNA targeting superoxide dismutase, in which mutations cause a subset of familial amyotrophic lateral sclerosis and provoke progressive paralysis. Following retrograde transport of AAV to the spinal cord after intramuscular injection in mice, mutant superoxide dismutase was downregulated in spinal motor neurons ameliorating the adverse effect of the disease.

1.9.8.7 Herpes simplex virus type 1 (HSV-1)

Herpes simplex virus type 1 (HSV-1) based vectors are increasingly being used for several gene therapy strategies (Epstein *et al.*, 2005). These vectors possess some inherent advantages over the other viral vectors in that the large capacity of HSV-1 particle allows to package and efficiently deliver up to 150 kilobases of DNA. Secondly, up to half of the 80 genes in the genome can be deleted without affecting virus production in cell culture. In addition, HSV can infect a broad spectrum of cell types and is naturally neurotropic. There are two main types of HSV-1 vector systems

for gene delivery, called amplicon and recombinant viruses. Amplicon viruses has been shown to suppress tumour growth in a nude mouse model through siRNA delivery into glioma cells (Saydam *et al.*, 2005), and successfully delivered polyomavirus BK T-antigen siRNA into human polyomavirus BK (BKV)-transformed cells inhibiting both the expression of BK T-Ag and tumourigenicity of BKV-transformed cells (Sabbioni *et al.*, 2007b).

1.9.9 The use of siRNA *in-vivo*

The function of a target gene can be validated by inhibiting the target protein and examining the induced phenotypic changes by biochemical or histological assays. Conventional target validation is time consuming because the screenings of small molecule inhibitors of a target protein and generation of knockout animals require extensive studies. As a potent and specific inhibitor, siRNA is being rapidly adopted as the preferred tool for functional genomic research (Bantounas *et al.*, 2004), and the success of siRNA *in-vitro* has led to growing interest in *in-vivo* applications of siRNA.

The route of siRNA administration chosen is mainly dependent on the organ or area of the body targeted, and considerations regarding the total dose required, possibility of repeated administration, the effectiveness of tissue distribution and potential side effects should all be taken into account. Delivery of siRNA *in-vivo* to animal tissues faces a lot of complications and often requires a combination of physical, chemical and biological approaches (Lu and Woodle, 2005). The main goal of *in-vivo* delivery is to achieve sufficiently stable accumulation of therapeutic molecules in target cells, which can exert an effect within the target cells without causing toxic or immunogenic effects. While the stability of siRNA in serum has been greatly increased by chemical modifications mentioned above, the choice of delivery routes is also important to ensure rapid and direct transportation of siRNA to target cells. However, it is impossible to design a universal *in-vivo* delivery system that is suitable for every scenario of siRNA delivery due to the accessibility of different tissue types and the variety of pharmacological requirements.

The routes of *in-vivo* delivery is generally categorised as either local or systemic (*Figure 1.12*). Some delivery vehicles and routes are very efficient for target validation in animals but not useful for the delivery of siRNAs in humans. Therefore, *in-vivo* siRNA delivery methods can also be classified as clinically or non-clinically viable. Systemic deliveries include intravenous and intraperitoneal administration, which is often considered for broadest tissue distribution, and local delivery can be used to achieve high concentrations at the intended target site while using a low dose and minimising the risk of systemic side-effects. Local delivery can be achieved by direct injection (e.g. intratumoural, intramuscular, intravitreous), or by topical application to a surface (e.g. transepithelial absorption through oral mucosa). Direct administration into the central nervous system (CNS) can also be achieved by intrathecal or intraventricular injection by-passing the issues with blood-brain barrier penetration (Xie *et al.*, 2006).

1.9.10 Systemic delivery

1.9.10.1 Intravenous administration using hydrodynamic delivery

Some of the initial studies of siRNA activity in mammals involved the delivery of siRNA into mouse livers using the hydrodynamic method (Lewis *et al.*, 2002; McCaffrey *et al.*, 2002; Zender *et al.*, 2003). Hydrodynamic delivery involves the rapid injection of a large volume of aqueous solution containing the therapeutic molecules e.g. siRNA into the mouse tail vein, which creates a high pressure in the vascular circulation, leading to delivery of the therapeutic molecules primarily into hepatocytes. Thus, this procedure is a useful method for functional genomic studies in the liver. However, because of the high risk of damaging the liver and other organs including the heart, hydrodynamic delivery is better suited to the study of liver function or liver infectious diseases (hepatitis) in animal models rather than for clinical treatments for humans (Giladi *et al.*, 2003). Song *et al.*, (2003) demonstrated the use of siRNA to protect mice from liver damage in two model systems involving Fas-mediated apoptosis. Anti-Fas siRNAs and control anti-EGFP siRNAs (50 μg per 1 ml PBS) were administered separately using hydrodynamic delivery for three

different doses. Both Fas mRNA and Ras protein levels were shown to be specifically reduced by 10 fold in recipient mouse hepatocytes relative to controls, and more surprisingly was that suppression lasted for ~10 days. Hydrodynamic delivery has also been used to study the antiviral potential of siRNAs *in-vivo*. Giladi *et al.*, (2003) demonstrated that a plasmid encoding the hepatitis B virus genome can be co-delivered with siRNAs to the liver of mice using the hydrodynamic method to study the effects of anti-HBV siRNA on viral replication (Giladi *et al.*, 2003). Five different HBV siRNAs were generated, and all showed great potency in reducing HBV titres produced in transfected livers.

1.9.10.2 Intraperitoneal administration

Injection of bacterial LPS into mice triggers secretion of tumour necrosis factor (TNF-α) and other cytokines by macrophages, resulting in a septic shock like syndrome and death from cardiovascular collapse. Administration of anti-TNF siRNA in cationic DOTAP (1,2-Dioleoyl-3-Trimethylammonium-Propane) liposomes by intraperitoneal injection 18 hrs prior to administration of 350 μg of lethal dose of bacterial LPS resulted in statistically significant survival rate and reduction of 75% of TNF-α in the anti-TNF siRNA treated animals (Sorensen *et al.*, 2003).

1.9.11 Direct injections

1.9.11.1 Intraocular

Direct injection of siRNAs into a target tissue can allow for lower dosing relative to systematic administration, reduce risk of systemic toxicity, and permit access to otherwise protected sites such as the CNS or the interior of the eye. Reich and Shen have both described the use of siRNA to disrupt the *VEGF* pathway via intraocular injection to inhibit neovascularisation following laser photocoagulation in mice (Reich *et al.*, 2003; Shen, 2006).

An increasing number of clinical trials have been approved for treating eye diseases with nucleic acid drugs. Sirna Therapeutics reported the study of Sirna-027, which is

a chemically modified siRNA drug targeting VEGFR-1 for the treatment of age-related macular degeneration (AMD). The treatment involves administration of a single escalating dose of the drug by direct intravitreal injection. During the phase I study of Sirna-027, it was observed that the drug was able to stabilise visual acuity in a dose-dependent manner (Shen, 2006). In addition, Acuity Pharmaceuticals reported the results of phase I clinical trial of Cand5, a siRNA drug targeting *VEGF* to treat AMD. 15 patients were administered Cand5 at five escalating doses by direct intravitreal injection and no adverse side effects were reported. Though, subconjuntival hemorrhage was observed as a side-effect which was deemed normal for this route of drug administration, and patients have now been enrolled in a Phase II clinical trial (Behlke, 2006). Delivery of unformulated siRNA specific to *VEGF* to the subretinal space in a mouse model of retinal neovascularisation resulted in significant reduction of angiogenesis in the eye. Using a murine model of herpetic stromal keratitis, which develops from the herpes simplex virus corneal infection, Kim *et al.*, (2004) showed that subconjunctival administration of siRNA targeting several genes in the *VEGF* pathway significantly inhibited the corneal angiogenesis and disease symptoms.

1.9.11.2 Intramuscular

The skeletal muscle tissue is readily accessible for local siRNA administration. A recent study showed that unformulated siRNA delivered by direct injection into mouse muscle followed by electroporation demonstrated significant gene silencing that lasted for 11 days (Golzio *et al.*, 2005). Hagstrom *et al.*, (2004) demonstrated an alternative method of hydrodynamic delivery to deliver siRNAs to skeletal muscle in rats, dogs and rhesus macaques. In this variant of hydrodynamic method, a limb is functionally isolated by application of a blood pressure cuff or tourniquet, and a large-volume bolus of nucleic acid solution is administered intravenously (Toumi *et al.*, 2006).

1.9.11.3 Direct injection in central nervous system (CNS)

Antisense oligonucleotides have a long history of successful use in neuroscience research (Ho and Hartig, 1999). Although charged nucleic acids do not readily cross the blood-brain barrier, oligonucleotides can be injected directly into the CNS. Similar to plasma and other tissues, the CNS is a relatively nuclease poor environment and antisense oligonucleotides with minimal modification have been employed with good results previously (Hebb and Robertson, 1997). Therefore, it is not surprising that direct injection of unmodified siRNAs into the CNS has met with success.

Non-viral infusion of siRNA in the brain has provided a unique approach to accelerate target validation for neuropsychiatric disorders that involve a complex interplay of genes from various brain regions. In one study, infusion of siRNA specific to an endogenous dopamine transporter (DAT) gene in regions (ventral midbrain) far distal to the infusion site resulted in a significant downregulation of DAT mRNA and protein in the brain and elicited a temporal hyperlocomotor response (Thakker *et al.*, 2004). Dorn *et al.*, (2004) reported the use of an implanted intrathecal pump in rat CNS to modulate chronic neuropathic pain. RNA duplexes had 2'-O-(2-methoxyethyl)-modification residues (MOE modified) with phosphorothioate linkages comprising the 2-base 3' overhangs on each strand and targeted the pain-related cation-channel P2X3. siRNAs were administered by continuous infusion at a dose of 400 µg/day for 7 days. Dorsal root ganglia showed up to 40% reduction in P2X3 mRNA and protein, and rats exhibited an attenuated pain response in several models of neuropathic pain, including tactile allodynia and agonist induced mechanical hyperalgesia. However, the difficulty of performing surgical implantation of an infusion pump and the exposure of delivering high doses of siRNA limits the usefulness of non-viral siRNA-infusion as a tool for functional genomics

1.9.11.4 Intratumoural

Malignant tumours grow fast and spread throughout the body via the blood and lymphatic systems. Metastatic tumours established at distant location are usually not encapsulated and, thus are more amenable for systemic delivery. A number of groups have reported successful use of direct injection into or adjacent to tumour masses using naked and complexed siRNAs. Aharinejad *et al.*, (2004) reported direct injection of unmodified siRNAs into subcutaneous masses of the human mammary tumour cell line MCF-7 in nude mice. Direct injections were administered after the tumour was established at a dose of 10 μg once every 3 days for 2 weeks. Two different siRNAs specific for murine colony stimulating factor (CSF-1) and the CSF-1 receptor (c-fms proto-oncogen) were generated. CSF-1 signaling functions in recruiting macrophage infiltration of tumours and several macrophage-derived factors facilitate metastasis and tumour growth. siRNAs were tested both *in-vitro* and *in-vivo,* and showed significant reduction of CSF-1 and CSF-1 receptor in tumour tissue, and tumour growth was reduced by 50%. A study in pancreas xenografts used the systemic administration of unmodified CEACAM6-specific siRNA, and demonstrated a significant suppression of primary tumour growth by 68% versus control siRNA, and also decreased the proliferation index of the tumour cells, and impaired angiogenesis with an apparent increase of apoptosis without apparent toxicity (Duxbury *et al.*, 2004). Leng and Mixon (2005) used cationic peptides to facilitate the delivery of unmodified siRNAs by direct injection into human breast cancer MDA-MB-435 implants in nude mice. The siRNA was designed to be specific for Raf-1, which is a member of Raf kinase family involved in Ras/MEK signalling. Each injection contained 12 μg of peptide complexed with 4 μg siRNA and was administered every 5 days with 3 doses. The peptide-anti-Raf-1 siRNA complex was effective in reducing tumour size by 60 % compared to treatment with the control siRNA.

1.19.12 Experimental controls for RNAi

The large number of examples given above has truly demonstrated that siRNAs are a powerful therapeutic tool to down-regulate specific gene expression *in-vivo.*

However, many publications that display RNAi data do not sufficient controls such as thorough investigation into the modes of siRNA action, secondary effects on genes within a biological pathway other than the target transcript, and the relationship between siRNAs and miRNAs in gene regulation. In 2003, the Nature Cell Biology editorial board presented a list of recommended controls that should be included, if possible, in RNAi experiments:

1. *Scrambled or non-specific siRNAs*: the use of siRNAs with scrambled sequences may not be a truly informative control as they are not functionally active. In addition, mismatched siRNAs with minor base changes can serve as useful negative controls, only if such changes render the siRNA inactive. However, such changes may have unforeseen effects by converting a siRNA into a miRNA that elicits translational repression.
2. *Basic controls:* Unlike long double-stranded RNAs (>30bp), siRNAs (~21 base-pairs) are not believed to activate the interferon response that leads to global translational inhibition. However, the use of siRNA preparations contaminated with long double-stranded RNAs may result in translational attenuation. Therefore it is important to show that siRNA-mediated down-regulation occurs at both the mRNA and protein levels, as well as functional or phenotypic readouts where possible. If suppression occurs at both mRNA and protein levels, then this is a true 'classical RNAi' response. In contrast, if only protein expression is down-regulated, then this may suggest that a miRNA-mediated translational repression is present.
3. *Quantitative controls*: Titration studies should be carried out to minimise the dosage of siRNA needed to reduce possible side effects as well as providing a graded readout of the effect.
4. *Mulitple siRNAs*: An effective method to enhance the validity of RNAi data is to demonstrate a similar silencing effect with two or more siRNAs targeted to different sites in the same transcript.
5. *Functional controls*: Introduction of vectors expressing target transcript refractory to RNAi is a useful functional control. Suppression-resistant transcripts can be generated by using one or more silent third-codon point

mutations within the siRNA targeted region, and if suppression is targeted to the 3'-untranslated region (UTR), replacement genes can be generated with modified UTRs.

1.9.13 Saturation of the RNAi pathway is lethal to cell survival

The enthusiasm around siRNA as a new therapeutic modality has been hampered by a growing awareness of its potential to cause unwanted side effects. RNAi has been found to induce off-target gene silencing, to trigger an interferon response leading to global translational inhibition, to stimulate non-specific RNA degradation by RNase L and to activate Toll-like receptors and retinoic acid-inducible gene 1 protein, both promote adverse immune responses (Barik, 2006). To add to this list of concerns, Grimm *et al.*, (2006) have reported that excessive RNAi can cause lethality in mice by clogging up the natural RNAi/ miRNA pathway. Initially in a systematic experiment to investigate the long term effects of high-level of shRNA expression in mouse livers, 49 distinct recombinant AAV8-shRNA vectors, each being unique in its length and sequence, were delivered into mouse livers by intravenous injection. Surprisingly, 36 AAV8-shRNA sequences showed dose-dependent chronic hepatopathy as characterised by lobular collapse or multifocal hepatocyte necrosis, and the remaining sequences killed the treated mice within two months of injections. A detailed study was then followed which led to the discovery that at high doses, the overexpressed recombinant shRNAs overwhelmed and saturated the nuclear karyopherin exportin-5 (whose main function is nuclear export and stabilisation of shRNAs/miRNAs). The saturation of exportin-5 could possibly have abrogated the exit of normal cellular pre-miRNAs, preventing cytoplasmic maturation and function of the pre-miRNA, leading to the shut down of global miRNA and lethality. Furthermore, RNA analyses supported this hypothesis by showing simultaneous decrease of two mature miRNAs of the liver, miR-122 (representing 70% of all liver miRNAs) and let-7a. In order to further assess whether shRNA over-expression compromised miRNA functionality, the authors co-transfected an EGFP-reporter fused to a miR-122 target site with toxic and non-toxic shRNAs into Huh7 cells. As expected, decreased GFP expression was observed in the presence of non-toxic

shRNAs, indicating efficient miR-122 mediated cleavage of the fusion mRNA. In contrast, co-delivery of toxic shRNAs hampered miR-122 processing, demonstrated by greater GFP expression. Moreover, over-expression of recombinant exportin-5 in transfected livers largely restored shRNA/miRNA function, suggesting that over-saturation of the nuclear export system was the cause of lethality. A variety of control experiments were also carried out to exclude other possible scenarios as the cause of death. First, protein analyses were carried out to show that transfected livers exhibited normal interferon-α/β/γ, tumour necrosis factor-α, interleukin-6 and p-21/p53 levels, and a lack of eIF2-α phosphorylation, suggesting that lethality was not the result of RNA-dependent protein kinase/interferon pathway activation. Secondly, lethality did not require the presence of a target mRNA, thus excluding the formation of RISC complexes or gene silencing as a contributing factor. However, in order to conclusively unravel all the possible mechanisms for causing lethality due to oversaturation of the RNAi pathway, it is essential to examine a number of other proteins upstream and downstream of exportin-5, such as DICER and other parts of the RISC complex that play important roles in RNAi. The evidence provided by Grimm *et al.,* (2006) have suggested that strict controlling of intracellular shRNA levels is crucial for ensuring safe and stable *in-vivo* gene silencing, where the use of inducible shRNA or tissue specific RNA polymerase II promoters may serve as good alternatives (Ventura *et al.*, 2004).

1.10 Micro-RNAs

All multicellular eukaryotes use evolutionarily conserved mechanisms, ranging from signalling pathways to transcriptional regulation to carry out developmental programs and important cellular functions. In recent years evidence has accumulated that small non-coding RNAs are also used in a conserved manner to regulate key developmental events. Currently there are four distinct classes of regulatory small non-coding RNAs have been described, including short interfering RNAs, repeat associated small interfering RNAs (rasiRNAs), piwi-associated RNAs (piRNAs) and micro-RNAs (miRNAs) (Aravin and Tuschl, 2005; Kim, 2006). Micro-RNAs represent a large family of the most phylogentically conserved non-coding genes that function as post-transcriptional regulators of many physiological processes, including embryonic development (Brennecke *et al.*, 2003; Zhao *et al.*, 2005). The first known mammalian miRNA, *lin-4*, was discovered in a screen of *Caenorhabditis. Elegans* heterochronic genes, which distinguished one larval developmental stage from another (Lee *et al.*, 1993). Subsequently, analysis of the heterochronic pathway revealed the first miRNA target, *lin-14* (Wightman *et al.*, 1993). The first mechanistic analysis of miRNA function was also performed in *C. elegans* where it was found that the levels of miRNA-regulated mRNAs did not change, but rather the abundance of proteins encoded by those mRNAs markedly decreased, thus, indicating the role of miRNA in post-transcriptional regulation (Olsen and Ambros, 1999). Later, the discovery that another miRNA, *let-7*, is conserved from worms to mammals resulted in the acknowledgement that miRNAs represent a near-universal mechanism for regulating protein expression in almost every species (Pasquinelli *et al.*, 2000). Over the past years, greater than 400 miRNAs have been identified in the human and mouse genomes and estimates suggest their actual number may be close to 1000 (*http://www.sanger.ac.uk/software/Rfam/mirna*) (Griffiths-Jones, 2004; Berezikov *et al.*, 2005; Bentwich *et al.*, 2005). Systematic analysis of the spatial expression of miRNAs has shown that many miRNAs are expressed in a tissue specific manner (Lagos-Quintana *et al.*, 2002), and as each of the miRNA is thought to regulate on average the expression of approximately 100-200 target genes through translation repression, it is possible that a significant percentage of the mammalian

transcriptomes and proteome are regulated by miRNAs. The genomic organisation of miRNAs is extremely diverse. In particular, miRNA genes may contain their own independent promoters and enhancers (*Figure 1.13*). In humans and mice, approximately 40% of miRNAs are located within the introns of either non-protein coding or protein coding transcription units, and 10% are located within exons. A further 30% have uncertain transcriptional origins, and the remaining 20% are derived from genomic repeats (Rodriguez *et al.*, 2004).

1.10.1 A mechanistic view of miRNAs

Mature miRNAs are generated via a two-step pathway to yield single stranded 21-23 nucleotide RNAs that regulate at the post-transcriptional level in developmental and differentiation processes of multicellular organisms. miRNAs are found either as individual miRNA genes or in tandemly arrayed clusters that may be transcribed as polycistrons (Lee *et al.*, 2002a). The first step of miRNA processing is the excision of short hairpin miRNA intermediates of ~70 nucleotide with two nucleotide 3'-overhangs, called *pre-miRNA*, from the long primary transcript termed a *pri-miRNA* (*Figure 1.14*) (Lee *et al.*, 2002a). This cleavage occurs exclusively in the nucleus and is mediated by an enzyme called *Drosha* (a member of the RNase III family). The next step in the formation of mature miRNA is export of the pre-miRNA to the cytoplasm, which is mediated by the nuclear export factor Exportin 5 (a member of the karyopherin family of nucleocytoplasmic transport factors) (*Figure 1.14*) (Yi *et al.*, 2003). Previously, Exportin 5 has been associated with nuclear transport of a whole range of small non-coding RNAs, including the adenovirus VA1 RNA and the human Y1 RNA (Gwizdek *et al.*, 2003). Similar to other members of the karyopherin family, Exportin 5 is dependent on the GTP-bound form of Ran co-factor for specific binding to its export substrate, and it is predicted to release its RNA cargo in the cytoplasm via hydrolysis of Ran-GTP to Ran-GDP by the cytoplasmic Ran GTPase activating protein. Once inside the cytoplasm, Dicer is responsible for processing pre-miRNAs into active 21-22 nucleotide mature miRNA duplexes with characteristic 3'-dinucleotides overhangs (Provost *et al.*, 2002), which are then incorporated into the micro-ribonucleoprotein RISC (miRNP) complex in an asymmetric fashion and the

antisense strand is used to repress mRNA translation by partial base-pairing to the target mRNA, often within the 3' UTR (*Figure 1.14*). However, in plants, a majority of miRNAs have extensive complementarity to their target sites and act as siRNA to elicit endonucleolytic cleavage of the target mRNA. Generally, in all other systems studied, miRNAs suppress gene expression not by endonucleolytic cleavage of mRNA, but by partial binding to target transcript (often within the 3' UTR, typically 50-85%) and blocking target mRNA translation. siRNAs and miRNAs appear to be functionally interchangeable: whether cleavage or translational repression of target mRNA occurs lies in the degree of sequence complementarity between the guide strand and its target (*Figure 1.14*). Similar to siRNA, miRNA is also a component of the functional RISC complex, which suggests that RISC might be a bi-functional complex that is capable of inducing two types of post-transcriptional regulations, i.e. target cleavage of mRNA in the case of siRNA and translational arrest in miRNA.

In the degradative pathways of siRNA and miRNA, cleavage of target RNA is governed by the endonuclease or 'slicer' activity of the RISC complex. The endonuclease activity of the RISC complex has been mapped to the PIWI domain in AGO proteins through mutagenesis (Liu *et al.*, 2004a). Interestingly, different human AGO proteins (AGO 1, 2 and 3) can be recruited by siRNA or miRNA to form RISC complexes, although only AGO2 can direct target mRNA cleavage (Meister *et al.*, 2004). On the basis of the type of AGO proteins being recruited to a RISC, these complexes are categorised into two main types: a cleaving RISC and a non-cleaving RISC (Tang, 2005). A cleaving RISC complex has dual functions that can direct the guide strand to elicit target mRNA cleavage or translational repression, depending on the base-pairing features between the target mRNA and small RNA (Hutvagner and Zamore, 2002). However, if the base-pairing between the siRNA or miRNA and the corresponding target mRNA is less extensive, then the target mRNA might be physically unreachable by the active endonuclease core in the cleaving RISC due to distorted helical formation as a result of non-complementarity (Haley and Zamore, 2004). This will subsequently lead to translational repression rather than efficient cleavage of target mRNA. In contrast, non-cleaving RISCs lacking enodonuclease

activity in the PIWI domain of AGO proteins can only direct translational repression of target mRNA. The exact mechanisms determining the assembly of a cleaving or non-cleaving RISC has yet to be fully elucidated, but it is likely governed by modes of regulation required for a particular gene, or even by the sequence context of the suppressor itself.

1.10.2 MicroRNA target recognition and RNA accessibility

It has been difficult to predict miRNA targets by nucleotide sequence matching because of limited sequence complementarity even in the setting of efficient translational inhibition. There is good evidence that a high degree of complementarity with the 5' end of the miRNA, particularly nucleotides 2-7 are important for target mRNA recognition (Lai, 2002; Stark *et al.*, 2003; Lewis *et al.*, 2005). However, even among these six nucleotides, non-matching still occur *in-vivo* which makes the use of sequence matching as a predominant criterion for target prediction extremely difficult. Several computational programs based on bioinformatic approaches have been used to identify miRNA targets, but the number of targets predicted for a given miRNA ranges from 100-500, making validation studies difficult (Alvarez-Garcia and Miska, 2005). Not all mRNA targets with sequences matching those of miRNAs are likely to be true targets. Much of the mRNA sequences are hidden and only local single stranded regions are accessible for binding to other RNAs, indicating that local target accessibility might lend specificity to the more promiscuous predictions of sequence matching. Another challenge is that the 3' untranslated regions (UTRs) of mRNAs form complex secondary and tertiary structures *in vivo* depending on the intracellular environment. Unknown interactions with RNA transcripts or with proteins might result in further alterations of the 3' UTR secondary structure, creating further obstacles for miRNA target site prediction (*Figure 1.15*) (Zhao and Srivastava, 2007).

1.10.3 The similarities between miRNAs and other regulatory pathways

Post-transcriptional downregulation of gene expression is not exclusive to miRNAs with many other mechanisms having been observed to share similar translational

regulatory pathways. The similarities of regulation mediated by miRNAs and PUF proteins (a family of proteins named from the founding members in *D. melanogaster* 'Pumilio' and *C. elegans* 'FBF') are strikingly similar. PUF protein family is widespread with family members found in many eukaryotes, including both plants and animals, and unicellular metazoan organisms. Several species including *C. elegans*, *Saccharomyces cerevisiae* and *Arabidopis thaliana* possess multiple PUF proteins, whereas *Drosophila* only possess one and vertebrates such as humans and mice have two. PUF proteins have been identified to bind to 3' UTR and mediate repression either by increasing de-adenylation, promoting mRNA degradation or by inhibiting translation (Wickens *et al.*, 2002). PUF proteins have multiple target sites and their activities can be modulated by multiple binding partners. Although the mechanism by which PUF proteins exert their effects is not fully understood, the parallels between the end points of their regulation and miRNA mediated regulation suggest that common factors are involved in these pathways.

Another potentially important connection between miRNA mediated regulation pathway and other translational control pathways comes from the finding that RCK/p54, a DEAD box helicase that interacts with argonaute proteins, Ago1 and Ago2, is involved in miRNA mediated translational repression (Chu and Rana, 2006). The *D. melanogaster* homolog of RCK, Me31B, is required for suppression of *oskar* mRNA translation (Nakamura *et al.*, 2001a), and the budding yeast homolog of RCK, Dhh1p, is involved in general translation repression (Coller and Parker, 2005).

1.10.4 The role of miRNA in animal development

In animals, early embryonic patterning and organ morphogenesis involve coordinated differentiation, migration, proliferation and programmed cell death. These complex cellular developmental events are dependent upon precise spatiotemporal regulation of mRNA and protein levels of key regulatory factors. During the past few years, several examples of miRNA regulation of developmental events have emerged. Progress in understanding the transcriptional regulation of miRNAs and identification of their targets may provide an opportunity to dissect the complex networks involved in the regulation of protein translation during cell fate decisions and further

embryogenesis (Zhao and Srivastava, 2007). Recent studies have demonstrated tissue specific roles of miRNAs during embryonic development, and with specific focus on the pivotal function of miRNAs on the regulation of cardiac cells, skeletal muscles, neurons and hematopoietic lineages.

Cardiogenesis: The heart is the first organ to function in the embryo and proper function of cardiovascular system is crucial for embryonic survival during development. Cardiac morphogenesis in mice involves intricate coordination of multiple cell types at precise time windows (Srivastava, 2006). Both miR-1-1 and miR-1-2 are abundant in the developing heart (Zhao *et al.*, 2005). Enrichment of miR-1-1 is initially observed in the atrial precursors before becoming ubiquitous in the heart, whereas a miR-1-2 enhancer is specific for the ventricles in the developing heart, and both are highly expressed in the cells of the cardiac outflow tract, therefore miR-1-1 and miR-1-2 might have chamber specific effects *in-vivo*.

Myogenesis: miR-01 and miR-206 promote the differentiation of skeletal myoblasts in culture, whereas mi133a has the opposite effect in inhibiting differentiation and promoting myoblast proliferation. Both miR-206 and miR-133a target a variety of factors that are important for myogenesis such as histone deactylase 4 (HDAC4), SRF, Fst1, Utrn, Pola 1 and Cx 43 (Chen *et al.*, 2006; Anderson *et al.*, 2006; Rosenberg *et al.*, 2006; Kim *et al.*, 2006).

Neurogenesis: miRNAs regulate key events during neurogenesis in multiple species. In *C. elegans*, two bilaterally symmetric gustatory neurons, ASE left (ASEL) and ASE right (ASER) exhibit left and right asymmetric molecular features with respect to one another. Auto-regulatory feedback loops involving distinct miRNAs control the cell fate decision between the two asymmetric states (Johnston and Hobert, 2003; Johnston *et al.*, 2005). In mammals, miR-134 is specifically expressed in rat dendritic spines in hippocampal neurons. It binds to the 3' UTR of Limk1 and represses local LimK1 translation, which results in inhibition of dendritic spine growth. Stimuli such as brain derived neurotrophic factor can relieve this suppression. This finding has

revealed that miRNAs can be important regulators of neuronal structure and plasticity, and respond to external signals (Schratt *et al.*, 2006).

Haematopoiesis: During embryogenesis, active haematopoiesis begins in the yolk sac and then moves to the liver and in later stages to the bone marrow. In normal adult mice, haematopoiesis occurs in marrow and lymphatic tissues, where the mechanisms governing changes in the site of haematopoiesis involve sequential cell fate diversification and cell differentiation. miR-181 is highly expressed in B-lymphoid cells of the bone marrow and ectopic expression of miR-181 in progenitor cells increases the fraction of B-lineage cells *in-vitro* and in adult mice (Chen *et al.*, 2004b).

1.10.5 Identification and characterisation of miRNAs in the mouse eye

Most miRNAs are expressed in a highly tissue specific manner in vertebrates (Lagos-Quintana *et al.*, 2003; Wienholds *et al.*, 2005). A given cell type expresses a defined subset of miRNAs, which in turn control a specific set of genes, thus a specific miRNA code appears to provide the signature that allows the differentiation of specialised cells from common precursors (Karali *et al.*, 2007). Hence to define the miRNAs code in the eye, it is necessary to determine a high resolution profile of the spatial and temporal distribution of miRNAs (Hobert, 2004). Karali *et al.*, (2007) have generated a high resolution expression atlas of miRNAs significantly expressed in the mammalian eye. This analysis has demonstrated that RNA *in-situ* hybridisation can be effectively performed on mouse embryos and tissue sections using probes that specifically recognise the mature sequence of miRNAs using locked nucleic acid-modified DNA oligonucleotide templates, whose specificity can distinguish single-base mismatches (Kloosterman *et al.*, 2006). Out of the 13 miRNAs that were found to be expressed at significantly high levels in the zebra fish eye by RNA *in-situ* hybridisation or microarray analysis (Wienholds *et al.*, 2005), seven miRNAs were expressed in the adult mouse eye with diverse and partially overlapping patterns, suggesting their role in controlling cell differentiation of the retina and other ocular structures. Most miRNAs expressed in the eye either overlapped or were in proximity

to transcripts derived predominantly from eye cDNA libraries. Mi-124a was expressed in all differentiated neurons but not in the glial Muller cells (Nelson *et al.*, 2006; Deo *et al.*, 2006; Smirnova *et al.*, 2005). miR-9 was detected only in the middle part of inner nuclear layer, reflecting its expression in Muller glia cells. miR-182 appeared to be expressed exclusively in photoreceptors. miR-29c, miR-181a and miR-204 were also expressed in the adult retina with variable patterns. Finally miR-184 was not detectable in the retina, but was strongly expressed in non-neural tissues such as the lens and cornea. These observations provided a detailed characterisation of expression of eye enriched miRNAs. Validation of the spatiotemporal distribution of miRNAs is an essential step towards the identification of their targets and understanding of their biological role in eye development and function.

1.10.6 The use of miRNAs as suppressive reagents

Boden *et al.*, (2004) have reported a novel suppression system where the sequences encoding for siRNA directed against HIV-1 transactivator protein (*tat*) were incorporated into a human miR-30 pre-microRNA (pre-miRNA) backbone. The *tat* siRNA delivered as pre-miRNA precursor into 293 cells showed significantly higher reduction of HIV-1 p24 antigen production than *tat* siRNA expressed from conventional shRNA backbone. Furthermore, possible explanations for a more enhanced potency achieved with miR-30 siRNA constructs compared to conventional shRNAs were also explored. Interestingly, it was found that the secondary structure of the shRNA expressed from miR30-backbone possessed a greater local folding potential than shRNA expressed from the conventional backbone. The higher folding potential might have created a greater structural stability of the stem-loop structure, leading to a higher rate of shRNA folding and subsequently, a faster rate of RISC/miRNP formation with the end result of a more potent gene silencing. Although the precise sequence and structural requirements of the loop structure of shRNA/miRNA precursors have not been fully elucidated, McManus *et al.*, (2002) have shown that the processing of shRNA stem-loop structures are highly dependent on the loop sequences. Thus there might be yet an unidentified structural motif in the pre-miRNA loop that is better recognised by Dicer or other related nucleases. Zeng *et*

al., (2002) have also demonstrated that the miR-30 miRNA backbone can be altered to include siRNA encoding sequences and have used this system to effectively downregulate endogenous human polypyrimidine tract binding protein. Furthermore, McManus *et al.*, (2002) have showed that siRNA sequences included into the stem of mir-26a effectively degrade homologous mRNA.

1.11 P-bodies

1.11.1 Introduction

The control of mRNA translation and degradation plays an important role in post-transcriptional regulation of eukaryotic gene expression and global mRNA quality control. Cellular mRNA quality control is responsible for the recognition and degradation of defected mRNAs formed as a result of failure to initiate translation, stalling of translation elongation or early termination of translation. In eukaryotes, mRNA turnover is regulated by two major decay pathways; 1) initially the decay of mRNA is carried out by a 5' to 3' exonucleolytic process, where the 3'-polyadenosine (poly-A-tail) is deadenylated by the predominant deadenylase, Ccr4p/Pop2p/Not complex; 2) Following deadenylation, the 5' mRNA cap is irreversibly removed by the decapping enzyme, Dcp1p/Dcp2p, and subsequently the entire body of the unprotected mRNA is degraded by the 5' to 3' exonuclease, Xrnp1 (Parker and Sheth, 2007). These translationally repressed mRNAs, along with other translation repressors and mRNA decaying proteins all localise in cytoplasmic foci known as Processing (P)-bodies.

Electron microscopy has identified P-bodies as cytoplasmic electron-dense structures that are 100-300nm in diameter, comprising 1-10nm strands of fibrils lacking a membrane. (Yang *et al.*, 2004; Eystathioy *et al.*, 2002). The protein composition of P-bodies has also been studied extensively and interestingly, all organisms were found to possess a conserved core of proteins consisting of a decapping enzyme (Dcp1p/DCp2p), activators of decapping (Dhh1p/RCK/p54, Pat1p, Scd6p/RAP55, Edc3p), the Lsm1p-7p complex and the 5' to 3' exonuclease Xrn1p (A full list of P-bodies compositional components can be found in *Table 1.3*). Collectively, the core components of P-bodies function mainly in translation repression and mRNA degradation, thus they are referred to as the 'repression/ decay machinery' (Parker and Sheth, 2007). Initially, P-bodies were thought to be conserved in yeasts, mammals and other species because they all contain the same activators of mRNA and degrading enzymes (Cougot *et al.*, 2004; Eystathioy *et al.*, 2002). However,

under closer examination, P-bodies are found to contain elements that are specific only to certain organisms. For example, metazoans possess proteins involved in regulating miRNA function which are lacking in Saccharomyces cerevisiae (Liu *et al.*, 2005a). Furthermore, mammalian P-bodies differ from yeast P-bodies in that they contain translation initiation factors and other proteins that have no counterparts in yeasts, such as GW182 and Argonaute proteins that are involved in RNA interference. Therefore, P-bodies found in mammalian cells are termed as GW bodies (GWBs), because they contain the distinctive mRNA binding protein, GW182 (Jakymiw *et al.*, 2007). GW182 is characterised by glycine (G) and trytophan (W) repeat rich domains and canonical RNA recognition motif that have been shown to associate with mRNAs in HeLa cells (Eystathioy *et al.*, 2002). Furthermore, mammalian GWBs and yeast P-bodies react differently to stress and cell growth. For example, yeast P-bodies increase in size and number during stress due to increased cell density or growth limitation (Teixeira *et al.*, 2005), whereas mammalian GWBs increase in size and number in proliferating cells and may interact with stress granules (Kedersha *et al.*, 2005). Explanations for the observed diversity and significance of P-bodies still remain undetermined, but it is likely the different composition of P-bodies may be dictated by individual factors associated with mRNAs targeted to these structures.

Recent studies have shown that some other RNA storage granules in eukaryotic cells are also closely associated with P-bodies. Maternal mRNA storage granules that function in translation repression and transport of maternal mRNAs have been shown to contain many of the components found in P-bodies, including the mRNA decapping enzyme and Dhh1 orthologs (Barbee *et al.*, 2006). Moreover, maternal mRNA storage granules require these proteins for their proper functions, for example Dhh1 orthologs are required for translation repression of maternal mRNA both in *Xenopus* and *Drosophila* (Nakamura *et al.*, 2001a). Neuronal granules found in *Drosophila* that function in the translation and transport control of mRNAs also contain many of the components found in P-bodies, including the decapping enzyme Xrn1p, Argonautes, Dhh1p ortholog, Scd6p/RAP55 ortholog Tral and Upf1 (Barbee

et al., 2006). The similarities in the compositional make-up of P-bodies, maternal RNA storage granules and neuronal granules, suggest that the general translational repression/decay machinery at the core of P-bodies is highly conserved in both germ cells and neurons. This observation suggests a possibility that maternal mRNA granules and neuronal granules may also function in mRNA degradation. Despite the similarities in different types of RNA granules, there can be different classes of P-body-like granules within a single cell. For example, the major class of P-body-like granules in Drosophila neurons exhibits the key protein components such as Dcp1 and dFMR, but subclasses of granules found within the same neuronal cells have been identified to lack such individual components (Barbee *et al.*, 2006).

1.11.2 The formation of GWBs/ P-bodies in mammalian cells

Mammalian GWBs/P-bodies are dynamic structures enriched in mRNA decay factors and pools of stored messenger ribonucleoproteins (Sheth and Parker, 2006), whose size and number appear to depend on specific intracellular processes. Cell proliferation and cellular stress such as inhibition of translational initiation are all correlated to the increase in the pool size of P-bodies (Kedersha *et al.*, 2005; Yang *et al.*, 2004; Andrei *et al.*, 2005; Brengues *et al.*, 2005). In contrast, blocking of transcription, deadenylation of mRNAs and translational elongation all decrease the size and number of P-bodies (Cougot *et al.*, 2004; Sheth and Parker, 2003). Therefore, there is a direct correlation between the pool size of cytoplasmic mRNA to the size and number of P-bodies.

The exact mechanism of mammalian GWBs/P-bodies formation remains unclear, but speculations have indicated that GWBs are formed by the assembly of different heteromeric protein complexes on mRNAs that can accumulate into larger mRNP structures. In particular, a powerful model has been put forward showing that RNAi shares a close relationship with GWB formation and function (Jakymiw *et al.*, 2007). In brief, RISC complexes containing the antisense strand of either siRNA/miRNA interact with target mRNA to form a specific ribonucleoprotein (RNP) structure that is dependent on the type of suppression to be carried out (mRNA cleavage or

translational repression). Subsequently, specific types of proteins are recruited to the RNP complex depending on the composition of the initial RNP. Furthermore, this model has been supported by evidence showing that suppression of Drosha or its counterpart, DGCR8 [Drosha+DGCR8 are responsible for the cleaving of long primary miRNA (pri-miRNA) to ~70nt hairpin precursor miRNA (pre-miRNA)], causes a depletion in the level of GWBs. Interestingly, siRNA transfected into Drosha-deficient cells served as a substitute for miRNA and increased the level of GWBs, indicating that miRNA is an integral component for the formation of GWBs/P-bodies (Pauley *et al.*, 2006).

1.11.3 RNAi in P-bodies

Concurrent studies have established a direct link between RNAi and mammalian GWBs, where a high concentration of Ago family proteins (Ago1-4), were found to be localised in GWBs. (Jakymiw *et al.* 2005; Liu *et al.* 2005a; Sen and Blau, 2005). In particular, the hAgo2 protein, which is the catalytic component of the RISC enzyme, has been shown to associate with several GWB compositions, including the miRNA-repression factor GW182 (Jakymiw *et al.* 2005; Liu *et al.*, 2005a). Furthermore, depletion of GW182 disrupts both siRNA and miRNA-mediated gene silencing by blocking the ability of hAgo2 to localise to GWBs (Jakymiw *et al.* 2005; Liu *et al.*, 2005a). Additional evidence for the involvement of GWBs in RNAi has come from studies carried out in *Drosophila melanogaster* orthlogs, where the interaction of GW182 with AGO1 promotes the degradation of a subset of miRNA-mediated decay mRNA targets. In addition, depletion of GW182 resulted in alterations of mRNA expression profiles to a similar level seen in cells depleted of the *Drosophila* miRNA effector Ago 1. Moreover, miRNAs ablate mRNAs in a manner that is dependent on the decapping enzyme and 5' to 3' exonuclease, Xrn1p. This suggests that the only method by which miRNAs can mediate gene silencing is by recruiting GWBs, where GW182 may act as a bridge connecting the components of the miRNA pathway to mRNA decay enzymes (Behm-Ansmant *et al.*, 2006).

The discovery of active RNAi-related components in mammalian GWBs and that P-body assembly is closely linked with RNAi have suggested that RISC activation and activity may take place within these cytoplasmic foci. Jakymiw *et al.*, (2005) have previously shown that fluorophore-labeled siRNA antisense strands transiently transfected into mammalian cells associated with GW182 and localised to GWBs. This has provided evidence that perhaps the antisense strand localises to GWBs independent of the target mRNA, and that the cleavage of a siRNA duplex and subsequent incorporation of the antisense strand into RISC may take place within GWBs (Liu *et al.*, 2005a; Liu *et al.*, 2005b).

1.11.4 Alternative quality control mechanisms targeted by GWBs/ P-bodies

Apart from the involvement of GWBs/ P-bodies in RNAi, they have also been shown to operate in other mRNA decay pathways, such as 1) nonsense mediated decay (NMD), 2) AU rich element (ARE)-mediated decay and 3) stress induced decay (SID).

1. Nonsense mediated decay (NMD) is a surveillance mechanism that removes abnormal mRNA transcripts containing premature termination codons. Several protein structures involved in NMD include UPF1-3, SMG5 and SMG7, which have also been found to localise to GWBs/ P-bodies. (Fukuhara *et al.*, 2005).
2. GWBs have also been linked to AU rich element ARE-mediated decay, which is a decay process involving mRNAs containing AU-rich elements in the 3' UTR. GWBs have been linked to ARE-mediated decay because depletion of three GWBS protein components (Xrn1, LSm1 and E-T) has been shown to inhibit AMD (Ferraiuolo *et al.*, 2005; Stoecklin *et al.*, 2006).
3. The observation that the size and number of P-bodies increases during stress in budding yeast cells, and that stress in mammalian cells can induce GWBs formation and interaction with stress granules have demonstrated their importance in stress induced decay (SID) (Kedersha *et al.*, 2005). However

budding yeast cells lack stress granules, therefore this mechanism is most likely to be exclusive to higher eukaryotes.

1.11.5 The interaction of GWBs/ P-bodies with stress granules

In mammalian cells, GWBs/ P-bodies and stress granules are compositionally, functionally and morphologically linked (Cougot *et al.*, 2004, Kedersha *et al.*, 2005). Both complexes share an assortment of functional proteins (CPEB1, Rck/p54, FAST, Xrn1, eIF4 and TTP) and also a single class of reporter mRNA (Cougot *et al.*, 2004; Kedersha *et al.*, 2005). In particular, both miRNAs and Ago proteins have been found to localise in stress granules during translation inhibition or stress induction. However, stress granules are only present during intracellular stress response, whereas GWBs/ P-bodies are continuously present in cells (Teixeira *et al.*, 2005).

Upon inhibition of translation initiation or induction of stress, affected mRNAs are either shuttled to stress granules for storage or targeted to GWBs for decay, and these mRNAs may exit to re-enter translation when conditions improve (Brengues *et al.*, 2005). Therefore, stress granules may serve as mRNA refuge sites where transcripts are sorted for storage, re-initiation of translation and subsequent export to GWBs for degradation (Kedersha *et al.*, 2005). This observation has been demonstrated in the endogenous cationic amino acid transporter (CAT-1) mRNA, which is regulated by the liver-specific miR-122a in Huh7 cells and is localised in GWBs under normal conditions. During cellular stress induced by serum starvation, the CAT-1 mRNA is released from GWBs to re-enter the cytoplasm for translation (Obernosterer *et al.*, 2007).

Parker and Shelth (2007) have proposed a dynamic model known as the 'mRNA cycle', which depicts the movement of cytoplasmic mRNAs between polysomes, P-bodies, stress granules and the nucleus under different cellular conditions. The steps involved in the 'mRNA cycle' are outlined in *Figure 1.16*, and some interesting observations made from this proposed model include; 1) The decapping machinery is only active or "switched on" when it is assembled into a larger mRNP that can

accumulate in P-bodies, this effectively protects functional mRNAs from inappropriate degradation due to non-specific interactions with degradation machinery. 2) The aggregation of mRNAs in P-bodies and stress granules may provide a storage system for balancing the ratio of translation capacity to the pool of mRNAs to be translated. An excessive amount of translatable mRNAs may compete for limiting translation factors, thereby preventing effective translation. 3) The cycling of mRNAs through P-bodies and re-entry into translation might be important in restoring translation back to mRNAs that has defective translation complexes. For instance, if a translational complex becomes defective, removal to a P-body will eliminate this defect, and re-entry into translation allows the recruitment of a new translational complex. The cycling of mRNA through P-bodies is quite similar to that of chaperones, where unfolded protein can either be refolded or targeted for degradation.

1.11.6 Functional interactions between GWBs and miRNAs

Recently, several groups have shown that Argonaute proteins, which bind to the active RISC complex in siRNAs and miRNAs, localise to P-bodies (Pillai *et al.*, 2005). Argonaute proteins interact in an RNA-independent pathway with the known P-body components DCPIA and GW182, and in *D. melanogaster* there is evidence that Ago 1 interact specifically with GW182 directly (Behm-Anasmant *et al.*, 2006). An attractive model for the mechanism of miRNA function in GWBs has been proposed by several groups (Behm-Anasmant *et al.*, 2006; Valencia-Sanchez *et al.*, 2006; Eulalio *et al.*, 2007). First, a miRNA bound to an Argonaute protein recognises its mRNA targets by partial base-pairing, the Argonaute protein in turn interacts with GW182, and the mRNA-miRNA Argonaute protein complex is then delivered to GWBs. When it reaches the GWB, the targeted mRNA is de-adenylated by resident de-adenylases, then either decapped and degraded or held in stasis by spatial removal from the translational machinery as GWBs are devoid of ribosomes (Valencia-Sanchez *et al.*, 2006; Eulalio *et al.*, 2007). The latter stasis condition was first illustrated by experiments in budding yeast showing the use of P-bodies as a repository for untranslated mRNAs (Brengues *et al.* 2005), and was also supported by

examples in mammalian cells where specific mRNAs were sequestered into GWBs from ribosomes in a miRNA dependent manner (Bhattacharyya *et al.*, 2006).

Although this hypothesis is appealing and is supported by multiple lines of evidence, several observations seem to be incompatible with the idea that GWB independent processes account for all miRNA mediated regulation. Specifically a quantitative microscopic analysis of Argonaute protein localisation has shown that only a small proportion (<2%) of Argonaute proteins are localised in GWBs (Leung *et al.*, 2006). Also knockdown of a GWB component was found to cause disappearance of visible foci but did not compromise miRNA function (Chu and Rana, 2006). The finding that a minority of Argonaute proteins and miRNAs localised to GWBs also indicated that the bulk regulation might take place elsewhere.

1.12 Aptamers

Over the past two decades, different strategies have been developed to manipulate gene expression and function at the RNA level. These include antisense oligonucleotides, ribozymes, small interfering RNAs and more recently, micro-RNAs have been shown to be active as translational protein inhibitors. Although these strategies enable rational design of regulatory sequences, they are not well-adapted to target protein expression in a controlled and specific manner. Aptamers are small single stranded nucleic acid (DNA or RNA) based ligands of 20mers to 80mers that fold into unique 3-dimensional conformations upon binding to target proteins or random sequences of RNA molecules (Ellington and Szostak., 1990). The 3-dimensional structures of aptamers distinguish them from conventional antisense oligonucleotides and ribozyme, which are linear and act to ablate mRNA by H-bond interactions. Aptamers are generated by the SELEX (systematic evolution of ligands by exponential enrichment), which is an iterative *in-vitro* evolution technology consisting of two sequential steps, 'selection' and 'amplification'. SELEX is capable of reducing a complex library of nucleic acids with randomized sequences (complexity ~10^{14}) to a minimised subset of sequences that bind specifically to the targeted protein.

From a therapeutic standpoint, aptamers are highly attractive alternatives to monoclonal antibodies in that they possess positive attributes of high affinity and exquisite specificity for cognate ligands. Aptamers are also much more cost efficient than antibodies, possess a lower immunogenicity, and can be chemically modified to improve bioavailability and stability. The first generation of aptamers have been hampered by nuclease sensitivity, poor bioavailability, fast renal clearance and limited cellular uptake. However, recent advances in the preparation of aptamers with 2'-Fluoro, 2'-amino pyrimidines, phosphorothioate or 2'-O-methyl nucleotides have greatly improved both metabolic stability and nuclease resistance in the serum (Burmeister *et al.*, 2005). The major advantages of aptamers are that they are can function at low concentrations and can be subcloned into expression cassettes for different applications. Moreover, aptamers possess better accuracy and specificity

than siRNAs, where they can distinguish between closely related members of a protein family and even different conformational states. Therefore, aptamers are becoming the preferred nucleic acid tool for both extracellular and intracellular validation of targets.

To date, many pharmaceutical companies have successfully translated aptamer technology into clinical trials (*Table 1.4*). The first aptamer drug that has gained FDA approval is Macugen (Pegaptanib sodium), which is currently used to treat wet-age related macular degeneration (AMD). Macugen is a pegylated, nuclease-resistant aptamer that acts as a selective antagonist against $VEGF_{165}$, which is a major inducer of abnormal blood vessel growth and leakage. *In-vivo* studies carried out by Lee *et al.*, (2005) in human umbilical vein endothelial cells (HUVEC) have illustrated the efficacy of Macugen in preventing abnormal blood vessel growth and retarding vision loss. Furthermore, Macugen is currently being used in clinical trials for diabetic macular edema and retinal vein occlusion (*Table 1.4*).

Other aptamer-based drugs that are also in clinical development phase are transcription factor decoys (TFD), which are small structured RNAs or double-stranded DNAs containing consensus binding sequences specific to transcription factors. Transcription factor decoys inhibit gene expression by occupying its target transcription factor's binding sites, which prevents binding of the transcription factor to promoter regions, thus the promoter remains switched off. An example of a transcription factor decoy is Avrina, which mimics the binding sequence of NF-κB on chromosomal DNA, inhibiting the production of several pro-antiinflammatory cytokines. Avrina have been tested in arthritis models and endotoxin-induced mouse models of liver failure, and is now in Phase I/II trials for the treatment of moderate atopic dermatitis (*Table 1.4*).

The ability to reverse the inhibitory property of aptamers with the introduction of short complementary sequences known as antidotes have also been proven to be a major advantage of this technology (*Figure1.17a*). The aptamer-antidote complex

would be particularly useful in surgical applications that demand the use of reversible drugs. Further developments of aptamer regulation have seen the use of light sensitive photolabile nucleobases to regulate thrombin (clotting factor) activity in plasma clotting pathways (*Figure 1.17b*).

The strategy of combining RNA-based therapies- ribozyme, siRNA and decoy RNA aptamer into a single therapy seems like an attractive approach that exploits the best potentials of individual tools to overcome the limitations of each. Li *et al.*, (2005) have recently described a triple element combinatorial lentiviral construct that harboured: (a) a VA1- derived polymerase III anti-CCR5 ribozyme targeting HIV-1 cells surface co-receptors; (b) an U6 transcribed nucleolar-localising TAR RNA decoy aptamer targeting viral TAT-activated transcription; (c) a U6-Pol III promoter driven-shRNA specific for *rev* and *tat* of HIV-1. The application of this triple-combinatorial RNA-based therapeutic approach greatly hampered HIV-1 replication in CD34 (+) hematopoietic progenitor cells, high-lighting the feasibility of combinatorial RNA-based gene therapy for the treatment of other viral infections.

1.13 Gene therapy for ocular diseases

1.13.1 Introduction

The eye is a relatively isolated compartment which makes it an ideal target organ for gene therapy of both inherited and acquired ocular disorders, and offers a valuable model system for gene therapy. The highly compartmentalised anatomy of the eye facilitates accurate delivery of vector suspensions to specific tissues under direct visualisation using microsurgical techniques. This enables precise positioning of vector at target sites within the globe while minimising systemic dissemination and unwanted systemic effects. Vectors injected into the vitreous cavity readily diffuse throughout the eye, and the amounts used for intraocular injections are small compared to those used for systemic application. This allows local targeting of a gene with minimal concern of targeting the same gene outside the eye, reducing the concern of remote effects in other tissues. Immune responses following intraocular administration are typically attenuated compared to those following systemic administration: anatomical barriers and a unique immune environment maintain a degree of protection from immune responses directed against vector antigens. The eye's optical transparency enables phenotypic examination and investigation of therapeutic effects by using fundus imaging *in-vivo*. Visual function is also quantifiable by examining psychophysical and electrophysiological parameters, and the contralateral eye often provides an invaluable experimental control (Campochiaro, 2006; Bainbridge *et al.*, 2006).

The clinical and genetic heterogeneity of retinitis pigmentosa have brought about the development of different strategies to target degenerating cells. Conventional treatments for RP as discussed in section 1.8 have been explored extensively, but the effect is often indirect and transient. As specific genes are being identified, there is a great potential for the use of gene-mediated therapy to treat RP. In autosomal recessive and X-linked recessive retinal degenerations, the principle of therapy is to correct the genetic defect by introducing the wild-type version of a mutated gene into cells where normal function of this gene is required. In autosomal dominant retinal

degeneration, the principle of therapy is to inhibit the expression of the gene responsible for deleterious effects. Gene silencing can be achieved through the use of single stranded antisense oligonucleotides, ribozymes and small-interfering RNAs (siRNA) (Millington-Ward *et al.*, 1997; LaVail *et al.*, 2000; Kiang *et al.*, 2005).

1.13.2 Gene replacement therapies

Currently, many studies have reported successful gene replacement strategies in models of inherited retinal degenerations resulting from loss-of-function mutations in genes encoding important proteins in photoreceptors and retinal pigment epithelium. In particular, recombinant adeno-associated viral (rAAV) vectors are increasingly being used to mediate efficient transduction of retinal pigment epithelium, photoreceptor cells and ganglion cells (Rolling, 2004). The tissue specificity and expression kinetics of recombinant AAV vectors are highly dependent on the vector serotype, and the anatomical compartment to which they are being delivered to. The development of hybrid pseudotype rAAV vectors in which a rAAV vector is packaged into a capsid derived from AAV of a different serotype, has considerably expanded the available repertoire of AAV vectors. rAAV-2/2 (rAAV-2 plasmid packaged in rAAV-2 capsid) mediated expression is typically of delayed onset, and gradually increases to reach stable levels of expression after two to four months. AAV-2/2 and AAV-2/5 are the most commonly used combinations because they transduce both photoreceptors and retinal pigment epithelium cells, whereas AAV-2/4 and AAV-4/4 mediate expression that is restricted to the retinal pigment epithelium only (Weber *et al.*, 2003). AAV-5 pseudotype vectors are mostly used to mediate gene replacement in rodent and large animal models of inherited retinal degenerations (Acland *et al.*, 2005). Schlichtenbrede *et al.*, (2003) shown that rAAV-mediated delivery of *peripherin* restored retinal structure and function for 14 weeks in the *rds* mouse model. Similarly, rAAV-mediated delivery of *Mertk*, an RPE receptor tyrosine kinase responsible for phagocytosis and shedding of photoreceptor outer segments, significantly restored phagocytic function and decreased the rate of photoreceptor degeneration in the Royal College of Surgeons rat model (Smith *et al.*, 2003). In a murine model of mucopolysaccharidosis (MPS) VI, in which the ocular

phenotype is associated with systemic lysosomal storage diseases, rAAV-mediated gene replacement of 4-sulfase reduced the accumulation of dermatan sulfate in retinal pigment epithelium cells. Furthermore, in MPS VII, replacement of the lysosomal enzyme β-glucuronidase reduced the accumulation of degraded glycosaminoglycans in retinal pigment epithelium cells, and improved overall retinal electroretinographic responses (Hennig *et al.*, 2004). Pawlyk *et al.*, (2005) demonstrated that rAAV-mediated delivery of retinitis pigmentosa GTPase regulator interacting protein (RPGR, a photoreceptor protein anchored within the connecting cilia) restored normal RPGR localisation, and also preserved photoreceptor cell functions in a Leber Congential Amaurosis mouse model. In addition, *in-utero* intraocular vector delivery of rAAV expressing RPE65 was capable of rescuing photoreceptor degeneration in the $RPE65^{-/-}$ knockout mouse model (Dejneka *et al.*, 2004). Furthermore, gene replacement therapy has also been demonstrated in the Swedish Briard dog model, which is homozygous for a null mutation in RPE65 that causes one form of Leber congenital night blindness. The defect in the dog model manifests a phenotype similar to that in human, with poor vision from early life and reduced dark/light-adapted electroretinographic responses. rAAV-mediated expression of wild type RPE65 gene in the retinal pigment epithelium following subretinal injection showed significant improvement in visual function following both electroretinographic and behavioural assessments (Narfstrom *et al.*, 2003a; Narfstrom *et al.*, 2003b).

Lentivirus based vectors are also attractive candidates for ocular gene transfer because of their ability to stably transduce non-dividing cells. Human immuno-deficiency virus-1 (HIV-1) and feline immunodeficiency virus (FIV)-based lentiviral vectors have been shown to transduce corneal endothelium and trabecular meshwork efficiently after delivery into the anterior chamber, and can also stably transduce the retinal pigment epithelium for up to 2 years following subretinal delivery into rodents (Challa *et al.*, 2005; Cheng *et al.*, 2005; Tschernutter *et al.*, 2005). The theoretical risk of recombinant mediated lentiviral replication may be minimised by using highly deleted vectors generated by re-coded packaging constructs in a four plasmid system (Molina *et al.*, 2004), and through the use of self-inactivating vectors (Bainbridge *et*

al., 2001). Vectors based on non primate lentiviruses such as FIV, equine infectious anaemia virus and bovine immunodeficiency virus have transduction efficiencies and expression durations in ocular tissues that are similar to HIV-based vectors, and may provide alternatives with safety advantages (Poeschla, 2003). Furthermore, insertional mutagenesis may be minimised by development of non-integrating vectors, such as integrase-deficient vectors which have been shown to persist as episomal ds-DNA plasmids that can transduce retinal cells *in-vitro* and mediate efficient sustainable levels of expression *in-vivo* (Saenz *et al.*, 2004).

1.13.3 RNAi in the treatment of autosomal dominant retinitis pigmentosa (adRP)

As discussed before, mutations in the human rhodopsin gene are the most common cause of autosomal dominant RP, and more than 120 different mutations have previously been identified in the rhodopsin gene (*www.retina-international.com*). Furthermore, mutations in rhodopsin may cause other forms of retinal diseases such as congential stationary night blindness (CBNS) and retinitis punctata albescens (RPA) (Dryja *et al.*, 1993; Souied *et al.*, 1996). Therefore, the proposition for a suppression therapy for RP patients is to develop tailor-made, specific suppressors targeted to each mutation. However, sequence specific therapy is impractical because of the need to evaluate and to optimise the efficacy of each therapy separately in corresponding animal models, prior to use in patients, which is both economically inefficient and time consuming. As an alternative, the enormous heterogeneity among rhodopsin mutations can be addressed by the use of mutation-independent suppression and replacement strategies. This strategy involves silencing of both mutant and wild type transcripts of a given gene using a suppressor that targets a commonly accessible site independent of the mutation, and simultaneously providing delivery of suppression resistant replacement genes (based on 3rd base wobble substitution or non-coding 5' or 3' UTR sequences) that encode wild type protein. (Farrar *et al.*, 2002). Initially, this approach was reported with the use of hammerhead ribozymes to suppress genes involved in autosomal dominant RP, such as rhodopsin and rds/peripherin (Millington-Ward *et al.*, 1997; Lewin *et al.*, 1998; O'Neill *et al.*,

2000; Gorbatyuk *et al.*, 2005). More recently, the focus has turned to the adaptation of RNA interference into the mutation-independent suppression and replacement approach for the treatment of dominantly inherited disorders. Kiang *et al.*, (2005) have successfully reported the use of an RNAi-based mutation independent and replacement approach as a therapeutic strategy for suppressing mutant rhodopsin transcripts. Initially, short hairpin RNAs showed significant suppression of murine rhodopsin in cell cultures, murine retinal explants and also in mouse liver *in-vivo*. Subsequent use of replacement rhodopsin genes engineered at degenerate third-codon wobble positions showed great resistance to the suppressor shRNA both in cell cultures and mouse liver *in-vivo*. Similarly, Cashman *et al.,* (2005) demonstrated potent silencing of both wild type and mutant (P23H) human rhodopsin alleles in human retinal retinoblasts using more than one short hairpin RNAs. Subsequent use of a codon exchanged rhodopsin mRNA conferred complete resistance to silencing by the shRNAs. In another investigation, Palfi *et al.*, (2006) successfully illustrated mutation independent suppression and replacement of *rds*/peripherin transcripts in cell cultures and murine retinal explants.

It is only recently that gene therapy directed to rhodopsin has been attempted in the retina using AAV-mediated delivery of siRNA. Tessitore *et al.*, (2006) have shown successful reduction of mouse P23H rhodopsin transgene expression following subretinal injection of rAAV-2/5 vectors encoding an allele specific shRNA in P23H transgenic rats. However, suppression of the P23H rhodopsin allele did not lead to the prevention of photoreceptor degeneration, and the authors concluded that more robust shRNA expression in the retina may be required for achieving therapeutic efficacy *in-vivo*. Likewise, Gorbatyuk *et al.*, (2007) also demonstrated that rAAV-2/5-mediated siRNA delivery into the subretinal space of heterozygous rhodopsin knockout mice caused a reduction of retinal function as a result of diminished rhodopsin mRNA and protein. Similarly, O'Reilly *et al.,* (2007) successfully demonstrated greater than 90% suppression of rhodopsin in murine photoreceptors following subretinal delivery of AAV-2/5 expressing shRNAs. The results obtained from these studies have proven

the potential for this strategy to be translated into therapies for a large variety of other inherited retinal diseases.

1.13.4 RNAi in the treatment of ocular neovascularisation

Neovascularisation complicates several different eye diseases and constitutes one of the most common and difficult pathological processes (Campochiaro, 2000). Three types of ocular neovascularisation are extremely common causes of blindness and visual morbidity include choroidal, retinal and corneal neovascularisation. Choroidal neovascularisation (CNV) is characterised by the growth of new blood vessels below the retina, and occurs in diseases of the Bruch's membrane/ retinal pigment epithelium (RPE). In particular, the wet form of neovascular age-related macular degeneration is the most prevalent cause of severe vision loss in people over the age of 60 in developed countries (Klein and Klein, 1993). While multiple pro-angiogenic proteins have been found to be involved in CNV, both clinical and experimental studies have shown that the vascular endothelial growth factor (*VEGF*) is a critical stimulus of the pathophysiology involved in CNV (Kwak *et al.*, 2000). *VEGF* is an essential growth factor for angiogenesis and has been shown to be up-regulated in a CNV animal model (Shen *et al.*, 1998). Although the balance between pro- or anti-angiogenic factors may regulate angiogenesis, inhibition of *VEGF* alone has been shown to completely prevent retinal angiogenesis (Ozaki *et al.*, 2000). Retinal neovascularisation occurs in ischemic retinopathies, such as diabetic retinopathy, and it is the most common cause of vision loss in working age in America (Klein *et al.*, 1984). In contrast, corneal neovascularisation occurs as a consequence of corneal infection or inflammation, such as herpes simplex keratitis.

One of the first uses of siRNA in ocular diseases was related to the study of choroidal neovascularisation. In a murine model of choroidal neovascularisation induced by rupture of Bruch's membrane with laser photocoagulation (Tobe *et al.*, 1998), the area of choroidal neovascularisation at sites of rupture of Bruch's membrane was significantly less in eyes that received a subretinal injection of *VEGF* siRNA compared to those injected with a control siRNA. Similarly, Reich *et al.*, (2003)

successfully demonstrated the use of *VEGF* specific siRNAs to inhibit hypoxia-induced *VEGF* in HeLa cells, and subretinal injection of the siRNA significantly decreased the extent of CNV in a murine laser-induced model of CNV. Although subsequent studies investigating the effect of intravitreal injection of *VEGF* siRNA in a primate model of choroidal neovascularisation were inconclusive, these studies have shown that the use of siRNA against *VEGF* has great therapeutic value, and its potential is being explored in a phase I clinical trial using intravenous injection of *VEGF*-targeting siRNA in patients with subfoveal choroidal neovascularisation due to neovascular AMD (Tolentino *et al.*, 2004a; Tolentino *et al.*, 2004b; Maguire *et al.*, 2005).

Kim *et al.*, (2004) reported that systemic administration using a polymer delivery system or topical administration of siRNAs directed against *VEGF-A, VEGF* receptor 1 (*VEGFR1*) and *VEGFR2* caused significant reduction of corneal neovascularisation induced by herpes simplex infection or CpG oligodeoxynucleotides. Murata *et al.*, (2006) also demonstrated successful inhibition of *VEGF* using diced siRNAs in human retinal pigment epithelial cells (ARPE-19). Subconjunctiva injection of these siRNAs into rat eyes was effective in attenuating the growth of corneal angiogenesis *in-vivo*, and most significantly, histological analysis showed no signs of toxicity or adverse effects on the tissues near the injection site.

1.13.5 RNAi-mediated downregulation of apoptotic mediators in ganglion cells

Apoptosis plays a central role in photoreceptor degenerations and glaucoma. There have been numerous attempts to understand the pro-apoptotic genes involved in apoptotic pathways to develop retinal cell survival therapies. Transection of optic nerves is an established model for apoptotic cell death, usually resulting in 80-90% of retinal ganglion cells (RGC) death 14 days post-nerve transection in adult rats (Kermer *et al.*, 2001). Axotomy-induced retinal ganglion cell (RGC) death is closely associated with the activation of an apoptotic signaling cascade involving pro- and anti-apoptotic genes of the *Bcl-2* and caspase family. Increased expression of immediate early genes in axotomised RGCs include *c-Fos* and *c-Jun*, where

inhibition of c-Jun in neurodegeneration models was successful in attenuating neuronal cell death, thus indicating an active role of c-Jun in early apoptosis induction (Crocker *et al.*, 2001). Further downstream in the apoptotic cascade is *Bax*, which acts as a proapoptotic stimulator of the multidomain subfamily of the *Bcl-2* family proteins, leading to the activation of caspases via cytochrome c release (Brady and Gil-Gomez, 1998). In addition, the mammalian cell death abnormality-4 (CED-4) homologue apoptotic protease-activating factor-1 (*Apaf-1*) is a major mediator of caspase-induced cell death, and activates downstream caspases via apoptosome formation (Zou *et al.*, 1999). Previous studies have already provided evidence to indicate that downregulation of c-*Jun, Bax* and *Apaf-1* may effectively interfere with the initiation of the apoptotic cascade in retinal ganglion cells (Lassus *et al.*, 2002; Crocker *et al.*, 2001; Isenmann *et al.*, 1999). In particular, Lingor *et al.*, (2005) have demonstrated that injection of siRNAs directed against *c-Jun, Bax* and *Apaf-1* into the optic nerve stump following axotomy, was able to sustain the survival of retinal ganglion cells *in-situ.* A single injection of *c-Jun, Bax* and *Apaf-1* targeting siRNAs proximal to the stump of the optic nerve increased retinal ganglion cells survival in the retina for two weeks after transfection, implicating their roles in apoptotic regulations.

1.13.6 RNAi in the treatment of oxidative damage in the retina

Oxidative damage has been implicated in several ocular diseases including age-related macular degeneration (The age-related eye disease study research group, 2001), and cone cell death in retinal pigmentosa (Shen *et al.*, 2005). Wu *et al.*, (2005) reported the use of siRNA directed against the p66 isoform of *Shc* adaptor protein to investigate its oxidative role in oxidative damage in retina. In *in-vitro* studies, transfection of RPE cells with p66 targeting siRNA reduced H_2O_2-induced generation of reactive oxygen species and apoptosis. Furthermore, intravitreous injection of paraquat (dimethyl dipyridilium) in mice provides an acute model of oxidative damage-induced retinal degeneration (Cingolani *et al.*, 2005). Subretinal injection of p66Shc siRNA in BALB/c mice prior to oxidative damage induced by paraquat preserved retinal function as assessed by electroretinograms. These studies provided

the evidence that siRNA targeting p66Shc may be feasible for treatment of oxidative damage in the retina.

1.13.7 RNAi as a therapeutic approach for ocular fibrosis

Excessive wound repair resulting in fibrosis scarring is a major cause of ocular disease. For example, after retinal re-attachment surgery, ~10% of patients develop a complication called proliferative vitreoretinopathy in which scar tissue occurs on the surface of the retina and exerts traction. Occasionally, this may lead to the redetachment of the retina, and addition surgery is required subsequently, substantially reducing visual prognosis (Campochiaro, 1997). In addition following filtration surgery for glaucoma which involves creation of an opening between the anterior chamber and the periocular space to allow exit of fluid to reduce intraocular pressure, excessive scarring causing the flap of sclera and conjunctiva to seal down can prevent the exit of fluid (Campochiaro, 2006). Transforming growth factor-β (TGFβ) and its receptors have been implicated in wound repair and fibrotic diseases. Nakamura *et al.*, (2004) used TGFβ receptor II specific siRNAs to suppress TGFβ receptor II expression, halting the production and migration of fibronectin in cultured human corneal fibroblasts. Furthermore, in a mouse model with subconjunctival scarring induced by injection of latex beads underneath the conjuntiva, co-injection of TGFβ receptor II specific siRNAs significantly reduced inflammatory and matrix deposition.

1.13.8 Genetic tests for RP

The large number of recently discovered RP genes and causative mutations has provided useful information for the establishment of genetic markers, which may help to establish the risks to family members based on the mode of inheritance and molecular genetic testing. However, the genetic and phenotypic heterogeneities of RP have created difficulties in genetic testing, where generally each known mutation accounts for only small percentage of patients. Mutation patterns may also be specific to certain ethnic groups, as exemplified in the much lower prevalence of RHO and RP1 mutations in Chinese patients than in Caucasians (Wang *et al.*, 2005a). Today,

predictive genetic testing for RP is still controversial (Mackey *et al.*, 2003). Nevertheless, genetic counseling aiming to provide information for making decisions regarding medical management or pregnancy, can be given based on risk assessment determined by family history, or by directly testing for a mutation. There is the issue of psychological burden on the carrier and family since no effective prevention or curative therapy exist (Wang *et al.*, 2005a).

Careful planning should be made as to the clinical features of patients who may benefit from gene therapy. For example, rhodopsin P23H mutation has been extensively studied and is of particular interest because it is the most common mutation that causes RP in North America. From an economic standpoint, many patients could benefit from a gene therapy tailored for this disease, but its phenotypes are relatively mild and patients have good vision well into adulthood. In comparison, RP that is caused by null mutations in PDE6B manifest severe symptoms with early onset in childhood. However being less frequent in the population this mutation has received less attention. Therefore it is important to balance the need for a gene-based treatment for a particular mutation from an economic and a humanitarian point of view and also to determine whether or not it will be possible to identify patients early enough in the course of their disease to benefit from gene therapy (Dejneka and Bennett, 2001).

Gene-based therapies have offered a means to correct gene defects in inherited ocular diseases by gene replacement and/or gene silencing and with broad applications in many sophisticated systems. Numerous studies in recent years have demonstrated proof of principle that gene-based therapies can mediate significant quantifiable improvements in ocular morphology and visual function in experimental and preclinical models. These advances have enabled the development of proposals for clinical trials of gene therapies for both inherited and acquired ocular diseases. This has culminated in the first clinical trials for Leber Congenital Amaurosis (LCA) being conducted in UK using AAV-mediated subretinal delivery of RPE65 (Ali R., Institute of of Ophthalmology, University College London, Moorefields Eye Hospital), with

future trials expected in the near future in the US (Bennett J., F. M. Kirby Center for Molecular Ophthalmology, University of Pennsylvania; and Hauswirth W. W., Departments of Ophthalmology, Neurology and Molecular Genetics and Microbiology, Center for Gene Therapy, University of Florida) and France (Rolling F., Faculty of Medicine, University of Nantes).

1.14 Mutations in inosine 5'-monophosphate dehydrogenase type 1 (IMPDH1) cause the RP10 form of autosomal dominant retinitis pigmentosa

1.14.1 Introduction

To date, mutations in 16 genes have been localised in individuals with autosomal dominant retinitis pigmentosa (adRP), but mutations have only been characterised in ~50% of adRP cases (http://www.sph.uth.tmc.edu.RetNet). In adRP, the majority of mutations identified occur in genes that encode photoreceptor specific proteins involved in phototransduction such as rhodopsin, *rds*/peripherin or RP1. In contrast, other forms of adRP are caused by mutations in more widely expressed genes whose mechanisms of action are essential for cellular regulation (*Table 1.1*), and one such gene is inosine 5'-monophosphate dehydrogenase type 1 (IMPDH1).

Initial genetic linkage mapping carried out in our laboratory (Jordan *et al.*, 1993) localised an adRP gene referred to as the RP10 locus, segregating in a Spanish family, to the long arm of chromosome 7. The investigation involved a genome-wide search using DNA from a large Spanish family (FA84), segregating classic adRP with a range of onset from 5-28 years of age. Patients exhibited typical symptoms of RP including nyctalopia (night blindness), constriction of visual field, bone-spicule pattern pigmentary deposits and diminished cone/ rod electroretinograms (ERGs). Following this, the disease locus in a large unrelated American family (UTAD045), exhibiting a later onset and a slower progression symptoms, was mapped to the RP10 region (McGuire *et al.*, 1995). Linkage data from both families (FA84 and UTAD045) were then combined to map the RP10 locus with greater precision and placed the disease gene in an interval of 4.7 Mb between two genetic markers on chromosome 7q.31.1 (McGuire *et al.*, 1996). Subsequently, Bowne *et al.*, (2002) reduced this linkage interval to 3.45 Mb in two unrelated American families. In addition, a number of smaller RP10 families originating from Scotland, Spain, Ireland and Poland have been reported, indicating that the RP10 locus comprises a significant proportion of all adRP cases (Mohamed *et al.*, 1996; Millán *et al.*, 1995; Grover *et al.*, 2004).

Following the localisation of RP10, efforts to identify the disease gene were impeded by the large size of the interval containing the RP10 gene, which contained approximately 60 genes listed in the interval and a considerable number of sequences with predicted coding functions (http://genome. ucsc.edu). Early attempts at screening for potential disease causing candidates in the interval excluded many genes including those encoding blue cone pigment (BCP), ADP ribosylation factor 5 (ARF5), metabotrophic glutamate receptor 8 (GRM8), diacylglycerol kinase iota (DGKI), the human homolog of the *Drosophila rdgA* gene (a ubinuclein-like gene) and a zinc finger-like gene as the RP10 gene (Bowne *et al.*, 2000; McGuire *et al.*, 1997). Following this, Kennan *et al.*, (2002) reported the use of a global gene expression approach to identify the disease causing gene within the large RP10 interval. Also in our laboratory, a mouse model carrying a targeted disruption of the rhodopsin gene was generated which displayed a severe retinopathy with the complete loss of photoreceptors after a 3 month period (Humphries *et al.*, 1997; Humphries *et al.*, 2001). This $Rho^{-/-}$ mouse model has enabled comparative transcriptional profiling in mouse retinas with or without functional photoreceptors, and changes in the level of expression of transcripts reflect the destruction of primary neurons and response by the surviving retinal cells undergoing the degenerative process. The gene encoding inosine 5'-monophosphate dehydrogenase type 1 (IMPDH1) showed a 5.8-fold downregulation in $Rho^{-/-}$ retinas and maps to the RP10 locus, while no other genes in the disease interval showed a similar degree of reduction (Kennan *et al.*, 2002). This result indicated that IMPDH1 is expressed at higher levels in photoreceptor cells compared to other retinal cell types in mouse. In parallel to our studies, Bowne *et al.*, (2002) used positional candidate cloning and refined linkage mapping to prioritise retinal-specific candidates based on differential transcriptional expression in wild type mice compared to $crx^{-/-}$ knockout mice retinas, and the gene encoding IMPDH1 showed a six-fold reduction in expression. Since many of the known genes responsible for causing RP are under CRX control in photoreceptors, IMPDH1 became a high-priority candidate for mutation screening. Collectively these data presented IMPDH1 as a strong candidate for the RP10 form of adRP gene.

1.14.2 Characterisation of Inosine 5'-monophosphate dehydrogenase (IMPDH)

Enzymes of the nucleotide biosynthesis pathway are essential for supporting cell growth and proliferation. Typically, cells can synthesise nucleotides through two different pathways: (a) the *de novo* pathway which involves the assembly of the purine or pyrimidine ring system in a stepwise manner or (b) the salvage pathway which recycles preformed nucleobases, nucleosides and nucleotides (Kornberg and Baker, 1992). The first enzyme located at the branch point of the purine *de novo* synthetic pathway is inosine 5'-monophosphate dehydrogenase (IMPDH), which is responsible for catalysing the rate-limiting step of *de novo* guanine nucleotide synthesis by oxidising inosine 5'-monophosphate (IMP) to xanthosine 5'-monophosphate (XMP) with the reduction of nicotinamide adenine dinucleotide (NAD) (Collart and Huberman, 1988) (*Figure 1.18*). IMPDH has been described in prokaryotes and eukaryotes, and both the gene and amino acid sequences are highly conserved across different species, with 36% sequence identity between *E. coli* and human proteins (Natsumeda and Carr, 1993). IMPDH controls the size of cellular guanine deoxy- and ribonucleotide pools, which in turn controls many physiological processes, including replication, transcription, cellular signalling and glycosylation (Weber *et al.*, 1992). The level of IMPDH1 enzyme activity varies with the cell cycle, exhibiting maximal enzymatic activity during the S-phase (Szekeres *et al.*, 1992).

In humans, IMPDH activity is governed by two separate but very closely related isoforms, termed type I and type II, that are encoded by separate genes located on chromosomes 7 and 3 respectively (Gu *et al.*, 1994; Glesne *et al.*, 1993). The human IMPDH type I and II cDNAs have been isolated and found to contain open reading frames encoding 514 amino acid proteins of 56 kilodaltons (Natsumeda *et al.*, 1990; Collart and Huberman, 1988). The two IMPDH proteins are 84% identical at the amino acid level, and are indistinguishable in their catalytic activities, substrate affinities and K_i values (Carr *et al.*, 1993; Natsumeda *et al.*, 1990; Collart and Huberman, 1988; Hager *et al.*, 1995). The mRNA transcripts are differentially regulated in different cell types, where IMPDH type 1 is constitutively expressed and is the predominant isoform in normal cells (Gu *et al.*, 1997). Regulation of IMPDH

activity during cellular growth and differentiation has been largely attributed to changes in the expression of the type II gene. IMPDH type II transcript is the predominant species in neoplastic cells and is selectively upregulated in replicating cells (Collart *et al.*, 1992; Nagai *et al.*, 1991; Nagai *et al.*, 1992). Conversely, when neoplastic cells are induced to differentiate, the enhanced levels of the type II transcript and total cellular activity are down-regulated (Kiguchi *et al.*, 1990a; Kiguchi *et al.*, 1990b; Olah *et al.*, 1988). In contrast, IMPDH type I transcript remains constitutively expressed during cell proliferation and induction of cell differentiation (Collart *et al.*, 1992; Nagai *et al.*, 1991; Nagai *et al.*, 1992). The presence of two different isoforms has been explained by observing the vastly different guanine nucleotide level requirements of differentiated and proliferating cells (Yalowitz and Hiremagalur, 2000). A study of relative mRNA levels in human tissues demonstrated significant differences in the pattern of distribution of the type I transcript, with relatively high levels in fetal heart, brain, retina, kidney, pancreas, colon and peripheral blood lymphocytes (Senda and Natsumeda, 1994). In contrary, the expression levels of the type II transcript are generally higher than type I, and far less variable in different tissue types. Both IMPDH type I and type II mRNA levels also increase with T-cell activation. Dayton and Zimmermann have shown that activation of peripheral blood T-lymphocytes with the mitogens PMA and inomycin resulted in a 10-15 fold induction of IMPDH mRNA expression and total cellular enzymatic activity respectively (Dayton *et al.*, 1994; Zimmermann *et al.*, 1998). These observations have indicated that the two genes are expressed in a tissue-specific manner, and are regulated in a different manner in resting, proliferating and neoplastic cells, and these differences may have important consequences for cellular function. In addition, the modulation of cellular IMPDH activity during cell growth and differentiation suggests a critically important role for the regulation of IMPDH type II gene expression in the progression of normal cell development.

In order to better understand the relative contributions of the *de novo* and salvage pathways, as well as the corresponding roles of both IMPDH isoforms, for guanine nucleotide biosynthesis, murine models with targeted disruption of either IMPDH

isoforms have been generated (Gu *et al.*, 2003). A mouse model harbouring the loss of both IMPDH type II alleles as a result of homologous recombination has shown early embryonic lethality despite normal levels of IMPDH type I and hypoxanthine guanine phosphoribosyltransferase (HPRT), a key enzyme in the salvage pathway of guanine nucleotide synthesis) activity (*Figure 1.18*) (Gu *et al.*, 2000). In addition, tissues from two types of double knockout mice (IMPDH type $I^{-/-}$ + type$II^{+/-}$ and IMPDH type$I^{-/-}$ + HPRT $^{-/-}$) showed undetectable levels of IMPDH type I mRNA, while IMPDH type II mRNA was approximately 50% lower in the IMPDH type $I^{-/-}$ + type$II^{+/-}$ mice than in wild-type mice, and IMPDH type II expression in IMPDH type $I^{-/-}$ + HPRT $^{-/-}$ mice was equivalent to that observed in wild type mice. These findings have demonstrated that IMPDH type I enzymatic activity is not essential for normal mouse development or fertility, and that the expression of IMPDH type II is not increased in response to the loss of IMPDH1 and HPRT activity (Gu *et al.*, 2003). Furthermore, the proliferation of lymphocytes was significantly reduced in mice harbouring the IMPDH type $I^{-/-}$ genotype or a double knockout (the IMPDH type $I^{-/-}$ + type$II^{+/-}$ and IMPDH type$I^{-/-}$ + HPRT $^{-/-}$ genotype) following activation by anti-CD3 or antiCD28 antibodies. Interestingly, lymphocyte proliferation was less impeded in both single and double knockout mice in response to other stimuli such as LPS, PMA or inomycin, suggesting a more selective inhibitory effect on lymphocyte activation through the T-cell signalling pathway (Gu *et al.*, 2003).

1.14.3 Gene regulation of IMPDH type I and II

The co-existence of two IMPDH iso-enzymes in mammalian cells with striking conservation of coding sequence and amino acid structure suggests that each subserves an important and non-overlapping function in cellular physiology and development. There are also other examples of multigene families that display tissue-specific differences in the expression of human enzymes essential for nucleotide metabolism. For example, phosphoribosyl pyrophosphate synthetase (PRPS) catalyses the synthesis of phosphoribosyl pyrophosphate, the primary precursor of the ribose monophosphate moiety of all nucleotides and a critical regulator of *de novo* purine and pyrimidine biosynthesis (Becker and Roessler, 1995). PRPS contains three

distinct isoforms: the first two isoforms termed PRPS subunits I and II, are encoded by distinct genes (PRPS1 and PRPS2) (Taira *et al.*, 1989a) and are expressed in a tissue specific manner (Taira *et al.*, 1989b), whereas the third isoform is exclusively expressed in the testes (Taira *et al.*, 1990). The differential expression of these isoforms has been attributed to the differences in 5'-flanking sequences and corresponding differences in transcriptional activity (Ishizuka *et al.*, 1992). Similarly, there are four isoforms of AMP deaminase encoded by three AMP deaminase genes (Sabina and Holmes, 1995). Transcriptional studies have shown that each isoform expresses multiple RNA transcripts in mutually exclusive patterns (van Den Bergh and Sabina, 1995), and is regulated by different promoters in the 5' flanking region (Mahnke-Zizelman *et al.*, 1996).

The human IMPDH type II gene is a relatively small gene of approximately 5.8 kb in length and has 14 exons (Collart and Huberman, 1988). The expression of IMPDH type II is regulated by a single core promoter region that contains tandem cAMP-response element binding sites, a Sp1 site, and a novel palindromic octamer sequence (Zimmerman *et al.*, 1995). In addition, the activation of peripheral blood T-lymphocytes with the mitogens PMA and ionomycin resulted in a 6-fold increase in IMPDH type II promoter activity (Zimmerman *et al.*, 1995). In contrast, the regulation of IMPDH type I is more complex and is governed by three alternative promoters in the 5'-flanking region (*Figure 1.19A*) (Gu *et al.*, 1997). Three major RNA transcript variants for IMPDH type I have been identified in human cells and various tissues suggesting that the enzyme is regulated in a cell type-specific manner. These IMPDH type I transcripts vary in size (4kb, 2.7kb and 2.5kb) but contain identical coding sequences derived from 14 exons, which encode an identical 55.6kDa IMPDH1 protein, and identical 3' untranslated regions (UTR) (*Figure 1.19B*). The only difference between the three transcripts lies in the splicing of three alternate untranslated 5'-exons, traditionally termed A, B, and C. In contrast, the IMPDH2 gene does not contain sequences homologous to the 5' exons A, B and C of IMPDH1, and lacks any additional exons preceding exon 1. The IMPDH1 P1-promoter produces a 4.0kb transcript that is primarily found in peripheral blood

lymphocytes (PBLs) and the expression of this transcript has a direct correlation with activated T-cells. An NFκB binding site is located within the P1-region and may be of relevance to this observation, because NFκB is involved in directing the transcription of a number of genes upon T and B-cell activation and inflammatory cytokine responses (Baldwin, 1996). The GC-rich P2-promoter produces the 2.7kb IMPDH1 transcript and is speculated to be tissue-specific, since it has shown different expression patterns in various cell lines. The P3-promoter regulates the expression of the 2.5kb transcript and contains a large number of Sp1 and AP2 binding sites that may account for the basal expression of this gene. Furthermore, the presence of several NGFI-A/ Egr-1 binding sites in close proximity to the transcription initiation sites promotes the upregulation of the 2.5kb transcript with T-cell activation. The Egr-1 is a zinc finger protein that is induced following interleukin-2 stimulation of T lymphocytes which is essential for subsequent cellular proliferation (Perez-Castillo *et al.*, 1993).

1.14.4 Localisation of IMPDH type I and type II in the retina

The two types of human IMPDH enzymes have previously been found by immunofluorescence experiments to localise in both the cytoplasm and nucleus of prostate cancer cells (PC-3), leukaemia cells (K562) and HeLa cells using a polyclonal antibody that could not distinguish between the two isoforms of IMPDH (McLean *et al.*, 2004). Furthermore, subcellular fractionation studies carried out by Aherne *et al.*, (2004) showed that wild-type IMPDH1 protein localised predominantly in the cytosolic fraction of HEK293T cells. Since human IMPDH enzymes do not possess a standard nuclear localisation signal (NLS), the signal directing the enzyme to the nucleus still remains to be deciphered (Cokol *et al.*, 2000). However the fact that nuclear localisation signals of many nuclear proteins have still not been identified, and recognition motifs have yet to be determined for ~50% of the known nuclear import factors (Chook and Blobel, 2001), renders the absence of knowledge of an NLS in IMPDH not unusual.

In order to determine the expression levels of IMPDH1 and IMPDH2 in various retinal regions, and to compare these levels with those from other regions of the body, Bowes Rickman *et al.*, (2006) have examined the expression data from the EyeSAGE database (*http://neibank.nei.nih.gov/EyeSAGE/index.shtml*). On average, IMPDH1 is expressed at a 10-fold higher level in the human retina than in other tissues, and is also expressed at levels ten times greater than IMPDH2 in the retina. However, in other tissues apart from the retina, IMPDH2 is two-fold higher than that of IMPDH1. In particular, the enzyme is expressed at higher levels in the peripheral retina than in the macula. In addition, *in-situ* mRNA expression pattern, immunofluorescence and SAGE analysis have shown that IMPDH1 is present in both rod and cone photoreceptor cells, and that the level of IMPDH1 mRNA expression is distinctively higher in rod-enriched segments, indicating that photoreceptors have a high demand for IMPDH1 (Aherne *et al.*, 2004; Bowne *et al.*, 2006a). Moreover, the expression of both human and mouse IMPDH1 has been localised to the inner segment and synaptic terminals of photoreceptors, with the major IMPDH1 mRNA being the 2.5 kb transcript (Gu *et al.*, 1997; Aherne *et al.*, 2004; Bowne *et al.*, 2006a).

1.14.5 IMPDH inhibitors

The inhibition of cellular IMPDH activity has been shown to induce differentiation and apoptosis through an abrupt cessation of DNA synthesis (Duan and Sadee, 1987), and premature termination of cell cycling at the G_1-S interface (Cohen and Sadee, 1983). This antiproliferative effect has presented IMPDH as an important drug target for immunosuppressive, antiviral and antitumour therapies (Allison *et al.*, 1991; DeClerq, 1993; Franchetti and Grifantini, 1999). The interest of IMPDH as a target for antitumour agents came from the observation that IMPDH is upregulated in rapidly proliferating tumour cells (Weber, 1983). Furthermore, the observation that IMPDH activity is highly induced upon mitogenic and antigenic stimulation in human peripheral blood lymphocytes (Gu *et al.*, 2003), and that T-lymphocytes activation is highly dependent on *de novo* pathway of nucleotide biosynthesis have made IMPDH1 an attractive target for immunosuppressive therapy. Mizoribine and Ribavirin represent a class of IMPDH inhibitors that contain nucleoside analogs

which are phosphorylated to 5'-monophosphates to inhibit IMPDH competitively (Kusumi *et al.*, 1988; Streeter *et al.*, 1973). Examples of uncompetitive inhibitors include mycophenolic acid (MPA) and the nucleoside tiazofurin, which need to be activated to its dinucleotide form before becoming active inhibitors (Cooney *et al.*, 1982). The pharmacological effects of IMPDH inhibition have been exploited by a number of commercial drug companies. An ester pro-drug of mycophenolic acid (MPA), mycophenolate mofetil (CellCept®) has been shown to prolong the survival of allografts and to reverse acute allograft rejection in animal studies, and has been approved as an immunosuppressant for the prevention of acute rejection in both heart and kidney transplantations (Kobashigawa *et al.*, 1998; Sollinger *et al.*, 1995). An oral formulation of ribavirin called Rebetol® has gained approval as a combination product with interferon-alpha (Rebetron®) for the treatment of hepatitis C patients who have relapsed after interferon monotherapy (Davis *et al.*, 1998). However, the use of currently available IMPDH inhibitors is still limited due to non-specificity for both iso-enzymes, and cellular toxicities that are likely to be compound-specific. For example, the administration of CellCept® has been associated with gastrointestinal (GI) tolerability problems in numerous patients, and the toxicity effect is likely being caused by the metabolism and disposition of the drug (Sollinger *et al.*, 1995; Bullingham *et al.*, 1998). Following the administration of the ester pro-drug, mycophenolate mofetil is rapidly hydrolysed to produce the active metabolite MPA, which in turn becomes extensively glucuronidated. This has a negative impact on the overall pharmacological activity since MPA glucuronide does not inhibit IMPDH, and large daily doses of 2–3 g are required to achieve clinical efficacy. Furthermore, the glucuronide is excreted in the bile and MPA is liberated by the glucuronidase of bacteria residing in the lower gastrointestinal tract. MPA then undergoes enterohepatic recirculation that leads to the build up of high concentrations of free MPA in the GI tract, which may cause of GI tolerability problems.

1.14.6 Mutations in IMPDH1 cause the RP10 form of adRP

Mutations in IMPDH1 cause the RP10 form of autosomal dominant RP and are also a rare cause of isolated Leber Congenital Amaurosis (LCA) (Bowne *et al.*, 2006b). It has been estimated that mutations in IMPDH1 alone cause approximately 2% of adRP, which is consistent throughout the American and Japanese population (Wada *et al.*, 2005a). A missense mutation, which is a trademark of adRP, has been revealed in exon 7 of IMPDH1 gene, and has been shown to segregate in all affected individuals of the Spanish family (FA84) (Kennan *et al.*, 2002). This specific mutation results in an arginine to proline substitution (CGC→CCC) at codon 224, where arginine in codon 224 is highly conserved among four species (human, mouse, Drosophila and Chinese hamster). Thus, this amino acid may be crucial for maintaining the functionality of IMPDH1 protein.

The most common missense mutation identified to date is the substitution of an asparagine for an aspartic acid (GAC→AAC) at codon 226 (Asp226Asn), which has been identified in two American and one British RP10 families (Bowne *et al.*, 2002; Wada *et al.*, 2005). This missense mutation is present in all affected individuals and has not been found in other unaffected family members. Moreover, the Asp226Asn mutation alone causes approximately 1% of adRP cases, and haplotype result suggests that this mutation has arisen multiple times; hence, it is a hot-spot for adRP mutations (Bowne *et al.*, 2006b). The aspartic acid at codon 226 is highly conserved in all IMPDH genes, and across a wide range of species including bacteria, indicating that this mutation is highly deleterious. Functional studies have revealed that patients with Asp226Asn mutation have an early onset of symptoms (<20 years of age) with severe reduction in rod and cone functions and aggressive progression of retinopathy (Bowne *et al.*, 2002). Bowne *et al.*, (2002) also reported another substitution, Val268Ile, in the American family where the Asp226Asn mutation was first discovered. The Val268Ile change occurs at a less conserved site and additional family members are required to determine whether this substitution segregates with disease.

A novel missense mutation was described by Grover *et al.*, (2004) in a family of Irish and Polish descent. The mutation occurs at codon 231 with a substitution of arginine to proline (Arg231Pro). Functional data from affected members of this family showed an aggressive form of adRP with night blindness in the first decade of life, reduced visual acuity, marked narrowing of the visual field and nondetectable ERGs at an early age. Furthermore, Wada *et al.*, (2005b) reported that a family of Japanese patients did not contain the most commonly reported Asp226Asn mutation, but described two novel mutations, Lys238Arg and Leu227Pro. These patients also have early onset of severe retinal degeneration and progressed to legal blindness after the age of ten. In addition, the common Asp226Asn and a novel missense mutation, Lys238Glu, have both been shown to co-segregate in a single North American family that co-segregated with dominant RP. However, the segregation analysis was not definitive due to small family size, so that it was not statistically possible to compare the clinical features consistent with those in Asp226Asn. Therefore Lys238Glu was categorised as an allele of uncertain pathogenicity (Wada *et al.*, 2005b). In summary, the combination of functional data reported has demonstrated three convincingly pathogenic mutations (Asp226Asn, Arg224Pro, and Arg231Pro) and two substitutions (Lys238Glu and Val268Ile) that are possibly pathogenic.

Interestingly, the three pathogenic IMPDH1 mutations (Arg224Pro, Asp226Asn, and Arg231Pro) (Bowne *et al.*, 2002; Kennan *et al.*, 2002; Grover *et al.*, 2004), as well as the two potentially pathogenic substitutions (Val268Ile and Lys238Glu), are all missense mutations that are localised in exon 10 of the IMPDH1 gene (*Figure 1.20A*). All of these mutations affect amino acid residues within a 45-residue stretch in the middle of the primary protein sequence, and no apparent null alleles (e.g., nonsense, frameshift, or splice-site mutations) have been uncovered in previously reported screens of adRP patients (Wada *et al.*, 2005a). The clustering of the identified mutations reveals that changes in this region of the protein have negative functional consequences that lead to retinal degeneration. Most of the adRP-linked genes encode proteins such as rhodopsin that are expressed exclusively in the retina and photoreceptor-specific functions. In contrast, IMPDH1 plays an essentially

housekeeping role in many tissues, so the photoreceptor-specific effects of these mutations are perplexing and have not yet been fully elucidated.

Although IMPDH1 is the predominant form of IMPDH enzymes in murine retina, homozygous deletion of IMPDH1 *in-vivo* only causes a slow and mild retinopathy (Aherne *et al.*, 2004). Aherne *et al.*, (2004) have shown that the structural integrity of the outer nuclear layer of 10 month old IMPDH1 knockout mouse retinas is almost indistinguishable from that of 10 months old wild type retinas (*Figure 1.21A*). Furthermore, ERG disturbances recorded in IMPDH1 knockout mice over a period of 13 months were much milder than those recorded in humans with dominant IMPDH1 mutations. In particular, the ERG disturbances of a 4-month IMPDH1$^{-/-}$ mouse (equivalent to the teenage years of human) were much less compromised than a 17 year old human patient from the FA-84 RP10 family (*Figure 1.21B*). Similarly, Gu *et al.*, (2003) demonstrated that the retinas of knockout mice lacking functional IMPDH1 protein have no histological evidence of retinal degeneration, and exhibited only a mild decrease in ERG amplitudes at 12 months of age. In contrast, mouse models carrying targeted disruption of other adRP-linked genes such as rhodopsin and CRX displayed more deleterious phenotypes, with undetectable photoreceptor activity at 5 months of age (Humphries *et al.*, 1997; Furukawa *et al.*, 1999). Therefore these observations suggest that IMPDH1 is not critical for retinal development and early photoreceptor function.

The adRP-linked mutations, Arg224Pro and Asp226Asn, are located within the second CBS domain that forms part of a smaller flanking subdomain of the IMPDH1 enzyme, whereas Val268Ile is situated closely to the catalytic subdomain interface (*Figure 1.20B*) (Aherne *et al.*, 2004; Mortimer and Hedstrom, 2005). The entire flanking domain lies adjacent to the catalytic domain and is not thought to be required for enzymatic activity (Sinctak and Nimersgern, 2000). The finding that IMPDH1 is more abundantly expressed in both human and murine retinas than IMPDH2, has suggested that IMPDH1 is responsible for the bulk GTP supply in photoreceptor cells for maintaining normal retinal functions (Aherne *et al.*, 2004). Therefore, a reasonable assumption is that the IMPDH1 missense mutations cause photoreceptor

degeneration through reduced enzyme activity, and subsequent decrease in guanine nucleotide concentration. However, two studies have demonstrated that these mutations do not affect enzyme activity or tetramer formation (Aherne *et al.*, 2004; Mortimer and Hedstrom, 2005).

A study has previously reported that ATP induces a 5-fold increase in the activity of human IMPDH type II isoform (Scott *et al.*, 2004). The Arg224Pro mutation has been shown to abrogate this effect, which suggests that the adRP-linked mutations could perturb the regulation of IMPDH1 by ATP. However, kinetic studies demonstrated that the activity of wild type and mutant IMPDH1 enzymes do not vary in the presence of various concentrations of ATP (Mortimer and Hedstrom, 2005). Therefore RP10 does not result from a change in the regulation of IMPDH1 by ATP.

Computational modelling of wild type and mutant IMPDH1 proteins has also revealed that the Arg224Pro mutation cause significant tertiary structure distortion of the helical arrangements in the CBS domain (*Figure 1.21C*) (Aherne *et al.*, 2004). The outcome of such a structural disruption has also affected protein solubility and subsequently results in protein aggregation. This is further supported by subcellular fractionation studies carried out by Aherne *et al.*, (2004) showing that mutant IMPDH1 protein harbouring the Arg224Pro or Asp226Asn mutations co-localised predominantly in the insoluble cellular fractions. In contrast, western blot analysis carried out by Mortimer and Hedstrom, (2005) showed that mutations in IMPDH1 did not affect protein stability or turnover in HeLa cells. However, cellular fractionation studies were not performed in this study to examine the solubility level of mutant protein. Therefore the results reported by Aherne *et al.*, (2004) strongly suggested that RP10 is likely to be the result of altered IMPDH1 protein solubility or formation of protein aggregates. Protein aggregation as the cause of photoreceptor cell death is not uncommon and has previously been reported in other adRP-linked mutations, including the P23H mutation in rhodopsin (Illing *et al.*, 2002), and the R14W mutation in the gene encoding carbonic anhydrase IV (CA4) that causes RP17 (Rebello *et al.*, 2004).

Recently, *in-vitro* and *in-vivo* studies have shown that both IMPDH type I and II enzymes bind single-stranded nucleic acids of ~100 nucleotides via interactions with the CBS domains (McLean *et al.*, 2004). In addition, immunoprecipitation experiments have demonstrated that both IMPDH enzymes bind DNA and RNA with nanomolar affinity *in-vivo*. Several other dehydrogenases have previously been reported to possess nucleic acid binding properties, and the most noticeable example is glyceraldehydes 3-phosphate dehydrogenase (GAPDH). GAPDH has been independently isolated as a tRNA, RNA, DNA and transcriptional regulatory element binding protein (Singh and Green, 1993; Zang *et al.*, 1998; Morenegg *et al.*, 1986). In addition, GAPDH has been characterised to possess uracil glycohydrolase activity (Meyer-Siegler *et al.*, 1991), and is involved in nuclear/cytoplasmic transport of tRNA and oligonucleotides (Singh and Green, 1993), activation of ribozymes (Sioud and Jesperen, 1996) and RNA cleavage (Evguenieva-Hackenberg *et al.*, 2002). These activities appear to be important in transcription, DNA repair, apoptosis and viral replication (Ishitani *et al.*, 1998; Saunders *et al.*, 1999; Sawa *et al.*, 1997), and may be mediated by different GAPDH isoforms (Choudhary *et al.*, 2000).

In contrast to other dehydrogenases, the NAD site of IMPDH1 is not involved in nucleic acid binding; rather the interaction is mediated through the regulatory domain of CBS. Mutations in the CBS domain have been implicated in a wide range of inherited diseases, including myotonia (Ponting, 1997) and familial hypertonia cardiomyopathy (Blair *et al.*, 2001). It seems likely that nucleic acid binding is a functional property of CBS domains, and alterations in nucleic acid binding activity may be a potential mechanism underlying the pathologies of RP10.

Following the discovery that IMPDH1 binds nucleic acids *in-vivo*, Mortimer and Hedstrom (2005) investigated the adRP-associated mutations to identify the functional property that correlates with disease. Both pathogenic mutations, Arg224Pro and Asp226Asn, have shown significantly decreased affinities for single stranded DNA, whereas a non-pathogenic mutation, A285T, initially identified in an unaffected RP family member, has no effect on single stranded DNA affinity (Bowne *et al.*, 2006b). The A285T mutation is situated on the catalytic domain far from both

the active site and subdomain (*Figure 1.20B*); thus, it is not surprising that this mutation does not affect nucleic acid binding. The Asp226Asn mutation also decreases the specificity of nucleic acid binding by increasing the binding affinity of a random pool of oligonucleotides from 4% to 70%. This alteration in the specificity of nucleic acid binding could be unique to photoreceptors and represents a gain-of-function that is often associated with autosomal dominant mutations. However, this effect is not observed in the Arg224Pro and A285T mutations, suggesting that its relevance to disease is still unclear. Furthermore, immuoprecipitation studies have shown that both adRP-linked mutations, Arg224Pro and Asp226Asn, reduce the association of IMPDH1 with RNA *in-vivo*. Conventional methods for determining the pathogenicity of IMPDH1 mutations is to demonstrate the co-inheritance of a mutation and disease, but this is often restricted by small family size and lack of records or loss of patient contacts. However, the observations reported above have clearly shown that nucleic acid binding provides a direct functional assay for determining the adRP pathogenicity of IMPDH1 mutations. For example, currently genetic linkage has failed to establish the pathogenicity of the V268I mutation due to small family size. However, the V268I mutation has been shown to cause significant decrease in both single stranded DNA affinity and specificity, and also disruption of RNA binding *in-vivo*. The presence of all these functional alterations has indicated that V268I is also likely to be pathogenic. Furthermore, the R231P mutation described by Grover *et al.*, (2004) may also be pathogenic because of its close proximity to Arg224Pro and Asp226Asn, which perturb nucleic acid binding.

Furthermore, Bowne *et al.*, (2006a) showed that the predominant RNA and protein isoforms of IMPDH1 identified in the retina are different from those identified in other tissues. The sequencing of IMPDH1 retinal transcripts has also revealed that both human and mouse photoreceptors contain multiple IMPDH1 transcripts that give rise to different protein isoforms (*Figure 1.22 and 1.23*). These unique isoforms are generated from a combination of alternate splicing, the use of alternate transcription initiation sites, and the inclusion of a novel exon (exon 13b) through alternative splicing. In human and mouse, the presence of exon 13b, which is a 17bp exon

located in the genomic sequence between exon 13 and 14, causes a reading frame shift that obliterates the stop codon in exon 14, and increases the number of amino acids in the carboxyl terminus of the protein (*Figure 1.22 and 1.23*). Interestingly, apart from the original IMPDH1 isoform identified by Gu *et al.*, (1997) (*Figure 1.19B*), the human retina has also been found to contain three additional isoforms generated by alternative splicing (*Figure 1.22*). Currently, the functional consequences of these novel isoforms are not known, but their presence in human photoreceptors have suggested that the pathophysiology of retinal degeneration is not caused by alteration of the function of the original IMPDH1 isoform alone, but maybe through the alteration of the function of one or more of the unique retinal IMPDH1 isoforms. Perhaps, like GAPDH, the multiple IMPDH1 isoforms found in human retinas are responsible for associating with proteins involved in transcription, translation, nuclear transport or DNA repair. Therefore, the pathological effects of IMPDH1 mutations could very well be the result of the disruption of nucleic acid binding and delineation of the many nucleic acid metabolisms governed by different isoforms of this enzyme, which may subsequently reveal a novel regulatory mechanism that could be crucial for photoreceptor function.

1.15 Objectives of this study

The apparent clustering of dominant missense mutations between residues 224 and 268, the lack of obvious null alleles, as well as the mild phenotypes observed in the IMPDH1 knockout mouse model (Aherne *et al.*, 2004), have indicated that the disease pathology is unlikely to be caused by haploinsufficiency for normal IMPDH1. Furthermore, the observation that the pathogenic mutations do not affect IMPDH1 enzyme activity, but rather decrease the affinity of nucleic acid binding and perturbation in RNA metabolism (Mortimer and Hedstrom, 2005), and the identification of novel IMPDH1 isoforms through alternate splicing, have suggested that the dominant segregation pattern associated with RP10 is likely to be caused by a gain-of-function mechanism. Alternatively, data from our laboratory (Aherne *et al.*, 2004) suggest a dominant negative phenotypic effect exerted by mutant IMPDH1 proteins. Regardless of the mechanism, the mild phenotype observed in IMPDH1 knockout mice, as opposed to the severe phenotype seen in humans with the dominant mutations, presents RP10 as a potential target for therapeutic intervention. The aim of this study to simultaneous ablate both wild type and mutant IMPDH1 transcripts by siRNA molecules, without the need to introduce a replacement allele, may be sufficient to abolish the effect exerted by the mutant protein, decreasing the rate of photoreceptor degeneration to a similar extent to that observed in the IMPDH1 knockout mouse model (Aherne *et al.*, 2004).

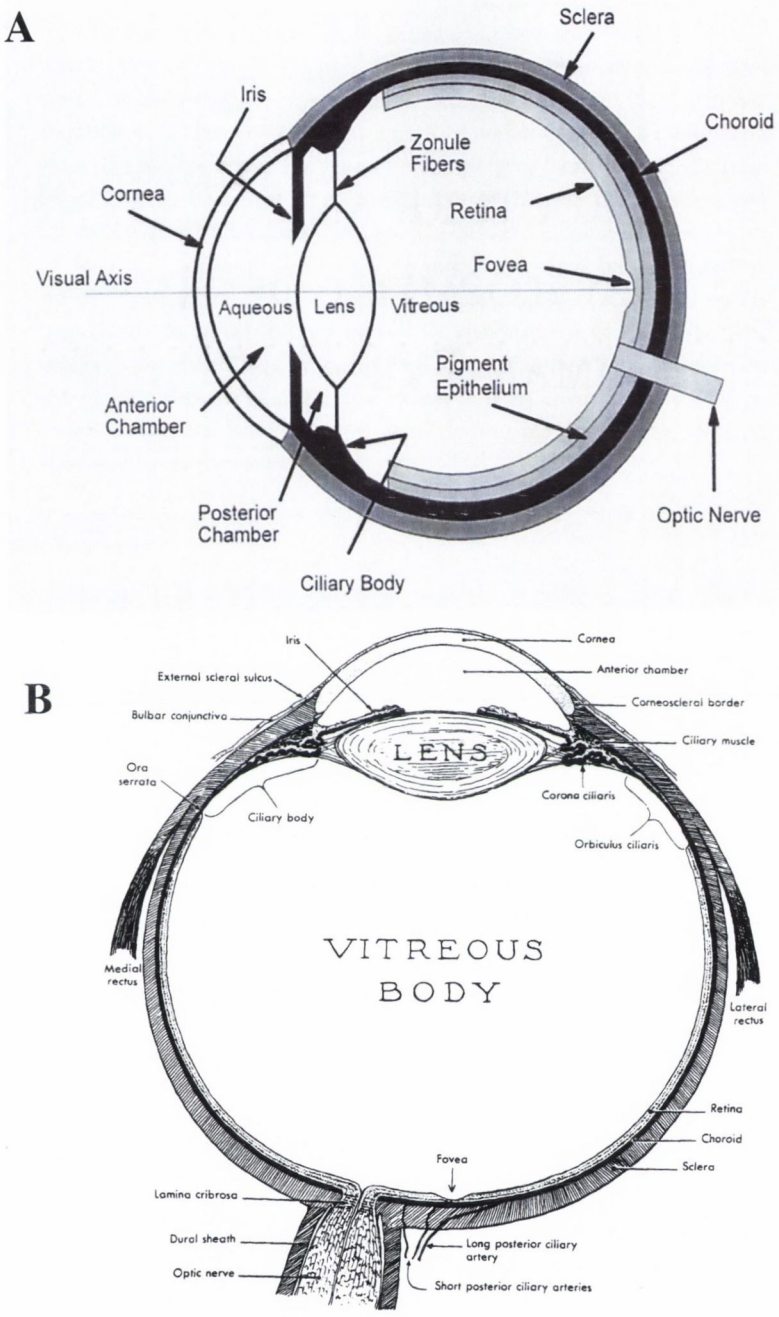

Figure 1.1: (A) Schematic diagram of the major components of the human eye (Printed from JT McIlwain. An Introduction To The Biology Of Vision. Cambridge University Press). (B) An overview of the human eye (Printed from Remington. Clinical Anatomy Of The Visual System).

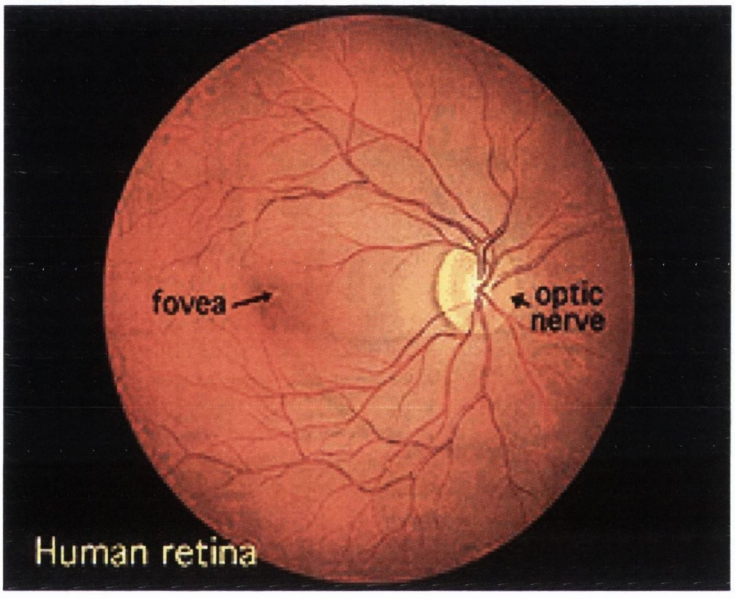

Figure 1.2: Fundus photograph of the living human eye. The central retinal artery and vein are seen as they penetrate the optic disc. The fovea lies at the centre of the macula lutea, and the pigmented area to the left. Picture obtained from http://www.webvision.med.utah.edu.

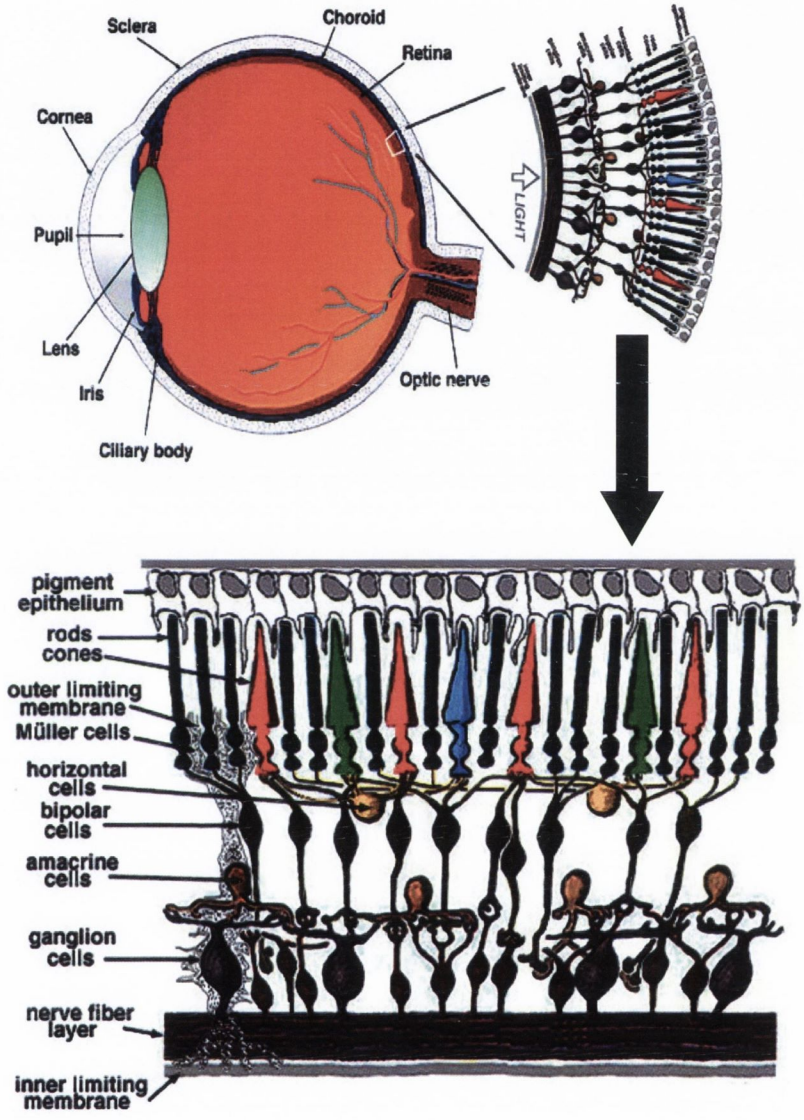

Figure 1.3: A schematic enlargement showing the structural compositions of the retina. Pictures obtained from http://www.webvision.med.utah.edu.

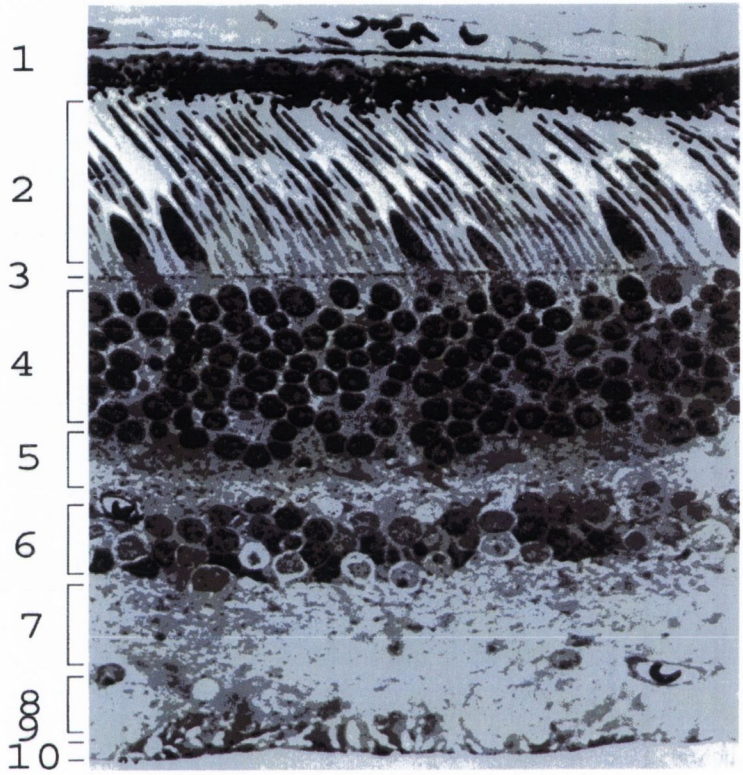

Figure 1.4: Light micrograph of a plastic-embedded retinal section. The layers are designated by numbers: (1) retinal pigment epithelium layer; (2) photoreceptor layer (3) external limiting membrane; (4) outer nuclear layer; (5) outer plexiform layer; (6) inner nuclear layer; (7) inner plexiform layer; (8) ganglion cell layer; (9) nerve fiber layer; (10) internal limiting membrane. (Printed from Remington. Clinical Anatomy Of The Visual System)

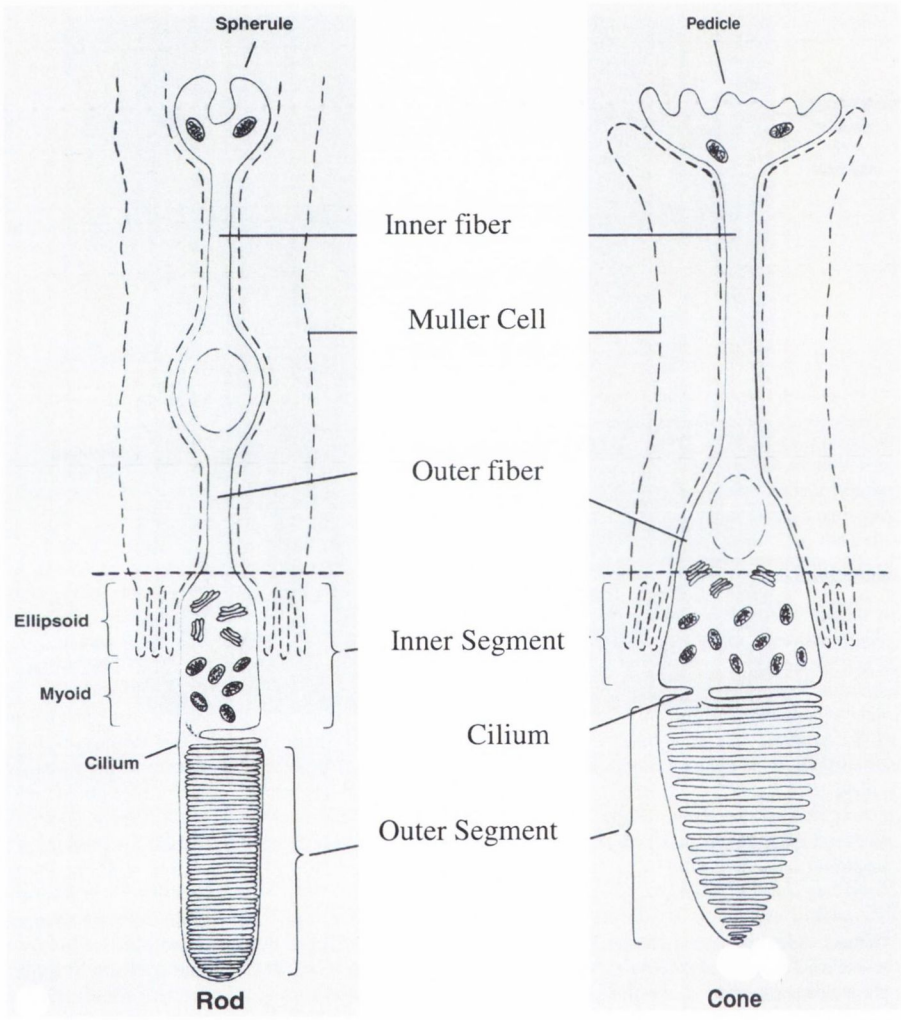

Figure 1.5: Photoreceptor cells (Printed from Remington. Clinical Anatomy Of The Visual System).

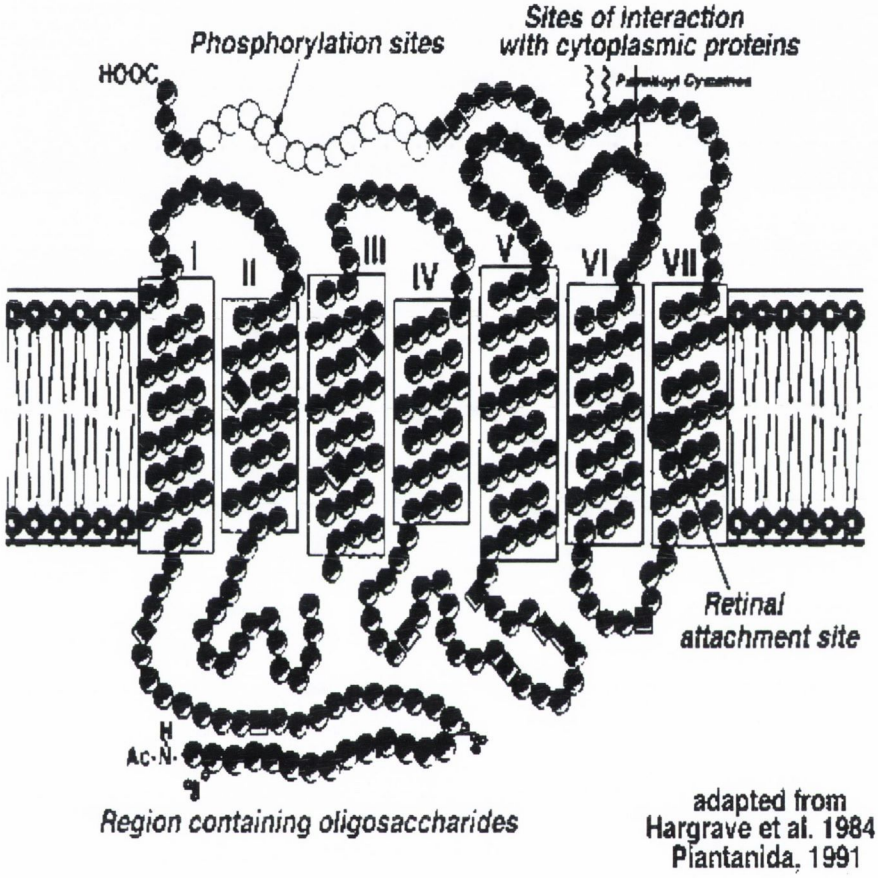

Figure 1.6: A schematic diagram illustrating the structural model of rhodopsin. Diagram obtained from http://www.webvision.med.utah.edu.

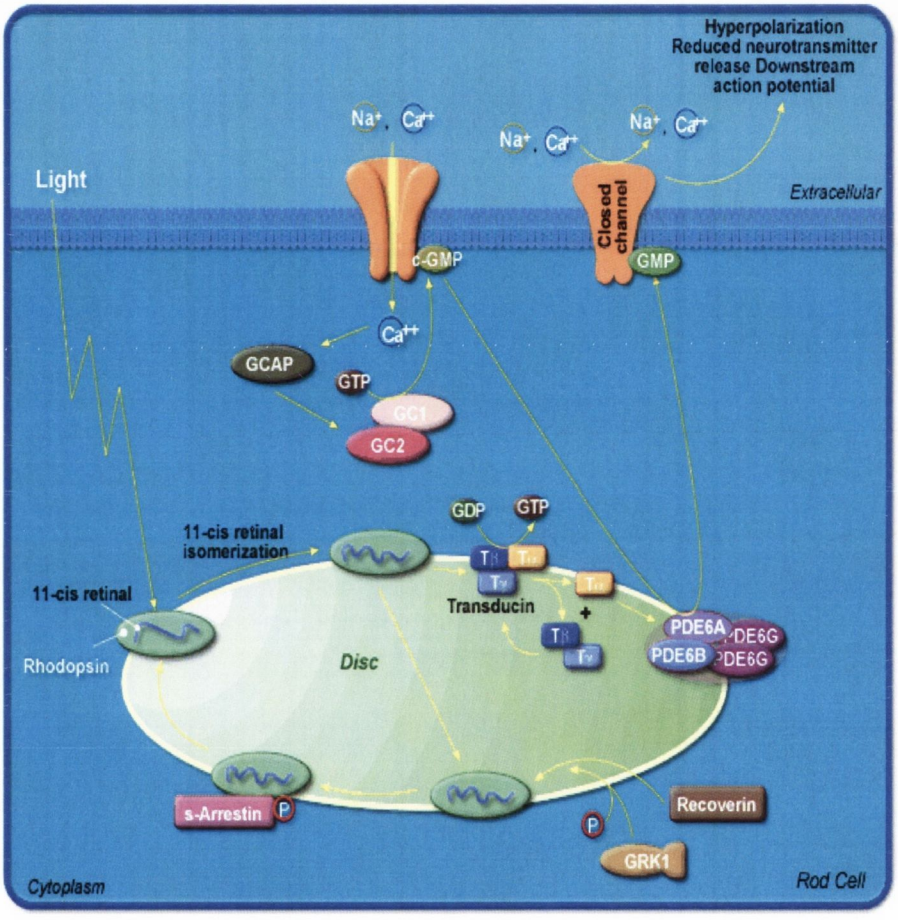

Figure 1.7: Activation of rhodopsin by light and the phototransduction cascade. Diagram obtained from *http://www.biocarta.com/pathfiles/h_rhodopsinPathway.asp.*

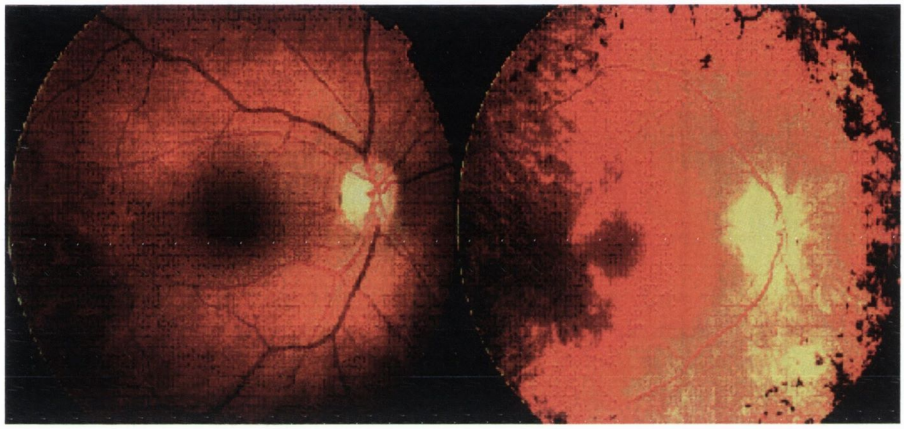

Figure 1.8: A photograph comparing a normal human retina (left) to a RP human retina (right). As can be seen in the RP retina, blood supplies radiating out from the optic disc have almost been demolished, and pigment epithelial thinning and intraretinal pigmentary deposits are also noticeable. (Photograph provided by Dr. Paul F. Kenna. Ocular Genetics Unit. Dept. of Genetics. Trinity College Dublin).

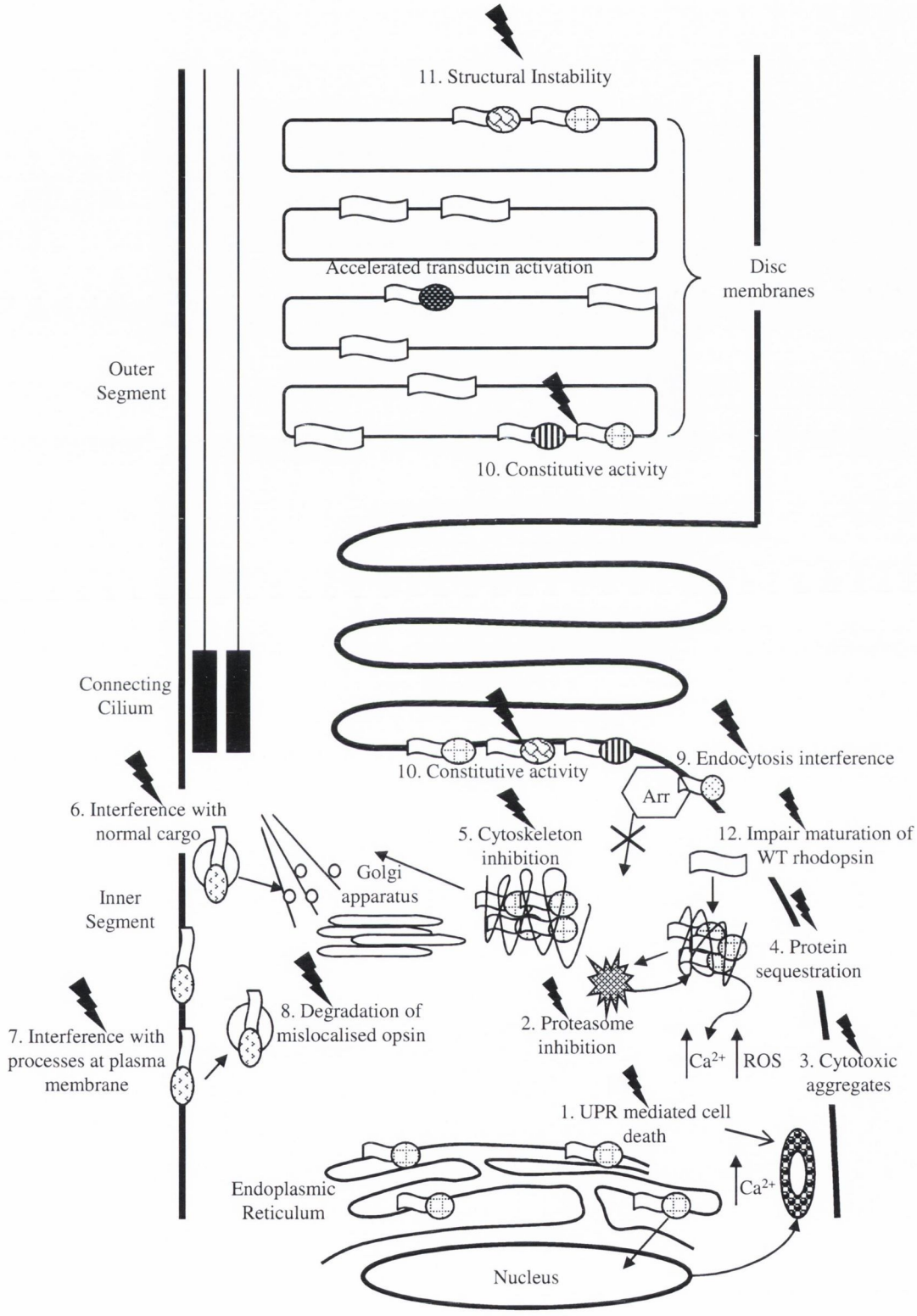
11. Structural Instability
Accelerated transducin activation
Disc membranes
Outer Segment
10. Constitutive activity
Connecting Cilium
10. Constitutive activity
9. Endocytosis interference
Arr
6. Interference with normal cargo
5. Cytoskeleton inhibition
12. Impair maturation of WT rhodopsin
Golgi apparatus
Inner Segment
4. Protein sequestration
8. Degradation of mislocalised opsin
2. Proteasome inhibition
7. Interference with processes at plasma membrane
Ca2+
ROS
3. Cytotoxic aggregates
1. UPR mediated cell death
Endoplasmic Reticulum
Ca2+
Nucleus

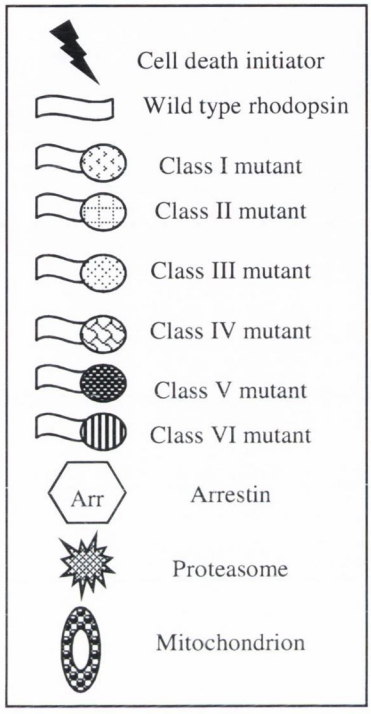

Figure 1.9: A schematic illustration of rhodopsin-mediated cell death pathways. The potential apoptotic pathways are numbered from 1-12; 1. UPR-mediated cell death; 2. Proteasome inhibition by protein aggregates; 3. Build up of cytotoxicity by protein aggregates; 4. Sequestration of photoreceptor proteins by aggregates and inclusions; 5. Aggregates and inclusions inhibition of cytoskeleton function; 6. Disruption of normal vascular traffic 7. Interference with processes at the plasma membrane and synapses; 8. Mislocalised opsin degradation; 9. Interference with normal cellular endocytosis; 10. Constitutive or dysregulated activation; 11. Structural instability of rod opsin in the outer segment; 12. Dominant-negative mechanisms induced by mutant rhodopsin. (Adapted from Mendes *et al.*, 2005)

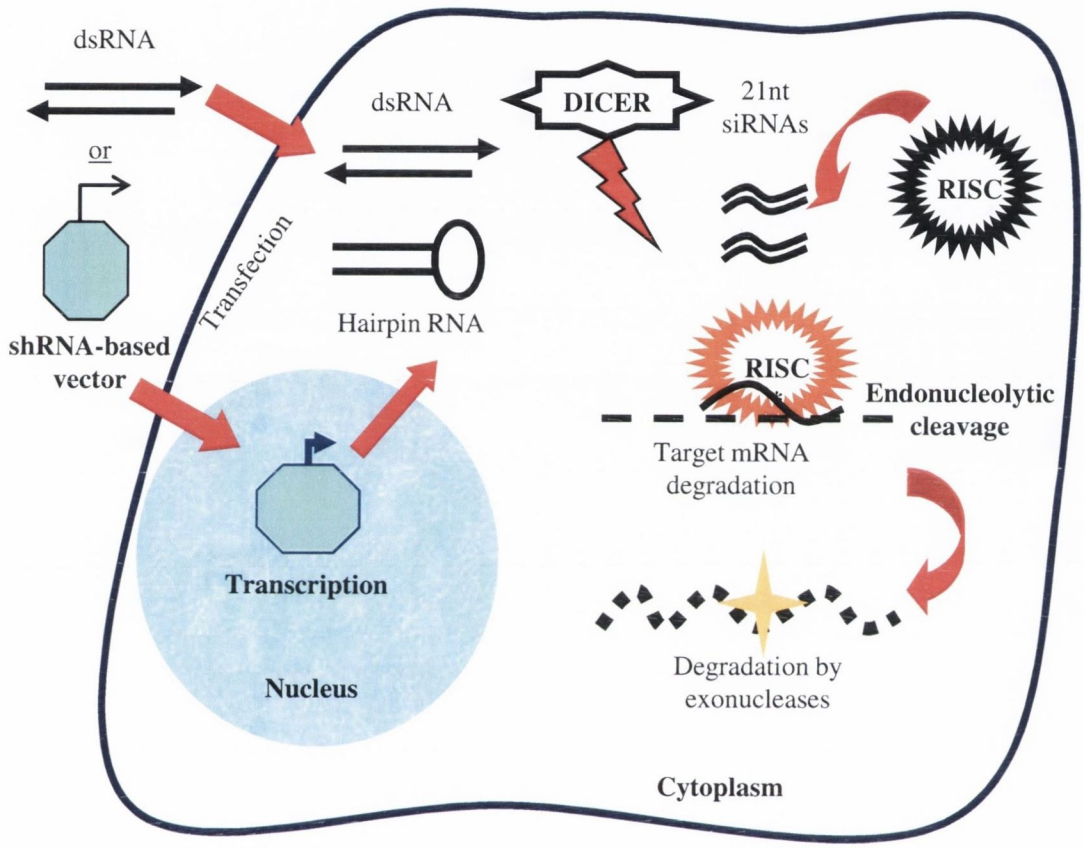

Figure 1.10: Mechanism of RNA interference (RNAi) in mammalian cell systems.

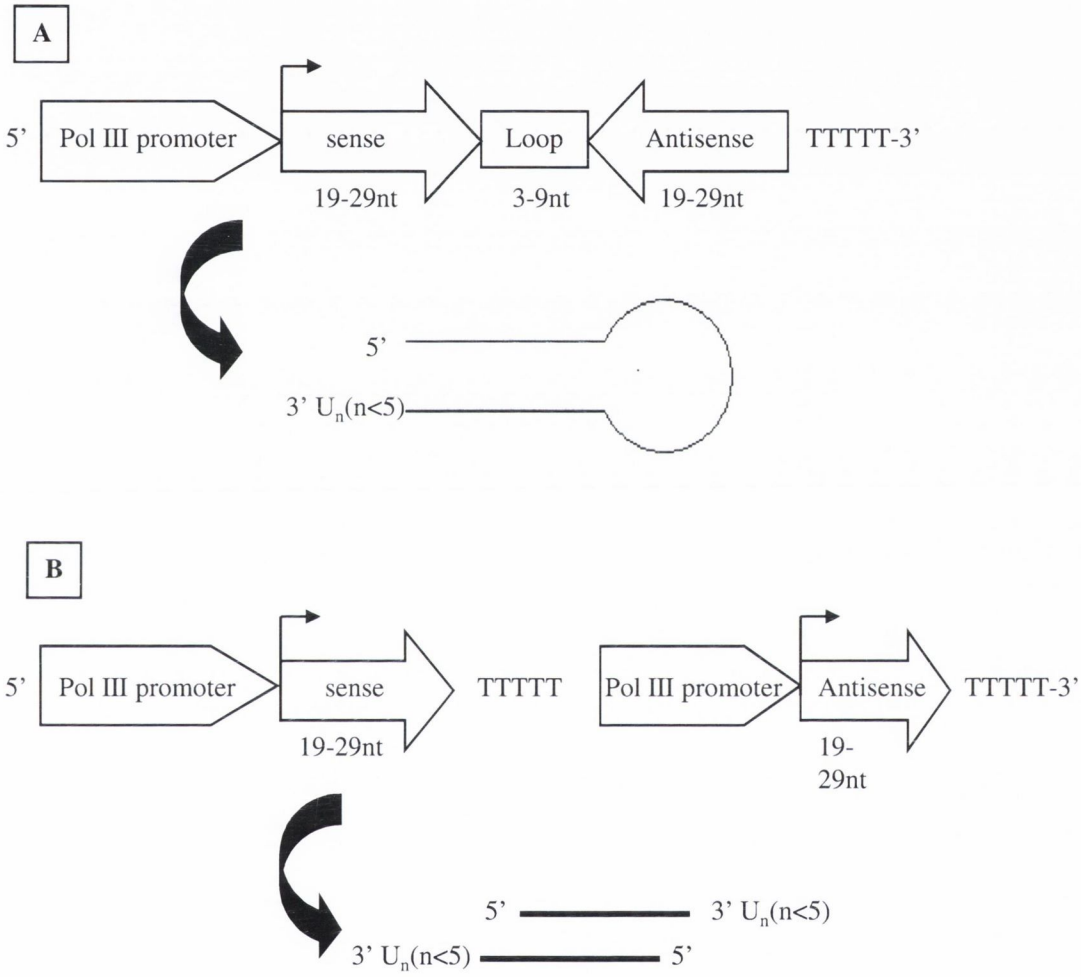

Figure 1.11: The DNA vector-based RNA interference system. (A) Generation of a short hairpin RNA (shRNA) directed by a polymerase III promoter (U6 or H1). (B) Diagrammatic presentation of tandem type vector driven siRNA constructs.

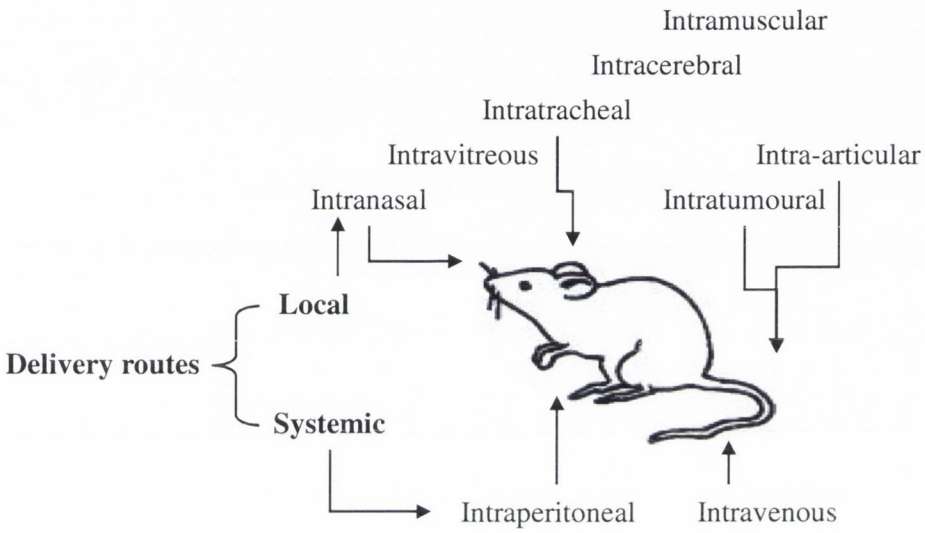

Figure 1.12: The routes of *in-vivo* siRNA delivery into animal models. The choice of delivery routes of siRNA is dependent on disease types and targeted tissues (Xie *et al., 2006).*

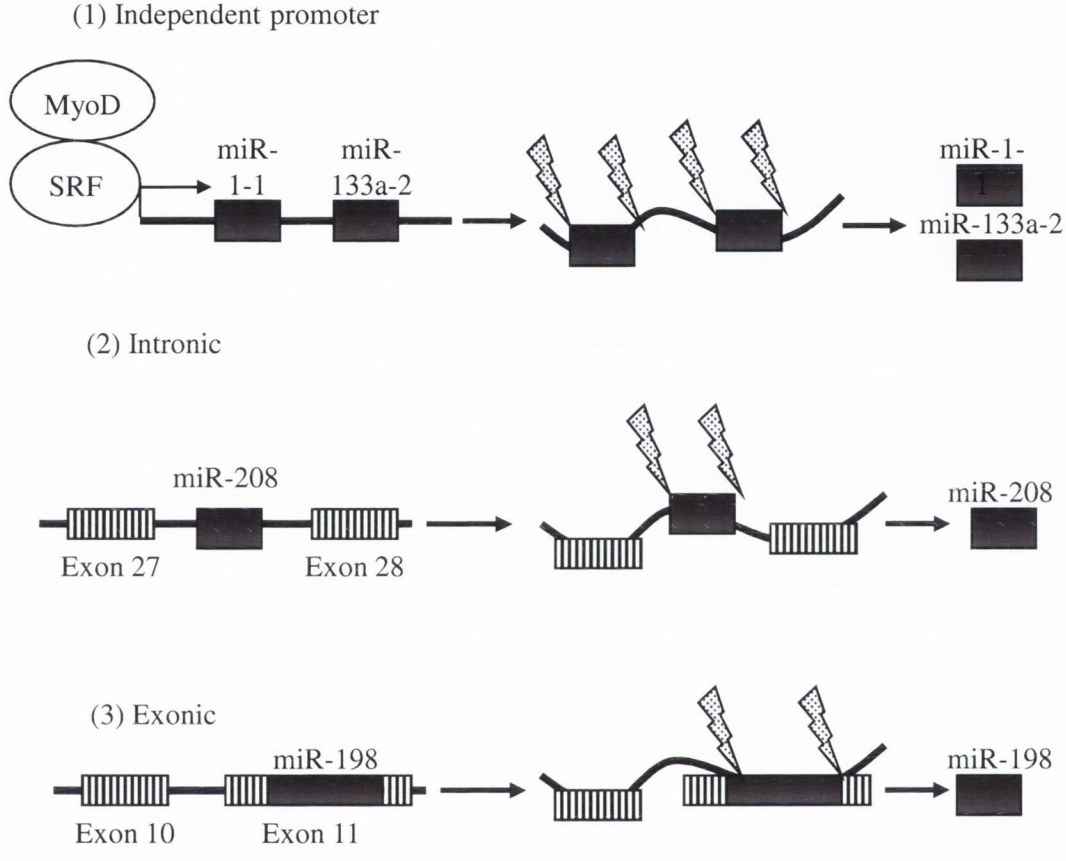

Figure 1.13: Genomic organisation of miRNAs (Zhao *et al.*, 2007). (1) Transcription of miRNAs can be independently regulated by separable promoters, as seen for miR-1-1 and miR-133a-2, which are regulated by the transcription factors SRF and MyoD. (2) Most intronic miRNA precursors have the same orientation as their host gene and are initially transcribed as part of its precursor RNA. miR-208 is expressed specifically in the mouse and human heart, and resides in intron 28 of human cardiac alpha-myosin heavy chain. (3) In exceptional cases, miRNAs that are embedded in or overlap with exons of known transcripts are always in the same orientation, and most of these known transcripts are in the non coding 5' or 3' UTRs (e.g. miR-198 in follistatin-like 1) (Cullen *et al.*, 2004).

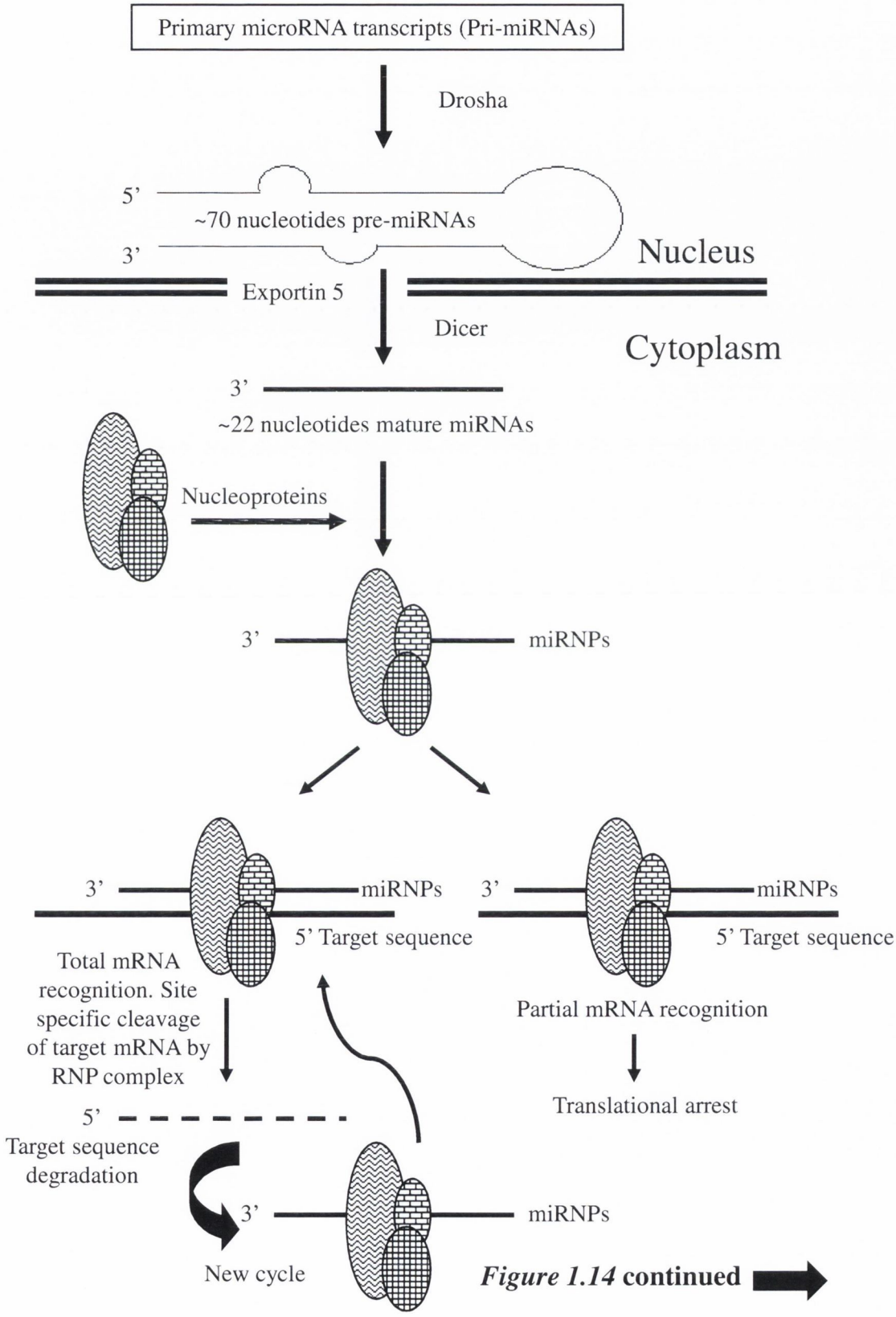

***Figure 1.14* continued**

Figure 1.14: Gene silencing by miRNAs. In the nucleus, miRNAs are initially derived from precursor transcripts that form multiple stems and hairpin structures. The processing of primary transcripts by Drosha yields pre-miRNAs of ~70 nucleotides in length, which are transported to the cytoplasm via Exportin 5. Pre-miRNAs are processed into ~22 nucleotides miRNAs by Dicer, which are then incorporated into ribonucleoprotein (RNP) complex that direct either RNA cleavage or translation arrest depending on the degree of homology between miRNA and target sequence.

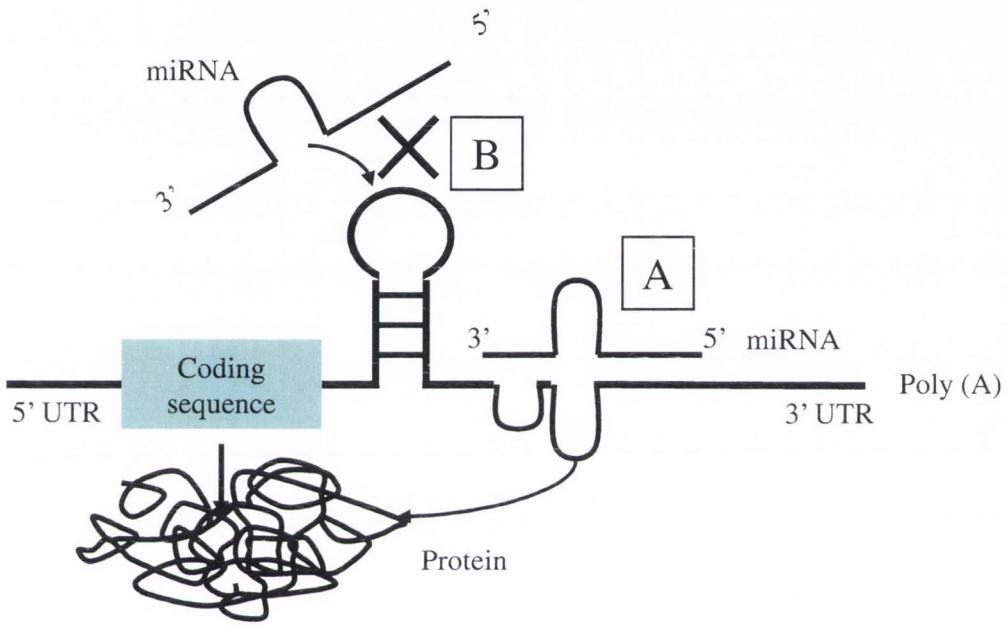

Figure 1.15: Model of miRNA target accessibility (Adapted from Zhao *et al.*, 2007). (A) miRNA binding to target sequence through limited complementarity to repress translation. (B) miRNAs can only access their target sites when they are physically accessible. Despite a high degree of sequence complementarity between miRNA and target mRNA, stem-loop or hairpin structure formed by mRNA may render miRNA inaccessible to its binding site, and thus unable to repress translation.

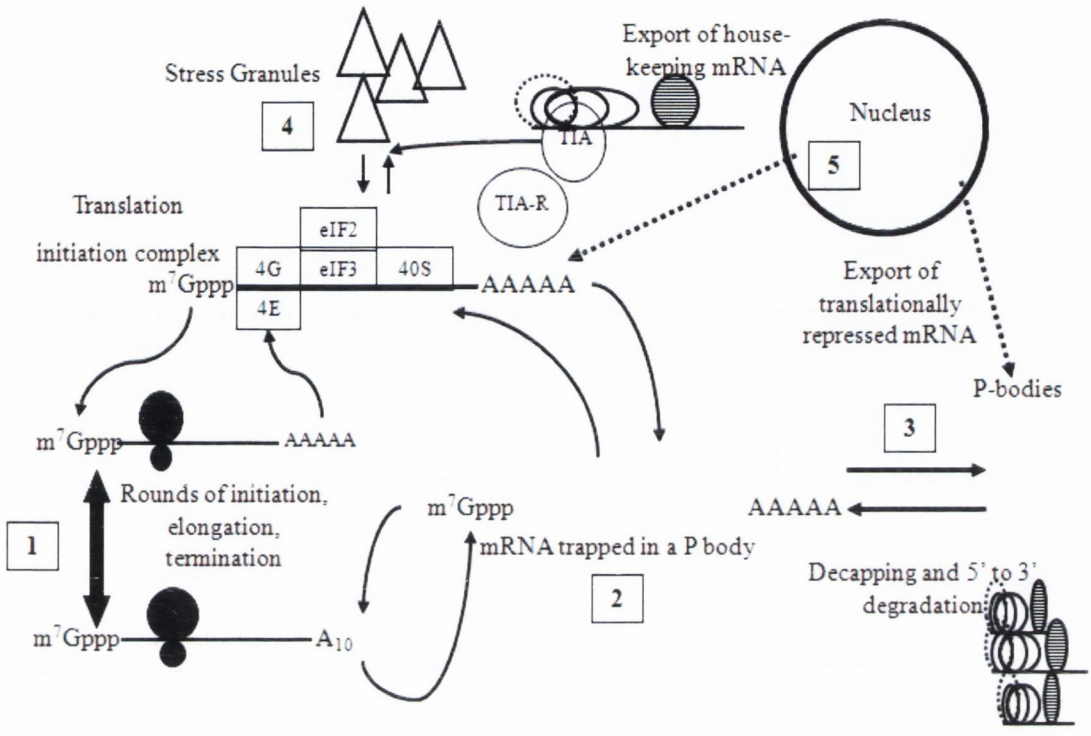

Figure 1.16: The mRNA cycle proposed by Parker and Sheth, 2007. A schematic diagram illustrating the cycling of mRNA through different subcellular compartments. 1) mRNAs present in polysomes may undergo numerous rounds of translation initiation, elongation and termination to produce polypeptides. 2) When defects in translation initiation or termination occurs through mutations or other stress related specific factors, mRNAs localised in polysomes are presented to components of the repression/decay machinery and translation is terminated. Thereby, a mRNA is formed that assembles into P bodies. 3) mRNAs localised with the repression/decay complex can be decapped and degraded by 5' to 3' exonuclease, retained in P-bodies or exit to re-enter translation. 4) When translation is halted, mRNAs may associate with specific factors that promote their accumulation in stress granules. mRNAs localised in stress granules can re-enter translation when conditions improve. 5) Housekeeping mRNAs are exported from the nucleus and enter translation directly. A subset of mRNAs may form a different type of nuclear mRNA that includes proteins targeting the mRNA directly to P-bodies.

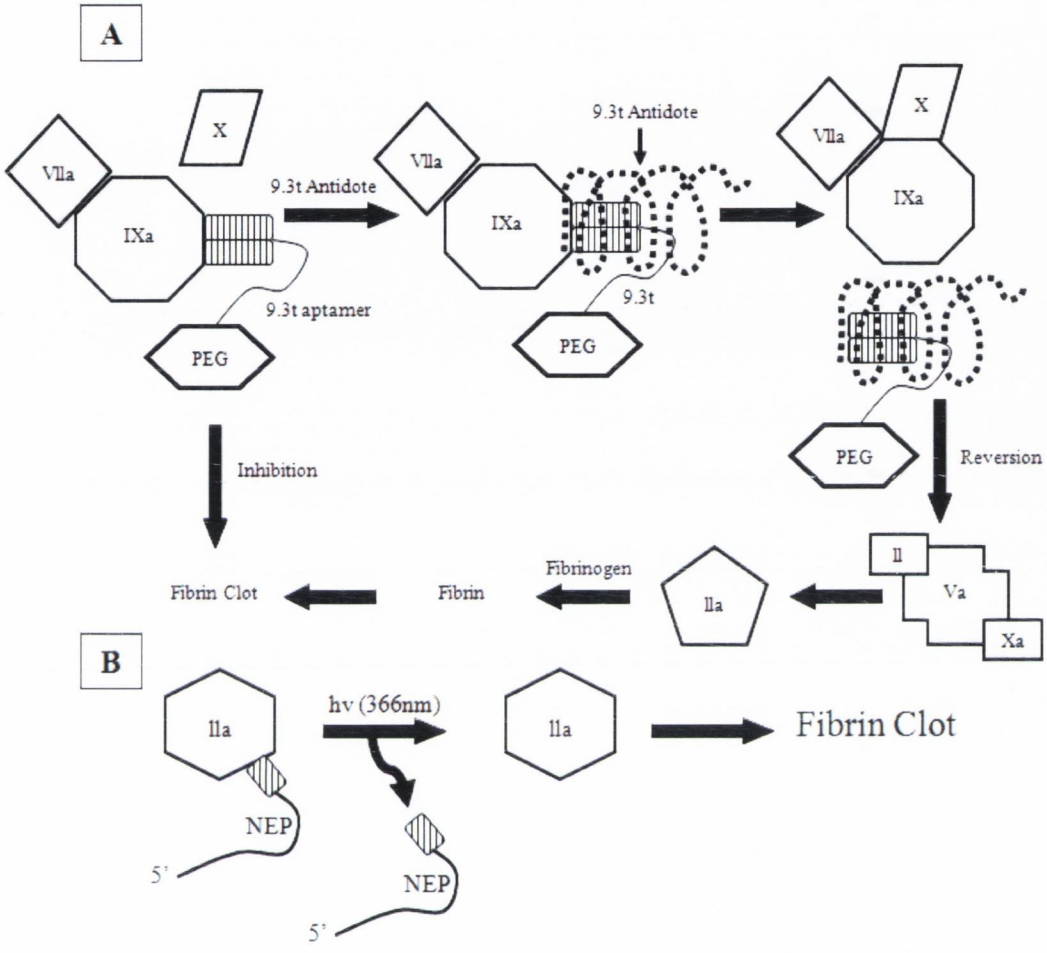

Figure 1.17: (A) The reversal of aptamer activity by a classical antisense oligonucleotide antidote. In brief, fibrin clotting was inhibited upon the formation of an anti-Factor IXa aptamer 9.3t complex. However, when the 9.3t antidote was added, the anticoagulating effect of 9.3t aptamer was abolished and clotting parameters resumed. The 9.3t antidote has been shown to be successful in a porcine systematic anticoagulation model and a murine arterial injury model (Rusconi *et al.*, 2004). (B) An aptamer-caged antidote chimera, containing both an anti-thrombin DNA aptamer and an inactivated 'caged' antisense antidote, blocked fibrin clotting activity. Upon irradiation, the antisense antidote was 'uncaged', inhibiting thrombin aptamer activity to restore normal clotting parameters. NPE = photolabile 1-(2-nitrophenyl)ethyl (Heckel *et al.*, 2006).

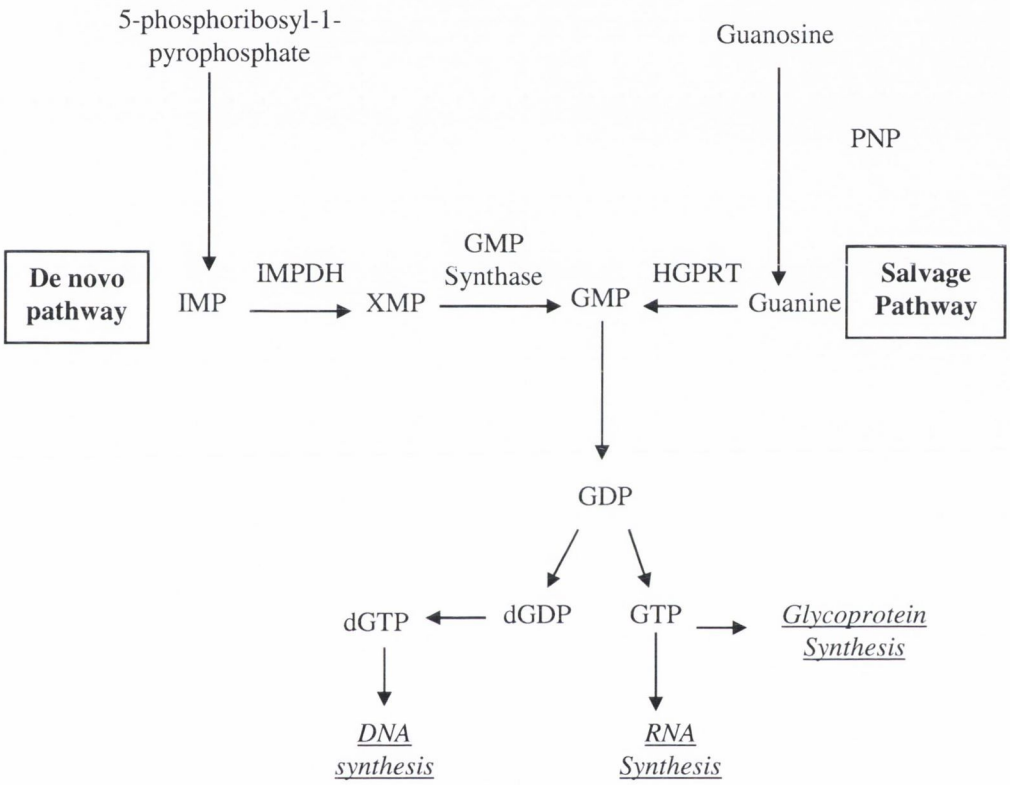

Figure 1.18: Schematic diagram illustrating the *de novo* guanine nucleotide synthesis and salvage pathways of GTP converging on GMP. Enzymes of the *de novo* pathway include inosine 5'-monophosphate dehydrogenase (IMPDH) and GMP synthase, and the salvage pathway involves hypoxanthine guanine phosphoribosyltransferase (HPRT) (Sintchak *et al.*, 2000).

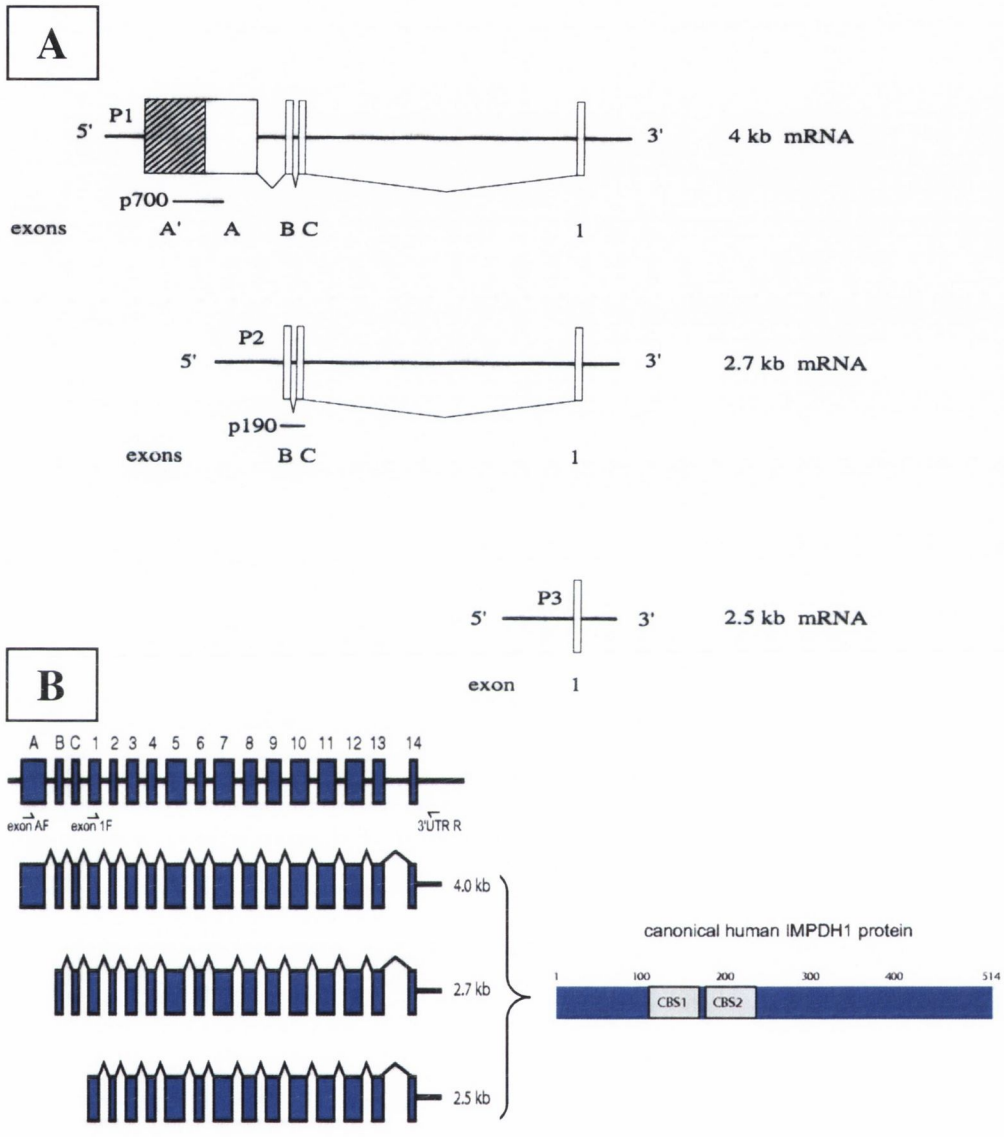

Figure 1.19: (A) Schematic diagrams illustrating the use of alternative promoters for the expression of the three different IMPDH type I transcripts. (B) Schematic diagrams of the genomic structure and the three IMPDH1 transcripts initially reported by Gu *et al.*, 1997.

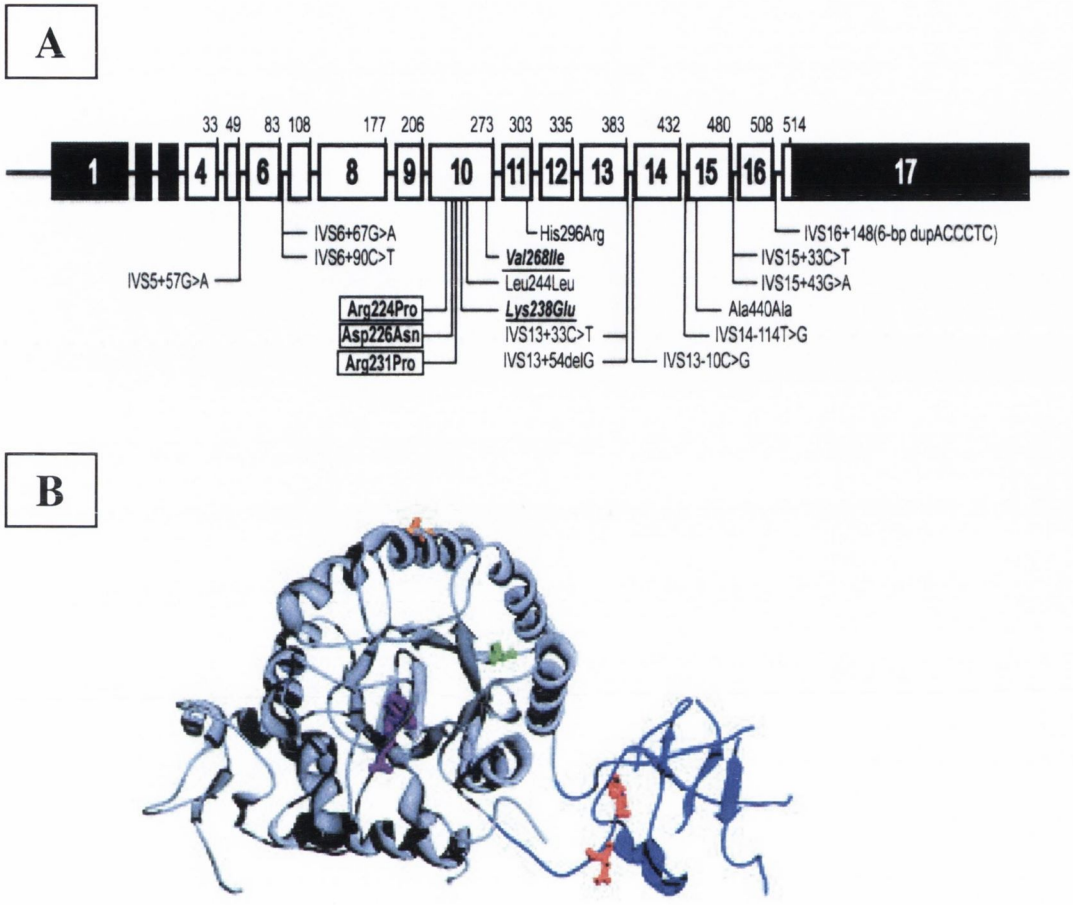

Figure 1.20: (A) A schematic map illustrating the 17 exons of the IMPDH1 gene. All the missense mutations involved in the RP10 form of adRP are shown in their corresponding exonal positions. The mutations in boxes are interpreted as causes of dominant RP, whereas those in italics and underlined are of uncertain pathogenicity. All other changes are interpreted as nonpathogenic rare variants or polymorphisms. Regions of exons in black are the 5' and 3' noncoding regions. The lengths of the exon boxes are in proportion to the lengths of their DNA sequences. At the top right corner of each box for exons 4 to 17 is the number of the codon at the 3' end of that exon (Wada *et al.*, 2005). (B) A monomer of the human IMPDH1 crystal structure (Protein Data Bank code 1JCN). The catalytic domain is shown in grey and the subdomain in blue. Both the Arg224 and Asp226 mutations are shown in red. The Val 268 mutation is shown in green, and the non-pathogenic mutation Ala 285 is shown in orange.

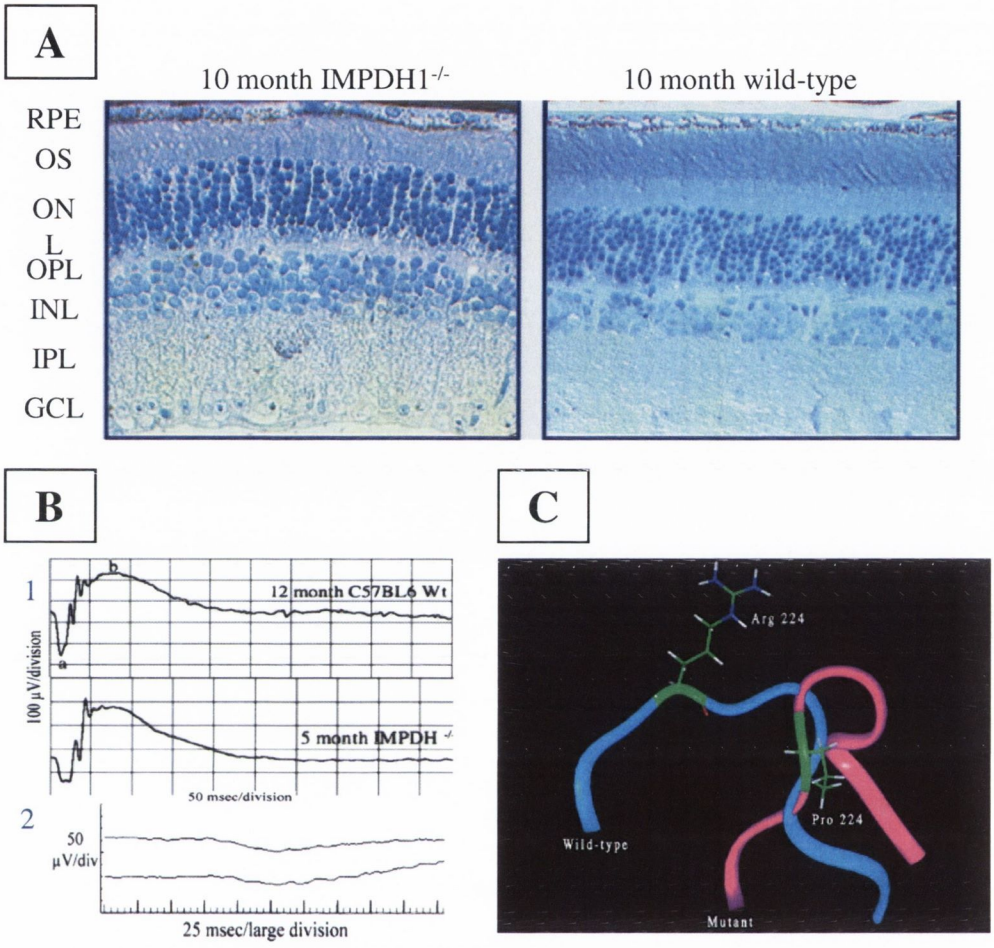

Figure 1.21: (A) Light micrographs of retinal sections. The structure of the outer nuclear layer of a 10-month-old IMPDH1$^{-/-}$ mouse retina is indistinguishable from that of a 10-month-old wild type mouse retina (B) (1) The maximal, dark-adapted, combined rod and cone responses recorded in a 5-month-old IMPDH1-/- mouse (≈ teenage human subject in terms of lifespan) displayed no functional degeneration when compared to a 12-month-old C57 wild-type mouse. (2) The combined rod and cone response in a 17 year old RP10 patient displayed non-recordable photoreceptor activity. (c) Computer modeling of wild type and mutant Arg224Pro IMPDH1 proteins. Mutant IMPDH1 protein exhibits significant structural perturbation near the region of the Arg224Pro mutation (pink) when compared to wild type protein (blue). Diagrams were obtained from Aherne *et al.*, 2004.

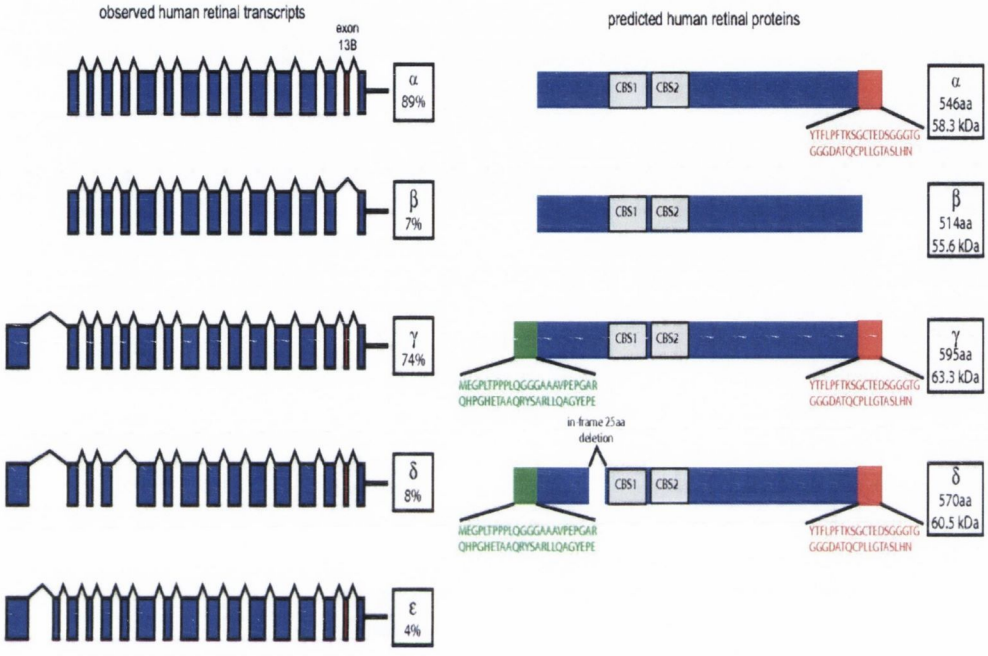

Figure 1.22: Schematic diagrams illustrating novel human IMPDH1 transcripts and proteins determined by Bowne *et al.*, (2006a). Transcript α is generated by splicing from exon 1 through to exon 13 and includes exon13b, thus giving rise to protein α containing additional amino acids in the C-terminal. Protein β represent the original IMPDH1 isoform identified by *Gu et al.*, (1997). Transcripts γ and δ are both directly spliced from exon A to 3'UTR and includes exon 13b, but with the latter lacking exon 4 which causes an in-frame deletion of 75 bp and 25 amino acids. The inclusion of exon C in transcript ε results in a premature stop codon that is predicted to undergo non-sense mediated decay only if the initiation codon in exon A is used. Green represents novel protein regions in exon A and red represents additional amino acids resulting from the inclusion of exon 13b. Transcript percentages reflect results of separate subcloning experiments.

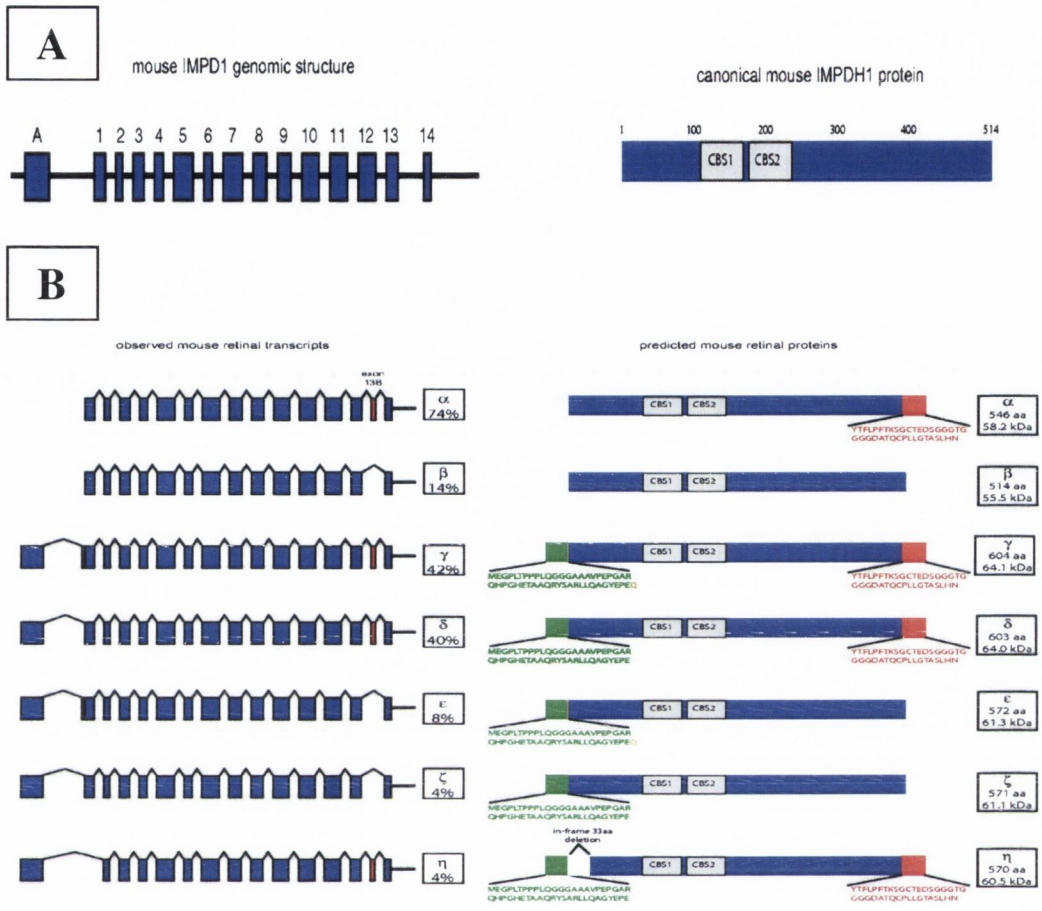

Figure 1.23: Mouse IMPDH1 transcripts and proteins identified by Bowne *et al.,* (2006a). (A) Genomic structures of mouse IMPDH1transcript and protein. In contrast to human, mouse does not possess an IMPDH1 exon B or exon C. (B) Mouse retinal IMPDH1 transcripts and protein isoforms predicted by sequence analysis and western blot analysis. Transcript α is spliced from exon 1 to 3'UTR with the inclusion of exon 13b, which results in an alteration of the C-terminus of the protein similar to the product of the equivalent human transcripts. Transcript β is similar to transcript α, but without the presence of exon 13b. Transcripts γ and δ are spliced from exon A to 3'UTR with the inclusion of exon 13b. The only difference is that transcript γ includes an additional 3 base pairs in 5' of exon 1, which results in an addition of one amino acid. Transcript ε is similar to transcript γ ,but without exon 13b. Transcript ζ is spliced from exon A to 3'UTR and exclude exon 13b, whereas transcript η is spliced from exon A to 3'UTR, but excludes exon 1, which results in an in-frame deletion of 33 amino acids encoded by exon 1. Orange denotes the additional amino acid caused by the inclusion of 3 bp 5' of exon 1. Green represents novel protein regions in exon A and red represents additional amino acids resulting from the inclusion of exon 13b. Transcript percentages reflect results of separate subcloning experiments.

Genes involved in Retinitis Pigmentosa	Inheritance pattern
Phototransduction cascade	
Rhodopin, RHO (G-protein coupled photon receptor)	Dominant, recessive
PDEA6B, rod cGMP phosphodiesterase β-subunit (G-protein effector enzyme)	Recessive
PDEA6A, rod cGMP phosphodiesterase α-subunit (G-protein effector enzyme)	Recessive
CNGA1, rod cGMP gated cation channel α-subunit	Recessive
CNGB1, rod cGMP gated cation channel β-subunit	Recessive
SAG, arrestin (rhodopsin deactivation)	Recessive
Vitamin A metabolism	
ABCA4, ATP-binding cassette protein A4 (photoreceptor disc membrane flippase for vitaminA)	Recessive
RLBP1, retinaldehyde binding protein (11-cis-retinaldehyde carrier)	Recessive
RPE65 (vitamin A trans-cis isomerase)	Recessive
LRAT, lecithin retinal acetyltransferase (synthesis vitamin A esters)	Recessive
RGR, RPE vitamin A G-protein coupled receptor (photon receptor in RPE)	Recessive
Structural or cytoskeletal	
RDS, peripherin (outer disc segment membrane protein)	Dominant, digenic
ROM1, rod outer segment protein	Digenic
FSCN2, fascin (actin bundling protein)	Dominant
TULP1, tubby like protein 1	Recessive
CRB1, crumbs homologue	Recessive
RP1, microtubule associated protein	Dominant, recessive
Signalling, cell-cell interaction, or synpatic interaction	
SEMAA, semaphorin B, transmembrane immune system protein	Dominant
CDH23, caherin 23	Recessive
PCDH15, protocadherin 15	Recessive
USH1C, Usher's syndrome type 1C	Recessive
USH2A, Usher's syndrome type IIA	Recessive
MASS1, monogenic audiogenic seizure susceptibility 1	Recessive
USH3A, Usher's syndrome type IIIA	Recessive
RP2, plasma membrane associated protein	X-linked
RNA-intron-splicing factors	
PRPF31, precursor mRNA-processing factor 31 (spliceosome component)	Dominant
PRPF8, precursor mRNA-processing factor 31 (spliceosome component)	Dominant
PRPF3, precursor mRNA-processing factor 31 (spliceosome component)	Dominant
RP9, PIM1-associated protein (RNA-splicing factor)	Dominant

Trafficking of intracellular proteins	
MYO7A, myosin 7A (melanosome motility protein)	Recessive
USH1G, scaffold protein containing ankyrin repeats and SAM domain (Usher's type I protein traffic regulator)	Recessive
Maintenance of cilia/ciliated cells	
BBS1, Bardet-Biedl syndrome 1	Recessive
BBS2, Bardet-Biedl syndrome 2	Recessive
ARL6, ADP-ribosylation factor like 6	Recessive
BBS4, Bardet-Biedl syndrome 4	Recessive
BBS5, Bardet-Biedl syndrome 5	Recessive
MKKS, McKusick-Kaufman syndrome	Recessive
BBS7, Bardet-Biedl syndrome 7	Recessive
TTC8, tetratricopeptide hormone-responsive B1 gene	Recessive
RPGR, trafficking of proteins in the cilia	X-linked
pH regulation (choriocapillaries)	
CA4, carbonic anhydrase IV (carbon dioxide/ bicarbonate balance)	Dominant
Phagocytosis	
MERTK, mer tyrosine kinase proto-oncogen (RPE receptor involved in outer segment phagocytosis)	Recessive
Other	
CERKL, ceramide kinase-like (ceramide converting enzyme)	Recessive
IMPDH1, inosine 5'-monophosphate dehydrogenase type 1 (guanine nucleotide synthesis)	Dominant
BBS10, vertebrate-specific chaperonin-like protein	Recessive

Table 1.1: Identified genes responsible for retinitis pigmentosa and functions of their protein products (Hartong *et al.*, 2006).

Classification	Characteristics	Location of point mutation	Protein Misfolding
Class I	Fold normally but are not transported to the outer segment	L328, T342, Q344, V345, A346, P347	No
Class II	Retained in the endoplasmic reticulum and cannot reconstitute with 11-cis-retinal	T17, P23, G51, T58, V87, G89, G106, C110, L125, A164, C167, P171, Y178, E181, G182, C187, G188, D190, H211, C222, P267, S270, K296	Yes
Class III	Affect endocytosis	R135	No
Class IV	Major effects on rod-opsin stability and post-transcriptional modification	T4	No
Class V	Increased activation rate for transducin	M44, V137	No
Class VI	Increased activation rate of opsin in the absence of chromophore and in the dark	G90, T94, A292	No

Table 1.2: A classification of known mutations in rhodopsin (Mendes *et al.*, 2005)

Core components	Function	Organisms
Dcp1p/DCAP-1	Decapping enzyme subunit	Yeast, Worm, Fly, Human
Dcp2p/DCAP-2	Catalytic subunit of decapping enzyme	Yeast, Worm, Fly, Human
Dhh1p/Me31B/RCK/p54	DEAD box helicase required for translational repression, decapping activator	Yeast, Fly, Human
Pat1p	Decapping activator and translation repressor	Yeast, Fly
Lsm1-7p	Sm-like proteins involved in decapping	Yeast, Human
Xrn1p	5' to 3' exonuclease	Yeast, Mouse, Human
Edc3p	Decapping activator	Yeast, Fly, Human
Hedls/Ge-1	Component of mammalian decapping complex	Human
Scd6p/CAR-1/RAP55	Protein containing Sm-like and FDF domain; involved in translation repression	Yeast, Worm, Human
Ccr4p/Pop2p/Not1-5p	Major cytoplasmic deadenylase	Yeast, Human
Additional components of P-Bodies: miRNA Repression Factors		
Argonautes/ALG-1	miRNA/siRNA silencing	Worm, Fly, Human
GW 182/AIN-1	Autoantigen containing multiple GW repeats, miRNA/siRNA silencing	Worm, Human
TNRB6B	Paralog of GW182, miRNA/siRNA silencing	Human
MOV10	DEAD box helicases, miRNA/siRNA silencing	Human
RNA-binding proteins and translation repressors		
Spb1p	Facilitates mRNA decapping	Yeast
CPEB	Cytoplasmic polyadenylation element binding protein, translational regulator	Human
Staufen	RNA-binding protein	Fly
Rbp1	RNA-binding protein, localises P bodies during cellular stress	Yeast
TTP	AU-rich element-binding prtoein observed in P bodies when overexpressed	Human
eIF4E	CAP-binding protein, regulates translation	Human
eIF4-T	eIF4E-binding protein, translation repressor	Human
Germin5	translation repressor	Human
Proteins involved in NMD		
Upf1p	ATP-dependent helicase required for NMD, accumulates in yeast P bodies in dcp1Δ xrn1Δ,dcp2Δ and upf3Δ strains, accumulates in mammalian P bodies when SMG7 is overexpressed	Yeast, Human
Upf2p	Component required for NMD, accumulates in P bodies in dcp1Δ dcp2Δ and xrn1Δ mutants	Yeast
Upf3p	Component required for NMD, accumulates in P bodies in dcp1Δ, dcp2Δ and xrn1Δ in yeast	Yeast
SMG-7	Factor required for phosphorylation of UPF1, accumulates in P bodies when overexpressed	Human
SMG-5	Factor required for phosphorylation of UPF1, accumulates in P bodies when SMG7 is overexpressed	Human
Proteins affecting Viral Function		
APOBEC3G, APOBEC3F	Antiviral host factos with deoxycytidine deaminase activity	Human
Vif	APOBEC3 inhibitor, accumulates in P bodies when APOBEC3G is overexpressed	Human
PKR	dsRNA dependent protein kinase, accumulates in P bodies when HPV E6 protein is expressed	Human
Miscellaneous		
FAST	FAS-activated serine/threonine phosphoprotein	Human
Dsc2p	Nutrient stress-dependent regulator of the scavenger enzyme Dcs1	Yeast
Rpb4p	Subunit of RNA polmerase II	Yeast

Table 1.3: P-bodies compositional components (Parker and Sheth, 2007).

Aptamers	Targets	Developer	Clinical Trial Developments
Pegaptanib (Macugen)	VEGF/ AMD	Eyetech (ISIS pharmaceuticals)	FDA approved (2004)
Edifoligide (E2F/, CABG surgery)	E2F/ CABG surgery	Anesiva (San Francisco, CA, USA)	No improvement over placebo in Phase III
Avrina (NF-κB decoy)	NF-κB/ eczema	Anesiva (San Francisco, CA, USA)	Phase III
AS1411	Nucleolin/ anticancer	Antisoma (London, UK)	Phase I/II
REG1	FIX/ anticoagulation	Regado Biosciences (Durham, NC, USA)	Phase I completed
ARC183	Thrombin/ anticoagulation	Archemix (Cambridge, MA, USA)	Phase I completed not in development
NU172 (ARC2172)	Thrombin/ anticoagulation	Nuvelo/ Archemix (San Carlos, CA/ Cambridge, MA, USA)	Pre-clinical

Table 1.4: Aptamers currently in the clinical pipeline (Que-Gewirth *et al.*, 2007).

Chapter 2
Materials and Methods

2. Materials and Methods

2.1 General materials and reagents

2.1.1 Materials and reagents used for general molecular cloning procedures

(i) Agarose gel: Agarose powder w/v (Sigma-Genosys, Pampisford, Cambridgeshire, UK) was weighed out depending on percentage gel required and dissolved in 1X Tris-acetate-EDTA (TAE) buffer.

(ii) Antibiotics: Ampicillin, Tetracycline and Kanamycin were supplied by Sigma-Aldrich, Stenheim, Germany.

	Stock Concentrations (mg/ml)	Final working concentrations (μg/ml)
Ampicillin	100	100
Tetracycline	10	25
Kanamycin	50	50

(iii) β-galactosidase staining solution (pH7.2): 5 mM potassium ferricyanide, 2 mM $MgCl_2$, 0.02% NP-40 and 0.01% SDS. 1 mg/ml X-gal (added prior to use).

(iv) DNA kits: EndoFree Plasmid Maxi-prep Kit, Qiaquick Gel Extraction Kit, Qiaquick PCR Purification Kit, RNeasy Mini Kit and Big Dye Terminator v3.1 Cycle Sequencing kits were purchased from Applied Biosystems were supplied by Qiagen, Hilden, Germany.

(v) DNA Loading Buffer is made up of 0.25% Bromophenol blue, 0.25% Xylene cyanol and 30% Glycerol. Ethidium Bromine was added to a final concentration of 0.5 ug/ml

(vi) DNA oligonucleotides were supplied by Sigma-Genosys (Pampisford, Cambridgeshire, UK), and resuspended in the appropriate volume with nuclease free water at a final concentration of 100 μM.

(vii) EDTA 0.5 M at pH 8.0: 93.6 g of disodium ethylenediaminetetra-acetate·$2H_2O$ was added to 400 ml ddH_2O. The pH was adjusted to pH 8.0 with NaOH and the final volume was made up to 500 ml with ddH_2O.

(viii) Luria-Bertani medium (LB medium): 10 g Tryptone (Oxoid Ltd, Basingstoke, Hampshire, UK) , 5 g Yeast (Oxoid Ltd., Basingstoke, Hamsphire, UK), 10 g NaCl (Scharlau Chemie, S.A., Barcelona, Spain) → made up to 1 L with ddH_2O and autoclaved at 15 lbs pressure for 20 min.

(ix) Lysozyme (10 mg/ml) was supplied by Sigma-Aldrich Chemical Corporation, Stenheim, Germany.

(x) Gel Loading Dye: 0.25% Bromophenol Blue, 0.25% Xylene Cyanol, 30% w/v glycerol → made up to 6X

(xi) Molecular weight markers: 100 bp and 1 kb ladders were supplied by New England Biolabs, Frankfurt, Germany.

(xii) M-Stet Buffer: 5% Triton X-100, 50 mM EDTA pH 8.0, 100 mM Tris pH 5.0, 5% sucrose.

(xiii) Nuclease-free water was obtained from Ambion, Huntingdon, UK.

(xiv) PCR buffers: 10X PCR Buffers – 500 mM KCL, 100 mM TrisCl (pH 8.8), 0.1% gelatine & 1% Triton (pH 9.0) supplemented with either 5mM, 10mM, 15 mM or 20 mM $MgCl_2$. dNTP mix (Roche, West Sussex, UK) 10 µl of dATP, dTTP, dCTP and dGTP in 160 µl dH_20 were added to PCR reaction to give a final concentration of 1.25 mM.

(xv) Plasmid mini-preparation Resuspension Buffer: 50 mM Tris pH 5.0 dissolved in 25% w/v sucrose.

(xvi) Restriction enzymes and corresponding buffers were supplied by New England Biolabs, Frankfurt, Germany.

(xvii) Sodium dodecyl sulfate (SDS) 10%: 100 g of electrophoresis-grade SDS was dissolved in 900 ml of ddH_2O and heated to 68°C. The pH was adjusted to 7.2 with concentrated HCl and the final volume was adjusted to 1 Litre with ddH_2O.

(xviii) Taq DNA polymerase, Pfu Turbo DNA polymerase, T4 DNase ligase and RNaseIT were supplied by Stratagene, La Jolla, CA, USA.

(xix) Tris-acetate/ EDTA electrophoresis buffer (50X TAE): 242 g Tris Base, 57.10 ml glacial acetic acid, and 100 ml 0.5 M EDTA pH 8.0, made up to 1 L with ddH_2O.

(xx) Vectors: pcDNA3.1(+) was obtained from Invitrogen. EGFP-1 was provided by Clontech. EGFP1 with a CMV promoter was kindly provided by Dr. A. Palfi*. pBluescript+H1 promoter vector was kindly provided by Dr. A-S Kiang* (*Department of Genetics, Trinity College Dublin).

(xxi) X-Gal stock solution: 40 mg/ml X-gal dissolved in DMSO

2.1.2 Materials and reagents for Tissue Culture

(i) 10 ml/ 25 ml pipettes, 6-well/ 24-well flat bottom tissue culture plates were obtained from Sarstedt Ltd, Nümbrecht, Germany.

(ii) DNase enzyme and buffer were obtained from Promega, Madison, WI, USA.

(iii) Freezing Medium: 2 ml Fetal Calf serum (FCS), 1 ml Dimethyl sulfoxide (DMSO), 2 ml $DMEM^{+}$.

(iv) Lipofectamine 2000® was obtained from Invitrogen, Paisley, UK.

(v) Mammalian cell lines: Human embryonic kidney cells (HEK293T; ATCC Number: CRL-1573), HeLa cells (ATCC Number: CCL-2) and N2a cells (mouse neuroblastoma cells; ATCC Number: CCL-131) were obtained from The American Type Culture Collection.

(vi) Opti-MEM I (serum-free medium) was obtained from Gibco-Invitrogen, Paisley, UK.

(vii) Tissue culture solutions: Dulbecco's modified Eagle medium (D-MEM), fetal calf serum (FCS), 1% L-glutamine, sodium pyruvate, trypsin-EDTA, phosphate buffered saline (PBS, pH 7.2), Hank's balanced salt solution (HBSS) were obtained from BioWhittaker, Cambrex, Bioscience, Verviers, Belgium. $DMEM^{+Abs}$ supplemented with 10% fetal calf serum (FCS), 1% L-gluatamine (2 mM), sodium pyruvate (2 mM) and 1% streptomycin/penicillin, whereas DMEM medium without antibiotics was regarded as $DMEM^{-Abs}$.

2.1.3 Materials and reagents for RNA study

(i) RNeasy Mini Kit (50) was obtained from Qiagen, Hilden, Germany.

(ii) RNase Away was obtained from Invitrogen, Paisley, UK.

(iii) QuantiTech™ Sybr Green RT-PCR reaction kit was obtained from Qiagen, Hilden, Germany.

(iv) Trizol Reagent was supplied by Molecular Research Center, Cincinnati, OH, USA.

2.1.4 Materials and reagents for protein study

(i) All IMPDH1 and IMPDH2 primary antibodies were kindly provided by Dr Sara J. Browne (*Human Genetics Centre, School of Public Health, University of Texas HSC, Houston, TX 77030, USA*). Refer to Bowne *et al.*, (2006a) for information regarding the generation of IMPDH1 and IMPDH2 antibodies.

- Rabbit polyclonal anti-N-IMPDH1 JK010305 (1.68 mg/ml) was designed to recognise canonical IMPDH1 residues 38-50 (Peptide sequence: GFIDFIAFEVDLT). This antibody was diluted at 1:7000 with Blocking buffer prior to use.
- Rabbit polyclonal anti-N-IMPDH2 JK010306 (2 mg/ml) was designed to recognise IMPDH2 residues 38-50 (Peptide sequence: GYIDFTADQVDLT). This antibody was diluted at 1:6000 with Blocking buffer prior to use.
- Rabbit polyclonal anti-β-actin (batch dependent 0.2-0.2 mg/ml) was diluted at 1:5000 with Blocking buffer prior to use (Abcam ab8227)

Secondary Antibodies

- Goat polyclonal to Rabbit IgG H&L conjugated with Horse-Radish Peroxidase (2 mg/ml) was obtained from Abcam (Cambridge, UK), and diluted at 1:5000 with Blocking buffer prior to use.

(ii) BCA Protein Assay Kit and Bovine Serum Albumin standards at a final concentration of 2mg/ml were supplied by Pierce, IL, USA.

(iii) Biotinylated Protein Ladder Detection Pack was obtained from Cell Signalling Technology, Danvers, MA, USA.

(iv) Blocking buffer solution (5% skimmed milk TBST): 5% non-fat dried skimmed milk (Marvel), 1X TBS, 0.05% Tween-20.

(v) Coomassie Blue staining solution (Sigma-Aldrich, Stenheim, Germany): 0.1% (w/v) Coomassie Blue R350, 20% (v/v) methanol, 10% (v/v) acetic acid, and brought to a final volume of 1 Litre with dH_2O.

(vi) Commassie Blue destaining solution: 100 ml acetic acid, 400ml methanol and made up to 1 Litre with dH_2O.

(vii) FUGI Medical Super RX X-ray film (18 x 24 cm) (Duesseldorf, Germany)

(viii) Nitrocellulose membrane was supplied by Schleicher and Schuell, Dassel, Germany.

(ix) Protease Inhibitors: Complete Mini-Protease Inhibitor Cocktail was obtained from Roche Diagnostics, West Sussex, UK.

(x) Protein Lysis Buffer: 50 mM Tris (pH7.5), 150 mM NaCl, 1% Nonidet P-40 (Sigma), 0.5 mM EDTA, 0.1% SDS, and 1 protease inhibitor cocktail tablet per 10 ml Protein Lysis Buffer (Roche Diagnostics, West Sussex, UK).

(xi) Protein Marker: Kaleidoscope pre-stained Protein Ladder was supplied by Bio-Rad Laboratories, Munich, Germany.

(xii) Protein SDS-Loading Buffer (5X): 0.5% (w/v) bromophenol blue, 10% (w/v) SDS, 50% glycerol, 250mM Tris-HCl pH6.8, 500 mM DTT and 5% β-mercaptoethanol.

(xiii) <u>Resolving gel for SDS-PAGE electrophoresis (10%)</u>

1.5M Tris-HCl, pH 8.8	2.5 ml
Acrylamide/Bis, 30% (Sigma-Aldrich)	3.33 ml
10% SDS	100 µl
10% Ammonium persulfate	50 µl
TEMED (N,N,N',N'-tetramethylethylethylene-diamine)	5.0 µl
Sterile ddH_2O	4.0 ml

(xiv) Restore Western Blot Stripping Buffer was obtained from Pierce, IL, USA.

(xv) SDS-PAGE Electrophoresis Running Buffer (1X)

25mM Tris	3.02 g
250mM Glycine	18.8 g
0.1% SDS	1 g

Made up to 1 Litre with ddH_2O and adjusted to pH 8.3.

(xvi) SDS-PAGE Transfer Buffer (1X)

30mM Glycine	2.90 g
48mM Tris	5.80 g
0.037% SDS	0.37 g
25% methanol	200 ml

Made up to 1 Litre with ddH_2O and adjusted to pH 8.3

(xvii) 5% Stacking Gel SDS-PAGE electrophoresis

0.5M Tris-HCl, pH 6.8	2.5 ml
Acrylamide/Bis, 30%	1.3 ml
10% SDS	100 µl
10% Ammonium persulfate	100 µl
TEMED (Sigma-Aldrich)	10 µl
Sterile ddH_2O	6.1 ml

(xviii) SuperSignal West Pico Chemiluminescent substrate was supplied by Pierce, IL, USA

(xix) 10X TBS

Sodium Chloride	292 g
Tris-Cl (1M, pH 7.5)	250 ml

Made up to 1 Litre and adjusted pH to 7.2-7.4 with HCl

(xx) 1X TBST: 100 ml 10X TBS and 500 µl Tween 20 (0.05%) made up to 1 Litre with dH_2O.

2.1.5 Materials and reagents used for immunohistochemistry

(i) Antibodies:

- Cleaved caspase-3 (Asp175) polyclonal antibody was obtained from Cell Signaling Technology, Danvers, MA, USA. Diluted at 1:300 in PBS prior to use.
- Cy3-conjugated AffiniPure Goat Anti-Rabbit IgG (cross reacts with human, mouse and rabbit serum proteins) was obtained from Jackson ImmunoResearch Laboratories Inc., PA, USA. Diluted at 1:500 in PBS prior to use.
- Rabbit polyclonal anti-C-IMPDH1 JK010307 (2mg/ml) was a kind gift from Dr Sara J. Browne (*Human Genetics Centre, School of Public Health, University of Texas HSC, Houston, TX 77030, USA*). This antibody was designed to recognise canonical IMPDH1 residues 426-438 (Peptide sequence: SQKRYFSEGDKVK) and was diluted at 1:300 with PBS containing 1% goat serum prior to use. Refer to Bowne *et al.*, (2006a) for information regarding the generation of this antibody.

(i) Aqua Poly/Mount was obtained from Polysciences, Inc., Warrington, PA.

(ii) DAPI (4'-6-Diamidino-2-phenylindol) nuclear staining solution was obtained from Sigma, Stenheim, Germany. Diluted at 1:5000 in PBS prior to use.

(iii) 4% paraformaldehyde: 16 g of paraformaldehyde (Sigma-Aldrich, Stenheim, Germany) was added to 40 ml of 10X PBS (BioWhittaker, Cambrex, UK), and brought up to 100 ml with ddH_2O. NaOH was added to the solution under constant stirring to solublise paraformaldehyde. The pH was then adjusted to 7.4 with HCl and made up to a final volume of 400 ml with ddH_2O.

(iv) Polysine glass slides (25 x 75 x 1.0 mm) were obtained from Menzel-Glaser, Braunschweig, Germany.

(v) Propidium Iodide solution was obtained from Sigma-Aldrich, Stenheim, Germany.

2.1.6 Animals

All animal experiments were conducted in compliance with the Association for Research in Vision and Ophthalmology (ARVO) statement regarding the use of animals in ophthalmic and vision research. C57B6/CBA and 129 S2/SvHsd mice (Harlan Laboratories, Oxfordshire, UK) were bred for several generations on site and maintained in a 12 hour light-dark cycle, with an ambient room temperature between 19-22°C. Both inbred mouse strains are readily available in our animal facility and are commonly used in eye research, particularly in the generation of transgenic, knock-out and knock-in mice (Reynolds *et al.*, 2008). Both sexes of mice were used in *in vivo* studies. Strain-specific variation in ERG between C57BJ6 and 129 S2/SvHsd mice has been reported, where 129 S2/SvHsd mice exhibited slower cone a- and b- wave single flash and flicker implicit times compared to C57BJ6 mice (Reynolds *et al.*, 2008). However, the main interest in this study was to examine rod response in the mouse retina as IMPDH1 is predominantly localised in rod photoreceptor cells (Aherne *et al.*, 2004; Bowne *et al.*, 2006a). A recent study has reported that commonly used wild-type laboratory inbred mouse strains (C57B6 or 129 S2/SvHsd) between 4- 15 weeks of age showed no differences between the size parameters of left and right eyes of both sexes of mice (Puk *et al.*, 2006), and differences in retinal function between male and female mice have not yet been reported in literatures.

2.2 General molecular methods

2.2.1 Determination of DNA and RNA concentration using UV spectrometer

UV spectrometer was used to determine the concentration of DNA and RNA. 1 µl of DNA/RNA was diluted in 100 µl ddH_2O and mixed by vortexing. The spectrometer was zeroed using ddH_2O as blank and the absorbance was measured at 260_{nm}. The final DNA or RNA concentration was calculated using the following the equations:

DNA concentration (µg/µl) = Absorbance at 260_{nm} x 50 x 100 (dilution)

RNA concentration (µg/µl) = Absorbance at 260_{nm} x 40 x 100 (dilution)

2.2.2 Agarose Gel Electrophoresis

Agarose powder was weighed out 0.8-2% (w/v) and dissolved in 1X TAE buffer. Agarose gel was then heated and ethidum bromide was added to a final concentration of 0.5 µg/ml. The gel was allowed to set with a comb inserted and DNA samples (with 0.1 volumes of DNA loading dye) were loaded into the wells accompanied by a DNA size marker. The gel was electophoresed at a constant voltage of 100V. DNA was visualised with a UV transilluminator (Hoeffer) and photographs were captured with Polaroid type 667 black and white film.

2.2.3 Phenol-chloroform extraction and ethanol precipitation of nucleic acids

Nucleic acids were mixed with an equal volume of buffer-saturated phenol (pH 7.5), vortexed and left standing on ice for 1min. The samples were then centrifuged at 13,000rpm in a Micromax centrifuge (Internatioinal Equipment Company: Thermo-Electron, Waltham, Ma, USA) at 4°C for 15 min. The upper aqueous phase containing the nucleic acids was transferred to a 1.5 ml eppendorf. An equal volume of a 1:1 buffer-saturated phenol and chloroform mix was added to the sample, vortexed and centrifuged as before. The upper phase was then removed to a new eppendorf and the nucleic acids were ethanol precipitated.

Nucleic acids were precipitated by adding one tenth volume of 3M sodium acetate and 3X volume of 100% ethanol. The samples were incubated at -20°C for 1-2 hrs and centrifuged at 13,000 rpm for 15 min. The supernatant was removed and the pellet was washed in 400 µl of 70% ethanol, centrifuged at 13,000rpm for 15 min. The ethanol was removed and resuspended in 20 µl of dH_2O.

2.2.4 XL1-Blue *E. coli* Competent Cells preparation

A loopful of XL1-blue *E. coli* was cultured in 10 ml Luria- Bertani (LB) broth containing 25 µg/ml of tetracycline with constant shaking in an orbital shaker at 37°C overnight. 250 µl overnight cultures were then used to inoculate 50 ml LB broth with 25 µg/ml of tetracycline until an OD_{600} of 0.3 to 0.5 (≈ 2 hrs) was reached. The cells were then centrifuged at 3,000 rpm for 10 min at room temperature. The supernatant was discarded and the pellet was resuspended in 25 ml of pre-chilled 50 mM $CaCl_2$. The cell suspension was incubated on ice for 20 minutes and then centrifuged at 3,000 rpm for 10 min. The cells were resuspended in 5ml pre-chilled 50 mM $CaCl_2$ and kept on ice overnight at 4°C for maximum competency.

2.2.5 Transformation of XL1-Blue competent cells

5 µl ligation mix were added to 100 µl XL-1 Blue *E.coli* competent cells and left on ice for >20 min. The cells were subjected to heat-shock at 42°C for 90 sec and returned to ice for 2 min. 1 ml of LB was added to the cells and agitated for 1 hr at 37°C. 200 µl of transformed cells were inoculated on LB selective agar plates and incubated overnight at 37°C. Transformants were selected by vectors ability to resist designated antibiotics. Suitable single colonies were picked and inoculated in 10 ml selective LB overnight.

2.2.6 Plasmid Mini-Prep Boiling Method

Single transformed colonies were picked and inoculated overnight in 10ml LB selective medium with agitation in an orbital shaker at 37°C. Cultures were centrifuged at 3,000rpm for 10minutes. The supernatant was discarded at the pellet was re-suspended in 60 µl Plasmid mini-preparation Resuspension buffer (section

2.1.1) and 20 µl lysozyme (10 mg/ml). The cell suspension was transferred to a 1.5 ml eppendorf tube and incubated on ice for 15 min. 500 µl of M-stet buffer (section 2.1.1) was added to the cell suspension and were left standing at room temperature for 10 min. The cell suspension was then placed in a water bath at 90°C for 40 sec, and centrifuged at 13,000 rpm at 4°C for 15mins. The coagulants were discarded and 5 µl RNaseIT (10 mg/ml) was added to each sample and incubated at 42°C for 15 min. 400 µl phenol and 100 µl chloroform were added to each sample and centrifuged at 13,000rpm for 10 min. The upper phase was transferred to a new eppendorf to which an equal volume of isopropanol was added, and was left at room temperature for 10 min. The samples were centrifuged at 13,000rpm for 10mins and pellets were washed in 75% ethanol. Subsequent to another centrifugation step, the pellet was resuspended in 20 µl sterile dH_2O and stored at -20°C. The presence of desired DNA insert was then determined by restriction enzyme digest analysis (section 2.2.10) or DNA sequencing (section 2.2.13).

2.2.7 DNA Ligations

Ligations were carried out in a 15 µl reaction volume at various ratio of vector: insert, (normally 1:1 to 1:10). Appropriate digest, ligase and insert controls were included in each reaction. One tenth volume of 10X ligase buffer and rATP were added along with 1unit of ligase enzyme per µg of DNA plasmid to the reaction. The final volume was made up to 15 µl with ddH_2O and incubated overnight at 16°C.

2.2.8 Design of oligonucleotides

Primer sequences were designed to 21 nucleotides in length, and were checked to ensure low secondary structure and primer dimmer formation using design software provided by Sigma-Genosys. GC % was also maintained between 50-60%. All oligonucleotidess were resuspended in nuclease free sterile water at concentration of 100 pmoles/ul or 100 µM.

2.2.9 Polymerase Chain Reaction (PCR)

Standard PCR reaction was carried out in a 20 µl reaction volume comprising of the following components: 1 unit Taq polymerase, 10 pmoles forward and reverse primers, 0.2 mM dNTPs, 20 ng DNA template, 20 mM $MgCl_2$ buffer and the final volume was made up to 20 µl with ddH_2O. The following PCR cycling steps were used: denaturing step at 94°C for 5 min followed by 35 cycles of 94°C for 1 min, 55°C for 1 min and 72°C for 1 min and 20 sec. A 10 min cycle at 72°C was added to enhance product yield. The cycling conditions varied slightly depending on the fragment being amplified.

For rapid screening of positive clones following transformation, single colonies were picked and resuspended in 5 µl 1X Tris-Triton lysis buffer. The following heat cycles were then applied: 94°C for 5 min, 15° for 2 min followed by 86°C for 1 min. The PCR reaction components described above was then added to the samples followed by normal PCR cycling steps.

PCR reaction carried out using PFU turbo Taq was performed in a 50µl reaction: 1 unit of PFU turbo Taq, 10 pmoles forward and reverse primers, 50 ng DNA template, 1.25 mM dNTPs, 1X PFU buffer and the final volume made up to 50 µl with ddH_2O. The PCR cycle was 94°C for 5 min followed by 35 cycles of 94°C for 30 sec, 55°C for 30 sec, 72°C for 1 min, and ending with 72°C for 10 min.

2.2.10 Restriction Enzyme Digestions

Enzyme digestions were carried out in 20-100 µl reaction volumes. Restriction enzymes were used at 1 unit per µg DNA with the appropriate buffer at 1X concentration. Enzyme digestions were incubated at 37°C for one to two hrs and examined by agarose gel electrophoresis.

2.2.11 Qiaquick (Qiagen) PCR purification

Five volumes of Buffer PB were added to one volume of DNA PCR products. The samples were placed in Qiaquick filter columns and centrifuged at 13,000rpm for 1

min. The flow through was discarded, 750 µl Buffer PE was then added to the column and centrifuged at 13,000rpm for 1 min. The Qiaquick column was transferred to a 1.5 ml eppendorf. DNA was eluted with 35 µl EB buffer by centrifuging 13,000rpm for 1 min.

2.2.12 Qiagen maxi-preps

After verifying that the recombinant clones were of the correct sequences, final vectors were prepared using the Qiagen maxi-prep kit in accordance with manufacturer's instructions. In brief, a single colony containing the plasmid of interest was inoculated in 10ml of selective LB and grown for 8 hrs with constant shaking at 37°C. 1 ml of this 10ml stock culture was transferred to 500 ml selective LB and grown for 16 hrs with constant shaking at 37°C. The bacterial cells were collected by centrifugation at 3,000rpm for 15 min at room temperature. The bacterial pellets were resuspended in 10 ml Buffer P1, and 10 ml of Buffer P2 was added with gentle mixing by 4-5 inversions. The cell suspension was incubated in Buffer P2 for 5 min and 10 ml of pre-chilled Buffer P3 was added. The cell lysate was then transferred to a cylindrical injection syringe and incubated for 10 min. During the incubation, the High Speed Maxi Tips were equilibrated by the flow through of 10 ml Buffer QBT under gravity. The cell lysate was then poured into the Maxi Tip and the bound DNA was then washed with 60 ml Buffer QC. DNA was then eluted with 15 ml Buffer QF and collected in a fresh 50 ml tube. The eluted DNA was precipitated with 10.5 ml of isopropanol and incubated at room temperature for 5 min. The QIA precipitator maxi module was attached to a 30 ml syringe and the precipitate was flushed through the module under constant pressure. The DNA bound to the module was washed with 2 ml 70% ethanol. The module membrane was air-dried by forcing air through the syringe plunger, and the DNA was eluted with 1ml Buffer TE.

2.2.13 DNA Sequencing

Sequencing was carried out using the 373A DNA Sequencing Machine (Applied Biosystems, Santa Clara, CA, USA). Sequencing reactions were carried out in a final volume reaction of 20µl. Each reaction contained 500 ng DNA, 5 pmoles of forward

or reverse primers, 4 µl BigDye® Taq mix and 4 µl BigDye® Buffer (PerkinElmer, Boston, MA, USA). Sequencing reactions were then cycled 26 times under the following conditions: 96°C for 30 sec, 50°C for 15 sec and 60°C for 4 min. PCR products were then precipitated with a solution containing 3 µl 3M sodium acetate, 62.5 µl 100% ethanol and 14.5 µl ddH_2O for 15 min at room temperature and centrifuged at 13,000rpm for 20 min. The pellets were washed with 75% ethanol and resuspended in 25 µl Template Suppressing Reagent. The resuspended samples were heated at 95°C for 5 min and returned to ice immediately. Samples were then loaded onto the ABI 373A Genetics Analyser and sequenced according to manufacturer's protocol. DNA sequences were collected using ABI data analysis software.

2.3 Tissue Culture Methods

2.3.1 Cell culture maintenance

All mammalian cell cultures (American Type Culture Collection, Manassas, VA, USA) were cultured in Dulbecco's modified Eagle medium ($DMEM^{+Abs}$) (GIBCO/BRL) in a 5% CO_2 incubator at 37°C.

2.3.2 Cell Passaging

Cells were passaged routinely to maintain exponential cell growth and minimise cell death due to excess confluency. DMEM media was aspirated off and cells were washed with phosphate buffered saline (PBS) at pH 7.2 for 2-3 min. The PBS was aspirated off and 2 ml of trypsin-EDTA (Gibco-BRL) was added to dissociate cells from cultured plates. The plates were then incubated at 37°C for 5 min to enhance trypsinisation. The degree of dissociation was monitored by visual inspection under light microscope. The action of trypsin was terminated by the addition of 10 ml $DMEM^{+Abs}$ per ml of trypsin used. Cells were centrifuged at 1,000 rpm for 5 min in a swing bucket centrifuge. Pellets were resuspended in 2 ml $DMEM^{+Abs}$ and plated at a concentration of ~$1x10^6$ cells/ml per 10 cm dish.

2.3.3 Haemocytometer cell counting

Cells were trysinised as described in section 2.3.2 and an aliquot was diluted at 1:10 in DMEM. A glass coverslip was first placed on top of the haemocytometer, and the diluted cell suspension was pippetted along the edge of the haemocytometer to allow dispersion through the counting area by capillary action. Cells present within the four 16-square areas were counted. The total number of cells present in the original cell stock was calculated using the following equation: Average number of cells from the four 16-square areas X 10 (dilution) = cells 10^4/ml.

2.3.4 Cryopreservation of cells

In order to maintain a healthy cell stock, cells were frozen down during their exponential growth phase or at low passage numbers. Pre-chilled freezing ampoules

were labeled with date of freezing, cell type and passage number. Subsequent to trypsinisation, cells were resuspended in 500 µl of DMEM+^{Abs} at a concentration of $5x10^6$ to $1x10^7$ cells/ml. Equal volume of cells and freezing medium (total volume = 1 ml) were added to pre-chilled ampoules and stored at -80°C or in liquid nitrogen. To regenerate a frozen stock, cells were thawed at room temperature for 10 min. The freezing ampoules were then placed in sterilised universals for centrifugation at 1,000rpm for 5 min. Freezing medium was then aspirated off and the pellet was resuspended in 10ml DMEM$^+$.

2.3.5 Poly-L-Lysine coating of coverslips

Coverslips (1000 x 13 mm. SLS, Nottingham) were placed in 100% ethanol overnight at room temperature with gentle shaking. The coverslips were then washed 3-4 times for 15mins in sterile water and incubated overnight in a tissue culture dish carrying a 2% Poly-L-Lysine solution (Sigma-Aldrich, Stenheim, Germany) diluted to 1:50. After incubation, the coverslips were washed three times with sterile water, air dried in a tissue-culture cabinet overnight without exposure to UV light and stored at 4°C.

2.3.6 General transfection protocol using Lipofectamine 2000®

Mammalian cells were trypsinised, counted and plated at the appropriate cell density in DMEM^{-Abs} so that the cells will be ~80-90% confluent at the time of transfection. All transfections were carried out in either 24- (RNA analysis) or 6-well plates (Protein analysis). The appropriate amounts of plasmid DNA or chemically sythesised siRNA were diluted in Opti-MEM (serum free medium). The required amount of Lipofectamine 2000® (Invitrogen) was diluted in Opti-MEM and incubated at room temperature for 5mins. The diluted Lipofectamine 2000® was then combined with the plasmid DNA or siRNA dilutions and complexes allowed to form at room temperature for 25 min. Suitable amounts of the Lipofectamine + DNA/RNA complex were added to each well, swirled and incubated at 37°C for 24-72 hrs.

2.3.7 RNA extraction from cultured cells

Trizol Reagent® was used for the isolation of total RNA from cultured cells. Approximately 1 ml of Trizol was added to every well containing 1-5 x 10^6 cells/ml. The cells were initially incubated in Trizol for 5 min at room temperature and homogenised by repetitive pipetting. The homogenates were then transferred to fresh RNase-free eppendorfs (Axygen Scientific Inc., USA). 200 µl chloroform was added to each homogenate and vortexed for 15 sec. The homogenates were then left standing for at room temperature for 2-3 min and centrifuged at 13,000rpm for 15 min at 4°C. Approximately 500 µl of upper aqueous phase (Volume of aqueous phase is ≈60% of Trizol used for homogenisation) was transferred to a new RNase-free eppendorf. RNA was then precipitated with 500 µl isopropanol and incubated at room temperature for >10 min. RNA samples were centrifuged at 13,000rpm for 10 min and the isopropanol was discarded. The RNA pellets were then washed with 500 µl 75% ethanol, centrifuged and resuspended in 20 µl RNase free water (Ambion).

2.3.8 DNase treatment of RNA samples

RNA samples were DNase-treated in a 50 µl volume reaction as follow: 20 µl RNA + 5 µl DNase enzymes (Promega) + 5 µl DNase buffer and made up to 50µl with RNase-free water. The reaction mixture was then incubated at 37°C for 1 hr. 250 µl Trizol and 85µl chloroform were added to each sample and vortexed for 15 sec. The samples were left at room temperature for 2-3 min and centrifuged at 13,000rpm for 15 min. The upper aqueous phase was transferred to a new RNase-free eppendorf. 200 µl isopropanol was then added to the upper aqueous phase and incubated at room temperature for >10 min. The samples were centrifuged at 13,000rpm and the pellets were washed in 500 µl 75% ethanol. The RNA was then resuspended in 20 µl RNase-free water (Promega) and stored at -80°C for further use.

2.4 Real Time RT-PCR analysis using SYBR Green I dye (Qiagen) on a Light-Cycler (Roche Diagnostics, Lewes, UK)

In this study, RNA was quantified using Real Time PCR technology on a Light-Cycler system (Roche Diagnostics) with SYBR Green I as fluorescent dye (Qiagen). QuantiTech™ was capable of supporting reverse transcription and gene specific amplification in a one-tube format. PCR reactions were carried out in 20 µl borosilicate glass. The optical properties of borosilicate glass were well suited for use as cuvettes for fluorescence and the high surface to volume ratio allowed equilibration between air and reaction components. The Light Cycler (Roche) was able to monitor 32 capillaries per run in a rotating carousel within the thermal chamber. For all cell culture experiments measuring the suppression of IMPDH1 expression, two-master mixes were prepared. The first master mix contained primers for amplifying IMPDH1, and the second contained primers of the housekeeping gene. Complementary DNA PCR primers (Sigma-Genosys Ltd) for RT-PCR were HPLC-purified and designed to span an intron yielding a product of 100 – 150bp to assist discrimination between RNA amplification or contamination from genomic DNA.

The reaction components of a master mix for 16 capillaries included the following:

Component	Volume/reaction
2x QuantiTect SYBR Green	180 µl (1x final concentration)
QuantiTect RT Mix	3.60 µl (0.2 µl /reaction)
Forward primer	9 µl (10 pmoles)
Reverse primer	9 µl (10 pmoles)
RNase-free water	158.40 µl
Total volume	**360 µl**

Both master mixes were vortexed and 17 µl of each reaction mix was dispensed into the glass capillaries. 3 µl of diluted RNA samples (1:1000) were then dispensed into the capillaries to give a total reaction volume of 20 µl. White caps were gently placed onto the capillaries and centrifuged at 3,500 rpm for 1 min to mix and settle all the reaction components into the capillary ends. The capillaries were then placed into the

rotating carousel of the light-cycler machine for RT-PCR. Standard curves were generated from PCR products made from serial dilutions of increasing concentrations of total RNA (1/5000, 1/2000, 1/1000, 1/500, 1/200 and 1/100). RT-PCR reaction conditions for the Light-Cycler system (Roche Diagnostics) were as follow: 50°C for 20 min for the reverse transcription phase, cDNA fragments were amplified following an initial denaturing step at 95°C for 15 min, followed by 35 cycles of amplification at 95°C for 15 sec (denaturing), 57°C for 20 sec (annealing) and 72°C for 8 sec (elongation). Fluorescence signals were measured after each elongation step. A melting curve was obtained by constant measurement of fluorescence during a warming cycle followed by gradual cooling from 95°C to 65°C for 10 sec, and 40°C for 30 sec.

Fluorescence data was analysed by the LightCycler quantification software (Version 3.3, supplied by Roche Molecular Biochemicals). The quantification of target mRNA, evaluation of the efficiency of PCR reactions and prevention of primer dimer formation were the main parameters in post RT-PCR analysis. *Figure 2.1Ai* and *2.1Bi* show the real-time amplification curve measured at the end of each elongation step plotted against the cycle number. The baseline indicated the first PCR cycle where the log linear fluorescence was distinguished from the background signal. The cycle number at which the fluorescence signal elevated above the baseline level was determined as the C_T value. Regression curves were then obtained by plotting the C_T values against the log concentration of standard RNA (*Fig. 2.1Aii* and *Fig. 2.1Bii*). PCR reaction efficiency was optimal when the slope values approached –3.33, the error value being less than 0.01 and the correlation co-efficient (r) being ≈1 as in *Figure 2.1Aii* and *Bii*. The melting curve generated at the end of the PCR reaction also indicated great primer specificity as all the amplified products of the RNA standards had the same melting temperatures (82 °C for β-actin and 86°C for IMPDH1), and the absence of a second peak of different melting points indicated the absence of genomic DNA contamination and the lack of primer dimmer formation during the reaction (*Fig. 2.1C).* For all suppression experiments, the same parameters were used and the level of IMPDH1 expression was in general standardised to the

housekeeping gene, β-actin, although other housekeeping genes such as IMPDH2 and transcription binding protein (TBP) were also tested and yielded similar results. In all studies, the results were expressed as a percentage to control samples transfected with control suppressors normalised to β-actin. The reciprocal values represented percentage suppression of IMPDH1 expression.

2.5 Western blot analysis

2.5.1 SDS-PAGE electrophoresis

For western blot analysis, HeLa cells were plated at a concentration of $3x10^5$cells/ml on 6-well plates a day prior to transfection. In general, 1.5 µg of plasmids expressing the gene of interest and 100 pmoles of siRNAs were co-transfected into HeLa cells in duplicates using Lipofectamine 2000® (Invitrogen) according to manufacturer's instructions. After 72 hrs of transfection, the cells were washed once with PBS and harvested by adding 500 µl trypsin per well. Trysinised cells were added to 10 ml DMEM and centrifuged at 1,000rpm for 5 min. The medium was removed and the pellet was washed twice with PBS. The pellets were then resuspended in 500 µl of protein lysis buffer solution. Lysed protein was incubated on ice for 10 min and homogenised by passing through 21G gauge needles to reduce the viscosity of the protein solution. The homogenised protein solution was then centrifuged at 13,000rpm for 15 min at 4°C and the supernatant containing soluble cytosolic proteins was stored at –20°C.

2.5.2 Determination of protein concentration with BCA protein assay

Protein concentration was determined by BCA Protein assay kit (Pierce) with bovine serum albumin (BSA) at 2mg/ml as standards on 96-well plates according to manufacturer's guidelines. The BSA standard curve was set up with the following concentrations; 0 mg/ml, 0.25 mg/ml, 0.75 mg/ml, 1.0 mg/ml, 1.5 mg/ml and 2 mg/ml. Samples were diluted at a 1:5 dilution and plated in triplicates. In brief, the 96-well plate was loaded with 10 µl of each of the BSA standards, 10 µl of diluted protein lysate samples and 10 µl of protein lysis buffer as blanks. 200 µl BCA working reagent (50:1 dilution of BCA reagent: Copper sulphate solution) was then added to each well being used. Plates were read on Rosys 2010 Anthos Plate reader at 595 nm and data were retrieved using Anthos 2010 platereader MS-DOS according to manufacturer's protocol. The concentration of protein was established using the equation: $y=slope(x+yk)$, where y=OD, x=concentration of protein (mg/ml), *slope* and *yk* were determined by the standard curve.

2.5.3 Gel cassette assembly

The Mini-Protean 3 gel cassette sandwich module was set up for hand cast gels according to manufacturer's instructions (Bio-Rad). A comb was completely submerged into the assembled gel cassette and the glass plate was marked 1cm below the comb teeth to signify the level to which the resolving gel was to be poured. 10% resolving polyacrylamide gel was prepared and poured to the mark on the glass plate. The gel was then overlaid with ethanol and allowed to polymerize for 30 min at room temperature. The overlaying ethanol was poured off carefully and a freshly prepared 5% stacking gel was poured between the glass plates until the top of the short glass was reached. The comb was then inserted into the stacking gel where the comb ridge was aligned with the top of the short plate. The stacking gel was allowed to polymerise for 15 min and the comb was removed before loading.

2.5.4 Mini-Protean 3 electrophoresis module assembly and sample loading

The Mini-Protean 3 electrophoresis module containing 500 ml SDS-PAGE electrophoresis running buffer was assembled according to manufacturer's guidelines (Bio-Rad). Sample loading buffer was first prepared by adding 50 µl β-mercaptoethanol to 950 µl protein loading buffer. Aliquots of samples containing equal amounts of total protein (30-50 µg) were diluted at 1:3 with sample loading buffer and heated at 95°C for 5 min. The optimal angle for visualising the wells was obtained and the samples were loaded gently avoiding air-bubbles. Kaleidoscope pre-stained standards (Bio-Rad) were loaded into the extreme left lane of each gel. SDS-PAGE electrophoresis was carried out at 120 volts for approximately 1.5 hrs.

2.5.5 Coomassie-Blue Staining

Subsequent to SDS-PAGE electrophoresis, the electrophoresis module was disassembled and the gels were carefully removed from the glass plates. Approximately 25 ml 1X TBS was added to the gel and incubated at room temperature for 1 hr with gentle agitation. The washing solution was discarded and the gel was stained in 30 ml coomassie staining solution for 2-3 hrs at room temperature with gentle shaking. The coomassie-blue staining solution was removed

and the gel was bathed in 30 ml destaining solution at room temperature for 24 hrs with mild agitation. The gel was visualised on a UV transilluminator (Hoeffer) under white light and photographs were taken with Polaroid type 667 black and white film.

2.5.6 Electrophoretic transfer of protein onto nitrocellulose membrane

The Mini Trans-Blot cell module was assembled according to manufacturer's instructions. Nitrocellulose membranes (Bioscience) were cut out to the dimension of the gel and were soaked in dH_2O. The gel was removed from the electrophoresis module and dipped in transfer buffer. The gel sandwich cassette was set up according to manufacturer's guidelines and inserted into the Mini Trans-Blot cell module. Sufficient SDS-PAGE transfer buffer was then poured into the module to leave the assembled gel sandwich cassette 0.5 cm below the surface of the buffer. The transfer module was placed at 4°C and power was supplied at 100 V for 2 hrs or 30 mA overnight.

2.5.7 Blocking of immunoblots

At the end of the transfer period, the blot was removed from the gel sandwich cassette (the resolved Kaleidoscope pre-stained standards was now visible on the blot) and washed twice in 1X TBS for 10 min with gentle agitation. 30 ml blocking solution (5% non-fat dry milk) was added to the blot and incubated at room temperature for 1 hr with gentle rocking.

2.5.8 Antibody probing of immunoblots

The blot was first probed with a primary antibody at the appropriate dilution and incubated in a sealed plastic bag at 4°C overnight on a rocker. The blot was washed 3 x 10 min in 1X TBS solution. The blot was then probed with the corresponding secondary antibody at the appropriate dilution and incubated in a sealed plastic bag at room temperature for 1 hr on a rocker. The blot was washed 3 x 10 min in 1X TBST. The immunoblots were submerged in 1 ml of SuperSignal Chemiluminescence Substrate (Pierce) solution for 5 min for the detection horseradish-peroxidase (HRP)

signals, and exposed to Fugi X-ray films in the dark-room facility or using FujiFilm Luminescent Image Analyser (LAS-3000).

2.5.9 Stripping of immunoblots

Immunoblots to be stripped after chemiluminescence detection were washed thoroughly 3x10 min in 1X TBS at room temperature. The blots were then incubated in Restore Western Blot Stripping Buffer (approximately 20 ml was required for an 8 x 10 cm blot) for 15mins at room temperature with gentle shaking. After stripping, the blot was re-blocked in blocking solution and re-probed with the appropriate antibodies as described above.

2.5.10 Densitometry

Band intensities on western blots were quantified by scanning with Epson Stylus CX3200 and analysed with the software, *ImageJ* (www.imagej.com).

2.6 Retinal Explants

2.6.1 *In-vitro* electroporation and retinal explants culture

Electroporation and maintenance of retinal explant cultures were carried out according to protocols described by Matsuda and Cepko, (2004), Kiang *et al.*, (2005) and Palfi *et al.*, (2006). In two independent experiments, 12 retinas were dissected from six new born C57B6/CBA mouse pups and transferred to a micro-electroporation chamber (Nepagene, Chiba, Japan, 3 mm x 10 mm x 5 mm) filled with 100 µl of pshLuc.EGFP or psh2048.EGFP at a final concentration of 1 µg/µl in Hank's balanced salt solution (HBSS). Five square pulses (30V) of 50-ms duration with 950-ms intervals were applied to the retinal tissues from the scleral side using a pulse generator (ECM 830 BTX). Electroporated retinas were cultured *in vitro* at 37°C on Costar Transwell polycarbonate membrane (0.2 µm pore, Corning Life Sciences, Acton, MA, USA) in neurobasal medium (Invitrogen) containing 2 mM taurine, 10% Fetal calf serum, Penicillin/streptomycin, and B-27 supplements (Invitrogen) for 14 days.

2.6.2 Fluorescent Activated Cell Sorting (FACS) analysis of cultured retinal explants

Neurobasal media were discarded latter to *in-vitro* culturing and retinal tissues were washed twice with 4 ml HBSS solution for 1 min. For cell sorting, six cultured retinal explants per construct per experiment were pooled together and dissociated into single cells by digestion with 2 ml of trypsin (1 mg/ml) (Roche) at 37°C for 20 min. 2-3 µl of DNaseI was added to the dissociated cells and was further incubated at 37°C for 10 min. 200 µl of trypsin inhibitor (Roche) was added to the cell suspension and centrifuged for 5 min at 1,200rpm. The pellet was then resuspended in 2 ml HBSS solution per pair of retinas. Furthermore, 10 µl of DNaseI was added to the cell suspension and incubated at 37°C for 10 min. Dissociated retinal cell suspensions (6 retinas pooled together) were then sieved through 50 µm Filcon filters (Dakocytomation). EGFP positive and EGFP negative cells were collected in a

Beckman-Coulter Altra Fluorescence Activated Cell Sorter (Beckman-Coulter, Inc., Fullerton, CA, USA) at a rate of 1000 cells/s. Approximately 100,000 to 540,000 EGFP positive cells per experiment were collected. The FACS sorter was incorporated with three lasers at 488 nm (blue), 633 nm (red) and 407 nm (violet) that enabled detection of two scattered signals. The sorting flow rate of 4 was used to maximise the purity of the final sample. Subsequent to FACS sorting, the isolated cells were concentrated through 0.45 µm Ultrafree-MC filter units (Amicon, PTFE membrane) by centrifuging at 1,300rpm for 1 min at a concentration of ≤ 200,000 cells/unit. The filter units were then stored at –20°C (dry ice) for transportation from the facility.

2.6.3 RNA extraction from retinal explant tissues using Qiagen RNeasy Kit

FACS-sorted cells were eluted by adding 350 µl RNA lysis buffer (RLT), to which 1% v/v β-mercaptoethanol had been added (Qiagen RNeasy Kit). RLT buffer was passed through the filters by centrifuging at 6,600rpm for 2 min; the filtrate was reapplied to the filters and centrifuged under the same conditions 4 times. 250 µl 100% ethanol was added to the diluted RNA and mixed thoroughly by pipetting. 700 µl of the sample was applied to an RNeasy MinElute Spin Column in a 2 ml collection tube, and centrifuged for 15 sec at 10,000rpm. The flow-through was discarded and the spin column was transferred to a new 2 ml collection tube. 500µl Buffer RPE was applied to the spin column and centrifuged for 15 sec at 10,000 to wash the column. The flow-through as discarded and 500 µl 80% ethanol was added to the RNeasy MiniElute Column. The column was centrifuged for 2 min at 10,000rpm to dry the silica-gel membrane. The RNeasy Elution MiniElute Spin Column was then transferred into a new 2 ml collection tube and centrifuged at 13,200 rpm for 5 min. The RNeasy Elution Spin Column was transferred to a new 1.5 ml eppendorf and 14 µl RNase-free water was added directly onto the center of the silica-gel membrane. RNA was then eluted by centrifuging the spin column for 1 min at 13,200 rpm, and stored at -80°C for further use.

2.7 Adeno-associated virus (AAV)

2.7.1 Adeno-associated virus production

All adeno-associated viral vectors used in this study were produced in our laboratory with the help of Dr. Naomi Chadderton (O'Reilly *et al.,* 2007). Recombinant AAVs were generated using the helper virus free, triple transfection method according to (Xiao *et al.*, 1998). Production of high-titre recombinant adeno-associated virus vectors in the absence of helper adenovirus). The IMPDH1 suppressor and non-targeting shRNA were sub-cloned into pAAV-MCS (Stratagene; *Figure 2.5*), flanked by the inverted terminal repeats (ITRs) of AAV2. The adenoviral helper plasmid, pHelper (Stratagene), and a second helper plasmid, pRep2/Cap5 (Hildinger *et al.*, 2001) (AAV-2 Rep and serotype capsid 5 proteins) were used to generate AAV-2/5. HEK-293 cells (ATCC accession number: CRL-1573) were seeded in fifty 150 mm plates at $5x10^6$ cells/ml and grown to confluency in 20ml DMEM containing 10% FCS. For each plate, 12.50 µg pAAV-MCS, 12.50 µg pRep2/Cap5 and 25 µg pHelper (at a ratio of 1:1:2) were prepared in 1 ml volume of 150mM NaCl, pH5. 1 ml of polyethylenimine (0.1 g/L 150 mM NaCl, pH 5) (Reed *et al.*, 2006) was then added to the mixture and was left incubating at room temperature for 8 min before adding to HEK293 cells (10% final volume → 2mls + 18mls). 7 hrs post transfection, the media was replaced with 20 ml of fresh DMEM containing 10% FCS and incubated for a further 48 hrs.

2.7.2 Caesium chloride purification method (Auricchio *et al.*, 2001a)

Forty-eight hrs post transfection, infected HEK-293 cells were collected by scraping and centrifugation at 1000g for 30 min. Cell pellets was then resuspedned in 10 ml PBS and subjected to 3 rounds of freeze thawing (-80°C → 37°C). 10 mg RNaseA and 10,000U DNase I were added to the cell suspension and incubated at 37°C for 30 min. The cell suspension was then centrifuged for 15mins at 1000g and the supernatant was transferred to a new tube. 0.5% (final concentration) of deoxycholic acid was added to the supernatant and incubated for 30 min at 37°C. $CsCl_2$ 0.454 g/ml was added to the supernatant (4.45 g $CsCl_2$ to 10 ml supernatant) and incubated on

ice for 5 min. A density gradient was prepared in Polyallomer Beckman tubes (89 mm height x 24 mm diameter) by layering 9ml of 1.40 density $CsCl_2$ (548.3 mg/ml) over 9 ml of 1.6 density $CsCl_2$ (816.5 mg/ml) pippeted below. The supernatant containing $CsCl_2$ was then applied to the top of the gradient. The tubes were equilibrated and centrifuged at 25,000rpm in a Beckman SW28 rotor for 18 hrs at 4°C. 1 ml fractions were collected using a 16G syringe needle and the refractive index was recorded on a retractometer. Fractions within the range of 1.373-1.368 were collected and pooled together in polyallomer Beckman tubes (6 ml volume, 13 mm height x 51 mm diameter), equilibrated with the 1.4 density $CsCl_2$ and centrifuged at 59,000rpm in a Beckman fixed angle rotor VTi65 for 18 hrs at 4°C. 0.5 ml fractions were collected and those possessing a refractive index from 1.373 to 1.368 were pooled into a single pollyallomer Beckman tube and centrifuged as before. 0.5 ml fractions with a refractive index of 1.373 to 1.368 were collected and dialysed in Slide-aLysers (Pierce) against 10 Litres of PBS over 40 hrs (1 Litre per 4 hrs).

2.7.3 Determination of genomic viral titre

AAV genomic titres were established post-dialysis using quantitative Real Time RT-PCR according to the method described by Rohr *et al.*, (2002). A 1 µl sample was treated before measurement with 7U DNaseI (30 min at 37°C, 10 min at 70°C, cool to 4°C), and 7 µg ProteinaseK (60 min at 50°C, 20 min at 95°C). Quantitative Real Time RT-PCR was carried out on the DNaseI + Proteinase K treated viral sample with primers specific for the transgene using the following parameters (10 min pre-incubation at 95°C → 36 cycles of amplification: 15 sec at 95°C, 5s at 67°C and 10 sec at 72°C) (7300 Q-PCR, Applied Biosystems). In order to determine the copy number of the transgene-containing viral DNA, a standard curve was generated using a five log spanning serial dilution (10^4-10^8) of the vector plasmid containing the transgene. Genomic titres i.e. viral particles (vp/ml) were determined by the following calculation: Copy number in quantitative Real Time RT-PCR x Dilution (100) x dilution of template (50) x factor to yield genomic particles/ml (222).

2.8 Statistical Analysis

For all experiments presented in this study: mean values, standard deviations (SD), standard error of the mean (S.E.M) were paired student *t*-tests were calculated using Data Desk 6.0 PPC (Data Description, Inc., New York, NY, USA). Analysis of Variance (ANOVA) post-hoc tests for multiple comparisons were calculated using GraphPad Prism. Differences were considered statistically significant at P-values $\leq$ 0.05.

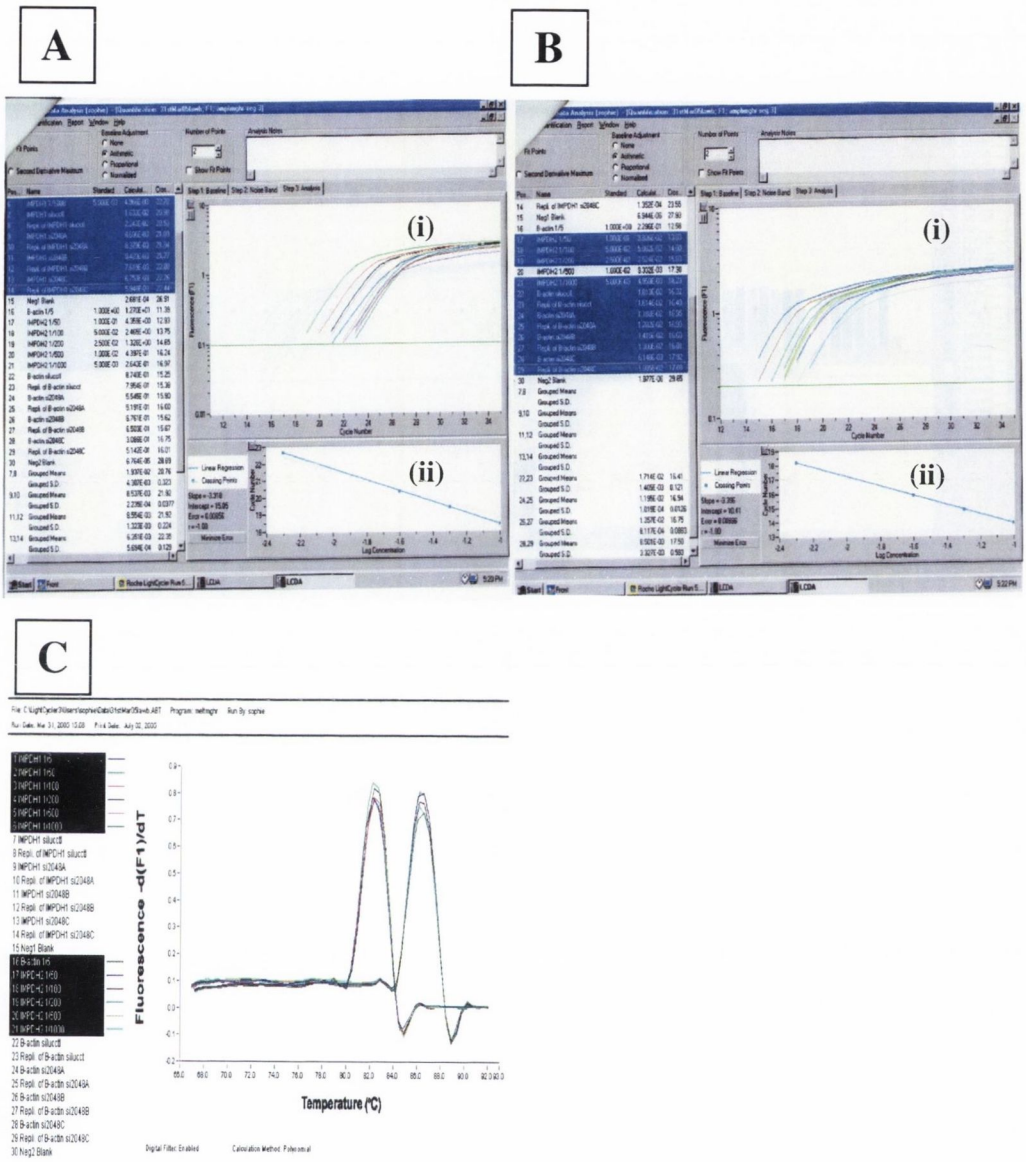

Figure 2.1: (A and B) Amplification and regression curves for IMPDH1 and β-actin quantification obtained from the Lightcycler® software. Regression curves were calculated with six standard values ranging from 1/5 to 1/1000 RNA copies and served for the quantification of RNA in unknown samples. (C) Melting curve analysis, showing specificity of the PCR reaction and the lack of primer dimmers.

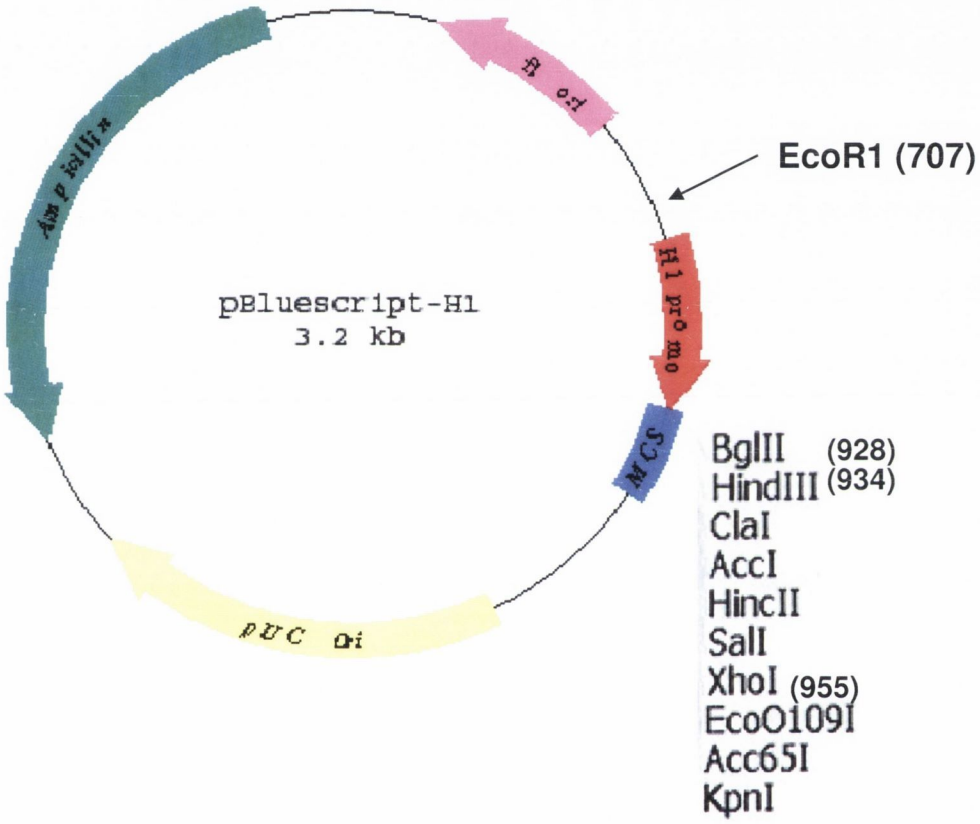

Figure 2.2: Vector map of pBluescript-H1 provided by Dr. A-S Kiang. The key restriction enzyme sites and the polymerase III H1 promoter are also illustrated.

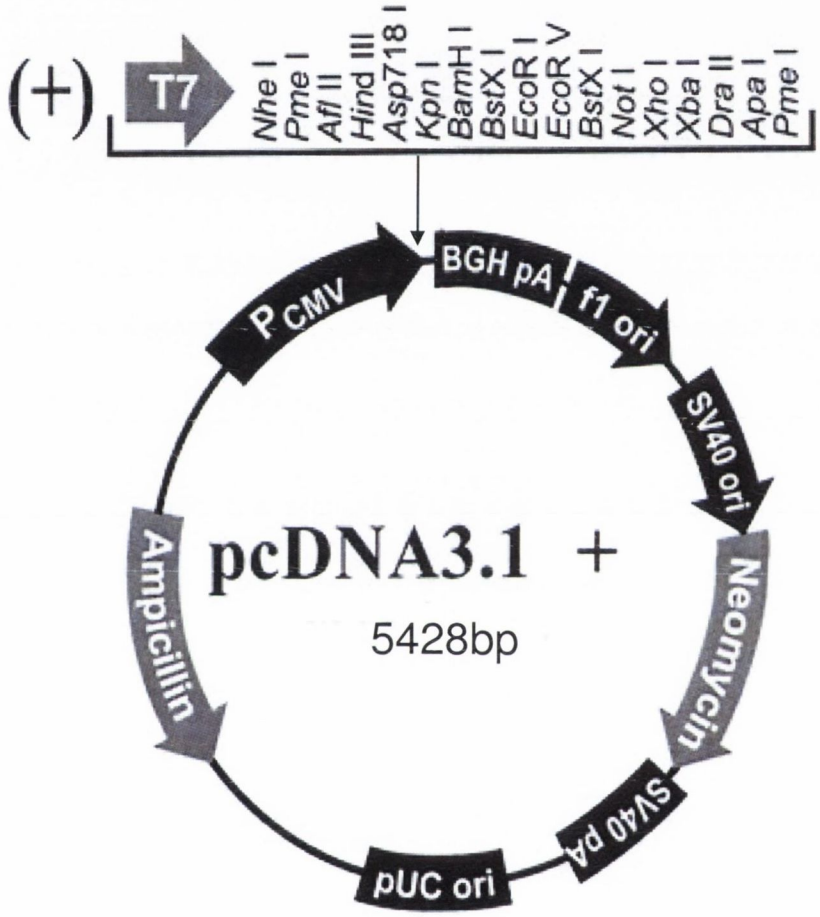

Figure 2.3: Vector map of CMV-promoter driven pcDNA3.1(+) from Invitrogen. The key restriction enzyme sites located within the multiple cloning sites are illustrated.

GenBank Accession #: U55761

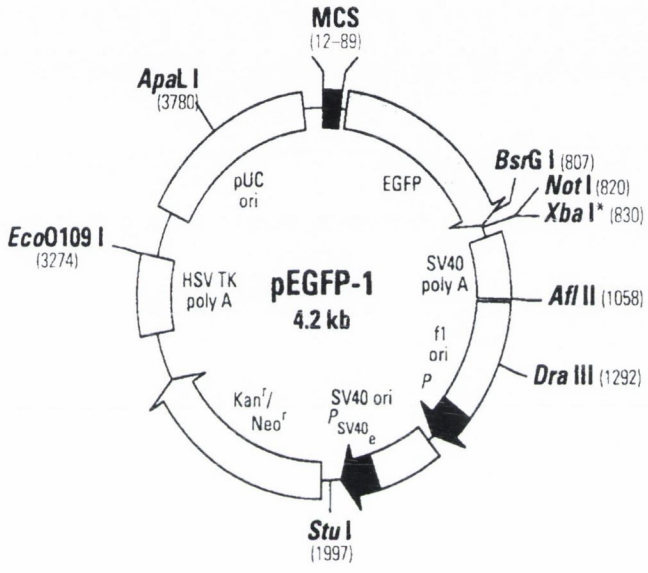

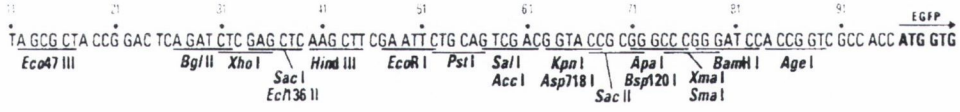

Figure 2.4: Restriction map and multiple cloning sites of pEGFP-1 (Clontech).

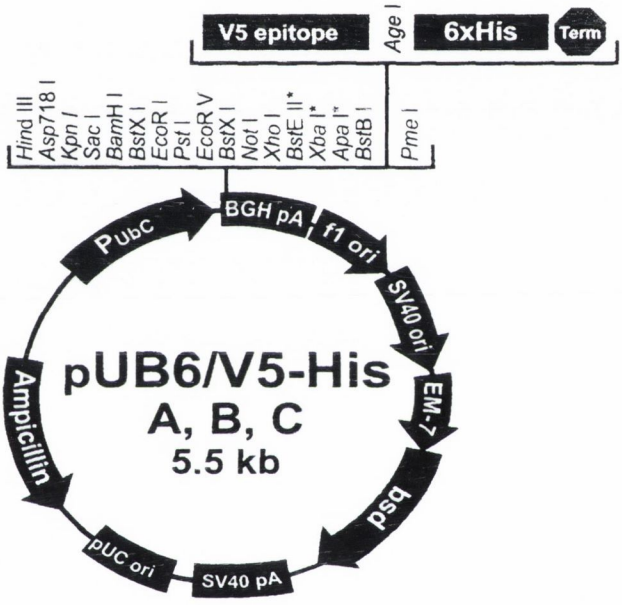

Figure 2.5: Vector map and multiple cloning sites of pUb6/V5-His A, B, C (Invitrogen). Vector sequence is available at *www.invitrogen.com*.

left inverted terminal repeat 1–141
CMV promoter 150–812
β-globin intron 820–1312
multiple cloning site 1319–1394
hGH polyA 1395–1873
right inverted terminal repeat 1913–2053
f1 origin 2145–2451
ampicillin resistance (*bla*) ORF 2970–3827
pUC origin 3978–4645

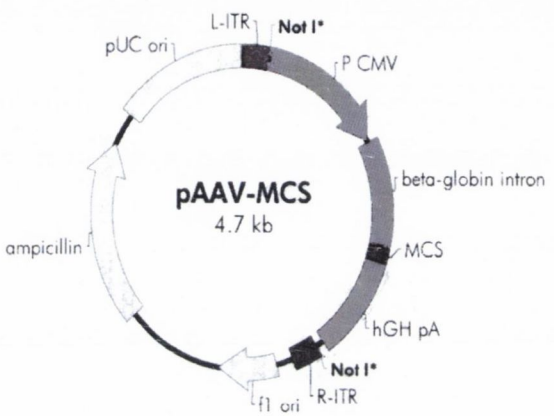

*Non-unique sites used to release the expression cassette

pAAV-MCS Multiple Cloning Site Region
(sequence shown 1319–1394)

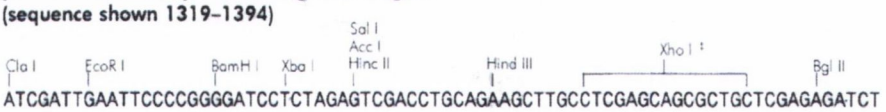

Figure 2.6: Vector map and multiple cloning sites of pAAV-MCS (Stratagene).

Chapter 3
Evaluation of IMPDH1-Specific siRNAs and shRNAs in Mammalian Cell Culture

3. Evaluation of IMPDH1-specific siRNAs and shRNAs in mammalian cell cultures

3.1 Introduction

RNA interference (RNAi) is an evolutionarily conserved post-transcriptional gene silencing process, in which double-stranded RNAs suppress the expression of genes by inducing degradation of mRNAs or blocking of mRNA translation (Fire *et al.*, 1998; Hannon, 2002; Elbashir *et al.*, 2001a and b). In this process, double-stranded RNA is cleaved by the enzyme Dicer into 21-25 nucleotide small interfering RNA (siRNA) duplexes with 2 nucleotide overhangs at the 3' ends. Processed siRNA duplexes are then incorporated in to a protein complex called RNA-induced silencing complex (RISC). Following this, the two strands of the siRNA duplex are separated by a helicase, and the retained RNA strand guides the activated RISC to identify complementary mRNA sequences. Identified mRNAs are then targeted for cleavage by an Argonaute protein, which has been shown to adopt an RNase-H structure (Hannon, 2002; Hammond *et al.*, 2001). Initially, RNAi was thought to possess the potential to become a powerful tool to knockdown gene expression in a wide range of cells. However, the introduction of long dsRNAs (>30bp) into mammalian cells was shown to cause general translational inhibition triggered by an interferon response mediated upon the activation of protein kinase PKR (Der *et al.*, 1997; Stark *et al.*, 1998). Shortly, Elbashir *et al.*, (2001a) demonstrated that synthetic 21 nucleotide dsRNAs with 2 nucleotide 3' overhangs, which were designed to mimic the products of the Dicer enzyme, evaded the host interferon response, resulting in a specific suppression of endogenous and exogenous gene expression in a variety of mammalian cells (HeLa and HEK293T cells). Furthermore, Caplen *et al.*, (2001) also presented supportive data on RNAi-mediated by synthetic siRNAs to induce gene specific inhibition in *C. elegans* and in cell lines of mice and human. Immediately after the publication of these reports, the use of synthetic siRNAs to transiently suppress the expression of target genes quickly became the method of choice for functional genomics research in mammals, and beyond their value of target

validation, siRNAs also possessed great potential as gene-specific therapeutic reagents. Although synthetic siRNA is a functional molecule itself, which can bypass the Dicer processing step, and enter directly into the RNA inducing silencing complex to induce target mRNA suppression of a complementary sequence, direct application of synthetic siRNA is accompanied by several disadvantages including the transient knockdown effect due to the lack of siRNA amplification mechanisms in mammalian cells, difficulty in regulating its activities, and the high expense associated with its use (Zamore, 2002; Zeng and Cullen, 2002; Chiu and Rana, 2002). In particular, the transient effect of synthetic siRNAs is a major drawback in studies of gene function that often requires the establishment of cell lines or transgenic organisms. In order to circumvent these problems, many groups have developed a vector-based siRNA expression system driven by polymerase III promoter such as U6, H1 or transfer RNA^{Val} promoter and demonstrated effective induction of vector-based RNAi in mammalian cells (Brummelkamp *et al.*, 2002; Paddison *et al.*, 2002a; Yu *et al.*, 2002; Miyagishi and Taira , 2002a and b; Kawasaki and Taira, 2003). A commonly used RNAi-based expression system in mammalian cells consists of a H1-polymerase III promoter that expresses a short hairpin siRNA in which two complementary siRNA strands are connected by a short loop sequence (Brummelkamp *et al.*, 2002; Paddison *et al.*, 2002a). These short hairpin RNAs have been reported to be cleaved into 21-23nt siRNAs in mammalian cells by a Dicer dependent processing event (Brummelkamp *et al.*, 2002; Paddison *et al.*, 2002a), which is similar to the processing of miRNA precursors (Hutvagner *et al.*, 2001). Concurrently, a related approach that uses an RNA polymerase III promoter to express synthetic hairpin microRNA precursors that are processed into siRNAs has been described (Zeng *et al.*, 2002). Subsequently, these short hairpin siRNAs are termed as shRNAs as they mimic the structure of the endogenously encoded natural pre-microRNAs, which are processed by Dicer in the cytoplasm and complex with Argonaute proteins to form RISC to mediate target mRNA suppression. In comparison to synthetic siRNAs, transfection of RNAi-based vectors has some advantages such as low cost, easiness of preparation and long-term and stable expression of siRNAs. In particular, the advantages of these promoters are that they

direct high levels of shRNA expression, which in turn mediates highly efficacious silencing. Moreover, the use of RNAi-based vector system can also facilitate RNAi in cell types that are difficult to transfect through incorporation into viral vectors, as well as advancing the generation of cell lines that stably express siRNAs. However, the limitations that surround the use of vector-based RNAi are that most polymerase III promoters lack cell specificity and exceedingly high levels of shRNA expression increases the probability of off-target silencing and eliciting of non-specific effects such as cellular toxicity and interferon response (Bridge *et al.*, 2003; Jackson *et al.*, 2003). Recently, an alternative method for expression of siRNAs using ribosomal transcription units driven by RNA polymerase I (Pol I) promoters has been reported. Similar to polymerase III-driven transcription, polymerase I-mediated transcription is very robust, ubiquitous, devoid of extensive RNA modifications and is characterised by clearly defined transcription start and termination sites (Grummt, 1999). In addition, polymerase I promoters have no limits for transcript size, and even more importantly, possesses a high species specificity (Heix and Grummt, 1995). This latter feature, which is unique among all RNA polymerases, provides an interesting potential regarding biosafety of experiments. Furthermore, inducible siRNA vector systems have been developed that allow stringent control over the expression of siRNAs in mammalian cells (Ma *et al.*, 2007). For example, van de Watering *et al.*, 2003 have designed a doxycyclin regulated form of the H1-promoter to inducibly knockdown β-catenin in colorectal cancer cells.

The remarkable potency of RNAi has led to its widespread use as a genetic tool for the inactivation of gene function and holds great potential as a genetic therapy for the treatment of infectious viral diseases (Giladi *et al.*, 2003), cancer (Duxbury *et al.*, 2004), and dominant diseases perpetuated by aberrant gene expression (Xia *et al.*, 2004). To date, many concurrent developments of similar hairpin siRNA designs and expression vectors in independent laboratories using different model systems have successfully demonstrated the power of RNAi as a therapeutic strategy for a wide range of ocular diseases, as discussed in detail in Chapter 1. Furthermore, mutation-independent suppression and replacement strategy has previously been successfully

demonstrated in our laboratory for targeting mutations in the rhodopsin and *rds*/peripherin genes which are involved in autosomal dominant retinitis pigmentosa (Kiang *et al.*, 2005; Palfi *et al.*, 2006). In particular, the identification of dominant negative phenotypic effects exerted by mutant IMPDH1 protein in our laboratory has presented RP10 as an excellent candidate for RNAi as a therapeutic strategy (Aherne *et al.*, 2004). Given the potential of RNAi and the urgent need for establishing a possible therapeutic strategy for the RP10 form of adRP, the aim of this chapter is to develop si/shRNAs to silence both wild type and mutant IMPDH1 expression at the mRNA and protein levels in mammalian cell cultures.

As a first step to explore RNAi in the treatment of RP10, five different recombinant DNA vectors that employ polymerase III H1-promoter for the synthesis of short hairpin RNAs against both human and mouse IMPDH1 were constructed. The ability of these shRNAs to suppress IMPDH1 mRNA expression was quantified using quantitative Real-Time fluorescent RT-PCR (Roche), which has proven to be a sensitive and specific method to quantitate nucleic acids over a vast dynamic range (Klein, 2002). Initially, the five IMPDH1-specific shRNAs tested exhibited maximal IMPDH1 mRNA silencing ranging from 16% to 45% in HEK293T cells. One of the major obstacles in using RNAi to knockdown gene expression is target sequence selection. Frequently siRNAs targeting different sites of the same gene can elicit varying inhibition of gene expression and target selection is empirical (Chalk *et al.*, 2004; Reynolds *et al.*, 2004). Subsequently, two additional target sites were chosen using more refined and stringent selection criteria (Reynolds *et al.*, 2004). Interestingly, two synthetic siRNAs generated against these newly selected targets showed more potent silencing of wild type and mutant IMPDH1 at the mRNA and protein level in HeLa cells as quantified by Real-Time RT-PCR analysis and western blots. The two effective synthetic IMPDH1-specific siRNAs were then subcloned into the polymerase III H1-vector system, and further testing illustrated that the two shRNAs mediated gene silencing of IMPDH1 with high efficiency comparable to that of synthetic counterparts. In summary, this chapter has demonstrated that two shRNAs expressed from H1-driven RNAi vector system suppressed wild type and

mutant IMPDH1 expression efficiently at the mRNA and protein levels in mammalian cells, and these results have provided the basis for further retinal explant *ex-vivo* (Chapter 4) and mouse *in-vivo* (Chapter 5) studies towards a RNAi-mediated gene therapy for RP10.

3.2 Methods

3.2.1 Construction of small hairpin RNAs targeting IMPDH1 using pSuper DNA-vector based approach

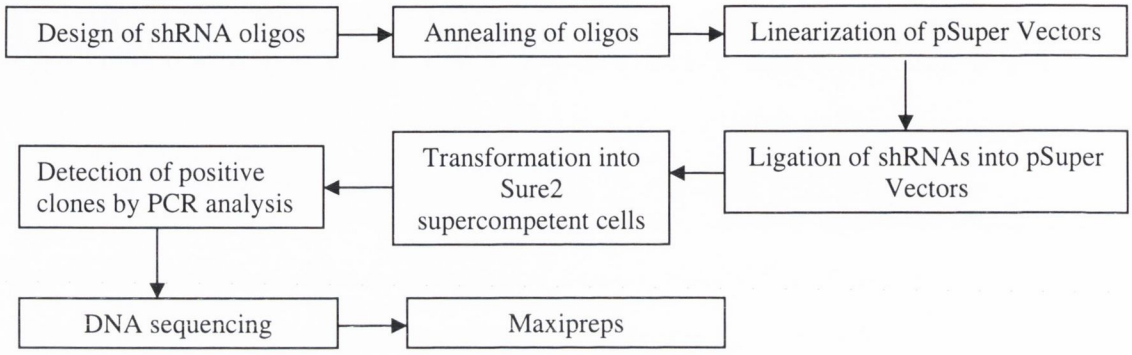

3.2.1.1 Design of short hairpin RNAs

By following the guidelines provided by *www.oligoengine.com* for the expression of short hairpin RNAs from pSuper RNAi vector system, five different sequences encoding shRNAs with 19 bases of homology to human (NM_000883) and mouse IMPDH1 (NM_011829) were synthesised as oligonucleotides (Sigma-Genosys Ltd). The selection of the sequences targeting IMPDH1 was determined using the search-engine supplied by *www.oligoengine.com*, and analysed by BLAST search (www.ncbi.nlm.nih.gov/BLAST) to minimise sequence homology with other genes (*Table 1*, Appendix).

3.2.1.2 Annealing of oligonucleotides

The annealing reaction was carried out by combining 2 µl of each forward and reverse oligonucleotide (100 pmoles) with 46 µl RNase free Universal Buffer. The mixture was heated to 90°C for 4 min and annealed at 70°C for 10 min. The annealed oligonucleotide inserts were then step-cooled to 37°C for 15 min and 10°C for 10 min. 1 µl of the annealed oligonucleotide was used immediately in the ligation reaction, which the remainder was stored at -20°C.

3.2.1.3 Linearisation of pSuper vector

The following enzyme digestion was set up for linearising pSuper vectors:

Components	Volumes/Concentrations
pSuper Vector	5 µl (1 µg)
Hind III	1 µl
Bgl II	1 µl
Buffer 3	5 µl
ddH_2O	88 µl
Total Volume	100 µl

The digestion was incubated at 37°C for 90 min.

3.2.1.4 Ligation of annealed oligonucleotide inserts into linearised pSuper Vector

Ligations were carried out in 15 µl reaction volumes at a vector to insert ratio of 1:5 (w/w) and incubated at 16°C overnight. Negative controls were also included to verify the complete digestion pSuper vector. The components of a ligation reaction included the following:

Components	Volumes			
	Experiment	Negative Controls A	Negative Controls B	Negative Controls C
Linearised pSuper Vector	1 µl	1 µl	1 µl	-
Annealed oligo inserts	5 µl	-	5 µl	5 µl
T4 Ligase	1 µl	1 µl	-	1 µl
T4 Ligase Buffer	1 µl	1 µl	1 µl	1 µl
ddH_2O	7 µl	12 µl	8 µl	8 µl
Total Volume	15 µl	15 µl	15 µl	15 µl

3.2.1.5 Transformation of Sure®2 Supercompetent Cells

100 µl Sure 2 supercompetent cells were aliquoted into pre-chilled 15 ml Falcon 2059 polypropylene tubes and transformation was carried out as outlined by the manufacturers (Stratagene). In brief, 2 µl of 1.22 M of β-mercapthoethanol was added to each of the 100µl aliquots of cells and incubated on ice for 10 min (gentle mixing every 2 min). Approximately 50 ng ligation mix were added to the cells and

incubated on ice for 30 min. During the incubation, NZY^+ broth was preheated in a 42°C water bath. The cells were then heat-shocked at 42°C for 30 sec and returned to ice for 2 min. 900 µl preheated NZY^+ broth was added to the cells and incubated the tubes at 37°C for 1 hr with shaking. 200 µl transformation mixtures were plated on the appropriate antibiotic LB agar plates and incubated overnight at 37°C.

3.2.1.6 Detection of positive recombinant clones

For rapid screening of positive clones following transformation, single colonies were picked carefully (so that only half of a colony was dislodged) and dispersed in 5µl 1XTT. The following heat cycles were applied: 94°C for 5 min, 15° for 2 min followed by 86°C for 1 min. Subsequent to the heat cycles, 20 µl PCR mix (1 unit Taq polymerase, 10 pmoles T7 forward and reverse primers, 0.2 mM dNTPs, 20 ng DNA template, 20 mM $MgCl_2$ buffer and the final volume was made up to 20 µl with ddH_2O) were added to each PCR reaction tubes. The following PCR cycling steps were then used: a denaturing step of 94°C for 5 min followed by 35 cycles of 94°C for 1 min, 55°C for 1 min and 72°C for 1 min 20 sec. A 10 min cycle at 72°C was added to enhance product yield. A positive control (pSuper vector with insert, shMR3 provided by *Dr. Sophie Kiang*) was included in the PCR reaction. After the PCR reaction, amplified DNA was detected using gel electrophoresis with a 1kb DNA ladder (New England Biolabs) as size marker. Positive clones yielded a PCR fragment of 530 bp, which was identical in size to the positive control. Negative clones yielded a product of 466 bp.

Colonies that yielded the correct size PCR product were minipreped and the pSuper vectors were sequenced (ABI Prism) as per section 2.2.13 using specific primers listed in Table 4 (Appendix). Correct recombinant clones were produced in bulk using Qiagen Maxi-prep kit in accordance to manufacturer's instructions.

3.2.2 An 8-criterion algorithm method for the design of chemically synthesised siRNA

The selection of the IMPDH1 targeting sequences for chemically synthesised siRNAs was determined by submitting the IMPDH1 sequence (NM_000883) to the search-

engines supplied by www.dharmacon.com/ www.ambion.com. The resulting sequences were then filtered using the 8 criterion algorithm method devised by Reynolds *et al.*, (2004) to select optimal siRNAs. The algorithm method was as follow: each siRNA target was assigned a score according to each of the logic listed below. A score of six or more points was a benchmark for yielding functional siRNAs.

1. Low G/C content (30-52%).....Plus 1 point
2. Absence of internal repeats.....Plus 1 point
3. An "A" base at position 19 of sense strand.....Plus 1 point
4. An "A" base at position 3 of sense strand.....Plus 1 point
5. An "U" base at position 10 of sense strand.....Plus 1 point
6. An "A/U" base at position 15-19.....Plus 1 point for each A/U
7. A base other than "G" at position 13 of sense strand.....Minus 1 point
8. A "G/C" at position 19 of sense strand.....Minus 1 point

Two siRNA sequences denoted as si1224 and si2048, scoring greater than 6 points, and sharing 19 bases of homology to human IMPDH1 (NM_000883) were selected. si2048 also shared 100% homology to mouse IMPDH1 (BC_053416). The siRNAs were synthesised by Dhamarcon, resuspended to a final concentration of 20pmoles in RNase-free water (Promega). The two siRNAs were also selected on the basis of minimal homology to human (NM_000884) and mouse (BC_052671) IMPDH2. Both IMPDH1-targeting siRNAs were generated as oligonucleotides and subcloned into the pSuper RNAi vector system to create psh1224 and psh2048, respectively, as outlined in section 3.2.1 (*Figure 3.4A*). Rhodopsin targeting siRNA duplexes and H1-driven shRNAs (siMR3 and shMR3) were provided by *Dr. A-S Kiang* (Dept. of Genetics, Trinity College Dublin) as non-targeting controls (Kiang *et al.*, 2005). A commercial synthetic siRNA duplex targeting luciferaseGL3 (siLuc) serving as a non-targeting control was obtained from Qiagen (Elbashir *et al.*, 2001). An additional siRNA duplex targeting luciferaseGL2 (Qiagen) was generated as oligonucleotides and sub-cloned into pSuper RNAi vector system to create pshLuc as outlined in section 3.2.1. Correct insertions of shRNA oligonucleotides were verified by DNA

sequencing as per section 2.2.13 using specific primers as listed in (*Table 4*, Appendix).

3.2.3 Construction of wild type and mutant IMPDH1 expression vectors

All IMPDH1 expression vectors were provided by Dr. Aileen Aherne and detailed cloning steps can be found in Aherne *et al.*, (2004). In brief, the wild-type IMPDH1 cDNA (NM_000883) in pGEM was originally received as a gift from Dr. Beverly Mitchell, University of North Carolina at Chapel Hill, USA. Primers were designed to introduce *Xho*I sites at either end of the wild-type IMPDH1 cDNA sequence and the 1.5 kb IMPDH1 cDNA was amplified by PCR with *Pfu* DNA polymerase (Stratagene). Wild type IMPDH1 cDNA inserts were then cloned into the *Xho*I site of the pcDNA3.1 (+) vector (Invitrogen) to produce pWtIMPDH1 (*Figure 3.1A*). The missense mutations CGC to CCC (Arg224Pro) and GAC to AAC (Asp226Asn) were introduced by amplification of the pET15b-IMPDH1 vector using IMPDH-Arg224 and IMPDH-Asp226 specific primers and the Quikchange XL site-directed mutagenesis kit (Stratagene). Primers were designed to introduce *Xho1* sites at either end of the mutant IMPDH1 cDNA sequences and the mutant IMPDH1 cDNAs were amplified by PCR with *Pfu* DNA polymerase (Stratagene). Both mutant IMPDH1 cDNA inserts were excised and sub-cloned into the Xho1 site of the pcDNA3.1(+) vector, generating pMutIMPDH1(224) and pMutIMPDH1(226) which are driven by the cytomegalovirus promoter (*Figure 3.1A*). In order to generate IMPDH1-EGFP reporter plasmids, the EGFP gene was first excised from pEGFP-N1 (Clontech, BD Biosciences, Inc.) and inserted in between the Hind III and Not I sites of pWtIMPDH1, pMutIMPDH1(224) and pMutIMPDH1(226), which was upstream of the IMPDH1 cDNAs, creating pWtIMPDH1.EGFP, pMutIMPDH1(224).EGFP and pMutIMPDH1(226).EGFP (*Figure 3.1A*). The EGFP gene was also excised from pEGFP-N1 and inserted in between the Hind III and Not I sites of pcDNA3.1(+), creating pcDNA.EGFP. All constructs were sequenced using specific primers (*Table 5*, Appendix) prior to use as shown in *Figure 3.1B.*

3.2.4 Determination of Transfection efficiency

3.2.4.1 β-galactosidase method

HEK293T cells were plated on 24-well plates at $1x10^5$cell/ml (500 µl per well) with $DMEM^{-Abs}$ medium a day prior to transfection. HEK293T cells at 80-90% confluency were transfected with 0.5 µg to 5 µg of pCMV-β mammalian reporter vectors (GIBCO-BRL) using Lipofectamine 2000® (Invitrogen) according to manufacturer's protocol. After 24 hrs of transfection, cells were fixed with 25% glutaldehyde and stained with X-gal and β-galactosidase staining solution at a final concentration of 1mg/ml. Cells were then incubated for 24 hrs in a 37°C incubator, and the number of blue cells in three randomly selected areas per well was counted under a light microscope at 10X magnification to determine the transfection efficiency, and each concentration was performed in triplicates.

3.2.4.2 Determination of vector-based RNAi transfection efficiency by transfection of EGFP expression plasmids in HeLa cells

HeLa cells were plated onto poly-L-lysine coated coverslips in 24-well plates at $1x10^5$cell/ml with $DMEM^{-Abs}$ medium. After 24 hrs, HeLa cells at 80-90% confluency were transfected with 0.1, 0.5, 1, 1.5 and 2 µg/µl pcDNA.EGFP using Lipofectamine 2000® (Invitrogen) according to manufacturer's protocol. 24hrs post-transfection, the cells were washed once in PBS for 5 min and stained with DAPI solution. The cells were washed with PBS and fixed with 4% paraformaldehyde for 20 min at room temperature. After fixing, the cells were washed 3 X 5 min with PBS and the poly-L-lysine coverslips were transferred onto glass slides. Coverslips were then placed onto the glass slides with a few droplets of aqua/polymount solution deposited on top of the cells. The total number of blue cells (total number of cell nuclei stained by DAPI) and green cells (EGFP trasnfected cells) were counted in three randomly selected areas per coverslip under a fluorescence microscope (Zeiss, Axioplan 2) at 20X magnification, and each concentration was performed in quadruplicates. Average percentage transfection efficiency was calculated by: Total number of EGFP positive cells/ Total number of DAPI stained cells X 100.

3.2.5 Transfection protocols

3.2.5.1 Transfection of chemically synthesised siRNAs and pBluescriptH1-driven shRNAs in HEK293T and HeLa cells for RNA analysis

HEK293T and HeLa cells were plated at $1x10^5$cells/ml (500 µl per well) onto a 24-well plate with $DMEM^{-Abs}$ medium one day before transfection. For each transfection sample, 1µg/µl pBluescriptH1 expressing IMPDH1-shRNAs or 20 pmoles chemically synthesised siRNAs were diluted in 50 µl of Opti-MEM-reduced serum medium and mixed gently. 1 µl Lipofectamine 2000® was then diluted to 50 µl Opti-MEM-reduced serum medium and incubated at room temperature for 5 min. The diluted pBluescriptH1 vectors/chemically synthesised siRNA molecules were combined with the diluted Lipofectamine 2000® (total volume is 100 µl) and incubated at room temperature for 25 min for complex formation. 100 µl shRNA/siRNA+Lipofectamine 2000® complex was then added to each sample well. The plate was mixed by gentle rocking and incubated at 37°C in a CO_2 incubator. Each sample was carried out in quadruplicates that were pooled together during RNA extraction (section 2.3.7). IMPDH1 mRNA expression was analysed by Real Time RT-PCR using IMPDH1-specific primers (*Table 2*, Appendix) 24 hrs post-transfection as outlined in section 2.4, and the average of three independent experiments was illustrated. For each transfection experiment, a control group was transfected with either LuciferaseGL3-directed (Qiagen) or rhodopsin-targeting control si/shRNA as non-targeting controls (*Table 1*, Appendix). IMPDH1 expression was standardised per unit house-keeping gene expression (IMPDH2 or β-actin) and expressed as a percentage of that for the non-targeting control as in Kiang *et al.*, (2005).

3.2.5.2 Co-transfection of pWtIMPDH1 and chemically synthesised siRNA in HeLa cells

HeLa cells were seeded at a density of $1x10^5$cells/ml onto a 24-well plate with $DMEM^{-Abs}$. After 24 hrs, 1 µg/µl pWtIMPDH1 was diluted in 50 µl Opti-MEM reduced serum medium with 20pmoles of si1224/si2048. 1 µl Lipofectamine 2000®

was then diluted to 50 µl Opti-MEM-reduced serum medium and incubated at room temperature for 5min. The plasmid/siRNA diluents were combined with Lipofectamine 2000® and incubated at room temperature for 25 min. 100 µl of this mixture was then added to each sample well and mixed by gentle rocking. Transfected cells were incubated at 37°C for 24 hrs prior to RNA extraction. Each sample was carried out in quadruplicates and pooled during RNA extraction as outlined in section 2.3.7. A non-targeting siRNA (siLuciferaseGL3) was included in each transfection experiment. Analysis of IMPDH1 suppression was carried out with RT-PCR using IMPDH1 specific primers, and the average of three independent experiments was taken.

3.2.5.3 Inhibition of wild type and mutant IMPDH1.EGFP fusion proteins by siRNAs in HeLa cells

HeLa cells were seeded onto poly-L-lysine coated coverslips in 24-well plates at a density of $1x10^5$cell/ml with $DMEM^{-Abs}$ medium. After 24hrs, HeLa cells at 80-90% confluency were separately co-transfected with the following combinations of siRNAs and plasmids: 20 pmoles of siLuciferaseGL3 or si1224 as background fluorescence control; 1 µg/µl pcDNA3.1.EGFP and 20 pmoles siLuciferaseGL3 or si1224 as negative controls; four experiments using all plasmid/siRNA combination of 1 µg/µl pWtIMPDH1.EGFP or pMutIMPDH1(224).EGFP and 20pmoles si1224 or si2048. All transfection was carried out using Lipofectamine 2000® (Invirtogen) according to manufacturer's protocol. 72 hrs post-transfection, the cells were fixed with 4% paraformaldehyde (pH 7.4) for 20 min at room temperature and stained with DAPI. The poly-L-lysine coverslips were transferred onto glass slides and plastic cover-slides were placed on top of the coverslips with a few droplets of aqua/polymount solution. Expression of EGFP in transfectants was examined by fluorescence microscope (Zeiss, Axioplan 2) at 20X magnification. Each group of samples was carried out in duplicates and the transfection experiment was repeated two times under the same experimental conditions.

3.2.5.4 Western blot analysis of wild type and mutation protein suppression by IMPDH1-specific si/shRNAs in HeLa cells.

HeLa cells were plated at $1.5x10^5$cells/ml (2 ml per well) onto 6-well plates with $DMEM^{-Abs}$ medium one day prior to transfection. After 24 hrs, separate wells of HeLa cells at a confluency of 80-90% confluency were co-transfected with the following components: 1.5 µg/µl pWtIMPDH1 or pMutIMPDH1(224) or pMutIMPDH1(226) with 100pmoles si1224 or si2048, or 1 µg/µl pBluescriptH1-driven sh1224/sh2048, diluted in 250 µl of Opti-MEM-reduced serum medium and mixed gently. 5 µl Lipofectamine 2000® was then diluted in 250 µl of Opti-MEM-reduced serum medium and incubated at room temperature for 5mins. The diluted IMPDH1 expression vectors/siRNA/shRNA molecules were then combined with the diluted Lipofectamin 2000® (total volume is 500 µl) and incubated at room temperature for 25 min for complex formation. 500 µl of the combined complexes were added to each sample well. The plate was mixed by gentle rocking and incubated at 37°C in a CO_2 incubator for 72 hrs. Each sample was carried out in duplicates and was pooled together during protein extraction. A non-targeting control (si/shLucfieraseGL3) was included in each experiment, and IMPDH1 protein was detected by anti-N-IMPDH1 antibody with each blot being stripped and immunostained with β-actin as loading controls (section 2.5). Each transfection experiment was repeated twice under the same experimental conditions. Band intensities were quantified by scanning with Epson Stylus CX3200 and analysed with the software, *ImageJ*. The percentage reduction in band intensities of IMPDH1 was calculated relative to the non-targeting control, which was standardised to represent 100% IMPDH1 expression and normalised against β-actin.

3.2.5.5 Time-dependent protein expression profile

1.5 µg/µl of pWTIMPDH1.EGFP or pMutIMPDH1(224).EGFP was transfected into HeLa cells using Lipofectamine 2000® as outlined in 3.2.5.4 above. Total protein was extracted between 0 to 72 hrs time intervals and IMPDH1 protein was detected using anti-N-antibody as described in section 2.5. Each blot was stripped and immunostained with β-actin as loading controls.

3.2.5.6 Suppression of Mutant IMPDH1 transcripts in mouse neuronal N2a cells

N2a cells were plated at $1x10^5$cells/ml onto a 24-well plate with $DMEM^{-Abs}$ medium one day before transfection. For each transfection sample, 1 µg/µl pMutIMPDH1(224) and 20 pmoles IMPDH1-synthetic siRNAs were diluted in 50 µl of Opti-MEM-reduced serum medium and mixed gently. 1 µl Lipofectamine 2000® was then diluted to 50 µl Opti-MEM-reduced serum medium and incubated at room temperature for 5 min. The diluted IMPDH1 mutant expression plasmid and siRNA molecules were combined with the diluted Lipofectamin 2000® (total volume is 100 µl) and incubated at room temperature for 25 min for complex formation. 100 µl expression plasmid+siRNA+Lipofectamine 2000® complex was then added to each sample wells. The plate was mixed by gentle rocking and incubated at 37°C in a CO_2 incubator. Each sample was carried out in quadruplicates and pooled together during RNA extraction (section 2.3.7). The level of IMPDH1 mRNA expression was analysed by Real Time RT-PCR using IMPDH1-specific primers (*Table 2*, Appendix) 24 hrs post-transfection (section 2.4), and the average of three independent experiments was taken. For each transfection experiment, a control group was transfected with LuciferaseGL3-directed (Qiagen) siRNA as non-targeting controls (*Table 1*, Appendix). IMPDH1 expression was standardised per unit β-actin expression and expressed as a percentage of that for the non-targeting control.

3.2.6 Detection of apoptosis

HeLa cells were plated at $1x10^5$cells/ml in a 24-well plate containing poly-L-lysine coverslips one day prior to transfection. Cells were separately transfected with 1 µg/µl pcDNA.EGFP, pWtIMPDH1.EGFP and pMutIMPDH1(224).EGFP using Lipofectamine 2000® according to manufacturer's manual. Twenty-four hours later, cells on the poly-L-lysine were washed in PBS, and fixed in 4% paraformaldehyde for 15 min at room temperature. After extensive washing in PBS, the cells were stained with cleaved caspase-3 (Asp175) antibody (1:300 in PBS) overnight at 4°C in a humidity chamber, and counterstained with Cy3 secondary antibody (1:500 in PBS) the following day. The cells were then stained with 4',6-diamindino-2-phenylindole and visualised by using a fluorescence microscope (Zeiss, Axioplan 2). Transfected

cells were identified by green fluorescence and apoptosis was examined by 528 to 553 nm excitation filter to allow detection of red fluorescence. Positive cells fluorescing green and red in six different fields on two independent coverslips were scored blindly. The experiment was repeated twice under the same conditions, and transfection efficiency was calculated by standardising the number of positive EGFP cells against the total number of cells as stained by DAPI in a given field. Percentage cell death was quantified by standardising the number of positive cleaved caspase-3 cells against the number of transfect green cells.

3.2.7 Statistical analysis

All values are presented as mean ± standard deviation (S.D.) unless otherwise indicated. Experiments were done a minimum of three times with two to three repeats per sample. Statistical analysis was done using 2-sample *t*-test and was calculated using Data Desk 6.0 PPC (Data Description, Inc., New York, NY, USA) and Analysis of Variance (ANOVA) post-hoc tests for multiple comparisons (GraphPad Prism). Y-error bars on histograms denote standard error of the mean. Differences were considered statistically significant at $P \leq 0.05$.

3.3 Results

3.3.1 Initial design of short-hairpin RNAs targeting human and mouse IMPDH1

The first step to explore RNAi for the treatment of RP10 involved the selection of distinct siRNA target sites on the human IMPDH1 mRNA sequence (NM_000883). Initially, the human IMPDH1 mRNA sequence was submitted to commercial RNAi target selection softwares provided by *www.oligoengine.com*. Recommended target sites were then aligned against the mouse IMPDH1 mRNA sequence (BC_053416) and the top five target sequences sharing 100% homology between human and mouse IMPDH1 mRNAs were selected. Short hairpin RNAs generated against these targets were termed as sh1057, sh2056, sh2067, sh688, sh1969 (*Figure 3.2*), and their target regions were located on the human IMPDH1 mRNA secondary structure as shown in *Figure 3.3*. These shRNAs are capable of targeting both wild type and mutant IMPDH1 transcripts as their target sites do not coincide with the location of Arg224Pro and Asp226Asn missense mutations (*Figure 3.2*). Although, chemically synthesised siRNA is commonly used to elicit specific gene suppression in higher eukaryotes, the suppression effect is not only transient but also costly. In contrast, the use of conventional expression vectors is more cost-efficient and can result in long term stable down-regulation of mRNA. In this study, the pBluescriptH1 vector system containing a polymerase III H1-promoter, which is an adaptation of the pSuper vector system generated by Brummelkamp *et al.*, (2002) was used to evaluate the suppression of IMPDH1 transcripts in mammalian cells. H1-promoter driven RNAi-vectors directing the synthesis of shRNAs were constructed by inserting an siRNA sequence specific for IMPDH1, which consisted of two 21-nt complementary sequences placed in opposition to each other with the insertion of a 9mer spacer sequence and the attachment of 5 Ts at the 3' end of the sequence downstream of the H1-promoter. Transcription of RNA polymerase III begins immediately after the H1-promoter and is terminated by the insertion of the 5 thymidines. The resulting RNA transcript then folds back to form short hairpin RNAs with 5Us overhang at the 3'end, which are then processed *in-vivo* by DICER (*Figure 3.4*). The advantages of using the H1-promoter are that it contains a specific transcriptional start position and

a termination signal consisting of five thymidines in series (T5), producing small RNA transcripts lacking the polyadenosine tail. The selected length and sequence of the 9-base loop used in this experiment has been found to be the most effective in several micro-RNA precursors and has been evaluated in shRNA secondary structure studies (Castanotto *et al.*, 2002). In addition, the cleavage of the transcript at the termination site yields two uridines producing the two 3'U overhangs of siRNA.

3.3.2 Determination of transfection efficiency

One of the major obstacles in the experimental aspect of RNAi is efficient delivery of target molecules into the cells of interest. In order to determine the ability of plasmid DNA to transfect mammalian cells, 1 μg/μl of pCMV-β reporter plasmid was transfected into HEK293T cells using Lipofectamine 2000® and the number of transfected cells was determined by β-galactosidase staining. After 24 hrs of transfection, the counting of positive β-galactosidase stained cells showed that up to 80.92% ± 4.76% of cells were transfected (*Fig. 3.5*). In addition, no major differences were observed in the number and morphology of HEK293T cells as compared to non-transfected cells 24 hrs after transfection with Lipofectamin 2000®. Therefore, these transfection parameters were used for subsequent RNAi-vector based suppression experiments using HEK293T cells. In addition, transfection parameter for HeLa cells was also investigated. Dose-dependent effects on transfection of increasing amounts of pcDNA.EGFP ranging from 0.1 μg/μl to 2 μg/μl transfected into HeLa cells were determined by counting the number of positive GFP cells 24 hrs post-transfection. As shown in *Fig. 3.6,* transfection efficiency was clearly correlated with the dose of plasmid transfected, with an increasing number of cells being transfected by the use of 0.1 μg/μl to 1.0 μg/μl of plasmids, and a gradual decrease at 1.5 μg/μl and 2 μg/μl. These data have indicated that optimum transfection efficiency was achieved at 1 μg/μl of plasmids showing 56% ± 12.27% of cells being transfected, which differed most significantly from cells transfected with 2 μg/μl of plasmids (P=0.001). Therefore, 1 μg/μl of plasmid was used as a benchmark for future transfection experiments. The observation of lower transfection efficiency of HeLa cells with respect to HEK293T cells was thought to be due to leakiness of β-galactosidase

expression and staining rather than an intrinsic difference. Both cell types were subsequently used, although most experiments were performed using HeLa cells due to their robust nature.

3.3.3 Suppression of endogenous IMPDH1 transcripts by short-hairpin RNAs in HEK293T cells

HEK293T cells were separately transfected with 1 μg/μl of each of the IMPDH1-targeting shRNAs: sh1057, sh2056, sh2067, sh688 and sh1969. As a non-targeting control, shMR3 against rhodopsin (Kiang *et al.*, 2005) was used and the level of endogenous IMPDH1 transcripts was measured by quantitative Real-Time RT-PCR. IMPDH1 expression was standardised per unit IMPDH2 expression and expressed as a percentage of that for the non-targeting control. The suppression data observed in *Figure 3.7* illustrated that all five shRNAs: sh1057, sh2056, sh2067, sh688 and sh1969 downregulated IMPDH1 mRNA levels non-significantly to 55.10% ± 13.02%, 81.59% ± 14.45%, 63.28% ± 16.18%, 69.17% ± 21.77% and 62.76% ± 12.89% ($P>0.05$) respectively, as compared to the non-targeting control. The most efficient suppression (~45%) was achieved with sh1057, but it did not statistically differ from that of sh2056, sh2067, sh688 and sh1969 ($P>0.05$). Various possibilities may account for the incomplete suppression of IMPDH1 expression. First, the selection and accessibility of target sites in the target transcript contributes significantly to the effectiveness of shRNA. However, currently there are no reliable methods for predicting ideal target sequences. Secondly, a closer examination of the construction of the nine-nucleotide spacer arm linking the inverted repeats as constructed according to *www.oligoengine.com* revealed that the DNA sequences were not complementary to each other, possibly creating a secondary loop structure within the plasmid shRNA construct, which may have had an adverse effect on the transcription process (*Figure 3.4B*). Brummelkamp *et al.*, (2002) have demonstrated the importance of the size and nucleotide sequence of the loop on shRNA activity. To understand whether the poor silencing efficiency scored by the five IMPDH1-shRNAs was due to the possible adverse effect caused by the faulty loop secondary structure or by the selection of target sites, the ability of small hairpin RNAs to

inhibit IMPDH1 was compared to that of chemically synthesised siRNA duplex targeted against the same sequence of IMPDH1. The most efficient shRNA, sh1057 was obtained in a chemically synthesised form (*Table 1*, Appendix). Real Time RT-PCR data showed that si1057 reduced the level of IMPDH1 transcripts to 53% ± 17%, compared to the non-targeting control, which did not greatly improve the silencing activity as compared to its short-hairpin counterpart. Therefore the poor silencing activity of the 5 shRNAs was most likely due to the selection of target sites, and that any of the five shRNAs transfected singly is only capable of eliciting partial inhibition on IMPDH1 expression. Thus co-transfection of HEK293T cells with a combination of two or more IMPDH1-specific shRNAs targeting different regions of IMPDH1 transcript was investigated in an effort to increase the inhibitory effect. A combination of two to four IMPDH1-specific shRNAs were transfected into HEK293T cells at a final concentration of 1 μg/μl and the level of IMPDH1 mRNA downregulation was quantified by Real Time RT-PCR 24 hrs post-transfection. IMPDH1 expression was standardised per unit IMPDH2 expression and expressed as a percentage of that for the non-targeting control (shMR3). Sh2065 was excluded from this study because it showed poor suppression efficiency in the previous experiment. The data shown in *Figure 3.7* illustrated that up to 50% ± 7.74% (P=0.0021) suppression of IMPDH1 mRNA was reached when HEK293T cells were co-transfected by a combination of four different shRNAs (sh1057, 2067, 688 and 1969). However, co-transfection of three different shRNAs (sh1057, 2067 and 688) only yielded 42% ± 11% (P=0.2) inhibition of IMPDH1 transcripts. Furthermore, a combination of sh1057 and 1969 showed the highest suppression activity at 53% ± 7% (P<0.0026), but was not significantly different when compared to the use of three or four shRNAs in combinations (P=0.76 and P=0.37, respectively), or the single use of the most efficient sh1057 (P=0.53) (*Figure 3.7*).

3.3.4 Downregulation of endogenous IMPDH1 mRNA by chemically synthesised siRNAs in HeLa cells

The subtle silencing effects elicited by the initial set of shRNAs on IMPDH1 targets may have been the result of poor target selection, similar to that reported by Holen *et*

al., 2002, whereby siRNAs targeting distinct regions on the same mRNA elicited different silencing efficiencies due to accessibility of target sites. Improved criteria for siRNA selection described by Reynolds *et al.*, (2004) and Swarup, (2004) were used to design two additional chemically synthesised siRNAs, si1224 and si2048 (section 3.2.2) targeting different regions in exons 7 and 13 of human IMPDH1 (*Figure 3.2*), and their target regions were located on the human IMPDH1 mRNA secondary structure as shown in *Figure 3.3*. Most of the predominant missense mutations found in IMPDH1 are located in exon 10; therefore the target regions of si1224 and si2048 are independent of the mutations. In particular, si2048 was designed to target both mouse and human IMPDH1 transcripts for convenience of evaluation in both mammalian cell culture and mouse model systems (*Figure 3.2*). In addition, it was thought that an siRNA capable of suppressing both endogenous mouse and exogenous human IMPDH1 transcript would better serve in later gene therapy models of RP10 since, in theory, such a treatment in humans would lead to knockdown of both wild type and mutant endogenous IMPDH1.

Initially, HeLa cells were separately transfected with 20pmoles of si1224 and si2048, and the level of endogenous human IMPDH1 transcripts was quantified by comparison to the non-targeting siRNA (siLuciferase GL3) transfected control using Real Time RT-PCR, and normalised to the corresponding internal control β-actin. Transfection of si1224 and si2048 resulted in a potent reduction of IMPDH1 mRNA levels to 31% ± 12% and 25% ± 5% respectively, compared to the non-targeting control ($P \leq 0.0001$, *Figure 3.8*). Therefore, the most potent IMPDH1 suppressor was found to be si2048, which yielded up to 75% reduction of IMPDH1 transcripts, but it did not statistically differ from that of si1224 ($P=0.89$). In addition, co-transfection of si1224 and si2048 suppressed IMPDH1 mRNA to 20% ± 4% ($P \leq 0.0001$) compared to the non-targeting control (*Figure3.8*). Interestingly, the use of the two siRNA duplexes in combination performed significantly better than si1224 alone ($P=0.026$), but did not show any statistical difference when compared to si2048 ($P=0.959$). These data have suggested that the use of multiple specific siRNA duplexes enhanced the overall inhibitory effect, and that the higher suppression efficiency was not due to

an increase of the total concentration of siRNAs used, because the total quantity transfected was maintained at 20 pmoles. Furthermore, the potent inhibitory effects elicited by si1224 and si2048 have shown that the selection of target sequence using the eight-criterion algorithm method devised by Reynolds *et al.*, (2004) was more robust and effective than conventional algorithms, and that both synthetic siRNAs were capable of knocking down endogenous human IMPDH1 expression very efficiently.

3.3.5 Dose-dependent downregulation of IMPDH1 mRNA expression by synthetic siRNA duplexes

To examine any dose-dependence in the suppression effect of synthetic siRNAs, increasing amounts of si2048 ranging from 5 to 100 pmoles were transfected into HeLa cells. Non-targeting siRNAs targeting luciferaseGL3 were also transfected at concentrations corresponding to those of si2048 and the level of IMPDH1 mRNA expression was quantified by Real Time RT-PCR 24 hrs post-transfection. IMPDH1 mRNA expression was standardised per unit β-actin expression and expressed as a percentage of that for the non-targeting control. The titration curve with graded concentrations of si2048 demonstrated that si2048-mediated downregulation of IMPDH1 mRNA expression was dose-dependent (*Figure 3.9*). The maximal IMPDH1 inhibitory effect was observed at 20 pmoles, with 64% inhibition of IMPDH1 expression, and further increasing the concentration did not increase the inhibitory potential of si2048 (*Figure 3.9*). This finding is in accordance with the recommended concentration of synthetic siRNAs used to achieve optimal silencing efficiency as illustrated in commercial transfection protocols (Invitrogen, Ambion, Oligoengine etc).

3.3.6 Co-transfection of synthetic siRNA duplexes and wild type IMPDH1 expression vectors in HeLa cells

Tissue specific expression analysis (*http://.expression.gnf.org*) has shown that IMPDH1 is most highly expressed in the human and mouse retina. In order to evaluate the inhibitory effect of siRNA in an environment where IMPDH1 transcript

is highly expressed, relative expression levels of IMPDH1 transcripts in cells exogenously transfected with the CMV-driven mammalian expression vectors pWtIMPDH1 expressing wild type IMPDH1 and pMutIMPDH1(224) expression mutant IMPDH1 compared to endogenous IMPDH1 from untransfected cells were first ascertained (*Figure 3.10*). Interestingly, transfection of IMPDH1 expression vectors increased the level of IMPDH1 transcripts in HeLa cells significantly with respect to endogenous IMPDH1 expression. By comparing the ratio of IMPDH1 transcripts between untransfected and transfected cells using Real Time RT-PCR 24 hrs post-transfection (*Figure 3.10*), the level of IMPDH1 transcripts increased by 38 and 98 fold in cells transfected with pWtIMPDH1 and pMutIMPDH1(224), respectively, as compared to untransfected cells. The level of exogenously expressed human IMPDH1 mRNA downregulation was then quantified following co-transfection of pWtIMPDH1 with either si1224 or si2048 by Real Time RT-PCR against a non-targeting siRNA (siLuciferaseGL3). 24 hrs post-transfection, IMPDH1 expression was standardised per unit β-actin expression and expressed as a percentage of that for the non-targeting control. Both si1224 and si2048 downregulated exogenous IMPDH1 mRNA expression by 70% ± 7% (P=0.006) and 76% ± 4.10% (P=0.0027) respectively, as compared to non-targeting siRNA (*Figure 3.11*). This finding has indicated that both IMPDH1-specific siRNAs are capable of maintaining efficient silencing activities in the presence of high IMPDH1 transcript levels.

3.3.7 siRNA-mediated downregulation of wild type and mutant IMPDH1 tagged with enhanced green fluorescent protein (EGFP)

IMPDH1 cDNAs can be readily subcloned into an enhanced green fluorescent protein (EGFP) reporter vector system (pEGFP-N1, Clontech) to create EGFP fusion proteins, and examination of the knockdown of EGFP can then be used to infer knockdown of the fused target transcript. This method provides a rapid and qualitative readout for siRNA efficacy. To evaluate this simple approach for siRNA-mediated silencing of IMPDH1 using EGFP as a visible molecular reporter, pWtIMPDH1.EGFP and pMutIMPDH1(224).EGFP were separatly transfected into

HeLa cells with 20 pmoles of si1224 or si2048. A non-targeting control (siLuciferaseGL3) was also included in this experiment and the level of EGFP fluoresence was analysed with a fluorescence microscope (Zeiss, Axioplan 2). Background fluorescence was observed in HeLa cells separately transfected with the non-targeting siRNA (siLuciferaseGL3) and si1224 (panel A of *Figure 3.12*). For negative controls, the co-transfection of pcDNA.EGFP with siLuciferaseGL3 and si1224 into HeLa cells showed a high level of EGFP fluorescence as shown in panel B of *Figure 3.12*. Transfection of HeLa cells with with pWtIMPDH1.EGFP in the presence of cognate siRNAs inhibited EGFP expression in a majority of co-transfected cells (panels C2 and C3 of *Figure 3.12*) as compared to cells transfected with the non-targeting siRNA (panel C1 of Figure 3). Similarly, transfection of HeLa cells with pMutIMPDH1(224).EGFP and cognate siRNAs led to a strong reduction in the mutant IMPDH1 EGFP fluorescence signals (panels D2 and D3 of *Figure 3.12*), in contrast, the non-targeting siRNA did not mediate downregulation of mutant IMPDH1 EGFP fusion protein (panel D1 of *Figure 3.12*). These qualitative results have indicated that the two IMPDH1-specific siRNAs were capable of suppressing both wild type and mutant IMPDH1 (Arg224Pro) proteins in HeLa cells. In addition, the EGFP system described here has provided a rapid qualitiative readout for siRNA efficacy and may be adapted to a varitey of different cell lines for examining the level of siRNA function.

3.3.8 Downregulation of mutant IMPDH1 transcripts harbouring the Arg224Pro missense mutation in N2a mouse neuronal cell

In order to evaluate the suppression of mutant human IMPDH1 transcripts harbouring the Arg224Pro mutation in murine systems, 1 μg/μl of CMV-driven vectors driving the expression of the human form of IMPDH1 cDNA harbouring the Arg224Pro mutation (pMutIMPDH1224), was co-transfected into N2a mouse neuronal cells with 20pmoles of cognate IMPDH1-specific siRNAs. The level of mutant IMPDH1 expression was quantified by Real Time RT-PCR using primers that specifically discriminate endogenous mouse IMPDH1 mRNA (*Table 3*, Appendix) and standardised against the internal control β-actin. The specificity of these primers was

confirmed by the absence of PCR products detected in the melting curve (*Figure 3.13A*). After 24 hrs of transfection, both si1224 and si2048 showed significant downregulation of mutant IMPDH1 transcripts by 83% ± 8% and 72% ± 4%, respectively, compared to the non-targeting control ($P<0.05$, *Figure 3.13*). However, the silencing of si1224 and si2048 did not differ significantly from each other ($P=0.5$). This result has indicated that both IMPDH1-specific siRNAs can elicit strong silencing effect on exogenous mutant IMPDH1 transcripts in mouse cell lines.

3.3.9 Downregulation of IMPDH1 protein expression following IMPDH1 RNAi-mediated suppression

Analysis of target mRNA could show a downregulation of the corresponding message but the active protein may persist throughout the time of the functional assay. Therefore, western blot analysis was carried out to determine the silencing effect of the two IMPDH1-specific siRNAs on wild type IMPDH1 protein expression. HeLa cells were transfected with the appropriate target moelcules and whole cell extracts were prepared and analysed by western blots 72 hrs post-transfection. The anti-N-IMPDH1 antibody used for detection of the 55 kDa IMPDH1 protein in HeLa cells has previously been shown to be specific for denatured IMPDH1 in western blot analysis, and exhibited minimal cross-reactivity with IMPDH2 (Bowne *et al.*, 2006a). Wild type and mutant IMPDH1 proteins were expressed at high levels in transfected cells with a band clearly visible at 55 kDa (lanes 2 and 3 of *Figure 3.14A*), which were consistent with that reported by Aherne *et al.*, (2004). An absence of IMPDH1 protein bands were evident in untransfected cells (lane 1 of *Figure 3.13 A* and *B*) and also in cells transfected with a construct that did not contain an IMPDH1 cDNA insert (Lane 6, *Figure 3.14B*). The upper panels of *Figure 3.14A* (lanes 5 and 6) and *B* (lanes 4 and 5) illustrate marked reduction of wild type IMPDH1 protein levels by cognate siRNAs, whereas that of the non-targeting control was not affected by the treatment. Quantification of band intensities showed that IMPDH1 protein expression was reduced to 16% ± 6% and 15% ± 5.5% by si1224 and si2048, respectively, as compared to the non-target control ($P=0.0151$ and $P=0.011$, respectively; *Figure 3.14C*). Furthermore, to determine whether the

expression of wild type IMPDH1 protein persisted throughout different time points of transfection, HeLa cells were transfected with wild type IMPDH1 expression plasmids and whole cell lysates were prepared at different time points post-transfection as shown in *Figure 3.15*. The upper panel of *Figure 3.15* illustrated the detection of high levels of wild type IMPDH1 protein from 18-72 hrs after transfection. This observation has indicated the efficiency and stability of the CMV-promoter over time and further indicated that the reduction of IMPDH1 protein by siRNAs was not due to the lack of exogenous gene expression.

To examine the effect of siRNA on mutant IMPDH1 protein expression, HeLa cells were co-transfected with pMutIMPDH1(224) and IMPDH1-specific siRNAs, and whole cell lysates were extracted and analysed by western blots 72 hrs post-transfection in two independent experiments (*Figures 3.16A* and *B*). Mutant IMPDH1 protein was expressed at substantial levels (lanes 1 and 2 of *Figure 3.16A;* lane 1 of *Figure 3.16B*) while an absence of protein was observed in cells transfected with an empty vector (lane 6 of *Figure 3.16A*). Furthermore, mutant IMPDH1 proteins were reduced to undetectable levels by cognate siRNAs (lanes 4 and 5 of *Figure 3.16A*; lanes 2 and 3 of *Figure 3.16B*), whereas the mutant protein level was not influenced by the non-targeting siRNA (lane 3 of *Figure 3.16A*; lane 1 of *Figure 3.16B*). Quantification of band intensites also showed significant reduction of exogenous mutant IMPDH1 protein expression to 16% ± 8% and 20% ± 4% by si1224 and si2048, respectively, as compared to non-targeting control ($P<0.05$ and $P=0.0356$, respectively; *Figure 3.16C*). Collectively, these results have shown that both IMPDH1-specific siRNAs can elicit efficient silencing of both wild-type and mutant IMPDH1 protein expression, which correspond to the significant reduction observed at the mRNA level.

3.3.10 Sub-cloning of si1224/si2048 into pBluescriptH1 vector system and analysis of suppression activity

Although the two synthetic IMPDH1-specific siRNAs have been shown to be effective in suppressing IMPDH1 at the mRNA and protein levels in mammalian

cells, the transient silencing effect and high-cost of production associated with synthetic siRNAs greatly reduce their applicability in long-term *in-vivo* studies. To overcome this limitation, the sequences of the two synthetic IMPDH1-specific siRNAs (si1224 and si2048) were generated as oligonucleotides (*Table 1*, Appendix) and subcloned into the pBluescriptH1 RNAi-vector system to enable the generation of short hairpin RNAs *in-vivo* (*Figure 3.4*). As can be seen in *Figure 3.17*, the suppression efficiency was retained in the pBluescriptH1 vector system where both sh1224 and sh2048 suppressed endogenous IMPDH1 transcripts in HeLa cells by up to 76% ± 5% and 84% ± 4%, respectively, compared to the non-targeting control (P=0.0012 and P=0.0014, respectively). The most potent suppression of IMPDH1 was achieved with sh2048, which differed significantly to that of sh1224 (P<0.0058). Furthermore, the capacity of both sh1224 and sh2048 to silence wild type and mutant protein expression was evaluated in HeLa cells by western blot analysis. In *Figures 3.18A* (lanes 3 and 5) and *B* (lanes 2 and 3), IMPDH1-specific shRNAs showed potent suppression of wild type IMPDH1 protein as compared to the non-targeting control (lanes 2 and 4 of *Figure 3.18A*; lane 1 of *Figure 3.18*B). Quantification of band intensities showed that sh1224 and sh2048 significantly reduced exogenous wild type IMPDH1 protein expression to 23% ± 9% and 17% ± 0.3%, respectively, as compared to non-targeting controls (P=0.169 and P=0.347, respectively; *Figure 3.18C*). In addition, the expression of mutant IMPDH1 protein harbouring the Arg224Pro and Asp226Asn mutations were both reduced to undetectable levels compared to the non-targeting controls in *Figures 3.19* (*A*-lanes 4 and 5; *B*-lanes 3 and 4) and *3.20* (*A* and *B*: lanes 2 and 3), respectively. Furthermore, quantification of band intensities showed that sh1224 and sh2048 reduced exogenous mutant IMPDH1 harbouring the Arg224Pro mutation to 14% ± 2% and 12% ± 4%, respectively, as compared to non-targeting control (P=0.0112 and P=0.0217, respectively; *Figure 3.19C*). Similarly, band intensities showed that sh1224 and sh2048 reduced exogenous mutant IMPDH1 harbouring the Asp226Asn mutation to 29% ± 8% and 22% ± 0.2%, respectively, as compared to non-targeting control (P=0.06 and P≤0.0001, respectively; *Figure 3.20C*). Taken together, these data have demonstrated that by adopting the hairpin structure that mimics pre-miRNAs, polymerase III-H1

directed synthesis of shRNAs can mediate gene silencing of wild type and mutant IMPDH1 with high efficiency comparable to that of synthetic counterparts.

3.3.11 Induction of apoptosis by over-expression of wild type and mutant IMPDH1

In order to examine pathological effects induced by over-expression of wild type and mutant IMPDH1 constructs, HeLa cells were transfected with 1 μg/μl of pcDNA.EGFP, pWtIMPDH1.EGFP and pMutIMPDH1(224).EGFP. Twenty four hours post-transfection, HeLa cells were stained with cleaved caspase-3/Cy3 and scored blindly as shown in *Figure 3.21A* and *B*. Caspase-3 is one of the key executioners of apoptosis, as it is responsible for the proteolytic cleavage of many key proteins such as the nuclear enzyme poly ADP-ribose polymerase (PARP) (Fernades-Alnemri *et al.*, 1994). Activation of caspase-3 requires proteolytic processing of its inactive zymogen into activated p17 and p12 fragments and cleavage of caspase-3 requires aspartic acid at the P1 position (Nicholson *et al.*, 1995). The cleaved caspase-3 antibody used in this study detects endogenous levels of the large fragment of activated caspase-3 resulting from cleavage adjacent to Asp175. Upon examination of transfected cells, expressions of wild type IMPDH1 and EGFP fusion proteins co-localised in the cytoplasm of HeLa cells as shown in *Figure 3.21C*, which was consistent with the subcellular fractionation results reported by Aherne *et al.*, (2004). Moreover, the expression of mutant IMPDH1 EGFP fusion protein appeared to have co-localised with DAPI staining in the cytoplasm and possibly in the nucleus of HeLa cells (*Figure 3.21C*). The localisation of mutant IMPDH1 protein in the nucleus and cytoplasm of HeLa cells may reflect the decreased solubility associated with mutant protein as previously described by Aherne *et al.*, (2004). Interestingly, transfection of EGFP construct alone induced apoptosis in a mean of 1.09% ± 0.80% of transfected cells (*Figure 3.22*), which represents the base-level of apoptosis induced by the use of lipid-based transfectant or the general transfection treatment. Transfection of wild type IMPDH1 plasmid induced cell death in a mean of 4.04% ± 2.62% of transfected cells (*Figure 3.22*), which differed significantly to that of the EGFP construct (P=0.0004). Furthermore, expression of mutant IMPDH1 induced the

highest rate of cell death in a mean of 11.15% ± 5.8% of transfected cells (*Figure 3.22*), which was significantly higher than those induced by the expression of either EGFP or wild type IMPDH1 ($P \leq 0.0001$ and $P=0.0002$, respectively). These results indicated that over-expression of IMPDH1 induces an apoptotic effect in mammalian cells, and that this effect is greater for mutant than wild-type IMPDH1

3.4 Discussion

The demonstration that short double stranded RNA duplexes can induce sequence-specific silencing in mammalian cells has initiated a revolution in the manner in which gene function is examined in cultured mammalian cells. The use of small interfering RNAs mimics the products generated by Dicer in the initiation step of RNAi, and enters the endogenous silencing pathway without triggering non-specific translational suppression via PKR (Elbashir *et al.*, 2001a; Bernstein *et al.*, 2001). Although the conventional use of synthetic siRNAs has offered good silencing activity in mammalian cells, their action is temporarily restricted as their potency becomes diluted throughout several cell divisions when the concentrations fall below the threshold for activity. However this problem was resolved by the development of vector-based RNAi in which siRNA is expressed in the form of short hairpin RNAs mimicking pre-miRNAs (Brummelkamp *et al.*, 2002). In comparison to synthetic siRNAs, which function as short duplex RNA molecules, shRNAs consist of stems of 19 nucleotides, a loop of various sizes and a short 3' overhang (Brummelkamp *et al.*, 2002), and is capable of generating a larger amount of siRNA for a longer period of time. In addition, RNA polymerase III promoters for tRNA or human H1 and/or mouse U6 promoters have been used to transcribe short hairpin RNAs *in-vivo* which provided greater stability and prolonged expression over synthetic counterparts (Brummelkamp *et al.*, 2002; Miyagishi and Taira, 2002a; Paddison *et al.*, 2002a; Kawasaki and Taira, 2003). However, in contrast to synthetic siRNAs which are upon transfection released into the cytoplasm without the need for further processing, shRNAs are transcribed in the nucleus and require extensive transformation such as transportation into the cytoplasm via Exportin-5 and cleavage by the Dicer enzyme. To date, the high efficiency and specificity of RNAi have made it a widely used method to knockdown virtually any protein-coding genes in somatic cell types from both humans and mice, and also as novel therapeutic reagents especially for diseases where the production of aberrant proteins is the predominant feature (Harper *et al.*, 2005; Lewis *et al.*, 2002).

In this study, quantitative Real-Time RT-PCR was used to measure the silencing ability of si/shRNA to inhibit IMPDH1 expression in various mammalian cell types. Real Time RT-PCR has been widely used in both basic research and clinical diagnosis to quantitate nucleic acids over a vast dynamic range (Klein, 2002). In addition, it holds many advantages over conventional methods (e.g. Northern hybridisation and RNase protection assays) for the detection of RNA quantities such as reproducibility, sensitivity precision and accuracy. In addition, for all the RNAi experiments carried out in this study, three different siRNAs that have previously shown great efficacy and specificity against cognate targets were selected as non-targeting controls: siLuciferase GL3 (Qiagen), shLuciferase GL2 (Qiagen) and si/shMR3 (provided by Dr. Sophie Kiang). siRNAs targeting luciferaseGL3 and luciferaseGL2 were first reported by Elbashir *et al.*, (2001a) in a functional study of synthetic siRNAs in mammalian cells, and have also been used extensively in other studies for the suppression of the luciferase gene. The reasons of choice for siMR3 as a non-targeting control was that it had previously been shown in our laboratory to elicit efficient silencing against the mouse rhodopsin gene with no evidence regarding off-target effects, and was also readily available in the laboratory (Kiang *et al.*, 2005).

In an initial attempt to optimise gene suppression of IMPDH1 in a time-efficient and cost-effective manner, five shRNAs targeting distinct regions of human (NM_000883) and mouse (BC_053416) IMPDH1 mRNAs were designed using a computer-assisted software provided by www.oligoengine.com (*Figure 3.2*). These shRNAs were subcloned into the pBluescriptH1 RNAi-vector system (Kiang *et al.*, 2005), which was an adaptation of the earlier DNA-vector system developed by Brummelkamp *et al.*, (2002) that used polymerase III-H1 promoter to direct the synthesis of small inverted repeats separated by a spacer region. The resulting RNA transcript from this construct folds back to form short hairpin RNAs which are then processed *in-vivo* by Dicer enzyme to yield 21-nucleotide siRNA duplexes with two 3' overhangs (*Figure 3.14*). The advantages of using polymerase III-H1 promoter for the synthesis of shRNAs are that it contains a specific transcriptional start position and a termination signal consisting of five thymidines in series (T5), producing small

RNA transcripts lacking the polyadenosine tail. However, the expression of shRNA from DNA-vectors imposes a few sequence restrictions on the primary siRNA design. For example, there should not be more than three consecutive U nucleotides present within the hairpin or loop sequence, as RNA polymerase III terminates at runs of four or more thymidines in the DNA template. Templates should also include 5 thymidines at the 3' end for efficient transcription termination. Moreover, the first nucleotide of the hairpin should preferably be a G or possible an A as the RNA polymerase III requires initiation of transcription with a purine (Mattaj *et al.*, 1988). Conventionally, siRNA-expression systems can be divided into two main approaches: first the sense and antisense strands of siRNA are expressed from different cassettes aligned in tandem in the same construct (i.e. tandem-type) (Miyagishi and Taira, 2002a), or secondly, the sense and antisense strands are expressed as a connected RNA with several intermediate bases which form stem-loop structured siRNA (i.e. stem-loop type) (Brummelkamp *et al.*, 2002). However, comparative studies have shown that the stem-loop shRNA system produced more potent suppression than the tandem shRNA system *in-vivo* (Miyagishi and Taira, 2002a). This finding has indicated that despite the requirement of Dicer processing steps, stem-loop structured shRNA is more suitable for *in-vivo* suppression. Furthermore, the pBluescriptH1vector system has also been used in previous studies in our laboratory to successfully inhibit rhodopsin and *rds*/peripherin in mammalian cells and *ex-vivo* in retinal explants (Kiang *et al.*, 2005; Palfi *et al.*, 2006; O'Reilly *et al.*, 2007).

Initial suppression data have shown that the five IMPDH1-shRNAs selected by commercial algorithms, were only capable of suppressing 18% to 45% of endogenous IMPDH1 mRNA expression in HEK293T cells (*Figure 3.7*). Preliminary speculations for the incomplete inhibition could be the efficiency of shRNA transfection or that the concentration of shRNA transfected (1 μg/μl) was not the optimal. However, transfection control experiment using β-galactosidase staining (*Figure 3.5*) has shown that ~80% of cells were transfected when 1 μg/μl DNA vector was used. Secondly, using enhanced GFP as a reporter marker, transfection of DNA-vector was found to be dose-dependent as shown in *Figure 3.6*, and the most

efficient transfection was also obtained by the use of 1 μg/μl DNA vector. Thus neither poor transfection efficiency nor sub-optimal concentration of shRNA constructs appeared to be responsible for the observed limited suppression of IMPDH1. Interestingly, the titration curve also showed that increasing the dose of DNA-vector during the use of lipid-based transfectants did not lead to increased transfection ability (*Figure 3.6*), perhaps because the lipid-DNA ratio became too small for efficient transfection. To obtain optimal ratio, increasing amounts of lipid-based transfectants would be required, but might be detrimental to the cells as well-known cytotoxic effects related to lipid formulations have been reported (Felgner *et al.*, 1987). However, upon closer examination, non-standard loop sequences incorporated into the shRNA oligonucleotides (*Figure 3.4B*), which could have disrupted the transcription process or caused misfoldings among the oligonucleotides were noted. The importance of the size and loop sequence has been subjected to extensive testing and thorough discussion throughout the literature. The loop structure is a major determinant of successful export of pre-miRNA or shRNA from the nucleus (Zeng and Cullen, 2004), and it has a significant impact on the silencing efficiency (Brummelkamp *et al.*, 2002). Various artificial loops have been successfully tested and the most commonly used construct composition: 5'-$G(N)_{18-21}$TTCAAGAGA$(X)_{18-21}C(T)_5$-3' (G=transcription initiation nucleotide; N= nucleotides in the sense strand; X=nucleotides in the antisense strand), as devised by Brummelkamp and Liu was adopted in this study (Brummelkamp *et al.*, 2002; Liu *et al.*, 2004b). Furthermore, loops derived from naturally occurring miRNAs have been shown to enhance the silencing potential of shRNA. For example, loops derived from human miR-30 (5'-UAAGCCACAGG-3') and human miR-23 (5'-CTTCCTGTCA-3') have shown to increase silencing capacity as opposed to shRNAs bearing the common artificial loop sequence (5'-TTCAAGAGA-3') (Boden *et al.*, 2004; Kawasaki and Taira, 2003; Xia *et al.*, 2004). Interestingly, the miR-30 loop sequence can be shortened to up to nine nucleotides while still retaining the ability to interact with Exportin 5 (Zeng and Cullen, 2004). Although some studies have stressed the importance of loop sequence, other studies have shown that omitting the loop region has no major effect on Dicer machinery, and that efficacy was highly dependent on

the processing of shRNAs by the Dicer enzyme rather than the hairpin structure (Siolas *et al.*, 2005). In order to discriminate the effect contributed by the loop sequence, the most potent of the initial set of IMPDH1-specific shRNAs (sh1057) was generated as a synthetic siRNA duplex (si1057). However, transfection of si1057 into HEK293T cells did not enhance silencing of endogenous IMPDH1 transcripts when compared to that of sh1057. Given that high transfection efficiency was achieved, the suboptimal silencing effects of the five IMPDH1-shRNAs were most likely due to the target sequences selected and not the design of the loop structure. This finding indicates that shRNAs targeting distinct sites on the same mRNA express different silencing efficiencies and that the choice of target sequence contributes immensely to the success of RNAi-based therapies. Similarly, other studies have shown that different siRNAs targeting the same gene do not share equal efficacies and that efficiency was highly dependent on target position and mRNA secondary structures (Holen *et al.*, 2002). Furthermore, statistical analyses have shown that synthesizing four siRNAs at random would yield a 75% chance of obtaining an effective siRNA, whereas synthesising nine siRNAs would still leave a 5% chance of none being active (Khvorova *et al.*, 2003). In an attempt to increase the suppression of IMPDH1 transcripts, two or more IMPDH1-specific shRNAs were co-transfected into HEK293T cells. However, enhanced gene silencing was not achieved with the use of multiple specific shRNAs as shown in *Figure 3.7*. In particular, the silencing effects of using two, three and four shRNAs in combinations did not differ greatly from each other, and also did not show significant improvement when compared to the use of a single sh1057. These findings are different to those previously reported by Ji *et al.*, (2003) who showed that transfection of three independent synthetic siRNAs that shared similar suppression effects when used singly (~70%), significantly increased suppression efficiency to 90% when used in combination. The underlying reason for the lack of increased silencing through the use of multiple shRNAs is still unclear. However, toxic effects related to the use of increased concentrations of shRNAs was excluded as the total concentration was kept constant at 1 μg/μl. Possible explanation for this finding could be the selection of target sites, whereby combining poor target regions does not necessarily improve

overall silencing efficiency or accessibility of the mRNA secondary structure to shRNA binding. In comparison to the study carried out by Ji *et al.*, (2003), who reported enhanced suppression through the use of multiple synthetic siRNAs, the use of multiple vector-based shRNA constructs may have an unforeseen negative impact on the overall RNAi pathway. Pre-miRNAs are structurally analogous to shRNAs, and both are dependent on the karyopherin Exportin 5 (Exp5) for nuclear export (Yi *et al.*, 2003; Lund *et al.*, 2004). Since shRNAs utilise essentially the same cellular processing mechanism as endogenous miRNAs (Bartel, 2004), with the exception that Drosha is only required by the latter, there is a possibility that the accumulation of multiple shRNAs in the nucleus may exhaust the transportation system regulated by Exportin 5, and may also dilute the catalytic turnover rates of Dicer enzymes to cleave short-hairpin RNAs into active siRNA duplexes. Evidence to support of this hypothesis was provided by Yi *et al.*, (2005), who reported that the Exportin 5-mediated nuclear export of pre-miRNAs and the structurally analogous shRNAs represented a rate-limiting step in the biogenesis of mature, biologically active miRNA and shRNA in human cell lines. The authors showed that over-expression of Exportin 5 specifically enhanced target inhibition of gene expression by a shRNA and increased the cytoplasmic expression of mature miRNAs. In addition, over-expression of the RNA processing enzymes Drosha and Dicer did not have any detectable effect on the processing and activity of the human miRNA, miR-30a, which was not surprising as Drosha itself has already been shown to be expressed at high levels endogenously (Wu *et al.*, 2000). However, the lack of effect of Dicer over-expression was unexpected as over-expression of Exportin 5 leads to the cytoplasmic accumulation of pre-miRNAs. This could be rationalised by previous studies in invertebrates showing that Dicer may require additional co-factors for proper function which are also expressed at limited levels (Liu *et al.*, 2003a). These data imply that it would be possible to achieve better suppression of IMPDH1 in cultured cells by using shRNA expressing plasmids in conjunction with simultaneous over-expression of Exportin 5.

The finding that a substantial fraction of randomly computer-designed shRNAs showed poor functionality has suggested that the sequence of a siRNA is its most important functional determinant. Recently, statistical analysis of increasing larger sets of synthetic siRNA sequences have resulted in the identification of design rules that substantially improve the success rate of synthetic siRNA design (Amarzguioui & Prydz, 2004; Huesken *et al.*, 2005; Reynolds *et al.*, 2004). In order to devise siRNAs that elicit greater silencing on IMPDH1, the algorithm developed by Reynolds *et al.*, (2004) was used to improve the selection of more effective synthetic siRNAs. The algorithm of Reynolds *et al.*, (2004) was originally based on statistical analysis of duplex region motifs of 180 21-nucleotide siRNAs targeting two genes in cell cultures. The following motifs were found to be positively correlated with functionality and were incorporated into the selection of IMPDH1 synthetic siRNA sequences: (i) 30-52% G/C content; (ii) at least 3 A/U bases in position 15-19; (iii) absence of internal repeats; (iv) A/U at positions 19; (v) A in position 3; (vi) U in position 10; (vii) absence of G in position 13. Collectively, the consensus sequence for a functional sense strand of a 19-nucleotide siRNA with a 2-nucleotide 3' overhang could be summarised as follows: 5'-S_1-U_{10}-S_{11}-H_{13}-3x$W_{15\text{-}19}$-W$(A)_{19}$dT-dT-3' (subscript indicates a nucleotide position. An A is preferred in position 19; H, S, G, W-IUPAC degeneracies). These features were then incorporated into the design algorithm and siRNA sequences were scored on a point-based system where a point was awarded for every criterion satisfied. A score of more than six points was regarded as a potentially effective siRNA sequence. By applying this algorithm to commercial recommended sequences, two siRNAs scoring greater than six points, si1224 and si2048 (*Figure 3.2*), were selected, and were initially generated as synthetic siRNAs as the algorithm was originally developed through the use of synthetic suppressors. In addition, both IMPDH1-specific siRNAs were designed to bear minimum complementarity to the human IMPDH2 gene to minimise off-target effects (*Figure 3.2*), and in particular, si2048 was selected to target both human and mouse IMPDH1 gene (*Figure 3.2*), which would assist future evaluation of siRNA silencing activity in murine retinal explants and in mouse models which would ideally carry the human form of mutant IMPDH1. To date, other algorithms have also

shown an improvement in the success rate of siRNA design. For example, the algorithm designed by Amarzguioui and Prydz (2004) was based on statistical analysis of duplex region motifs of eighty 21-nucleotide siRNA duplexes targeting five distinct genes. The algorithm incorporated the certain selection features which are quite similar to the one designed by Reynolds *et al.*, (2004): the A/U differential for the three terminal base pairs at each end of the duplex; the positively correlated motifs W19 (A or U at position 19 of sense strand), S1 (G or C at position 1) and A6; and the negatively correlated motifs U1 and G19. Furthermore, the algorithm of Huesken *et al.*, (2005) is a neural network derived algorithm that was trained on the full 21-nt guide sequence of 2,182 distinct siRNAs targeting 34 genes. This algorithm is mainly based on machine learning and no distinct design rules can be formulated. As a result, it operates as a black box and this algorithm is currently the state of the art in siRNA target-site prediction. Recently, these prediction rules have been incorporated into several web-based tools such as Deqor (Henschel *et al.*, 2004) and siDirect (Naito *et al.*, 2004), which are commonly used along with other specialised commercial design tools (*www.dharamacon.com* and *www.qiagen.com*) to predict the cleavage efficacy of siRNAs. The first attempt to compare siRNA efficacy predictors was performed in 2004 by Sætrom and Snove (2004). But no clear indication was discovered as to which siRNA features or web-tool were crucial for optimal prediction (Aravin and Tuschl, 2005). Although some principles and sophisticated softwares have been put forward to facilitate selection, siRNA prediction is still largely an empirical matter and currently there are no fail-safe ways to predict optimal sequences. Therefore siRNAs designed for each specific sequence would still have to be experimentally tested to confirm their silencing efficiency. However one of the leading companies in RNAi, Qiagen, claims that recently developed novel computer prediction software can produce 100% functional siRNAs for any available sequences.

The two newly designed IMPDH1-specific siRNAs were generated as symmetric 21-nucleotide siRNA duplexes with 2 nucleotides 3' overhangs targeting different sites on IMPDH1 mRNA. The results of quantitative Real Time RT-PCR showed that the

two algorithmically designed siRNAs reduced IMPDH1 mRNA levels by 69% and 75% in HeLa cells, respectively (*Figure 3.8*), which outperformed previous shRNAs that had been randomly selected by computer-assisted softwares. Therefore the algorithm devised by Reynolds *et al.*, (2004) seemed to be more stringent and accurate for the selection of siRNA target sequence than the previously used automated predictors. It is well reported that different siRNAs function at vastly different concentrations. Potent siRNAs can be achieved at sub-nanomolar amounts, while others may require larger doses to achieve the same degree of silencing (Ji *et al.*, 2003). Apart from the search for optimal target sequence, it is equally important that optimal concentrations of siRNAs are used. Titration experiment has demonstrated that the silencing of IMPDH1 transcripts in mammalian cells was dose-dependent, with the most effective suppression being achieved at the lower concentration range of 5-20pmoles (*Figure 3.9*). The observation that higher concentrations of synthetic siRNAs failed to elicit stronger suppression could be explained by the fact that excessive amounts of synthetic siRNAs have a negative impact on the efficiency of transfection. Ji *et al.*, (2003) have previously reported that transfection efficiency was found to be dose-dependent, and that the number of transfected cells and inhibition partially correlated to the siRNA concentrations used. This emphasises the importance of the need to optimise siRNA concentration for each experiment to obtain maximum transfection efficiency and silencing activity. Furthermore, an 80% knockdown of IMPDH1 transcripts was achieved by co-transfection of the two synthetic IMPDH1-specific siRNAs in HeLa cells (*Figure 3.8*). This result has demonstrated that the use of multiple synthetic siRNAs elicited significantly greater suppression of IMPDH1 mRNA than the use of a single suppressor (*Figure 3.8*), which is consistent with the observation reported by Ji *et al.*, (2003). The underlying reason for this observation is still unclear, but perhaps the use of multiple synthetic siRNAs may alter the secondary structure of the target mRNA, making the target site more accessible and susceptible to siRNA cleavage. However, this enhancement effect was not observed previously in the use of multiple IMPDH1-specific shRNAs as discussed above (*Figure 3.7*). Possible explanation for this difference could be that the designed algorithms was more powerful in selecting

siRNA sequences than conventional computer-assisted softwares (www.oligoengine.com), and that combining good target regions significantly improved the overall silencing efficiency. Moreover, in comparison to the use of DNA-vector driven shRNAs, the transfection of synthetic siRNA molecules does not require Dicer enzyme processing, or transportation from the nucleus to the cytoplasm via Exportin 5 before incorporation into RISC. As a result, the use of synthetic siRNA duplexes may ultimately have prevented the negative impact of over-loading the RNAi pathway as compared to the use of multiple shRNAs. This hypothesis is further supported by evidence showing that over-expression of Exportin 5 does not enhance RNAi mediated by synthetic siRNA duplexes, which is predicted to gain direct access to the cytoplasm after transfection without requiring Exportin 5-mediated nuclear export (Yi *et al.*, 2005).

Tissue specific expression patterns (*http://expression.gnf.org*) and expression studies carried out by Bowes Rickman *et al.*, (2006) have indicated that the retina possesses the highest level of IMPDH1 expression compared to other tissues in both human and mouse. Tranfection of CMV-driven mammalian expression vectors directing the synthesis of wild type and mutant human IMPDH1 cDNAs resulted in a significant increase of IMPDH1 transcripts in HeLa cells as compared to non-transfected cells (*Figure 3.10*). Furthermore, intracellular localisation of the wild type IMPDH1 EGFP fusion proteins seemed to appear predominantly in the cytoplasm only, and mutant IMPDH1 protein harbouring the Arg224Pro mutation appeared to have localised in both the nucleus and cytoplasm of HeLa cells (*Figure 3.20B*). Previous subcellular fractionation studies carried out by Aherne *et al.*, (2004) showed that mutant IMPDH1 protein harbouring the Arg224Pro exhibited considerably decreased solubility, and as a result, the majority of the mutant protein only localised in the insoluble cellular fraction. Therefore the localisation of mutant IMPDH1 protein in the nucleus and cytoplasm observed in this study may represent the insoluble form of mutant protein. However, future studies involving subcellular fractionation in HeLa cells would have to be carried out to confirm these results. In addition, confocal microscopy may also give better insights into the localisation of wild-type and mutant

IMPDH1 protein in different cellular compartments. Interestingly, over-expression of mutant IMPDH1 harbouring the Arg224Pro mutation induced a strong apoptotic response in HeLa cells as detected by cleaved caspase-3 antibody staining, whereas over-expression of wild-type IMPDH1 induced a subtle apoptotic response when compared to the expression of EGFP alone (*Figure 3.21*). The induction of cell death by over-expression of mutant protein is not an uncommon pathological effect in the retina, as previously reported by Illing *et al.*, (2002) showing that over-expression of mutant rhodopsin harbouring the P23H mutation in cell culture causes apoptosis via protein aggregation. In another study, Rebello *et al.*, (2004) have demonstrated that over-expression of the R14W mutant gene encoding carbonic anhydrase IV (CA4) induced apoptosis via protein aggregation in mammalian cells. In this study, it remains to be deciphered whether the apoptotic effect observed in HeLa cells is due to the over-expression of mutant IMPDH1 protein alone, or as a result of an unknown pathological effect related to the expression of mutant IMPDH1. However, the observation that over-expression of wild type IMPDH1 and EGFP only induced a mild apoptotic response, and early data reported by Aherne *et al.*, (2004) regarding decreased mutant protein solubility in mammalian cells have strongly suggested that the formation of protein aggregates is likely to be the cause of the pathological effect. Apoptosis is a complex mechanism that can be mediated by numerous pathways involving intracellular and extracellular signals, and it is also difficult to monitor as only a small proportion of cells may show apoptosis at any given time. The results obtained in this study represented the induction of apoptosis after twenty hours of transfection, and additional time-points are required to determine further unknown pathological effects related to over-expression of mutant IMPDH1. In addition, immunostaining with cleaved caspase-3 antibody represents an early event in the apoptotic pathway, and perhaps future studies should also include other downstream apoptotic assays such as terminal deoxynucleotidyl transferase biotin-dUTP nick end labelling (TUNEL), which is a distinct marker for DNA fragmentation. Furthermore, HeLa cells used in this study as an apoptotic model do not represent a cellular system originating from the retina. Therefore, a thorough analysis in retinas is needed to investigate and evaluate *in-vivo* the role of mutant IMPDH1 expression in the

pathogenesis of RP10. Following this, co-transfection of pWtIMPDH1 and IMPDH1-specific siRNAs in HeLa cells reduced the level of endogenous and exogenous wild type IMPDH1 transcripts to approximately 24% when compared to the non-targeting control (*Figure 3.11*). This result has indicated that strong silencing was maintained among the two IMPDH1-specific siRNAs in a cellular environment where the target transcript is in excess to that of the suppressors. In addition, by using specifically designed primers to discriminate human IMPDH1 mRNA from that of mouse, the results obtained from Real-Time RT-PCR showed that the two IMPDH1-specific siRNAs were capable of eliciting strong suppression on exogenous mutant IMPDH1 transcripts harbouring the Arg224Pro mutation in mouse neuronal cells (*Figure 3.13*). This result has further indicated that the two rationally designed IMPDH1-specific siRNAs can elicit efficient silencing on exogenous mutant IMPDH1 transcripts in mammalian cell cultures.

Transfection of reporter EGFP marker and IMPDH1 cDNA fusion constructs into HeLa cells has permitted the use of live imaging to assess the suppression of IMPDH1 protein by fluorescence microscopy. This method has provided rapid screening of functional siRNAs by fusing target sequences to EGFP, and has also proven to be a convenient and reliable method for determining the impact of siRNAs on wild type and mutant IMPDH1 protein expression. Constitutive expression of wild type and mutant IMPDH1 tagged EGFP proteins were successfully silenced in a high proportion of transfected cells (*Figure 3.12*), suggesting that both normal and mutant allelic transcripts were susceptible to gene silencing at the same target regions. Furthermore, western blot analysis was used to examine the level of alteration in post-transcriptional and translational processes in HeLa cells treated with IMPDH1-specific siRNAs. The signals for the 55 kDa wild type and mutant IMPDH1 protein were suppressed to undetectable levels by the two IMPDH1-specific siRNAs when compared to the non-targeting controls (*Figure 3.13 and 3.15*), which strongly correlated with earlier results demonstrating the ability of IMPDH1-specific siRNAs to reduce IMPDH1 expression at the mRNA level. Interestingly, no IMPDH1 protein band of size 55kDa was detected by western blot analysis in untransfected HeLa

cells. Wild type IMPDH1 protein has a half life of ~30 hours (Expasy Protparam Tool) and is found to be stable in cell cultures. Initial speculation is that the anti-N-IMPDH1 antibody used in this study can only detect IMPDH1 protein that is expressed above a certain basal level. This assumption is supported by the detection of IMPDH1 protein in HeLa cells transfected with exogenous IMPDH1 constructs, but not detected in control (pcDNA3.1 vector only) or untransfected cells (*Figures 3.13, 3.15A, 3.17A, 3.18*). In addition, Bowne *et al.,* (2006a) showed that the anti-N-IMPDH1 antibody was able to detect endogenous IMPDH1 protein expression in human and mouse retinal tissues in a concentration-dependent manner. This observation further supports the assumption as IMPDH1 is found to be expressed highly in the retina compared to other tissues in the body. The issue regarding the sensitivity of the antibody and the minimum level of IMPDH1 protein expression that is required for detection will be evaluated in additional studies.

Although the two synthetic IMPDH1-specific siRNAs have offered good silencing activity against wild type and mutant IMPDH1 at the mRNA and protein levels in mammalian cell cultures, the silencing effect is temporarily restricted as their concentrations fall below the active threshold through cell division. Therefore, the two IMPDH1-specific siRNAs were generated as oligonucleotides and subcloned into the pBluescript-H1 vector backbone to achieve sustained gene silencing in *ex-vivo* and *in-vivo* systems. The conversion of synthetic siRNAs to vector-based shRNAs has been discussed extensively by Matveeva *et al.*, (2007), and various considerations should be taken into account during this transfer. The optimal duplex stability and relevant G/C content may vary between shRNAs and synthetic siRNAs due to differences in RNA secondary structures. Thermodynamic parameters of the 3' overhangs for shRNAs are most likely different from those for siRNAs since in the former they are represented by RNA and in the latter, by DNA nucleotides. The capacity of the two new IMPDH1-specific shRNAs to silence endogenous IMPDH1 transcripts were tested in HeLa cells and both shRNAs reduced IMPDH1 mRNA expression to 24% and 16%, respectively (*Figure 3.16*), which were more efficient than their synthetic counterparts (*Figure 3.8*). Moreover, the two IMPDH1-specific

shRNAs strongly suppressed both wild type and mutant IMPDH1 proteins harbouring the Arg224Pro and Asp226Asn mutations in HeLa cells (*Figure 3.17, 3.18 and 3.19*). These results have fully demonstrated that siRNA design rules can be transferred directly to shRNA without affecting the silencing efficacy, and that polymerase III H1-driven short hairpin RNAs, modeled conceptually on miRNAs, are potent experimental tools for inducing gene silencing of IMPDH1 in mammalian cells. Moreover, the ability to encode a constitutive silencing signal may permit the alliance of shRNA induced silencing with *ex-vivo* and *in-vivo* gene delivery methods for therapeutic approaches based on stable RNAi in humans.

3.5 Summary of current findings

The current study has provided strong evidence that IMPDH1-specific siRNAs can elicit a strong silencing effect on wild type and mutant IMPDH1 expression at the mRNA and protein levels in mammalian cell cultures. In addition, the selection of target sequence was found to play a major role in determining the efficiency of siRNA functionality. Recently developed prediction algorithms (Amarzguioui & Prydz, 2004; Huesken *et al.*, 2005; Reynolds *et al.*, 2004) and advanced commercial softwares (siDirect) have greatly improved the selection of optimal siRNA sequences. The selection of potent siRNAs in this study initially involved retrieval of potential IMPDH1 target sites through readily available commercial softwares (www.dharmacon.com), and subsequently filtered these through the prediction algorithm devised by Reynolds *et al.*, (2004). This prediction pathway has combined the advantages of both systems and has proven to be extremely valuable in selecting novel siRNAs in the future. The data have also demonstrated that the silencing efficiency of synthetic IMPDH1-specific siRNAs was retained in H1-driven shRNA constructs, indicating that siRNA design rules can be transferred directly to shRNA without affecting silencing efficacy. Moreover, over-expression of mutant IMPDH1 harbouring the Arg224Pro mutation triggered a significant apoptotic response in HeLa cells. However, the underlying pathological mechanism has not yet been fully deciphered and further studies into the aberrant production of mutant IMPDH1 protein aggregates may help decipher the pathophysiological process that leads to RP10 in photoreceptor cells. RNAi-mediated mRNA degradation is an active process that requires the proper function of a series of endogenous proteins. Whether the RNAi mechanism is preserved *ex-vivo* in murine retinal explants, as suggested by previous studies in our laboratory (Kiang *et al.*, 2005; Palfi *et al.*, 2006; O'Reilly *et al.*, 2007) is addressed in the next chapter.

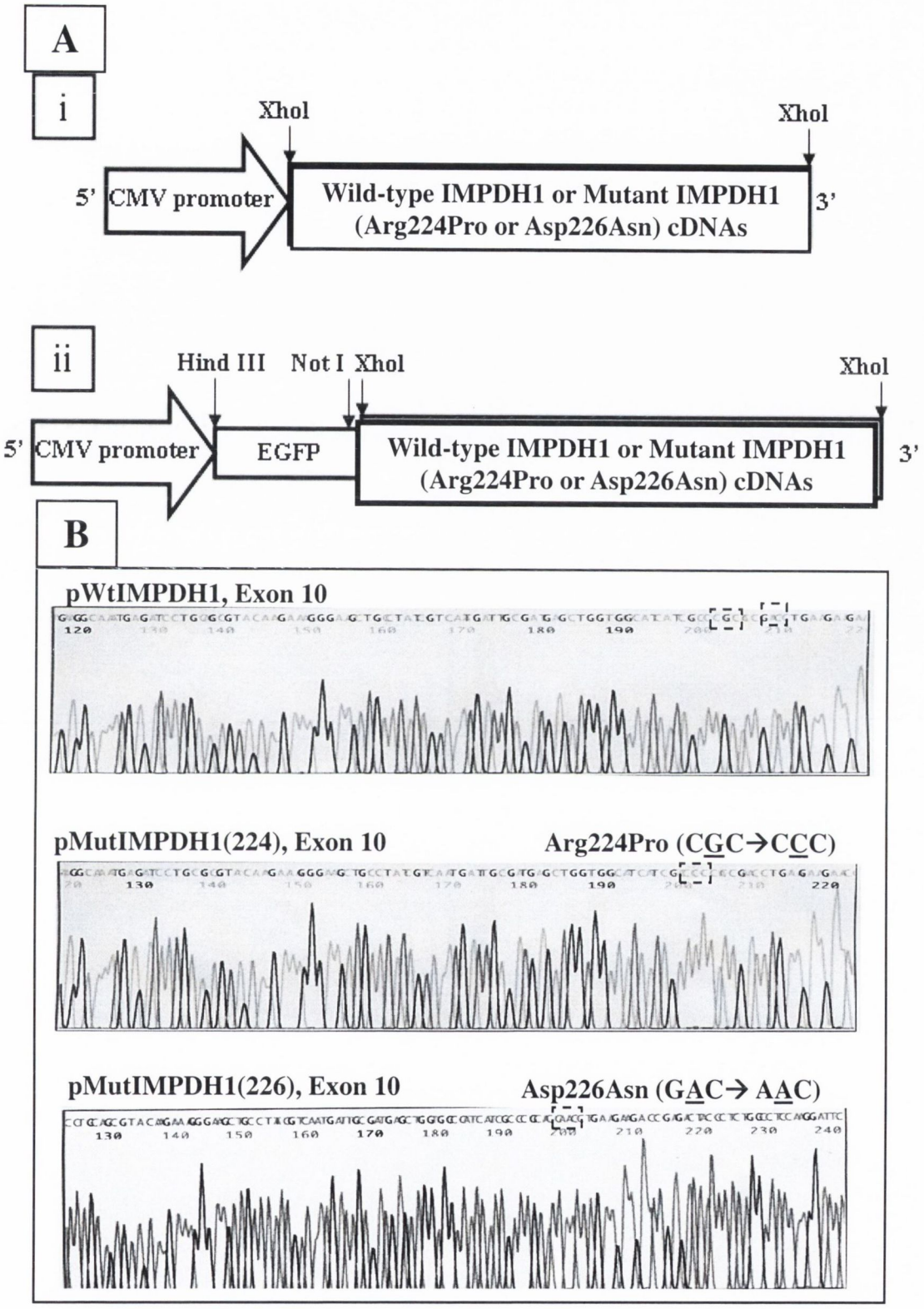

Figure 3.1: (A) Schematic diagrams illustrating the cloning of wild type and mutant IMPDH1 cDNAs into pcDNA3.1(+): (i) Vector maps of pWtIMPDH1, pMutIMPDH1(224) and pMutIMPDH1(226) (ii) Vector maps of pWtIMPDH1.EGFP, pMutIMPDH1(224).EGFP and pMutIMPDH1(226).EGFP (B) Sequencing of pWtIMPDH1, pMutIMPDH1(224) and pMutIMPDH1(226). Dotted areas indicate location of missense mutations.

The 19bp-target site of sh1057 is located on exon 5 of human IMPDH1 (NM_000883)

Human IMPDH1 5'-A·A·G·C·U·G·G·U·G·G·G·C·A·U·C·G·U·C·A-3'

Sh1057 antisense 3'-U·U·C·G·A·C·C·A·C·C·C·G·U·A·G·C·A·G·U-5'

Mouse IMPDH1 5'- A·A·G·C·U·G·G·U·G·G·G·C·A·U·C·G·U·C·A-3' (No mismatches)

The 19bp-target site of sh2065 is located on exon 12 of human IMPDH1 (NM_000883)

Human IMPDH1 5'-A·A·G·U·U·U·G·A·G·A·A·G·C·G·G·A·C·C·A-3'

Sh2065 antisense 3'-U·U·C·A·A·A·C·U·C·U·U·C·G·C·C·U·G·G·U-5'

Mouse IMPDH1 5'- A·A·G·U·U·U·G·A·G·A·A·G·C·G·G·A·C·C·A-3' (No mismatches)

The 19bp-target site of sh2067 is located on exon 12 of human IMPDH1 (NM_000883)

Human IMPDH1 5'-G·U·U·U·G·A·G·A·A·G·C·G·G·A·C·C·A·U·G-3'

Sh2067 antisense 3'-C·A·A·A·C·U·C·U·U·C·G·C·C·U·G·G·U·A·C-5'

Mouse IMPDH1 5'- G·U·U·U·G·A·G·A·A·G·C·G·G·A·C·C·A·U·G-3' (No mismatches)

The 19bp-target site of sh688 is located on exon 2 of human IMPDH1 (NM_000883)

Human IMPDH1 5'-C·U·C·A·C·C·U·A·C·A·A·C·G·A·C·U·U·C·C-3'

Sh688 antisense 3'-G·A·G·U·G·G·A·U·G·U·U·G·C·U·G·C·C·G·G-5'

Mouse IMPDH1 5'- C·U·C·A·C·C·U·A·C·A·A·C·G·A·C·U·U·C·C-3' (No mismatches)

The 19bp-target site of sh1969 is located on exon 12 of human IMPDH1 (NM_000883)

Human IMPDH1 5'-G·U·T·C·C·C·U·A·C·C·U·C·A·U·A·G·C·A·G-3'

Sh1969 antisense3'-C·A·U·G·G·G·A·U·G·G·A·G·U·A·U·C·G·U·C-5'

Mouse IMPDH1 5'-G·U·T·C·C·C·U·A·C·C·U·C·A·U·A·G·C·A·G-3' (No mismatches)

The 19bp-target site of si1224 is located in exon 7 of human IMPDH1 (NM_000883)
Human IMPDH1 5'-G·C·U·G·C·C·U·A·U·C·G·U·C·A·A·U·G·A·U-3'
sh1224 antisense 3'-C·G.A.C.G.G.A.U.A.G.C.A.G.U.U.A.C.U.A-5'
Mouse IMPDH1 5'-G·C·U·G·C·C·**C**·A·U·**A**·G·U·C·A·A·**C**·G·A·U-3' (3 mismatches)
Human IMPDH2 5'-G·**U**·U·G·C·C·**C**·A·U·**U**·G·U·**A**·A·A·U·G·A·**A**-3'(5mismatches)
Mouse IMPDH2 5'- G·**U**·U·G·C·C·**C**·A·U·**U**·G·U·**G**·A·A·T·G·A·**A**-3' (5 mismatches)

The 19bp-target site of si2048 is located in exon 13 of human IMPDH1 (NM_000883)
Human IMPDH1 5'-U·G·U·A·C·U·C·A·G·G·A·G·A·G·C·U·C·A·A-3'
sh2048 antisense 3'-A·C·A·U·G·A·G·U·C·C·U·C·U·C·G·A·G·U·U-5'
Mouse IMPDH1 5'- U·G·U·A·C·U·C·A·G·G·A·G·A·G·C·U·C·A·A-3' (No mismatches)
Human IMPDH2 5'-U·G·U·A·C·U·C·**U**·G·G·**G**·G·A·G·C·U·**U**·A·A-3' (3 mismatches)
Mouse IMPDH2 5'- U·G·U·A·C·U·C·**G**·G·G·**G**·G·A·G·C·U·**U**·A·A-3' (3 mismatches)

Figure 3.2: Alignments of IMPDH1 targeting shRNA target sites with human IMPDH1 (NM_000883), mouse IMPDH1 (BC_053416), human IMPDH2 (NM_000884) and mouse IMPDH2 (BC_052671). Human/mouse IMPDH1 and IMPDH2 cDNAs were obtained from NCBI nucleotide database (http://www.ncbi.nlm.nih.gov/sites/entrez) and aligned using Clustal W multiple sequence alignment (http://www.ebi.ac.uk/clustalw) provided in the public domain by the European Bioinformatics Institute, European Molecular Biology Laboratory, Heidelberg, Germany. shRNAs are named according to the relative positions of the 5' nucleotide within NM_000883.

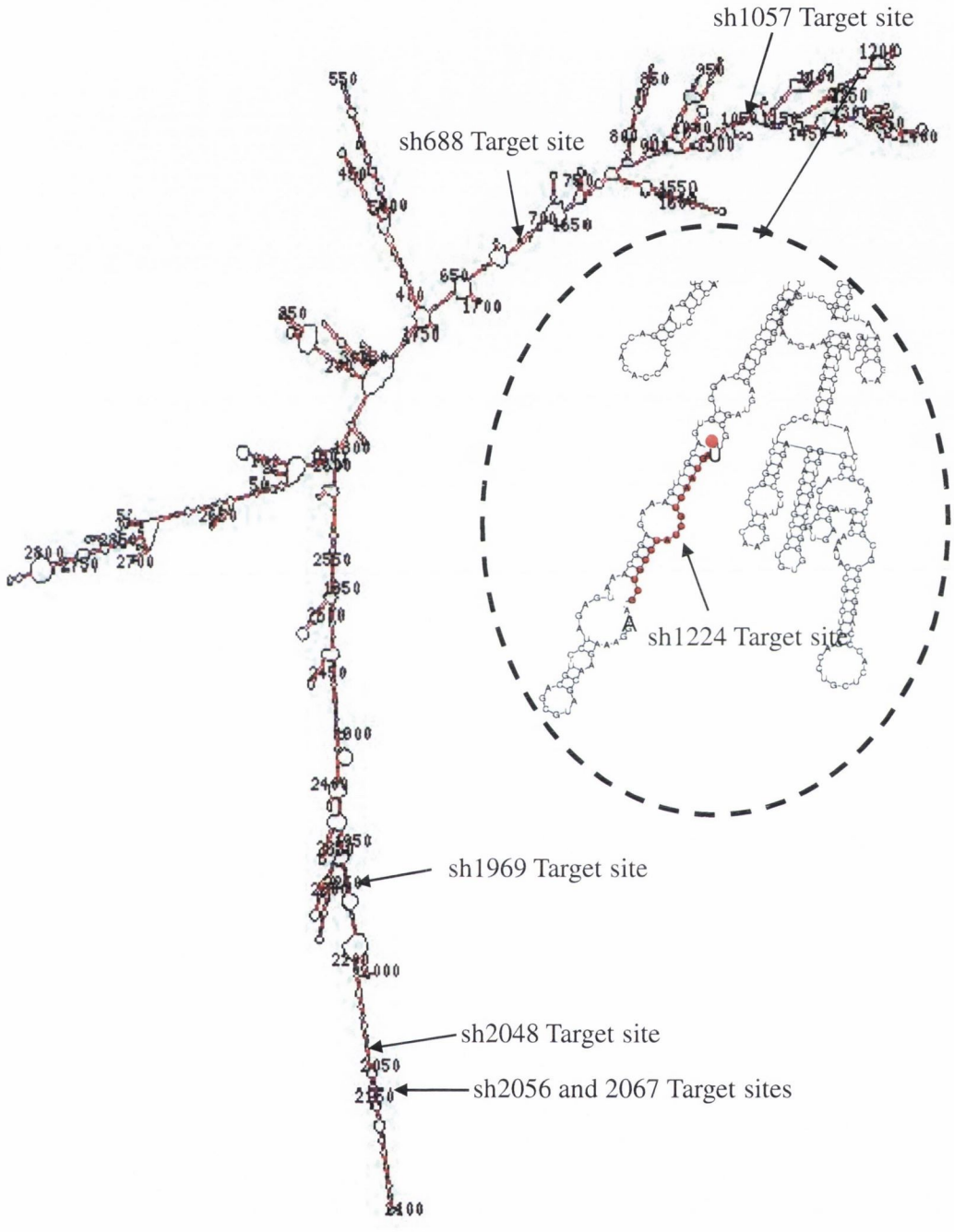

Figure 3.3: Human IMPDH1 mRNA (Accession Number: NM_000883) secondary structure folded by mFold software (http://www.mFold.com). Target sites of all IMPDH1-specific siRNAs designed in this study are located on the human IMPDH1 mRNA secondary structure. An enlargement of the detail around sh1224 target site is given.

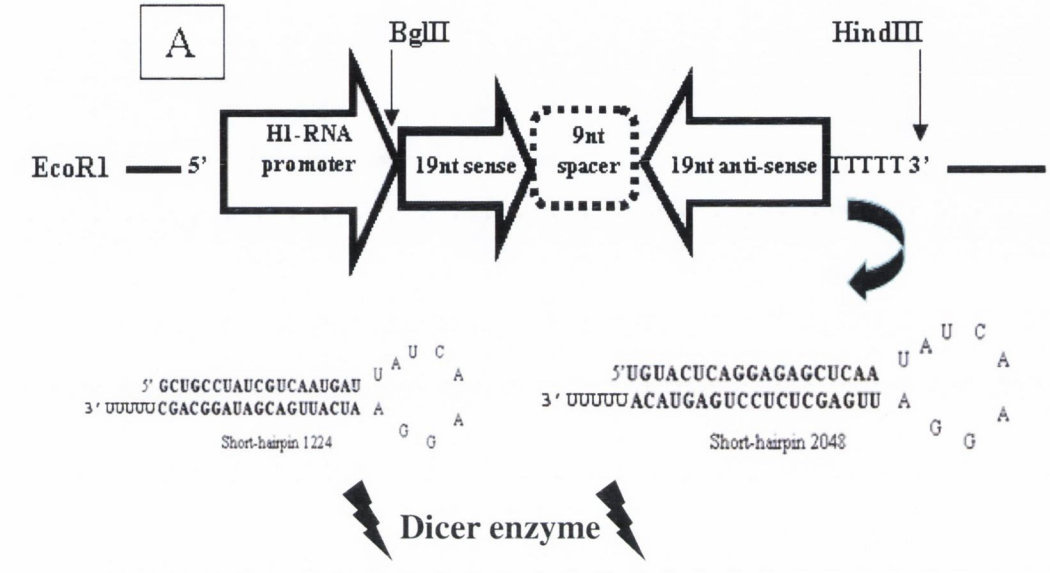

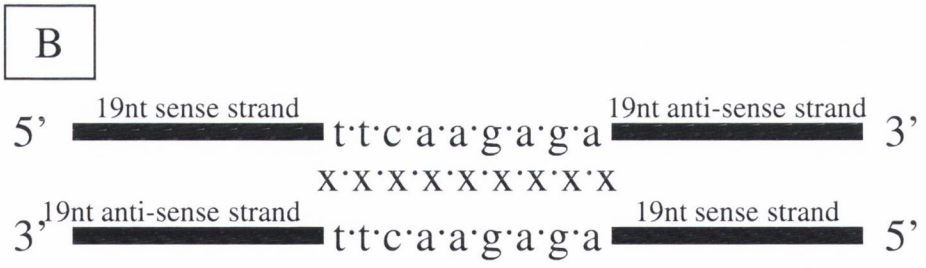

Figure 3.4: **(A)** Sub-cloning of shRNA oligonucleotides into pBluescriptH1 vector to construct the human H1 polymerase III promoter driven vector for short hairpin RNA. Schematic illustrations of short hairpin RNA transcripts. **(B)** The incorporation of a non-complimentary loop sequence in the antisense strand of the shRNA DNA template, where 'X' denotes non-complementarity.

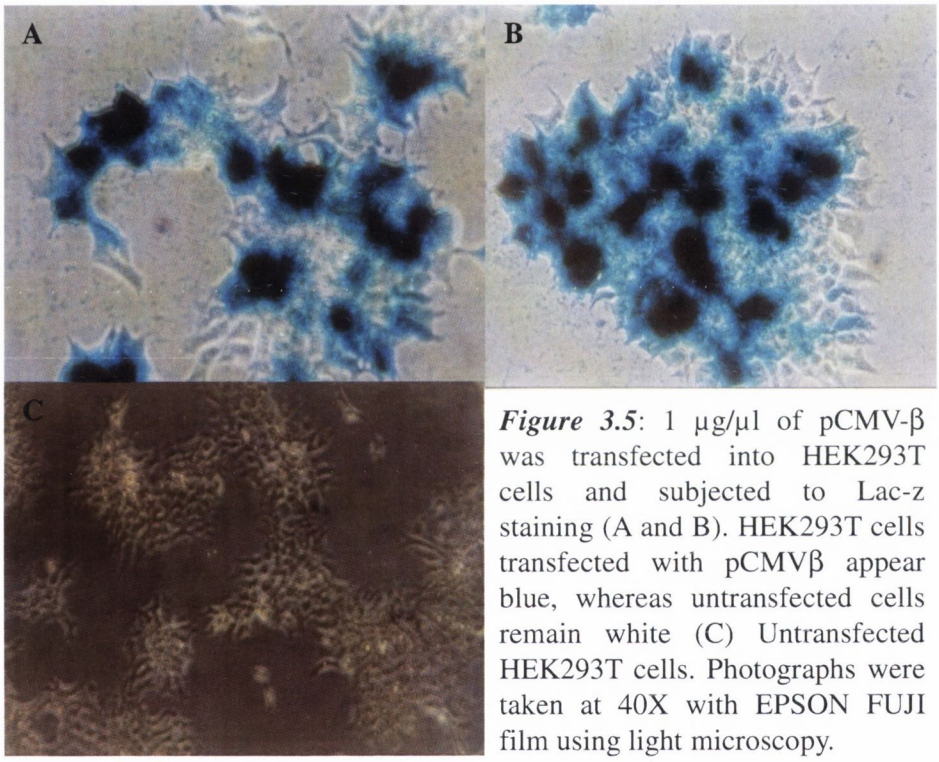

Figure 3.5: 1 µg/µl of pCMV-β was transfected into HEK293T cells and subjected to Lac-z staining (A and B). HEK293T cells transfected with pCMVβ appear blue, whereas untransfected cells remain white (C) Untransfected HEK293T cells. Photographs were taken at 40X with EPSON FUJI film using light microscopy.

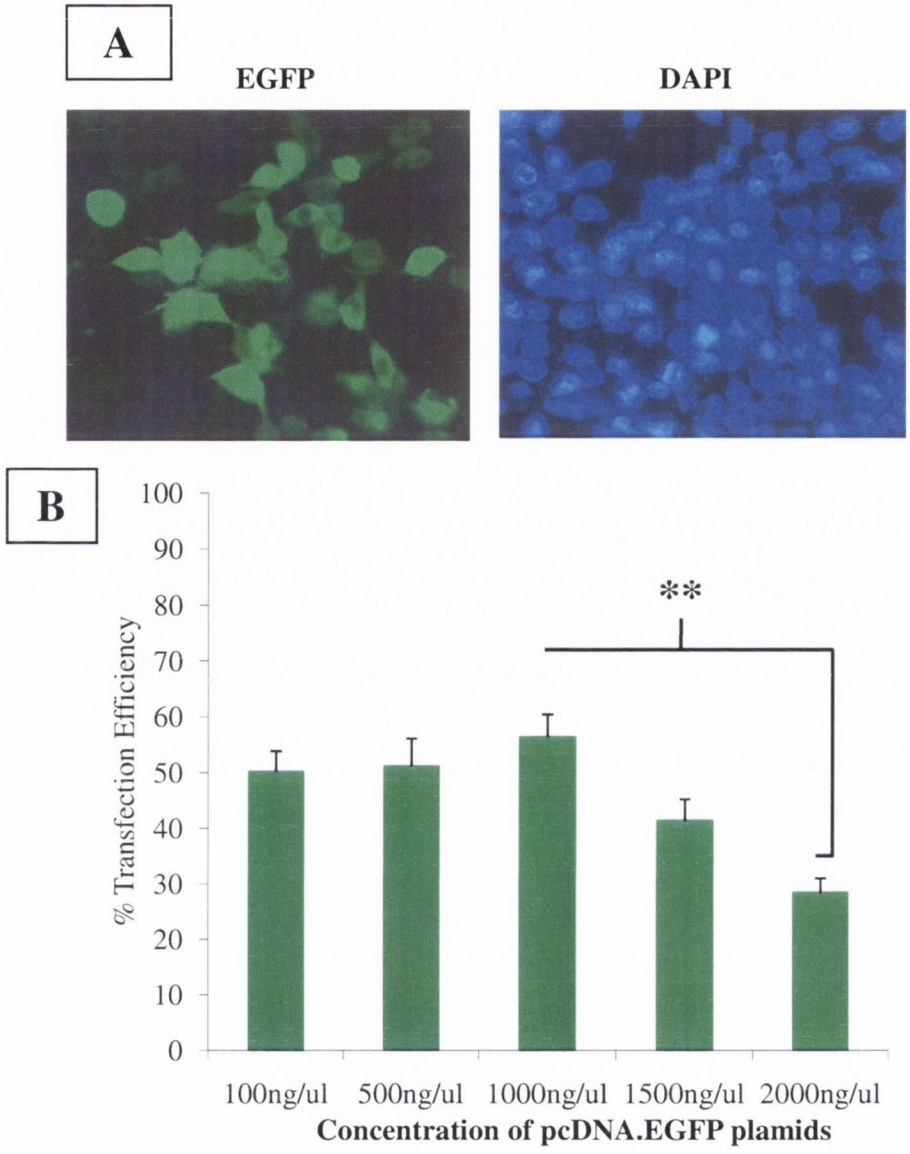

Concentrations of pcDNA.EGFP	100ng/µl	500ng/µl	1000ng/µl	1500ng/µl	2000ng/µl
% Transfection Efficiency	50.19%±3.7%	51.21%±4.95%	56.41%±4%	41.39%±3.83%	28.41%±2.6%

Figure 3.6: Effect of dose on the transfection efficiency of plasmid vectors in mammalian cells. HeLa cells were plated on cover-slides in a 24-well culture plate and transfected with 100 to 2000 ng/µl pcDNA.EGFP. 24 hrs post-transfection, cells were fixed in 4% paraformaldehyde and three random areas were selected for viewing under the fluorescence microscope. The number of positive EGFP and DAPI cells were counted blindly, and the percentage transfection was calculated by: (Number of EGFP cells/Number of DAPI-stained cells)x100. (A) Fluorescent pictures of HeLa cells 24 hrs post-transfection. (B) Histogram showing percentage transfection. The average of three independent experiments is shown; Y-error bars indicate standard of the mean (SEM). * $P < 0.05$. **$P<0.001$

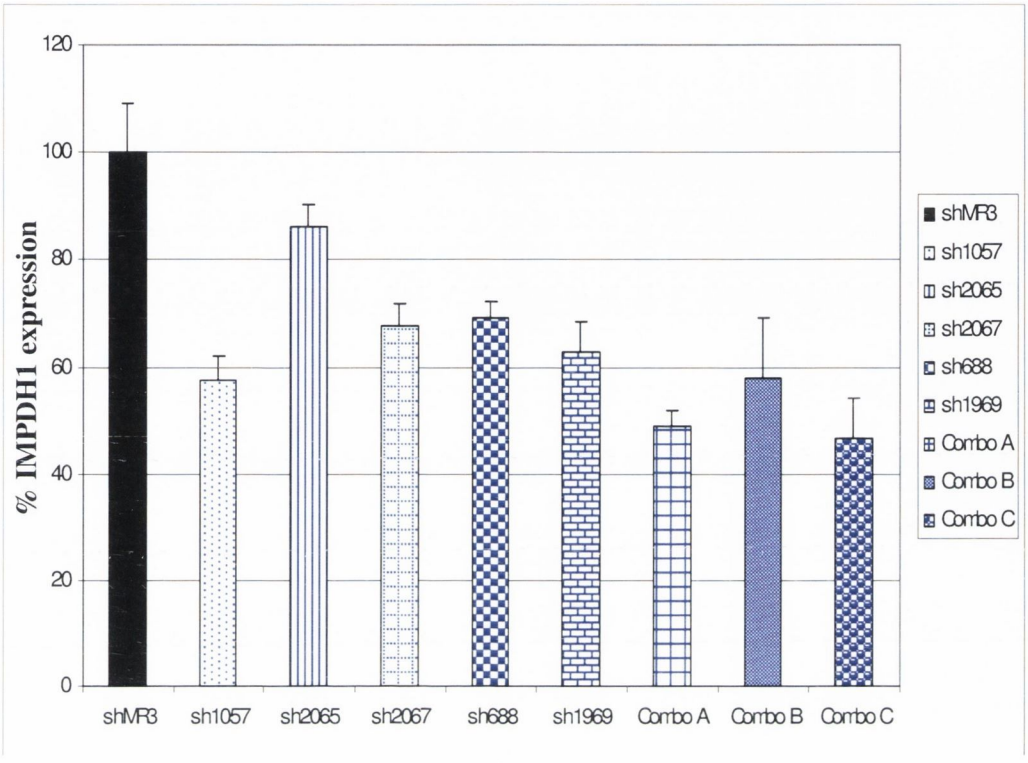

shRNAs	Sh1057	Sh2065	Sh2067	Sh688	Sh1969	Combo A	Combo B	Combo C
%IMPDH1 expression ± SEM	55% ± 5%	82% ± 6%	63% ± 7%	69% ± 8%	63% ± 6%	50% ± 7%	58% ± 11%	47% ± 7%

Figure 3.7: Suppression of endogenous IMPDH1 transcripts in HEK293T cells. HEK293T cells were separately transfected with 1 μg/μl of five different pBluescriptH1-based RNAi vectors directing the synthesis of IMPDH1-specific shRNAs (sh1057, sh2065, sh2067, sh688 and sh1969). In addition, HEK293T cells were co-transfected with a combination of shRNAs. Combo A represents a combination of sh1057, 2067, 688 and 1969. Combo B included sh1057, 2067 and 688, whereas Combo C denotes a combination of sh1057 and 1969. sh2065 was excluded from the combinational study because it showed poor suppression efficiency when transfected on its own. Percentage IMPDH1 expression was quantified by Real Time RT-PCR 24hrs post-transfection and normalised to the house-keeping gene, IMPDH2. A rhodopsin target shRNA, shMR3 (Kiang *et al.*, 2005), was used as a control and this was standardised to show 100% IMPDH1 expression (Black bar). The average of three independent experiments is shown; Y-error bars indicate standard error of the mean (SEM). * $P < 0.05$. ** $P \leq 0.0001$

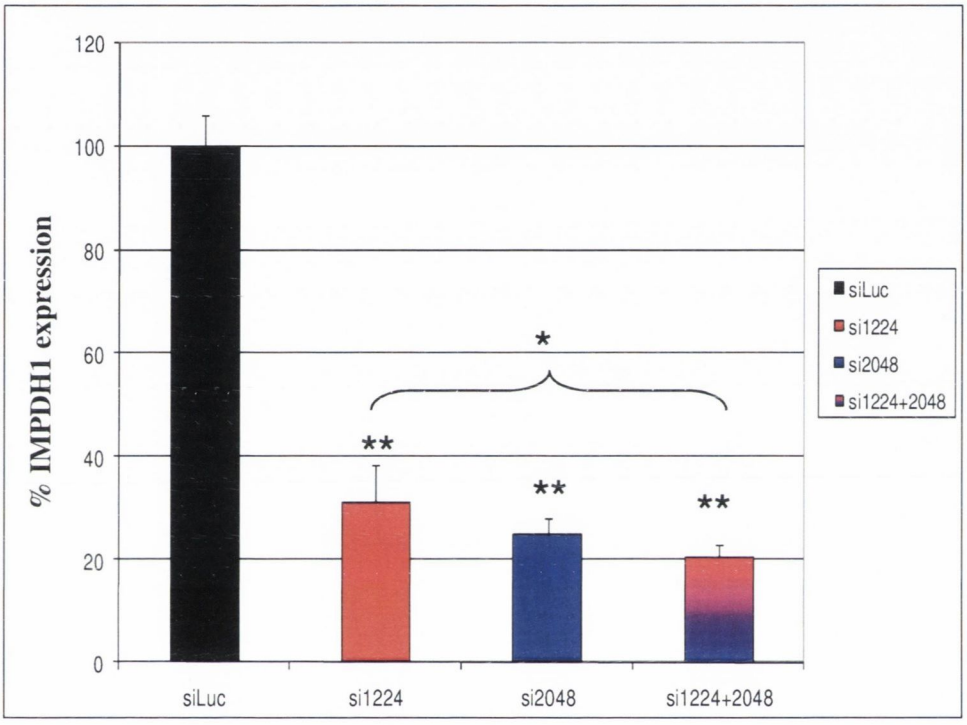

siRNA	si1224	si2048	si1224+2048
% IMPDH1 expression ± SEM	31.37%±7.25%	25%±2.98%	20.65%±2.25%

Figure 3.8: siRNA-mediated suppression of endogenous IMPDH1 mRNA expression in HeLa cells. HeLa cells were separately transfected with 20 pmoles of siRNAs (si1224 and si2048), or in combinations (total concentration=20 pmoles). Percentage IMPDH1 expression was quantified by Real Time RT-PCR and normalised to the house-keeping gene, β-actin. A control set was transfected with siRNAs directed at LuciferaseGL3, and this was standardised to represent 100% IMPDH1 expression (Black bar). The average of 3 independent experiments is shown; Y-error bars indicate standard error of the mean (SEM). * $P<0.05$, ** $P<0.0001$. siLuc=siLuciferaseGL3.

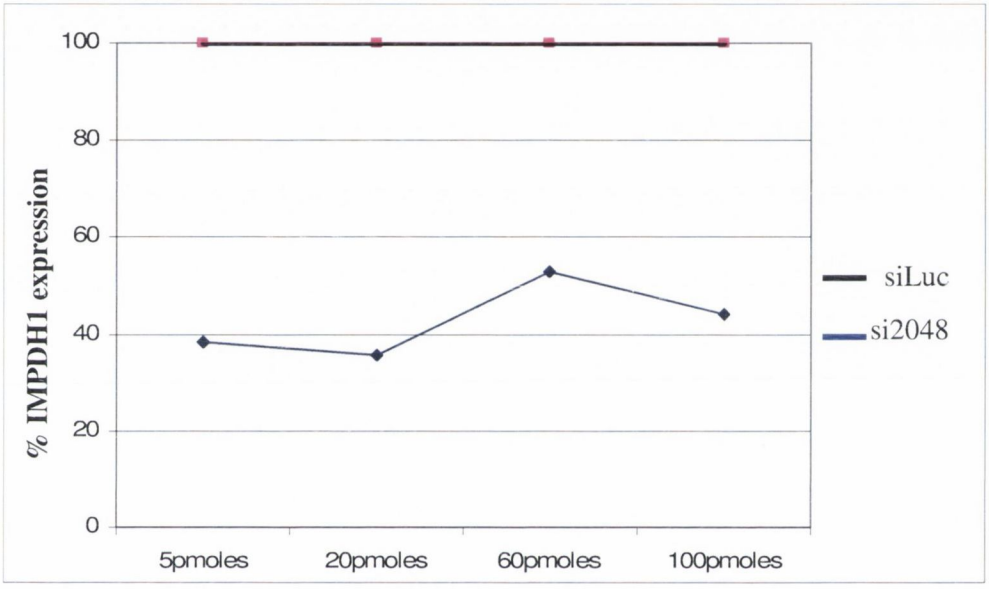

Concentrations of si2048	5pmoles	20pmoles	60pmoles	100pmoles
% IMPDH1 expression	38.26%	35.72%	52.78%	44.03%

Figure 3.9: Dose-dependent suppression of IMPDH1 transcripts by si2048 in HeLa cells. HeLa cells were transfected with different concentrations of si2048 ranging from 5 pmoles to 100 pmoles for 24 hrs. The level of IMPDH1 expression was quantified by Real Time RT-PCR and normalised to β-actin. A control set was transfected with the corresponding concentrations of siLuciferaseGL3, and standardised to represent 100% IMPDH1 expression. Percentage IMPDH1 expression is shown in the panel at the bottom.

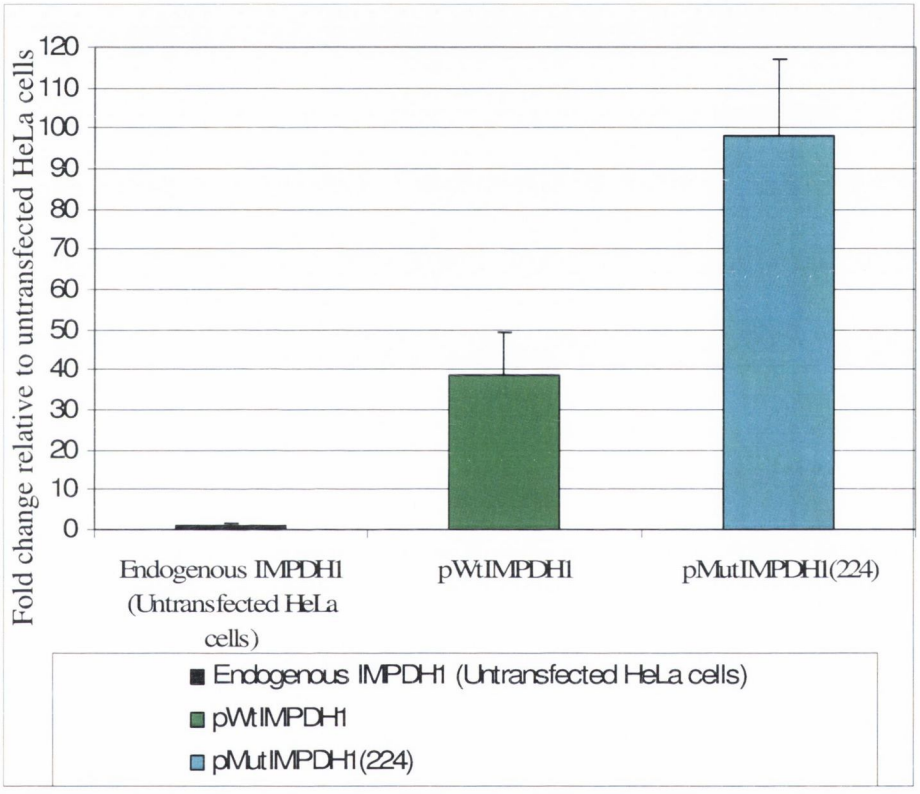

Figure 3.10: Comparisons of the levels of endogenous and exogenous IMPDH1 transcripts in HeLa cells by quantitative Real Time RT-PCR analysis. The level of endogenous IMPDH1 transcripts was normalised to 1 (black bar). Transfection of pWtIMPDH1 and pMutIMPDH1(224) increased the level of IMPDH1 transcripts by 38 and 98 fold, respectively, relative to untransfected cells. Y-error bars indicate standard error of the mean (SEM).

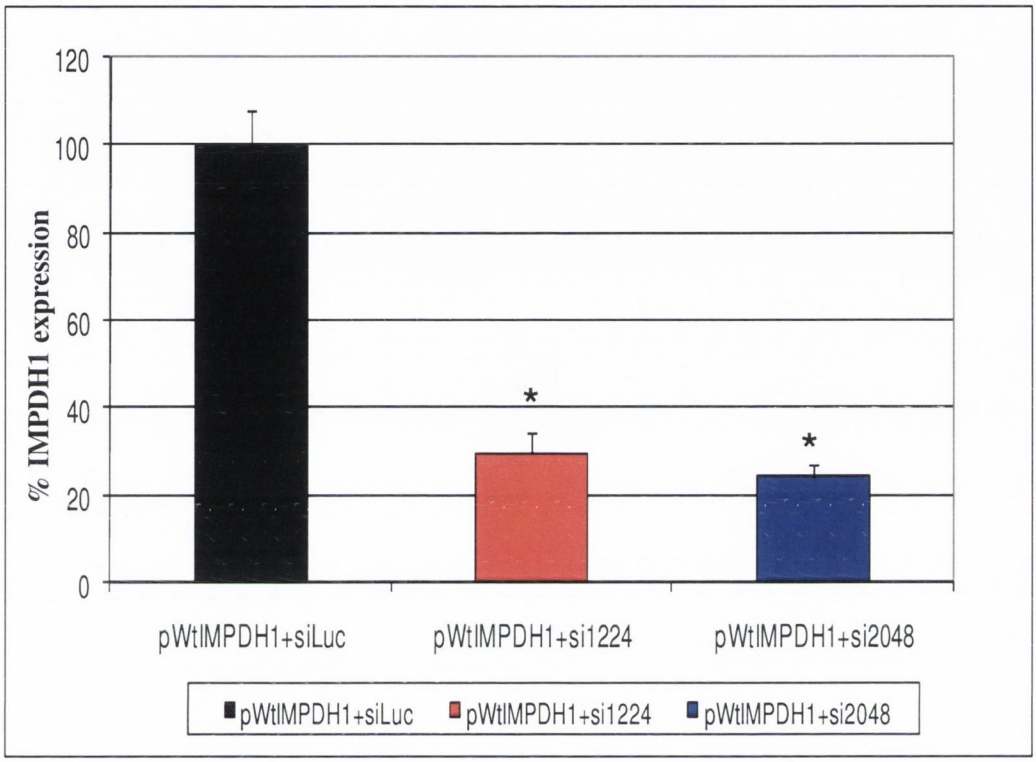

siRNA	pWtIMPDH1+si1224	pWtIMPDH1+si2048
% IMPDH1±SEM	29.81%±4.31%	24.21%±2.9%

Figure 3.11: Efficiency of IMPDH1-specific siRNAs in targeting total IMPDH1 (exogenous and endogenous transcripts) in HeLa cells. HeLa cells were co-transfected with 1 μg/μl pWtIMPDH1 and 20 pmoles of si1224/si2048. Percentage IMPDH1 expression was quantified 24 hrs post-transfection by Real Time RT-PCR and normalised to the housekeeping gene, β-actin. A control set was transfected with siLuciferaseGL3 and standardised to represent 100% IMPDH1 expression (Black bar). The average of 3 independent experiments is shown; Y-error bars indicate standard error of the mean (SEM). * $P<0.05$.

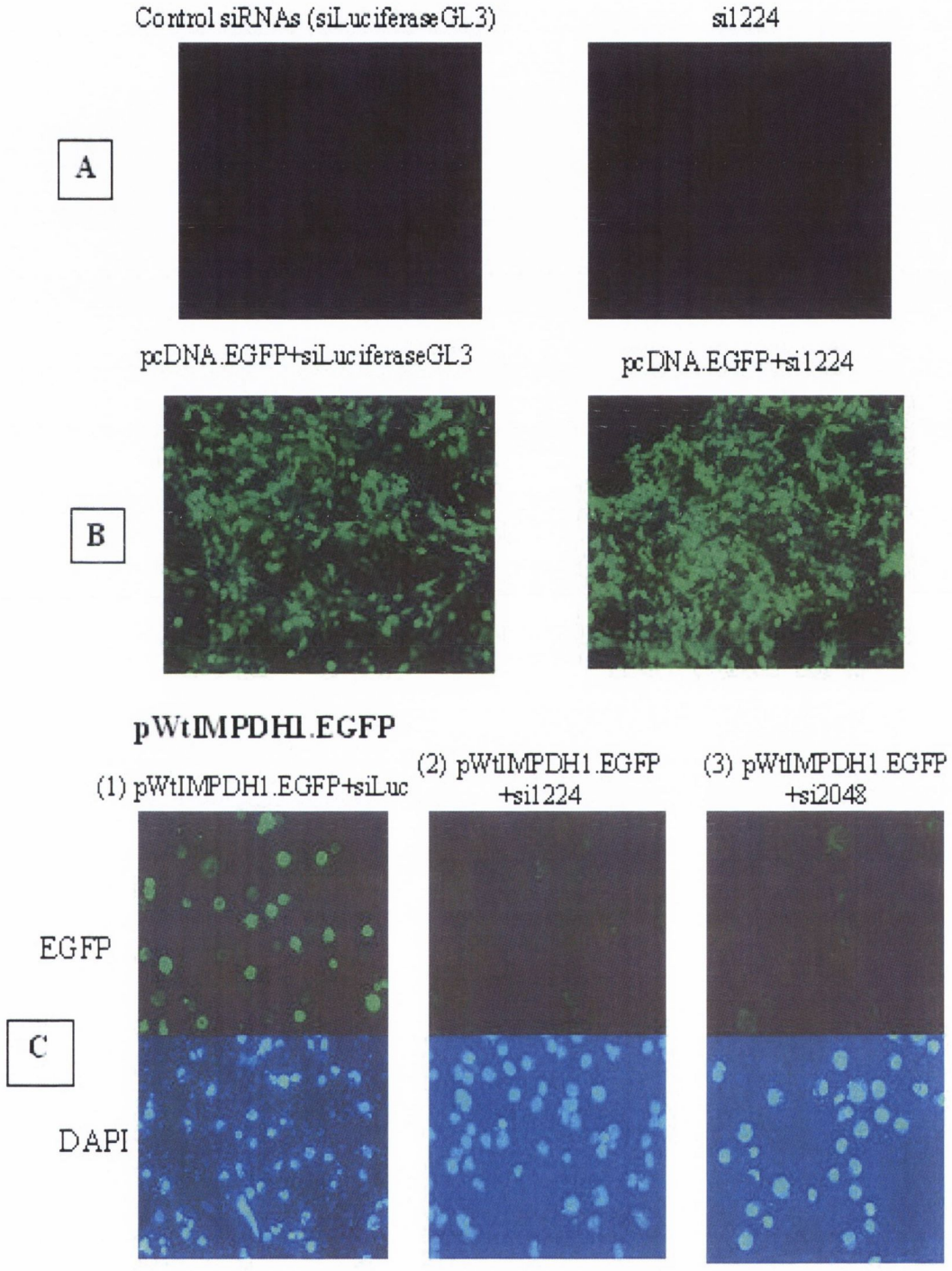

Figure 3.12 **continued**

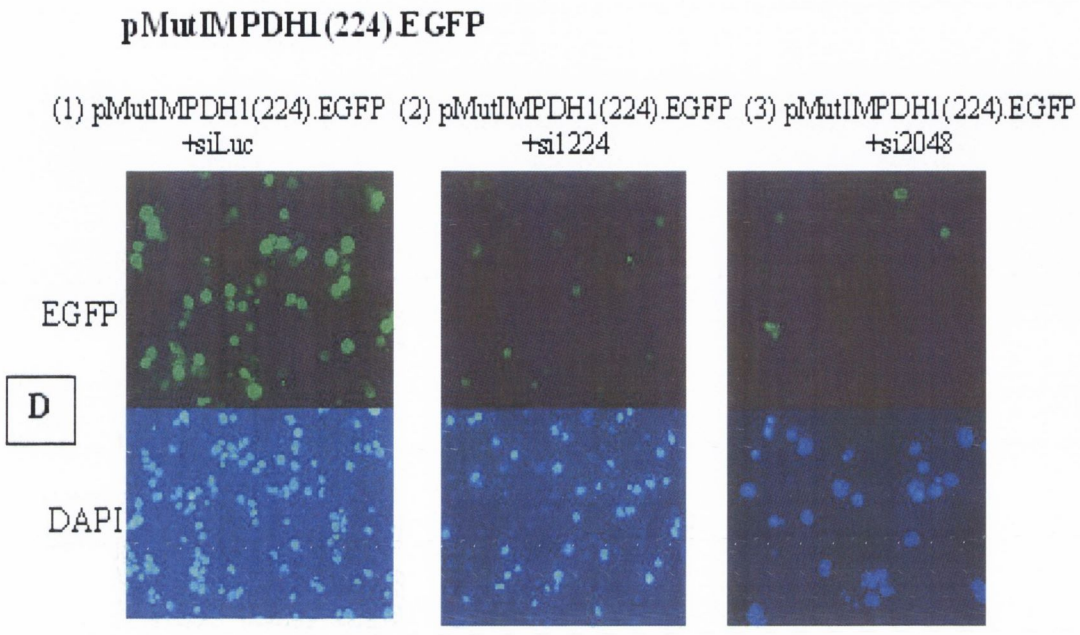

Figure 3.12: Analyses of EGFP expression by fluorescence microscopy. HeLa cells cultured on poly-L-lysine coated slides were transfected with the indicated molecules for 24 hrs, fixed with 4% paraformaldehyde and visualized under a fluorescent microscope. Single images of GFP were collected in three different fields of view per coverslip in the same sample using identical imaging settings. All corresponding images were taken at same exposure of magnification 20X. (A) HeLa cells separately transfected with 20 pmoles of either a non-targeting siRNA (siLuciferaseGL3) or IMPDH1-specific siRNAs as background fluorescence. (B) Co-transfection of 1 µg/µl of pcDNA.EGFP and 20 pmoles of either a control siRNA (siLuciferaseGL3) or IMPDH1-specific siRNAs as negative controls. (C) Co-transfection of 1 µg/µl pWtIMPDH1.EGFP and 20 pmoles of either control siRNAs (siLuciferaseGL3) or IMPDH1-specific siRNAs (si1224 and si2048). (D) Co-transfection of 1 µg/µl pMutIMPDH1(224).EGFP and 20 pmoles of either control siRNAs (siLuciferaseGL3) or IMPDH1-specific siRNAs (si1224 and si2048). DAPI staining in lower panels of (C) and (D) indicates all cell nuclei in the field. All the fluorescent images shown were randomly selected from three independent experiments. siLuc= siLuciferaseGL3

A

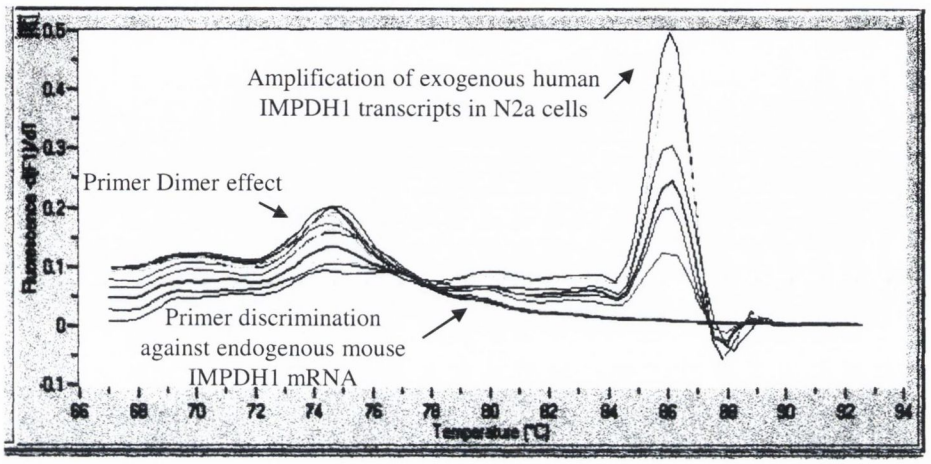

B

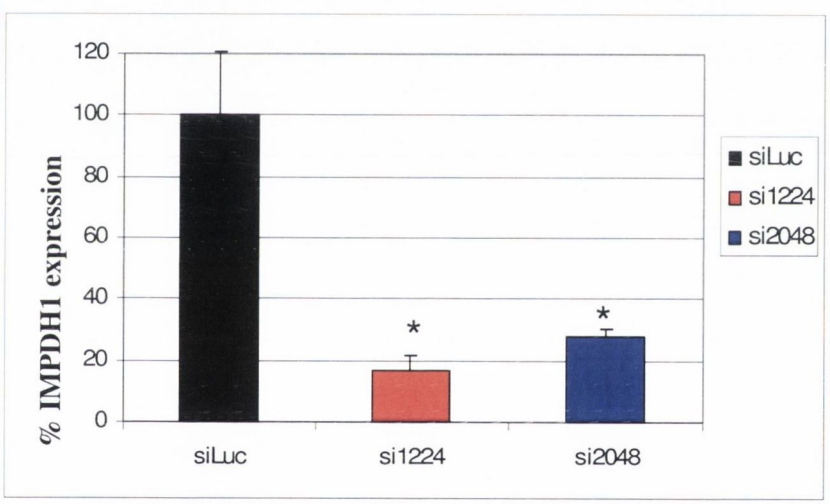

siRNA	MutIMPDH1+si1224	MutIMPDH1+si2048
%IMPDH1 expression ± SEM	16.70% ± 4.76%	27.75% ± 2.58%

Figure 3.13: (A) Real Time RT-PCR melting curve analysis showing the discrimination of human IMPDH1 primers against endogenous mouse IMPDH1 mRNA. (B) siRNA-mediated knockdown of mutant IMPDH1 transcripts in N2a cells. 1 µg/µl of mutant IMPDH1 expression plasmid (pMutIMPDH1(224)) was co-transfected with 20 pmoles of cognate siRNAs in N2a cells and the level of mutant IMPDH1 expression was quantified by Real Time RT-PCR 24hr post-transfection. A control set was transfected with siRNAs directed at LuciferaseGL3, and this was standardised to represent 100% IMPDH1 expression (Black bar). The average of 3 independent experiments is shown; Y-error bars indicate standard error of the mean (SEM). * $P<0.05$.

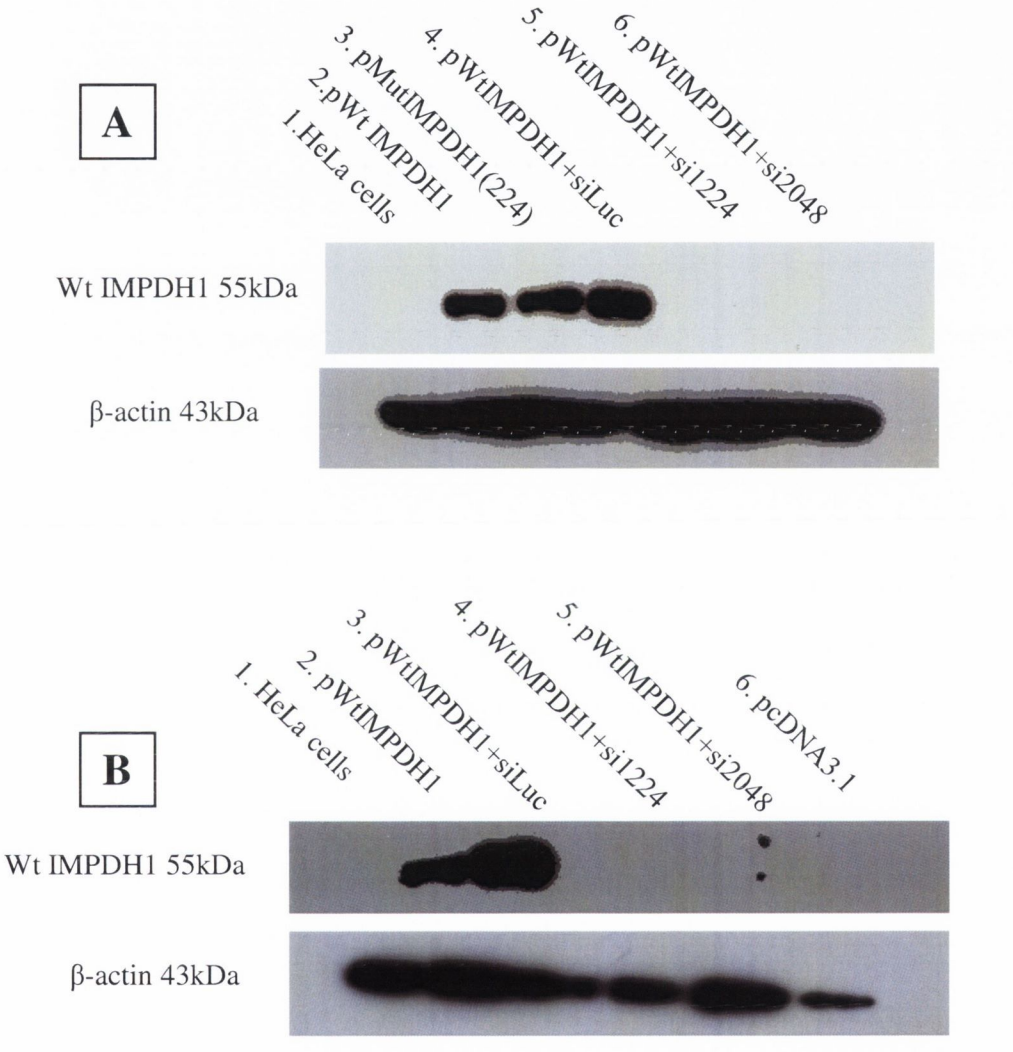

Note: Uneven and lateral distribution of β-actin proteins in A and B (lower panels) may have been caused by unequal sample loading and diffusion of protein samples out of the wells prior to electrophoresis. Detection of IMPDH1 protein clearly illustrates the suppression effect caused by both siRNAs

***Figure 3.14* continued**

C

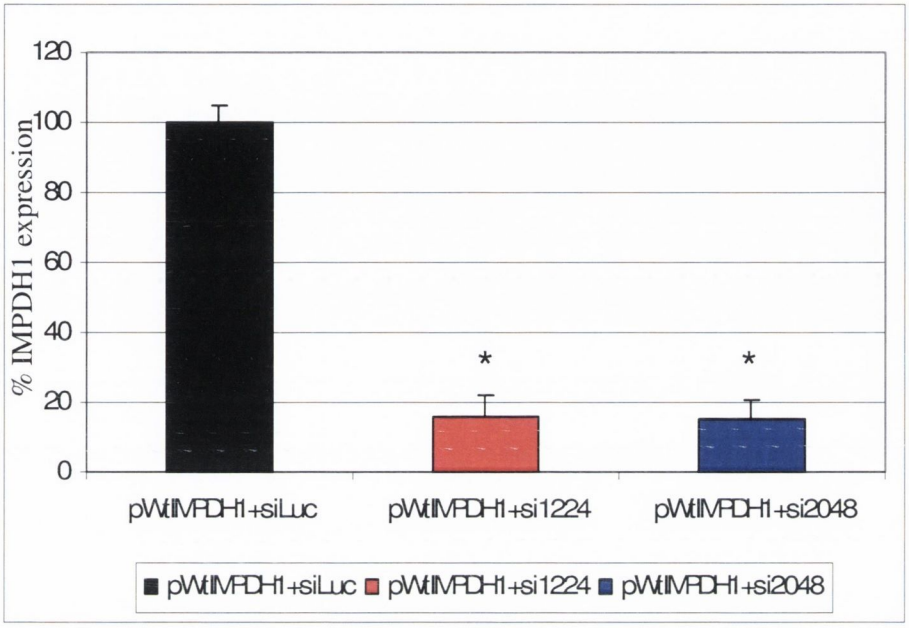

Densitometry (Band intensity)	**WtIMPDH1+si1224**	**WtIMPDH1+si2048**
% IMPDH1 expression ± SEM	16% ± 6%	15% ± 5.5%

Figure 3.14: (A) Western blot analysis of HeLa cells co-transfected with: Lane 1=Non-transfected cells; Lane 2=1.5 µg/µl pWtIMPDH1; Lane 3=1.5 µg/µl pMutIMPDH1(224); lane 4=1.5 µg/µl pwtIMPDH1 and 100pmoles siLuciferaseGL3; Lane 5=1.5 µg pwtIMPDH1 and 100 pmoles si1224; Lane 6- 1.5 µg/µl pwtIMPDH1 and 100pmoles si2048. (B) Western blot analysis of HeLa cells co-transfected with: Lane 1=Non-transfected cells; Lane 2=1.5 µg/µl pWtIMPDH1; Lane 3=1.5 µg/µl pWtIMPDH1 and 100pmoles siLuciferaseGL3; Lane 4= 1.5µg/µl pwtIMPDH1 and 100 pmoles si1224; Lane 5=1.5 µg pwtIMPDH1 and 100 pmoles si2048; Lane 6- 1.5 µg/µl pcDNA3.1 as negative control plasmid. Wild type IMPDH1 proteins were detected with anti-N-IMPDH1 antibody (Upper panels), and β-actin immunostaining was shown as loading controls (Lower panels). Each lane was loaded with 30 µg of total protein. The blots shown here represent two independent experiments carried out under the same conditions. **(C)** Quantification of band intensities in western blots. Histogram illustrates the average band intensity of two independent experiments from (A) and (B). Percentage wild type IMPDH1 expression in band intensity ± SEM was calculated relative to non-targeting control to represent 100% IMPDH1 expression (black bar), and normalised against β-actin. *P<0.05. Y-error bars denote standard error of the mean.

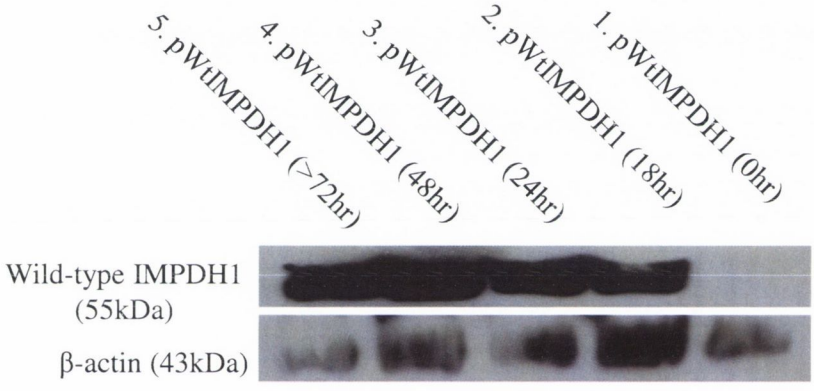

Figure 3.15: Western blot analysis of time-dependent expression of wild type IMPDH1 protein in HeLa cells. HeLa cells were transfected with wild type IMPDH1 expression plasmids (pWtIMPDH1) and whole cell lysates were extracted at the designated time-points as labeled on the blot. Wild type IMPDH1 protein was detected with anti-N-IMPDH1 antibody (upper panel), and β-actin as loading controls (bottom panel). Note: Poor detection of β-actin may have been caused by excessive washing with stripping buffer or inactivation of primary/ secondary antibody as a result of repeated freeze-thaw cycles. Top panel demonstrates continuous IMPDH1 protein expression measured throughout different time-points.

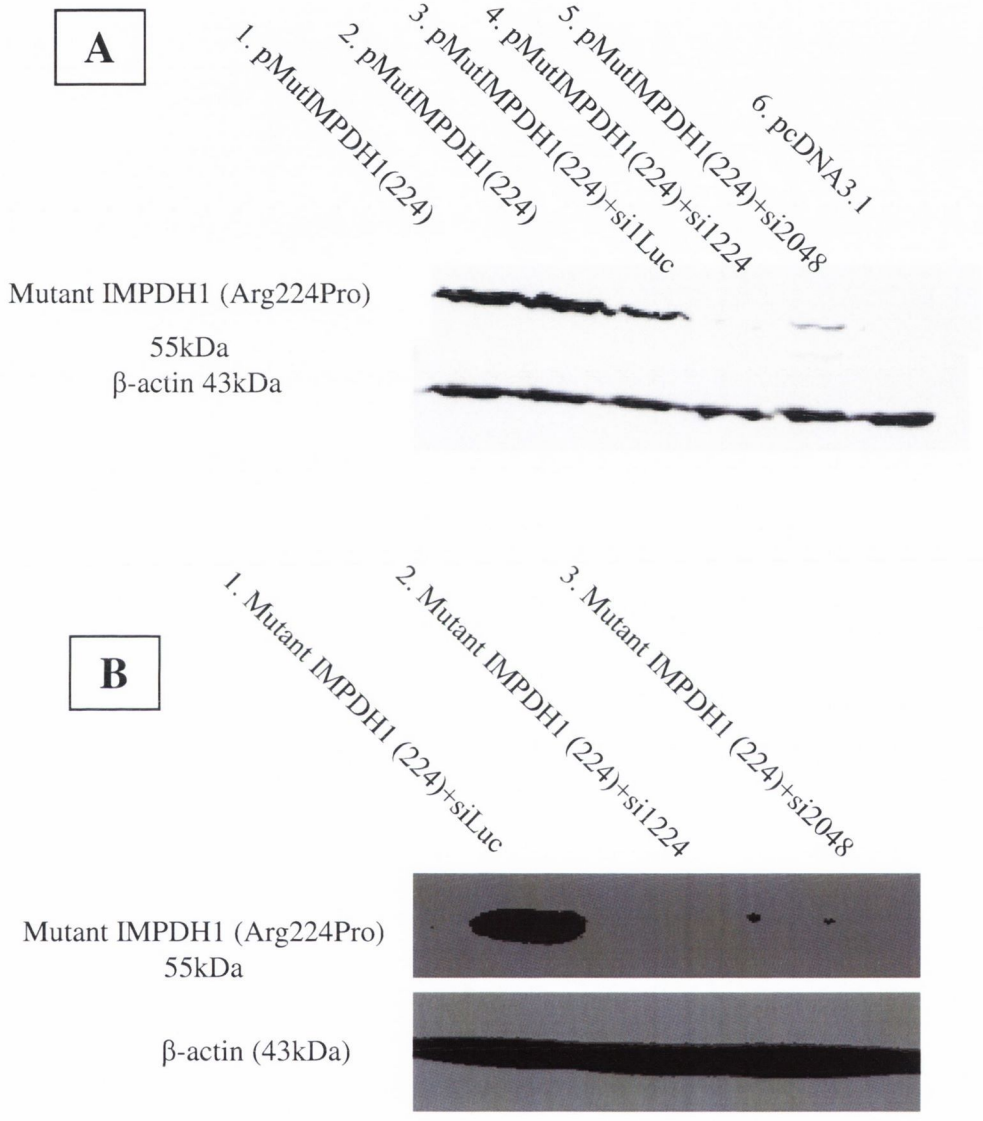

Note: Lateral band spreading of β-actin may have been caused by diffusion of protein samples out of the wells prior to electrophoresis (bottom panel). Top panel clearly demonstrated strong silencing of mutant IMPDH1 by both siRNAs

***Figure 3.16* continued**

C

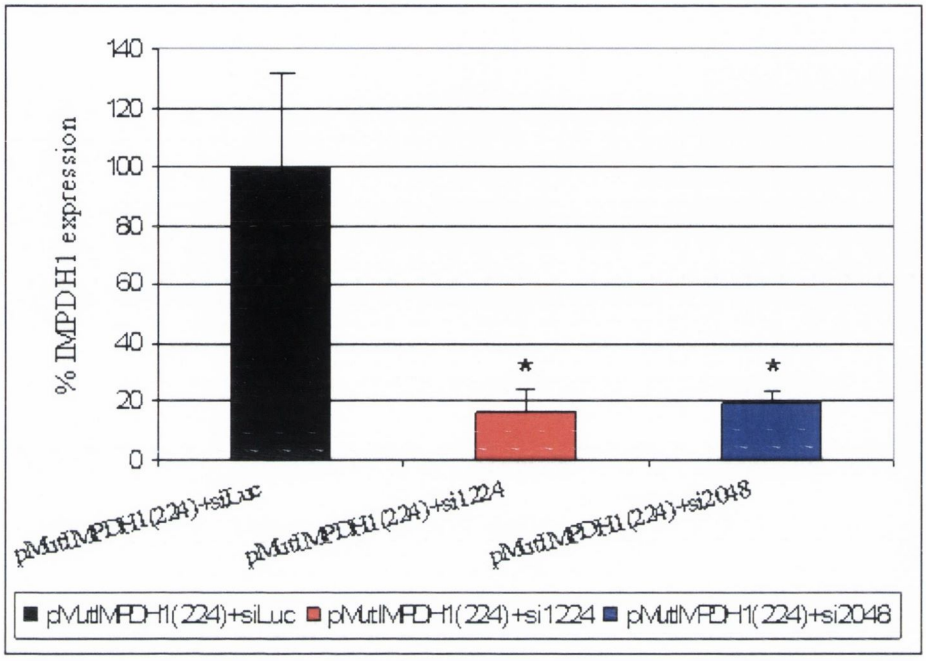

Densitometry (Band Intensity)	MutIMPDH1+si1224	MutIMPDH1+si2048
% IMPDH1 expression ± SEM	16% ± 8%	20% ± 4%

Figure 3.16: *(A and B)* Western blot analysis of HeLa cells co-transfected with the indicated mutant IMPDH1 expression plasmids harboring the Arg224Pro mutation and IMPDH1-specific siRNAs. The negative control plasmid, pcDNA3.1, lack the IMPDH1 cDNA insert. Mutant IMPDH1 proteins were detected with anti-N-IMPDH1 antibody (upper panels) and β-actin immunostaining was shown as loading controls (lower panels). The blots shown here represent two independent experiments carried out under the same conditions. **(C)** Quantification of band intensities in western blots shown in (A) and (B). Percentage mutant IMPDH1 expression from band intensities of the IMPDH1 signals were normalised to those of β-actin, and band intensities from non-targeting control was standardised to represent 100% IMPDH1 expression (black bar). *P<0.05. Y-error bars denote standard error of the mean.

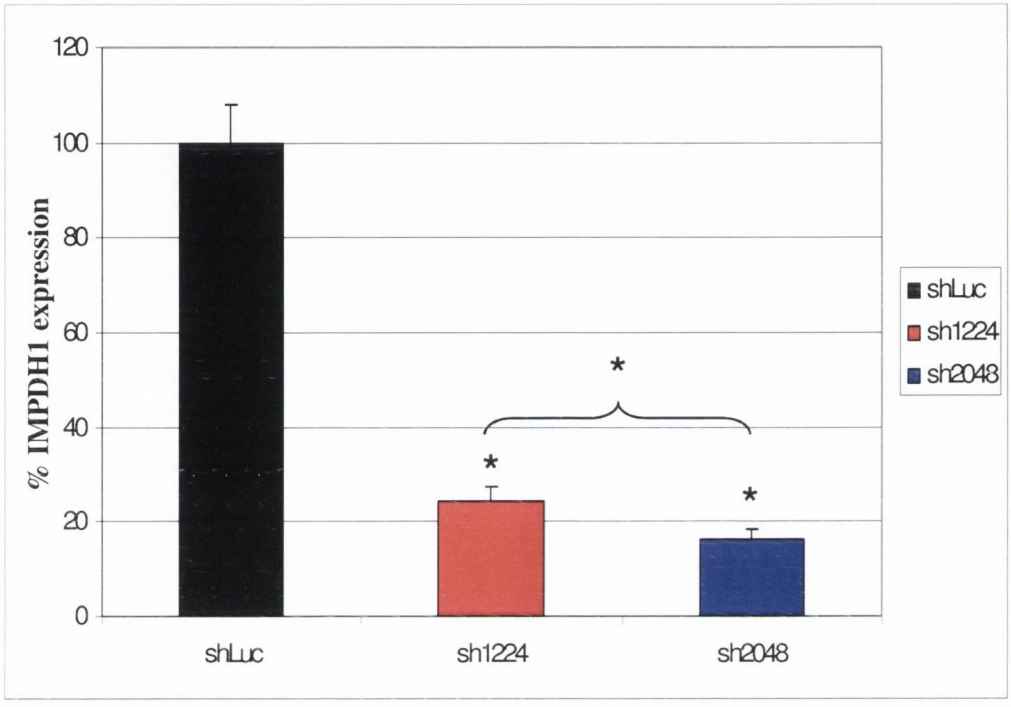

shRNA	sh1224	sh2048
% IMPDH1 expression ± SEM	24.4% ± 3%	16.07% ± 2%

Figure 3.17: Suppression of endogenous IMPDH1 mRNA in HeLa cells by polymerase III H1-promoter driven shRNAs. HeLa cells were separately transfected with 1 μg/μl of psh1224 and psh2048 and the level of IMPDH1 mRNA expression was quantified by Real Time RT-PCR 24 hrs post-transfection. A control set was transfected with shRNAs directed at LuciferaseGL2, and this was standardised to represent 100% IMPDH1 expression (Black bar). The average of 3 independent experiments is shown; Y-error bars indicate standard error of the mean (SEM). * $P<0.05$.

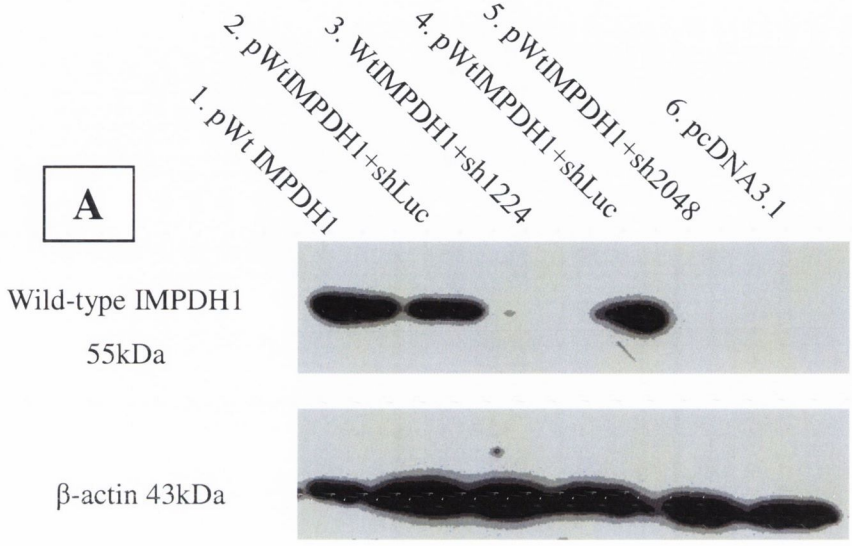

Note: Unequal and lateral band spreading of β-actin in the bottom panel may have been caused by unequal sample loading and diffusion of protein samples out of the wells prior to electrophoresis. Top panel clearly demonstrated strong suppression of IMPDH1 by shRNAs.

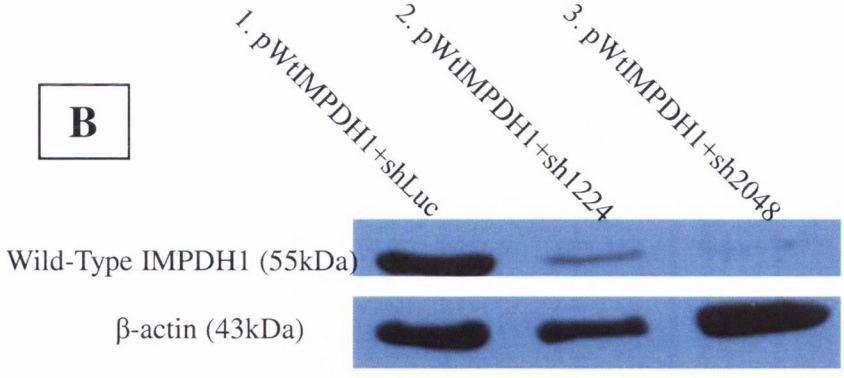

***Figure 3.18* continued**

C

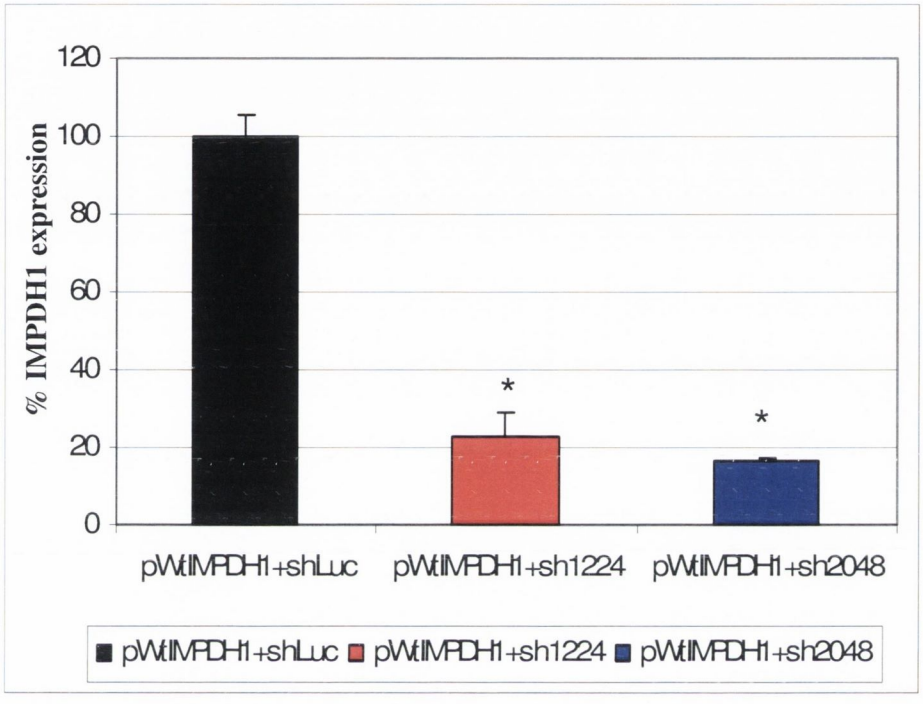

Densitometry (Band Intensity)	WtIMPDH1+sh1224	WtIMPDH1+sh2048
% IMPDH1 expression ± SEM	23% ± 9%	17% ± 0.36%

Figure 3.18: *(A and B).* Western blot analysis of knockdown of wild-type IMPDH1 protein expression in HeLa cells by Polymerase III H1-promoter driven IMPDH1-specific shRNAs. Lanes on each blot are labeled with the transfected constructs. The level of wild type IMPDH1 protein expression was detected by anti-N-IMPDH1 antibody, and the same membrane was stripped and probed again with the antibody recognising β-actin. Each lane was loaded with 30 μg of total protein. The blots illustrated here represent two independent experiments carried out under the same condition. (C) Quantification of band intensities in western blots shown in (A) and (B). Percentage wild type IMPDH1 expression from band intensities of the IMPDH1 signals were normalised to those of β-actin, and band intensities from non-targeting control was standardised to represent 100% IMPDH1 expression (black bar). *P<0.05. Y-error bars denote standard error of the mean.

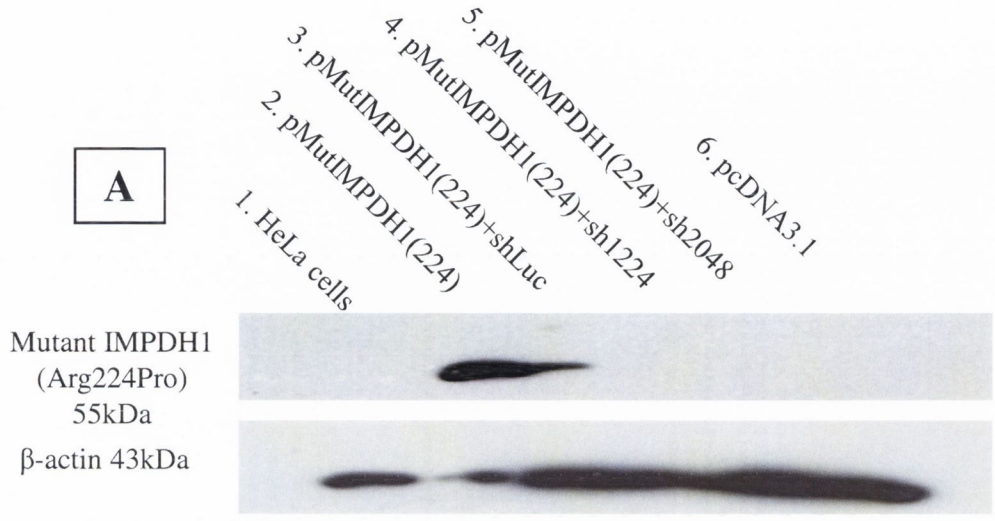

Note: Lateral band distribution of β-actin may have been caused by diffusion of protein samples out of the wells prior to electrophoresis (bottom panel). Top panel showed strong suppression of mutant IMPDH1 by both shRNAs.

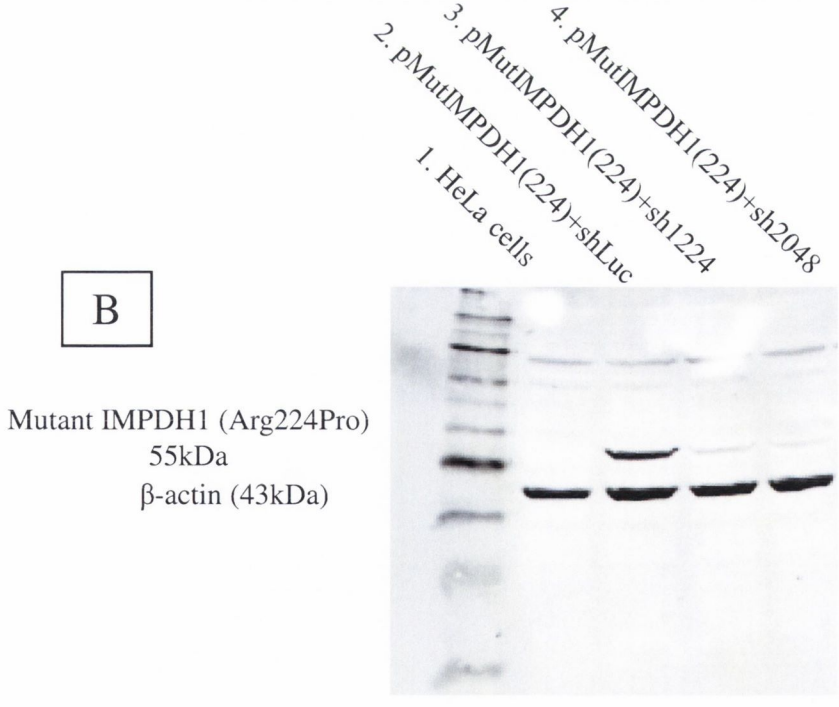

***Figure 3.19* continued**

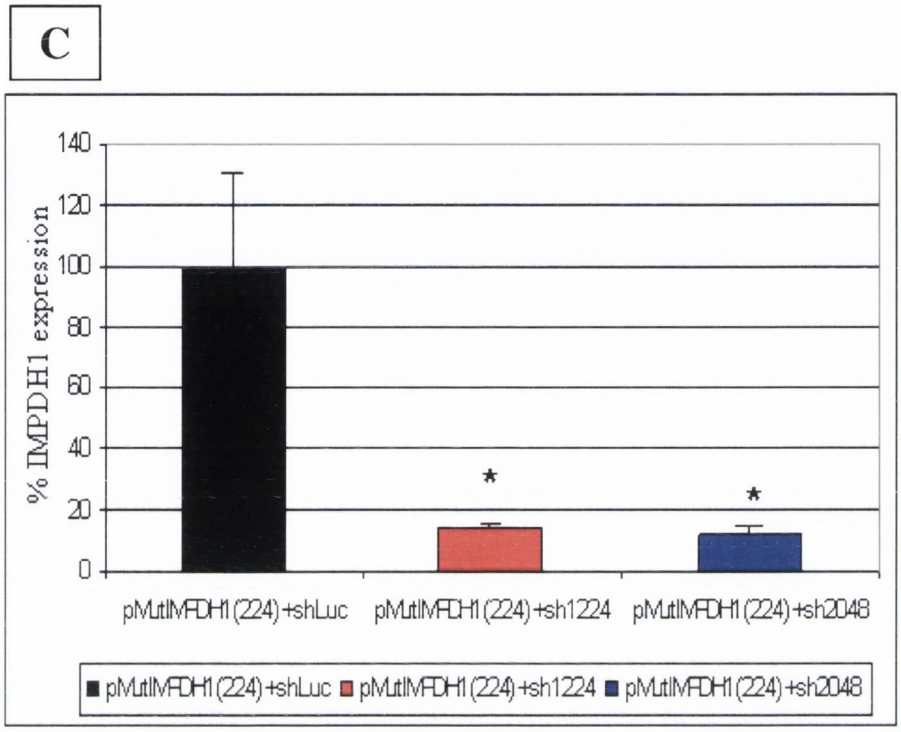

Densitometry (Band Intensity)	MutIMPDH1+sh1224	MutIMPDH1+sh2048
% IMPDH1 expression ± SEM	14% ± 2%	12% ± 4%

Figure 3.19: *(A and B)* Western Blot analysis of HeLa cells co-transfected with mutant IMPDH1 expression plasmids harboring the Arg224Pro and polymerase III H1-promoter driven IMPDH1-specific shRNAs. Lanes on each blot are labeled with the transfected constructs. The level of wild type IMPDH1 protein expression was detected by anti-N-IMPDH1 antibody, and the same membrane was stripped and probed again with the antibody recognizing β-actin. Each lane was loaded with 30 μg of total protein. The blots illustrated here represent two independent experiments carried out under the same condition. (C) Quantification of band intensities in western blots shown in (A) and (B). Percentage mutant IMPDH1 expression from band intensities of the IMPDH1 signals were normalised to those of β-actin, and band intensities from non-targeting control was standardised to represent 100% IMPDH1 expression (black bar). *P<0.05. Y-error bars denote standard error of the mean.

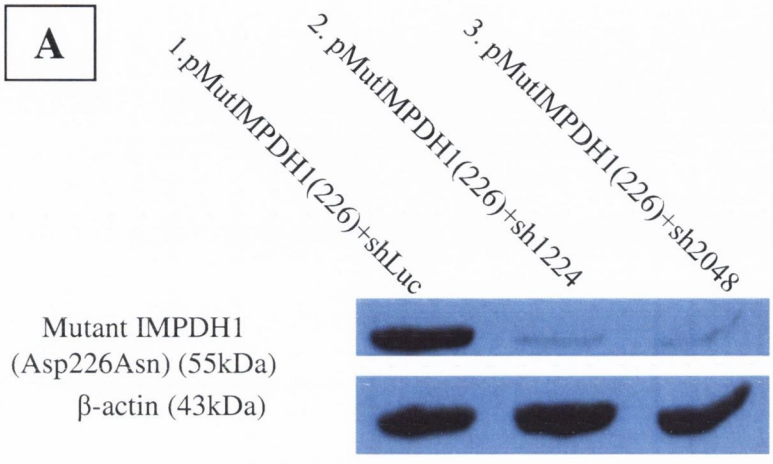

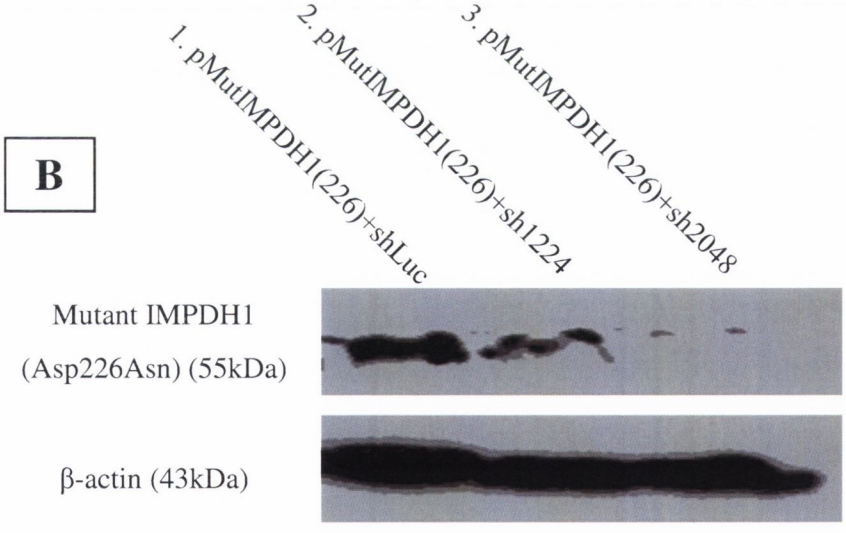

Note: Lateral band spreading of β-actin may have been caused by diffusion of protein samples out of the wells prior to electrophoresis (bottom panel). Top panel clearly demonstrated strong suppression of mutant IMPDH1 by both shRNAs.

***Figure 3.20* continued**

C

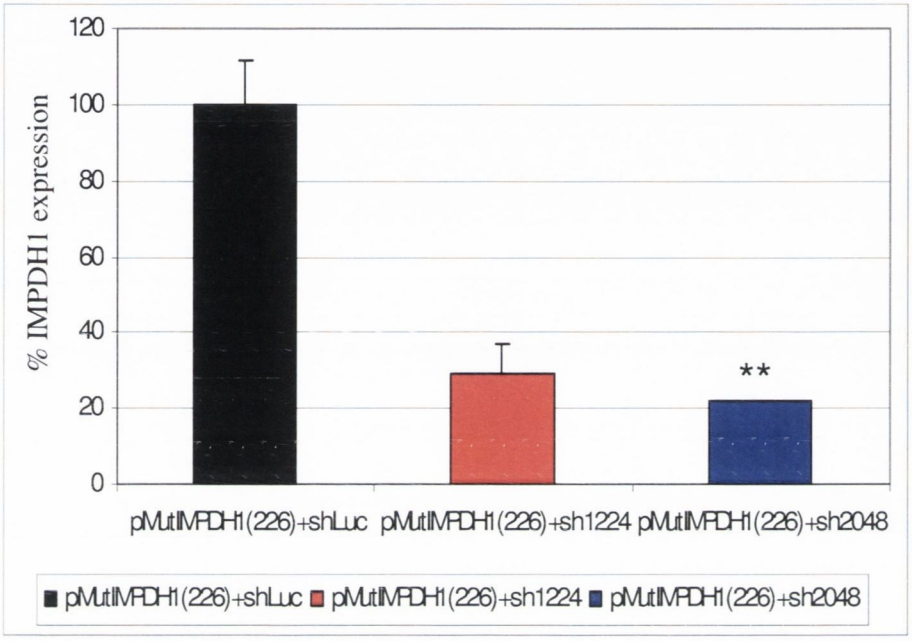

Densitometry (Band Intensity)	**MutIMPDH1+sh1224**	**MutIMPDH1+sh2048**
% IMPDH1 expression ± SEM	29% ± 8%	22% ± 0.2%

Figure 3.20: *(A and B)* Western Blot analysis of HeLa cells co-transfected with mutant IMPDH1 expression plasmids harboring the Asp226Asn and polymerase III H1-promoter driven IMPDH1-specific shRNAs. Lanes on each blot are labeled with the transfected constructs. The level of wild type IMPDH1 protein expression was detected by anti-N-IMPDH1 antibody, and the same membrane was stripped and probed again with the antibody recognizing β-actin. Each lane was loaded with 30 μg of total protein. The blots illustrated here represent two independent experiments carried out under the same condition. (C) Quantification of band intensities in western blots shown in (A) and (B). Percentage mutant IMPDH1 expression from band intensities of the IMPDH1 signals were normalised to those of β-actin, and band intensities from non-targeting control was standardised to represent 100% IMPDH1 expression (black bar). **$P \leq 0.0001$. Y-error bars denote standard error of the mean.

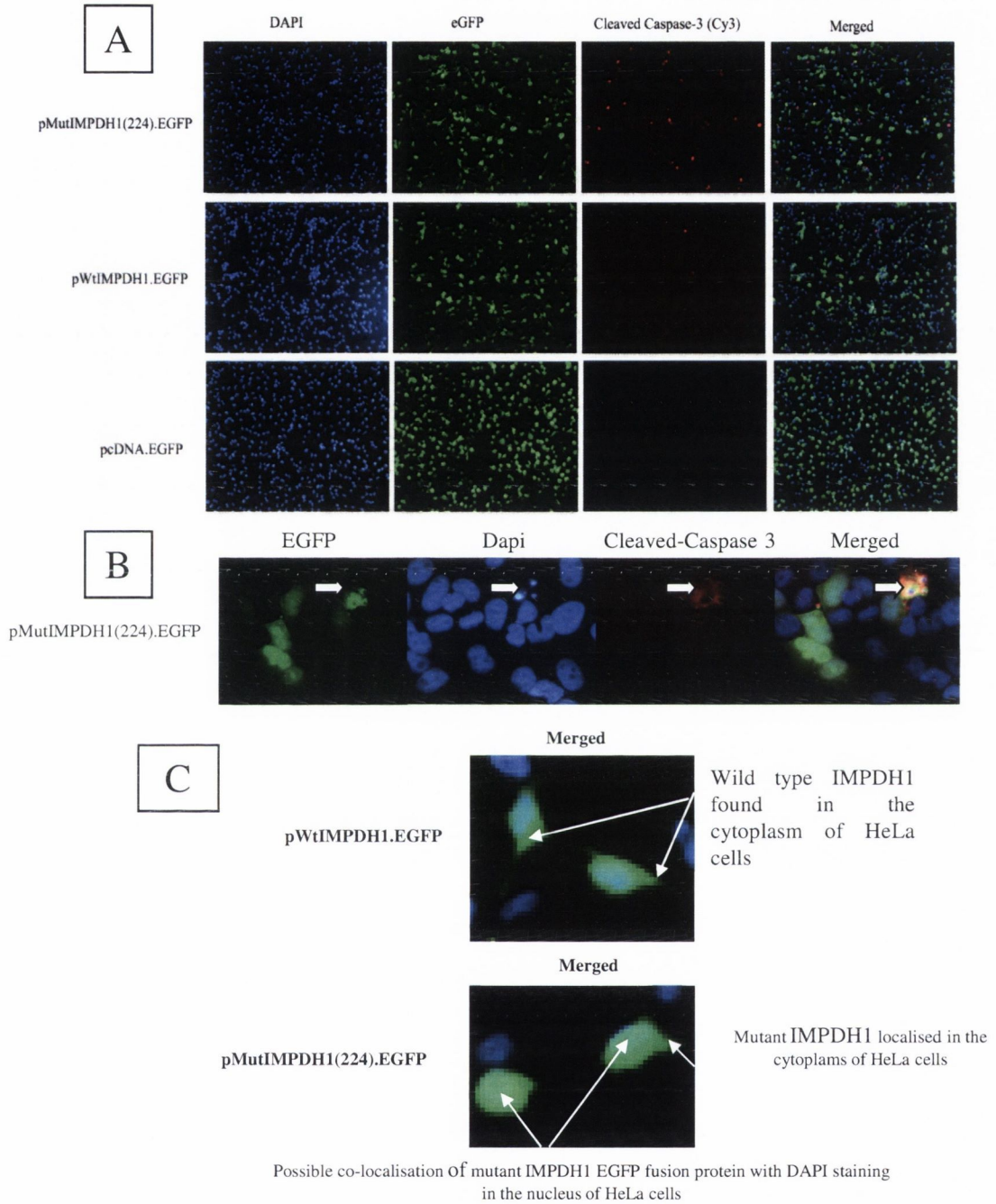

Figure 3.21: (A) Immunostaining of HeLa cells transfected with pcDNA.EGFP, pWtIMPDH1.EGFP and pMutIMPDH1(224).EGFP for cleaved caspase-3. HeLa cells were stained with DAPI to identify the nucleus. Transected cells were visualised by fluorescence microscopy at 20X magnification. Green = EGFP, red = apoptotic cells stained by cleaved caspase-3 primary antibody and followed by Cy-3 secondary antibody, blue = DAPI. (B) Superimposed images of HeLa cells transfected with mutant IMPDH1 EGFP fusion protein harboring the Arg224Pro mutation. (C) Superimposed images of nuclear and cytoplasmic localisation of wild type and mutant IMPDH1 EGFP fusion proteins in HeLa cells.

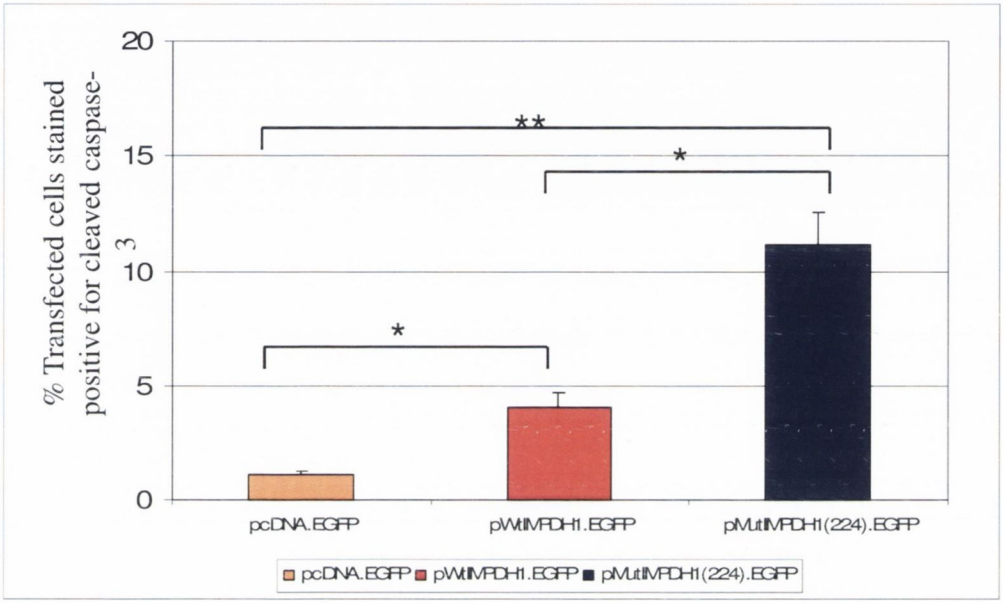

Plasmid vector	pcDNA.EGFP	WTIMPDH1.EGFP	MutIMPDH1.EGFP
% Apoptotic cells ± SEM	1.09% ± 0.8%	4.04% ± 2.62%	11.15% ± 5.80%

Figure 3.22: Overexpression of mutant IMPDH1 induces apoptosis in HeLa cells. HeLa cells transfected with either pcDNA.EGFP, pWtIMPDH1.EGFP and pMutIMPDH1(224).EGFP were stained with cleaved caspase-3 antibody, and followed by Cy3 staining (red). The percentage of apoptotic cells were calculated by standardizing the number of red cells against the percentage of transfected cells in two independent experiments. Y-error bars denote standard error of the mean. pMutIMPDH1 induced significantly more apoptosis than pcDNA.EGFP alone (** $P \leq 0.0001$), and differed significantly to wild-type IMPDH1 expression (* $P = 0.0002$).

Chapter 4
Suppression of IMPDH1 *ex-vivo* in Mouse Retinal Explants

4. Suppression of IMPDH1 *ex-vivo* in mouse retinal explants

4.1 Introduction

4.1.1 Background

The primary challenge for gene therapy is to develop a method that delivers therapeutic genes to targeted cells or tissues where adequate gene expression can be achieved. An ideal gene delivery method needs to meet three major criteria: (1) it should protect the transgene against degradation by nucleases in intercellular matrices, (2) it should bring the transgene across the plasma membrane and into the nucleus of target cells, and (3) it should have no detrimental effects (Gao *et al.*, 2007). To date, the majority of gene therapy clinical trials performed have used viral vectors for gene delivery. However, there are major practical limitations to viral gene delivery systems, including difficulties of scale-up production, lack of selectivity, inadequate infectivity *in-vivo*, susceptibility to neutralisation by serum antibodies (particularly on second and subsequent administrations) and inflammatory responses raised against successfully transduced cells. In addition, acute immune response and insertion mutagenesis uncovered in gene therapy clinical trials have raised serious safety concerns about commonly used viral vectors (Parker *et al.*, 2003). Consequently, considerable attention has turned towards the development of non-viral systems for gene delivery. To date, established methods of non-viral gene delivery can be divided into two main categories: chemical delivery (synthetic cationic polymer-based gene delivery) and physical delivery (carrier free gene delivery). Chemical approaches employ synthetic or naturally occurring compounds as carriers to deliver transgene into target cells (Liu *et al.*, 2003b), whereas physical approaches include microinjection of naked DNA, ballistic delivery, ultrasound, hydrodynamic delivery and electroporation and require physical force to permeate the cell membrane to facilitate intracellular gene transfer. Although significant progress has been made in the application and development of various non-viral gene delivery systems, the efficiency of transgene expression in a majority of non-viral approaches

are still several orders of magnitude lower than viral vectors, especially in the case of *in-vivo* gene delivery (Gao *et al.*, 2007; Parker *et al.*, 2003).

4.1.2 Gene delivery by chemical approaches

To date, the most frequently studied strategy for nonviral gene delivery is the formulation of DNA into condensed particles by using cationic lipids or cationic polymers. The DNA-containing particles are subsequently taken up by cells via endocytosis, macropinocytosis, or phagocytosis in the form of intracellular vesicles, from which a small fraction of the DNA is released into the cytoplasm and migrates into the nucleus for transgene expression. Since Felgner and colleagues first reported in 1987 that a double-chain monovalent quaternary ammonium lipid, N-[1-(2,3-dioleyloxy)propyl]-N,N,N-trimethylammonium chloride, effectively binds and delivers DNA to cultured cells, hundreds of new cationic lipids have been developed for lipid-based gene delivery approaches (Liu *et al.*, 2003b). Different classes of cationic lipids contain varying numbers of charges in their hydrophilic head groups and possess specific structure in their hydrophobic moiety. Cationic lipids are also highly soluble in aqueous solution, forming positively charged 'micellar' structures called liposomes. Although some cationic lipids alone exhibit good transfection activity, they are often formulated with noncharged phospholipids (e.g. dioleoylphosphatidylcholine, DOPE) or cholesterol as helper lipids to form liposomes. Upon mixing with cationic liposomes, plasmid DNA is condensed into small quasi-stable particles called lipoplexes, providing protection against nuclease degradation in intracellular environment. The major drawback of lipoplexes is that their hydrophobic and positively charged surface frequently leads to interactions with plasma proteins and other extracellular proteins, which bind non-specifically to the lipoplexes and inactivating its activity (Urtti *et al.*, 2000). Poly-L-lysine was one of the first groups of cationic polymers used in gene transfer *in-vivo* (Wu and Wu, 1988). Following this, a significant number of cationic polymers in linear or branched configuration have been explored as carriers for *in-vitro* and *in-vivo* gene delivery. These include polyethylenimine (PEI) (Boussif *et al.*, 1995; Goula *et al.*, 1998; Chemin *et al.*, 1998), polyamidoamine (Rudolph *et al.*, 2000) and polypropylamine

dendrimers (Schatzlein *et al.*, 2005), polyallylamine, cationic dextran (Hosseinkhani *et al.*, 2004), chitosan (Erbacher *et al.*, 1998; Venkatesh and Smith, 1997) cationic proteins (polylysine, protamine, and histones) (Balicki and Beutler, 1997) and cationic peptides (Balicki *et al.*, 2002; Park *et al.*, 2003). Although most cationic polymers share the same function of condensing DNA into small particles and facilitating cellular uptake via endocytosis through charge-charge interaction with anionic sites on cell surfaces, their transfection activity and toxicity differ dramatically.

4.1.3 Gene transfer by physical approaches

The concept of gene delivery using physical approaches involves the induction of transient injuries on cell membranes so that DNA can enter the cells by diffusion. Gene delivery employing mechanical (particle bombardment or gene gun), ultrasonic, hydrodynamic (hydrodynamic gene transfer) and electric (electroporation and iontophoresis) are discussed below.

4.1.3.1 Enhanced gene transfer by particle bombardments

Particle bombardment or ballistics was first reported by Klein *et al.*, (1987) as a gene delivery system to overcome the inherent difficulty of transgene expression in plant cells. This original method utilised a gunpowder acceleration system to propel DNA-coated tungsten particles at recipient cells, resulting in the penetration of the cell wall and membrane as shown by intracellular expression of reporter genes. Subsequently, helium-driven devices, such as the Helios™ gene gun (Bio-Rad Laboratories), have been developed, in which a helium pulse is used to accelerate DNA-coated gold microparticles through the cell membrane (Bulletin, B.R. Bio Rad Bulletin. 2084). The momentum allows the gold particles to penetrate a few millimetres deep into a tissue and release DNA into cells on the path. Further improvements have also been made by incorporating chemical modification on the surface of the gold particles to allow higher capacity for DNA coating and precise control of DNA deposition in to cells in various tissues (O'Brien and Lummis, 2002). Particle bombardment of

mammalian tissues *in-vivo* has not been investigated thoroughly, although currently there are many groups developing this technology. Skin conditions of genetic origin (genodermatoses) are favourable targets for gene therapy, as the skin is easily accessible (Lin *et al.*, 2000). A variety of cell types have shown a significant level of reporter gene expression *in-vitro* following particle bombardment (Heiser, 1994), whereas other studies, targeting brain neurons (Jiao *et al.*, 1992), skeletal muscle (Zelenin *et al.*, 1991), liver (Cheng, *et al.*, 1993) and cutaneous and subcutaneous tissue (Cheng *et al.*, 1993; Lin *et al.*, 2000), have shown varying levels of reporter gene expression.

4.1.3.2 Enhancement of gene transfer using ultrasound

The discovery made by Fechheimer *et al.*, (1987) showing the transfection of murine fibroblasts using sonication has expanded the methodology of gene transfer by physical methods. Ultrasound delivery involves the exposure of cells to low-intensity sound waves which create membrane pores and facilitates intracellular gene transfer through passive diffusion of DNA across the membrane pores (Kim *et al.*, 1996; Koch *et al.*, 2000). Recently, the transfection efficiency of ultrasound exposure has been enhanced by the addition of air-filled microbubbles in the transfection medium, which rapidly expand and shrink under ultrasound irritation, generating local shock waves that transiently permeate the nearby cell membranes. Lawrie *et al.*, (1999) demonstrated that ultrasound assisted transfection of primary porcine vascular smooth muscle cells (PVSMCs) with naked plasmid was associated with greater than two hundred fold enhancements in reporter gene expression when the transfection medium was supplemented with microbubbles, compared with 16-fold enhancements using ultrasound alone. Several studies have also shown that ultrasound assisted transfection also enhances non-viral gene delivery *in-vivo* without any indication of toxic effects (Amabile *et al.*, 2001; Huber *et al.*, 1999; Schratzberger *et al.*, 1999). Since ultrasound can penetrate soft tissue and can be applied to specific areas, it could become an ideal method for noninvasive gene transfer into cells of the internal organs. More recently, some reports have shown that substantial effects of

microbubble-enhanced ultrasound on the biological efficacy of therapeutic plasmid delivery to vascular and skeletal muscle (Taniyama *et al.*, 2002; Teupe *et al.*, 2002). In combination with the flexibility, general safety and repeatability of ultrasound delivery in most organs and tissues, these early *in-vivo* studies have proven the potential use of ultrasound-assisted transfection in clinical gene therapy protocols.

4.1.3.3 Hydrodynamic gene delivery

Hydrodynamic gene delivery is an injection-based delivery method that introduces naked plasmid DNA into cells of highly perfused internal organs (e.g. the liver) with an impressive efficiency (Liu *et al.*, 1999b; Zhang *et al.*, 1999). The gene delivery efficiency is mainly determined by the anatomic structure of the organ, injection volume, and the speed of injection. In a mouse model, the optimal condition involves 1.6 to 1.8 ml of DNA solution in saline for a 20 g mouse (8%-9% of the body weight) and an injection time of ~5 seconds via the tail vein. Mechanistically, the rapid tail vein injection of a large volume of DNA solution causes a transient overflow of injected solution at the inferior vena cava that exceeds the cardiac output. As a result, the injection induces a flow of DNA solution in retrograde into the liver, a rapid rise of intrahepatic pressure, liver expansion, and reversible disruption of the liver fenestrae (Zhang *et al.*, 2004). The gene transfer efficiency of this simple procedure is the highest so far achieved *in-vivo* among non-viral approaches with approximately 30% to 40% of hepatocytes being transfected by a single hydrodynamic injection of less than 50 μg of plasmid DNA (Liu *et al.*, 1999b). In addition, hydrodynamic delivery has also been used to express proteins of therapeutic value such as alpha-1 antitrypsin (Zhang *et al.*, 2000; Alino *et al.*, 2003), cytokines (Jiang *et al.*, 2001), hepatic growth factors (Yang *et al.*, 2001), erythropoietin (Maruyama *et al.*, 2004), and also of small interfering RNA molecules (Lewis *et al.*, 2002; McCaffrey *et al.*, 2002) in mouse and rat models. Depending on the plasmid construct and the regulatory elements driving expression of the transgene, the level of gene expression in some cases has reached or exceeded the physiological level (Zhang *et al.*, 2000; Alino *et al.*, 2003). However, the real obstacle that remains for gene transfer by the

hydrodynamic method is how to translate this effective procedure to one that is applicable to humans.

4.1.3.4 Enhanced gene transfer by electroporation

Neumann *et al.*, (1982) first demonstrated electroporation-mediated gene transfer which involves the local administration of plasmid DNA coupled with application of an alternating electrical field in mouse lyoma cells over 20 years ago. Subsequently electroporation has become a common delivery method for *in-vitro* transfection of bacterial and mammalian cells with plasmid DNA (Neumann *et al.*, 1989), and other nuclear material such as RNA or DNA oligonucleotides (Bergan *et al.*, 1993; Neumann *et al.*, 1999). The application of electric pulse in electroporation is thought to disrupt the cell membrane, forming transient pores of restricted sizes through which DNA complexes can pass through. However, high frequency electrical fields applied for a long duration can cause local tissue damage and inflammation (Mathiesen, 1999). Currently, electroporation has been extensively tested in many types of tissues *in-vivo* (Heller *et al.*, 2005), for example, Hasson *et al.*, (2005) demonstrated that electroporation substantially increased transgene expression in isolated lung in an *ex-vivo* organ culture setting. Dean *et al.*, (2003) also showed that similar transfer efficiency of a reporter plasmid was achieved in live animals when a pair of electrodes was placed directly on the chest. Ghartey-Tagoe *et* al., (2006) evaluated the ability of electroporation to efficiently transfect differentiated epithelial monolayers (T84 monolayers) with reported plasmids (luciferase and green fluorescent protein) and synthetic siRNAs targeting the nuclear envelop proteins lamin A/C. The authors demonstrated that optimised electroporation conditions resulted in strong reporter plasmid expression in T84 cells, and expression of reporter genes increased proportionally with increasing electroporation strength. In addition, it was shown that transfection of reporter plasmids by lipofection exhibited poorer transfection efficiency than electroporation. Moreover, electroporation was found to transfect monolayers with synthetic siRNAs, which resulted in ~90% inhibition of lamin A/C. These results have suggested that electroporation can provide a valuable delivery method for transfection of intestinal epithelial monolayers and other

differentiated cell systems. Akaneya and colleagues (2005) demonstrated local electroporation-mediated transfer of synthetic siRNAs into a specific brain region of mice results in a marked reduction of target genes such as the expression of GluR2 and Cox-1 in pyramidal cells in the CA1 region of the hippocampus. Interestingly, the knockdown mouse models generated by electroporation displayed physiological functions consistent with the downregulated genes such as glutamate release from presynaptic sites, long-term potentiation (LTP) and long-term depression (LTD). Collectively, these data have provided evidence that RNAi-induced gene silencing by electroporation holds great potential for disease therapy, and recently, electrotransfer has been adapted as a versatile delivery system for the treatment of eye diseases.

4.1.4 The application of electroporation and iontophoresis to ocular gene therapy

At present, electroporation and iontophoresis are being developed as an innovative non-viral mediated gene delivery mechanism for the treatment of eye diseases. These two techniques rely mainly on the use of varying electric current to allow transfection of different ocular cell types *in-vivo*. Electroporation has been found to be most efficient for the delivery of custom designed plasmids such as RNAi-based vector systems or viral vectors (André and Mir, 2004; Wells, 2004), whereas iontophoresis is being developed for the delivery of small nucleic acid fragments such as antisense oligonucleotides, ribozymes, or synthetic siRNAs. The mechanism of electroporation relies mainly on a relatively high intensity of electric field (>100 V/cm) and very short pulses (μ-msec duration) application. Application of these conditions induces reversible destabilisation and permeablisation of the cell membrane enabling drugs and genetic materials to gain access into different cells in various tissues (Teissie *et al.*, 2005; Babiuk *et al.*, 2002a and b; Banga *et al.*, 1999). Recent reports have also specified electroporation dramatically enhanced plasmid gene transfer *in-vivo* to different ocular cells and tissues (Oshima *et al.*, 1998; Sakamoto *et al.*, 1999). Iontophoresis technique, in contrary, is based on the application of low voltage (typically 10 V or less) continuous constant or alternative electric current (0.5-1.5 mA/cm^2) for enhanced tissue penetration of molecules (Banga *et al.*, 1999).

Therefore, iontophoresis is suitable when tissue penetration with low molecular weight ionized drugs is preferred. In addition, tissue penetration of higher molecular weight or non-charged molecules can also be improved by additional mechanisms such as electro-osmosis or tissue permeation (Pikal *et al.*, 1992). Currently, enhanced intraocular delivery of drugs and small charged oligonucleotides has been achieved in animal models using trans-corneal, corneoscleral and scleral iontophoresis (Asahara *et al.*, 2001; Behar-Cohen *et al.*, 2002; Berdugo *et al.*, 2003; Kralinger *et al.*, 2003; Voigt *et al.*, 2002a). The instrument required conventionally consists of a 'pulse generator' and an 'applicator', which includes the electrodes. The three dimensional geometry of the electrodes determines the strength, homogeneity, orientation and the shape of the electrical field transferred to the target tissue during electroporation (André and Mir, 2004). A two-type pulse technique using a combination of high voltage, followed by low-voltage pulses is commonly used with most electroporation instrumentation (Aihara and Miyazaki, 1998). Different electrodes have also been developed for various applications; for example surface and needle electrodes have been developed for deep tissues, electroporation catheters for hollow organs such as blood vessels, and tweezer-type electrodes for ocular tissues (Mehier-Humbert and Guy, 2005; Rabussay *et al.*, 2003; Wells, 2004; Matsuda and Cepko, 2004). In contrast, an iontophoresis device comprises a power source and two electrode compartments delivering a constant or alternating milliamp current. The drug to be iontophoresed is placed in the electrode compartment bearing the same charge. The stability of drug activity to ionization is an important factor when clinical use is considered. The intensity and duration of electricity applied, the shape of the electrode, and drug properties (molecular weight and chemical structure) are important to determine the efficiency of permeation enhancement (Yasukawa *et al.*, 2004).

In contrast to the homogeneity of muscle tissues, the heterogeneous tissue composition of the eyeball has added more complexity to electroporation with much less predictability of geometry and distribution of electric charges (Dezawa *et al.*, 2002). In particular, when excessive electrical voltages and extended electric pulses

are used, irreversible tissue damage may occur as a result of thermal heating (Durieux *et al.*, 2004), and fluctuation in Ca^{2+} influx due to disruption of cell membranes may also induce tissue damage due to Ca^{2+}-mediated protease activation (Gissel and Clausen, 2001). Therefore, electroporation parameters (i.e. electrode design, field strength and pulse duration and magnitude) are required to be specifically adapted to specific tissues in order to obtain optimal electrotransfer. These parameters are often adapted or improved on previous mechanistic research, mathematic modelling and empirical optimisation (Somiari *et al.*, 2000; Zampaglione *et al.*, 2005).

4.1.4.1 Electroporation-assisted gene transfer in ocular gene therapy

In 1998, Oshima and colleagues first reported targeted gene transfer to corneal endothelium *in-vivo* by electric pulses. Plasmid with the *lac-Z* gene encoding β-galactosidase was injected into the anterior chamber of rat eyes, and a series of eight electric pulses of 20 V with a pulse length of 50 msec was delivered through an electrode placed on the surface of the cornea. Beta-galactosidase was detected in the corneal endothelium for at least 21 days after the gene transfer, with a peak at 3 days, and gene expression was confined within the ring-shaped area of corneal endothelial cells. Using the same technique, a therapeutic gene (plasmid encoding tissue plasminogen activator) was transferred to the corneal endothelium, where the biologically active tPA was present for four days after treatment and induced a significant decrease in fibrin formation following YAG laser-generated bleeding in the anterior chamber (Sakamoto *et al.*, 1999). Electroporation of subconjunctivally and intracorneally injected plasmids (encoding luciferase or enhanced green fluorescent protein, EGFP) has been shown to yield high reporter gene expression on the entire surface of the cornea in both epithelial and stromal layers (Blair-Parks *et al.*, 2002). The parameters used in this study was later transferred to another study involving electroporation of a subconjunctivally injected plasmid encoding matrix metalloproteinase-3 (MMP-3) after glaucoma surgery, which caused significantly longer survival of the filtering bleb, and decreased levels of intraocular pressure as compared to controls (Mamiya *et al.*, 2004).

Electroporation method can be applied for both gain- and loss-of-function in the rodent retina. Matsuda and Cepko, (2004) showed that *in-vitro* and *in-vivo* electroporation after subretinal injection of plasmid encoding EGFP in newborn rats and mice, and also in mouse retinal explants resulted in widespread transduction of retinal cells with an average 80% (rats) and 50% (mice) of the retinal cells expressing EGFP. In wild type CD1 mice, electroporation application after subretinal injection of DNA-based RNA interference vectors directed against two transcription factors (Crx and Nrl) essential for photoreceptor development led to the induction of photoreceptor phenotypes similar to those of corresponding knockout mice (Matsuda and Cepko, 2004). Using identical experimental parameters, Matsuda and Cepko, (2007) have also characterised several retinal cell-type specific promoters such as the regulatory sequence for rhodopsin (Zack *et al.*, 1991), cellular retinaldehyde binding protein (Cralbp) (Matsuda and Cepko, 2004) and promoter regions of Nrl (Swaroop *et al.*, 1992) in the expression of EGFP in newborn rat retinas. In addition, Matsuda and Cepko, (2007) demonstrated the silencing of EGFP reporter gene by electroporation of a rhodopsin promoter-Cre-inducible RNAi vector using the miR-30 based shRNA expression system (Zeng *et al.*, 2002; Paddison *et al.*, 2004b) into rat retinas at P0, which has broadened the use of Cre/loxP system and cell-type specific promoters in the application range of *in-vivo* electroporation. Similarly, Rao *et al.*, (2004) showed that the combination of RNAi with *in-ovo* electroporation provided a powerful method for silencing the expression of retinoid-synthesising enzyme Raldh2 in chick embryo.

4.1.4.2 Iontophoresis –assisted gene transfer in ocular gene therapy

The original concept of using iontophoresis to enhance the delivery of drugs into the ocular tissues was developed by Hughes and Maurice (1984). Subsequently, Behar-Cohen *et al.*, (1997 and 1998) and Berdugo *et al.*, (2003) confirmed that controlled low-current density iontophoresis was safe and did not induce significant structural alterations in the cornea. Following this, Asahara *et al.*, (2001) reported on the use of iontophoresis for promoting intraocular penetration of topically applied nucleic acid. After transcorneal iontophoresis, a topically applied 6-FAM labeled 23-base antisense

oligonucleotides of human aldose reductase was detected in the aqueous humor, the vitreous, and retina after 5, 10, and 20 minutes of iontophoresis, respectively, and no sign of ocular toxicity was observed. Furthermore, using antisense-NOSII ODN, Voigt *et al.*, (2002b) successfully achieved significant down-regulation of NOSII expression in the iris/ciliary body tissues of rat eyes with endotoxin-induced uveitis.

Collectively, the wide range of strategies validated and the potential for targeting specific types of cells have strengthened the promising early observations made using electroporation and iontophoresis. These two non-viral delivery methods have proven to be safe to use and can be used efficiently for targeted gene delivery in ocular tissues *in-vivo*. To date, their application for the treatment of ocular human diseases is approaching its final stages of adaptation and practical implementation in clinical trials (Bejjani *et al.*, 2007).

4.1.5 Fluorescence-activated cell sorting (FACS)

Fluorescence-activated cell sorting (FACS) is a specialised type of flow cytometry that provides a sensitive method for sorting a heterogeneous mixture of biological cells, one cell at a time, based upon the specific light scattering and fluorescent characteristics of each cell. It is a useful instrument as it provides fast, objective and quantitative recording of fluorescent signals from individual cells as well as physical separation of cells of particular interest. The basic principles behind FACS can be categorised into the following steps (*Figure 4.1*): (1) first the cell suspension to be sorted is entrained in the center of a narrow, rapidly flowing stream of liquid. The flow is arranged so that there is a large separation between cells relative to their diameter, and a vibrating mechanism causes the stream of cells to break into individual droplets; (2) a beam of light (usually laser light) of a single wavelength is directed onto the hydro-dynamically focused stream of fluid. A number of detectors are aimed at the point where the stream passes through the light beam; one in line with the light beam (Forward Scatter or FSC), several perpendicular to the light beam (Side Scatter, SSC), and one or more fluorescent detectors. Each suspended particle passing through the beam scatters the light in a characteristic pattern, and fluorescent

chemicals found in the particle or attached to the particle may be excited into emitting light at a lower frequency than the light source. This combination of scattered and fluorescent light is picked up by the detectors, and by analysing fluctuations in brightness at each detector (one for each fluorescent emission peak), the detector can extrapolate various types of information about the physical and chemical structure of each individual particle; (3) an electrical charging ring is placed just at the point where the stream breaks into droplets and a charge is placed on the ring based on the immediately prior fluorescence intensity measurement and the opposite charge is trapped on the droplet as it breaks from the stream. The charged droplets then fall through an electrostatic deflection system that diverts droplets into containers based upon their charge. To date, fluorescence-activated cell sorting (FACS) is extensively used in immunology to determine the stage of proliferation, differentiation or activation of immunocompetent cells. Several other reports have emphasised the usefulness of FACS in the analysis of cells derived from the central nervous system (CNS). In particular, McLaren *et al.*, (2001) showed that flow cytometry can be used to characterise the physical parameters of neurons, astrocytes or oligodendrocytes, and other groups have used the FACS to purify neural stem cells producing green fluorescent protein under the control of a nestin promoter (Wang *et al.*, 2000; Junger and Junger, 1998; Sergent-Tanguy *et al.*, 2003).

4.1.6 Objectives

Previous chapter have already shown that two IMPDH1-specific si/shRNAs (sh1224 and sh2048) elicited strong silencing effect on wild type and mutant IMPDH1 at both mRNA and protein levels in human and mouse cell lines (HeLa and N2a cells, respectively). In this chapter, the silencing efficacy of sh2048 (specific for both human and mouse IMPDH1, *Figure 3.2*), was further evaluated *ex-vivo* in mouse retinal explants using a combination of *in-vitro* electroporation (Matsuda and Cepko, 2004) and FACS analysis for obtaining pure transfectant populations. Previous studies carried out in our laboratory have used identical techniques to illustrate successful suppression and replacement strategy for both the rhodopsin and *rds*/peripherin genes in organotypic retinal cultures (Kiang *et al.*, 2005; Palfi *et al.*, 2006; O'Reilly *et al.*, 2007). In order to evaluate the silencing efficiency of IMPDH1 *ex-vivo* in retinal explants, a dual expression vector system that co-expressed green fluorescence protein (CMV-driven) and sh2048 (H1-driven) simultaneously (psh2048.EGFP) was first evaluated in mouse neuronal cells (N2a), and then electroporated *in-vitro* into dissected new born wild type C57B6/CBA mouse retinas after which positively transfected cells were extracted by FACS analysis. Subsequently, RNA was extracted from these cells and Real Time RT-PCR analysis was carried out to determine the level of endogenous murine IMPDH1 transcripts.

4.2 Methods

4.2.1 Construction of pshLuc.EGFP and psh2048.EGFP

The cloning steps of dual expression plasmids: pshLuc.EGFP and psh2048.EGFP was adapted from Kiang *et al.*, (2005) and Palfi *et al.*, (2006). In brief, restriction fragments containing the H1-promoter, shRNA sequences and termination signal were excised from pshLuc and psh2048, respectively, by restriction enzyme digestion at EcoRI and Hind III. The fragments were then subcloned into pEGFP-1 (Clontech) into which the CMV-promoter (PCR amplified from pcDNA3.1+) had been inserted immediately 5' of the EGFP cDNA (provided by Dr. Alpad Palfi, Department of Genetics, Trinity College Dublin), to give pshLuc.EGFP and psh2048.EGFP, respectively (*Figure 4.2*). A 300bp Ubc intron was PCR amplified (*Table 6*, Appendix) from pUB6/V5-His A, B, C (Invitrogen) and inserted in between the polymerase H1 and CMV promoters (*Figure 4.2*). Correct insertions of restriction fragments were verified by DNA sequencing using specific primers (*Table 7*, Appendix) as described in section 2.2.13.

4.2.2 Suppression of IMPDH1 mRNA expression in N2a cells

N2a (mouse neuroblastoma) cells were plated at a density of $1x10^5$cells/ml onto a 24-well plate with $DMEM^{-Abs}$ medium one day before transfection. For each transfection sample, 1 µg/µl of pshLuc.EGFP or psh2048.EGFP was diluted in 50 µl of Opti-MEM-reduced serum medium and mixed gently. 1 µl of Lipofectamine 2000® was then diluted in 50 µl Opti-MEM-reduced serum medium and incubated at room temperature for 5mins. The diluted shRNA vectors were combined with the diluted Lipofectamin 2000® (total volume = 100 µl) and incubated at room temperature for 25 min for complex formation. 100 µl expression shRNA vector+Lipofectamine 2000® complex was then added to each sample wells. The plate was mixed by gentle rocking and incubated at 37°C in a CO_2 incubator. Each sample was carried out in quadruplicates and pooled together during RNA extraction as in section 2.3.7. The level of IMPDH1 mRNA expression was analysed by Real Time RT-PCR using IMPDH1-specific primers (*Table 2*, Appendix) 24 hrs post-transfection (section 2.4),

and the average of three independent experiments was illustrated. For each transfection experiment, a control group was transfected with pshLuc.EGFP as non-targeting controls (*Table 1*, Appendix). IMPDH1 expression was standardised per unit β-actin expression and expressed as a percentage of that for the non-targeting control.

4.2.3 Electroporation of murine retinal explants and fluorescence activated cell sorting (FACS)

Electroporation of cultured murine retinal explants and fluorescence activated cell sorting (FACS) were carried out according to protocols described by Kiang *et al.*, (2005) and Palfi *et al.*, (2006) as shown in *Figure 4.3*, and described in detail in sections *2.61*, *2.62* and *2.63*. In brief, 12 retinas were dissected from one day old wild type C57B6/CBA mouse pups and electroporated with 100 µl of pshLuc.EGFP or psh2048.EGFP (final concentration=1 µg/µl) in a micro-electroporation chamber (Nepagene, model CUY532, 3 mm x 10 mm x 5 mm) from the scleral side at 5 square pulses (30 V) of 50 ms duration with 950 ms intervals using a pulse generator (ECM 830 BTX) in two independent experiments. Retinal tissues were then cultured for 14 days *in-vitro* on Costar Transwell polycarbonate membrane and six retinas per construct were pooled together for dissociation by trypsin digest into single cells. Dissociated retinal cells expressing EGFP were collected using a Beckman-Coulter Altra Fluorescence Activated Cell Sorter (Beckman-Coulter, Inc., Fullerton, CA, USA). All FACS sorting procedures were carried out with the help of Dr. Alfonso Blanco (Conway Institute, University College Dublin). FACS-sorted EGFP positive retinal cells were concentrated through Amicon ultra-free-MC 0.45 µm filtration units (Millipore Corp., Billerica, MA) and RNA was extracted using the RNeasy Mini Kit (Qiagen).

4.2.4 Real Time RT-PCR analysis of endogenous mouse IMPDH1 transcript levels in retinal explants

The levels of endogenous mouse IMPDH1 mRNA (BC_053416) and β-actin mRNA (EF_095208) were determined by Real Time RT-PCR analysis using Quantitect

SYBR Green RT-PCR kit (Qiagen) on a LightCycler (Roche Diagnostics Ltd., Lewes, UK). RT-PCR analysis was carried out in 20 µl reactions using 10 pmoles of HPLC purified primers (*Table 2*, Appendix) as described in detail in section 2.4. Reverse transcription was performed at 50°C for 20 min, and cDNA was amplified in 38 cycles at 94°C for 15 sec, 57°C for 20 sec and 72°C for 5 sec. For all the retinal explant experiments, the level of endogenous IMPDH1 expression was standardised to house-keeping β-actin expression, and expressed as a percentage of that for the non-targeting control, pshLuc.EGFP.

4.2.5 Vibratome sectioning of retinal explant tissues

Electroporated retinal explant cultures were fixed in 4% paraformaldehyde (pH 7.4) for 30 min at 37°C and washed with PBS for 30 min. The outlines of retinal explants sitting on polycarbonate filter membranes were cut out and embedded in 4% agarose agar (Sigma) as shown in *Figure 4.4*. Agar blocks containing retinal explants were then sectioned with a vibratome sectioner (Leica VT 1000S, Leica Bioscience, DA, USA) at 50 µm thickness. Retinal sections were stained with 4'-6-Diamidino-2-phenylindoland, DAPI (1:5000 in PBS) and embedded on glass slides using Aqua-polymount (Polyscience Inc.). The slides were stored overnight at room temperature in the dark and transferred to 4°C for long-term storage. All fluorescence imaging was carried out on a fluorescence microscope (Zeiss, Axioplan 2) at an excitation wavelength of 350 nm. All images were captured at 40X magnification.

4.2.6 Statistical Analysis

For all graphs presented in this chapter, each data point represents the mean of two independent experiments. The standard deviation of the mean (S.D) and standard error of the mean (S.E.M) were calculated using Data Desk 6.0 PPC (Data Description, Inc., New York, NY, USA). Two sample student *t*-tests were applied for comparisons between the means of non-targeting and targeting shRNAs. Y-error bars denote standard error of the mean. Unless otherwise stated, *P*-value ≤ 0.05 was considered to indicate statistical significance.

4.3 Results

4.3.1 Construction of dual expression RNAi-vector systems

In order for easy identification of cells that express shRNA after transfection, a dual-vector RNAi vector system was constructed. This vector system contains two main expression units (*Figure 4.2*); (1) the silencing unit excised from pBluescriptH1 contains sequences encoding an shRNA under the control of human H1-RNA polymerase III promoter (as previously described in Chapter 3); and (2) the reporter gene, enhanced green fluorescent protein (EGFP) under the control of CMV promoter. Therefore, cells transfected with this construct can be directly detected by fluorescence of GFP at the single cell level. Previous studies carried out in our laboratory have successfully used an identical dual expression RNAi-vector system to express shRNAs targeting rhodopsin and *rds*/peripherin in retinal explants (Kiang *et al.*, 2005; Palfi *et al.*, 2006; O'Reilly *et al.*, 2007). In this study, only sh2048 was selected to be subcloned into the dual expression plasmid (psh2048.EGFP), as it was initially generated to target both human and mouse mRNA with full complementarity, whereas sh1224 was designed specifically for human IMPDH1 and contains three mismatches at the target site in mouse IMPDH1 (*Figure 3.2*). An additional dual-expression shRNA vector was constructed expressing shRNAs targeting luciferase2 (pshLuc.EGFP) as a non-targeting control for silencing experiments (section 3.22).

4.3.2 Suppression of endogenous IMPDH1 mRNA by psh2048.EGFP in N2a cells

In order to assess whether subcloning of sh2048 into the dual expression cassette has affected its silencing ability in mammalian cell cultures, N2a (mouse neuroblastoma) cells were transfected with 1 μg/μl of psh2048.EGFP and the level of endogenous IMPDH1 mRNA was quantified by Real Time RT-PCR analysis twenty-four hours post-transfection. Endogenous IMPDH1 expression was standardised to β-actin mRNA levels and expressed as a percentage of IMPDH1 mRNA levels in cells transfected with the non-targeting control. The suppression data represented in *Figure 4.5* showed that IMPDH1 expression was reduced to 35% ± 7% in N2a cells transfected with psh2048.EGFP compared to expression levels found in cells

transfected with the non-targeting control (P=0.0478). This result illustrated that sh2048 elicited efficient silencing on mouse IMPDH1 transcripts in N2a cells, and that subcloning of the H1-driven shRNA restriction fragment into the dual expression RNAi-vector system did not affect the silencing ability of sh2048.

4.3.3 RNAi-mediated suppression of IMPDH1 mRNA in retinal explants following *in-vitro* electroporation

One technical factor limiting the use of RNAi approach for studies of putative knockdown phenotypes in individual cells is that many cell types are only transfected with low efficiency, resulting unavoidably in a large fraction of untransfected cells which may contaminate the population, thus diluting the observed effect of the RNAi and obscuring the experimental outcome. In addition, it is critical to obtain pure transfectant populations when assessing RNAi-mediated silencing of a target gene, since untransfected cells will significantly mask the true knockdown effect. Therefore, the ability of fluorescence-activated cell sorting (FACS) to separate a heterogeneous mixture of cells based upon the specific light scattering and fluorescent characteristics of each cell was exploited to obtain a population of positive transfectants. Initially twelve retinas from new-born wild type C57B6/CBA mouse pups were dissected and six retinas were separately electroporated in a pool within a micro-chamber containing 100 µl of pshLuc.EGFP and psh2048.EGFP at a concentration of 1 µg/µl, respectively, as previously described by Matsuda and Cepko (2004). Retinal explants were then cultured *in-vitro* for 14 days, and six retinas electroporated with each plasmid were pooled prior to trypsin dissociation. Trypsin-dissociated single retinal cells expressing EGFP representing transfected cells were identified and sorted by FACS analysis. More specifically, electroporated photoreceptor cells were sorted by size fractionation and EGFP fluorescence levels in two independent experiments as shown in *Figures 4.6, 4.7; experiment 1* and *Figures 4.8 and 4.9; experiment 2*, and all FACS sorting parameters were calibrated according to previous studies reported by Kiang *et al.*, (2005) and Palfi *et al.*, (2006). The histograms of FITC versus cell number in *Figures 4.6* to *4.9* show that EGFP-fluorescent cells exhibited a greater than 2 log-scale difference in their fluorescence

level when compared to non-transfected cells, and accounted for 8-33% of the total cell population. RNA was then extracted from the EGFP-positive retinal cells for Real Time RT-PCR analysis, and the level of endogenous IMPDH1 mRNA in retinal cells transfected with psh2048.EGFP was significantly suppressed to 19% ± 4.9%, compared to levels found in cells transfected with the non-targeting control (*Figure 4.10*, P=0.0318). In addition, vibratome sections in *Figure 4.11* show that 14-day old electroporated retinal cultures have differentiated and morphologically resembled a normal retina *in-vivo*, displaying a defined outer nuclear layer, inner nuclear layer and ganglion cell layer. Moreover, the CMV-driven EGFP reporter gene was expressed ubiquitously in most retinal cell types (*Figure 4.11*). Collectively, these results show that significant downregulation of endogenous murine IMPDH1 gene expression was achieved *ex-vivo* in retinal explants using sh2048.

4.4 Discussion

The safety and efficacy of electroporation in humans has been shown in a variety of contexts, most notably as a means to target and enhance intracellular delivery of chemotherapeutic agents for treatment of malignant cutaneous or subcutaneous lesions (Gothelf *et al.*, 2003). Animal studies have further supported human studies and have additionally demonstrated delivery of a number of different genes into various animal models (Trezise, 2002). While stability issues surrounding the use of lipid- or polymer-based carriers suggest that they may not be well suited to *in-vivo* use (Gao *et al.*, 2007), viral-based delivery of siRNA has been shown to be effective *in-vivo* (Xia *et al.*, 2002), though it is often hampered by several limitations such as the difficulty in regulating the extent of infection, potential toxicity to cell types e.g. neurons, and being highly time consuming to construct (Ehrengruber *et al.*, 2001; Janson *et al.*, 2001). *In-vivo* electroporation may overcome these shortcomings by controlling the region where the effect of RNAi is reached by altering the lag time of electroporation after injection of siRNA and the positioning of the electroporation electrode.

In the previous chapter, transfection of IMPDH1-specific shRNAs to mammalian cell cultures has been successfully shown to reduce IMPDH1 expression at both mRNA and protein level with great efficiency. However, since the efficacy of RNAi-mediated silencing is highly dependent on the endogenous RNAi pathway which varies significantly between *in-vitro* and *in-vivo* systems, the robustness of the two IMPDH1 suppressors was further tested in retinal explants, which provide a cellular environment similar to that of *in-vivo* retinal tissues. Matsuda and Cepko, (2004) previously demonstrated that DNA can be readily introduced into retinal cells of newborn mouse and rat by electroporation *in-vitro* and *in-vivo*. Furthermore, Kiang *et al.*, (2005), Palfi *et al.*, (2006) and O'Reilly *et al.*, (2007) in our laboratory have both successfully demonstrated *in-vitro* electroporation of RNAi-based vector systems to suppress and replace the rhodopsin and *rds*/peripherin genes respectively, *ex-vivo* in retinal explants. Akaneya *et al.*, (2005) previously reported that the effect of synthetic siRNAs in the mouse brain was transient and was only present for one week after

local electroporation. To overcome this limitation, a dual expression RNAi-based vector system that produces IMPDH1-specific shRNAs driven by polymerase III H1-promoter and enhanced green fluorescence protein (EGFP) driven by CMV was constructed. The EGFP reporter gene allows for the identification and sorting of pure transfected cell populations from electroporated retinas, so preventing untransfected cells from masking the true knockdown effect of IMPDH1 achieved by the shRNA. In addition, only one of the previously validated IMPDH1-shRNAs, sh2048, was subcloned into the dual expression RNAi-vector system for further evaluation in retinal explants as it was initially designed to target both human IMPDH1 (NM_000883) and mouse (BC_053416) IMPDH1 transcripts (*Figure 3.2*). Transfection of the newly subcloned dual expression RNAi-vector system into N2a cells showed efficient silencing of endogenous IMPDH1 expression (*Figure 4.5*), indicating that the activity of sh2048 was not affected by this additional cloning step, and has also illustrated its specific silencing efficacy for both mouse and human IMPDH1 transcripts.

According to a study reported by Sukharev *et al.*, (1992) the ability of extracellular molecules to enter the cytosol is highly dependent on the paradigms of electrical pulses applied during electroporation. Conventionally in *in-vivo* electroporation studies, the parameters of the electrical pulse with 10- to 90-V intensity and $\geq$ 50 ms duration are generally used (Itasaki *et al.*, 1999). In addition, Akaneya *et al.*, (2005) have developed a novel pattern of electrical pulses for the introduction of synthetic siRNAs by *in-vivo* electroporation into specific brain regions. This method uses a combination of preceding electrical pulse of high intensity and short duration (poring pulse), followed by an electrical pulse of low intensity and long duration (driving pulse). The two electrical pulses are believed to have their own respective task where the poring pulse opens a pore in the membrane, and the driving pulse helps extracellular siRNAs to enter the cytosol. One of the major drawbacks of electroporation is the need to increase voltage to enhance the efficiency of transfection, which may increase the possibility of inducing cell death (Itasaki *et al.*, 1999). Strong electrical pulses increase the effectiveness of transfection by increasing

the size and number of pores in the membrane, but enhance cell death by increasing toxicity following the influx of external media, generation of free radicals (Bonnafous *et al.*, 1999) and inducing vascular effects (Gehl *et al.*, 2002). When the lifetime of pores is prolonged by electric pulses of long duration, intracellular contents may also leak out of the cell membrane (Gehl *et al.*, 1999). In this study, the electrical pattern used for electroporation-mediated delivery of shRNAs into retinal explants included five square pulses at 30 V of 50 ms duration with 950 ms intervals. These electrical parameters were shown not to have caused any significant detrimental damage on cultured retinal explants, as the histology in *Figure 4.11* showed normal morphological differentiation of cultured retinas to resemble a normal retina *in-vivo* with defined outer and inner nuclear layers, which was consistent with the observation reported by Matsuda and Cepko, (2004). Furthermore, the retinal explants were aligned in a specific position within the micro-electroporation chamber so that the current was applied from the scleral side of the retinas during *in-vitro* electroporation (*Figure 4.3*). The purpose of this specific arrangement was to achieve maximum electroporation efficiency since Matsuda and Cepko, (2004) previously reported that electroporation into the vitreal side of adult mouse retinas *in-vitro* was much less efficient than the scleral side. A possible explanation for this is that the presence of basal laminae in the inner limiting membrane might impede vector penetration; nonetheless, this method could serve to be a useful technique for transfecting the ganglion cell layer *in-vitro*. In particular, vibratome sections of electroporated retinas in *Figure 4.11* show the presence of EGFP fluorescence in cells of the outer nuclear layer, inner nuclear layer and also the ganglion cell layer. This observation has thus illustrated the effectiveness of *in-vitro* electroporation in delivering DNA plasmid throughout the different layers of the retina, and the robustness of the ubiquitous CMV promoter in driving the expression of EGFP in various retinal cell types.

The transfection efficiency of cells within the retinal explants was approximately 8-33% as observed by FACS analysis (*Figures 4.6 to 4.9*), and this variation was accounted by subtle differences in each independent electroporation experiments,

such as the positioning of explants in the micro-electroporation chamber or dissociation into single cell digests. For the assessment of RNAi-mediated silencing of a target gene, it is important to examine the pure transfectant population since untransfected cells can significantly mask the true knockdown effect. By extracting the pure transfectant population from retinal explants, the evaluation of the suppression of IMPDH1 was not masked by the 62-92% untransfected cells, and it was observed that up to 81% suppression of endogenous murine IMPDH1 mRNA was achieved with sh2048 (*Figure 4.10*). It is most likely that the suppression data obtained in retinal explants after FACS analysis represent the true silencing activity of sh2048, as only transfected cells were evaluated. This is supported by the previous observation in N2a cells where suppression of only 65% was achieved (*Figure 4.5*). This is most likely because untransfected cells have lowered the observed overall knockdown effect. Additional attempts have also been made to analyse the level of IMPDH1 suppression at the protein level in FACS sorted retinal explants by western blot analysis or immunostaining. However, the concentration of protein retrieved from FACS sorted retinal cells was insufficient for western blot analysis, and an antibody for immunostaining was not yet available at the time of the study. The suppression of IMPDH1 at the protein level *in-vivo* was however evaluated in mouse retina in the next chapter.

4.5 Summary of current findings

Many studies have confirmed the promising potential of electroporation as a powerful non-viral physical method for the enhancement of nucleic acid delivery into ocular tissues. The results obtained in this study have demonstrated that *in-vitro* electroporation can be used to efficiently deliver RNAi-based vectors into retinal explants to achieve stable and long-term downregulation of IMPDH1 gene expression. Furthermore, electroporation of sh2048 did not cause any significant pathological effect to the development of retinas *in-vitro*. The construction of a dual expression RNAi-vector system and FACS analysis have also provided a rapid and sensitive method for sorting positively transfected photoreceptor cells, which allowed for the evaluation of shRNA-mediated silencing of IMPDH1 in a true transfectant population. Although the basic instrumentation and modalities of application have been established for *in-vivo* electroporation (Matsuda and Cepko, 2004 and 2007), the long term safety, secondary effects of electrically assisted delivery into ocular tissues, and longevity and stability of shRNA expression remain to be carefully analysed in animal models. For these reasons, *in-vivo* electroporation may not yet be well suited as therapeutic delivery method for gene therapy of inherited retinal diseases. In order to achieve stable suppression of IMPDH1 *in-vivo*, the specificity and efficiency of adeno-associated viral vectors to mediate stable expression of transgene *in-vivo* will be exploited as discussed in the next chapter. Previous reports have successfully illustrated significant suppression of the mouse rhodopsin gene and VEGF *in-vivo* by AAV mediated siRNA delivery (Gorbatyuk *et al.*, 2007; Tessitore *et al.*, 2006; O'Reilly *et al.*, 2007; Cashman *et al.*, 2006), therefore the adaptation of the current shRNA vector into an AAV-mediated RNAi vector system promises to be even more powerful at silencing IMPDH1 gene expression in mouse retinas *in-vivo*.

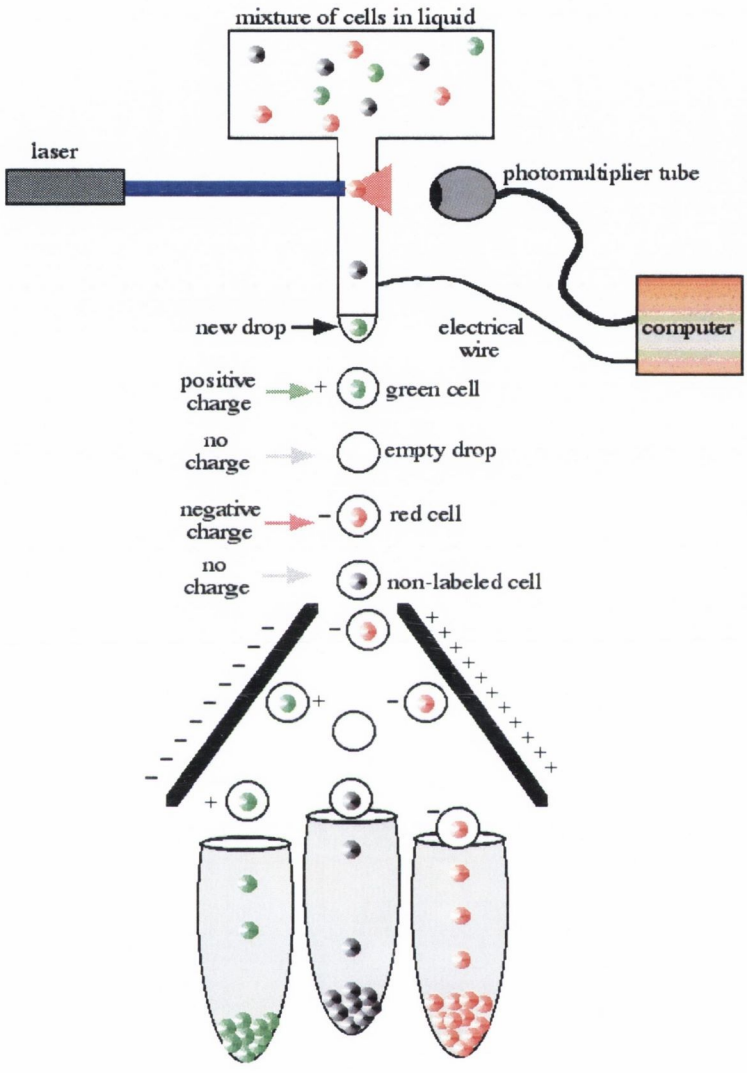

Figure 4.1: A schematic diagram showing the steps involved in fluorescence-activated cell sorting (FACS). The major components of FACS include**:** (1) A flow cell- liquid stream carries and aligns the cells so that they pass single file through the light beam for sensing. (2) a light source - commonly used are lamps (mercury and xenon); high power water-cooled lasers (argon, krypton, dye laser); low power air-cooled lasers (argon (488nm), red-HeNe (633nm), green-HeNe, HeCd (UV)); diode lasers (blue, green, red, violet). (3) a detector and Analogue to Digital Conversion (ADC) system - generating FSC and SSC as well as fluorescence signals. (4) an amplification system - linear or logarithmic. (5) A computer for analysis of the signals.

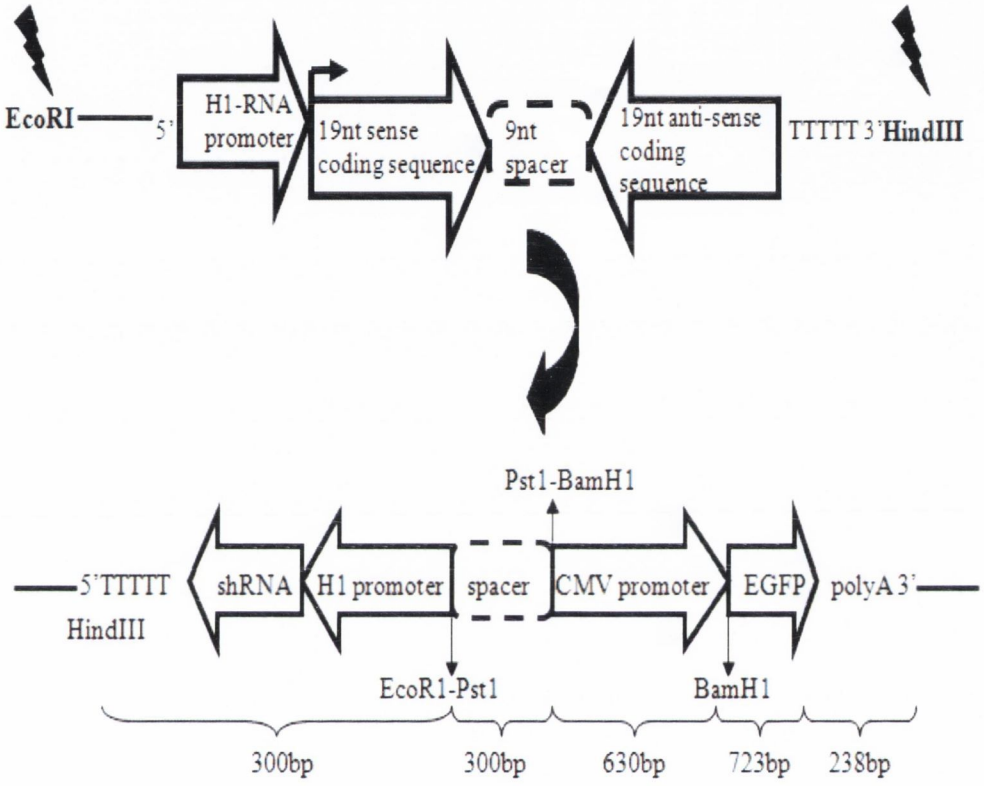

Figure 4.2: A schematic illustration of the dual-expression plasmid. Restriction fragments containing the H1 promoter, shRNA sequences and termination signal were excised from pshLuc and psh2048, respectively, at the designated restriction sites and subcloned into pEGFP-1 (Clontech) containing the EGFP cDNA driven by a CMV promoter. A Ubc intron was also inserted in between the two promoters. The size of each construct element is given in base pairs.

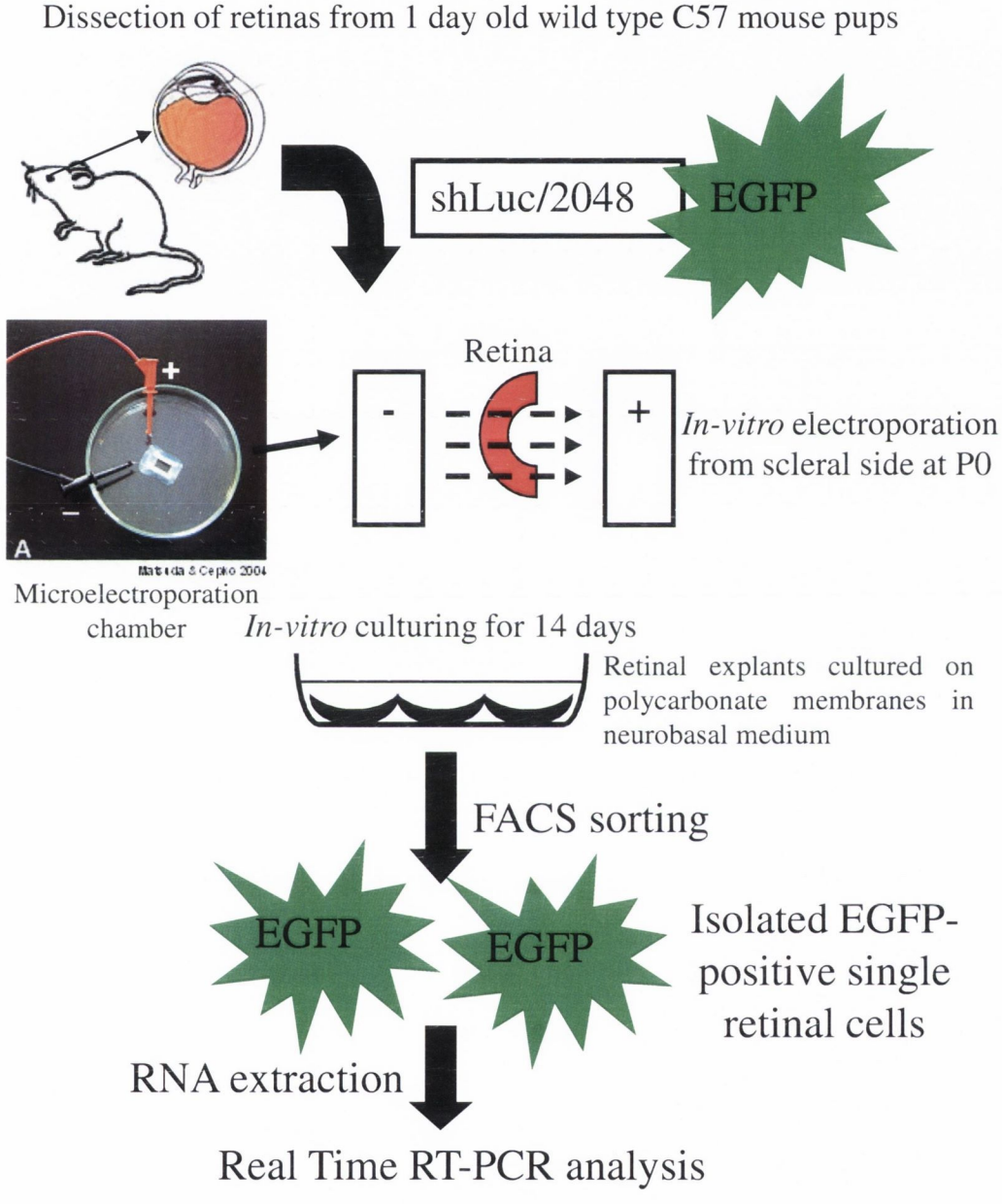

Figure 4.3: A schematic diagram illustrating the steps involved in the electroporation, maintenance, dissociation and fluorescence activated cell sorting (FACS) of cultured retinal explants.

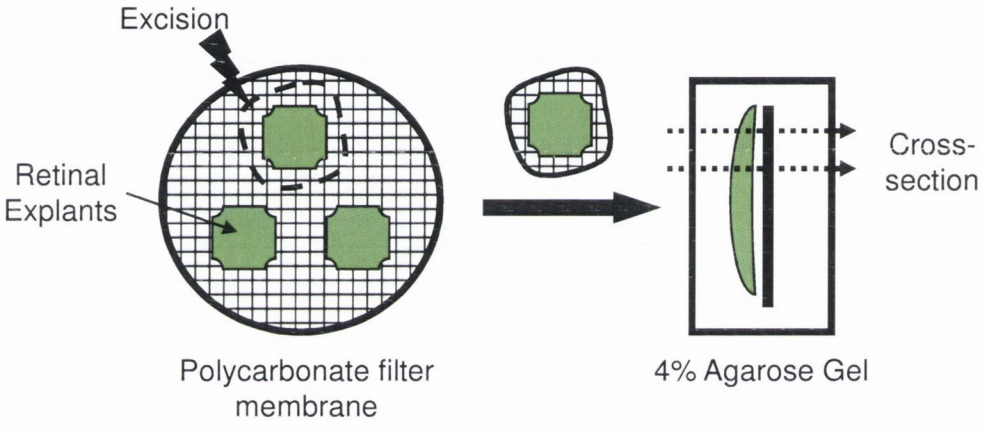

Figure 4.4: Vibratome sectioning of retinal explants. Retinal explants were excised from polycarbonate filter membranes and embedded in 4% agarose gel. Embedded retinal explants were then sectioned with a vibratome sectioner (Leica VT 1000S) at 50μm thickness

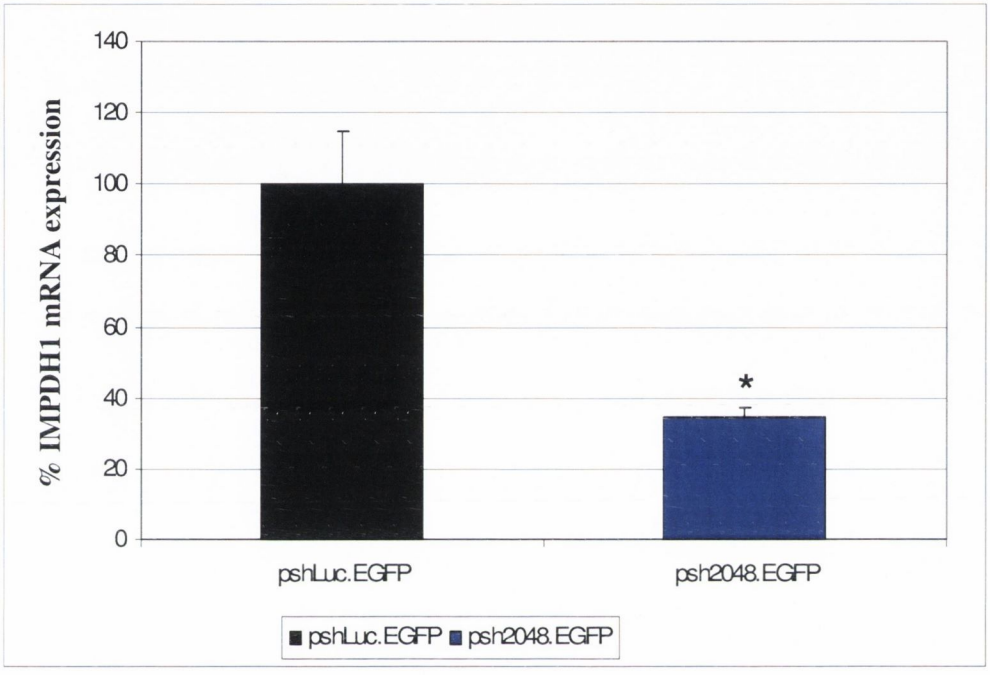

shRNA	psh2048.EGFP
% IMPDH1 expression ± SEM	35% ± 2.68%

Figure 4.5: Suppression of endogenous mouse IMPDH1 transcripts in N2a cells by sh2048. N2a cells were transfected with 1 μg/μl of psh2048.EGFP (blue bar) and pshLuc.EGFP (black bar) as control. Twenty-four hours after transfection, RNA was extracted from N2a cells and percentage IMPDH1 expression was quantified by Real Time RT-PCR and normalised to the house-keeping gene, β-actin. A control set was transfected with shRNAs directed at LuciferaseGL2, and this was standardised to represent 100% IMPDH1 expression (Black bar). The average of 3 independent experiments is shown; Y-error bars indicate standard error of the mean (SEM). Percentage IMPDH1 expression ± SEM is denoted in the bottom panel. * $P<0.05$.

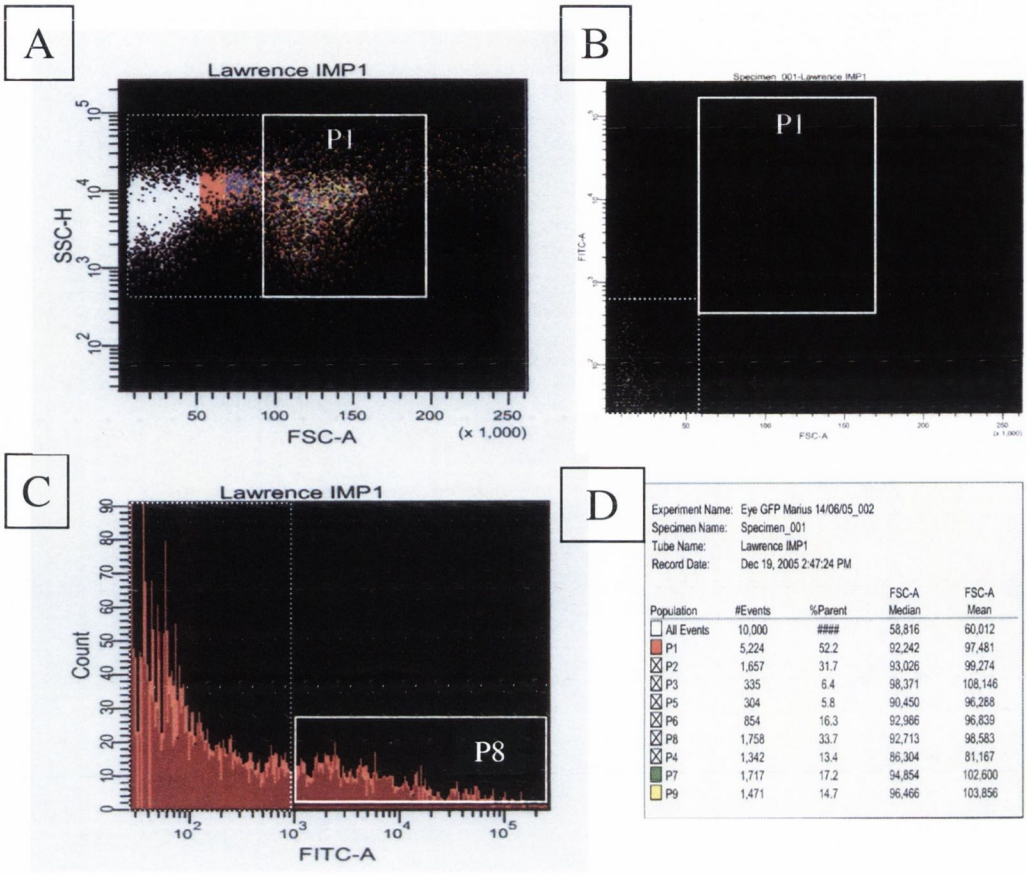

Figure 4.6; Experiment 1 (Non-targeting shRNA): Isolation of pshLuc.EGFP transfected cells from retinal explants by FACS. **(A)** A scatterplot of forward scatter (FSC, X-axis) versus side scatter (SSC, Y-axis). FSC correlates with the entire cell volume and SSC is dependent on the inner complexity of the particle (i.e. shape of the nucleus, the amount and type of cytoplasmic granules or the membrane roughness). pshLuc.EGFP transfected cells from dissociated retinal explants were initially sorted by size and granularity, and the boxed area (P1) depicts the population of intact photoreceptor cells. Dotted area represent a population of cells containing mainly of cell debris. **(B)** A scatterplot of forward scatter (FSC, X-axis) versus green fluorescence intensity (FITC, Y-axis). Individual dots represent each individual cells. Dotted area represents a population EGFP-negative cells. Boxed area (P1) represent the isolation of a population of retinal cells with fluorescence levels above an arbitrary threshold. **(C)** A histogram of green fluorescence intensity (FITC, x-axis) versus cell number. Dotted area represent a population of cells in P1 with fluorescence levels below an arbitrary level, whereas boxed area (P8) represent those above an arbitrary threshold. **(D)** A table illustrating percentage of different populations of cells sorted by size (SSC) and fluorescence (FITC). Up to 33% (P8) of cells in electroporated retinal explants expressed EGFP above the threshold. RNA were extracted from these cells for Real Time RT-PCR analysis to determine the level of endogenous murine IMPDH1 mRNA in shRNA-transfected cells. All parameters required for size fractionation and selection of fluorescence threshold were set by Dr. Alfonso Blanco (Conway Institute, UCD), and the same parameters were used for all other studies involving FACS.

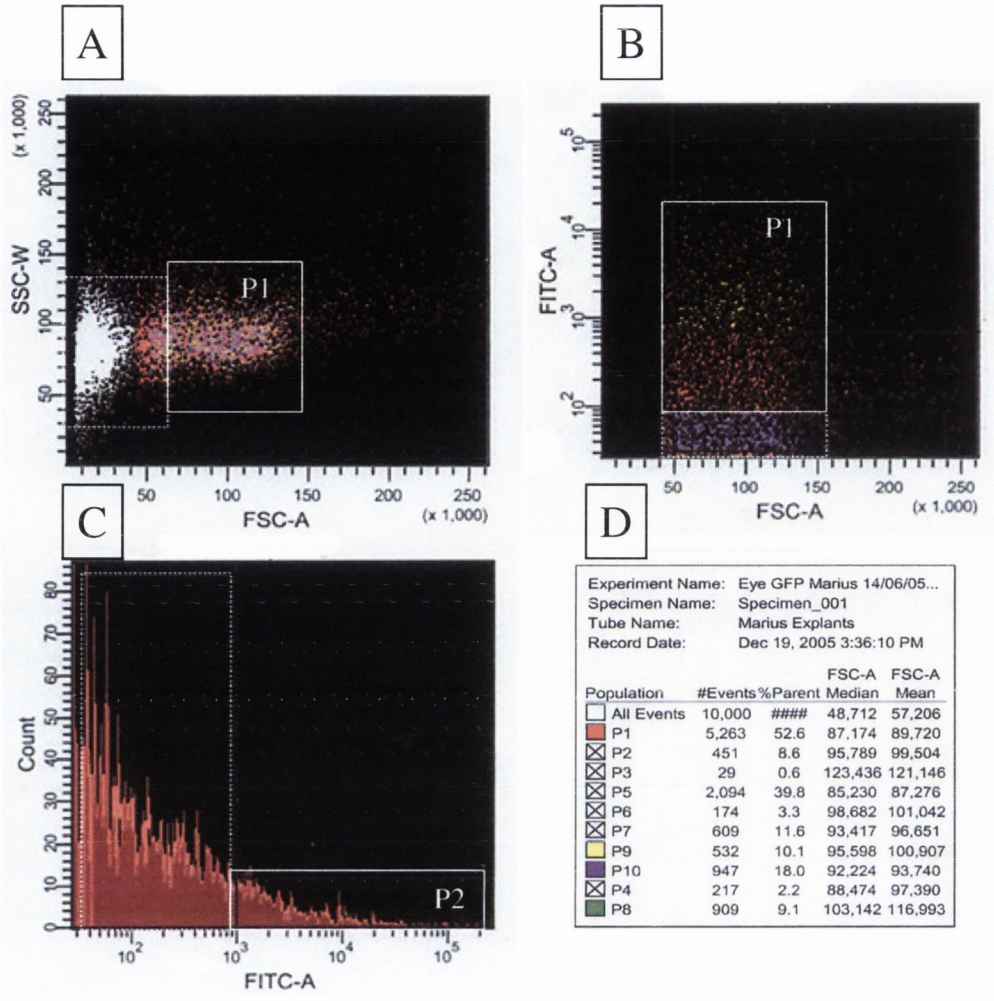

Figure 4.7; Experiment 1 (Targeting shRNA): Isolation of psh2048.EGFP transfected cells from retinal explants by FACS. **(A)** A scatterplot of forward scatter (FSC, X-axis) versus side scatter (SSC, Y-axis).psh2048.EGFP transfected cells from dissociated retinal explants were initially sorted by size, and the boxed area (P1) depicts the population of intact photoreceptor cells. Dotted area represent a population of cells containing mainly of cell debris. **(B)** A scatterplot of forward scatter (FSC, X-axis) versus green fluorescence intensity (FITC, Y-axis).Dotted area represents a population EGFP-negative cells. Boxed area (P1) represent the isolation of a population of retinal cells with fluorescence levels above an arbitrary threshold. **(C)** A histogram of green fluorescence intensity (FITC, x-axis) versus cell number. Dotted area represent a population of cells in P1 with fluorescence levels below an arbitrary threshold, whereas boxed area (P2) represent those above an arbitrary threshold. **(D)** Up to 8.6% (P2) of cells in electroporated retinal explants expressed EGFP above the threshold. RNA were extracted from these cells for Real Time RT-PCR analysis to determine the level of endogenous murine IMPDH1 mRNA in shRNA-transfected cells.

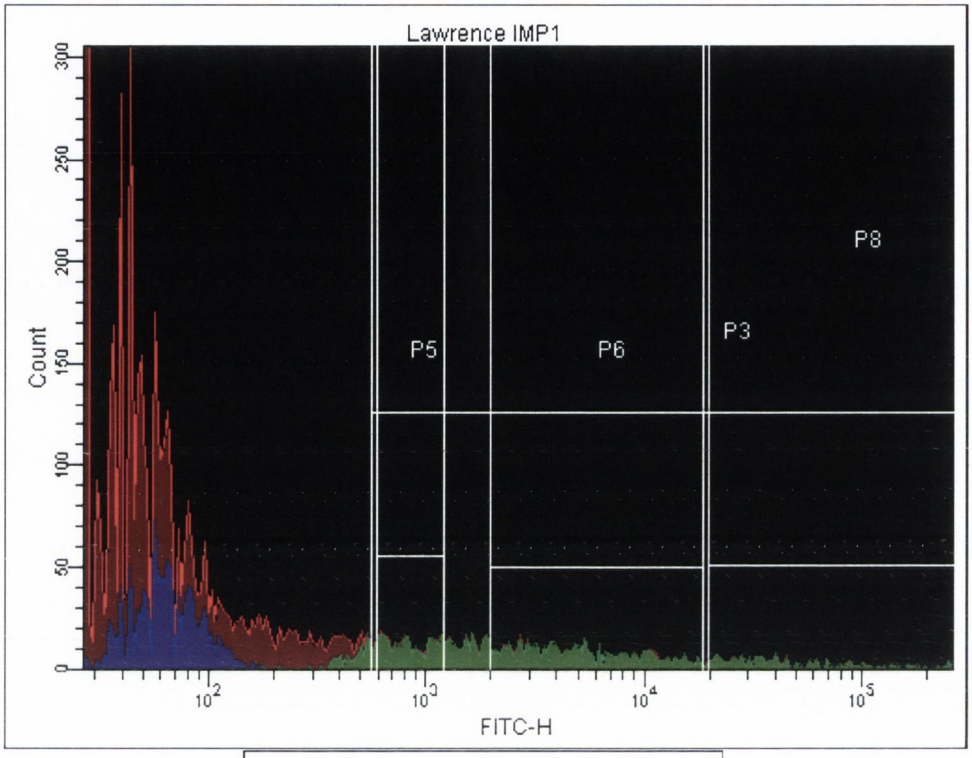

Tube: Lawrence IMP1

Population	#Events	%Parent	%Total
All Events	10,000		100.0
P1	5,706	57.1	57.1
P2	1,058	18.5	10.6
P3	172	3.0	1.7
P5	255	4.5	2.6
P6	501	8.8	5.0
P8	1,138	19.9	11.4
P4	738	7.4	7.4
P7	1,186	11.9	11.9
P9	1,007	10.1	10.1
P10	985	9.8	9.8

Figure 4.8; Experiment 2: FACS analysis of pshLuc.EGFP transfected cells from mouse retinal explants. A histogram of green fluorescence intensity (FITC, x-axis) versus cell number. Table below illustrates percentage of cells sorted based on fluorescence levels in different populations. Intact cells were initially selected by size fractionation using side scatter (SSC). Boxed area represent population of single retinal cells with fluorescence levels above an arbitrary threshold, and up to 20% (P8) of cells in electroporated retinal explants expressed EGFP. RNA were extracted from these cells for Real Time RT-PCR analysis to determine the level of endogenous murine IMPDH1 mRNA in shRNA-transfected cells.

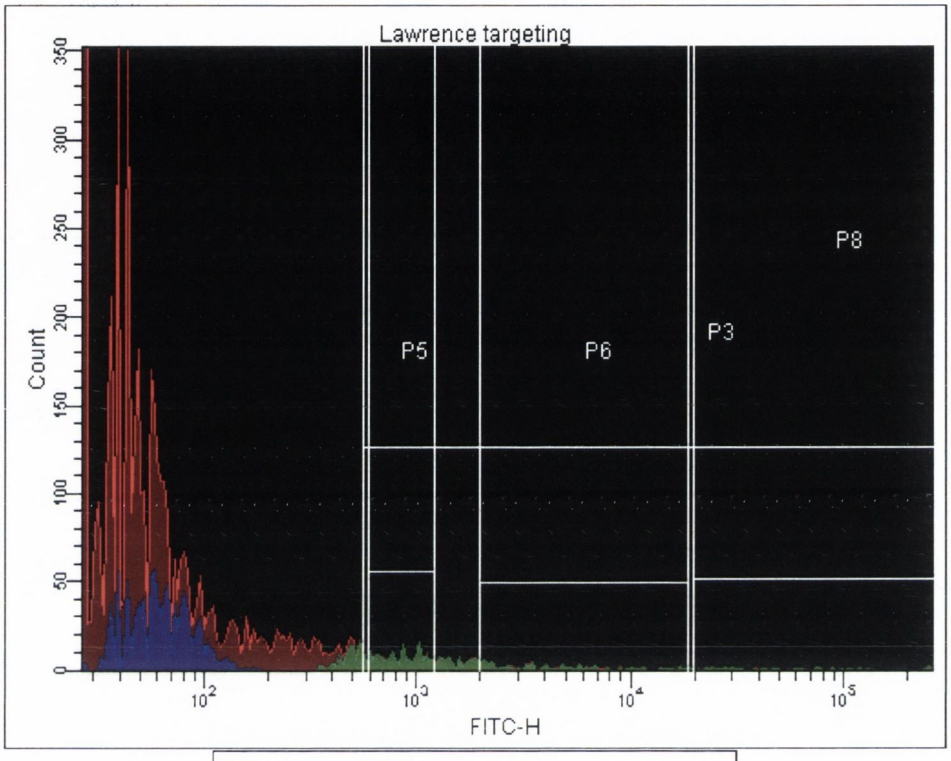

Tube: Lawrence targeting

Population	#Events	%Parent	%Total
All Events	10,000		100.0
P1	5,255	52.6	52.6
P2	372	7.1	3.7
P3	45	0.9	0.4
P5	153	2.9	1.5
P6	112	2.1	1.1
P8	412	7.8	4.1
P4	176	1.8	1.8
P7	486	4.9	4.9
P9	347	3.5	3.5
P10	976	9.8	9.8

Figure 4.9; Experiment 2: FACS analysis of psh2048.EGFP transfected cells from mouse retinal explants. A histogram of green fluorescence intensity (FITC, x-axis) versus cell number. Table below illustrates percentage of cells sorted based on fluorescence levels in different populations. Intact cells were initially selected by size fractionation using side scatter (SSC). Boxed area represent population of single retinal cells with fluorescence levels above an arbitrary threshold, and up to 7.8% (P8) of cells in electroporated retinal explants expressed EGFP. RNA were extracted from these cells for Real Time RT-PCR analysis to determine the level of endogenous murine IMPDH1 mRNA in shRNA-transfected cells.

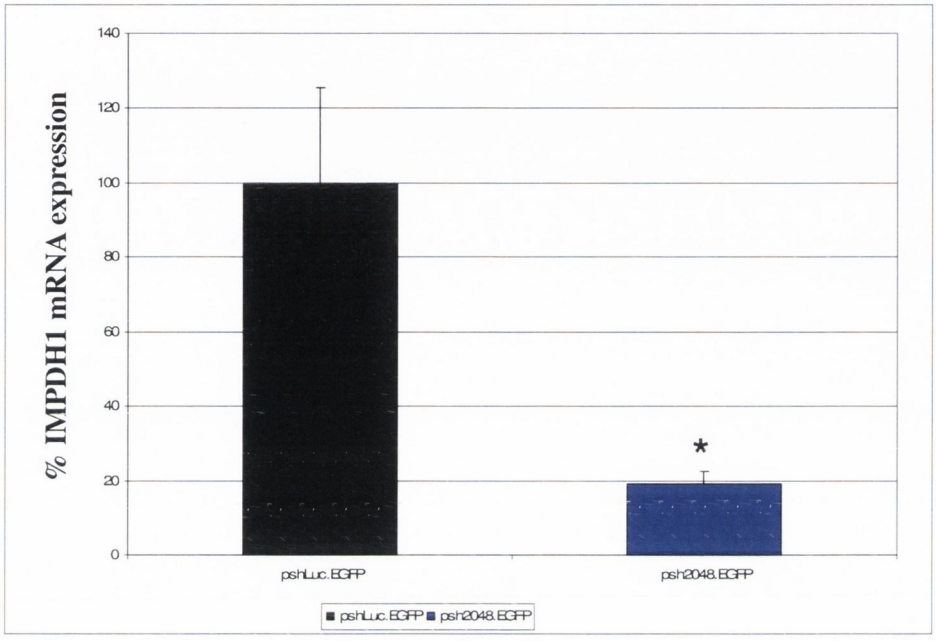

shRNA	psh2048.EGFP
% IMPDH1 expression ± SEM	19% ± 3.46%

Figure 4.10: Suppression of IMPDH1 transcripts in mouse retinal explants. For each experiment, 12 retinas from six newborn wild type C57B6/CBA pups were dissected and six retinas were electroporated with either pshLuc.EGFP (non-targeting control, black bar) or psh2048.EGFP (blue bar). Electroporated retinas were cultured for 14 days *in-vitro*, and pooled together before trypsin dissociation into single cell suspensions. Dissociated retinal cells were FACS sorted as described in *Figures 4.6 to 4.9*. RNA was extracted from EGFP-positive retinal cells and percentage IMPDH1 mRNA expression was quantified by Real Time RT-PCR analysis, and normalised to the house-keeping gene, β-actin. A control set transfected with luciferaseGL2 targeting shRNA (pshLuc.EGFP) was standardised to represent 100% IMPDH1 expression (Black bar). The average of 2 independent experiments is shown; Y-error bars indicate standard error of the mean (SEM). Percentage IMPDH1 expression ± SEM is denoted in the bottom panel. * $P<0.05$.

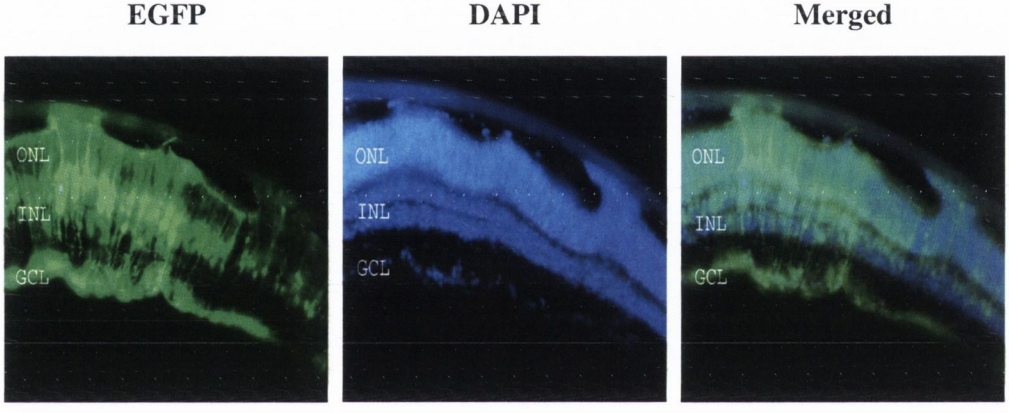

Figure 4.11: *In-vitro* electroporated mouse retinal explants. Wild-type C57B6/CBA mouse retinas at P0 were *in-vitro* electroporated with psh2048.EGFP from the scleral side and cultured for 14 days. *In-vitro* electroporated retinas were sectioned with a vibratome sectioner (Leica VT 1000s) at 50μm thickness and stained with DAPI (Sigma). Retinal sections were viewed under a fluorescence microscope (Zeiss, Axioplan 2) and all images were captured at 40X magnification.

Chapter 5
In-vivo Suppression of IMPDH1 in Mouse Retinas

5. *In-vivo* suppression of IMPDH1 in mouse retinas

5.1 Introduction

Since Elbashir *et al.,* (2001a), first discovered that transfection of short 21-nucleotide double-stranded RNA duplexes termed as small interfering RNAs (siRNAs) into mammalian cells effectively inhibited endogenous genes in a sequence-specific manner, post-transcriptional gene silencing by siRNAs has emerged as a powerful tool for genetic analysis in mammalian cells and possesses great potential to produce novel therapeutics. However, siRNA suppression suffers from several limitations such as high cost, nonspecific toxicity during transfection, and most notably, transient suppression of gene expression. To overcome these limitations, many groups have developed DNA vectors that utilize RNA polymerase III and U6 promoters to express short hairpin RNA in the form of an inverted repeat sequence containing a hairpin loop (Brummelkamp *et al.*, 2002; Miyagishi and Taira, 2002a and b; Paddison *et al.*, 2002b; Lee *et al.*, 2002b; Sui *et al.*, 2002). These small hairpin RNAs have been shown to be efficiently processed into siRNAs inside the cells and achieve sequence-specific gene silencing. However, RNAi-based vectors cannot be delivered to all tissues as plasmids and thus subsequently, several groups have developed retroviral-based vectors for the delivery of siRNA into mammalian cells (Brummelkamp *et al.*, 2002; Barton and Medzhitov, 2002; Devroe and Silver, 2002). Despite some success, these vectors suffer from limitations inherent to oncoretroviral vectors such as inability to infect non-dividing cells and low titres. Recently, adeno-associated virus (AAV) has been evaluated in several human gene therapy trials due to its unique features that distinguish it from other gene therapy vectors (Stilwell and Samulski, 2003). These include (i) the ability to infect both dividing and non-diving cells; (ii) a broad host range; (iii) wild-type AAV has never been associated with any disease and cannot replicate in infected cells; (iv) lack of cell-mediated immune response against the vector; (v) ability to integrate into a host chromosome or persist episomally, thereby creating potential for long-term expression; (vi) serotype and capsid combinations give tissue and cell specificity e.g. AAV-2/5 specifically transduces the retinal pigment epithelium and photoreceptor cells (Tomar *et al.*, 2003; Stilwell and

Samulski, 2003; Auricchio *et al.*, 2001b). Moreover, DNA microarray studies have shown that infection with AAV vectors has minimal influence on changing the pattern of cellular gene expression (Stilwell and Samulski, 2003).

5.1.1 Adeno-associated viruses (AAVs)

Adeno-associated virus (AAV) is a *Dependovirus* that belongs to the *Parvovirinae* subfamily of *Parvoviridae*, and was originally isolated as a contaminant of adenoviral cultures, thus given the name adeno-associated virus (Berns, 1996). AAV is non-enveloped with icosahedral symmetry and a diameter of 18–26 nm, and similar to other parvoviruses, AAV possesses a core with a beta barrel motif consisting of anti-parallel beta sheets (Rabinowitz and Samulski, 2002; Xie *et al.*, 2002). AAV is packaged as a 4.7 kb linear single-stranded DNA molecule and is relatively simple in its organisation, comprised of two genes that encode four replication (*rep*) proteins and three structural (*cap*) VP proteins (*Figure 5.1*). The *rep* and *cap* genes are situated between two sets of 145 nucleotide long open reading frames called inverted terminal repeats (ITRs), which typically assume a T-shaped hairpin secondary structure. ITRs play crucial roles in many steps of the virus life cycle; such as the expression and replication of the viral genome early in productive infection, and its packaging into the AAV capsid. Subsequently in infected cells, ITRs are also involved in the conversion of single-stranded viral DNA into the double-stranded form from which AAV gene expression occurs, and which becomes integrated into the host chromosome or persists episomally (Wang *et al.*, 1995; Weitzman *et al.*, 1994; Zhou and Muzyczka, 1998). Furthermore, another unique feature of AAV is that it requires a helper virus to complete its own life cycle (latent to lytic phase) in infected cells, and a detailed description of the life cycle of wild type AAV is described in *Figure 5.2i*. The helper virus, typically adenovirus or a member of the herpes virus family, provides products (RNAs and proteins) that stimulate gene expression from the AAV promoters, enhance transport and splicing of the AAV pre-mRNAs, and in case of herpes simplex virus 1 support replication of the AAV genome (Weindler and Heilbronn, 1991). However, in the absence of helper virus or helper functions, the AAV genome integrates into the host cell genome entering the

latent phase of its cycle. In human cells, integration occurs in a site-specific manner on human chromosome 19q13.3-qter (*AAVS1* locus) (Kotin *et al.*, 1992). In addition, AAV *rep* proteins are critical for controlling site-specific integration by mediating the interaction between the AAV ITRs and the *AAVS1* locus (Linden *et al.*, 1996).

5.1.2 Vectors based on adeno-associated viruses

The early discovery that AAV ITRs are the only sequences required *in-cis* to mediate packaging of DNA sequences embedded in between has paved the way for generating recombinant vectors derived from AAV. A direct method to produce recombinant AAV (rAAV) vector is to replace the entire *rep* and *cap* genes with any transgene and its associated regulatory sequences (*Figure 5.1*). However, the total size of the resulting recombinant AAV cassette, including both the transgene and the two ITRs, cannot greatly exceed the size of the wild type AAV genome (4.7 kb), to ensure efficient encapsidation. In order to package recombinant transgene into viral capsids, the AAV vector plasmid is typically transfected into cultured cells together with two other plasmids; (i) an AAV helper plasmid encoding the *rep* and *cap* genes *in trans* and, (ii) a helper adenoviral plasmid providing the respective helper virus gene products such as E1a, E1b, E2a, E4 & VA RNA from the adenovirus genome. Following the transfection of rAAV and helper plasmids into cells, the Rep and VP proteins expressed from the AAV helper plasmid replicate the recombinant genome to high copy numbers and form AAV capsids for its packaging, respectively. The products expressed from the helper adenoviral plasmid provide the same helper functions as do infectious adenovirus during growth of wild-type AAV, which is to enhance expression of the *rep* and *cap* genes as well as support AAV RNA transport and splicing. However, the adenoviral plasmid is not infectious, as it does not contain the adenovirus genome, thus ensuring that the final rAAV preparation is free from contaminating adenovirus. Likewise, the final rAAV stocks are also free from wild-type AAV virus, because the *rep* and *cap* expressing helper plasmid lacks the ITRs required for DNA encapsidation (*Figure 5.2ii*).

To date, eight different AAV serotypes (AAV 1-8) have been isolated and cloned (*Figure 5.3*) (Muramatsu *et al.*, 1996; Chiorini *et al.*, 1997; Rutledge *et al.*, 1998; Chiorini *et al.*, 1999; Xiao *et al.*, 1999; Gao *et al.*, 2002a), and possibly many more may be harboured in the genome of different mammalian tissues. The most divergent AAV sequence probably belongs to serotype 5 (Bantel-Schaal *et al.*, 1999; Chiorini *et al.*, 1999), which was isolated from a condylomatous lesion (i.e. genital warts caused by human papilloma viral infection) (Bantel-Schaal and zur Hausen, 1984). AAV7 and 8 sequences were isolated from rhesus monkeys tissues (Gao *et al.*, 2002b), and all other serotypes were isolated as contaminants of adenoviral cultures. Among all the AAV serotypes, adeno-associated virus type-2 (AAV-2) was the first recombinant form of AAV and has been used as a successful gene transfer vector in a variety of rodent and large animal models (Snyder, 1999; Monahan and Samulski, 2000) Recombinant AAV-2 vectors are capable of mediating efficient and prolonged transgene expression in a number of tissues and have been used to deliver therapeutic genes to correct gene defects in animal models of various human disorders (Elliger *et al.*, 1999; Xiao *et al.*, 2000; Bosch *et al.*, 2000; Jung *et al.*, 2001), and has been used in over twenty different clinical trials to date ranging from treatment for haemophilia B to retinoblastoma (Kay *et al.*, 2000; Hurwitz, 2001; Manno *et al.*, 2002), and including a recent trial currently underway by Ali and colleagues using rAAV-2/2 for the delivery of RPE65 gene for the treatment of Leber Congenital Amuarosis (LCA) in young adult patients (UCL Institute of Ophthalmology and Moorfields Eye Hospital).

Another major advantage of rAAV vectors is that the packaging plasmid can be interchanged between different AAV serotypes, resulting in the assembly of hybrid AAV vectors containing the genome of one serotype (i.e AAV-2), and different capsids (Duan *et al.*, 2001; Hildinger *et al.*, 2001). These hybrid or pseudotyped AAV vectors are designated AAV-2/1 to 8, where the first number indicates the ITRs of origin and the second represent the capsid (*Figure 5.3*). The capsid protein sequences exhibit significant variation among different AAV serotypes and are a key element in AAV-mediated transduction of different types of tissues. The benefit of

pseudotyping is that the resulting rAAV particles display the unique tropisms and serological properties of the capsid serotype which are different from those of AAV-2. In the case of AAV-2, the capsid interacts with a receptor complex on the surface of the target cells including heparan sulphate (Summerford and Samulski, 1998), fibroblast growth factor receptor 1 (Qing *et al.*, 1999) and integrin (Summerford *et al.*, 1999). However, these receptor complexes are absent from the luminal surface of airway epithelia, rendering in-efficient transduction of the lung using AAV-2. In contrast, the AAV-5 receptor complex including O-linked sialic acid is located on the surface airway epithelia (Walters *et al.*, 2001), thus AAV-2 virus pseudotyped with AAV-5 capsid has allowed efficient transduction of the lung *in-vivo* (Zabner *et al.*, 2000). In addition to cellular tropism, capsid proteins also influence the onset and intensity of gene expression. For example, studies have shown that AAV vectors harbouring the same genome but with different capsids showed different transduction efficiency and onset of transgene expression in the retina and muscles (Auricchio *et al.*, 2001b; Chao *et al.*, 2000). Furthermore, Wang *et al.*, (2005b) demonstrated differential global muscular transduction in rodent models by exploiting the natural diversity present in viral capsids. Therefore, exchanging capsids between various AAV serotypes impacts on vector's ability to enter and transduce different tissues efficiently. From an experimental point of view, the only modification required to produce an AAV vector based on an alternative serotype is the capsid gene (*cap*) within the AAV helper plasmid. In contrast, the *rep* gene in the helper and the ITRs in the AAV vector remains unchanged (Grimm, 2002). The benefit of pseudotyping has largely expanded the range of potential targets for AAV-mediated gene transfer and has circumvented many immunological issues, which should both be important with respect to the use of AAV vectors to deliver shRNAs.

Currently, the versatile functionality of recombinant AAV-mediated shRNA system has been demonstrated in a diverse range of gene function analyses and disease models. For example, Hommel *et al.*, (2003) demonstrated the use of AAV-mediated RNAi to generate specific knockdown of *Th*, the gene encoding the dopamine synthesis enzyme tyrosine hydroxylase within the midbrain neurons of adult mice.

This localised gene knockdown resulted in behavioural changes including a motor performance deficit and reduced response to a psychostimulant. Moore *et al.*, (2005) also showed that stable delivery of HBV-targeted RNAi AAV vectors successfully reduced the expression of the hepatitis surface antigen (HBsAg) in 293T cells and HepG2.2.15 cells containing full length clone of the HBV genome. By using a mouse model harbouring the human dominant neurodegenerative disease, spinocerebellar ataxia type 1 (SCA1), Xia *et al.*, (2004) showed that AAV-2/1 shRNA vectors efficiently reduced target protein ataxin-1 expression in the brain and documented improved cellular and behavioural characteristics.

5.1.3 Adeno-associated viral vectors for retinal gene transfer

The retina has many unique properties that make it particularly amenable for AAV-mediated gene transfer. It is a thin laminar structure that is accessible by multiple routes, consequently, different areas of the eye and various cell types may be exposed to a therapeutic intervention. The fact that the eye is small and enclosed limits the dose of vector necessary to achieve a therapeutic effect and prevents exposure of other tissues to the vector. In addition, the small size of the globe allows direct extrapolation of a treatment dosage from an animal experiment to a human study (Bennett, 2000). There are physical barriers in the retina, such as the blood retinal barrier (BRB), which further protect a widespread diffusion of the vector to the systemic circulation. In particular, the subretinal space is separated from the blood supply by the retinal pigment epithelium (RPE) and an intracellular junction in the inner retina. These barriers provide a beneficial effect in protecting the retina from the immune response by sequestering antigens from the systemic circulation (Surace and Auricchio, 2003). In addition there are a number of sophisticated means to evaluate the therapeutic efficacy of treatment over time. Retinal function can be monitored with non-invasive and quantitative tests such as ophthalmoscopy, electroretinography (ERG), optical coherence tomography (OCT) and the measurement of afferent pupillary responses and visual evoked potentials (VEPs).

AAV is a particularly promising vector for retinal gene therapy. Since the first demonstration of subretinal delivery of a recombinant AAV vector encoding a reporter gene (*lac Z*) to transduce retinal cells (Ali *et al.*, 1996), many aspects of AAV biology have been elucidated, including its retinal cell specificity, efficiency, immunogenicity and stability. In murine retinas, subretinal delivery of AAV-2 and AAV-5 vectors expressing reporter genes has been shown to transduce both retinal pigment epithelium (RPE) and photoreceptor cells (Ali *et al.*, 1996; Ali *et al.*, 1998; Yang *et al.*, 2002). In particular, the transduction efficiency of AAV-5 vectors appears to be greater than that of AAV-2, such that at five weeks post-injection, the ratio of transgene-expressing photoreceptor cells transduced with AAV-5 versus AAV-2 was 1000:1 (Yang *et al.*, 2002). Moreover, the onset of gene expression and the number of viral genome copies per eye was both faster and higher for AAV-5 vectors. Furthermore, both AAV-1 and AAV-6 vectors transduce predominantly the retinal pigment epithelium (RPE), being approximately 15 times more efficient than AAV-2 vectors (Xiao *et al.*, 1999; Auricchio *et al.*, 2001b; Yang *et al.*, 2002). Similarly, AAV-4 exhibits exclusive transduction of the RPE after subretinal delivery, whereas AAV-3 vectors transduce retinal cells with low efficiency (Weber *et al.*, 2003; Yang *et al.*, 2002). Subretinal delivery of AAV has also been carried out in larger animal models (dogs and non-human primates), which better mimic the cone and rod photoreceptor populations and retinal topography of the human eye. In non-human primates, subretinal administration of AAV-2 and AAV-5 vectors has resulted in specific transduction of rod photoreceptor cells and RPE cells, and AAV-5 vector appeared to be more efficient for the transduction of rod photoreceptors (Bennett *et al.*, 1999; Lotery *et al.*, 2003). In contrast, intravitreal injection of rAAV-2 leads to efficient transduction of ganglion cells, the trabecular meshwork and various cells of the inner nuclear layer (Ali *et al.*, 1996; Ali *et al.*, 1998; Auricchio *et al.*, 2001b; Liang *et al.*, 2001; Martin *et al.*, 2002). Interestingly, AAV delivery via intravitreal injection has also shown to transduce the optic nerve (Guy *et al.*, 1999; Dudus *et al.*, 1999), and subsequently this strategy was exploited to treat a form of optic neuritis in rodents as well as a model of glaucoma in rats (Guy *et al.*, 1998; McKinnon *et al.*, 2002).

Reports involving administration of the retina with AAV chimeric serotypes in which the vector is flanked by AAV-2 ITRs, but encapsidated in an AAV-1, -2, -3, -4 or -5 capsid generating rAAV-2/1-5 have also been extensively described. Subretinal injection of rAAV-2/1 expressing EGFP shows early onset of EGFP expression (3-4 days) and with transgene expression restricted to the RPE. Weber *et al.*, (2003) demonstrated that rAAV-2/4 allows exclusive and stable transduction of RPE cells, and that this feature is conserved among rodent, canine and non-human primate models. Moreover, AAV-2/2 and -2/5 vectors transduce both RPE and photoreceptor cells efficiently (Auricchio *et al.*, 2001b), and onset of transgene expression occurs at two to four weeks for both of these AAV vectors. Interestingly, an absence of transduced cells was noted following intravitreal injection of AAV-2/1 and AAV-2/5 vectors. This result highlights the effects of the mode of injection along with serotype on specific cell type transduction. Subretinal injection of AAV-2/1, -2/2, -2/3, -2/4 and –2/5 in rats results in a hierarchy in the levels of transgene expression with rAAV-2/4 and –2/5 capsids being the most efficient (Rabinowitz *et al.*, 2002). In particular, Yang *et al.*, (2002) reported that 30 times more viral genomic copies were detected in mouse eyes injected with AAV-2/5 than in those injected with AAV2. Additional studies have confirmed that AAV-2/5 transduces both RPE and photoreceptor cells in rat and dog, with photoreceptor cells being more efficiently transduced that with AAV-2/2 (Weber *et al.*, 2003). Similar to the chimeric rAAV-2/5 vector, subretinal injection of rAAV-5/5 vector in mouse retina shows faster expression kinetics as well as higher transduction efficiency rAAV-2/2 (Yang *et al.*, 2002), with RPE cells and photoreceptors being transduced in both case.

The selection of promoter in AAV is also a key determinant of specific retinal cell type transduction. A proximal mouse rhodopsin promoter was the first to be evaluated in the context of an AAV vector in murine and rodent retinas (Flannery *et al.*, 1997). The proximal sequence (-386/+85) of the murine rhodopsin gene was used to drive the expression of enhanced green fluorescent protein in AAV2, and reporter gene expression was found exclusively in rat photoreceptors. In addition, the use of the ubiquitously expressed immediate-early cytomegalovirus (CMV) enhancer-

promoter has also shown efficient and stable reporter gene expression in both murine RPE and photoreceptor cells following subretinal injections (Grant *et al.*, 1997). Recently, O'Reilly *et al* (2007) demonstrated the use of a mouse rhodopsin promoter in AAV-2/5 for the delivery of replacement rhodopsin gene in mouse retinas. Expression of the replacement gene was limited exclusively to the photoreceptor cells and conferred significant resistance to shRNA suppression. Furthermore, Allocca *et al.*, (2007) evaluated the ability of different serotypes in combination with constitutive or photoreceptor-specific promoters such as the human rhodopsin, CMV and the chicken β-actin promoters to transduce photoreceptor cells. The authors showed that the use of the rhodopsin promoter in combination with AAV-2/7 or 8 yielded the highest transduction efficiency of photoreceptor cells, compared to the use of AAV-2/5, which had previously been cited as the most efficient vehicle for photoreceptor targeting as described previously. These studies have demonstrated that the use of specific promoters in combination with the appropriate AAV serotype allows for efficient and exclusive cell-type transduction. The use of human RPE65 promoter has also shown high-level of RPE-specific expression in RPE65-deficient Briad dogs (Le Meur *et al.*, 2007), and is currently employed in a human clinical trial for the expression of the RPE65 gene by specific transduction of the RPE using rAAV-2/2 vectors in young adults (Ali and colleagues; UCL Institute of Ophthalmology and Moorfields Eye Hospital)

5.1.4 Important aspects in the use of AAV-mediated gene transfer for retinal gene therapy

5.1.4.1 Expression level of transgene is critical for gene therapy

The level of gene expression is particularly important for the development and treatment of retinal diseases. For example, rhodopsin is highly expressed in rod outer-segments suggesting that high levels must be achieved in order to correct a recessive mutation in this gene. However, transgenic mice overexpressing wild-type rhodopsin exhibit retinal degeneration (Olsson *et al.*, 1992). Similarly, over-expression of *rds*/peripherin in normal mice following somatic gene delivery also leads to cell death

(Sarra *et al.*, 2001). These findings suggest that there is a fine line between the therapeutic and toxic dose of specific transgenes, and that tight regulation of the level of gene expression is needed for successful retinal gene therapy. In order to circumvent such a drawback, many studies have attempted to develop pharmacologically regulatable viral systems that can tightly control the level and time of gene expression to obtain maximum safety and efficacy of viral delivery (Auricchio *et al.*, 2002a; Dejneka *et al.*, 2001; McGee *et al.*, 2001a). Several inducible viral expression systems, including rapamycin (Rivera *et al.*, 1996; Ye *et al.*, 1999), mifepristone (Serguera *et al.*, 1999), ecdysone (No *et al.*, 1996), and tetracycline (*tet*) (Gossen *et al.*, 1995; McGee *et al.*, 2001a) have been developed to control transgene expression *in-vivo*. In particular, rapamycin-mediated regulation of erythropoietin (Epo) expression has been demonstrated in rats and in one non-human primate following subretinal injection of two rAAV vectors, one encoding the transactivator, and the other Epo (Auricchio *et al.*, 2002a).

5.1.4.2 Time of delivery

An additional factor that needs to be considered is the time to deliver treatment. Retinal degeneration varies from early and severe to late and progressive. Slowly progressive diseases have a much wider therapeutic window than those with an earlier onset such as Leber Congenital Amaurosis (LCA) (Cremers *et al.*, 2002). For retinal disease with a severe early onset characteristic, it is critical to apply AAV-mediated gene transfer that allows for sustained expression over time and eventual re-administration (Anand *et al.*, 2000; Bennett *et al.*, 1999), and therapeutic intervention should be undertaken during early foetal development or in early childhood. Timely gene delivery in early onset and congenital retinal dystrophies would prevent the pathological consequences of the mutation to retinal function, and allow for the proper development of the local retinal network and visual cerebral circuitry that depend at least in part on visually evoked stimuli (Banin *et al.*, 1999; Huang *et al.*, 1999; Zack, 1999).

5.1.4.3 Safety and Biodistribution

AAV has been regarded to be one of the safest of all known viral-based vector systems, as it has never been associated with any human malignancy when compared to other viruses such as lentivirus and adenovirus. Furthermore, the high safety profile of AAV has recently been highlighted by a study carried out by Stilwell and Samulski, (2004) who used DNA microarray analysis to identify and directly compare genes modulated during AAV or adenovirus infection of cultured cells. Interestingly, AAV infection did not elicit pathogenic response whereas adenovirus infection resulted in induction of immune and stress-response genes associated with pathogenesis. Moreover, since AAV vectors derived from wild-type AAV retain only the ITRs and do not express any viral genes, they are gutless by design, and so evade cytotoxic cellular immune response in the transduced cells.

An accurate evaluation of vector biodistribution after subretinal or intravitreal administration is of primary importance for safe and successful ocular gene therapy using rAAV. A number of studies have evaluated the biodistribution of rAAV following various routes of administration. Most of these have shown that multiple cell types in a target organ are exposed to the viral vector, though others demonstrated scattering of virus to the systemic circulation. For example in non-human primate studies, delivery of rAAV-2/2 to the muscle (Favre *et al.*, 2001) or lung (Conrad *et al.*, 1996) resulted in detectable vector in the serum at 6 days (muscle) to 14 days (lung). Examination of tissue 18-months after rAAV intramuscular administration indicated the presence of rAAV genome in the liver, peripheral blood mononuclear cells (PBMC) and scattered lymph node sites. To date, biodistribution of viral vectors in distant organs following intraocular administration has not yet been reported. Weber *et al.*, (2003) reported that following subretinal delivery of rAAV in the dog and non-human primates, viral vector DNA could be detected in the serum as early as 15 minutes after rAAV administration and for up to 25 days in some instances. In lacrymal and nasal fluids, viral genome was also detected as early as 15 minutes after injection and up to 4 days postinjection. Furthermore, Dudus *et al.*, (1999) demonstrated that following intravitreal injection

of rAAV-2/2*gfp*, high levels of GFP protein persisted for six months in the optic nerves and brains of mice and dogs. In addition, injection of rAAV-2/2*lacZ* in the vitreous cavity of guinea pigs leads to β-galactosidase expression in fibers, glial cells and blood vessels of the optic nerve (Guy *et al.*, 1999). Recently, Rolling, (2004) reported the biodistribution of rAAV vectors in distant organs following subretinal or intravitreal injection in the rat, dog and non-human primate. Following subretinal and intravitreal injections, rAAV sequences were not detected in the liver or in the gonads of these animals, but were found in PBMC at early time points after vector delivery. The most striking result was the detection of rAAV sequences in different regions of the brain after intravitreal injection in dog. Although additional biodistribution studies in large animal are required, these preliminary results suggest the ability of rAAV-2/2 to be transported trans-neuronally.

5.1.5 AAV-based therapy for diseases due to loss-of-function mutations

Recessively inherited retinal degenerations represent a group of retinal abnormalities whose phenotype is due to the loss of function of a gene. AAV-mediated gene replacement therapy constitutes the most promising and direct strategy for the treatment of autosomal recessive retinal disease as pseudotyped rAAV vectors can provide selective transduction and prolonged expression of therapeutic gene in the retina. Ali *et al.*, (2000) reported the first successful rescue of retinal degeneration in *rds* null mice. These animals are characterised by an inability to form outer segments, and develop an early loss of retinal function with progressive photoreceptor cell death. Following AAV vector delivery of *rds*/peripherin gene, functional and morphological studies revealed outer segment restoration and proper disc formation. Unfortunately, the treatment was unable to halt the degenerative process and earlier improvements were lost over time (Sarra *et al.*, 2001). The authors concluded that this outcome might have been caused by a lack of homogeneous transduction, delayed onset of transgene expression or by toxic effects resulting from the over-expression of *rds*/peripherin. Recent developments in AAV vector delivery technologies have specifically addressed these issues and resulted in an improvement of treatment. In another study, AAV-mediated gene transfer

strategy been reported in the retina for the treatment of two forms of mucopolysaccharidosis (MPS). These lysosomal storage disorders result from deficiency of enzymes involved in the degradation of sulfated glycosaminoglycans (GAGs), leading to a progressive abnormal accumulation of GAGs in these organelles and eventual multi-organ failure. Accumulation of GAGs is evident in the retina by the presence of dilated lysosomes and inclusions in the RPE. Intraocular or intravenous administration of an AAV encoding the human β-glucuronidase gene lead to persistent activity of the enzyme in a murine model of MPSVII (Daly *et al.*, 1999). The treatment reverted the lysosomal phenotype in many tissues including the RPE. A similar result was also obtained following subretinal injection of AAV-4-sulphatase into a cat model of MPS VI (Ho *et al.*, 2002).

The Royal College of Surgeons (RCS) rat is a widely studied animal model of retinal degeneration in which the inability of the RPE to phagocytose shed photoreceptor outer segments leads to a progressive loss of rod and cone photoreceptors. This defect is caused by a mutation in the mertk gene that is normally expressed in the RPE (Gal *et al.*, 2000), and has also been described in patients with retinitis pigmentosa. The first demonstration of successful rescue of both functional cellular defect (phagocytosis) and photoreceptor degeneration was achieved by recombinant adenovirus-mediated gene transfer to the RPE (Vollrath *et al.*, 2001). More recently, it was demonstrated that rAAV-mediated gene transfer slows photoreceptor loss in this model, and subretinal injection of rAAV-2/2*mertk* prolonged photoreceptor cell survival in the RCS rat as shown by histological analysis. Moreover, electroretinographic analysis of treated eyes showed that functional photoreceptors were still present at 9 weeks, as opposed to the untreated control eye showing virtually no activity (Smith *et al.*, 2003). Similarly, gene replacement study using rAAV vectors was achieved in $Prph2^{Rd2/Rd2}$ mice. The $Prph2^{Rd2/Rd2}$ mouse is homozygous for a null mutation in peripherin-2 gene, and completely fails to develop photoreceptor discs and outer segments. Consequently, the photoreceptor cell layer undergoes progressive apoptotic cell loss, and ERG analyses showing the functionality of the photoreceptor cells decline to undetectable levels by 2 months.

Subretinal injection of rAAV-2 encoding peripherin-2 transgene resulted in the re-establishment of the structural integrity of the photoreceptor layer as well as in electrophysiological correction (Schlichtenbrede *et al.*, 2003; Schlichtenbrede *et al.*, 2004). Extended analysis of this treatment in the same model demonstrated that the potential for ultrastructural improvement was dependent upon the age at which animals were treated and that over-expression of peripherin-2 might be harmful to photoreceptor cells (Sarra *et al.*, 2001).

The first report of long-term success for the treatment of a retinal disease was described in the Swedish Briard dog model of Leber Congenital Amaurosis (LCA) possessing a null mutation in RPE65, which is the most common form of retinal degeneration in children and comprises of ~2% of autosomal recessive retinal dystrophy cases (Lorenz *et al.*, 2000; Acland *et al.*, 2001; Thompson *et al.*, 2003; Thompson *et al.*, 2000). The RPE65 gene encodes a highly conserved protein that is primarily expressed in the RPE and cone photoreceptors, and is essential for the synthesis of rhodopsin ligand 11-*cis*-retinal in the visual cycle. $RPE^{-/-}$ affected Briard dogs do not generate adequate levels of visual pigment, and suffer from poor vision and severely depressed light- and dark-adapted ERG responses. The fact that there are close similarities between the clinical characteristics of the disease resulting from RPE65 mutations in humans and the dogs have made the $RPE65^{-/-}$ Briard dog a valuable model for the evaluation of gene therapy. Currently, two studies have demonstrated delivery of AAV-2/2 delivery of canine RPE65 to the Swedish Briard dog resulted in stable restoration of visual function, as assessed by psychophysical and behavioral testing (Acland *et al.*, 2001; Narfstrom *et al.*, 2003a). However, Narfstrom *et al.*, (2003b) have observed the development of uveitis in 75% of the rAAV-2/2*rpe65*-treated eyes, which could be attributed either to the presence of a contaminant in the vector preparation or may result from an immune response to the RPE65 protein. In addition, the rAAV-2/2 vectors used in these two reports used a CMV-promoter for the high levels of RPE65 expression in both the RPE and photoreceptors cells. Since the long-term effects of this are not known, it might be safer to use a RPE-specific promoter or rAAV vector that target transgene expression

specifically to the RPE, such as serotype 4 or 1. In addition, it has recently been reported that restoration of visual function to the RPE65$^{-/-}$ mouse was achieved following *in-utero* administration of a rAAV-2/1*rpe65* vector (Dejneka *et al.*, 2004). However, many more steps, ranging from safety studies to discussion of ethical implications, must be taken before *in-utero* gene therapy for human retinal diseases can be envisaged. Recently, Le Meur *et al.*, (2007) reported successful restoration of rod and cone photoreceptor function in RPE65-deficient Briard dogs using rAAV-2/4 mediated delivery of RPE65 into the retinal pigment epithelium. In particular, treated animals remained stable after 8-11 months of age and showed improved physiological response to obstacle courses under dim and normal light. These promising data have culminated in the use of AAV in a recent clinical trial for LCA, where Ali and colleagues subretinally injected rAAV-2/2 carrying a human RPE65 promoter driving the expression of RPE65 cDNA into young adult patients (UCL Institute of Ophthalmology and Moorfields Eye Hospital). The awaiting results from this clinical trial will contribute immensely to the use of AAV vectors for treating retinal disease.

5.1.6 AAV-based therapy for diseases due to gain-of-function mutations

Several transgenic animal models of autosomal dominant RP (adRP) have been generated and these animals carry one copy of a mutated gene that encodes a misfolded or mislocalised protein. The expression of misfolded proteins in photoreceptors often leads to cell death through apoptosis. For example, transgenic rodents and pigs overexpressing the dominant rhodopsin P23H mutations (substitution of histidine for proline at rhodopsin codon 23) that recapitulate the human disease have been generated (Naash *et al.*, 1993; Steinberg *et al.*, 1996; Petters *et al.*, 1997; Machida *et al.*, 2000). The direct approach for therapy of adRP would be to eliminate or modulate the relative amounts of mutant protein using molecular suppressors such as ribozymes or siRNAs to restore normal function. The former has been successfully achieved with allele-specific inhibition of the P23H rhodopsin in transgenic rats using rhodopsin promoter-driven ribozymes delivered to photoreceptor cells via adeno-associated viral (AAV) vectors (Lewin *et al.*, 1998).

The treatment resulted in long-term morphological and functional rescue, and treatment was even effective in later stages of the degenerative process (LaVail *et al.*, 2000). However, this approach has the disadvantage of requiring the design of allele specific suppressors -a feat now known to be more difficult than initially proposed. In addition, in theory each particular mutation within a disease-associated gene would require a separate suppressor. In order to circumvent these problems, mutation independent suppression and replacement strategy has been developed whereby wild type allele as well as mutant transcripts are suppressed followed by or concomitant with the addition of a replacement gene which supplies wild type product, but is resistant to suppression (Millington-Ward *et al.*, 1997; Farrar *et al.*, 2002). While suppression of mouse P23H mutant transcript in a rat model of RP following introduction of AAV-delivered shRNA preferentially targeting murine rhodopsin has been achieved, retinal histology was not rescued by this suppression-only therapy (Tessitore *et al.*, 2006). The authors concluded that more robust shRNA expression in the retina may be required to achieve therapeutic efficacy *in vivo*. Gorbatyuk *et al.*, (2007) similarly demonstrated *in-vivo* suppression of rhodopsin following subretinal delivery of AAV-2/5 vectors containing H1-driven shRNA targeting murine rhodopsin transcripts into heterozygous $RHO^{+/-}$ mice. Moreover, in our laboratory, O'Reilly *et al.*, (2007) successfully demonstrated greater than 90% suppression of rhodopsin in photoreceptors of $NHR^{+/-}$ $RHO^{-/-}$ mice (human rhodopsin transgene on a null mouse rhodopsin background) following subretinal delivery of AAV-2/5 expressing shRNAs. In addition, subretinal delivery of AAV-2/5 vectors expressing codon-modified rhodopsin replacement genes into new born $P23H^{+/-}$ $RHO^{+/-}$ mice in the presence of rhodopsin-targeting shRNAs significantly protected the outer nuclear layer thickness from deterioration. This result represents the first successful *in-vivo* suppression and replacement strategy for dominantly inherited disorders.

5.1.7 AAV-based therapy for ocular neovascular diseases

In diabetic proliferative retinopathy (DPR), retinal vein occlusion, retinopathy of prematurity (ROP) and age-related macular degeneration (AMD), destabilisation of the retinal or choroidal microenvironment leads to the formation of new blood

vessels, which ultimately results in blindness. In diseases such as DPR and ROP, neovascularisation is mainly triggered by hypoxic conditions due to retinal microcapillary non-perfusion (Campochiaro, 2000), whereas the cause of aberrant vessel growth in choroidal neovascularisation (CNV) has not been fully deciphered.

Endostatin, angiostatin, and pigment epithelium-derived growth factor (PEDF) are negative regulators of angiogenesis and may prove beneficial in the treatment of neovascular diseases. AAV2 and AAV-2/1 mediated-delivery of PEDF, endostatin, angiostatin and TIMP3 has been successful in reducing angiogenesis in a mouse model of retinopathy of prematurity (ROP) (Auricchio *et al.*, 2002b; Raisler *et al.*, 2002). Intraocular injection of AAV-PEDF also significantly reduced angiogenesis in an experimental model of CNV where the lesions caused by laser photocoagulation-mediated rupture of Bruch's membrane were attenuated (Mori *et al.*, 2002). More recently, recombinant AAV-2/2 encoding fibroblast growth factor family members FGF-2, FGF-5 and FGF-18 have been evaluated using a transgenic rat model of retinitis pigmentosa (S334-ter-4, Ser to Ter substitution at 334 that results in a mutated rhodopsin gene). Despite the lack of significantly increased retinal function as shown by electroretinograms (ERGs), treated rats displayed a greater number of surviving photoreceptors following subretinal injection of AAV-vectors, suggesting the ability of these factors to protect photoreceptors from apoptosis in this rat model of RP (Lau *et al.*, 2000; Green *et al.*, 2001). The same RP rat model was used to evaluate the therapeutic potential of glial cell line-derived neurotrophic factor (GDNF). In rAAV-2/2*gdnf*-treated rats, photoreceptor cell death was attenuated for 45 days and animals exhibited greater ERG a-wave mean amplitudes (McGee *et al.*, 2001b). Alternatively, inhibition of the effects elicited by pro-angiogenic factors may also eliminate aberrant neovascularisation. VEGF is a potent mitogen for vascular endothelial cells, and stimulates vascular permeability. Lai and Bainbridge both introduced an AAV vector expressing the soluble truncated form of the VEGF receptor, sFlt-1, to inhibit angiogenesis in experimental models of both CNV and ROP (Lai *et al.*, 2002; Bainbridge *et al.*, 2002). Cashman *et al.*, (2006), also demonstrated attenuation of CNV by subretinal injection of AAV-2/5

expressing shRNAs targeting VEGF in a CNV mouse model caused by AAV-mediated over-expression of VEGF in the RPE (Spilsbury *et al.*, 2000).

5.1.8 Electroretinography (ERG)

The electroretinogram (ERG) is of immense clinical value in objectively assessing the status of the retina in eye diseases in human patients and in laboratory animal models of retinal disease. It is a mass electrical response of the retina to photic stimulation which is recorded from the corneal surface of the eye. The waveform generated by a brief flash reflects a complex combination of waveforms generated by various portions of the retina, and two distinctive components of the waveform that are most often measured in a normal ERG recording are the a- and b- waves (*Figure 5.4A*). Following flash stimulation, the a-wave represents the first large negative component, followed by the b-wave which is corneal positive and usually larger in amplitude. Extracellular ionic currents created by rod and cone photoreceptor cells generate the a-wave during phototransduction activity, and is a general reflection of the physiological health of photoreceptor cells in the outer retina. In contrast, the b-wave reflects the activity in cells post-synaptic to the photoreceptors and often represents the health of the inner layers of the retina, including the bipolar and Muller cells (Miller and Dowling, 1970). Another waveform that is sometimes recorded is the c-wave, which reflects the interaction between the responses of Muller cells and the hyperpolarisation of the apical membrane of the retinal pigment epithelium that occurs in response to a decrease in potassium concentration in the subretinal space (Marmor and Hock, 1982). ERG can be recorded using a number of different types of corneal electrodes such as carbon, wire of gold foil for detecting electrical activity. Most electrodes are monopolar, i.e., are referred to another electrode site most commonly on the forehead, whereas some are bipolar with the reference electrodes built into a metal surface on a speculum (http://webvision.med.utah.edu/ClinicalERG.html).

5.1.9 Objectives of this study

Following the observation that the IMPDH1-specific shRNA, sh2048, elicited strong silencing effects on IMPDH1 expression at the mRNA and protein level in mammalian cell cultures and in retinal explants, the aim of this study was to subclone sh2048 into templates of adeno-associated viral DNA backbones to achieve long-term suppression of IMPDH1 *in-vivo*. AAV-2 pseudotyped with AAV-5 capsids is used to generate the recombinant AAV-shRNA vector because previous studies carried out in our laboratory and those of others have shown efficient transduction of retinal pigment epithelium and photoreceptor cells with AAV-2/5 viral vectors (Ali *et al.*, 1996; Auricchio *et al.*, 2001b; O'Reilly *et al.*, 2007). Infectious viral particles expressing sh2048 were subretinally delivered into wild type mouse retinas to assess the level of suppression both at the mRNA and protein level *in-vivo*. Furthermore, studies undertaken in which an AAV vector over-expressing mutant IMPDH1 harbouring the Arg224Pro mutation which generates a disease model for RP10 was co-injected with AAV-vector expressing sh2048, protected retinal histology from the detrimental effect elicited by the mutant IMPDH1 protein *in-vivo*.

5.2 Methods

5.2.1 AAV vector production and purification

Restriction fragments containing H1-driven shLuc or sh2048 and CMV-driven EGFP cDNA were excised from pshLuc.EGFP and psh2048.EGFP, respectively, by restriction enzyme digestion using Afl II and BglII, and blunt cloned into pAAV-MCS (previously linearised and blunted with NotI) between the two AAV-2 internal terminal repeats (ITRs) (*Figure 5.5*). Expression cassettes were packaged into AAV-5 capsids and generated into recombinant AAV-2/5 viruses using a helper virus-free system as described in section 2.7.1 to 2.7.3. The generated recombinant AAVs included pAAVshLuc.EGFP (non-targeting shRNA) and pAAVsh2048.EGFP (IMPDH1-specific shRNA). A second AAV vector expressing a non-targeting shRNA, pAAVshNT.EGFP, was provided by Dr Naomi Chadderton. shNT is scrambled in sequence and has been shown by Qiagen not to interact with any known gene sequence, and has previously been used in an *in-vivo* study carried out in our laboratory (O'Reilly *et al.*, 2007). A restriction fragment containing the EGFP cDNA (p-EGFP, Clontech) was sucloned into the multiple cloning site (MCS) of pAAV-MCS (Stratagene) and generated as recombinant AAV-2/5 viruses to create pAAVEGFP (kindly provided by Dr. Naomi Chadderton). AAV-2/5 IRES hr-EGFP vectors containing rhodopsin promoter driven wild type IMPDH1 (NM_000883) and mutant IMPDH1 (Arg224Pro) cDNAs, designated as pAAVWtIMPDH1 and pAAVMutIMPDH1(224), respectively, were kindly provided by Dr. Avril Kennan. Viral titres (vp/ml) of all recombinant AAV-2/5 vectors used in this study are listed in the table below:

	Viral titres (viral particles/ml)	
Recombinant AAV-2/5 vectors	**1st Batch**	**2nd Batch**
pAAVshLuc.EGFP	$1x10^{13}$ vp/ml	$6.85x10^{12}$ vp/ml
pAAVsh2048.EGFP	$2.19x10^{13}$ vp/ml	$3.3x10^{12}$ vp/ml
pAAVshNT.EGFP	$5.7x10^{12}$ vp/ml	-
pAAVEGFP	$5.7x10^{12}$ vp/ml	-
pAAVWtIMPDH1.EGFP	$1.77x10^{12}$ vp/ml	-
pAAVMutIMPDH1(224).EGFP	$1.4x10^{12}$ vp/ml	-

5.2.2 Animals and subretinal AAV injections

The use of animals and subretinal injections carried out in this work were in accordance with the European Communities Regulations 2002 and 2005 (Cruelty of Animals Act) and the Association for Research in Vision and Ophthalmology statement for the use of Animals in Ophthalmic and Vision Research. C57B6/CBA and 129S2/SvHsd (Harlan, UK) mice were bred, and maintained in a 12-hour light-dark cycle. Both sexes of mice were used in *in vivo* studies. A registered ophthalmologist (Dr. Paul F. Kenna) performed all procedures in a barrier facility with sterile instruments and solutions. In brief, 2 weeks to 4 months old mice were anesthetized by intraperitoneal injection of Medetomidine and Ketamine (10 and 750 µg/10 g body weight, respectively). Pupils were dilated with 1% cyclopentolate and 2.5% phenylephrine, and, under local analgesia (Amethocaine), a small puncture was administered in the sclera. Under microscopic control, a 34-gauge blunt-ended microneedle attached to a 10 µl syringe (Hamilton, Bonaduz, Switzerland) was inserted through the puncture, and 1 to 3 µl of $10^{12\text{-}13}$ vp/ml recombinant AAV vectors in PBS was administered to the subretinal space, and a retinal detachment was induced (*Figure 5.4B*). In particular, all co-injections were carried out at a plasmid molar ratio of 1:5 (AAV-IMPDH1 expressing plasmid: AAV-shRNA). Following subretinal injection, a reversing agent (100 µg/10 g body weight, Atipamezole Hydrochloride) was delivered by intraperitoneal injection. Body temperature was maintained using a homeothermic heating device (O'Reilly *et al.*, 2007).

5.2.3 Electroretinographic analysis (ERG)

Animals were dark-adapted overnight and prepared for electroretinography under dim red light. Pupillary dilation was carried out by installation of 1% cyclopentalate and 2.5 % phenylephrine. Animals were anesthetized by intraperitoneal injection with ketamine (2.08 mg per 15 g body weight) and xylazine (0.21 mg per 15 g body weight). Standardised flashes of light were presented to the mouse in a Ganzfeld bowl to ensure uniform retinal illumination. The ERG responses were recorded simultaneously from both eyes by means of contact lens electrodes (Medical Workshop, Groningen, Netherlands) using 1% Amethocaine as topical anesthesia and

Vidisic (Dr Mann Pharma, Germany) as a conducting agent and to maintain corneal hydration. Reference and ground electrodes were positioned subcutaneously, ~1 mm from the temporal canthus and anterior to the tail respectively. Responses were analysed using a RetiScan RetiPort electrophysiology unit (Rolad Consulting Gmbh). The protocol was based on that approved by the International Clinical Standards Committee for human electroretinography. Rod-isolated responses were recorded using a dim white flash (-25 dB maximal intensity where maximal flash intensity was 3 candelas/m^2/s) presented in the dark-adapted state. Maximal combined rod-cone response to the maximal intensity flash was then recorded. a-waves were measured form the baseline to the trough and b-waves from the baseline (in the case of rod-isolated responses) or from the a-wave to the trough (Aherne *et al.*, 2004; O'Reilly *et al.*, 2007). All ERG analyses were carried out by a registered ophthalmologist (Dr. Paul F. Kenna) in a barrier facility with sterile instruments and solutions.

5.2.4 AAV-mediated gene transfer in retinal explant cultures

The eyes of two new born wild type C57B6/CBA mice were dissected under a dissecting microscope and each whole-mount retinal explants was infected for 24 hrs with 10^{13} vp/ml of pAAVsh2048.EGFP diluted with 1 ml of neurobasal medium (containing 2 mM taurine, 10% Fetal calf serum) on Costar Transwell polycarbonate membrane in a 6-well plate. Whole-mount retinal explants were then washed in PBS and cultured *in-vitro* at 37°C on Costar Transwell polycarbonate membrane (0.2 μm pore) in neurobasal medium (Invitrogen) containing 2 mM taurine, 10% Fetal calf serum, Penicillin/streptomycin, and B-27 supplements (Invitrogen) for seven days. Media was replenished daily. Transduced whole-mount retinal explants were fixed in 4% paraformaldehyde (pH7.4) and sectioned with a vibratome sectioner (Leica VT 1000S, Leica Biosciences, DA, USA) at 50μm thickness as described in section 4.2.5. Retinal sections were stained with propidium iodide (1:500 in PBS) and embedded on glass slides using Aqua-polymount (Polyscience Inc.). The slides were stored overnight at room temperature in the dark and transferred to 4°C for long-term storage. All fluorescence imaging was carried out on a fluorescence microscope (Zeiss, Axioplan 2) at 40X magnification.

5.2.5 Isolation of FACS sorted retinal RNA for quantitative analysis of IMPDH1 mRNA

Two weeks to one-month old wild type C57B6/CBA mice were subretinally injected with 1-3 µl of $10^{12\text{-}13}$ vp/ml pAAVshLuc.EGFP (left eyes) and pAAVsh2048.EGFP (right eyes). Four weeks post-injection, AAV-transduced retinas were dissected, pooled and dissociated by trypsin digestion. Dissociated single retinal cells expressing EGFP were FACS sorted using a Beckman-Coulter Altra Fluorescence Activated Cell Sorter (Beckman-Coulter, Inc., Fullerton, CA, USA), and RNA was extracted from FACS sorted retinal cells using a RNeasy Mini Kit (Qiagen) as described in sections 2.6.1 to 2.6.3. Quantitative Real Time RT-PCR analysis was performed by comparison of IMPDH1 and β-actin amplification products from right (Targeting shRNA) and left (Non-targeting shRNAs) pooled eyes. IMPDH1 expression was standardised per unit β-actin expression and expressed as a percentage of that for the non-targeting control.

5.2.6 Retinal protein extraction and western blot analysis of IMPDH1 protein levels

Adult wild type C57B6/CBA mice were subretinally injected with 3 µl of $10^{12\text{-}13}$ vp/ml pAAVshLuc.EGFP (left eyes) and pAAVsh2048.EGFP (right eyes) per eye. A second subretinal injection with the same concentrations of AAV shRNAs was administered into the same eyes at different regions of the retina one week after the primary injection. Four weeks after the second injection, mice were euthanized by carbon dioxide inhalation, and retinas were dissected. Protein extracts were obtained from dissected retinas by passing through 21-gauge syringes in protein lysis buffer. Protein concentration was quantified by BCA assay (Promega) and 30µg of total retinal protein was loaded into each lane. Protein samples were separated by electrophoresis on 10% SDS-polyacrylamide gels and transferred to nitrocellulose membranes. IMPDH1 protein was detected using anti-N-IMPDH1 antibody (kindly provided by Dr Sara J. Browne, *University of Texas HSC, Houston, USA*) at a concentration of 1:7000 in 5% skimmed milk, and secondary detection was performed using HRP-conjugated anti-rabbit antibodies (Abcam). The blots were

developed using Enhanced Chemiluminescent Kit (Pierce). Blots were stripped and re-probed with β-actin as loading control. Western blot band intensities were quantified using the Image processing web-tool, *Image J*. The percentage expression in band intensity for IMPDH1 was calculated relative to control virus to represent 100% expression, and normalised against β-actin.

5.2.7 Histological analysis and quantification of outer nuclear layer (ONL) thickness

Injected eyes were fixed in 4% paraformaldehyde (pH 7.4) overnight at 4°C on a rotating device. Eye cups were then washed in phosphate buffered saline for 1 hr and submerged in solutions of 10%, 20% and 30% sucrose. Eye cups were then embedded in optimum cutting temperature solution (OCT, Tissue Tek) and snap frozen by liquid nitrogen. Frozen eyes were sectioned on a cryo-sectioner (Leica CM 1900 Cryostat, Leica Biosciences, DA, USA) in 12 μm thickness and sections were collected on Polysine® slides (Menzel-Glazer). Sectioned eyes were mounted with Aqua-Polymount (Polyscience) mounting medium after nuclei-counterstaining with DAPI (1:5000 in PBS). Retinal sections were then visualised under fluorescence microscope (Zeiss, Axioplan 2) or confocal microscope (Olympus FU1000, Hamburg, Germany). Outer nuclear layer (ONL) thickness was evaluated in 12 μm cryostat sections. The number of rows of photoreceptor nuclei in the central and peripheral sides of nine independent cryostat sections from each eye co-injected with AAV-mutant IMPDH1 and AAV-sh2048 or AAV-shNT was counted blindly under a confocal microscope (Olympus FU1000), and the average ONL layers for AAV-sh2048 injected and AAV-shNT eyes were grouped.

5.2.8 Immunohistochemistry

Whole eyes were extracted from injected mice and immediately fixed in 4% paraformaldehyde (pH 7.4) for 4 hrs at 4°C on a rotating device. The paraformaldehyde was then removed, and the eyes were washed with Phosphate Buffer Saline every 15mins for 1 hr at 4°C. After washing, the eyes were cryo-protected in 10%, 20% and 30% sucrose in PBS, and were then suspended in

specimen blocks with optimum cutting temperature solution (OCT, Tissue Tek) and snap frozen by liquid nitrogen. Frozen eyes were cryo-sectioned on a cryo-sectioner (Leica CM 1900 Cryostat, Leica Biosciences, DA, USA) in 12 μm thickness and sections were collected on Polysine® slides (Menzel-Glazer). Sectioned eyes were then blocked for 20 min at room temperature in PBS containing 5% goat serum. Primary antibody anti-C-IMPDH1 (kindly provided by *Dr Sara J. Browne, University of Texas HSC, Houston, USA*) was made up in PBS at a concentration of 1:300 containing 1% goat serum and incubated with sectioned eyes over-night at 4°C in a humidity chamber. After primary antibody incubation, sectioned eyes were washed three times with PBS at 15 min intervals. Secondary antibody (Cy3-labeled anti-rabbit IgG antibody) was made up in PBS at a concentration of 1:500 containing 1% goat serum and incubated with sectioned eyes for 1 hr at 37°C in a humidity chamber. Following incubation, sectioned eyes were washed six times with PBS at 15min intervals and mounted with Aqua-Polymount (Polyscience) mounting medium after nuclei-counterstaining with DAPI (1:5000 in PBS). Retinal sections were then visualised under fluorescence microscope (Zeiss, Axioplan 2) or confocal microscope (Olympus FU1000, Hamburg, Germany).

5.2.9 Statistical analysis

Experimental data sets for all suppression data sets were pooled, averaged, and standard deviation values were calculated. 2-Sample Student's *t-test* (Data Desk 6.1, Data Descriptions) for paired data and Analysis of Variance (ANOVA) post-hoc tests (GraphPad Prism) for multiple comparisons were used to test the significance of ERG, protein and RNA measurements. $P \leq 0.05$ were considered statistically significant. Y-error bars on histograms illustrate standard error of the mean (SEM).

5.3 Results

5.3.1 Construction of rAAV-2/5 vectors expressing IMPDH1-specific shRNA and evaluation of transduction efficiency

In order to generate an AAV-based vector for shRNA delivery in this study, the AAV helper virus-free system (Xiao *et al.*, 1998) was used which allowed for the production of infectious recombinant human AAV-2 virions without the need of a helper virus (*Figure 5.6*). The *rep* and *cap* genes have been removed from the viral vector (pAAV-MCS) and are provided *in-trans* on the plasmid pRep2/Cap5 (Hildinger *et al.*, 2001). A second plasmid, pHelper, provides the adenovirus gene products required for the production of infective AAV particles, such as E2A, E4 and VA RNA genes. The remaining adenoviral gene products are provided by the HEK-293 cells that stably express adenovirus E1 gene. A recombinant AAV-2/5 vector was designed to express both H1-promoter driven sh2048 and CMV promoter-driven enhanced green fluorescent protein (EGFP) (pAAVsh2048.EGFP), which allowed for the direct identification of cells expressing shRNA *in-vivo*. A second rAAV-2/5 vector co-expressing luciferase GL2 targeting shRNA and EGFP (pAAVshLuc.EGFP) was constructed similarly and was used as a non-targeting control virus. As an initial step to evaluate the transduction efficiency of AAV-2/5 shRNA constructs, whole-mount retinal explants were prepared from newborn wild type C57B6/CBA mice and transduced with pAAVsh2048.EGFP (1 µl $2.19x10^{13}$ vp/ml diluted in 1 ml of neurobasal medium) for twenty-four hours. Seven days post-transduction, a substantial proportion of whole-mount retinal explants were observed to express EGFP as shown in *Figure 5.7A*. Upon examination of vibratome retinal sections, transduced retinal explants have differentiated *in-vitro* in a manner similar to normal *in-vivo* development as shown in *Figure 5.7B*, which is consistent with the observation reported by Ogilvie *et al.*, (1999), which showed that retinal explants at P7 possessed 8-9 nuclei of photoreceptor cells. In particular, strong EGFP fluorescence was observed in the outer nuclear layer of retinal explants illustrating the specificity of pAAVsh2048.EGFP in transducing photoreceptor cells. Furthermore, 3 µl of pAAVsh2048.EGFP ($2.19x10^{13}$ vp/ml) was subretinally injected

into the right eye of a 4-week old wild type C57B6/CBA mouse and the contralateral eye was injected with 3 µl of pAAVshLuc.EGFP ($1x10^{13}$ vp/ml). Four weeks post-injection, the animal was sacrificed and isolated retinas were embedded in OCT for cryostat sectioning. Upon examination under a fluorescent microscope, frozen fixed retinal sections injected with pAAVshLuc.EGFP or pAAVsh2048.EGFP both showed strong EGFP signals in the retinal pigment epithelium, outer segments and outer nuclear layer, whereas the inner nuclear layer and the ganglion cell layer were not transduced (*Figure 5.7C*). In particular, AAV-mediated expression of both viral vectors did not disrupt the retinal structure (*Figure 5.7C*). These results further illustrated the specificity and efficiency of rAAV-2/5 vectors in transducing the retinal pigment epithelium and photoreceptor cells, which is consistent with the observation reported by a previous study (Auricchio *et al.*, 2001b).

5.3.2 Immunolocalisation of IMPDH1 in mouse retina

Immunofluorescence staining was performed on frozen fixed retinal sections from one month old wild type C57B6/CBA mice using anti-C-IMPDH1 antibody, and immune complexes were detected with Cy3-labeled anti-rabbit IgG antibody. Anti-C-IMPDH1 staining showed that IMPDH1 was localised predominantly in the outer segment adjoining the outer nuclear layer, and weak staining was also detected in the retinal pigment epithelium and synaptic terminals of the photoreceptor cells (*Figure 5.8*). No staining was observed in retinas tested without anti-C-IMPDH1 antibody. This pattern of protein localisation is consistent with the *in-situ* mRNA expression pattern reported previously by Aherne *et al.*, (2004), and also with the immunofluorescence staining reported by Bowne *et al.*, (2006a).

5.3.3 AAV RNAi-mediated suppression of IMPDH1 transcripts *in-vivo*

In order to assess the long term suppression of IMPDH1 *in-vivo*, 1 µl of pAAVsh2048.EGFP ($2.19x10^{13}$ vp/ml) was subretinally injected into the right eyes of 14-day-old wild type C57B6/CBA mice, and contralateral eyes were injected with 1µl of pAAVshLuc.EGFP ($1x10^{13}$ vp/ml) (n=8). Two weeks post-injection, eyes from four injected mice were pooled and dissociated (i.e. two groups of dissociated retinas

injected with pAAVshLuc.EGFP (n=4 retinas/group); and two groups of dissociated retinas injected with pAAVsh2048.EGFP (n=4 retinas/group)). EGFP-positive cells were collected by FACS as shown in *Figure 5.9; injection #1* and RNA was extracted from these cells. The level of endogenous mouse IMPDH1 mRNA suppression was measured by Real Time RT-PCR analysis. IMPDH1 expression was standardised per unit endogenous β-actin and expressed as a percentage of that for the contralateral non-targeting control. According to the data shown in *Figure 5.10; injection #1*, which represents the average of all the pooled eyes (n=8), AAV-sh2048 significantly reduced endogenous IMPDH1 mRNA levels to 37% ± 5%, as compared to the contralateral non-targeting control ($P<0.05$).

To assess whether the age of animals and incubation period of AAV in the retina have any significant contribution to RNAi-mediated suppression *in-vivo*, 3 µl of pAAVsh2048.EGFP ($2.19x10^{13}$ vp/ml) was subretinally injected into the right eyes of three months old wild type C57B6/CBA mice, and contralateral eyes were injected with 3 µl of pAAVshLuc.EGFP ($1x10^{13}$ vp/ml) (n=6). Four weeks post-injection, eyes from three injected mice were pooled and dissociated (i.e. two groups of dissociated retinas injected with pAAVshLuc.EGFP (n=3 retinas/group); and two groups of dissociated retinas injected with pAAVsh2048.EGFP (n=3 retinas/group)). EGFP-positive cells were analysed and collected by FACS as described in *Figure 5.11; injection #2*. Similar to the previous experiment, the level of IMPDH1 mRNA expression was quantified by Real Time RT-PCR, standardised per unit endogenous β-actin and expressed as a percentage of that for the non-targeting control. The results shown in *Figure 5.12; injection #2* (an average of all the pooled eyes; n=6) demonstrated that AAV sh2048 strongly reduced the level of IMPDH1 mRNA to 29% ± 8%, as compared to the non-targeting control ($P\leq0.0001$). This result has suggested that the injection of 3 µl of AAV vector and an incubation period of 4 weeks may be optimal for achieving potent silencing of IMPDH1 *in-vivo*, and was therefore used as a benchmark for future suppression experiments. In order to determine whether the age of mice at injection affects the suppression efficiency of pAAVsh2048.EGFP, further six 2-week-old wild-type C57B6/CBA mice were

subretinally injected. Due to the size of the retinas at this stage of development, only a single micro-litre was injected, i.e. 1 µl of pAAVsh2048.EGFP ($2.19x10^{13}$ vp/ml) into the right eyes and 1 µl of pAAVshLuc.EGFP ($1x10^{13}$ vp/ml) into contralateral eyes. Four weeks post injection, eyes from three animals were pooled and dissociated (i.e. two groups of dissociated retinas injected with pAAVshLuc.EGFP (*n*=3 retinas/group) and two groups of dissociated retinas injected with pAAVsh2048.EGFP (*n*=3 retinas/group)). Following FACS analysis (*Figure 5.13; injection #3*), the level of IMPDH1 mRNA expression in EGFP-positive cells was quantified by Real Time RT-PCR, and AAV-sh2048 significantly reduced IMPDH1 to 22% ± 3%, as compared to non-targeting control (*Figure 5.14*; *injection #3*; P=0.0271). Upon comparison of the result obtained in *Figure 5.12; injection #2*, the observation made in *Figure 5.14*; *injection #3* suggests that the suppression efficiency of IMPDH1 *in-vivo* by sh2048 is not dependent on the age of animals injected, as the use of younger animals did not reduce silencing activity.

In the above suppression experiments, the high viral titre of rAAV-sh2048 at $2.19x10^{13}$ vp/ml was exploited to obtain maximum silencing efficiency *in-vivo*. However, since 3 µl is the largest volume possible to inject subretinally, it was not possible to compensate for the lower titre of control virus injected into control eye and therefore over twice as much AAV-sh2048 was used in comparison to AAV-shLuc. In order to determine whether the suppression achieved previously was due to this bias towards the use of a higher AAV suppressor viral titre than the AAV non-target control in this experiment, the concentration of rAAV-sh2048 was diluted to match that of AAV-shLuc. In addition, it was of interest to evaluate whether suppression of IMPDH1 at the transcript level *in-vivo* caused any detrimental effect on normal photoreceptor function. Therefore 3 µl of pAAVsh2048.EGFP (stock concentration diluted to 1:3 to yield ~$6.85x10^{12}$ vp/ml) was injected into six 4-month-old wild type C57B6/CBA mice, while contralateral eyes were injected with 3µl of an equal concentration ($6.85x10^{12}$ vp/ml) of pAAVshLuc.EGFP. Four weeks post-injection, photoreceptor activity in the retinas of injected mice was evaluated using electroretinography (ERG). The b-wave amplitudes of rod-isolated response and

combined rod and cone response to maximal intensity flashes presented in the dark-adapted state from all six animals were recorded as shown in *Figures 5.15A* and *5.16A,* respectively. b-wave amplitudes of both rod-isolated and maximal rod and cone responses in mouse #1 to #4 showed an almost 60% reduction in eyes treated with pAAVsh2048.EGFP relative to those treated with the control virus (P=0.0057 and P=0.0028, respectively: *Figure 5.15B* and *C*; *injection #4*). Reduced b-wave amplitudes observed in AAV-sh2048-injected eyes of mouse #1 to #4 were not unexpected since the knockdown of IMPDH1 transcripts might have a negative impact on the high level demand of GTP by photoreceptor cells. However, the rate of functional deterioration occurred at a more rapid rate than those recorded in IMPDH1$^{-/-}$ mouse, where progressive reduction in retinal function was not observed until five months of age (Aherne *et al.,* 2004). In contrast, b-wave amplitudes of both rod-isolated and maximal rod and cone responses in mouse #5 and #6 showed opposite recordings to mice #1 to #4, where functional responses were moderately and markedly higher in AAV-sh2048-injected eyes of mouse #5 and #6, respectively, as compared to contralateral control eyes (*Figure 5.16B (i) and (ii)*). Reasons for the opposing b-wave amplitudes observed in AAV-sh2048 injected eyes of mouse #5 and #6 compared to mouse #1 to #4, and the low ERG recordings in AAV-shLuc injected eyes have not yet been fully elucidated, but a possible explanation could lie in variation of injection efficiency. Based on the trend of observed ERG recordings, eyes from mouse #1 to #4 which showed deterioration of retinal function in AAV-sh2048 injected eyes were pooled and dissociated for FACS analysis as shown in *Figure 5.15D* and *E*. The level of IMPDH1 mRNA expression in EGFP-positive cells collected from mouse #1 to #4 was quantified by Real Time RT-PCR, and AAV-sh2048 significantly reduced IMPDH1 mRNA to 32% ± 8%, as compared to control virus (*Figure 5.15F*; P=0.001). This result has shown that diluting the concentration of rAAV-sh2048 from 2.19×10^{13} vp/ml to 6.85×10^{12} vp/ml did not have any negative impact on the silencing efficiency when compared to previous suppression experiments. Furthermore, rAAV-mediated suppression of IMPDH1 transcripts by ~68% *in-vivo* can lead to a 60% reduction in b-wave amplitudes. Eyes from mouse #5 and #6 which showed no deterioration of retinal function in AAV-sh2048 treated eyes

were FACS sorted individually as shown in *Figures 5.16C (i)* and *(ii)*. Interestingly, less than 10% suppression of IMPDH1 transcripts was observed in EGFP-positive cells from mouse #5 and #6, as compared to control virus (*Figures 5.16D (i)* and *(ii)*, respectively). The lack of reduced b-wave amplitudes and suppression effects observed in rAAV-sh2048 injected eyes of mouse #5 and #6 may have been the result of poor *in-vivo* AAV-mediated expression of shRNAs or poor subretinal delivery of AAV vectors. Collectively, excluding mouse #5 and #6 from injection number four, Real Time RT-PCR analyses carried out from these four sets of injections have indicated that subretinal delivery of rAAV-2/5 sh2048 vectors elicited long-term and efficient suppression of IMPDH1 transcripts in photoreceptor cells, and that transduction efficiency did not directly correlate with silencing efficiency as shown in *Table 5.17*.

5.3.4 AAV shRNA-mediated suppression of IMPDH1 protein *in-vivo*

Endogenous mouse IMPDH1 protein was initially evaluated by western blot analysis using anti-N-antibody on native wild type C57B6/CBA mouse retinal protein. A single correctly sized band of 55 kDa was clearly visible (*Figure 5.18A*). Similarly, a band also of 55 kDa specific to anti-N-IMPDH2 antibody was observed on a second western blot (*Figure 5.18B*). These results are consistent with those reported previously by Bowne *et al.*, (2006a). To evaluate the effect of AAV-mediated shRNA delivery on the expression of IMPDH1 protein *in-vivo*, 3 µl of pAAVsh2048.EGFP ($2.19x10^{13}$ vp/ml) was subretinally injected into two-month-old wild type C57B6/CBA mice, and contralateral eyes were injected with 3 µl of pAAVshLuc.EGFP ($1x10^{13}$ vp/ml) (n=3). As previously discussed in Chapter 4, the amount of material collected from FACS analysis does not suffice for use in western blot analysis. Therefore in an attempt to maximise the area of AAV transduction in the retina, a second subretinal injection was administered to a different area of the retina one week after the primary injection using the same concentrations of AAV-vectors (the one-week gap would have allowed the bleb formed by the first injection to settle down before the administration of the second injection to minimise damage to the retina). Four-weeks after the second injection, total protein was extracted from

the retinas of three injected animals and pooled for western blot analysis. Western blot in *Figure 5.19A* showed that robust downregulation of IMPDH1 protein in photoreceptor cells transduced with pAAVsh2048.EGFP as compared to the non-targeting control had occurred. Furthermore, in two repeat experiments, 3 µl of pAAVsh2048.EGFP (diluted $2.19x10^{13}$ vp/ml at 1:3 to yield ~$6.85x10^{12}$ vp/ml) was subretinally injected into four-month-old wild type C57B6/CBA mice, and contralateral eyes were injected with 3 µl of pAAVshLuc.EGFP ($6.85x10^{12}$ vp/ml), *n=3* and *n*=4, respectively. Similarly, a second subretinal injection was administered one week after the first injection using the same concentrations of AAV-vectors, and four weeks after the second injection, total protein was extracted and pooled for western blot analysis. Consistent with the first finding, western blots from the two repeat experiments showed strong reduction of IMPDH1 protein by AAV-sh2048 in *Figure 5.19B* and *5.19C*, respectively. Densities of the IMPDH1 protein bands were measured by densitometry software (*Image-J*) and normalised to the density of β-actin protein bands from the same samples. The histogram in *Figure 5.19D* illustrates the mean of three independent experiments (*Figure 5.19 A, B and C*) showing that 22% ± 6% suppression of endogenous IMPDH1 in total retinal protein was achieved in eyes treated with AAV-sh2048, as compared to those treated with the non-targeting control (P=0.355).

5.3.5 Detection of AAV-mediated RNAi suppression of IMPDH1 *in-vivo* by immunohistochemistry

To qualitate the levels of IMPDH1 protein reduction in AAV-treated eyes, 3 µl of pAAVsh2048.EGFP ($2.19x10^{13}$ vp/ml) was subretinally injected into one-month-old wild type C57B6/CBA mice, and contralateral eyes were injected with 3 µl of pAAVshLuc.EGFP ($1x10^{13}$ vp/ml) (*n*=2). Four weeks post-injection, sections from frozen retinas were probed with anti-C-IMPDH1 antibody and immune complexes were detected using Cy3-labeled anti-rabbit IgG antibody. Representative fluorescent images in *Figure 5.20B* showed near complete downregulation of IMPDH1 expression in the outer segment and outer nuclear layer of retinas injected with pAAVsh2048.EGFP, as compared to the retinas of non-targeting control (*Figure*

5.20A), which showed normal IMPDH1 expression pattern similar to that observed in previous immunolocalisation assay (section 5.3.2). Furthermore, the EGFP expression patterns observed in *Figure 5.20* further assured the specificity of rAAV-2/5 viral vectors in transducing the outer segment and outer nuclear layer of injected animals. Collectively, this result demonstrates that rAAV-sh2048 can elicit specific and potent silencing of IMPDH1 expression in the outer segment and outer nuclear layer of injected mice.

5.3.6 Time-dependent analysis of the effect elicited by AAV shRNA-mediated suppression of IMPDH1 on retinal histology

It is evident that long-term suppression of IMPDH1 *in-vivo* is required for successful therapy for a progressive retinopathy such as RP10, therefore the impact of long-term suppression of IMPDH1 on photoreceptor structure and function was evaluated *in-vivo*. 3 µl of pAAVsh2048.EGFP ($2.19x10^{13}$ vp/ml) was subretinally injected into four one-month-old wild type C57B6/CBA mice, and contralateral eyes were injected with 3 µl of pAAVshLuc.EGFP ($1x10^{13}$ vp/ml) (n=4). The first time-point examined was four weeks post-injection, which would have represented the incubation period used for previous suppression experiments. Two mice (designated as mouse #1 and #2) were sacrificed and frozen fixed retinal sections from these animals were immunostained with anti-C-IMPDH1 antibody. Representative fluorescent images of retinas injected with pAAVshLuc.EGFP (*Figure 5.21Ai*) showed normal IMPDH1 expression pattern and healthy retinal structure with 11-12 layers of photoreceptor cell nuclei in the outer nuclear layer (n=2). Furthermore, retinas injected with pAAVsh2048.EGFP illustrated knockdown of IMPDH1 expression in both the outer segment and outer nuclear layer (*Figure 5.21Aii; n*=2). Interestingly, the thickness of the outer nuclear layer appeared to be very slightly reduced as a result of IMPDH1 suppression by AAV-sh2048 (*Figure 5.21Aii*), which was consistent with the diminished ERG b-wave amplitudes of rod-isolated and maximal, rod and cone responses observed previously in AAV-sh2048 injected eyes (section 5.3.3; *Figure 5.15A; injection #4*). The second time-point examined was four months post-injection, and ERG analyses were performed on these two mice (designated as mouse

#3 and #4) before they were sacrificed for histological examination. Similarly, frozen fixed retinal sections were immunostained with anti-C-IMPDH1 antibody for the detection of IMPDH1 expression *in-vivo*. The retinal structure of the eye in mouse #3 injected with pAAVsh2048.EGFP exhibited low levels of IMPDH1 expression and a mildly compromised outer nuclear layer with 8-9 rows of photoreceptor cell nuclei (*Figure 5.21Bii*), and with reduced b-wave amplitudes of rod-isolated and maximal rod and cone responses. In particular, the histology observed in mouse #3 did not differ greatly to that of mouse #1 and #2, which was analysed four weeks post injection (*Figure 5.21Aii*). In the contralateral eye of mouse #3 which was injected with control virus (rAAV-shLuc), normal retinal histology with 10-11 layers of photoreceptor cell nuclei in the outer nuclear layer was visible, but b-wave amplitudes of rod-isolated response and maximal, cone and rod were both completely diminished (*Figure 5.21Bi*). A possible explanation for this inconsistency could be variation among ERG recordings or physical injury induced by subretinal injection, which may have consequently affected ERG recordings without visibly damaging the structure. Interestingly, the eye from mouse #4 injected with pAAVsh2048.EGFP exhibited the most significant detrimental effect elicited by the suppression of IMPDH1 *in-vivo*. Photoreceptor cell nuclei in the outer nuclear layer were reduced to 3-4 layers (*Figure 5.21Cii*), as opposed to that observed in the contralateral eye injected with control virus, which possessed 10-11 rows of photoreceptor cell nuclei (*Figure 5.21Ci*). Furthermore, b-wave amplitudes of both rod-isolated response and maximal, cone and rod response were reduced to near-undetectable levels in the eye injected with AAV-sh2048 (*Figure 5.21Cii*), whereas contralateral eye injected with AAV-shLuc showed normal ERG b-wave amplitudes (*Figure 5.21Ci*). This result suggests that in some cases long-term downregulation of IMPDH1 may cause significant cell death *in-vivo* and that further long-term studies must be carried out to determine the frequency of occurrence of this potential problem.

5.3.7 Induction of retinopathy by AAV-mediated over-expression of mutant IMPDH1

Animal models are valuable tools to study *in-vivo* the disease pathogenesis and to evaluate experimental therapies. Unfortunately, a RP10 mouse model displaying the pathological effect of mutant IMPDH1 protein has not yet been generated. Previous studies carried out in our laboratory by *Dr. Avril Kennan* have shown that subretinal delivery AAV vector expressing the human mutant IMPDH1 cDNA harbouring the Arg224Pro mutation causes significant thinning of the outer nuclear layer in wild type 129 S2/SvHsd mice (data not published). Therefore a series of co-injections was carried out in wild type 129 S2/SvHsd mice to assess whether suppression of mutant IMPDH1 protein by rAAV-sh2048 *in-vivo* could rescue the retina from degeneration. A novel AAV non-targeting shRNA, designated as pAAVshNT.EGFP, which has previously been applied in *in-vivo* studies (O'Reilly *et al.,* 2007) was used as a non-targeting control in this study. Adult wild type 129 S2/SvHsd mice (3-4 months old) were subretinally co-injected at a viral particle ratio of 1:5 (pAAVIMPDH1 or pAAVEGFP cDNA:shRNA) with one eye being injected with rAAV-sh2048 and the contralateral eye with rAAV-shNT in groups of five animals (n=5) as follows; (i) uninjected; (ii) 2 µl of either pAAVsh2048.EGFP or pAAVshNT.EGFP ($3.3x10^{12}$ vp/ml) with 1 µl pAAVEGFP ($1.8x10^{12}$vp/ml); (iii) 2 µl of either pAAVsh2048.EGFP or pAAVshNT.EGFP ($3.3x10^{12}$ vp/ml) with 1 µl pAAVWtIMPDH1.EGFP ($1.77x10^{12}$ vp/ml); (iv) 2 µl of either pAAVsh2048.EGFP or pAAVshNT.EGFP ($3.3x10^{12}$ vp/ml) with 1 µl pAAVMutIMPDH1(224).EGFP ($1.4x10^{12}$ vp/ml) (*Table 5.22*).

Four weeks post-injection, ERG analyses were carried out on all injected animals and the pooled effects of expression of different AAV vectors on rod-isolated response are shown in *Figure 5.23*. The reduction in b-wave amplitudes of rod-isolated response observed in eyes co-injected with AAV-EGFP vector and AAV-shNT, as compared to uninjected eyes, was most likely to be caused by the combinatorial effects of subretinal injection and AAV expression in photoreceptor cells (P>0.05; *Figure 5.23*). In addition, no significant difference in b-wave amplitudes was

observed between eyes co-injected with AAV-EGFP and either AAV-sh2048 or AAV-shNT (P>0.05; *Figure 5.23*). b-wave amplitudes of eyes co-injected with AAV-wild type IMPDH1 and AAV-shNT or AAV-sh2048 were significantly reduced as compared to uninjected eyes (P<0.05, *Figure 5.23*), suggesting a trend of further deterioration by expression of wild type IMPDH1 *in-vivo* (*Figure 5.23*). Interestingly, b-wave amplitudes of rod-isolated response recorded in eyes co-injected with AAV-sh2048 and (i) AAV-wild type IMPDH1; (ii) or AAV-mutant IMPDH1 were all reduced significantly, as compared to uninjected eyes (P<0.05 and P=0.001, respectively; *Figure5.23*). This observation is consistent with previous findings described in *sections 5.3.3* and *5.3.6*, which showed that suppression of IMPDH1 *in-vivo* 4-week post-injection has a negative impact on retinal function. ERG b-wave amplitudes of rod-isolated response were significantly reduced in eyes co-injected with AAV-mutant IMPDH1 and AAV-shNT as compared to uninjected eyes (P=0.001; *Figure 5.23*), indicating that over-expression of mutant IMPDH1 *in-vivo* has a detrimental effect on retinal function. Furthermore, co-injection of mutant IMPDH1 with rAAV-sh2048 showed no significant rescue of retinal function based on the ERG data, as compared to contralateral eyes co-injected with AAV-shNT (P>0.05; *Figure 5.23(iv)*).

In order to further investigate the pathological effect elicited by AAV-mediated expression of mutant IMPDH1 and the consistency between functional response and histological changes, all injected animals described above were sacrificed immediately after ERG analyses and frozen fixed retinal sections were visualised under a confocal microscope. A representative fluorescent image from uninjected eyes show a normal retinal structure with 11-12 rows of photoreceptor cell nuclei in the outer nuclear layer as shown in *Figure 5.24A*, which is consistent with the normal ERG response recorded in *Figure 5.23(i)*. Similarly, eyes treated with AAV-EGFP vector and AAV-sh2048 or AAV-shNT did not show any histological differences, but the thickness of the outer nuclear layer was mildly reduced to ~10 rows (*Figure 5.24B*), as compared to the sections of uninjected eyes (*Figure 5.24A*). As discussed previously, this subtle reduction probably represents the effects of subretinal injection

and AAV expression in the retina, and is consistent with the mildly reduced ERG response recorded in *Figure 5.23(ii)*. Moreover, representative images of eyes co-injected with AAV-wild type IMPDH1 and rAAV-shNT or rAAV-sh2048 illustrated a more notable reduction in the thickness of outer nuclear layer (*Figure 5.24C*), as compared to uninjected eyes (*Figure 5.24A*), which is also consistent with the reduction in b-wave amplitudes shown in *Figure 5.23(iii)*. Fluorescent images from four mice (designated as mouse #6, 7, 9, 10) co-injected with rAAV-mutant IMPDH1 and rAAV-shNT showed significant reduction in outer nuclear layer thickness compared to uninjected eyes (*Figure 5.25*), which is compatible with the highly reduced ERG wave amplitudes observed previously in *Figure 5.23(iv)*. The main finding of this experiment was that contralateral eyes of these mice treated with AAV-mutant IMPDH1 and AAV-sh2048 showed a modest increase in outer nuclear layer thickness (*Figure 5.25*), indicating that suppression of mutant IMPDH1 *in-vivo* provided a moderate protection effect with respect to retinal structure, which is however not reflected in the ERG wave amplitudes in *Figure 5.23(iv)*. Nevertheless, one mice (designated as mouse #8) did not show any histological difference between eyes co-injected with rAAV-Mutant IMPDH1 and rAAV-sh2048 or rAAV-shNT (*Figure 5.26B*). Upon examination of retinal sections from mouse #8, a low level of EGFP fluorescence expressed in a small area of the retina was observed, as opposed to the widespread EGFP fluorescent signal seen in retinal sections of Mouse #6 (*Figure 5.26A*). This observation may possibly suggest that the lack of mutant IMPDH1-induced retinal degeneration observed in Mouse #8 was caused by poor subretinal delivery of AAV or low AAV transduction efficiency.

The number of rows of photoreceptor cell nuclei in the central and peripheral sides of retinas co-injected with rAAV-mutant IMPDH1 and rAAV-shNT were compared to those co-injected with rAAV-mutant IMPDH1 and rAAV-sh2048 in mouse #6, 7, 9 and 10. The number of rows of photoreceptor nuclei in the central and peripheral sides of nine independent cryostat sections from each eye co-injected with rAAV-mutant IMPDH1 and rAAV-sh2048 or rAAV-shNT was counted blindly, and the average number of ONL layers for rAAV-sh2048 injected and rAAV-shNT eyes

were grouped (*n=4*) as shown in *Figure 5.27*. Eyes treated with rAAV-sh2048 yielded a 3-fold increase in the average number of photoreceptor nuclei layers in the central region of the retina as compared to contralateral eyes (P=0.0465, *Figure 5.27*). Similarly, the average number of photoreceptor nuclei layers in the peripheral region of the retina in rAAV-sh2048 treated eyes was 4-fold greater than eyes treated with AAV-shNT (P=0.03, *Figure 5.27*). Collectively, the total number of rows of photoreceptor cell nuclei in both the central and peripheral sides of the retina in rAAV-sh2048 treated eyes showed a significant 4-fold increase when compared to rAAV-shNT treated eyes (P=0.0269, *Figure 5.27*).

5.4 Discussion

For autosomal dominant retinitis pigmentosa (adRP), the feasibility of achieving persistent shRNA expression from a viral vector is highly desirable, especially when long-term and stable suppression of mutant protein is required to obtain therapeutic benefits (O'Reilly *et al.*, 2007; Gorbatyuk *et al.*, 2007). In this study, adeno-associated viral vectors were chosen to express IMPDH1-specific shRNA based on its safe, non-pathogenic and stable characteristics *in-vivo* (Phillips, 2001; Phillips *et al.*, 2002). The use of the gutless AAV system and the fact that AAV vectors display only a modest frequency of integration into the host genome have contributed to the overall safety of this particular vector system. In addition, the property of AAV to persist in infected cells as extrachromosomal forms has allowed stable and strong expression of shRNA *in-vivo*. Numerous reports have previously demonstrated prolonged expression of AAV-delivered transgenes for over 18 months in mice and canine models (Mount *et al.*, 2002; Snyder *et al.*, 1999). Injection of recombinant AAV-2/5 vectors into the subretinal space has delivered shRNA exclusively to the retinal pigment epithelium, photoreceptor outer segment and outer nuclear layer of wild type mouse retinas (*Figure 5.7C*), with no significant damage to the overall retinal structure. This finding is consistent with the transduction pattern reported by Aurrichio *et al.*, (2001b) and O'Reilly *et al.*, (2007), using rAAV-2/5 viral vectors. Immunolocalisation studies have shown that IMPDH1 is predominantly localised in the outer segment, outer nuclear layer and inner nuclear layer (*Figure 5.8*), which is consistent with the *in-situ* mRNA expression pattern previously reported by Aherne *et al.*, (2004), and with the immunofluorescence staining reported by Bowne *et al.*, (2006a). The presence of IMPDH1 predominantly in photoreceptor cell layers is not surprising as IMPDH1 is largely responsible for the production of guanine nucleotides within photoreceptor cells (Aherne *et al.*, 2004; Bowne *et al.*, 2006a). This observation also offers a plausible reason as to why mutations in IMPDH1 exclusively affect photoreceptor cells only. The IMPDH1 localisation pattern observed in the retina, and previous reports showing that subretinal injection provided a safer and more direct route of delivery into the retinal pigment epithelium and photoreceptor cells (Bennett *et al.*, 1996), indicated that subretinal delivery of

IMPDH1-specific shRNAs would offer the most efficient downregulation of IMPDH1 *in-vivo*. In addition, delivery into the subretinal space has been shown to offer immunological privilege that minimises the immune-mediate clearance of AAV and the transduced cells (Jiang *et al.*, 1993).

Real Time RT-PCR analyses from RNA extracted from pure transfectant populations obtained following FACS analysis from four independent experiments, showed that expression of AAV-sh2048 in the retinas of wild type C57B6/CBA mice led to ~70% *in-vivo* suppression of IMPDH1 at the mRNA level (*Table 5.17*). A single injection was capable of transducing ~3-50% of total retinal cells, and the discrepancy in transduction efficiency was possibly due to variations between subretinal injections (*Table 5.17*). Interestingly, transduction efficiency did not directly correlate with shRNA suppression of IMPDH1 *in-vivo* (*Table 5.17*), indicating that once a cell is transduced with AAV-sh2048, IMPDH1 transcript suppression ensues and that this is a linear response, thus more cells transduced does not mean more suppression per transduced cell. Furthermore, the efficiency of AAV-mediated shRNA suppression was not dependent on either the age of animals, or the volume of AAV vectors injected, but an incubation period of 4 weeks yielded slightly more efficient suppression than that of 2 weeks (*Table 5.17*). However, only two time points at two- and four-week post-injection were analysed in this study, and subsequent longer incubation periods would be required to justify this finding. In order to evaluate the effect of IMPDH1 suppression *in-vivo* on photoreceptor cell function, ERG measurements were recorded in six mice prior to Real Time RT-PCR analysis. The b-wave amplitudes of rod-isolated response recorded in this study reflects the rod photoreceptor cell function exclusively, whereas the b-wave amplitudes of maximal, rod and cone response depict the collective functions of both rod and cone photoreceptor cells. Interestingly, b-wave amplitudes in four out of six mice showed approximately 60% reduction in rod-isolated response and maximal, rod and cone response when endogenous IMPDH1 transcripts were suppressed by 68% as compared to control virus (*Figure 5.15B, C and F*). This result suggests that there may be a direct correlation between endogenous IMPDH1 expression and retinal

function, where significant suppression of IMPDH1 *in-vivo* leads to a proportional decrease in retinal function. This hypothesis is supported by the observation that IMPDH1 is predominantly co-localised in rod photoreceptor cells, and is largely responsible for the production of guanine nucleotides within photoreceptor cells (Aherne *et al.*, 2004). However, two other animals showed higher b-wave amplitudes in eyes injected with AAV-sh2048, as compared to control eyes injected with AAV-shLuc (*Figure 5.16B (i) and (ii)*). Moreover, Real Time RT-PCR analysis showed that less than 10% IMPDH1 mRNA suppression was achieved in these animals (*Figure 5.16D (i) and (ii)*). Poor transduction efficiency can be ruled out since approximately 6-30% transduction of retinal cells was achieved in these animals (*Figure 5.16C (i) and (ii)*). Thus the discrepancy in ERG response observed in these animals may possibly be explained by the lack of AAV-mediated RNAi suppression of IMPDH1 transcripts *in-vivo* in these two cases, although the reason for this remains obscure.

Western blot analyses showed that up to 22% suppression of IMPDH1 at the protein level was achieved in total retinal protein following two sequential subretinal injections (*Figure 5.19D*). Lotery *et al.*, (2003) previously demonstrated the use of controlled multiple subretinal injections to allow wide-spread transduction of non-human primate retinas and showed that this method reduced surgical trauma to the retina. The apparently subtle silencing effect elicited by AAV-sh2048 at the protein level would have been masked by the abundance of endogenous mouse IMPDH1, since protein was extracted from total retina including non-transduced areas rather than from FACS sorted cells as for Real Time RT-PCR analysis. However, considering that a single subretinal injection only transduces approximately 3-50% of the entire retina (*Table 5.17*), the level of IMPDH1 protein suppression achieved in these experiments using double subretinal injections could be more than 22% when transduction efficiency is taken into account (Average transduction efficiency per injection is ~3-50% as shown in *Table 5.17*, and two injections would transduce ~6-100% of total retina. Therefore the average suppression efficiency could possibly be from 22-100%). Similarly, immunohistochemical analysis showed that endogenous

IMPDH1 protein expression was significantly suppressed in the outer nuclear layer of AAV-sh2048 treated eyes (*Figure 5.20*). An additional observation made in this experiment was that no severe damage of retinal structure was detected following suppression of endogenous IMPDH1 at the protein level 4 weeks post-injection, despite earlier results showing that a 68% reduction in IMPDH1 transcripts yielded a proportional decrease in retinal function (*Figure 5.15B, C and F*). A similar observation has been reported in the retinas of Briard dogs homozygous for the RPE65 mutation, which showed an early and severe impairment of retinal function with a relatively preserved retinal structure early in life, with photoreceptors slowly degenerating over time (Wrigstad *et al.*, 1992). RPE65 is an abundant protein found in the RPE and plays an important role in vitamin A metabolism and is necessary for the synthesis of the visual pigment chromophore 11-*cis*-retinal (Thompson and Gal, 2003). Therefore, possibly similar to the RPE65 Briard dog model, the loss of IMPDH1 may primarily affect retinal function, since phototransduction activity most likely requires a high level of GTP supply. In contrast, retinal structure may be relatively preserved in the early stages of IMPDH1 depletion, but may begin to degenerate slowly as time progresses.

In order to further evaluate the long-term effect of IMPDH1 suppression on retinal morphology, histological examination was carried out on eyes treated with rAAV-sh2048 at two different time-points post-injection. First, histological analyses of retinas from two animals treated with AAV-sh2048 showed relatively well preserved retinal structure with intact outer nuclear layers four weeks post-injection as shown in *Figure 5.21A (i) and (ii)*. Unfortunately, ERG analyses were not carried out on these animals, however the histological finding is consistent with the immunohistochemistry result obtained previously (*Figure 5.20*). Examination of the retinas from one mouse treated with AAV-sh2048 four months post-injection showed slight variations between retinal function and structure. Interestingly, this mouse showed normal retinal structure in both AAV-sh2048 and AAV-shLuc treated eyes (*Figure 5.21 B (i) and (ii)*). However, b-wave amplitudes of rod-isolated and maximal, rod and cone responses were dramatically decreased in the eye injected

with the control virus, as compared to the eye treated with rAAV-sh2048 showing normal retinal function (*Figure 5.21 B (i) and (ii)*). The underlying reason for the discrepancy observed between retinal function and structure has not yet been fully deciphered, but could possibly be explained by complications in retinal detachment and adhesion following subretinal injection, which may have affected subsequent ERG measurements. In contrast, retinas from another animal treated with rAAV-sh2048 showed both significant reductions in outer nuclear layer thickness and diminished retinal function after four months of injection, as compared to the control virus which showed normal retinal structure and function (*Figure 5.21C (i) and (ii)*). The rapid deterioration in both retinal structure and function following IMPDH1 downregulation *in-vivo* was not expected, since the IMPDH1$^{-/-}$ mouse model only began showing signs of retinopathy after five months of age (Aherne *et al.*, 2004). One possible explanation for this is that in newly born IMPDH1$^{-/-}$ mouse, photoreceptor cells may be able to adjust to the absence of endogenous IMPDH1 with a compensatory mechanism such as the use of IMPDH2, thus exhibiting a slower retinopathy over time. However, suppression of endogenous IMPDH1 *in-vivo* may cause a scenario where the retina is unable to adapt to the sudden loss of IMPDH1, resulting in a more rapid degeneration. In addition, another speculation is that photoreceptor degeneration may have been caused by non-specific silencing of IMPDH2 in AAV-sh2048 treated eyes. It has been previously reported that a mouse model harbouring the loss of both IMPDH2 alleles as a result of homologous recombination showed early embryonic lethality despite normal IMPDH1 expression (Gu *et al.*, 2000). Therefore, it is possible that AAV-mediated non-specific silencing of IMPDH2 may have a negative impact on photoreceptor survival. This will be further evaluated in chapter 6. Additional knockdown studies at different time points are needed to understand the role of IMPDH1 at different stages of retinal development. In the continuation of this study, mice younger than P7 will be subretinally injected with rAAV-sh2048 to evaluate whether suppression of IMPDH1 prior to full retinal development will lead to a slower rate of degeneration as seen in the IMPDH1$^{-/-}$ mouse model (Aherne *et al.*, 2004). In addition, over-expression of shRNA has been shown to exert lethal effects in mice by competing with endogenous

micro-RNAs for limiting cellular factors required for the processing of various small regulatory RNAs (Grimm *et al.*, 2006). Therefore, further titration studies are desired to evaluate the lowest concentration of AAV-sh2048 needed to obtain a beneficial therapeutic effect, and shRNA expression through the use of inducible and tissue specific promoters may allow greater temporal and spatial control in knockdown of IMPDH1 (Lebherz *et al.*, 2005).

AAV-mediated delivery of human mutant IMPDH1 harbouring the Arg224Pro mutation has been shown to induce aggressive retinopathy similar to that observed in transgenic mice bearing the P23H rhodopsin mutation (Olsson et al., 1992) with significant distortion of the outer nuclear layer and diminished retinal function (*Figure 5.23 and 5.25*). Similarly, Cashman *et al.*, (2006) demonstrated adenovirus-mediated subretinal delivery of human VEGF165 [a major stimulant of choroidal neovascularisation (CNV)] into murine retinas induced pathologies comparable to some of the hallmarks of wet age-related macular degeneration (AMD). In particular, it was determined that CNV could be stimulated within five days in this VEGF165-induced CNV animal model. Although the pathological effect induced by over-expression of mutant IMPDH1 has not yet been fully elucidated in the retina, early studies in our laboratory has shown that mutation in IMPDH1 causes significant disruption to its protein structure, resulting in the formation of protein aggregates (Aherne *et al.*, 2004). Photoreceptor cell death caused by protein aggregation has previously been reported in other adRP-linked mutations, including the P23H mutation in rhodopsin (Illing *et al.*, 2002), and the R14W mutation in the gene encoding carbonic anhydrase IV (CA4) that causes RP17 (Rebello *et al.*, 2004). In addition, protein aggregation caused by polyglutamine expansion has also been identified as the underlying disease mechanism for several neurological disorders such as Huntington's disease and six forms of spinocerebellar ataxia (Zoghbi and Orr, 2000; Nakamura *et al.*, 2001b; Xia *et al.*, 2002). Nonetheless, persistent AAV-mediated expression of mutant human IMPDH1 in the retina has provided a rapid retinal degeneration model for RP10 that can be established within four weeks of injection. Interestingly, AAV-mediated expression of wild type IMPDH1 *in-vivo* also

appeared to result in degeneration of both retinal structure and function when compared to uninjected eyes (*Figures 5.23 and 5.24C*), but the degree of functional degeneration was insignificant compared to eyes injected with mutant IMPDH1. Although IMPDH1 is highly expressed in photoreceptor cells, over-expression of exogenous wild type IMPDH1 may have a negative impact on the endogenous IMPDH1 pool. Tan *et al.*, (2001) previously described that over-expression of replacement rhodopsin transgene causes a toxic effect *in-vivo* (Tan *et al.*, 2001). In order to further understand this phenomenon, additional studies involving AAV-mediated expression wild type IMPDH1 in other organs, such as the liver via hydrodynamic delivery, may provide an insight as to whether this effect is specific to over-expression of IMPDH1 in photoreceptor cells only.

Lastly, evidence indicating therapeutic benefit after co-injection of AAV vectors expressing mutant IMPDH1 and sh2048 at a viral particle ratio of 1:5 (IMPDH1 cDNA: shRNA) has been obtained in wild type 129 S2/SvHsd mice. Cashman *et al.*, (2006) also demonstrated a therapeutic effect following co-injection of adenoviral vectors expressing *VEGF* and shRNA at viral particle ratios of 1:5 and 1:10 (VEGF cDNA: shRNA) in the VEG165-induced CNV murine model described above. In particular, choroidal flatmounts revealed that co-injection of *VEGF* and *VEGF*-targeting shRNA at a viral particle level of 1:10 reduced CNV by up to 84% relative to the control virus. Although the ERG data shown in *Table 5.22 (iv)* illustrated that b-wave amplitudes was only rescued in two out of five mice (IMP-02A #6 and IMP-02A #7) following co-injection of AAV-sh2048 and AAV-mutant IMPDH1, histopathological analyses showed that significant protection of outer nuclear layer was achieved in four out of five mice (IMP-02A #6, 7, 9 and 10; *Figure 5.25*). In particular, these animals showed a four-fold increase in outer nuclear layer thickness around the peripheral and central regions of the retina in eyes treated with AAV-sh2048 and AAV-mutant IMPDH1, as compared to control virus (*Figure 5.27*). However, one mouse (IMP-02A #8) showed no significant histological difference between eyes co-injected with AAV-mutant IMPDH1 and AAV-sh2048 or AAV-shNT (*Figure 5.26B*), which may have been the result of poor AAV transduction

efficiency as shown by limited EGFP expression in *Figure 5.26A*. It is important to note that ERG measurements provide an overall electrical response from the entire retina, which may not reflect the true impairment in retinal function possibly when only a small proportion of the retina is transduced per injection. This may possibly explain the discrepancy observed between ERG response and histological analyses observed in mouse #9 and #10 (*Table 5.22 (iv)*). Technical variations and complications (e.g. traumatic lesion) between each subretinal injection can also cause modification to retinal structure that may affect ERG recordings. Natural variations between different ERG measurements may also contribute to the discrepancy seen between ERG response and histological analyses, since a 10% fluctuation is observed in b-wave amplitudes between the left and right eyes of uninjected animals (IMP05-#18, 19 and 20; *Table 5.22 (i)*). Moreover, the AAV-mutant IMPDH1: shRNA (1:5) ratio used in this study was empirically determined, thus it may have favoured AAV-mutant IMPDH1 so that there was not enough shRNA to compensate for the pathological effect. Therefore, additional titration studies are required to determine the optimal ratio of AAV-mutant IMPDH1 and shRNA in order to provide better protection of both retinal function and structure in animal models stimulating human RP10.

5.5 Conclusions

Collectively, the central findings of the present study are that IMPDH1-specific shRNA expressed from rAAV-2/5 efficiently transduced the retinal pigment epithelium, outer segment and outer nuclear layer of murine retinas. In addition, rAAV-mediated expression of sh2048 elicited strong and stable silencing of endogenous murine IMPDH1 at both the mRNA and protein levels for up to four weeks *in-vivo*. Moreover, AAV-mediated expression of mutant human IMPDH1 harbouring the Arg224Pro mutation in retinas of wild type 129 S2/SvHsd mice simulated a disease model of human RP10 with extensive deterioration of retinal structure and function over four weeks of time. Co-injection of AAV-2/5 mutant IMPDH1 with rAAV-sh2048 has provided a modest increase in ERG response and protected the outer nuclear layer from extensive deterioration.

Although the results obtained in this study have revealed that shRNA expressed from rAAV-2/5 for silencing IMPDH1 *in-vivo* may hold great potential for the treatment of RP10, some important issues still remain to be resolved. Firstly, the time-frame of treatment for RP10 will need to be further explored, since the therapeutic potential of IMPDH1 downregulation was validated in a mouse model generated by AAV-delivery of mutant IMPDH1 in this study, in which it is most likely that the co-delivery of rAAV-sh2048 prevented the initiation of substantial retinal degeneration, rather than correcting early retinal damage. In the case of treating a transgenic mutant IMPDH1 mouse model or indeed, a human patient, rAAV-sh2048 would be required to be delivered early enough to prevent massive loss of photoreceptor cells. In particular, the appropriate timing of treatment may vary with individual models and treatments. The finding that long-term suppression of endogenous murine IMPDH1 by rAAV-sh2048 causes a significant degeneration in both retinal structure and function has suggested that studies to develop further IMPDH1-targeting shRNAs which may overcome these complications should be carried out. Alternatively, mutation-independent suppression and replacement strategy (Farrar *et al.*, 2002) may provide a more appropriate approach to therapy for RP10. Successful suppression and

replacement strategies have previously been demonstrated as a therapeutic approach for adRP in our laboratory. For example, Kiang *et al.*, (2005) demonstrated potent suppression of rhodopsin gene and subsequent use of a resistant rhodopsin gene with seven mismatches at the shRNA target site provided resistance to suppression in both *in-vitro* and *in-vivo* systems. Palfi *et al.*, (2006) have also illustrated mutation-independent suppression and simultaneous replacement of *rds*/peripherin transcripts in mammalian cell cultures and murine retinal explants. Recently, O'Reilly *et al.*, (2007) demonstrated the first successful application of *in-vivo* suppression and replacement strategy by showing that an AAV-delivered codon modified rhodopsin replacement gene resisted the suppression effect of targeting RNAi molecules, and provided both structural and functional retinal protection in Pro23His mice. Therefore, AAV-mediated simultaneous suppression of wild type and mutant IMPDH1, and delivery of suppression resistant replacement IMPDH1 genes (based on 3rd base wobble substitution or decaying non-coding 5' or 3' UTR sequences) may potentially resolve the negative effect associated with long-term suppression of IMPDH1 *in-vivo*. In order to achieve a successful RNA replacement strategy, the delivery of shRNA and the replacement gene should originate from the same recombinant AAV vector, otherwise some cells may receive the suppressor agent without the replacement gene, while other cells may overexpress IMPDH1 without limiting the production of the endogenous protein. Finally, a genome-wide transcriptional profile should be carried out to determine whether there is non-specific downregulation of other mRNA in photoreceptor cells apart from the silencing of IMPDH1. Although all our experimental data were relative to a luciferase-targeting or scrambled-sequence shRNA, and no major gross morphological changes were observed in eyes injected with control virus. Nonetheless, the possibility of non-specific silencing of unrelated mRNAs by sh2048 in both *in-vitro* and *in-vivo* systems cannot be ignored and will be addressed in the next chapter.

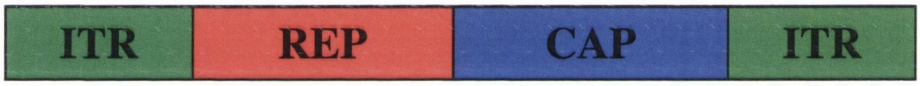

Figure 5.1: A schematic diagram illustrating the wild type genome of AAV, which is composed of a single stranded DNA molecule, two genes; rep, coding for proteins which control viral replication, structural gene expression & integration into the host genome, & cap, which codes for capsid structural proteins (VP). At either end of the genome is a 145 bp inverted terminal repeat (ITR), containing a promoter:

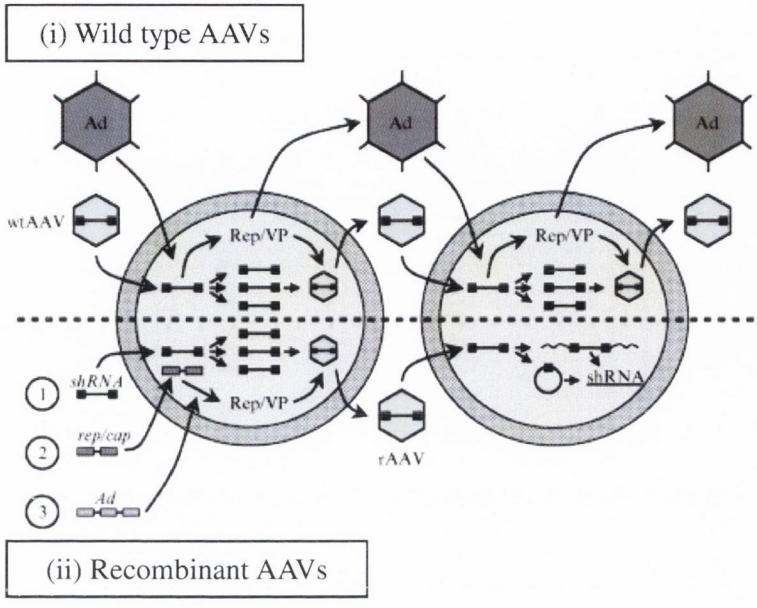

Figure 5.2: Life cycles of wild type AAVs and recombinant AAVs: (i) Propagation of wild-type AAV. Cells are coinfected with the virus and a helper virus, and the AAV capsid traffics to the nucleus, where it releases its genome [black line with boxes at the both ends indicate ITRs]. Products expressed from the helper virus support expression of the AAV genes, resulting in large amounts of AAV replication (Rep) and capsid (VP) proteins. In parallel, the wild-type AAV genome replicates to high copy numbers in the nucleus and eventually becomes encapsidated in virions formed by assembled VP proteins. The helper virus finally induces cell lysis, and progeny AAV as well as replicated adenovirus are released to start a fresh infection cycle in another cell. (ii) For recombinant AAV production, the components required for propagation are provided from three separate plasmids, which are triple transfected into cells: (1) an AAV vector plasmid comprising the transgene (labelled as shRNA) flanked by the AAV-2 ITRs, (2) an AAV helper plasmid encoding the *rep* and *cap* genes, and (3) an adenoviral helper plasmid (typically encoding the E2A, VA, and E4 genes). In the cell nucleus, the AAV helper expresses Rep and VP proteins *in trans*, whereas the ITRs replicate the transgene (shRNA) sequences *in-cis*. The VP proteins then assemble into capsids, which take up the amplified viral DNA. In contrast, the cells do not produce progeny helper virus and thus do not get lysed, allowing the rAAV particles to be harvested from the intact cell. In a reinfected cell, the rAAV particle releases its genome, which subsequently does not get replicated (because of the absence of AAV or adenoviral gene expression), but instead can integrate into the host chromosome or assume extrachromosomal circular or linear forms, either of which results in rAAV genome persistence. Diagram was obtained from Grimm *et* al., (2005).

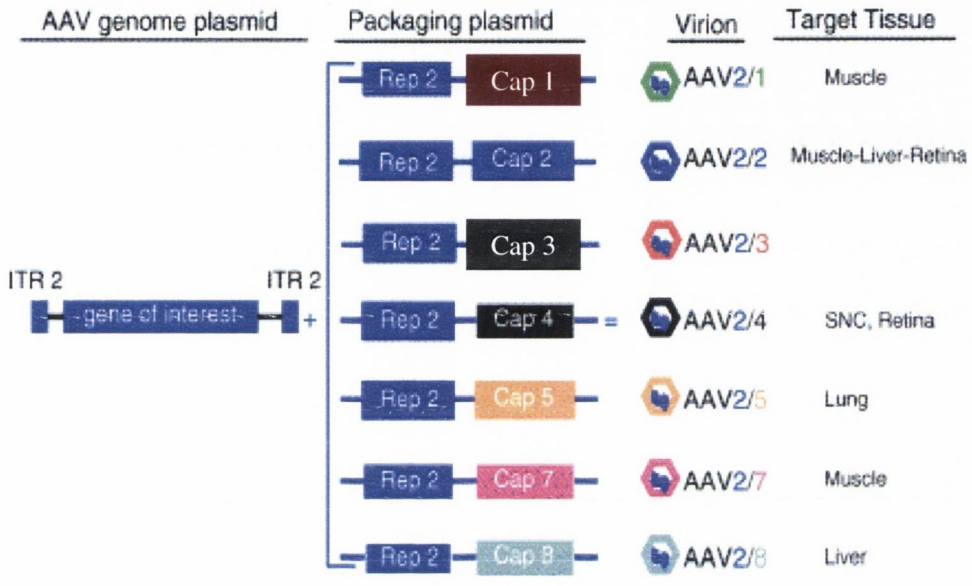

Figure 5.3: A schematic diagram illustrating pseudotyped AAV production and target tissues. Transfection of rAAV plasmid containing the therapeutic gene situated within the viral ITRs, the packaging sequences (*cap* genes encoding for the capsids), and the *rep* open reading frames belonging to the serotype 2 to allow efficient packaging of a viral genome with AAV-2 ITRs. The pseudotyped virions containing the genome of one serotype (AAV-2) and a different capsid (AAV-2/1-8) have tropism dependent on the capsid sequence. Diagram was obtained from Surace *et al.*, (2003).

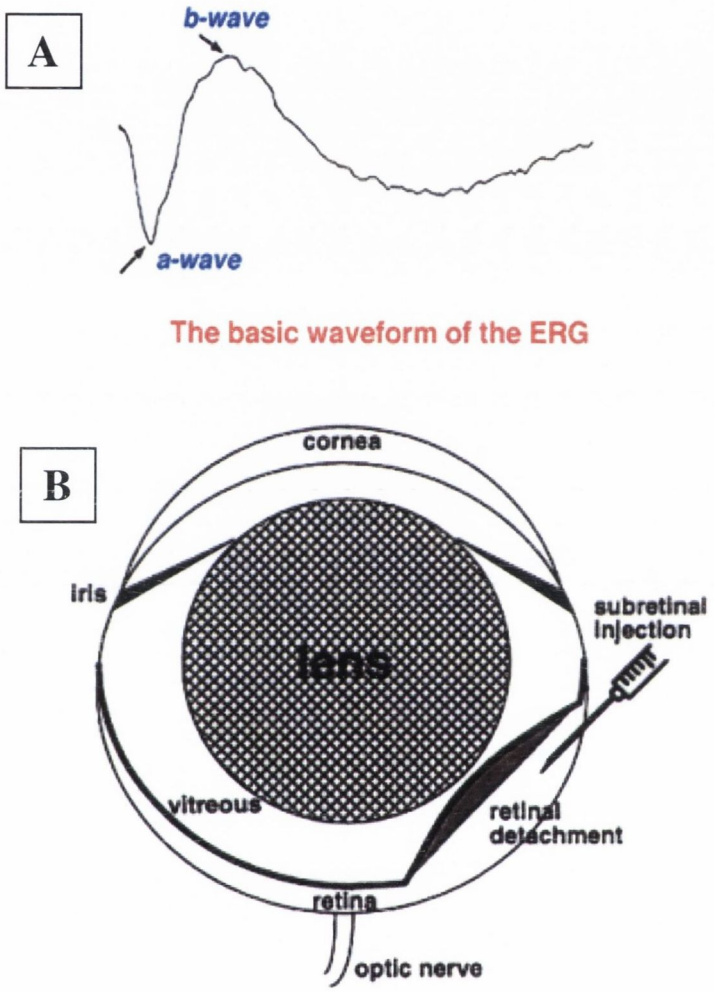

Figure 5.4: (A) The biphasic ERG waveforms of a normal patient (B) A schematic diagram illustrating the route of subretinal injection. Diagram was obtained from Ali *et* al., (1996).

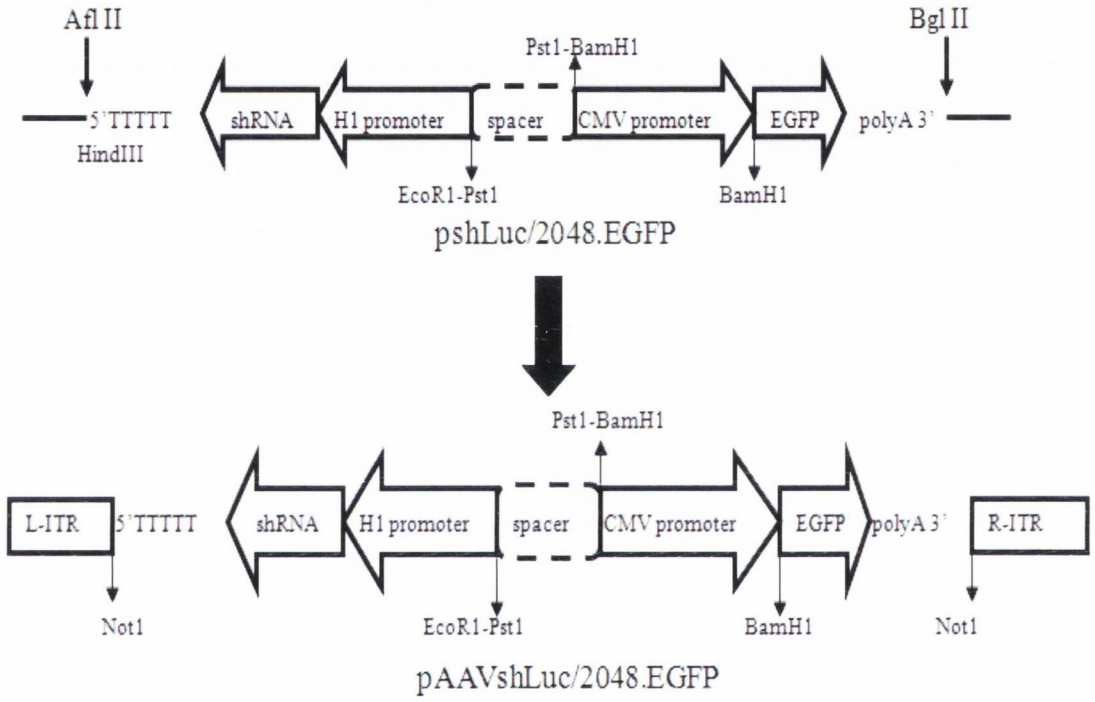

Figure 5.5: A schematic representation of pAAVshRNA.EGFP vector expressing either shLuc (non-targeting control) or sh2048 under the control of the human H1-RNA polymerase III promoter and an EGFP cDNA under the control of the CMV promoter. Restriction fragments containing the H1-promoter driven shRNA and CMV-promoter driven EGFP were excised from pshLuc/2048.EGFP (Chapter 4) and inserted between two AAV-2 derived inverted terminal repeats (ITRs) present in the pAAV-MCS vector (Stratagene).

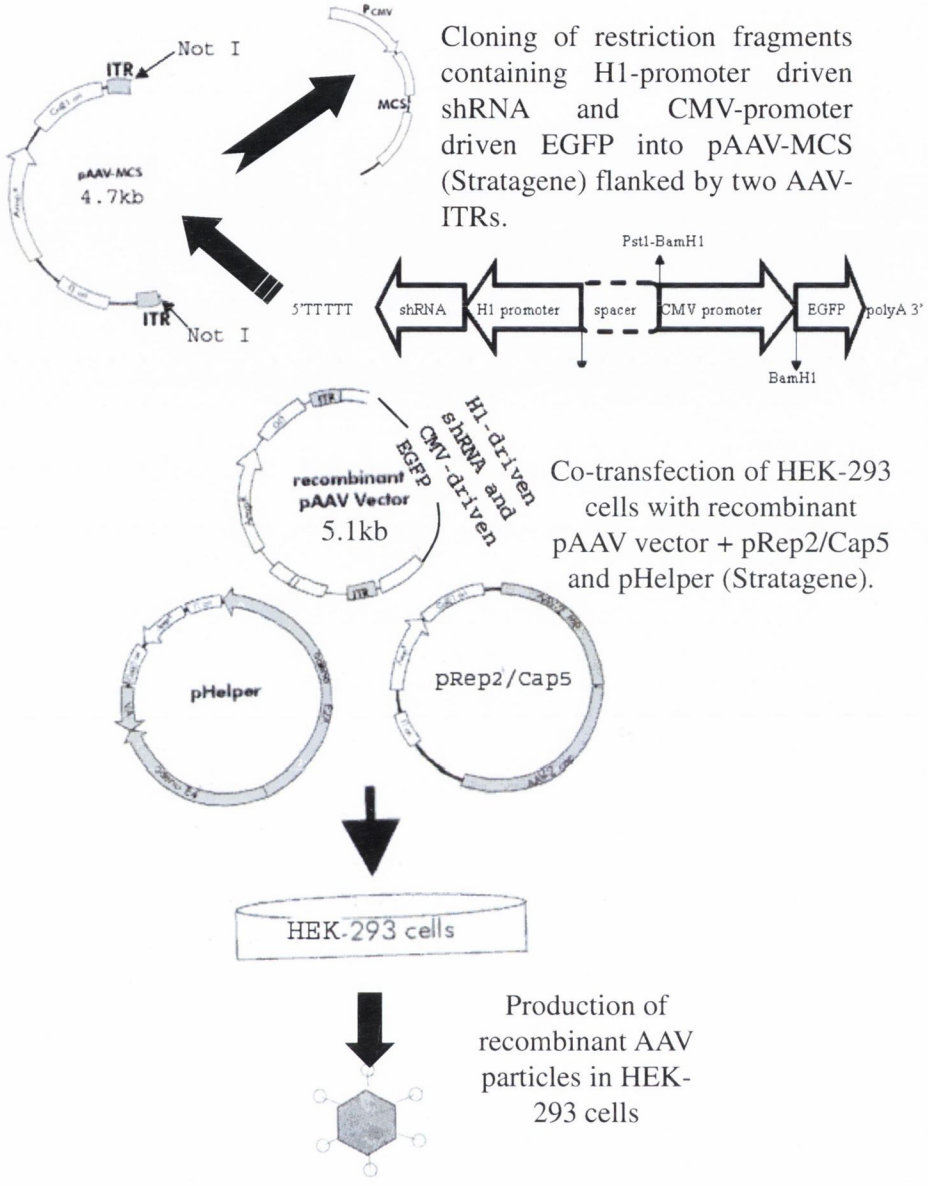

Figure 5.6: A schematic overview of the production of recombinant AAV particles expressing IMPDH1-specific shRNAs. Restriction fragments containing H1-driven shRNA and CMV-driven EGFP were cloned into pAAV-MCS (Stratagene). The ITR sequences present in pAAV-MCS provide all of the *cis*-acting elements necessary for AAV-2 replication and packaging. The recombinant AAV plasmid was co-transfected into HEK-293 cells with pRep2/Cap5 (carrying AAV-2 replication and AAV-5 capsid genes) and pHelper (providing most of the adenovirus gene products required for the production of infective AAV particles, i.e. E2A, E4 and VA RNA genes; Stratagene) at a ratio of 1:1:2. Recombinant AAV-2/5 viral particles were prepared from infected HEK-293 cells and purified by $CsCl_2$ gradient centrifugation.

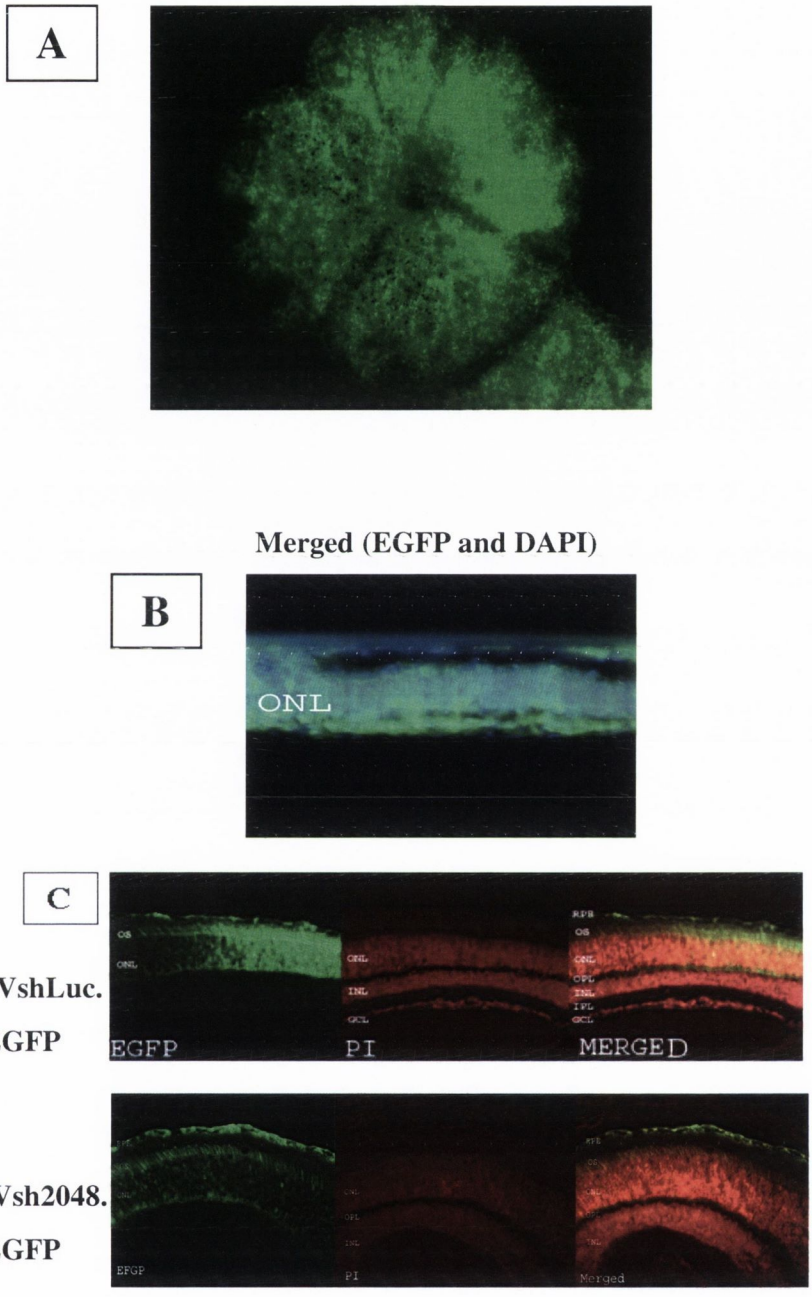

Figure 5.7: (A) A fluorescent image of retinal whole mount prepared from a newborn wild type C57B6/CBA mouse transduced with pAAVsh2048.EGFP for 7 days (Magnification 10X). (B) Vibratome section of retinal explants (50μM thickness) from new born wild type C57B6/CBA mice transduced with pAAVsh2048.EGFP for 7 days (Magnification 40X). PI= Cell nuclei staining with propidium iodide. Merged=PI overlaid with EGFP. **(C)** Cryostat sections of four-week old wild type C57B6/CBA mice (12 μm) subretinally injected with pAAVshLuc.EGFP (top panels) and pAAVsh2048.EGFP (bottom panels) for 4 weeks. (Magnification 40X). Merged=Propidium iodide overlaid with EGFP.

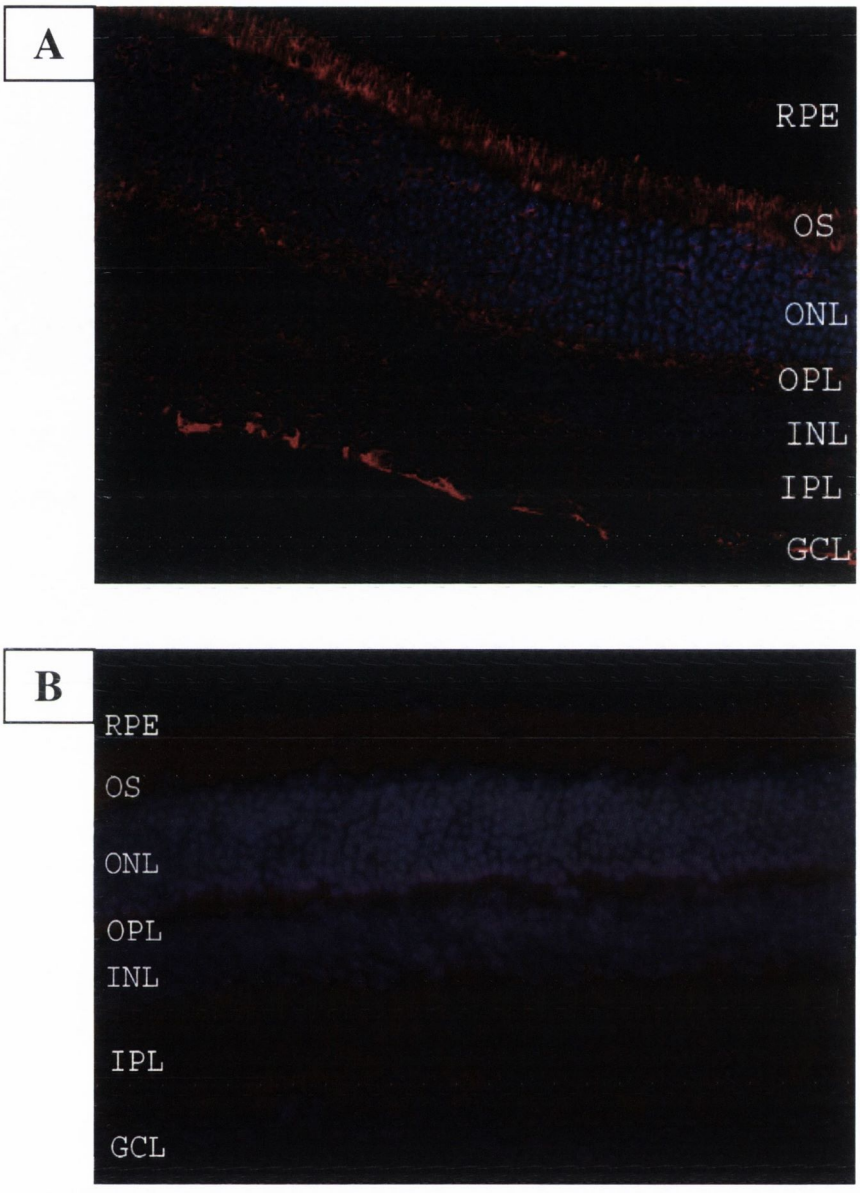

Figure 5.8: (A) Immunolocalisation of IMPDH1 in wild-type C57B6/CBA mouse retina. Frozen fixed retinas were incubated with anti-C-IMPDH1 antibody followed by incubation with Cy3-conjugated goat anti-rabbit secondary antibody (red). Cell nuclei were stained with DAPI (blue). IMPDH1 localised to the retinal pigment epithelium (RPE), outer segment (OS), outer nuclear layer (ONL) adjoining the inner nuclear layer (INL) and ganglion cell layer (GCL). (B) Negative control without anti-C-IMPDH1 primary antibody staining. All fluorescent images were taken with a confocal microscope at 40X magnification (Olympus FU1000, Hamburg, Germany).

A **Group 1**: Four wild type C57B6/CBA mice injected with pAAVshLuc.EGFP (left eyes) and pAAVsh2048.EGFP (right eyes)

(i) Pool of 4 animals (Non-targeting) (ii) Pool of 4 animals (Targeting)

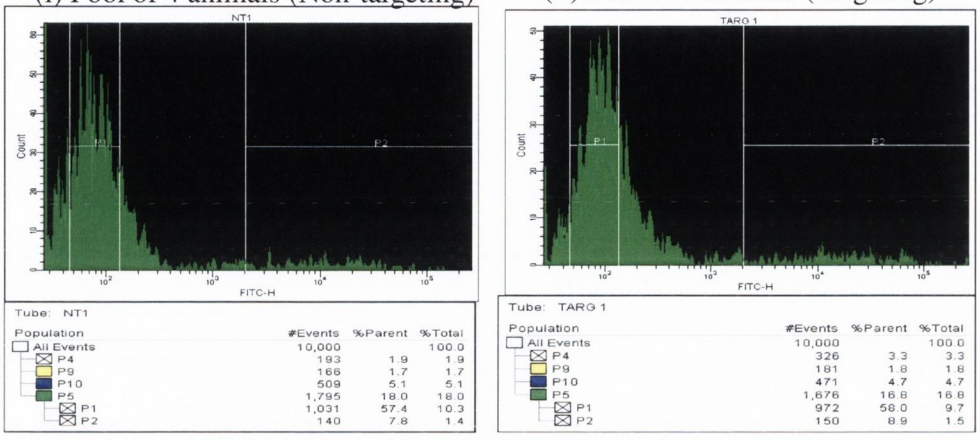

B **Group 2**: Four wild type C57B6/CBA mice injected with pAAVshLuc.EGFP (left eyes) and pAAVsh2048.EGFP (right eyes)

(i) Pool of 4 animals (Non-targeting) (ii) Pool of 4 animals (Targeting)

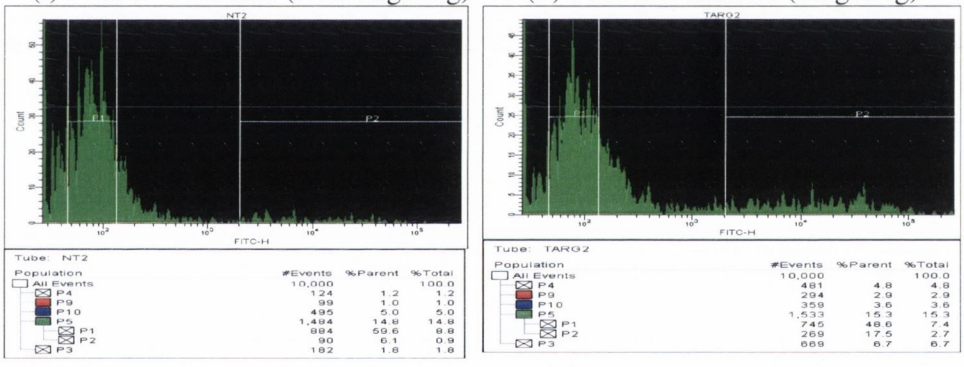

Figure 5.9: Injection #1; FACS analysis of eight 2-weeks old wild type C57B6/CBA mice subretinally injected with 1 µl $1x10^{13}$ vp/ml of pAAVshLuc.EGFP (non-targeting controls) in the left eyes, and 1 µl $2.19x10^{13}$ vp/ml of pAAVsh2048.EGFP in the right eyes. Four animals were pooled per group and dissociated retinas underwent FACS two weeks post-injection. (A) FACS data for the first group of four animals. Histograms of green fluorescence intensity (FITC, x-axis) versus cell number. The boxed area represents population 2 with fluorescence levels above an arbitrary level: (i and ii) 7.8% and 8.9% (P2) of retinal cells injected either with pAAVshLuc.EGFP or pAAVsh2048.EGFP, respectively. (B) FACS data for the second group of four injected C57B6/CBA mice; (i) up to 6.1% (P2) of retinal cells injected with pAAVshLuc.EGFP ;(ii) and 17.5% (P2) of retinal cells injected with pAAVsh2048.EGFP showed EGFP above an arbitrary level. RNA were extracted from these cells for Real Time RT-PCR analysis to determine the level of endogenous murine IMPDH1 mRNA in shRNA-transfected cells as shown in *Figure 5.10*. All parameters required for size fractionation and selection of the arbitrary fluorescence threshold were set by Dr. Alfonso Blanco (Conway Institute, UCD), and the same parameters were used for all other studies involving FACS.

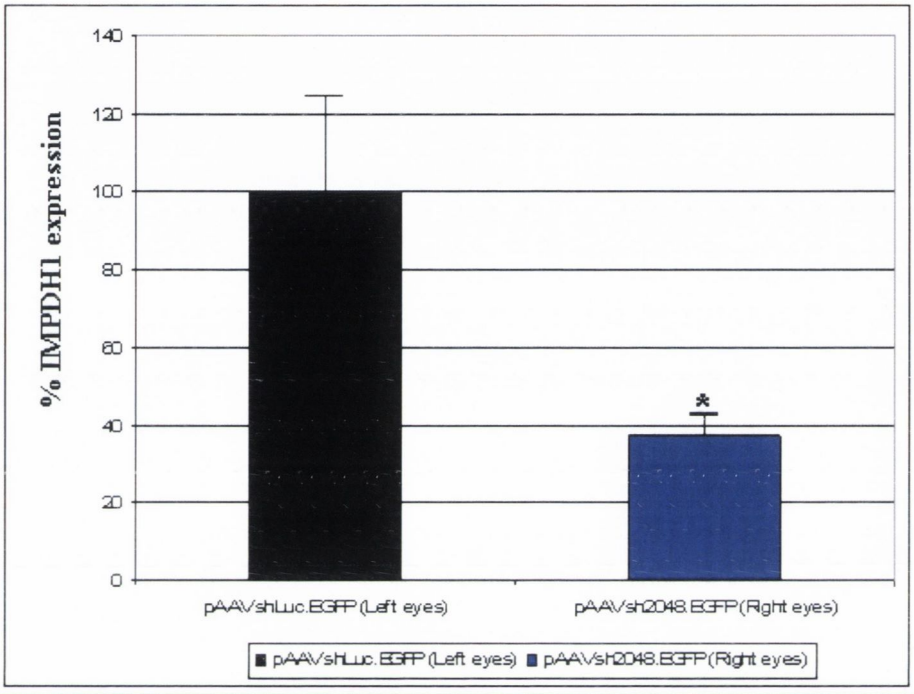

AAV plasmid	pAAVsh2048.EGFP
% IMPDH1 expression ± SEM	37% ± 5.14%

Figure 5.10: Injection #1; AAV-mediated shRNA suppression of IMPDH1 in wild type C57B6/CBA retinas. Eight 2-weeks old wild type C57B6/CBA mice were subretinally injected with 1 µl $1x10^{13}$ vp/ml of pAAVshLuc.EGFP (left eyes) and 1 µl $2.19x10^{13}$ vp/ml of pAAVsh2048.EGFP (right eyes) and FACS sorted two weeks post-injection as described above in *Figure 5.9*. The level of IMPDH1 mRNA expression in each group of four animals was quantified by Real Time RT-PCR analysis and normalised to the house-keeping gene, β-actin. Control AAV-shRNA (pAAVshLuc.EGFP) was standardised to represent 100% IMPDH1 expression (black bar). Histogram of IMPDH1 expression and percentage IMPDH1 expression ± SEM shown here represent the mean of the two groups of 4 injected C57B6/CBA mice (N=8). Y-error bars indicate standard error of the mean (SEM). *=$P<0.05$ The level of IMPDH1 mRNA expression in the pAAVsh2048.EGFP injected retinas was significantly different to that of the non-targeting control ($P<0.05$).

A

Group 1: Three wild type C57B6/CBA mice subretinally injected with pAAVshLuc.EGFP (left eyes) and pAAVsh2048.EGFP (right eyes)

(i) Pool of 3 animals (Non-targeting)

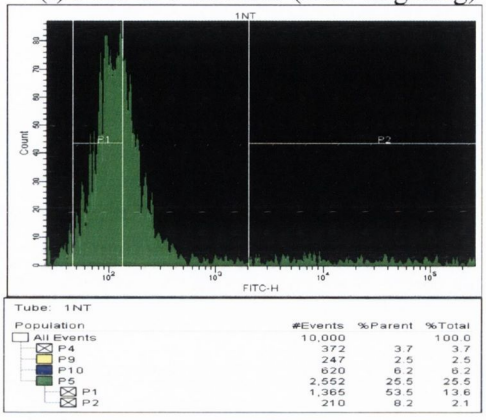

Tube: 1NT

Population	#Events	%Parent	%Total
All Events	10,000		100.0
P4	372	3.7	3.7
P9	247	2.5	2.5
P10	620	6.2	6.2
P5	2,552	25.5	25.5
P1	1,365	53.5	13.6
P2	210	8.2	2.1

(ii) Pool of 3 animals (Targeting)

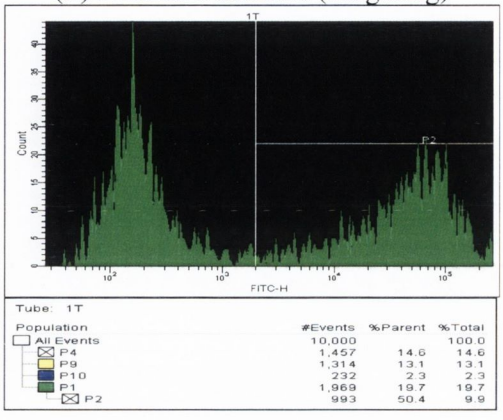

Tube: 1T

Population	#Events	%Parent	%Total
All Events	10,000		100.0
P4	1,457	14.6	14.6
P9	1,314	13.1	13.1
P10	232	2.3	2.3
P1	1,969	19.7	19.7
P2	993	50.4	9.9

B

Group 2: Three wild type C57B6/CBA mice subretinally injected with pAAVshLuc.EGFP (left eyes) and pAAVsh2048.EGFP (right eyes)

(i) Pool of 3 animals (Non-targeting)

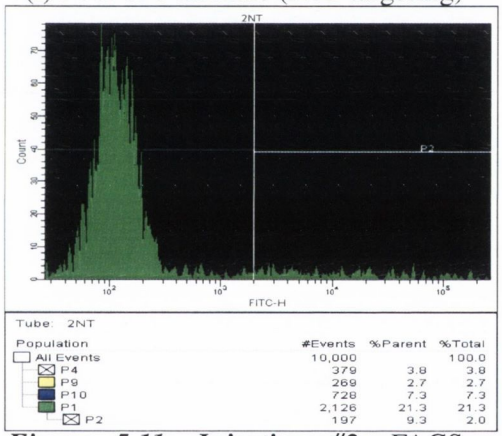

Tube: 2NT

Population	#Events	%Parent	%Total
All Events	10,000		100.0
P4	379	3.8	3.8
P9	269	2.7	2.7
P10	728	7.3	7.3
P1	2,126	21.3	21.3
P2	197	9.3	2.0

(ii) Pool of 3 animals (Targeting)

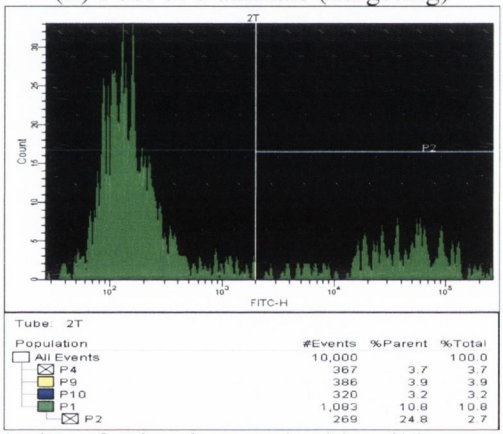

Tube: 2T

Population	#Events	%Parent	%Total
All Events	10,000		100.0
P4	367	3.7	3.7
P9	386	3.9	3.9
P10	320	3.2	3.2
P1	1,083	10.8	10.8
P2	269	24.8	2.7

Figure 5.11: Injection #2; FACS analysis of six 3 month-old wild type C57B6/CBA mice subretinally injected with 3 µl $1x10^{13}$ vp/ml of pAAVshLuc.EGFP (non-targeting controls) in the left eyes, and 3 µl $2.19x10^{13}$ vp/ml of pAAVsh2048.EGFP in the right eyes. Three animals were pooled per group and dissociated retinas underwent FACS four weeks post-injection. (A) FACS data for the first group of three animals. Histograms of green fluorescence intensity (FITC, x-axis) versus cell number. Boxed area represents cells in population 2 with fluorescence levels above an arbitrary level: (i) 8.2% (P2) of retinal cells injected with pAAVshLuc.EGFP; (ii) and 50.4% (P2) of retinal cells injected with pAAVsh2048.EGFP. (B) FACS data for the second group of three injected C57B6/CBA mice; (i) up to 9% (P2) of retinal cells injected with pAAVshLuc.EGFP; (ii) and 25% (P2) of retinal cells injected with pAAVsh2048.EGFP showed EGFP above an arbitrary level. RNA were extracted from these cells for Real Time RT-PCR analysis to determine the level of endogenous murine IMPDH1 mRNA in shRNA-transduced cells as shown in *Figure 5.12*.

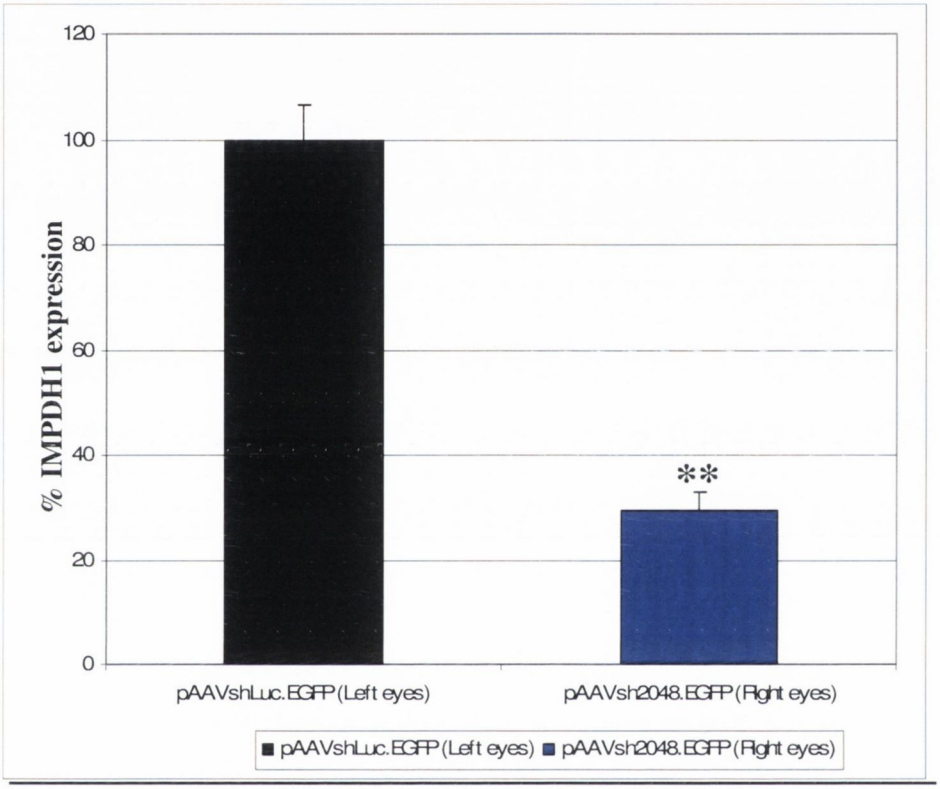

AAV plasmid	pAAVsh2048.EGFP
% IMPDH1 expression ± SEM	29% ± 3.56%

Figure 5.12*: *Injection #2; AAV-mediated suppression of IMPDH1 in six 3-month-old wild type C57B6/CBA mice subretinally injected with 3µl $1x10^{13}$vp/ml of pAAVshLuc.EGFP (left eyes) and 3 µl $2.19x10^{13}$ vp/ml of pAAVsh2048.EGFP (right eyes). Two groups of three injected mice were separately FACS sorted as described above in *Figure 5.11*. The level of IMPDH1 mRNA expression in each group of three mice was quantified by Real Time RT-PCR analysis and normalised to the house-keeping gene, β-actin. Control AAV-shRNA (pAAVshLuc.EGFP) was standardised to represent 100% IMPDH1 expression (black bar). Histogram of IMPDH1 expression and percentage IMPDH1 expression ± SEM shown here represent the mean of the two groups of three injected mice (N=6). Y-error bars indicate standard error of the mean (SEM). **=P ≤ 0.0001. The level of IMPDH1 mRNA expression in the pAAVsh2048.EGFP injected retinas was significantly different to that of the non-targeting control (P≤0.0001).

A

Group 1: Three wild type C57B6/CBA mice injected with pAAVshLuc.EGFP (left eyes) and pAAVsh2048.EGFP (right eyes)

(i) Pool of 3 animals (Non-targeting)

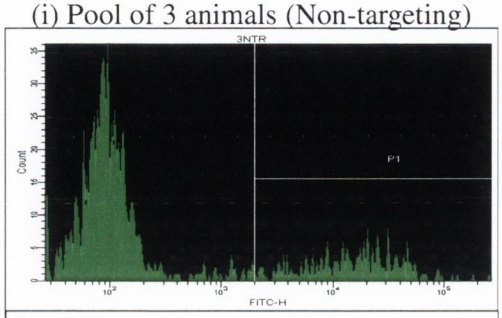

Tube: 3NTR

Population	#Events	%Parent	%Total
All Events	10,000		100.0
P4	583	5.8	5.8
P9	330	3.3	3.3
P10	395	4.0	4.0
P3	1,034	10.3	10.3
P1	233	22.5	2.3

(ii) Pool of 3 animals (Targeting)

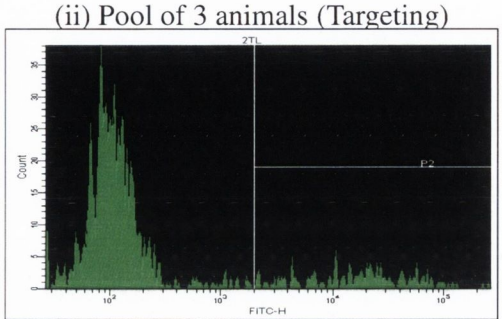

Tube: 2TL

Population	#Events	%Parent	%Total
All Events	10,000		100.0
P4	473	4.7	4.7
P9	246	2.5	2.5
P10	439	4.4	4.4
P1	952	9.5	9.5
P2	158	16.6	1.6

B

Group 2: Three wild type C57B6/CBA mice injected with pAAVshLuc.EGFP (left eyes) and pAAVsh2048.EGFP (right eyes)

(i) Pool of 3 animals (Non-targeting)

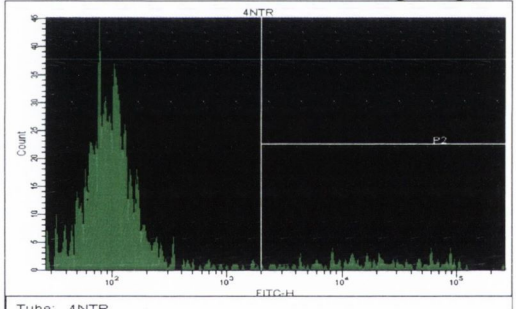

Tube: 4NTR

Population	#Events	%Parent	%Total
All Events	10,000		100.0
P4	270	2.7	2.7
P9	174	1.7	1.7
P10	462	4.6	4.6
P1	1,018	10.2	10.2
P2	115	11.3	1.2

(ii) Pool of 3 animals (Targeting)

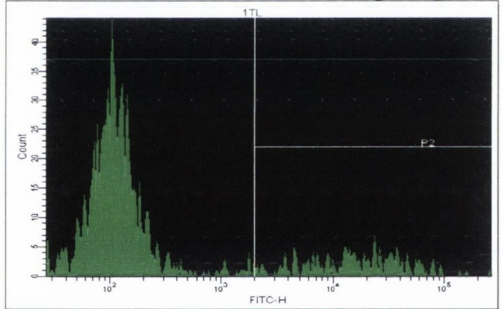

Tube: 1TL

Population	#Events	%Parent	%Total
All Events	10,000		100.0
P4	513	5.1	5.1
P9	270	2.7	2.7
P10	339	3.4	3.4
P1	1,116	11.2	11.2
P2	213	19.1	2.1

Figure 5.13: Injection #3; FACS analysis of six 2 week-old wild type C57B6/CBA mice subretinally injected with 1 µl $1x10^{13}$ vp/ml of pAAVshLuc.EGFP (left eyes), and 1 µl $2.19x10^{13}$ vp/ml of pAAVsh2048.EGFP (right eyes). Three animals were pooled per group and dissociated retinas underwent FACS four weeks post-injection. (A) FACS data for the first group of three animals. Histograms of green fluorescence intensity (FITC, x-axis) versus cell number. (i) 22.5% (P1) of retinal cells injected with pAAVshLuc.EGFP and (ii) 16.6% of retinal cells injected with pAAVsh2048.EGFP expressed EGFP above the threshold. (B) FACS data for the second group of three injected mice: (i) 11.3% (P2) of retinal cells injected with pAAVshLuc.EGFP and (ii) 19.1% (P2) of retinal cells injected with pAAVsh2048.EGFP showed EGFP above an arbitrary level. RNA were extracted from these cells for Real Time RT-PCR analysis to determine the level of endogenous murine IMPDH1 mRNA in shRNA-transduced cells as shown in *Figure 5.14*.

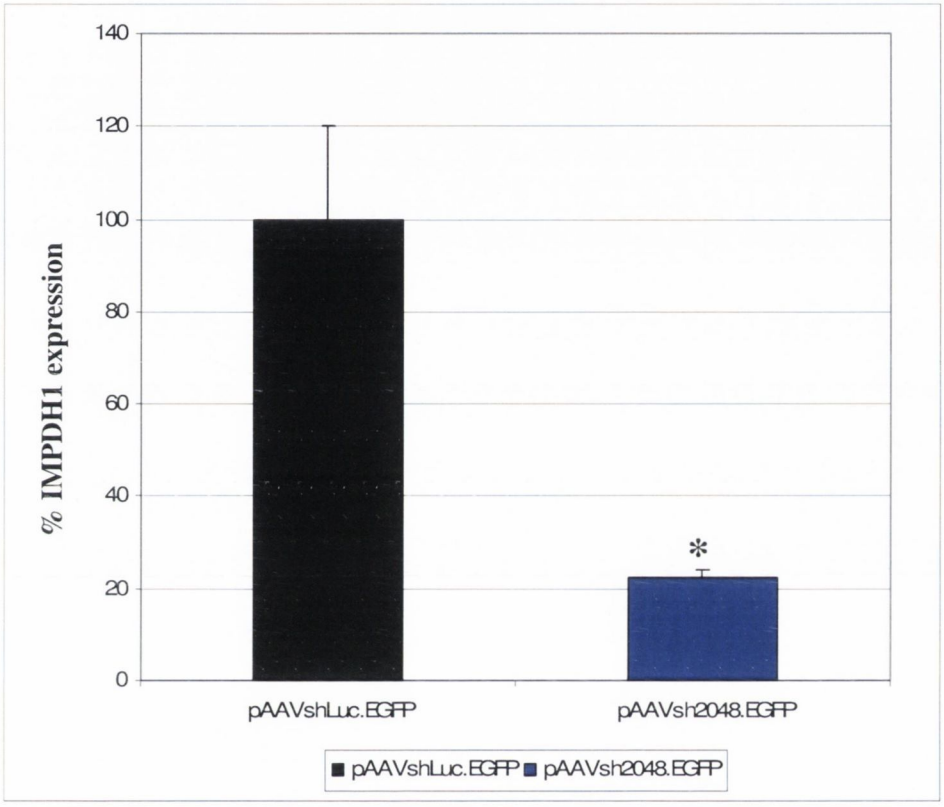

AAV plasmid	pAAVsh2048.EGFP
% IMPDH1 expression ± SEM	22% ± 1.5 %

Figure 5.14: Injection #3; AAV-mediated suppression of IMPDH1 in six 2-weeks old wild type C57B6/CBA mice subretinally injected with 1 µl $1x10^{13}$ vp/ml of pAAVshLuc.EGFP (left eyes) and 1 µl $2.19x10^{13}$ vp/ml of pAAVsh2048.EGFP (right eyes). Two groups of three injected mice were separately FACS sorted as described above in *Figure 5.13*. The level of IMPDH1 mRNA expression in each group of three mice was quantified by Real Time RT-PCR analysis and normalised to the house-keeping gene, β-actin. Control AAV-shRNA (pAAVshLuc.EGFP) was standardised to represent 100% IMPDH1 expression (black bar). Histogram of percentage IMPDH1 expression and percentage IMPDH1 expression ± SEM shown here represent the mean of the two groups of three injected mice (N=6). Y-error bars indicate standard error of the mean (SEM). *=$P<0.05$. The level of IMPDH1 mRNA expression in the pAAVsh2048.EGFP injected retinas was significantly different to that of the non-targeting control ($P=0.0271$).

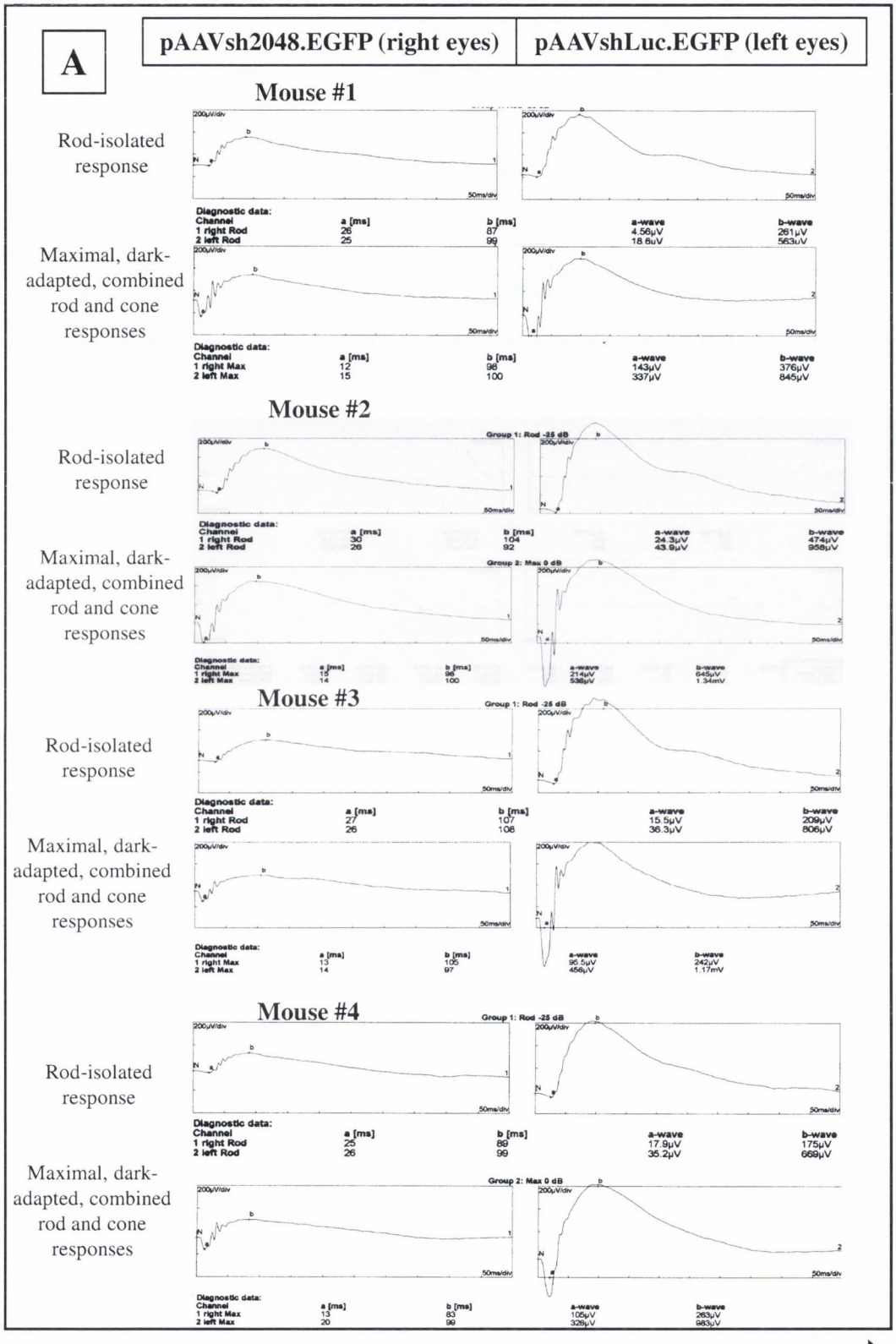

Figure 5.15 **continued**

B

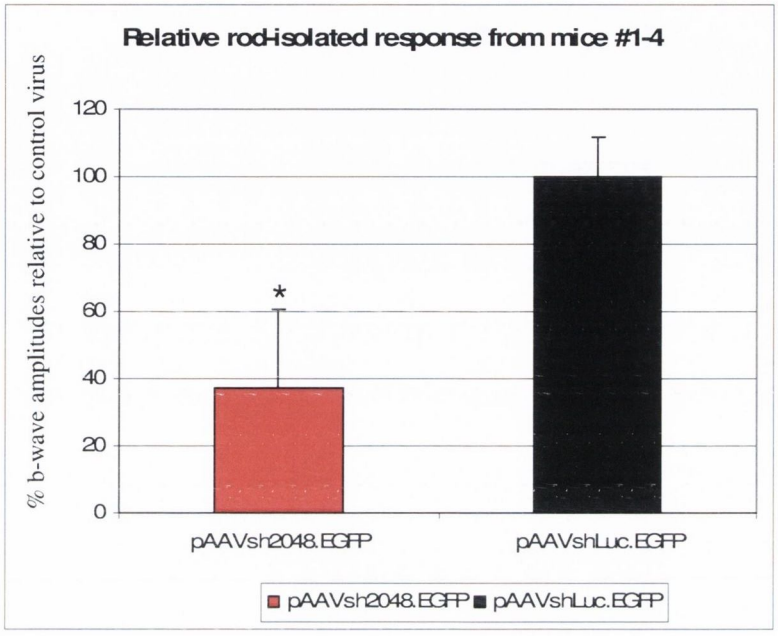

C

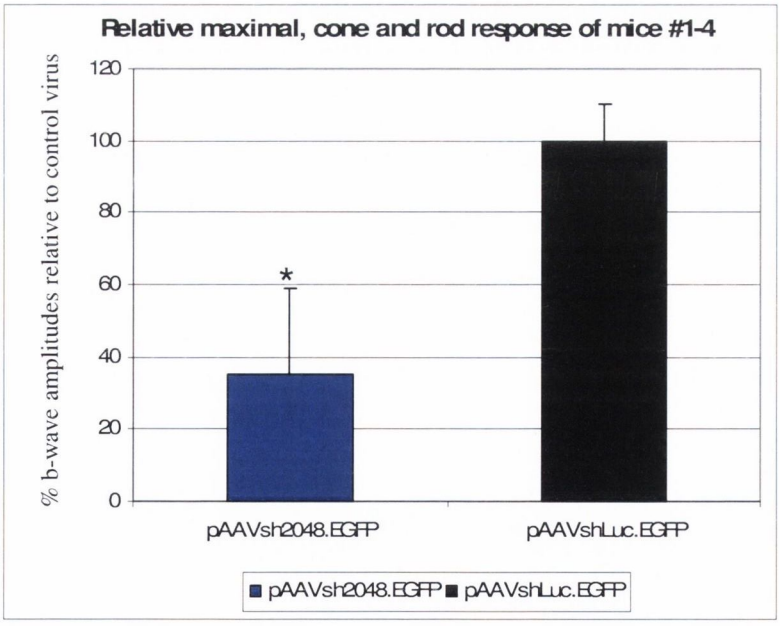

Figure 5.15 **continued**

Group 1: Combination of Mouse #1 and 2

(i) Pool of 2 mice (AAV-shLuc) (ii) Pool of two mice (AAV-sh2048)

D

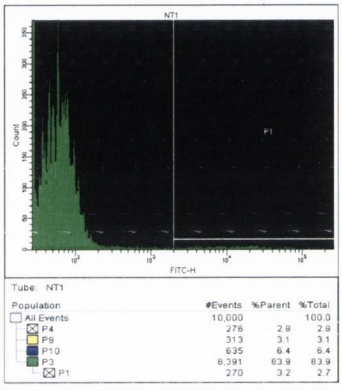

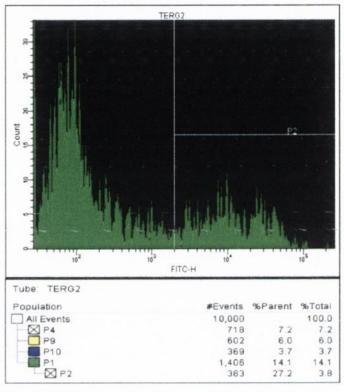

Group 2: Combination of Mouse #3 and 4

(i) Pool of 2 mice (AAV-shLuc) (ii) Pool of two mice (AAV-sh2048)

E

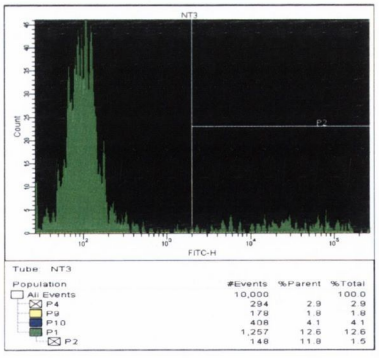

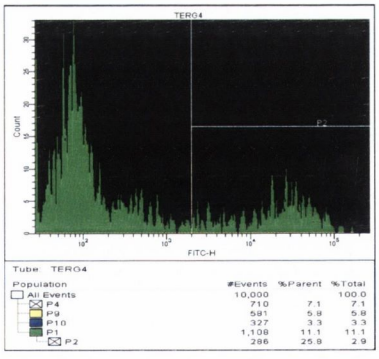

***Figure 5.15* continued**

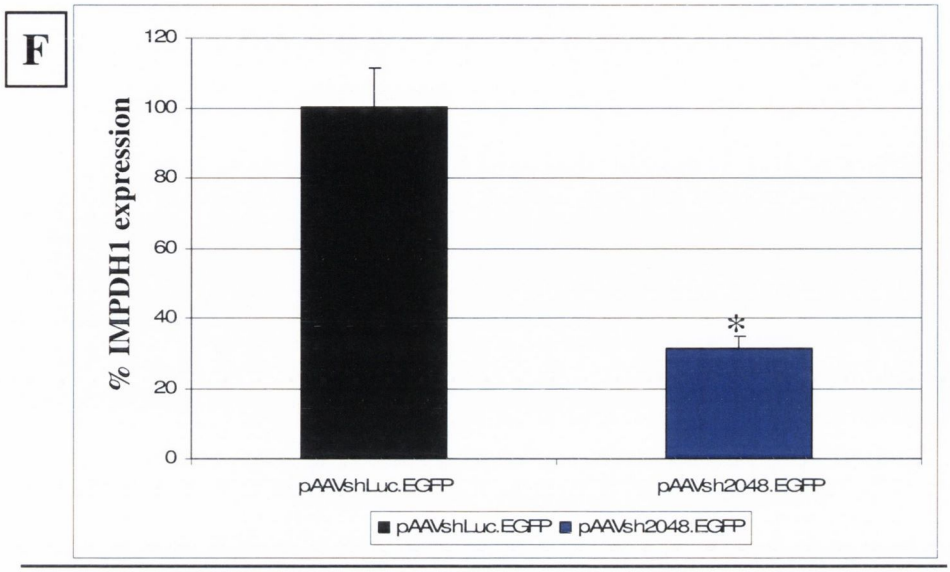

AAV plasmid	pAAVsh2048.EGFP
% IMPDH1 expression ± SEM	32% ± 3.5%

Figure 5.15; Injection #4: *In-vivo* suppression of IMPDH1 transcripts. (A) ERG analysis in wild type C57B6/CBA mice. Rod-isolated response and maximal, dark-adapted combined rod and cone responses were recorded in four 4-months old wild type C57B6/CBA (designated as Mouse # 1, 2, 3, 4) four weeks after subretinal injection with 3 µl of pAAVshLuc.EGFP (left eyes) and pAAVsh2048.EGFP (right eyes) at equal concentrations ($6.85x10^{12}$ vp/ml). (B) Histograms illustrate percentage rod-isolated b-wave amplitudes of AAV-sh2048 injected eyes in Mouse #1, 2, 3 and 4 against AAV-shLuc injected eyes normalised to represent 100% (black bars). Y-error bars denote standard error of the mean (SEM). *P<0.05. (C) Histograms illustrate percentage maximal, rod and cone b-wave amplitudes of AAV-sh2048 injected eyes in Mouse #1, 2, 3 and 4 against AAV-shLuc injected eyes normalised to represent 100% (black bars). Y-error bars denote SEM. *P<0.05. (D) FACS analysis of Mouse #1, 2, 3, 4. Dissociated retinas from group 1 (Mouse #1 and 2) were pooled together for FACS sorting. (i) 3.2% (P2) of retinal cells were positively transduced with pAAVshLuc.EGFP and (ii) 27.2% (P2) were transduced by pAAVsh2048.EGFP. (E) Dissociated retinas from group 2 (mouse #3 and 4) were pooled together for FACS analysis. (i) 11.8% (P2) were transduced with pAAVshLuc.EGFP; and (ii) 25.8% with pAAVsh2048.EGFP. (F) Following FACS analysis, the level of IMPDH1 mRNA expression in group 1 (Mouse #1 and 2) and group 2 (Mouse #3 and 4) was quantified by Real Time RT-PCR analysis and normalised to the house-keeping gene, β-actin. Control AAV-shLuc was standardised to represent 100% IMPDH1 expression (black bar). The histogram of percentage IMPDH1 expression and percentage IMPDH1 expression ± SEM shown here represent the mean of the two groups (N=4). Y-error bars indicate standard error of the mean (SEM). *P<0.05. The level of IMPDH1 mRNA expression in the pAAVsh2048.EGFP injected retinas was significantly different to that of the non-targeting control (P<0.001).

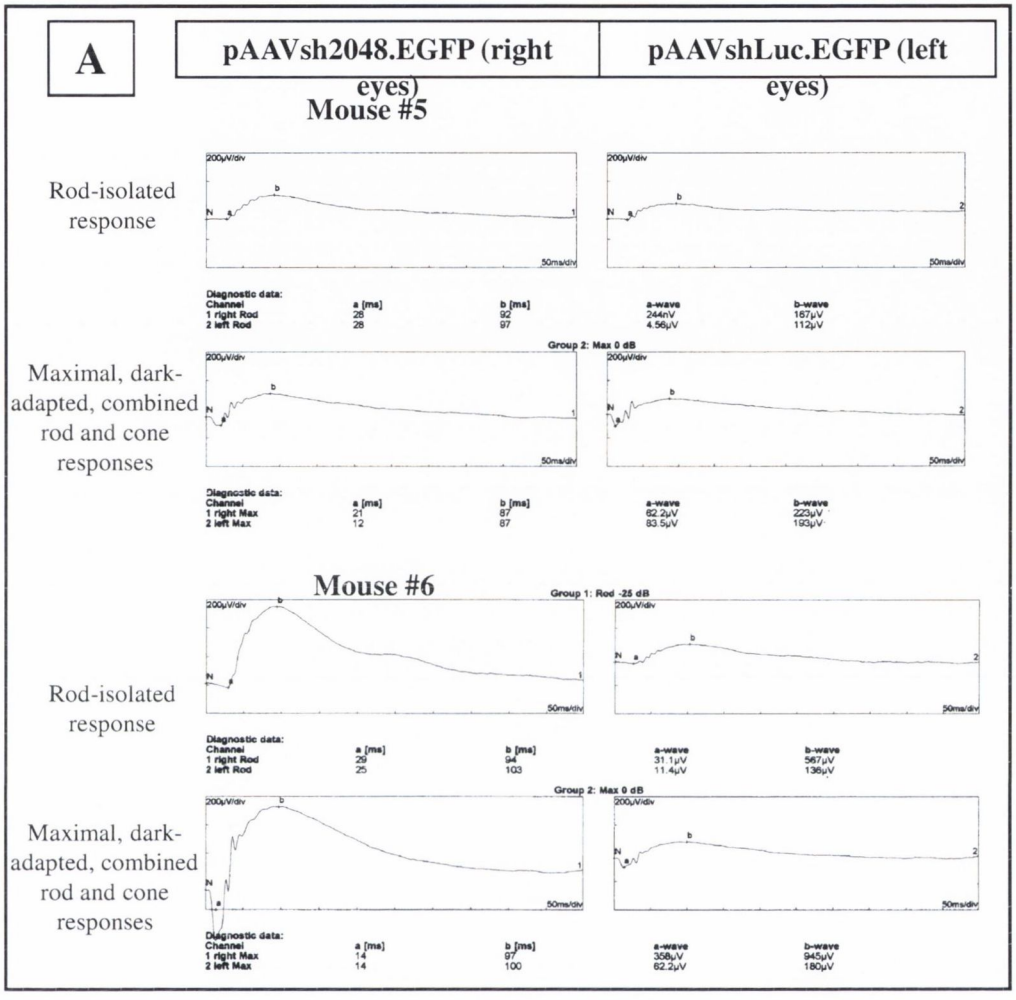

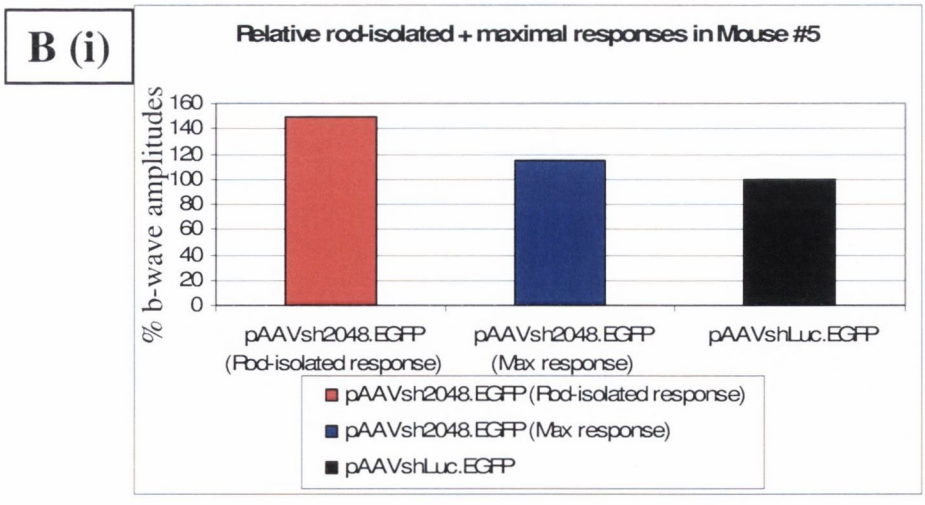

Figure 5.16 **continued**

B (ii)

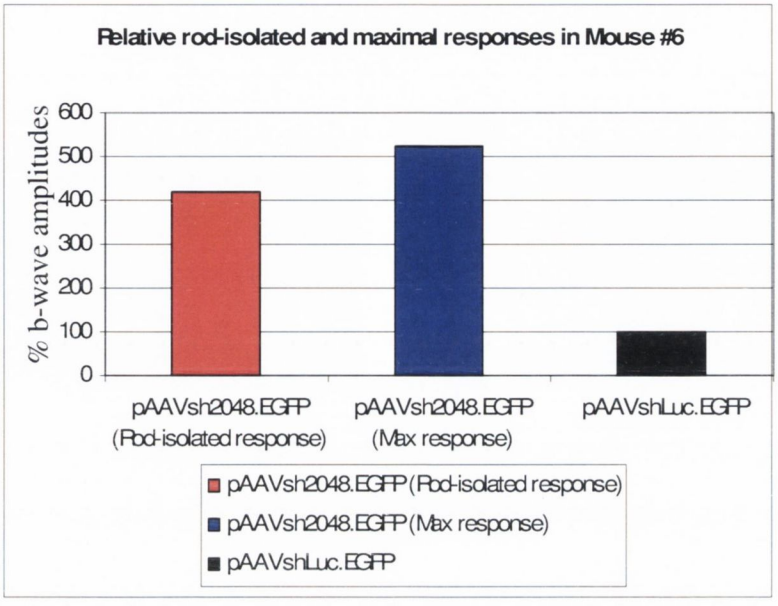

Mouse #5

C (i)

(i) pAAVshLuc.EGFP

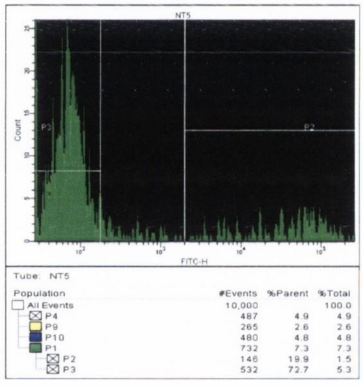

(ii) pAAVsh2048.EGFP

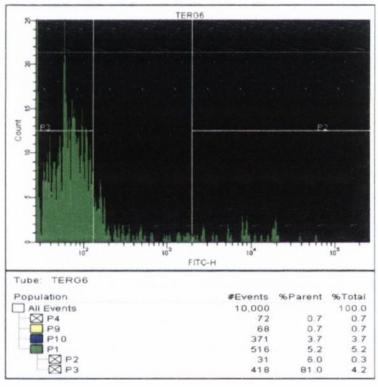

Mouse #6

C (ii)

(i) pAAVshLuc.EGFP

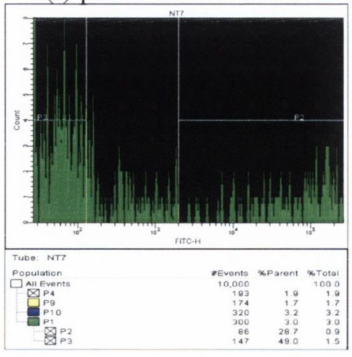

(ii) pAAVsh2048.EGFP

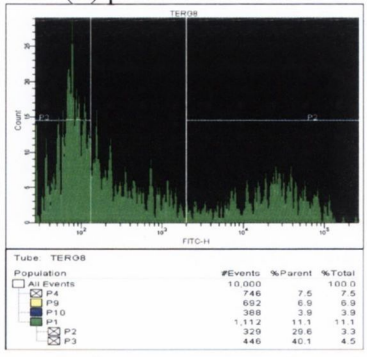

Figure 5.16 **continued**

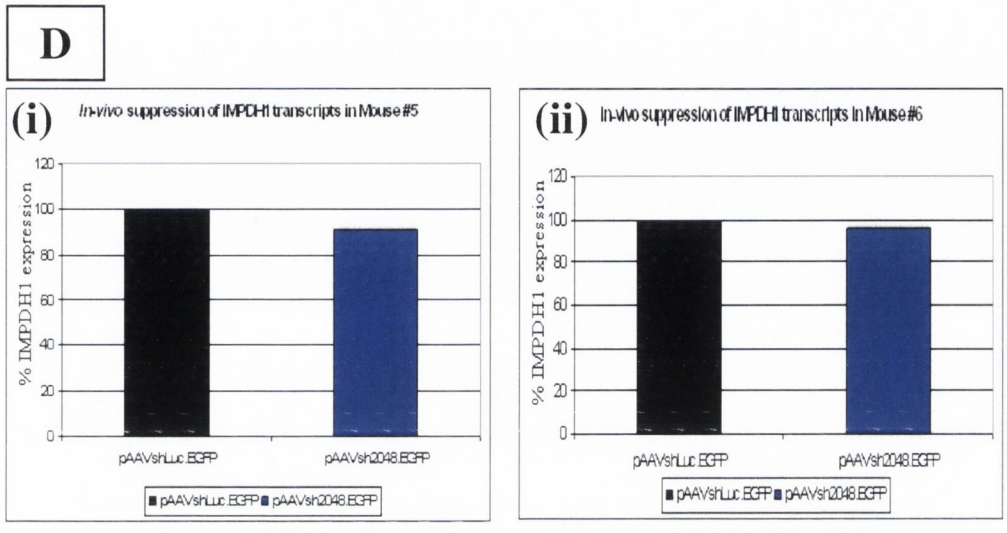

Figure 5.16; Injection 4: (A) ERG analysis in wild type C57B6/CBA mice. Rod-isolated responses and maximal, dark-adapted combined rod and cone responses were recorded in two 4-months old wild type C57B6/CBA (designated as Mouse #5 and 6) four weeks after subretinal injection with 3 µl of pAAVshLuc.EGFP (left eyes) and pAAVsh2048.EGFP (right eyes) at equal concentrations ($6.85x10^{12}$ vp/ml). (B) Histograms illustrate percentage of rod-isolated and maximal b-wave amplitudes in AAV-sh2048 injected eyes of Mouse (i) # 5 and (ii) #6 against AAV-shLuc injected eyes normalised to represent 100% (black bars). (C) FACS analysis (i) Up to 19.9% and 6% (P2) of retinal cells were transduced with pAAVshLuc.EGFP and pAAVsh2048.EGFP, respectively, in Mouse #5. (ii) 28.7% and 29.6% (P2) of retinal cells were transduced with pAAVshLuc.EGFP and pAAVsh2048.EGFP, respectively, in Mouse #6. RNA was extracted from these cells for Real Time RT-PCR analysis to determine the level of endogenous murine IMPDH1 mRNA. (D) Following FACS analysis, the levels of IMPDH1 mRNA expression in (i) Mouse #5 and (ii) Mouse #6 were quantified by Real Time RT-PCR analysis and normalised to the house-keeping gene, β-actin. Control AAV-shLuc was standardised to represent 100% IMPDH1 expression (black bar).

				FACS analysis		RT-PCR analysis
	Age of Animals	Incubation period		% AAV retinal transduction		Pooled effect
Injection #1				pAAVsh2048.EGFP (Right eyes)	pAAVshLuc.EGFP (Left eyes)	% IMPDH1 suppression ± SD
(n=8)	2 weeks	2 weeks	Group 1 (n=4)	9%	9%	63% ± 5%
			Group 2 (n=4)	17.50%	6%	
Injection #2				pAAVsh2048.EGFP	pAAVshLuc.EGFP	% IMPDH1 suppression ± SD
(n=6)	3 months	4 weeks	Group 1 (n=3)	50%	8%	71% ± 9%
			Group 2 (n=3)	25%	9%	
Injection #3				pAAVsh2048.EGFP	pAAVshLuc.EGFP	% IMPDH1 suppression ± SD
(n=6)	2 weeks	4 weeks	Group 1 (n=3)	17%	23%	78% ± 3%
			Group 2 (n=3)	19%	11%	
Injection #4	mice #1-4			pAAVsh2048.EGFP	pAAVshLuc.EGFP	% IMPDH1 suppression ± SD
(n=4)	4 months	4 weeks	Group 1 (n=2)	26%	3%	68% ± 9%
			Group 2 (n=2)	26%	12%	
Injection #4	mouse #5 and #6			pAAVsh2048.EGFP	pAAVshLuc.EGFP	% IMPDH1 suppression ± SD
(n=2)	4 months	4 weeks	mouse #5	6%	20%	9%
			mouse #6	30%	29%	4%

Table 5.17: A summary of FACS analyses data and corresponding % IMPDH1 mRNA suppression obtained from the four separate injection experiments described above.

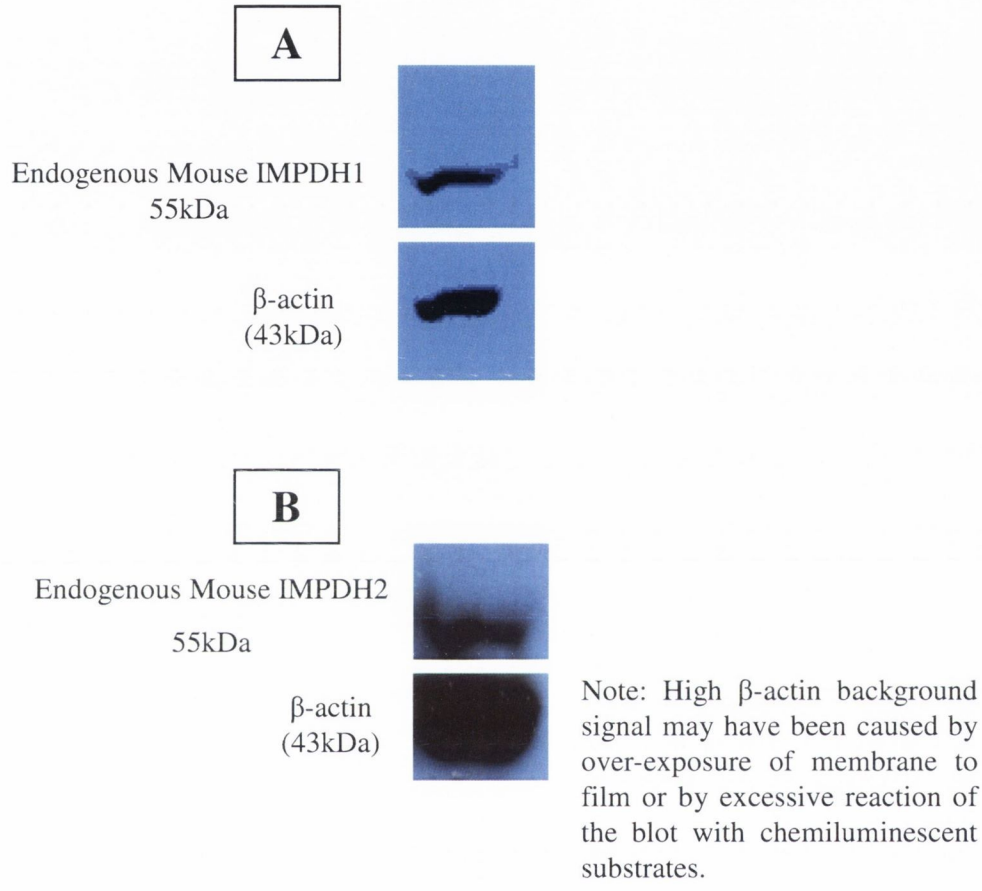

Figure 5.18: Detection of endogenous mouse IMPDH1 and IMPDH2 proteins in wild type C57CBA/B6 mouse retinas. Protein was extracted from three adult wild type C57CBA/B6 mouse retinas and pooled together for western blot analysis using; (A) anti-N-IMPDH1 antibody for the detection of IMPDH1 protein; and (B) anti-N-IMPDH2 for the detection of IMPDH2 protein.

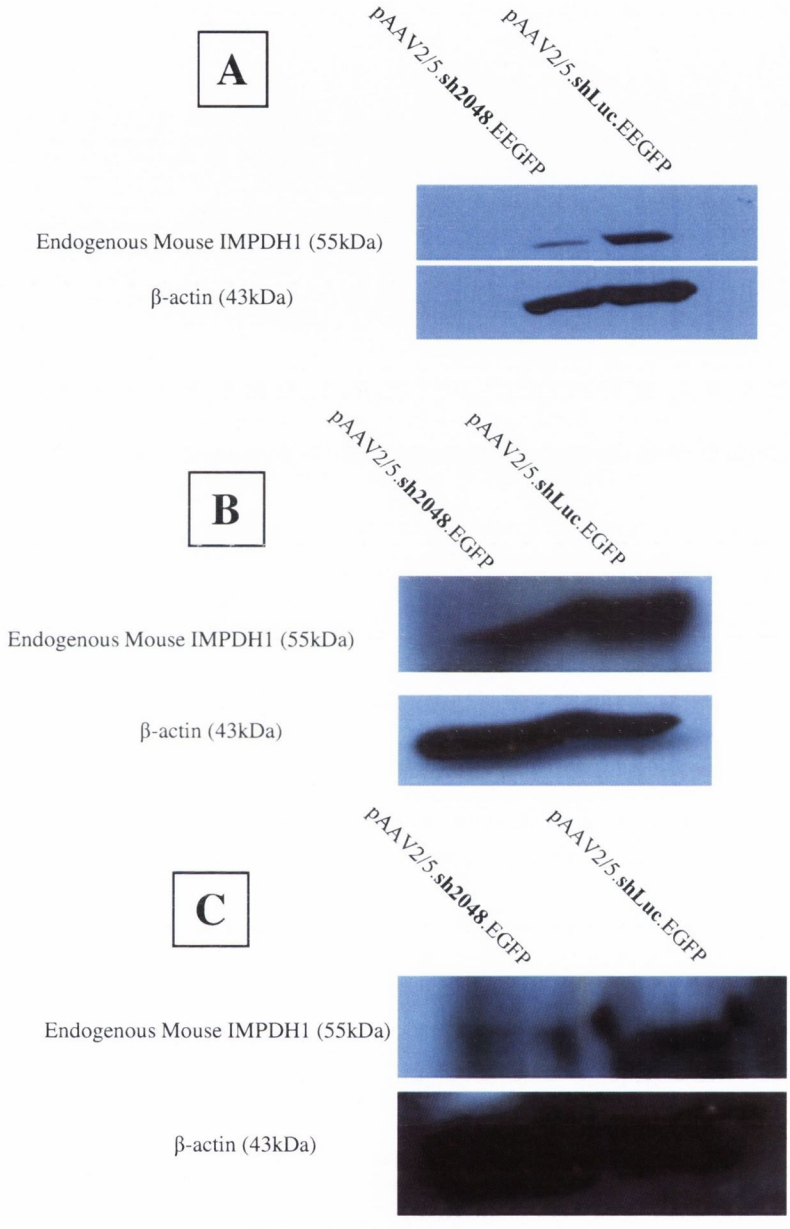

Note: High IMPDH1 and β-actin backgrounds signal may have been caused by over-exposure of membrane to film or insufficient washing protocols. However, the top panel clearly demonstrated rAAV-shRNA-mediated suppression of IMPDH1.

Figure 5.19 **continued**

D

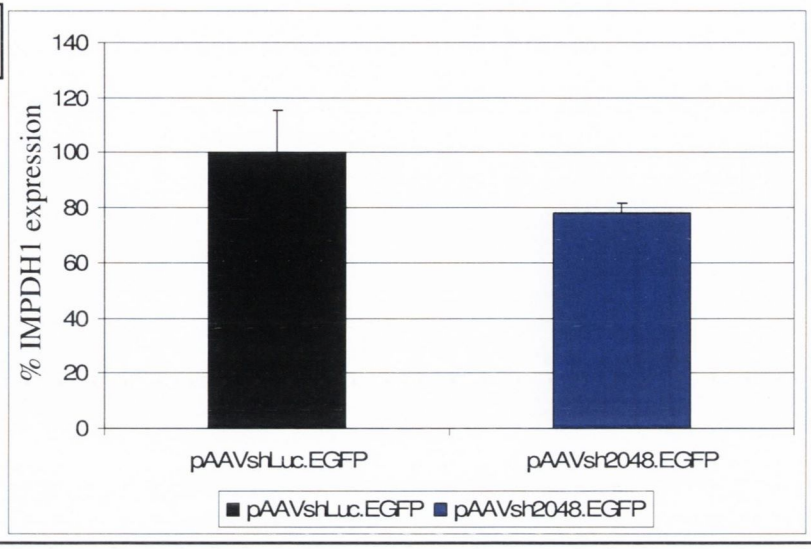

Densitometry (Band Intensity)	pAAVshLuc.EGFP	pAAVsh2048.EGFP
% IMPDH1 expression ± SEM	100% ± 15%	78% ± 3.34%

Figure 5.19: Western blot analysis of AAV-mediated shRNA suppression of IMPDH1 protein in wild type C57CBA/B6 mouse retinas. (A) Three 2-months old wild type C57B6/CBA mice were subretinally injected with 3 µl $1x10^{13}$ vp/ml pAAVshLuc.EGFP (left eyes) and 3 µl $2x10^{13}$ vp/ml pAAVsh2048.EGFP (right eyes). One week post-injection, a second subretinal injection was administered in a different region of the retina with the same volume and concentration of AAV suppressors as before. Four weeks after the second injection, retinas were dissected from the animals, and left and right eyes were pooled into separate samples. (B) In a second experiment, three 4-months old wild type C57B6/CBA mice were subretinally injected with 3 µl of pAAVshLuc.EGFP and pAAVsh2048.EGFP at equal concentrations ($6.85x10^{12}$ vp/ml). One week post-injection, a second subretinal injection was administered in a different region of the retina with the same volume and concentration of AAV suppressors as before. Four weeks after the second injection, retinas were dissected from the animals, and left and right eyes were pooled into separate samples. (C) In the third experiment, four 4-months old wild type C57B6/CBA mice were subretinally injected with 3 µl of pAAVshLuc.EGFP and pAAVsh2048.EGFP at equal concentrations ($6.85x10^{12}$ vp/ml). One week post-injection, a second subretinal injection was administered in a different region of the retina with the same volume and concentration of AAV suppressors as before. Four weeks after the second injection, retinas were dissected from the animals, and left and right eyes were pooled into separate samples. All IMPDH1 protein was detected using anti-N-IMPDH1 antibody, and the same blot was stripped and re-probed with β-actin as loading control. (D) Quantification of band intensities from western blots. The histogram illustrates the average band intensity of three independent experiments from (A), (B) and (C) (n=10). Percentage IMPDH1 expression in band intensity for IMPDH1 was calculated relative to that resulting from the control to represent 100% IMPDH1 expression (black bar), and normalised against β-actin. The panel below gives the percentage of IMPDH1 expression based on band intensity ± SEM. Y-error bar denotes standard error of the mean (SEM).

A

Wild-type C57CBA/B6 subretinally injected with pAAVshLuc.EGFP (left eyes)

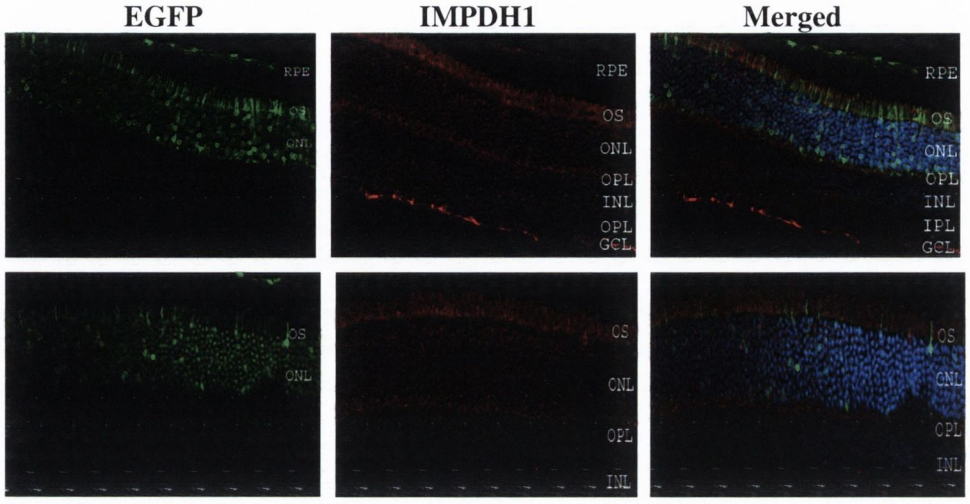

B

Wild type C57B6/CBA subretinally injected with pAAVsh2048.EGFP (right eyes)

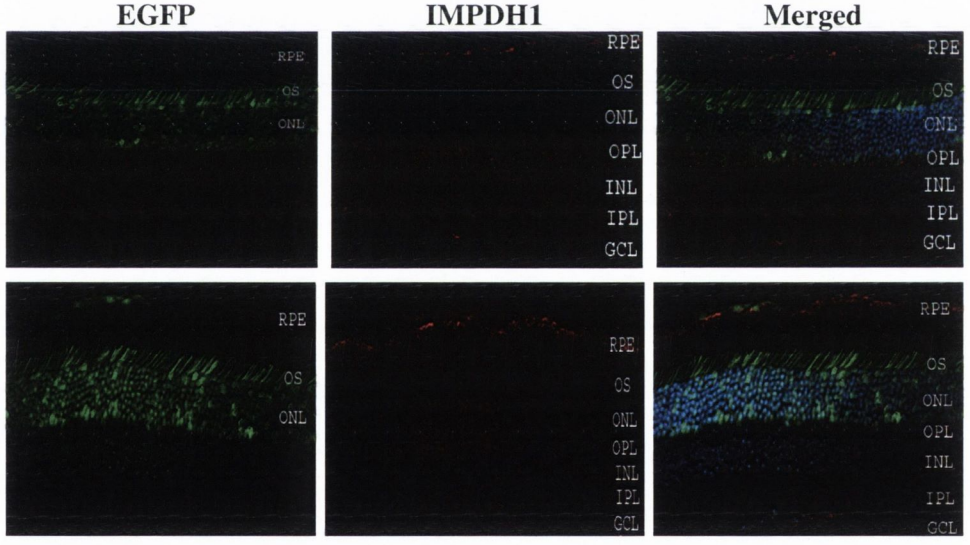

Figure 5.20: Immunohistochemical analysis of AAV-mediated shRNA suppression of IMPDH1 in wild type C57B6/CBA mouse retinas. Two 1-month old wild type C57B6/CBA mice were subretinally injected with (A) 3 µl of pAAVshLuc.EGFP (left eyes) and (B) 3 µl of pAAVsh2048.EGFP (right eyes) at equal concentrations ($6.85x10^{12}$ vp/ml). Four weeks post-injection, retinas were dissected and frozen in OCT for cryostat sectioning. Frozen fixed retinal sections (at 12 µm thickness) were incubated with anti-C-IMPDH1 antibody followed by further incubation with Cy-3 conjugated anti-rabbit IgG secondary antibody (red). Cell nuclei were stained with DAPI (blue) as appeared in merged photographs. Fluorescence images were captured using confocal microscopy (Olympus FU1000) at 40X magnification, and represent two independent injected mice.

A (i)

Wild type C57B6/CBA mice (Mouse #1 and 2) subretinally injected with pAAVshLuc.EGFP (left eyes) and dissected four-weeks post injection

Merged; EGFP+DAPI+IMPDH1; (40X Magnification)

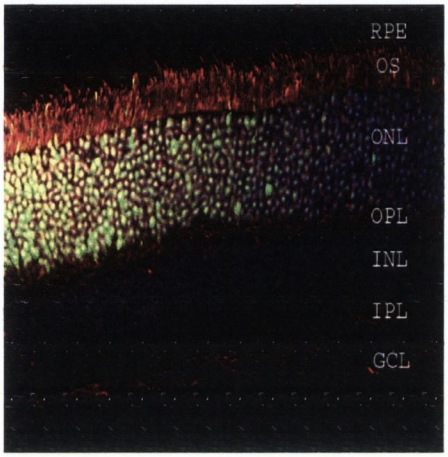

Merged; EGFP+DAPI+IMPDH1; (60X Magnification)

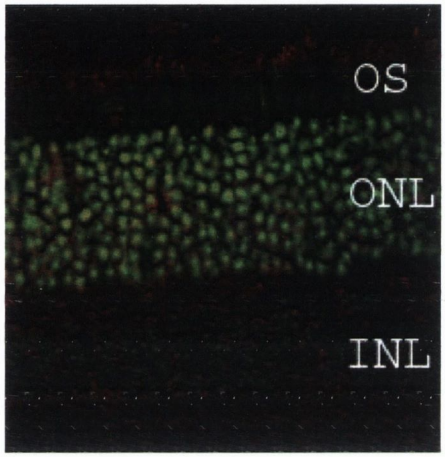

A (ii)

Wild type C57B6/CBA (Mouse #1 and 2) subretinally injected with pAAVsh2048.EGFP (right eyes) and dissected four weeks post injection

Merged; EGFP+DAPI+IMPDH1 (40X Magnification)



Merged; EGFP+DAPI+IMPDH1 (60X Magnification)



Figure 5.21 **continued**

B (i) **Wild type C57B6/CBA (Mouse #3) subretinally injected with pAAVshLuc.EGFP (left eye) and dissected four months post-injection.**

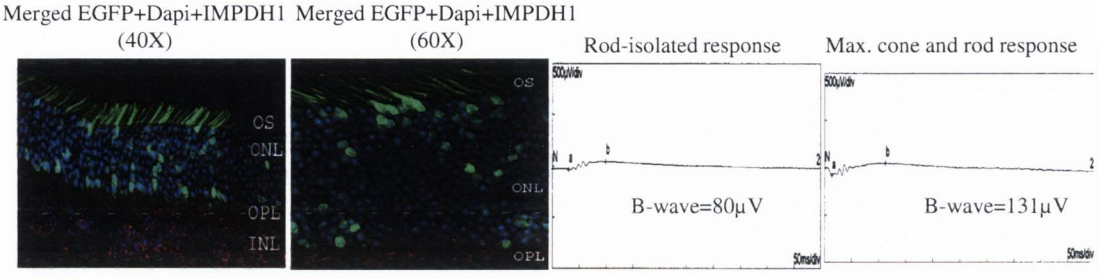

B (ii) **Wild type C57B6/CBA (Mouse #3) subretinally injected with pAAVsh2048.EGFP (right eye) and dissected four months post-injection**

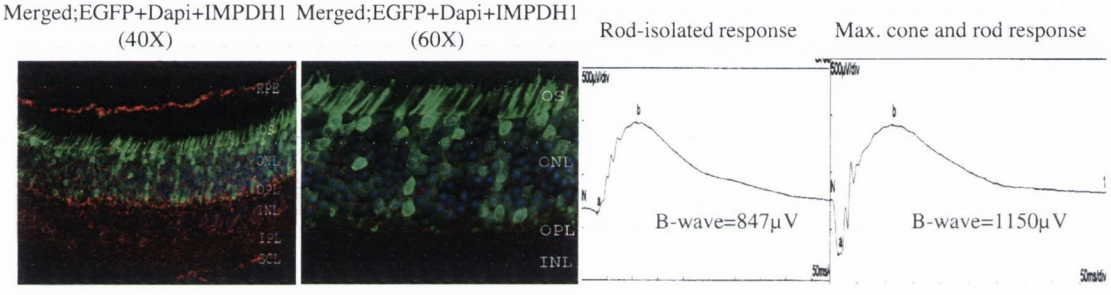

C (i) **Wild type C57B6/CBA (Mouse #4) subretinally injected with pAAVshLuc.EGFP (left eye) and dissected four months post-injection**

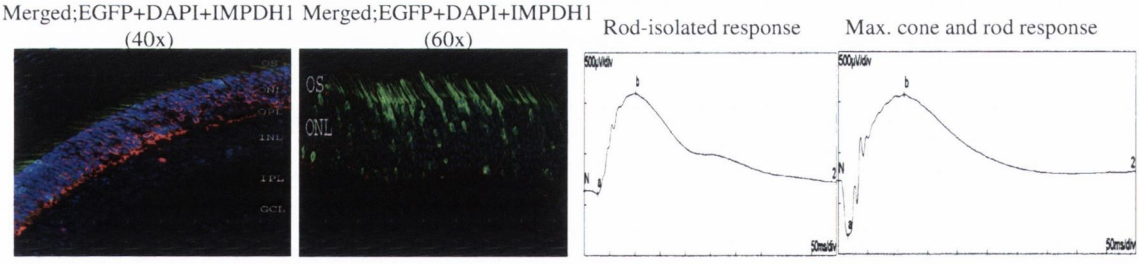

C (ii) **Wild type C57B6/CBA (Mouse #4) subretinally injected with pAAVsh2048.EGFP (right eye) and dissected four months post-injection**

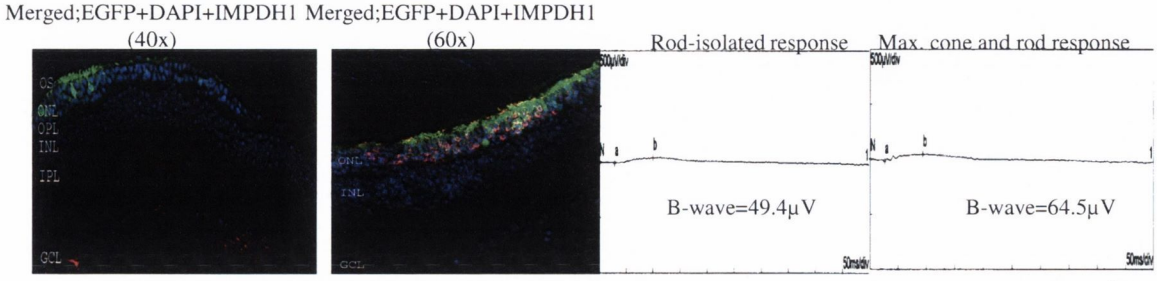

Figure 5.21 **continued**

Figure 5.21: Time-course analysis of the effect of AAV-mediated suppression of IMPDH1 on retinal histology. Four 1-month old wild type C57B6/CBA mice (Mouse #1, 2, 3, 4) were subretinally injected with 3 µl of pAAVshLuc.EGFP and 3 µl of pAAVsh2048.EGFP at equal concentrations ($6.85x10^{12}$ vp/ml). (A i and ii) Retinas from the left and right eyes of Mouse #1 and 2 were dissected four weeks post-injection and embedded in OCT for cryostat sectioning. (B i and ii, and C i and ii) ERG analysis measuring rod-isolated response and maximal, dark adapted cone and rod responses was first performed on Mouse #3 and 4 four months post-injection. Retinas were subsequently dissected from these animals for OCT embedding. All frozen fixed retinas (12 µm thickness) were immunostained with anti-C-IMPDH1 antibody followed by Cy3 secondary antibody (red). Cell nuclei were stained with DAPI (blue). Fluorescence images were captured using a confocal microscope (Olympus FU1000) at 40X or 60X magnifications. Merged images represent overlaying of IMPDH1 (red), cell nuclei (blue) and AAV-transduced cells (green).

ERG b-wave amplitudes Animals		Constructs injected	Rod-isolated response (b-wave, μV)
(i) Uninjected Controls			
IMP-04 #16	Right eye	Uninjected	868
	Left eye	Uninjected	867
IMP-04 #17	Right eye	Uninjected	1420
	Left eye	Uninjected	1420
IMP-05 #18	Right eye	Uninjected	1340
	Left eye	Uninjected	1580
IMP-05 #19	Right eye	Uninjected	1870
	Left eye	Uninjected	1760
IMP-05 #20	Right eye	Uninjected	1260
	Left eye	Uninjected	1450
(ii) Empty Vector Controls		1μl 1.8x10^{12}vp/ml : 2μl 3.3X10^{12}vp/ml	
IMP-03 #11	Right eye	pAAV.EGFP+pAAVsh2048.EGFP	545
	Left eye	pAAV.EGFP+pAAVshNT.EGFP	954
IMP-03 #12	Right eye	pAAV.EGFP+pAAVsh2048.EGFP	786
	Left eye	pAAV.EGFP+pAAVshNT.EGFP	1470
IMP-03 #13	Right eye	pAAV.EGFP+pAAVsh2048.EGFP	1130
	Left eye	pAAV.EGFP+pAAVshNT.EGFP	1210
IMP-03 #14	Right eye	pAAV.EGFP+pAAVsh2048.EGFP	865
	Left eye	pAAV.EGFP+pAAVshNT.EGFP	866
IMP-03 #15	Right eye	pAAV.EGFP+pAAVsh2048.EGFP	650
	Left eye	pAAV.EGFP+pAAVshNT.EGFP	379
(iii) Wild type IMPDH1		1μl 1.77x10^{12}vp/ml : 2μl 3.3X10^{12}vp/ml	
IMP-01 #1	Right eye	pAAV.WtIMPDH1.EGFP+pAAVsh2048.EGFP	1160
	Left eye	pAAV.WtIMPDH1.EGFP+pAAVshNT.EGFP	935
IMP-01 #2	Right eye	pAAV.WtIMPDH1.EGFP+pAAVsh2048.EGFP	796
	Left eye	pAAV.WtIMPDH1.EGFP+pAAVshNT.EGFP	1040
IMP-01 #3	Right eye	pAAV.WtIMPDH1.EGFP+pAAVsh2048.EGFP	568
	Left eye	pAAV.WtIMPDH1.EGFP+pAAVshNT.EGFP	379
IMP-01 #4	Right eye	pAAV.WtIMPDH1.EGFP+pAAVsh2048.EGFP	602
	Left eye	pAAV.WtIMPDH1.EGFP+pAAVshNT.EGFP	758
IMP-01 #5	Right eye	pAAV.WtIMPDH1.EGFP+pAAVsh2048.EGFP	310
	Left eye	pAAV.WtIMPDH1.EGFP+pAAVshNT.EGFP	340
(iv) Mutant IMPDH1 (Arg224Pro)		1μl 1.4x10^{12}vp/ml : 2μl 3.3X10^{12}vp/ml	
IMP-02A #6	Right eye	pAAV.MutIMPDH1.EGFP+pAAVsh2048.EGFP	578
	Left eye	pAAV.MutIMPDH1.EGFP+pAAVshNT.EGFP	292
IMP-02A #7	Right eye	pAAV.MutIMPDH1.EGFP+pAAVsh2048.EGFP	631
	Left eye	pAAV.MutIMPDH1.EGFP+pAAVshNT.EGFP	313
IMP-2A #8	Right eye	pAAV.MutIMPDH1.EGFP+pAAVsh2048.EGFP	203
	Left eye	pAAV.MutIMPDH1.EGFP+pAAVshNT.EGFP	396
IMP-2B #9	Right eye	pAAV.MutIMPDH1.EGFP+pAAVsh2048.EGFP	409
	Left eye	pAAV.MutIMPDH1.EGFP+pAAVshNT.EGFP	622
IMP-2B #10	Right eye	pAAV.MutIMPDH1.EGFP+pAAVsh2048.EGFP	42.6
	Left eye	pAAV.MutIMPDH1.EGFP+pAAVshNT.EGFP	54.1

Table 5.22: A table illustrating b-wave amplitudes of rod-isolated response from wild type 129 S2/SvHsd mice co-injected with; (i) uninjected; (ii) pAAV.EGFP and pAAVsh2048.EGFP or pAAVshNT.EGFP; (iii) pAAVWtIMPDH1.EGFP and pAAVsh2048.EGFP or pAAVshNT.EGFP; (iv) pAAVMutIMPDH1(224) and pAAVsh2048.EGFP or pAAVshNT.EGFP.

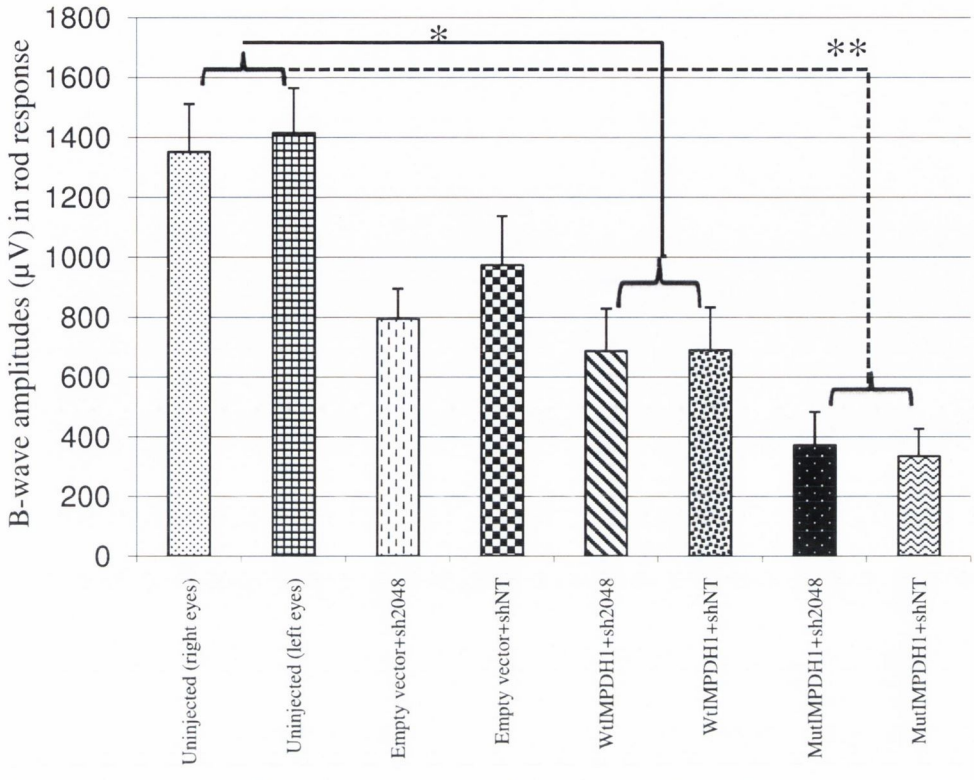

Average b-wave amplitudes (µV) in rod-isolated response ± SEM	Uninjected (Right eyes)	Uninjected (Left eyes)	Empty Vector+sh2048	Empty vector+shNT	WtIMPDH1+sh2048	WtIMPDH1+shNT	MutIMPDH1+sh2048	MutIMPDH1+shNT
	1351 ± 160	1415 ± 149	795 ± 100	974 ± 163	687 ± 141	690 ± 142	372 ± 111	335 ± 91

Figure 5.23: The effect of AAV-mediated co-expression of IMPDH1 and shRNA on b-wave amplitudes of rod-isolated response in wild-type 129 S2/SvHsd mice. Histograms illustrating the average b-wave amplitudes of rod-isolated response measured by ERG analysis; (i) Rod-isolated response from five uninjected adult wild-type 129 S2/SvHsd mice; (ii) Rod-isolated response from five adult wild-type 129 S2/SvHsd mice co-injected with 1µl $1.8x10^{12}$vp/ml of pAAVEGFP and 2µl $3.3x10^{12}$ vp/ml of pAAVshNT.EGFP (left eyes), and 1 µl $1.8x10^{12}$vp/ml of pAAVEGFP and 2 µl $3.3x10^{12}$ vp/ml of pAAVsh2048.EGFP (right eyes); (iii) Rod-isolated response from five adult wild-type 129 S2/SvHsd mice co-injected with 1 µl $1.77x10^{12}$ vp/ml of pAAVWtIMPDH1.EGFP and 2 µl $3.3x10^{12}$ vp/ml of pAAVshNT.EGFP (left eyes), and 1 µl $1.77x10^{12}$ vp/ml of pAAVWtIMPDH1.EGFP and 2 µl $3.3x10^{12}$ vp/ml of pAAVsh2048.EGFP (right eyes); **(iv)** Rod-isolated response from five adult wild type 129 S2/SvHsd mice co-injected with 1 µl $1.4x10^{12}$ vp/ml of pAAVMutIMPDH1(224).EGFP and 2 µl $3.3x10^{12}$ vp/ml of pAAVshNT.EGFP (left eyes), and 1 µl $1.4x10^{12}$ vp/ml of pAAVMutIMPDH1(224).EGFP and 2 µl $3.3x10^{12}$ vp/ml of pAAVsh2048.EGFP (right eyes). Subsequent to ERG analysis, all mice were sacrificed and retinas were dissected for histological analysis. Empty vector = pAAVEGFP. Error bar denotes standard error of the mean. *$P<0.05$. **$P\leq0.0001$. Solid line describes significant ERG difference between uninjected eyes and eyes co-injected with wild-type IMPDH1 and shNT or sh2048. Broken line depicts signficant ERG difference between uninjected eyes and eyes co-injected with mutant IMPDH1 and shNT or sh2048.

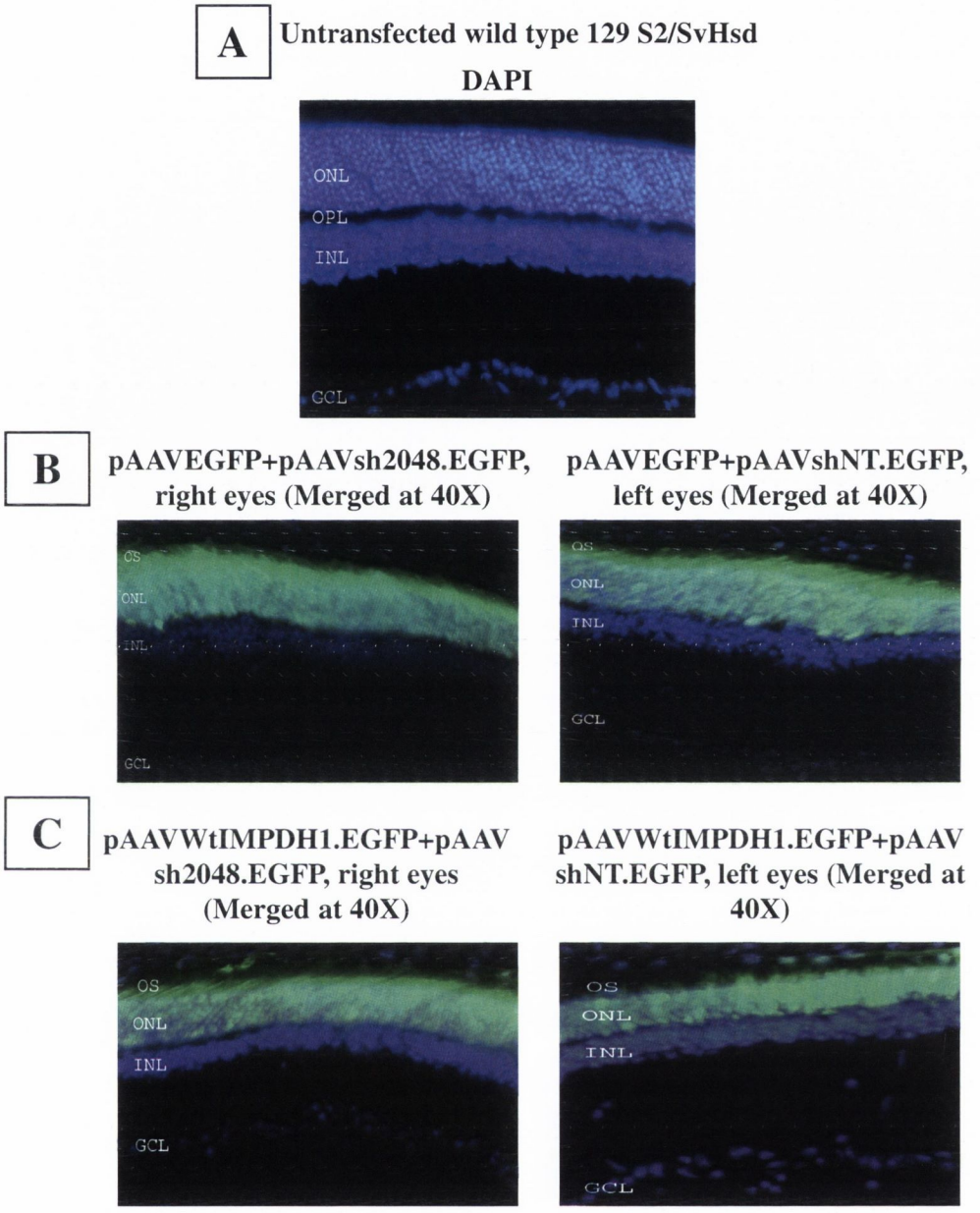

Figure 5.24: Histological analysis of wild type 129 S2/SvHsd retinas co-injected with AAV vectors expressing wild type IMPDH1 and shRNAs. Following ERG analysis as described above in *Figure 5.23*, all mice were sacrificed and retinas were dissected for cryostat sectioning. Frozen fixed retinal sections (12 μm) were visualised under a confocal microscope (Olympus FU1000) at 40X magnification. All merged fluorescence photographs shown here depict representative images of retina sections observed in all animals. Merged = overlaying of cell nuclei staining with DAPI (blue) and AAV-transduced cells (green). (A) Untransfected wild type 129 S2/SvHsd mice; (B) co-injection of EGFP and non-targeting shRNA (shNT) (right panel), and sh2048 (left panel); (C) co-injection of wild type IMPDH1 and non-targeting shRNA (shNT) (right panel), and sh2048 (left panel).

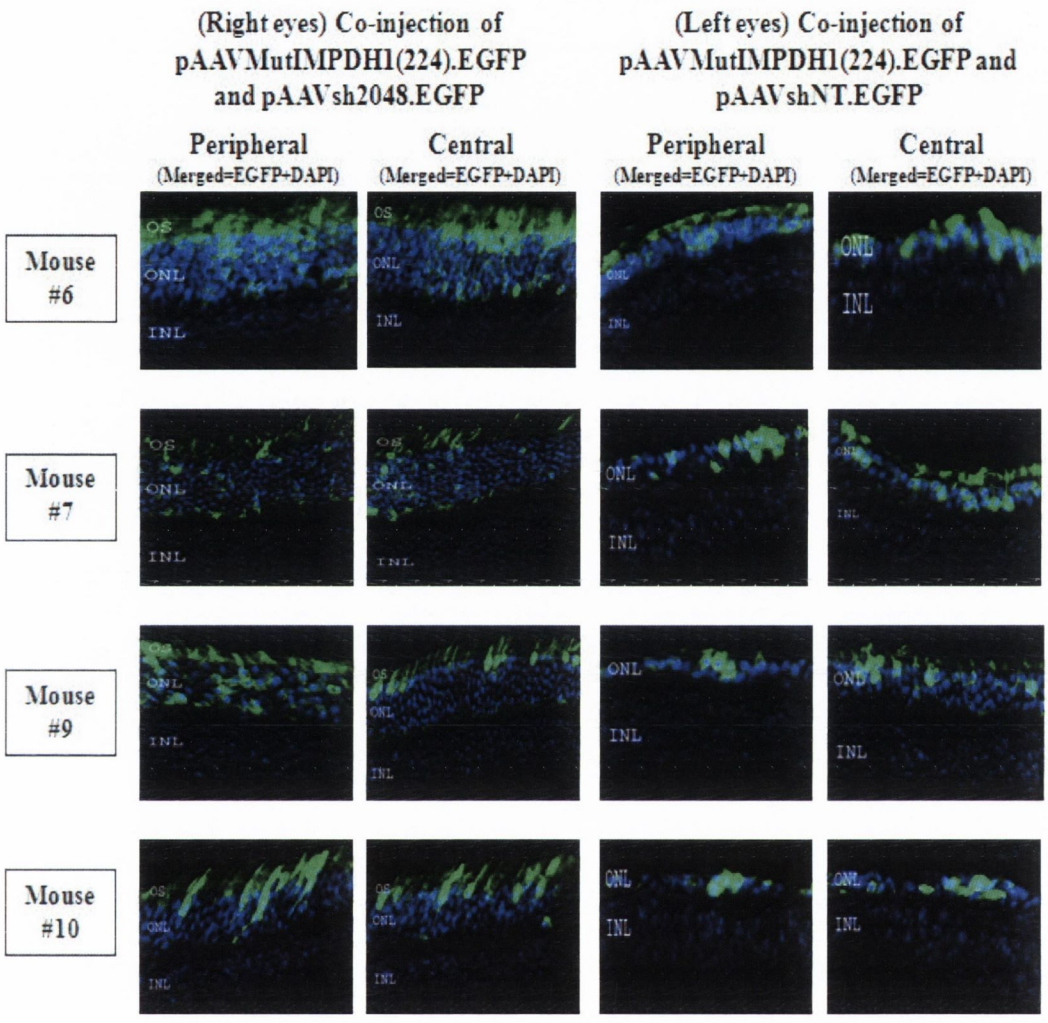

Figure 5.25: Expression of Mutant IMPDH1 in the mouse retina causes reduction of ONL thickness. Histological analysis of wild type 129 S2/SvHsd retinas co-injected with AAV vectors expressing mutant IMPDH1 harboring the Arg224Pro mutation and IMPDH1-specific shRNAs. Subsequent to ERG analyses as described above in *Figure 5.23*, all five wild type 129 S2/SvHsd mice (Mouse #6 to 10) co-injected with pAAVMutIMPDH1(224).EGFP and pAAVsh2048.EGFP or pAAVshNT.EGFP were sacrificed and retinas were dissected for cryostat sectioning. Central and peripheral regions of frozen fixed retinal sections (12 μm) were visualised under a confocal microscope (Olympus FU1000) at 40X magnification. Fluorescent pictures of central and peripheral regions of retinal sections shown here are representative images of the general observation made throughout the entire dissected eye. (OS=outer segment; ONL=outer nuclear layer; INL=inner nuclear layer; GCL=ganglion cell layer).

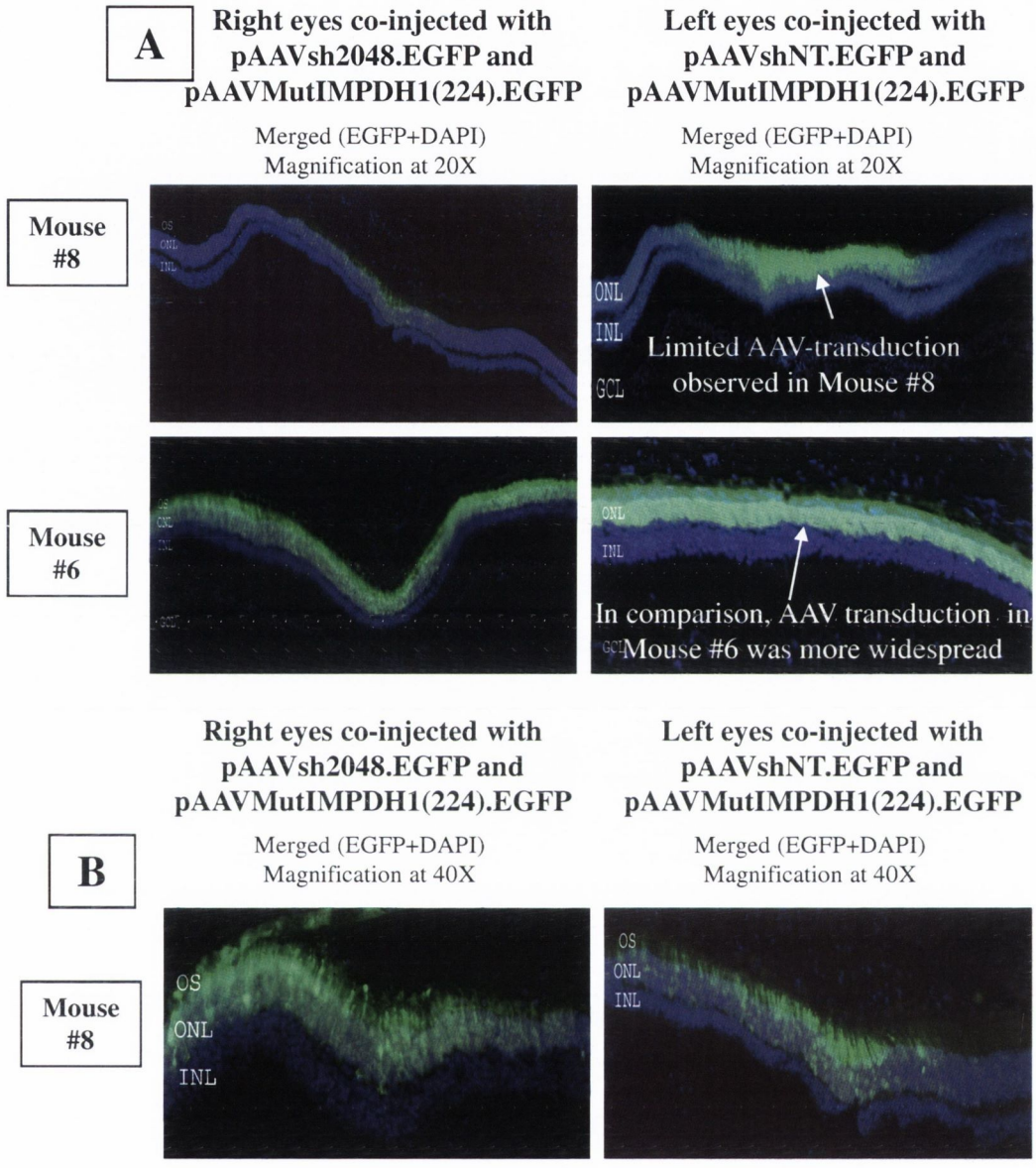

Figure 5.26: Limited AAV transduction was observed in retinal sections of Mouse #8, possibly due to poor AAV delivery. (A) Comparisons of retinal sections from Mouse #6 and Mouse #8. Magnification at 20X. (B) Superimposed areas of retinal sections transduced with AAV-mutant IMPDH1 and AAV-shNT or AAV-sh2048. Magnification at 40X. Merged=DAPI overlaid with EGFP.

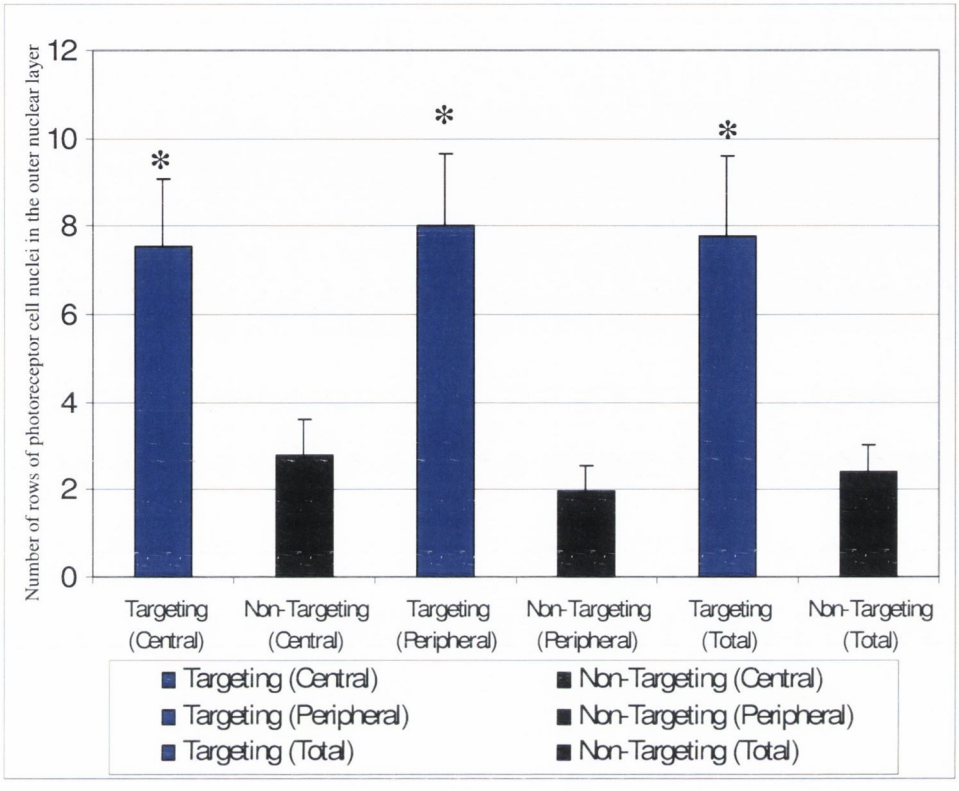

Regions of retina	Central		Peripheral		Total	
AAV construct injected	pAAVsh2048.EGFP	pAAVshNT.EGFP	pAAVsh2048.EGFP	pAAVshNT.EGFP	pAAVsh2048.EGFP	pAAVshNT.EGFP
	Right eye	Left eye	Right eye	Left eye	Right eye	Left eye
Number of rows of photoreceptor cell nuclei ± SEM	8 ± 1.54	3 ± 0.82	8 ± 1.66	2 ± 0.59	8 ± 1.81	2 ± 0.64

Figure 5.27: AAV-mediated shRNA suppression of mutant IMPDH1 protects retinal histology. Following histological analysis of mice #6, 7, 9 and 10 in *Figure 5.26*, the number of rows of photoreceptor cell nuclei in nine randomly selected central and peripheral regions of frozen fixed retinal sections were scored blindly. Histograms show the average number of rows of photoreceptor cell nuclei found in the central, peripheral regions (N=4). Total = average of central and peripheral. Y-error bar denotes standard error of the mean (SEM). *P<0.05. Co-injection of pAAVsh2048.EGFP with pAAVMutIMPDH1(224).EGFP significantly protected the outer nuclear layer from deterioration in the central and peripheral regions of the retina (P=0.0465 and P=0.03, respectively), as compared to the non-targeting control.

Chapter 6
Evaluation of Off-target Effects Against IMPDH2

6. Evaluation of off-target effects against IMPDH2

6.1 Introduction

Short hairpin RNAs (shRNAs) expressed from exogenously introduced RNAi-vector systems and endogenous pre-mircoRNA (pre-miRNA) are both cleaved in the cytoplasm by the Dicer enzyme to form 21- to 25-nucleotide double-stranded RNAs (dsRNA) (*Figure 6.1A*) (Ambros and Chen, 2007; Nilsen, 2007). The antisense strands of siRNAs or miRNAs are incorporated into the RNA-induced silencing complex (RISC) where they provide specificity for target transcript cleavages. In particular, the antisense strand of siRNAs generally recognises target transcripts with perfect complementarity to elicit mRNA cleavage (Filipowicz *et al.*, 2005). In contrast, most miRNAs show partial complementarity (e.g. 3' untranslated regions of mRNAs) to target regions and mediate gene silencing at the translational level. In order to achieve effective siRNA- or miRNA-mediated suppression, the antisense or guide strand of siRNA/ miRNA duplexes is required to be incorporated into RISC efficiently, in preference to the sense strand (*Figure 6.1A*). Thermodynamic profiling experiments have revealed that the strand selection of RISC incorporation is highly dependent on the thermodynamic stability, which is contributed by the level of G/C contents, between the sense and antisense strand of siRNA duplex (Reynolds *et al.*, 2004; Khovorova *et al.*, 2003) (*Figure 6.1B*). In particular, these studies have shown that the lowest stability between the strands of highly functional siRNAs was located at the 5' terminus of the antisense strand, and less functional siRNAs were found to possess 5' terminal instability in the sense strand. This implies that the energy profile of the siRNA determines its entry into RISC.

Target recognition by siRNA was initially thought to be a highly sequence specific gene silencing mechanism where a single mismatch between the guide strand of the siRNA and the target mRNA was able to terminate gene silencing. However, this theory was considerably challenged when significant off–target effects were observed in a microarray study showing the ability of siRNAs to cross-react with targets of

partial sequence similarity, causing non-specific global up-regulation or down-regulation of hundreds of genes and with protein products involved in diverse cellular functions (Jackson *et al.*, 2003; Persengiev *et al.*, 2004) Several mutational studies carried out in *Drosophila* and mammalian cells have also indicated that central mutations between the siRNA antisense strand and the target mRNA were more detrimental to the silencing activity than mismatches occurring at both terminal ends of the siRNA. (Elbashir *et al.*, 2001c; Amarzguioui *et al.*, 2003). Holen *et al.,* (2005) have systematically introduced a wobble mutation into the central region of siRNA targeting Flap endonuclease 1 (Fen 1) and Aquaporin 4 (Aqp 4), which led to a G: U interaction between the siRNA antisense stand and the mRNA target. The results revealed that such a mutation made in the central region of the siRNA was deleterious to the silencing effect, but in contrast, introduction of mutations into the terminal nucleotides was tolerated to a much greater extent. Furthermore, Haley and Zamore, (2004) demonstrated in Drosophila extracts that mutations in the 3' end of the antisense strand rather than in the 5' end were tolerated by the RISC enzyme, signifying that the position of the mismatch in the siRNA affects the severity of silencing loss.

Additional concern regarding off-target effects was raised in a large-scale knockdown experiment using a synthetic siRNA library to identify novel druggable regulators of the HIF-1 pathway (involved in tumour growth), where all top three hits were due to siRNA off-target effects (Lin *et al.*, 2005). In particular, two of the top three hits mediated non-specific gene silencing through a specific seven nucleotide motif, and further analysis showed that the generation of off-target effect through this 7-nt motif depended on the characteristics of the target mRNA, position and sequence context surrounding the complementarity region. This finding is in agreement with that of Jackson *et al.,* (2003) where gene silencing can occur with minimal complementation. Furthermore, siRNAs showing significant off-target effects have been found to possess a high G/C content at positions 2-8 of the antisense strand, indicating that high thermodynamic stability in the 5' region of the siRNA antisense strand rather than complementarity at the 3' end was only needed for suppression. The 'seven-

nucleotide complementation' has been observed in the 5' end of many miRNAs antisense strands that are complementary to specific sequence motifs that mediate negative post-transcriptional regulation (Lai, 2002). The ability of siRNA to enter the miRNA translational repression pathway, (Saxena *et al.*, 2003), and that miRNAs can associate with RISC complex to downregulate a number of genes at mRNA level have previously been reported. (Lim *et al.*, 2005). Therefore it is possible that siRNAs could behave like miRNAs to interact with undesired targets through minimal sequence complementation, resulting in the recruitment of RISC complex to target mRNA. This interchangeable relationship between siRNA and miRNA makes predictions of off-target effect extremely difficult.

Currently, siRNA has been used extensively in mammalian cells to inhibit the expression of specific genes for experimental and therapeutic purposes. However, a critical question to be answered is whether non-specific gene silencing by siRNA is concentration-dependent or not. Persengiev *et al.*, (2004) have analysed the expression of a subset of genes following transient transfection of siRNAs ranging from 0 to 200 nM in HeLa S3 cells. As expected, non-specificity decreased as concentrations went down, indicating that off-target effects are dependent upon siRNA concentration in a gene specific manner. Interestingly, non-specific silencing induced by siRNAs is not a transient effect; evidence has shown that once the mechanism is initiated, the effect is sustained throughout the course of the siRNA treatment (Persengiev *et al.*, 2004)

The conclusions drawn from the majority of mutational studies have raised certain questions because mismatched nucleotides were introduced into the siRNA rather than the targeted mRNA sequence. Since the efficacy of siRNA silencing activity is governed by the ability of siRNA to enter the RNA-induced silencing complex (RISC), and the ability of the antisense strand to locate target sequences, alteration of the siRNA sequence has raised uncertainty as to whether the loss of silencing activity was due to alterations in RISC entry or target recognition. Du *et al.*, (2005) carried out an extensive off-target study to investigate the silencing activity of a functional

siRNA on all 57 permutations of its cognate wild type target site where each mutated site forms different single nucleotide mismatches to the guide strand (*Figure 6.2*). In contrast to other studies, mutations were introduced to the target mRNA rather than modifying the siRNA molecule, assuring that the siRNA was not differently unwounded to avoid complications in the RISC loading process. Although alteration of the target mRNA sequence may introduce changes to the mRNA secondary structure, any possible effects related to this were not investigated by the author. In brief, a total of 57 different fusion luciferase reporter plasmids carrying all possible single nucleotide mutations for each of the target site for a fully validated 19 nucleotide siRNA (siCD46), were separately co-transfected into HEK 293 cells. The level of suppression was then quantified by dual-luciferase activity 24 hours post transfection. Interestingly, 73% of the 57 mutated fusion luciferase reporters carrying target sites forming mismatches with cognate siRNA showed significant reduction in silencing efficiency, and variable levels of off-target effects were found. Furthermore, based on the silencing efficacies of different mismatches caused by single nucleotide variation, the target site of siCD46 was found to have three different tolerance regions towards mismatches, and these were categorised as low, medium and high regions. Mismatches occurring at position 5-11 of the target region were categorised as the low tolerance region because incompatibility at these positions completely abolished suppression activities. This finding was consistent with earlier reports claiming that perfect base-pairing in the central region was crucial for optimal silencing activity, and siRNA was highly sensitive to mismatches at these positions (Elbashir *et al.*, 2001c; Jackson *et al.*, 2003). However, even at this low tolerance region, mismatches at positions 5, 7, 8, 11 were found to be well tolerated. These high tolerance mismatches have sparked speculations as to whether this region of the siRNA-mRNA interaction bears an important role in transcript silencing. This observation has also been found in the 5' end of many miRNAs that contain seven core nucleotides that are fully complementary to the target regulatory regions in the 3' untranslated regions. Sequence complementarity between the core nucleotides of the miRNA to target regulatory regions suggests a role in stablisation of the miRNA-mRNA interaction. Therefore this may also be true for the siRNA-mRNA interaction.

Positions 3, 4 and 12 to 17 were considered as medium tolerance regions because mismatches at these positions were moderately tolerated, and suppression activity was still significant (>40%). Interestingly, the silencing efficiency for the mutations at positions 13 and 14 (13→T; 14→A), was not altered and was similar to that of the wild type. This observation suggested that the silencing efficiency was determined not only by the position of the mismatch, but possibly by the identity of the substituted nucleotide as well. Lastly, the two terminal nucleotides at both ends of the target region at position 1, 2, 18 and 19 were classified as high tolerance regions, where none of these substitutions affected silencing. Further examination of the silencing profile also found that the G: U wobble base-pair [G (target site) → U (guide strand)] was the best tolerated mismatch, as previously reported by Saxena *et al.*, (2003).

To date, absolute siRNA specificity cannot be guaranteed, implying that risk assessment for off-target silencing has to be of a case to case analysis of individual siRNAs. One of the most common methods used to prevent the possibility of off-target effects in the design of siRNAs is to perform computational searches to minimise sequence similarities with unrelated genes. Fast and sensitive bioinformatic tools such as 'BLAST', 'siDirect' or 'DEQOR' have been used extensively to align short oligonucleotide sequence with unrelated genes (Naito *et al.*, 2004). However, many search engines may miss important alignments for such short oligonucleotides when the parameters are not stringent enough, therefore search engines using algorithms with higher sensitivity are needed. Naito *et al.*, (2005) have developed a new online system that provides fast and accurate off-target searches for potential targets by mimicking the biochemical process of double-stranded mediated gene silencing *in-vivo*. The unique feature of this software is that it breaks up the input sequence into siRNA cocktails, imitating the Dicer enzyme, and performs exhaustive scans for each of the siRNA to locate off-target candidates.

Apart from the careful design of siRNA through computational softwares, chemical modifications made to siRNA molecules have also improved non-specificity. A

collaborative study carried out by Dharmacon Research (Lafayette, CO) and Rosetta Inpharmatics (Seattle, WA) have shown that methyl groups added to the 2' position of the ribosyl ring of the second base of siRNA significantly reduced off-target effects, and silencing efficiency was not compromised. In addition, the 2'-O-methyl modification was much more effective at reducing off-target effects when it was added to position 2 of the antisense strand of siRNA (Jackson *et al.*, 2006; Amarzguioui *et al.*, 2003).

In order to prolong the expression of siRNAs *in-vivo,* many studies have adopted expression plasmids harbouring polymerase II or III promoters for the expression of siRNAs. However, the use of short hairpin RNA constructs provides additional complexity and risk to off-target effects. Although Brummelkamp *et al.*, (2002) have demonstrated specific production of sense and antisense strands from hairpin siRNA transcripts, the exact position of double-stranded hairpin cleavage has not yet been studied extensively, and the exact hairpin secondary structure has only been predicted theoretically. In order to overcome this limitation, the generation of more than one shRNA targeting the same sequence will ensure that the suppression effect is true. Although many limitations still surround the issue of absolute siRNA specificity, some of the studies examined above have broadened our understanding of the off-target mechanism elicited by siRNA partial complementation with target mRNA, which may be important for the design of more specific siRNAs, and for the development of siRNAs as therapeutic drug candidates.

Understanding of off-target effects is not only important for siRNA design, but is also crucial for the development of siRNAs as therapeutic tools. In order to investigate the specificity of IMPDH1-specific si/shRNAs, the silencing effects of these suppressors are assayed against another isoform of human IMPDH enzymes, inosine 5'-monophosphate dehydrogenase type II (IMPDH2), which shares 70% and 84% homology to IMPDH1 at the DNA sequence and amino acid levels, respectively. In addition, the two isoforms also have indistinguishable substrate affinities, catalytic activities and K_i values (Carr *et al.*, 1993; Collart and Huberman, 1988; Natsumeda *et*

al., 1990; Hager *et al.*, 1995). Due to the striking similarities between these two isoforms in many aspects, evaluation of functional IMPDH1-specific si/shRNAs against IMPDH2 expression at the mRNA and protein level in mammalian cells and *in-vivo* would prove to be useful for providing an insight into the level of specificity of these suppressors, and also an understanding of siRNA-mediated non-specific off-target effects.

6.2 Methods

6.2.1 Construction of IMPDH2 expression vectors

To construct a CMV-driven IMPDH2 mammalian expression vector, IMPDH2 cDNA (NM_000884) was excised from pET-30 Ek/LIC+IMPDH2 (Novagen), a kind gift from *Dr Sara J. Bowne, Human genetics centre, school of public health, University of Texas HSC, Houston, TX 77030, USA*), and IMPDH2 template cDNA was PCR-amplified using PFU DNA polymerase (Stratagene) with IMPDH2-specific primers (*Table 4*, Appendix). The IMPDH2 primers were designed to introduce a Not I site at the 5' end, and an *XhoI* site at the 3' end of wild-type *IMPDH2* cDNA sequence (*Table 3*, Appendix). Amplified PCR fragments were then digested with *NotI* and *XhoI* and inserted in-frame into the respective restriction sites in pcDNA3.1(+) (Invitrogen), to create pWtIMPDH2. To create EGFP-tagged IMPDH2 constructs, amplified IMPDH2 cDNAs were digested with *NotI* and *XhoI* and inserted in-frame downstream of EGFP in the vector pcDNA.EGFP, to create pWtIMPDH2.EGFP. All positive clones were checked by DNA sequencing to ensure the fidelity of all the PCR and cloning steps using specific primers (*Table 4*, Appendix).

6.2.2 Transfections and quantitative Real Time RT-PCR analysis

HeLa cells were plated at $1x10^5$cells/ml (500 µl per well) onto a 24-well plate with $DMEM^{-Abs}$ medium one day before transfection. For each transfection sample, 20pmoles chemically synthesised siRNAs were diluted in 50 µl of Opti-MEM-reduced serum medium and mixed gently. 1 µl Lipofectamine 2000 was then diluted to 50µl Opti-MEM-reduced serum medium and incubated at room temperature for 5 min. The diluted chemically synthesised siRNA molecules were combined with the diluted Lipofectamine 2000® (total volume is 100 µl) and incubated at room temperature for 25 min for complex formation. 100 µl shRNA/siRNA+Lipofectamine 2000® complex was then added to each sample well. The plate was mixed by gentle rocking and incubated at 37°C in a CO_2 incubator. Each sample was carried out in quadruplicates that were pooled together for RNA extraction by Trizol as outlined in section 2.3.7. IMPDH2 mRNA expression was analysed by Real Time RT-PCR using

IMPDH2-specific primers (*Table 2*, Appendix) 24 hrs post-transfecton as described in section 2.4, and the average of five independent experiments was illustrated. For each transfection experiment, a control group was transfected with LuciferaseGL3-directed (Qiagen) siRNA as non-targeting controls (*Table 1*, Appendix). IMPDH2 expression was standardised per unit house-keeping gene expression (β-actin) and expressed as a percentage of that for the non-targeting control.

6.2.3 Inhibition of wild type IMPDH2 and EGFP fusion proteins by siRNAs in HeLa cells

HeLa cells were seeded onto poly-L-lysine coated coverslips in 24-well plates at a density of $1x10^5$cell/ml with $DMEM^{-Abs}$ medium. After 24hrs, HeLa cells at 80-90% confluency were separately co-transfected with 1 μg/μl pWtIMPDH2.EGFP and 20 pmoles siLuciferaseGL3 or si2048. All transfection was carried out using Lipofectamine 2000® (Invitrogen) according to manufacturer's protocol. 72 hrs post-transfection, the cells were fixed with 4% paraformaldehyde (pH 7.4) for 20 min at room temperature and stained with DAPI. The poly-L-lysine cover-slips were transferred onto glass slides and plastic cover-slips were placed on top of the glass slides with a few droplets of aqua/polymount solution. Expression of EGFP in transfectants was examined by fluorescence microscope (Zeiss, Axioplan 2) at 20X magnification. Each group of samples was carried out in duplicates and the transfection experiment was repeated twice under the same experimental conditions.

6.2.4 Western blot analysis of IMPDH2 protein levels *in-vitro* and *in-vivo*

6.2.4.1 *In-vitro* analysis of IMPDH2 protein levels

HeLa cells were plated at $1.5x10^5$cells/ml (2 ml per well) onto 6-well plates with $DMEM^{-Abs}$ medium one day prior to transfection. After 24 hrs, separate wells of HeLa cells at a confluency of 80-90% confluency were co-transfected with 1.5 μg/μl pWtIMPDH2 and 1 μg/μl of psh1224 or psh2048, diluted in 250 μl of Opti-MEM-reduced serum medium and mixed gently. 5 μl Lipofectamine 2000® was then diluted in 250 μl of Opti-MEM-reduced serum medium and incubated at room temperature

for 5 min. The diluted IMPDH2 and shRNA vectors were then combined with the diluted Lipofectamine 2000® (total volume is 500 µl) and incubated at room temperature for 25 min for complex formation. 500 µl of the combined complexes were added to each sample well. The plate was mixed by gentle rocking and incubated at 37°C in a CO_2 incubator for 72 hrs. Each sample was carried out in duplicates and was pooled together during protein extraction. A non-targeting control (shLucfieraseGL3) was included in each experiment, and IMPDH2 protein was detected by anti-N-IMPDH2 antibody (section 2.1.4) with each blot being stripped and immunostained with β-actin as loading controls (section 2.5). Transfection experiments were repeated twice under the same experimental conditions. IMPDH2 protein levels were quantified by densitometry using *ImageJ*, and percentage IMPDH2 expression in band intensity for IMPDH2 was calculated relative to non-targeting control and normalised against β-actin.

6.2.4.2 *In-vivo* analysis of IMPDH2 protein levels

Retinal protein extracts obtained from subretinally injected adult wild type C57B6/CBA mice were subjected to western blot analyses as previously described in section 5.2.6. IMPDH2 protein was detected using anti-N-IMPDH2 antibody (kindly provided by *Dr Sara J. Browne, University of Texas HSC, Houston, USA*) at a concentration of 1:6000 in 5% skimmed milk, and secondary detection was performed using HRP-conjugated anti-rabbit IgG antibodies (Abcam). The blots were developed using Enhanced Chemiluminescent Kit (Pierce). Blots were stripped and re-probed with β-actin as loading control. Western blot band intensities were quantified using the Image processing web-tool, *Image J*. The percentage expression in band intensity for IMPDH2 was calculated relative to control virus to represent 100% expression, and normalised against β-actin.

6.2.5 Statistical analysis

Experimental data sets for all suppression data sets were pooled, averaged, and standard deviation values were calculated. 2-sample Student's *t-test* (Data Desk 6.1, Data Descriptions) for paired data was used to test the significance of RNA and

protein quantitation. P-values ≤ 0.05 were considered statistically significant. Y-error bars on histograms illustrate standard of the error mean (SEM).

6.3 Results

6.3.1 Alignment of IMPDH1-specific siRNAs against human and mouse IMPDH2 transcripts

Upon alignment of the antisense strands of IMPDH1-specific siRNAs against target sites in human and mouse IMPDH2 transcripts, it was found that: (i) si1224 antisense strand carried five nucleotide mismatches at positions 1, 7, 10, 13 and 18, where numbering is for 5' of antisense strand, against human and mouse IMPDH2 transcripts; whereas (ii) si2048 antisense strand possessed three nucleotide mismatches at positions 3, 9 and 12 against human and mouse IMPDH2 mRNA (*Figure 6.3*).

6.3.2 siRNA-mediated suppression of IMPDH2 mRNA in HeLa cells

To study the effect of mismatches between IMPDH1-specific siRNAs and its mRNA target on RNAi silencing activity, HeLa cells were separately transfected with 20pmoles of si1224 or si2048. Twenty-four hours post-transfection, the level of endogenous IMPDH2 transcripts was measured by quantitative Real-Time RT-PCR. IMPDH2 expression was standardised per unit β-actin expression and expressed as a percentage of that for the non-targeting control (siLuc). HeLa cells treated with si1224 and si2048 only showed non-significant reduction of IMPDH2 mRNA to 90% ± 21% and 89% ± 17%, respectively, as compared to non-target control (P=0.7681 and P=0.7372, respectively; *Figure 6.4*). This result has indicated that both IMPDH1-specific siRNAs show at most a very limited trend for off-target effects against IMPDH2 at the mRNA level.

6.3.3 siRNA-mediated suppression of IMPDH2–tagged enhanced green fluorescent protein (EGFP) protein in HeLa cells

The target cDNA-EGFP fusion based assay outlined in *section 3.3.7* was used to investigate the specificity of si2048 towards IMPDH2 expression. 20pmoles of siLuc or si2048 was co-transfected with 1μg/μl of pWtIMPDH2.EGFP into HeLa cells and EGFP was visualised under a fluorescence microscope 72 hours post-transfection.

No qualitative difference in EGFP expression levels was observed between cells co-transfected with si2048 and those with non-targeting control (*Figure 6.5*).

6.3.4 shRNA-mediated suppression of IMPDH2 protein in HeLa cells

To determine whether the mismatches between IMPDH1-specific shRNAs and IMPDH2 would provoke a micro-RNA response by inducing translational blockade, HeLa cells were separately co-transfected with 1μg/μl pWtIMPDH2 and psh1224 or psh2048. The expression levels of IMPDH2 were analysed by western blot analysis 72hrs after transient transfection using anti-N-IMPDH2 antibody. Consistent with quantitative Real Time RT-PCR analysis (section 6.3.2), HeLa cells co-transfected with sh1224 or sh2048 showed no significant reduction of IMPDH2 protein, as compared to the non-targeting control (*Figure 6.6A and B*). In particular, average densitometry measurements taken from two independent experiments showed no significant changes of IMPDH2 expression at the protein level by sh1224 (90% ± 13%) and sh2048 (101% ± 5%), as compared to the non-targeting control (P=0.43 and P=0.86, respectively; *Figure 6.6C*). Subtle silencing of IMPDH2 at the protein level has further illustrated the specificity of both IMPDH1-specific shRNAs in mammalian cells and has also provided strong evidence that mismatches between IMPDH1-specific shRNAs and IMPDH2 do not induce a miRNA-related protein translational inhibition response.

6.3.5 AAV-mediated shRNA inhibition of IMPDH2 *in-vivo*

Following the efficient silencing of endogenous murine IMPDH1 protein achieved in retinas sub-retinally injected with pAAVsh2048.EGFP as described in section 5.3.4, equal total protein extracts from three groups of animals were subjected to western blot analysis for the detection of IMPDH2 using anti-N-IMPDH2 antibody. In contrast to *Figure 5.19*, no variations in the levels of IMPDH2 protein were detected between retinas injected with AAV-sh2048 and the control virus (AAV-shLuc) as shown in *Figures 6.7A, B and C*. In particular, average band intensities from three groups of animals (n=10) showed that AAV-sh2048 did not significantly affect IMPDH2 expression (95% ± 5%), as compared to control virus (P=0.82; *Figure*

6.6D). Consistent with *in-vitro* findings, AAV-sh2048 did not elicit non-specific silencing effects or miRNA-related translational inhibition on IMPDH2 expression *in-vivo*.

6.4 Discussion

To date, increasing evidence has indicated the potential of RNAi as a therapeutic strategy for the treatment of virus-mediated diseases (Wantanabe *et al.*, 2006), neurological disorders (Xia *et al.*, 2006) and cancer prevention (Ko *et al.*, 2006). In particular, the exclusive target specificity of siRNA against disease-related mRNAs is an essential prerequisite for successful administration of this technology in humans. It has been reported that a single mismatch between siRNA molecules and target transcripts can abolish degradation (Elbashir *et al.*, 2001c; Semizarov *et al.*, 2003), further emphasising the specificity of this technique as a potential therapeutic approach. However, enthusiasm about the specificity and selectivity of siRNA-mediated gene silencing has been subjected to critical re-evaluation. Recently, a growing body of evidence has indicated that siRNA specificity is not guaranteed and off-target silencing can occur through various mechanisms such as; (i) global up- or downregulation of genes using high dosages of siRNA (Semizarov *et al.*, 2004; Persengiev *et al.*, 2004); (ii) the induction of interferon (IFN) response (Sledz *et al.*, 2003); (iii) miRNA-like translational inhibition (Scacheri *et al.*, 2004; Saxena *et al.*, 2003; Zeng *et al.*, 2003); and (iv) mRNA degradation by partial sequence complementation (Jackson *et al.*, 2003). Although some of the off-target effects can be eliminated by using lower concentrations of siRNA (Semizarov *et al.*, 2004; Persengiev *et al.*, 2004; Jackson *et al.*, 2003), monitoring the level of OAS1 expression, a classic IFN target gene that is induced greater than 50-fold on activation of an IFN response (Bridge *et al.*, 2003), following siRNA transfection, or the use of bioinformatics tools such as siDirect (Naito *et al.*, 2004) in the design of siRNA to minimise sequence homology in unrelated genes, prediction of off-target effects for a particular siRNA still remains difficult and great variability exists between individual cases. Although DNA microarray studies may provide a rapid and sensitive platform for measuring siRNA specificity at the global mRNA transcription level, it can not provide an accurate evaluation of off-target effects at the protein level, including off-target effects due to the action of siRNAs acting as micro-RNAs due to partial sequence homology.

In the initial steps of siRNA design in this study, the specificity of siRNAs against IMPDH1 transcripts was determined using BLAST searches. However, recent data have raised doubts on the value of BLAST searches for general siRNA specificity determination (Birmingham *et al.*, 2006). Experimentally determined siRNA off-target effects have previously been shown to correlate strongly with mismatches between positions 2 to 8 within the guide strand (known as the seed sequence) and sequences in the 3'UTR of affected genes (Du *et al.*, 2005; Holen *et al.*, 2005). These seed sequences may be too short to be confidently detected by BLAST search, as BLAST searches are only useful for identifying near-perfect matches. Recently a commercial web-based tool has been made available for identification of all possible seed matches for any given siRNA (*http://www.dharmacon.com/seedlocator/default.aspx*), however, the predictive value of such software remains limited at present, as only a small fraction of seed matches result in actual off-target effects (Amarzguioui *et al.*, 2006). Although BLAST and seed-match searches can be used to eliminate poor sequences on the basis of potential off-target effects, it seems that there is no substitute for experimental determination of specificity, preferably by genome-wide gene expression profiling in combination with verification of phenotypes to avoid miRNA-mediated translational inhibition effect.

IMPDH2 has presented itself as an excellent validation candidate for the study of off-target effects because of its close resemblance with IMPDH1 at both the amino acid identity and enzymatic properties (Carr *et al.*, 1993; Collart and Huberman, 1988; Natsumeda *et al.*, 1990; Hager *et al.*, 1995). In addition, validation of IMPDH1-specific siRNA silencing activities against IMPDH2 may also provide intrinsic information about the relationship between IMPDH type I and II. Through Real Time RT-PCR and western blot analyses, it was found that both si/sh1224 and 2048 showed little silencing effects on IMPDH2 expression at the mRNA and protein levels in mammalian cells and *in-vivo*. Previous studies have shown that non-specific silencing was influenced by both the position of the mismatched base and the identity of the nucleotides forming the mismatch (Du *et al.*, 2005; Holen *et al.*, 2005). The excellent specificity observed in both IMPDH1-specific siRNAs may have been

contributed by the presence of mismatches located within the seed region (equivalent to nucleotide positions 2 to 8) of the antisense strands of si1224 and si2048 (*Figure 6.3*). Du *et al.*, (2005) previously demonstrated that the seed region represents a low tolerance region, implying that mismatches at these positions significantly abolish most of the suppression activity. Furthermore, mismatches found in more central regions of the antisense strand, such as positions 10 and 13 for si1224, and positions 9 and 12 of si2048, represent a medium tolerance region (Holen *et al.,* 2005), where mismatches are fairly well tolerated with a slight reduction in silencing activity (*Figure 6.3*). A single mismatch at position 18 of si1224 antisense strand has been located in a high tolerance region (position 18 and 19 of antisense strand), where single nucleotide substitution at these positions has no detrimental effect on silencing activity. However, the high tolerance effect of this single mismatch might have been masked by the other four which are located in low and medium tolerance regions (*Figure 6.3*). In addition, the degree of off-target effect is also determined by the identity of the mismatched nucleotides. For example, mismatches between the antisense strand of siRNA and target sites that result in the formation of G:U, U:U or A:C base pairing have been shown to be well tolerated (Saxena *et al.*, 2003). A number of G:U and A:C wobbles have been located across different positions between the antisense strands of si1224/2048 and IMPDH2 mRNA target sites (*Figure 6.3*), but no significant reduction in transcript level was observed in *Figure 6.4*. The reason for this phenomenon has not yet been fully deciphered, but possibly the tolerance level of G:U or A:C wobbles are highly dependent on specific positions in mRNA-siRNA pairing. Furthermore, Holen *et al.*, (2005) illustrated that the existence of greater than two mismatches in the antisense strand of siRNA, even when combining positions with good tolerance levels, exceeds the limit of tolerance causing an ablation of silencing activity. This result may possibly explain the lack of off-target effect against IMPDH2 observed in this study as both antisense strands of si1224 and si2048 possess greater than three mismatches against target transcript (*Figure 6.3*).

The ability of siRNAs to enter the miRNA pathway to inhibit a target at the translational level (Saxena *et al.*, 2003; Zeng *et al.*, 2003), and recent findings that some miRNAs can downregulate large numbers of target mRNAs have added an extra degree of difficulty in predicting off-target effects (Lim *et al.*, 2005). The 5' ends of many miRNAs have been shown to contain a specific seven nucleotide sequence motif that are complementary to several classes of sequence motifs known to mediate negative post-transcriptional regulation (Lai, 2002; Lewis *et al.*, 2003). In addition, two separate reports have demonstrated that miRNAs with high G/C content at positions 2-8 of the antisense strand, which induces a high thermodynamic stability in the 5' region of the miRNA antisense strand, is sufficient to inhibit the translation of targets without requiring extensive complementation at the 3' region of the antisense strand (Doench and Sharp, 2004; Lin *et al.*, 2005). Considering the importance of thermodynamic stability in the 5' region of a miRNA for target recognition, it might be possible to improve the selectivity of siRNA by choosing siRNAs with lower thermodynamic stability at the 5' region of the antisense strand (Lin *et al.*, 2005). Therefore the lack of miRNA-mediated translational repression observed between IMPDH1-specific shRNAs and IMPDH2 in mammalian cells and mouse retinas (*Figures 6.6 and 6.7*) was probably due to the low G/C content (>30%, *Figure 6.2*) observed in positions 2-8 in the 5' regions of both shRNA antisense strands.

The specificity of AAV-sh2048 *in-vivo* shown in *Figure 6.7* has provided evidence for supporting the hypothesis that the deterioration of retinal function observed in *Figure 5.15A* following *in-vivo* suppression of IMPDH1 by AAV-sh2048, was not caused by non-specific silencing of IMPDH2, but rather by ablation of IMPDH1 alone or some other essential house-keeping genes. If this speculation is true, then the lack of non-specific silencing of IMPDH2 in AAV-sh2048 treated eyes (*Figure 6.7*) may also support another hypothesis proposing that IMPDH2 does not provide a compensatory effect in retinas in response to the loss of IMPDH1, which is supported by the finding reported by Gu *et al.*, (2003) showing that IMPDH2 expression is not increased in response to the loss of IMPDH1 activity. To evaluate whether other

adRP-linked genes (i.e. *rds*/peripherin, rhodopsin, NRL or PRPF 3/8/31) may be downregulated by off-target effects elicited by AAV-sh2048, and thus may contribute to the observed retinal degeneration, further studies including genome-wide transcriptional profiling are required.

6.5 Conclusions

Collectively, the results obtained in this chapter have provided a preliminary insight into the high level of shRNA specificity towards IMPDH1. However, off-target effects were only evaluated against IMPDH2 at the mRNA and protein level, which bears close resemblance to IMPDH1 in many aspects. Furthermore, the lack of non-specific silencing by rAAV-sh2048 against IMPDH2 *in-vivo* has supported the hypothesis that suppression of IMPDH1 was the main cause of retinal function deterioration reported previously in section 5.33, and suggested that IMPDH2 may not provide a compensatory effect in response to the loss of IMPDH1 in the retina. In order to understand the full magnitude of off-target effects, genome-wide gene expression profiling should be carried out to provide a broader view of off-target effects elicited by sh2048 at global transcriptional levels. However, since siRNA may also act as miRNA in eliciting translational repression through partial complementation to target transcripts, a proteomics study should ideally also be carried out in conjunction with transcriptome analysis. The findings made in this study have significant implications for future siRNA design with respect to specificity and activity. Firstly, siRNAs with lower thermodynamic stability and minimal homology in the seed region (positions 2-8 at the 5' end of antisense strand) should be analysed in detail since these sequences play a central role in the recognition of miRNA (Jackson *et al.*, 2006). Secondly, the position of the mismatched base and the identity of nucleotides forming this mismatch between the antisense strand of siRNA and target transcript should be analysed with reference to mismatch tolerance studies carried out by Du *et al.*, (2005) and Holen *et al.*, (2005) to minimise off-target effects. Thirdly, since a partial complementation between a siRNA and the 3'-UTR of a gene appeared to trigger off-target silencing, designing siRNAs with minimal complementation to the 3'-UTR may also improve the specificity of siRNA (Lin *et al.*, 2005). Irrespective of the design of siRNAs, the observed biological effects subsequent to specific inhibition of target genes using RNAi should always be statistically analysed compared to appropriate non-targeting siRNA controls (Tschaharganeh *et al.*, 2007). This procedure guarantees that

monitored functional consequences after RNAi treatment reflect authentic and target-specific biological effects.

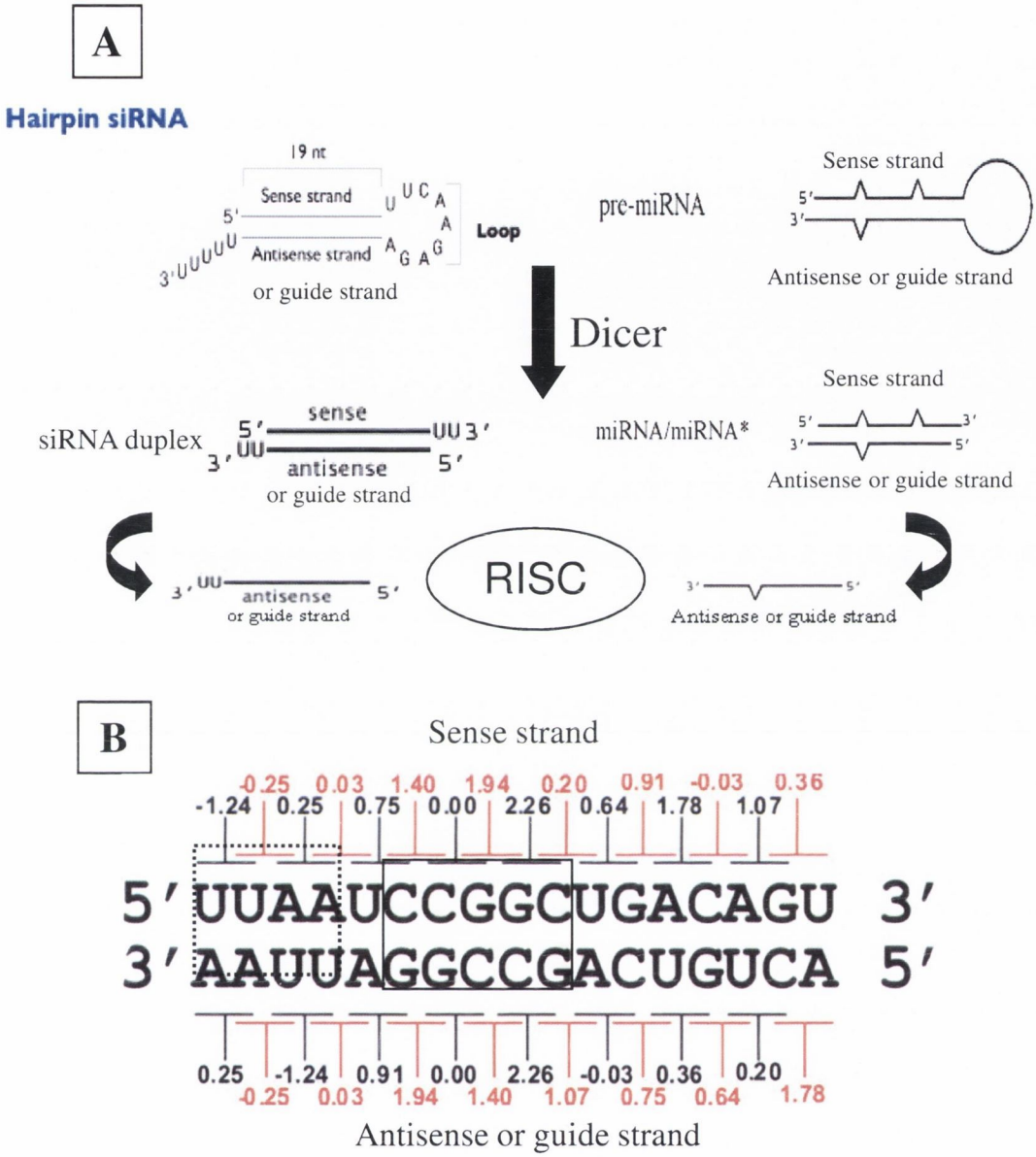

Figure 6.1: (A) A schematic diagram illustrating the formation of siRNA and miRNA duplexes. Short hairpin RNAs and precursor-miRNA (pre-miRNA) are processed by Dicer to form duplexes of siRNA and miRNA containing sense and antisense/ guide strands. The antisense or guide strand of siRNA or miRNA is then incorporated into RISC to induce target transcript cleavage or translational inhibition, depending on the level of complementarity between antisense strand and target mRNA. (B) Thermodynamic stability (ΔG) of the nearest-neighbour interactions in siRNA or miRNA duplexes. Boxed region represents an area of high thermodynamic stability in the centre of the RNA duplex as conferred by high G:C contents. Dotted region shows an area of low thermodynamic stability near the 5' terminus of sense strand (low G/C contents), as compared to the 5' terminus of antisense strand, thus the antisense strand is less likely to be incorporated into RISC.

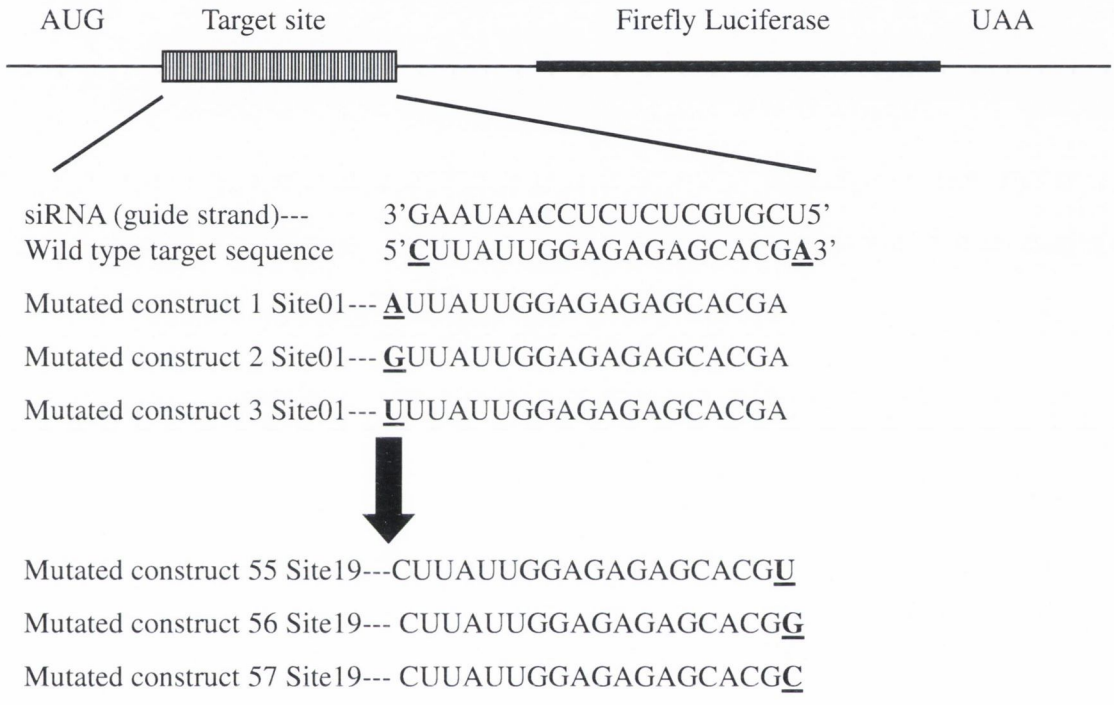

Figure 6.2: A schematic diagram of the fusion firefly luciferase reporter system used in the off-target study carried out by Du *et al.*, (2005). Each nucleotide within the target site sequence is mutated from positions 1 to 19 etc, and the wild type sequences are shown as examples.

The 19bp-target site of si1224 in exon 7 of human (NM_000884) and mouse IMPDH2 (BC_052671)

Human IMPDH2 5'-G·**U**·U·G·C·C·**C**·A·U·**U**·G·U·**A**·A·A·U·G·A·**A**-3'(5mismatches)

Mouse IMPDH2 5'-G·**U**·U·G·C·C·**C**·A·U·**U**·G·U·**G**·A·A·T·G·A·**A**-3' (5 mismatches)

sh1224 antisense 3'-C·**G**^{18}·A·C·G·G·**A**^{13}·U·A·**G**^{10}·C·A·**G**^{7}·U·U·A·C·U·**A**^{1}**-5'**

The 19bp-target site of si2048 in exon 13 of human (NM_000883) and mouse IMPDH2 (BC_052671)

Human IMPDH2 5'-U·G·U·A·C·U·C·**U**·G·G·**G**·G·A·G·C·U·**U**·A·A-3' (3 mismatches)

Mouse IMPDH2 5'- U·G·U·A·C·U·C·**G**·G·G·**G**·G·A·G·C·U·**U**·A·A-3' (3 mismatches)

sh2048 antisense 3'-A·C·A·U·G·A·G·**U**^{12}·C·C·**U**^{9}·C·U·C·G·A·**G**^{3}·U·U-5'

Figure 6.3: Alignments of IMPDH1-specific shRNA target sites with human IMPDH2 (NM_000884) and mouse IMPDH2 (BC_052671). Human and mouse IMPDH2 cDNAs were obtained from NCBI nucleotide database (http://www.ncbi.nlm.nih.gov/sites/entrez) and aligned using Clustal W multiple sequence alignment (http://www.ebi.ac.uk/clustalw) provided in the public domain by the European Bioinformatics Institute, European Molecular Biology Laboratory, Heidelberg, Germany. Bolded and underlined nucleotides represent positions of mismatches between antisense strand of siRNA and target mRNA.

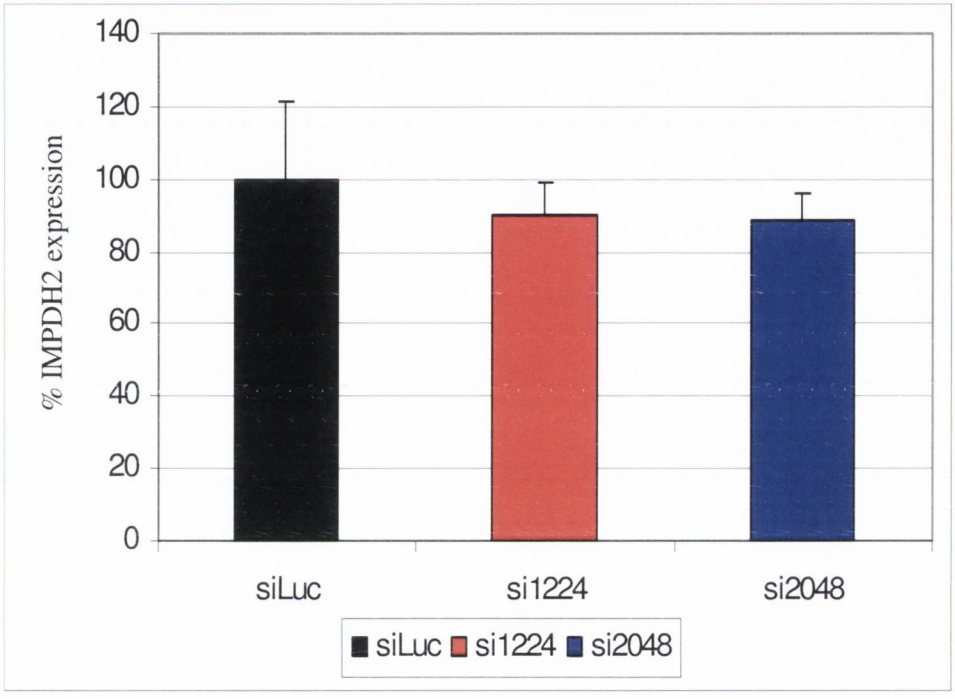

siRNAs	si1224	si2048
% IMPDH2 expression ± SEM	90% ± 9.5%	89% ± 7.2%

Figure 6.4: Off-target silencing of IMPDH2 mRNA in HeLa cells. HeLa cells were separately transfected with 20 pmoles of the indicated siRNAs using Lipofectamine 2000® reagent. Percentage expression of endogenous IMPDH2 transcript was determined by Real Time RT-PCR 24 hours post-transfection and normalised to the house-keeping gene, β-actin. A control set was transfected with siRNAs targeting LuciferaseGL3, and this was standardised to represent 100% IMPDH2 expression (Black bar). The average of 5 independent experiments is shown; Y-error bars indicate standard error of the mean (SEM).

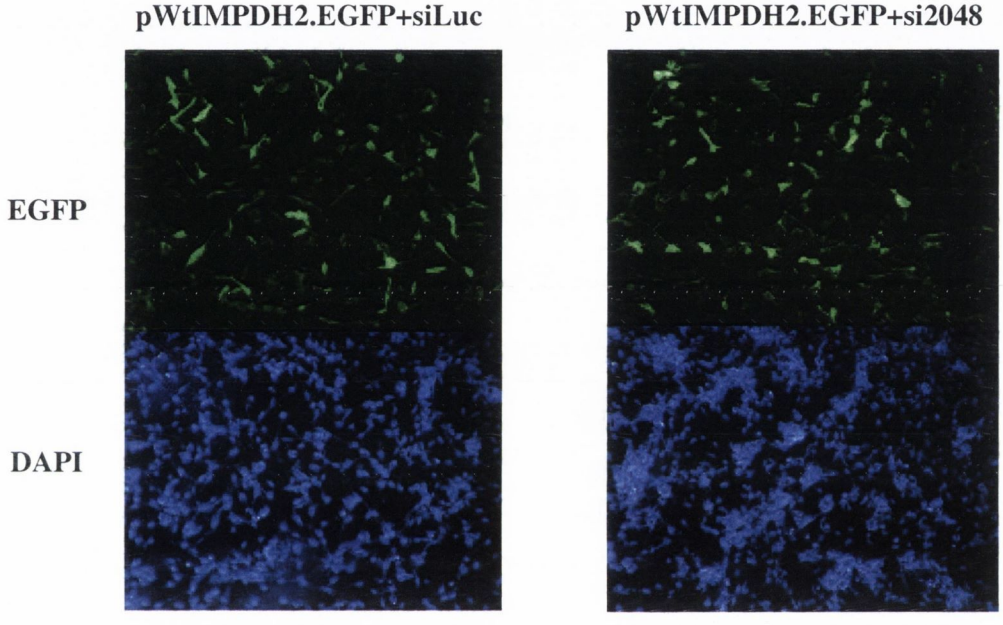

Figure 6.5: Off-target silencing of IMPDH2 and EGFP fusion protein in HeLa cells. HeLa cells were co-transfected with 1µg/µl of pWtIMPDH2.EGFP and 20pmoles of siLuc or si2048. At 72 hours of post-transfection, single images of EGFP were collected in three different fields of view per coverslip in the same sample under a fluorescence microscope. All corresponding images were taken at 20X magnification. DAPI staining in lower panels indicates cell nuclei. Representative fluorescent images shown here were selected from two independent experiments. siLuc= siLuciferaseGL3.

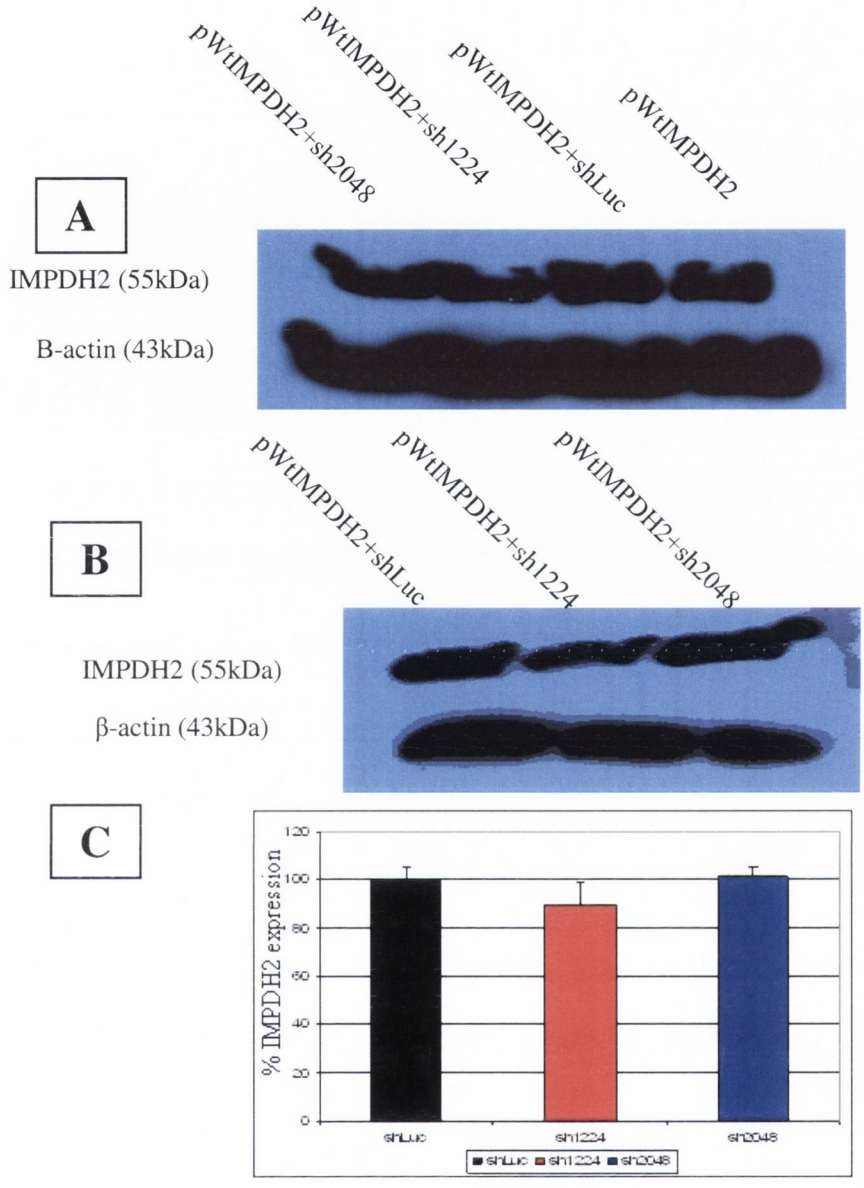

Densitometry (Band Intensity)	**si1224**	**si2048**
% IMPDH2 expression ± SEM	89.88% ± 9%	101.72% ± 3.7%

Figure 6.6: Western blot analysis of IMPDH2 expression in HeLa cells. (A and B) HeLa cells were co-transfected with 1.5 µg/µl pWtIMPDH2 and 1µg/µl psh1224 or psh2048. Protein was extracted 72 hrs post-transfection and analysed by western blotting using anti-N-IMPDH2 antibody. All blots were stripped and re-probed with β-actin as loading controls. (C) Quantification of IMPDH2 and β-actin band intensities by densitometry. Percentage IMPDH2 expression in band intensity was calculated with respect to non-targeting control, which was standardised to represent 100% IMPDH2 expression, and normalised against β-actin. Average band intensities from (A) and (B) are shown in histograms. Y-error bars denote standard error of the mean.

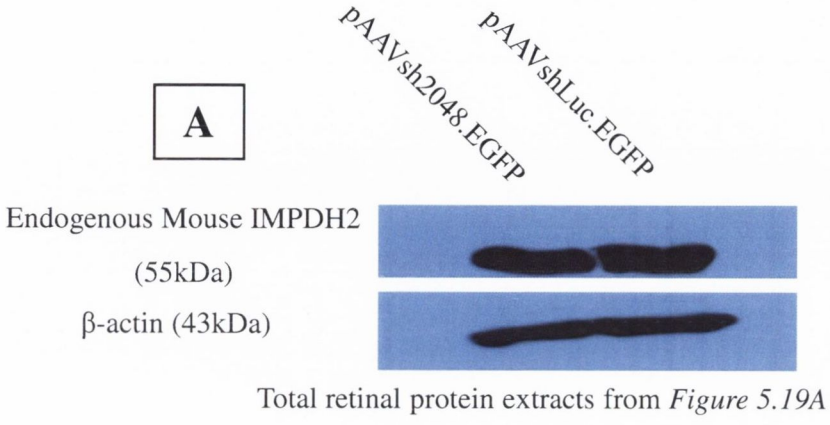

Total retinal protein extracts from *Figure 5.19A*

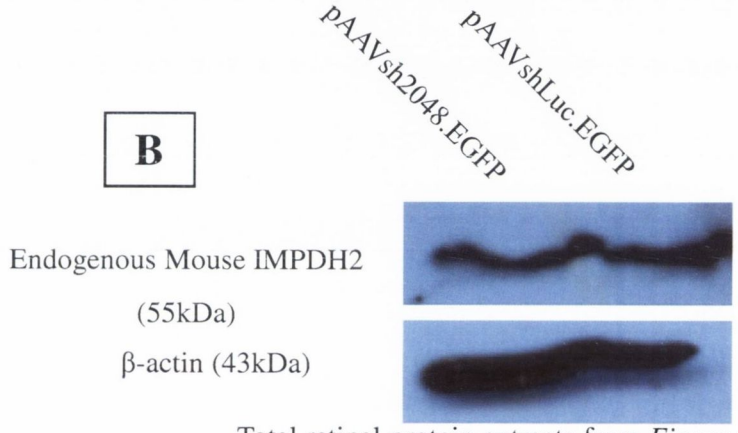

Total retinal protein extracts from *Figure 5.19B*

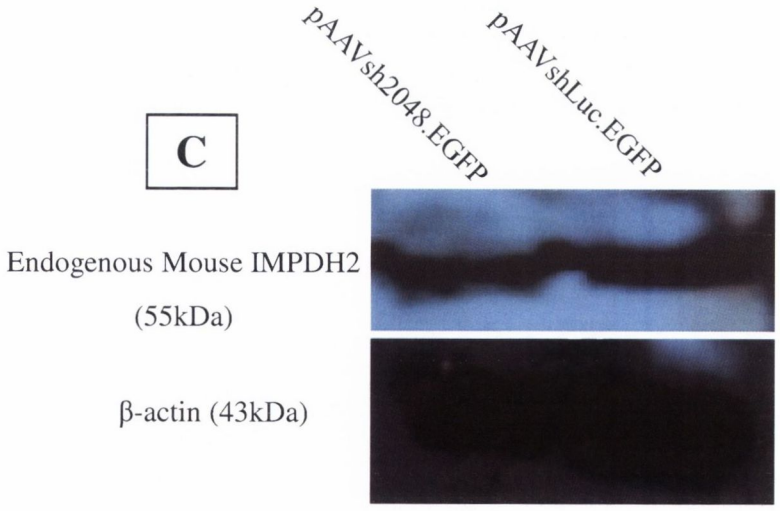

Total retinal protein extracts from *Figure 5.19C*

***Figure 6.7* continued**

D

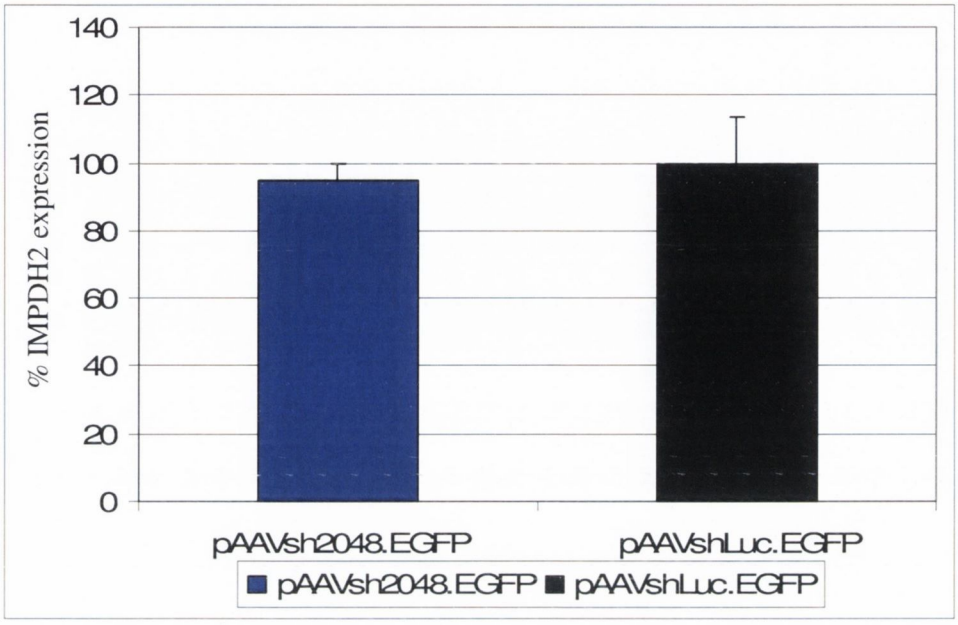

Densitometry (Band Intensity)	pAAVsh2048.EGFP	pAAVshLuc.EGFP
Percentage IMPDH2 expression ± SEM	95% ± 5%	100% ± 13.45%

Figure 6.7: Western blot analysis of IMPDH2 expression *in-vivo.* (A, B and C) Following the detection of endogenous murine IMPDH1 in subretinally injected wild type C57B6/CBA mice as described in *Figure 5.19*, the same protein extracts from each group of injected animals were subjected to western blotting and IMPDH2 was detected using anti-N-IMPDH2 antibody. All blots were stripped and re-probed with β-actin as loading controls. (D) Quantification of IMPDH2 and β-actin band intensities by densitometry. Percentage IMPDH2 expression in band intensity was calculated with respect to control virus (pAAVshLuc.EGFP), which was standardised to represent 100% IMPDH2 expression (black bar), and normalised against β-actin. Average band intensities from (A), (B) and (C) are shown in histograms. Y-error bars denote standard error of the mean.

Chapter 7
Concluding Remarks and Future Studies

7 Concluding remarks and future studies

During the initial stages of this study, it became apparent that selection of optimal siRNA target sequences could be achieved by combining commercial prediction softwares (*www.dharmacon.ie*) with the prediction algorithm designed by Reynolds *et al.*, (2004). Two synthetic siRNAs, designated as si1224 and si2048 targeting distinct regions of human and mouse IMPDH1 shared efficient and sequence specific suppression of IMPDH1 transcripts and protein in mammalian cell culture. Transfection of HeLa cells with the corresponding siRNA oligonucleotides cloned into H1-promoter driven RNAi-vector system resulted in similar levels of IMPDH1 suppression. Furthermore, both shRNAs suppressed IMPDH1 harbouring the Arg224Pro and Asp226Asn mutations in a mutation-independent manner. Over-expression of mutant Arg224Pro IMPDH1, but not wild-type IMPDH1, was found to induce a significant apoptotic response in HeLa cells. The underlying pathological effect has not yet been fully deciphered, but as suggested in a previous study, an alteration in the folding and solubility of the mutant IMPDH1 protein in mammalian cells may cause aberrant protein aggregation leading to cell death (Aherne *et al.*, 2004). *In-vitro* electroporation of dual-expression plasmids containing H1-driven sh2048 and CMV-driven EGFP into murine retinal explants followed by fluorescent activated cell sorting (FACS) analysis brought about robust suppression of endogenous IMPDH1 transcript in true transfectant retinal cell populations *ex-vivo.*

The use of pseudotyped rAAV-2/5 viral vectors expressing sh2048 and EGFP has allowed exclusive transduction of retinal pigment epithelium, photoreceptor outer segment and outer nuclear layer in wild type C57B6/CBA mice following subretinal injection. Furthermore, photoreceptor-specific expression of sh2048 using the rAAV-2/5 viral vector demonstrated significant downregulation of IMPDH1 at the mRNA and protein level *in-vivo* at four weeks post-injection, with no significant adverse effects on retinal function or structure. However, continuous AAV-mediated RNAi suppression of endogenous IMPDH1 by sh2048 caused deteriorations in retinal function and structure four months post-injection. Interestingly, the rate of photoreceptor degeneration occurred at a faster rate than that observed in the

IMPDH1 knockout mouse model (Aherne *et al.*, 2004). Initial investigations centered on the hypothesis that photoreceptor degeneration was caused by non-specific silencing of IMPDH2 in AAV-sh2048 treated eyes, as early embryonic lethality has previously been shown in IMPDH2$^{-/-}$ mice (Gu *et al.*, 2000). However, protein analyses showed that IMPDH2 expression was not affected in AAV-sh2048 treated eyes, suggesting that photoreceptor degeneration was not linked to a lack of IMPDH2. Furthermore IMPDH2 did not provide a compensatory effect for the diminution of IMPDH1 levels, but remained static regardless of the suppression status of IMPDH1. The expression of mutant human IMPDH1 harbouring the Arg224Pro mutation delivered by rAAV-2/5 viral vectors in wild type 129 S2/SvHsd mice has provided a disease model for RP10. Photoreceptor degeneration can be invoked within 4 weeks after subretinal injection, and is characterised by a complete ablation of the outer nuclear layer and an undetectable electroretinographic (ERG) response (Dr. Avril Kennan, unpublished data). Compared to other mouse models with targeted disruption of a dominant RP-associated gene such as rhodopsin or *rds*/peripherin (Humphries *et al.*, 1997; Sanyal *et al.*, 1980), in which completely diminished ERG amplitudes are not observed until after five months of age, this mutant IMPDH1-induced RP10 mouse model appears much more aggressive. The cause of rapid photoreceptor degeneration observed in these mice has not yet been investigated, but it is likely to be caused by IMPDH1 protein misfolding and subsequent aggregation as postulated above by Aherne *et al.*, (2004), and previously shown in a wide range of other hereditary or multifactorial neurodegenerative diseases such as Alzheimer's and Parkinson's disease (Kopito, 2000; Sherman and Goldberg, 2001). Interestingly in this study, simultaneous delivery of AAV-mutant IMPDH1 with rAAV-sh2048 by subretinal injection in wild-type 129 S2/SvHsd mice prolonged the integrity of photoreceptor function and structure. Therefore a similar scenario could be envisaged in patients with RP10 whereby delivery of AAV-sh2048 might be able to attenuate the rate of photoreceptor degeneration by suppressing the mutant protein. Nonetheless, a number of issues regarding the safety of AAV-mediated retinal gene transfer, such as the risk of long-term suppression of IMPDH1,

will need to be addressed, and it remains a considerable challenge to translate the results from small murine models to large animals, and ultimately to human patients.

Evaluation of rAAV-mediated RNAi suppression of IMPDH1 in eyes of large animal models such as non-human primates is an important step towards future clinical development as such eyes are anatomically and physiologically more similar to the human eye than the mouse counterpart. In addition, reliable surgical procedures for vector delivery such as subretinal injection and dosage of injected vector in primate are likely to be similar to those required for use in humans. Most importantly, the therapeutic effect of gene delivery can be safely evaluated in primates by non-invasive methods to monitor retinal function, such as electroretinography (ERG), ophthalmoscopy and optical coherence tomography (OCT). Many reports have shown successful AAV-mediated transgene expression in the retinal pigment epithelium (RPE) and photoreceptor cells of dogs and primates (Bennette *et al.*, 1999; Bainbridge *et al.*, 2003; Lotery *et al.*, 2003). For example, Le Meur *et al.*, (2007) showed that subretinal injection of rAAV-2/4 vector carrying human RPE65 cDNAs driven by a human RPE65 promoter into $RPE65^{-/-}$ purebred Briard dogs restored photoreceptor function. Recently, Ali and colleagues (UCL Institute of Ophthalmology and Moorfields Eye Hospital) reported the first human clinical trial in young adult patients who have developed Leber Congential Amaurosis (LCA) in childhood by subretinal injection of clinical grade rAAV-2/2 carrying RPE65 genes driven by a human RPE65-promoter. The results from this human clinical trial are likely to provide an important basis on which to build further refine results for future clinical trials involving gene therapy.

Although IMPDH1-specific siRNA to elicit silencing effect against IMPDH2 at the mRNA and protein level in mammalian cells and *in-vivo* mouse retinas has been investigated and found to be lacking, it is important to compare transcriptional profiles of mice injected with rAAV-shLuc and rAAV-sh2048 to study potential non-specific silencing of other genes. In addition to the importance of possible changes at the transcriptional level, it is imperative to investigate any secondary changes in

retinal miRNAs following the introduction of AAV-shRNAs, as it has been reported that excessive RNAi can cause lethality in mice by oversaturation of the natural RNAi/ miRNA pathway (Grimm *et al.*, 2006). Recently, many research studies have adopted a new approach for safer RNAi by subcloning siRNA sequences into the backbone of naturally occurring miRNAs to overcome the concern about obstructing the endogenous RNAi machinery. shRNAs bearing a miRNA backbone are processed through a more natural and efficient pathway similar to those of endogenous miRNAs (Chang *et al.*, 2006). In particular, Silva *et al.*, (2006) showed that siRNAs subcloned into the backbone of a natural miRNA (miR-30) can be transcribed efficiently by both polymerase II and III promoters. Interestingly, Castanotto *et al.*, (2007) reported that shRNA bearing the miR-30 backbone maintained its silencing efficiency and did not compete for endogenous RNAi components when compared to the use of normal shRNAs. Therefore in future studies, sh2048 will be cloned into the miRNA backbone to form rAAV-mir2048, and this may maintain the same silencing efficiency as its original counterpart, and may also provide safer long-term application of shRNA expression *in-vivo*. Another aspect to be addressed is the quantification of the levels of AAV delivered mutant IMPDH1 transcripts and shRNAs *in-vivo*. RNase protection assays followed by densitometric analysis of autoradiographs will enable the levels of mutant IMPDH1 and shRNA transcripts expression in the mutant IMPDH1-induced RP10 mouse model to be determined, thus enabling the study of the dynamics and kinetics of interaction between the shRNA and its target transcript. Experiments will be carried out to investigate long-term effects of AAV-mediated shRNA expression in mouse retinas. These will include the analysis of histology, immunohistochemistry, ERG, transcriptional and miRNA profiling at time points of up to one year post-injection, thus extending observations beyond four months post-injection, the furthest time point examined in the current study.

The observation that a single mouse treated with rAAV-sh2048 developed significant photoreceptor degeneration by four months post-injection has suggested that there may be good reason to design a suppression resistant IMPDH1 gene as part of a

combined suppression and replacement strategy as has been developed for rhodopsin (Kiang *et al.*, 2005; Tessitore *et al.*, 2006; Gorbatyuk *et al.*, 2007; O'Reilly *et al.*, 2007). However, future studies including those outlined above may reveal that improved shRNA constructs and strategies do not cause retinal degeneration in mice even after prolonged expression *in-vivo* and thus negate the requirement for a replacement gene. If required however, an important issue to address is the determination of the optimal level of the replacement IMPDH1 gene so that IMPDH1 expression remains sufficiently high to sustain photoreceptor cell survival, but does not exceeding the toxic threshold (Tan *et al.*, 2001).

Collectively, these data have demonstrated that IMPDH1-specific siRNAs expressed from H1-driven vectors and rAAV-2/5 viral vectors can elicit efficient and sequence specific suppression of wild type and mutant IMPDH1 at the mRNA and protein levels in mammalian cells, *ex-vivo* retinal explants and *in-vivo* mouse retinas. Furthermore, the proof-of-principle of rAAV-mediated gene therapy in the mutant IMPDH1-induced RP10 murine model, in conjunction with accumulating evidence that AAV represents a safe and efficient means for delivering molecular therapies to photoreceptors (Rolling *et al.*, 2004), suggest that AAV-mediated RNAi suppression of IMPDH1 holds great promise for future therapies for RP10 patients.

Appendix

Name		Target positions on Human IMPDH1 (NM_000883)	Sequences 5'→3'
sh1057	**Sense** **Antisense**	1057-1075	gatcccc**aagctggtgggcatcgtca**ttcaagaga**tgacgatgcccaccagctt**ttttggaaa agcttaaaaa**aagctggtgggcatcgtca**tagagaactt**tgacgatgcccaccagctt**ggg
sh2065	**Sense** **Antisense**	2065-2083	gatcccc**aagtttgagaagcggacca**ttcaagaga**tggtccgcttctcaaactt**ttttggaaa agcttaaaaa**aagtttgagaagcggacca**tagagaactt**tggtccgcttctcaaactt**ggg
sh2067	**Sense** **Antisense**	2067-2085	gatcccc**gtttgagaagcggaccatg**ttcaagaga**catggtccgcttctcaaac**ttttggaaa agcttaaaaa**gtttgagaagcggaccatg**tagagaactt**catggtccgcttctcaaac**ggg
sh688	**Sense** **Antisense**	688-702	gatcccc**ctcacctacaacgacttcc**ttcaagaga**ggaagtcgttgtaggtgag**ttttggaaa agcttaaaaa**ctcacctacaacgacttcc**tagagaactt**ggaagtcgttgtaggtga**gggg
sh1969	**Sense** **Antisense**	1969-1988	gatcccc**gtgccctacctcatagcag**ttcaagaga**ctgctatgaggtagggcac**ttttggaaa agcttaaaaa**gtgccctacctcatagcag**tagagaactt**ctgctatgaggtagggcac**ggg
si1057	**Sense** **Antisense**	2067-2085	**aagcuggugggcaucguca** **ugacgaugcccaccagcuu**
si1553	**Sense** **Antisense**	1553-1571	**gaaccugauugaugcuggu** **accagcaucaaucagguuc**
si1224	**Sense** **Antisense**	1224-1242	**gcugccuaucgucaaugau** **aucauugacgauaggcagc**
si2048	**Sense** **Antisense**	2048-2066	**uguacucaggagagcucaa** **uugagcucuccugaguaca**
sh1224	**Sense** **Antisense**	1224-1242	gatcccc**gctgcctatcgtcaatgat**ttcaagaga**atcattgacgataggcagc**ttttta agcttaaaaa**gctgcctatcgtcaatga**ttctcttgaa**atcattgacgataggcagc**ggg
sh2048	**Sense** **Antisense**	2048-2066	gatcccc**tgtactcaggagagctcaa**ttcaagaga**ttgagctctcctgagtaca**ttttta agcttaaaaa**tgtactcaggagagctcaa**tctcttgaa**ttgagctctcctgagtaca**ggg
siMR3	**Sense** **Antisense**	683-701	gccugaggucaacaacgaa uucguuguugaccucagga
shMR3	**Sense** **Antisense**	683-701	gatcccc**gcctgaggtcaacaacgaa**ttcaagaga**ttcgttgttgacctcaggc**ttttta agcttaaaaa**gcctgaggtcaacaacgaa**tctcttgaa**ttcgttgttgacctcaggc**ggg
siLuc	**Sense** **Antisense**	-	cuuacgcugaguacgucga ucgaaguacucagcguaag
shLuc	**Sense** **Antisense**	-	gatcccc**gcgtacggggaaacttcga**ttcaagaga**tcgaagtattccgcgtacg**ttttggaa agcttttccaaaaa**cgtacgcggaatacttcga**tctcttgaa**tcgaagttttccccgtacgc**ggg
siNT	**Sense** **Antisense**	-	uucuccgaacgugucacgu acgugacacguucggagaa

Table 1: Sequences of IMPDH1-specific shRNAs and synthetic siRNAs, and non-targeting control si/shRNAs. shRNA oligonucleotides were provided by Sigma-Genosys and chemically synthesised siRNAs were obtained from Dharmacon Ltd. siRNA target sequences are underlined in bold. Si/shMR3: Rhodopsin targeting si/shRNA. siLuc: siRNA targeting Luciferase GL3. shLuc: shRNA targeting Luciferase GL2. siNT: scrambled siRNA obtained from Qiagen.

Gene		Product Size	Sequences 5'→3'	Gene Bank Accession Number
Human and Mouse IMPDH1	Forward Reverse	99bp	cgtgaggatgacaaataccg accatggcgatctgatacac	NM_000883 (Human) BC_053416 (Mouse)
Human and Mouse IMPDH2	Forward Reverse	193bp	acacctgaattccaggccaa gaggagatgatgcccaccaa	NM_000884 (Human) BC_052671 (Mouse)
Transcription Binding Protein (TBP)	Forward Reverse	90bp	gcatattttcttgctgccagtct accacggcactgattttcagtt	NM_003194
Human β-actin	Forward Reverse	296bp	tcacccacactgtgcccatctacga cagcggaaccgctcattgccaatgg	XM_004814 (Human) EF_095208 (Mouse)
Human IMPDH1 only	Forward Reverse	215bp	tgcctatcgtcaatgattgc tcccttgggacgagtccaag	NM_000883

Table 2: Sequences of HPLC-purified primers for Real-Time RT-PCR amplification. Primers were HPLC purified and made up to 100pmoles according to manufacturer's instructions (Sigma-Genosys).

Name		Product Size	Sequences 5'→3'
T7 primers for shRNA oligo inserts in H1-promoter	Forward Reverse	466bp (without inserts) 530bp (+inserts)	aacagctatgaccatg cgccagggttttcccagtcacgac
Primers for IMPDH2 cDNA	Forward Reverse	1544bp	atttgcggccgctcatggccgactacctgattag ccgctcgagtcagaaaagccgcttctcat

Table 3: Sequences of primers for template-DNA amplification. Primers are desalted and made up to 100pmoles according to manufacturer's instructions (Sigma-Genosys).

Name		Sequence 5'→3'
H1-specific primers for determining (+ve) shRNA inserts	Forward	gaacgctgacgtcatcaacc
	Reverse	attaatgcagctggcacgac
Primers for sequencing IMPDH2-tagged EGFP constructs (NM_000884)		
IMPDH2GFPFr1	Forward	acggcaagctgaccctgaag
IMPDH2GFPFr2	Forward	acaacatcgaggacggcagc
IMPDH2seq2	Forward	gactttctcattctccctgg
IMPDH2seq3	Forward	ggtttctgcggtatcccaat
IMPDH2seq4	Forward	tagcctccaaagatgccaag
IMPDH2seq5	Forward	agcaacagcagtgtacaagg
IMPDH2seq6	Forward	gacaaaatcaaagtggccca

***Table 4**:* Sequences of primers used for sequencing of shRNAs subcloned into pBluescript-H1 and IMPDH2 cDNA subcloned into pcDNA3.1(+). Primers were desalted and made up to 100pmoles according to manufacturer's instructions (Sigma-Genosys).

Primers for sequencing **pWtIMPDH1, pMutIMPDH1(224), pMutIMPDH1(226), pWtIMPDH1.EGFP** and **pMutIMPDH1(224).EGFP**		5'→3'
IMPDH1fr1	Forward	caaatgggcggtaggcgtgt
IMPDH1fr2	Forward	acggcaagctgaccctgaag
IMPDH1fr3	Forward	ggtgaagttcgagggcgaca
IMPDH1fr4	Forward	ctgctgcccgacaaccacta
IMPDH1fr5	Forward	ctcacctacaacgacttcct
IMPDH1fr6	Forward	gaacagggcttcatcacgga
IMPDH1fr7	Forward	ccaaggattgaactggtggt
IMPDH1fr8	Forward	ataccgtctggacctgctga
IMPDH1fr9	Forward	aggaagtgatggcctgtggt
IMPDH1fr10	Forward	ggatcccatggagaagagca

Table 5: Primers used for sequencing pWtIMPDH1, pMutIMPDH1(224), pWtIMPDH1.EGFP, pMutIMPDH1(224).EGFP and pMutIMPDH1(226).EGFP. Primers were desalted and made up to 100pmoles according to manufacturer's instructions (Sigma-Genosys).

Primer names	Orientation	5' to 3'
Human UbC Fr	Forward	ctgttcccgagtcttgaatg
Human UbC Rv	Reverse	aacgggtgacgtcacgacac

Table 6: Primers used for PCR amplification of human Ubc intron from pUB6/V5-His A, B, C (Invitrogen).

Primer names	Orientation	5' to 3'
pCMVEGFPfr1	Forward	gtgtacggtgggaggtctat
pCMVEGFPfr2	Forward	atttccaagtctccacccca
pCMVEGFPrv1	Reverse	accgagttctccagtcagtg

Table 7: Primers for sequencing pshLuc.EGFP and psh2048.EGFP. Primers were desalted and made up to 100pmoles according to manufacturer's instructions (Sigma-Genosys).

References

Acland G. M, Aguirre G. D, Ray J, Zhang Q, Aleman T.S , Cideciyan A. V, Pearce-Kelling S. E, Anand V, Zeng Y, Maguire A. M, Jacobson S. G, Hauswirth W. W, Bennett J (2001) Gene therapy restores vision in a canine model of childhood blindness. *Nat. Genet.* **28**: 92–95

Acland G. M, Aguirre G. D, Bennett J, Aleman T. S, Cideciyan AV, Bennicelli J, Dejneka NS, Pearce-Kelling S. E, Maguire A. M, Palczewski K, Hauswirth W. W, Jacobson SG (2005) Long-term restoration of rod and cone vision by single dose rAAV-mediated gene transfer to the retina in a canine model of childhood blindness. *Mol Ther.* **12**: 1072–1082

Aharinejad S, Paulus P, Sioud M, Hofmann M, Zins K, Schafer R, Stanley E. R, Abraham D (2004) Colony stimulating factor-1 blockade by antisense oligonucleotides and small interfering RNAs suppresses growth of human mammary tumour xenografts in mice. *Cancer Res.* **64**: 5378-5384

Aherne A, Kennan A, Kenna P. F, McNally N, Lloyd D. G, Alberts I. L, Kiang A. S, Humphries M. M, Ayuso C, Engel P. C, Gu J. J, Mitchell B. S, Farrar G. J, Humphries P (2004) On the molecular pathology of neurodegeneration in IMPDH1-based retinitis pigmentosa. *Human Molecular Genetics.* **13(6)**: 641–650

Ahmad I, Tang L, Pham H (2000) Identification of neural progenitors in adult mammalian eye. *Biochem. Biophys. Res. Commun.* **270**: 517-521

Aihara H and Miyazaki J (1998) Gene transfer into muscle by electroporation *in-vivo*. *Nat Biotechnol.* **16**: 867–870

Akaneya Y, Jiang B, Tsumoto T (2005) RNAi-mediated gene silencing by local electroporation in targeting brain region. *J Neurophysiol.* **93**: 594-602

Ali R. R, Reichel M. B, Thrasher A. J, Levinsky R. J, Kinnon C, Kanuga N, Hunt D. M, Bhattacharya S. S (1996) Gene transfer into the mouse retina mediated by an adeno-associated viral vector. *Hum. Mol. Genet.* **5**: 591–594

Ali R. R, Reichel M. B, De Alwis M, Kanuga N, Kinnon C, Levinsky R. J, Hunt D. M, Bhattacharya S. S, Thrasher A. J (1998) Adeno-associated virus gene transfer to mouse retina. *Hum. Gene Ther.* **9**: 81–86

Ali R. R, Sarra G. M, Stephens C, Alwis M. D, Bainbridge J. W, Munro P. M, Fauser S, Reichel M. B, Kinnon C, Hunt D. M, Bhattacharya S. S, Thrasher A. J (2000) Restoration of photoreceptor ultrastructure and function in retinal degeneration slow mice by gene therapy. *Nat. Genet.* **25**: 306–310

Alino S. F, Crespo A, Dasi F (2003) Long term therapueitc levels of human alpha-1 antitrypsin in plasma after hydrodynamic injection of nonviral DNA. *Gene Ther.* **10**: 1672-1679

Allerson C. R, Sioufi N, Jarres R, Prakash T. P, Naik N, Berdeja A, Wanders L, Griffey R. H, Swayze E. E, Bhat B (2005) Fully 2'-modified oligonucleotide duplexes with improved in vitro potency and stability compared to unmodified small interfering RNA. *J. Med. Chem.* **48**: 901-904

Allison A. C, Almquist S. J, Muller C. D, Eugui E. M (1991) *In-vitro* immunosuppressive effects of mycophenolic acid and an ester prodrug RS-61443. *Transplant. Proc.* **23**: 10–14

Allocca M, Mussolino C, Garcia-Hoyos M, Sanges D, Iodice C, Petrillo M, Vandenberghe L. H, Wilson J. M, Marigo V, Surace E. M, Auriicchio A (2007) Novel adeno-associated virus serotypes efficiently transducer murine photoreceptors. *Journal of Virology*. **81 (20)**: 11372-11380

Alvarez-Garcia I and Miska E. A (2005) MicroRNA functions in animal development and human disease. *Development*. **132**: 4653-4662

Alves-Rodrigues A, Gregori L, Figueiredo-Pereira ME (1998) Ubiquitin, cellular inclusions and their role in neurodegeneration. *Trends Neurosci*. **21**: 516-520

Amabile P. G, Waugh J. M, Lewis T. N, Elkins C. J, Janas W, Dake M. D (2001) High-efficiency endovascular gene delivery via therapeutic ultrasound. *J Am Coll Cardiol*. **37**: 1975-1980

Amarzguioui M and Prydz H (2004) An algorithm for selection of functional siRNA sequences. Biochem. *Biophys. Res. Commun.* **316**: 1050–1058

Amarzguioui M, Holen T, Babaie E, Prydz H (2003) Tolerance for mutations and chemical modifications in a siRNA. *Nucleic Acids Res.* **31**: 589-595

Amarzguioui M, Lundberg P, Cantin E, Hagstrom J, Behlke M. A, Rossi J. J (2006) Rational design and in vitro and in vivo delivery of Dicer substrate siRNA. *Nat Protoc.* **1(2)**: 508-17

Ambros V and Chen X (2007) The regulation of genes and genomes by small RNAs. *Development*. **134**: 1635-1641

Anand V, N. Chirmule N, M. Fersh M, A.M. Maguire A. M, Bennett J (2000) Additional transduction events after subretinal readministration of recombinant adeno-associated virus. *Hum. Gene Ther.* **11**: 449–457

Anderson C, Catoe H, Werner R (2006) MIR-206 regulates connexin43 expression during skeletal muscle development. *Nucleic Acids Res*. **34**: 5863-5871

André F and Mir L. M (2004) DNA electrotransfer: its principles and an updated review of its therapeutic applications. *Gene Ther.* **11 (Suppl 1)**: S33–S42

Andrei M.A, Ingelfinger D, Heintzmann R, Achsel T, Rivera-Pomar R, Lubrmann R (2005) A role for eIF4E-transporter in targeting mRNPs to mammalian processing bodies. *RNA*. **11**: 717-727

Andrés A, Garriga P, Manyosa J (2003) Altered functionality in rhodopsin point mutants associated with retinitis pigmentosa. *Biochem Biophys Res Commun*. **303**: 294-301

Aravin A and Tuschl T (2005) Identification and characterization of small RNAs involved in RNA silencing. *FEBS Lett*. **579**: 5830-5840

Argrawal N, Dasaradhi P. V, Mohmmed A, Malhotra P, Bhatnagar R. K, Mukherjee S. K (2003) RNA interference: biology, mechanism, and applications. *Microbiol Mol Biol Rev*. **67**: 657-658

Armant M. A and Fenton M. J (2002) Toll-like receptors: a family of pattern-recognition receptors in mammals. *Genome Biol.* **29**: 3

Asahara T, Shinomiya K, Naito T, Shiota H (2001) Induction of gene into the rabbit eye by iontophoresis: preliminary report, *Jpn J Ophthalmol* **45**: 31–39

Auricchio A, Hildinger M, O'Connor E, Gao G. P, Wilson J. M (2001a) Isolation of highly infectious and pure adeno-associated virus type 2 vectors with a single-step gravity-flow column. *Hum Gene Ther.* **12**: 71–76

Auricchio A, Kobinger G, Anand V, Hildinger M, O'Connor E, Maguire A. M, Wilson J. M, Bennett J (2001b) Exchange of surface proteins impacts on viral vector cellular specificity and transduction characteristics: the retina as a model. *Hum. Mol. Gene.* **10 (26)**: 3075-3081

Auricchio A, Rivera V. M, Clackson T, O'Connor E. E, Maguire A. M, Tolentino M. J, Bennett J, Wilson J. M (2002a) Pharmacological regulation of protein expression from adeno-associated viral vectors in the eye. *Mol Ther.* **6**: 238-42

Auricchio A, Behling K. C, Maguire A. M, O'Connor E. M, Bennett J, Wilson J. M, Tolentino M. J (2002b) Inhibition of retinal neovascularization by intraocular viral-mediated delivery of anti-angiogenic agents. *Mol. Ther.* **6**: 490–494

Babiuk S, Baca-Estrada M. E, Foldvari M, Storms M, Rabussay D, Widera G, Babiuk L. A (2002a) Electroporation improves the efficacy of DNA vaccines in large animals. *Vaccine.* **20**: 3399–3408

Babiuk S, Baca-Estrada ME, Pontarollo R, Foldvari M (2002b) Topical delivery of plasmid DNA using biphasic lipid vesicles (Biphasix). *J Pharm Pharmacol.* **54(12)**: 1609-14

Bahasra O and Prilliman K. R (2004) RNA interference: the molecular immune system. *J Mol Histol.* **35**: 545-553

Bainbridge J. W, Stephens C, Parsley K, Demaison C, Halfyard A, Thrasher A. J, Ali R. R (2001) In vivo gene transfer to the mouse eye using an HIV-based lentiviral vector; efficient long-term transduction of corneal endothelium and retinal pigment epithelium. *Gene Ther.* **8**: 1665–1668

Bainbridge J. W, Mistry A, De Alwis M, Paleolog E, Baker A, Thrasher A. J, Ali R. R (2002) Inhibition of retinal neovascularisation by gene transfer of soluble vegf receptor sFlt-1. *Gene Ther.* **9**: 320–326

Bainbridge J. W, Mistry A, Schlichtenbrede F. C, Smith A, Broderick C, De Alwis M, Georgiadis A, Taylor P. M, Squires M, Sethi C, Charteris D, Thrasher AJ, Sargan D, Ali R. R (2003) Stable rAAV-mediated transduction of rod and cone photoreceptors in the canine retina. *Gene Therapy.* **10**: 1336-1344

Bainbridge J. W. B, Tan M. H, Ali R. R (2006) Gene therapy progress and prospects: the eye. *Gene Therapy.* **13**: 1191-1197

Baldwin A. S (1996) The NF-kappa B and I kappa B proteins: new discoveries and insights. *Annu. Rev. Immunol.* **14**: 649-81

Balicki D and Beutler E (1997) Histone H2A significantly enhances *in-vitro* DNA transfection. *Mol Med.* **3(11)**:782-7

Balicki D, Putnam C. D, Scaria P. V, Beutler E (2002) Structure and function correlation in histone H2A peptide-mediated gene transfer. *Proc Natl Acad Sci U S A.* **99(11)**: 7467-71

Banga A. K, Bose S, Ghosh T. K (1999) Iontophoresis and electroporation: comparisons and contrasts. *Int J Pharm.* **179**: 1–19

Banin E, Cideciyan A. V, Aleman T. S, Petters R. M, Wong F, Milam A. H, Jacobson S. G (1999) Retinal rod photoreceptor-specific gene mutation perturbs cone pathway development. *Neuron.* **23**: 549–557

Bantel-Schaal U and zur Hausen H (1984) Characterization of the DNA of a defective human parvovirus isolated from a genital site. *Virology.* **134**: 52–63

Bantel-Schaal U, Delius H, Schmidt R, zur Hausen H (1999) Human adeno-associated virus type 5 is only distantly related to other known primate helper-dependent parvoviruses. *J. Virol.* **73**: 939–947

Bantounas I, Phylactou L. A, Uney J. B (2004) RNA interference and the use of small interfering RNA to study gene function in mammalian systems. *J Mol Endocrinol.* **33**: 545-557

Barbee S. A, Estes P. S, Cziko A. M, Hillebrand J, Luedeman R. A, Coller J. M, Johnson N, Howlett I. C, Geng C, Ueda R (2006) Staufen-and FMRP-containing neuronal RNPs are structurally and functionally related to somatic P bodies. *Neuron.* **52**: 997-1009

Barik S (2006) RNAi in moderation. *Nature Biotechnology.* **24(7)**: 796-797

Bartel D. P (2004) MicroRNAs: Genomics, biogenesis, mechanism, and function. *Cell.* **116**: 281-297

Barton G. M and Medzhitov R (2002) Retroviral delivery of small interfering RNA into primary cells. *Proc. Natl. Acad. Sci. USA.* **99**: 14943-14945

Beales P. L, Elcioglu N, Woolf A. S, Parker D, Flinter F. A (1999) New criteria for improved diagnosis of Bardet-Biedl syndrome: results of a population survey. *J Med Genet.* **36**: 437–446

Beales P. L, Badano J. L, Ross A. J, Ansley S. J, Hoskins B. E, Kirsten B, Mein C. A, Froguel P, Scambler P. J, Lewis R. A, Lupski J. R, Katsanis N. (2003) Genetic interaction of BBS1 mutations with alleles at other BBS loci can result in non-Mendelian Bardet-Biedl syndrome. *Am J Hum Genet.* **72**:1187–1199

Becker M. A and Roessler B. J (1995) in The Metabolic and Molecular Bases of Inherited Disease (Scriver, C. R., Beaudet, A. L., Sly, W. S., and Valle, D., eds), **Vol. 2**; 1655-1677, McGraw-Hill Inc., New York

Behar-Cohen F. F, Parel J. M, Pouliquen Y, Thillaye-Goldenberg B, Goureau O, Heydolph S, Courtois Y, De Kozak Y (1997) Iontophoresis of dexamethasone in the treatment of endotoxin-induced-uveitis in rats. *Exp Eye Res.* **65**: 533–545

Behar-Cohen F. F, Savoldelli M, Parel J. M, Goureau O, Thillaye-Goldenberg B, Courtois Y, Pouliquen Y, de Kozak Y (1998) Reduction of corneal edema in endotoxin-induced uveitis after application of L-NAME as nitric oxide synthase inhibitor in rats by iontophoresis. *Invest Ophthalmol Vis Sci* **39**: 897–904

Behar-Cohen F. F, El Aouni A, Gautier S, David G, Davis J, Chapon P, Parel J. M (2002) Transscleral Coulomb-controlled iontophoresis of methylprednisolone into the rabbit eye: influence of duration of treatment, current intensity and drug concentration on ocular tissue and fluid levels. *Exp Eye Res.* **74**: 51–59

Behlke A. M (2006) Progress towards *in vivo* use of siRNAs. *Molecular Therapy.* **13 (4)**: 644-70

Behm-Ansmant I, Rehwinkel J, Doerks T, Stark A, Bork P, Izaurralde E (2006) mRNA degradation by miRNAs and GW182 requires both CCR4-NOT deadenylase and DCP:DCP2 decapping complexes. *Genes. Dev.* **20**: 1885-1898

Bejjani R. A, Andrieu C, Bloquel C, Berdugo M, BenEzra D, Behar-Cohen F (2007) Electrically Assisted Ocular Gene Therapy. *Survey of Ophthalmology.* **52 (2)**: 196-208

Bence NF, Sampat RM, Kopito RR (2001) Impairment of the ubiquitin-proteasome system by protein aggregation. *Science.* **292**: 1552-1555

Bennett J, Pakola S, Zeng Y, Maguire A (1996) Humoral response after administration of E1-deleted adenoviruses: immune privilege of the subretinal space. *Hum. Gene Ther.* **7**: 1763–1769

Bennett J, Maguire A. M, Cideciyan A. V, Schnell M, Glover E, Anand V, Aleman T. S, Chirmule N, Gupta A. R, Huang Y, Gao G. P, Nyberg W. C, Tazelaar J, Hughes J, Wilson J. M, Jacobson S. G (1999) Stable transgene expression in rod photoreceptors after recombinant adeno-associated virus-mediated gene transfer to monkey retina. *Proc Natl Acad Sci USA.* **96**: 9920-9925

Bennett J (2000) Gene therapy for retinitis pigmentosa. *Curr. Opin. Mol. Therapeutics* **2**: 420–425

Bentwich I, Avniel A, Karov Y, Aharonov R, Gilad S, Barad O, Barzilai A, Einat P, Einav U, Meiri E, Sharon E, Spector Y, Bentwich Z (2005) Identification of hundreds of conserved and nonconserved human microRNAs. *Nat. Genet.* **37**: 766-770

Berdugo M, Valamanesh F, Andrieu C, Klein C, Benezra D, Courtois Y, Behar-Cohen F (2003) Delivery of antisense oligonucleotide to the cornea by iontophoresis. *Antisense Nucleic Acid Drug Dev.* **13**: 107–114

Berezikov E, Guryev V, van de Belt J, Wienholds E, Plasterk RH, Cuppen E (2005) Phylogenetic shadowing and computational identification of human microRNA genes. *Cell.* **120**: 21-24

Bergan R, Connell Y, Fahmy B, Neckers L (1993) Electroporation enhances c-myc antisense oligodeoxynucleotide efficacy. *Nucl. Acids Res.* **21**: 3567–3573

Berger W, van de Pol D, Bachner D, Oerlemans F, Winkens H,Hameister H, Wieringa B, Hendriks W, Ropers H. H, Ploos van Amstel J. K, Bergman A. J, van Beurden E. A,

Roijers J. F, Peelen T, van den Berg I. E, Poll B. T, Kvittingen E. A, Berger R (1996) An animal model for Norrie disease (ND): gene targeting of the mouse ND gene. Hum Mol Genet. 5: 51-59

Berns K. I (1996) Paroviridae: the viruses and their replication. In: B.N. Fields, Editor. Fundamental Virology. Lippincot-Raven. Philadelphia, New York: 1017–1042

Berns K, Hijmans E. M, Mullenders J, Brummelkamp T. R, Velds A, Heimerikx M, Kerkhoven R. M, Madiredjo M, Nijkamp W, Weigelt B, Agami R, Ge W, Gavet G, Linsley P. S, Beijersbergen R. L, Bernards R (2004) A large scale RNAi screen in human cells identifies new components of the p53 pathway. *Nature.* **428 (6981)**: 431-437

Bernstein E, Caudy A. A, Hammond S. M, Hannon G. J (2001) Role for a bidentate ribonuclease in the initiation step of RNA interference. *Nature.* **409**: 363-366

Berson E. L, Rosner B, Simonoff E (1980) Risk factors for genetic typing and detection in retinitis pigmentosa. *Am J Ophthalmol.* **89**: 763–775

Berson E.L, Rosner B, Sandberg M. A, Dryja T. P (1991) Ocular findings in patients with autosomal dominant retinitis pigmentosa and a rhodopsin gene defect (Pro-23-His). *Arch. Ophthalmol.* **109**: 92–101

Berson E. L (1993) Retinitis pigmentosa: the Friedenwald lecture. *Invest Ophthalmol Vis Sci.* **34**: 1659–1676

Berson E. L, Rosner B, Sandberg M. A, Hayes K. C, Nicholson B. W, Weigel-DiFranco C, Willett W. I (1993a) A randomized trial of vitamin A and vitamin E supplementation for retinitis pigmentosa, *Arch Ophthalmol.* **111**: 761–772

Berson E. L, Rosner B, Sandberg M. A, Hayes K. C, Nicholson BW, Weigel-DiFrano C, Willett W (1993b) Vitamin A supplementation for retinitis pigmentosa. *Arch Ophthalmol.* **111(11)**: 1456-9.

Berson E. L (1998) Treatment of retinitis pigmentosa with vitamin A. *Digit J Ophthalmol.* **4**: 1–4

Berson E. L, Rosner B, Sandberg M. A, Weigel-DiFranco C, Moser A, Brockhurst R. J, Hayes K. C, Johnson C. A, Anderson E. J, Gaudio A. R, Willett W. C, Schaefer E. J (2004) Further evaluation of docosahexaenoic acid in patients with retinitis pigmentosa receiving vitamin A treatment: subgroup analyses. *Arch Ophthalmol.* **122**: 1306–1314

Bessant D. A, Payne A. M, Mitton K. P, Wang Q. L, Swain P. K, Plant C, Bird A. C, Zack D. J, Swaroop A, Bhattacharya S. S (1999) A mutation in NRL is associated with autosomal dominant retinitis pigmentosa. *Nat Genet.* **21**: 355-6

Bhattacharyya S. N, Habermacher R, Martine U, Closs E. I, Filipowicz W. (2006) Relief of microRNA-mediated translational repression in human cells subjected to stress. *Cell.* **125**: 1111-1124

Birch D. G, Anderson J. L, Fish G. E (1999) Yearly rates of rod and cone functional loss in retinitis pigmentosa and cone-rod dystrophy. *Ophthalmology.* **106** (1999):258–268

Birmingham A, Anderson E. M, Reynolds A, Ilsley-Tyree D, Leake D, Fedorov Y, Baskerville S, Maksimova E, Robinson K, Karpilow J, Marshall WS, Khvorova A (2006)

3'UTR seed matches, but not overall identity, are associated with RNAi off-targets. *Nat. Methods.* **3**: 199-204

Blair E, Redwood C, Ashrafian H, Oliveira M, Broxholme J, Kerr B, Salmon A, Ostman-Smith I, Watkins H (2001) Mutations in the g(2) subunit of AMP-activated protein kinase cause familial hypertrophic cardiomyopathy: evidence for the central role of energy compromise in disease pathogenesis. *Hum. Mol. Genet.* **10**: 1215–1220

Blair-Parks K, Weston B. C, Dean D. A (2002) High-level gene transfer to the cornea using electroporation. *J Gene Med.* **4**: 92–100

Bockaert J and Pin J. P (1999) Molecular tinkering of G protein-coupled receptors: An evolutionary success. *EMBO J.* **18**: 1723-1729

Boden D, Pusch O, Silbermann R, Lee F, Tucker L, Ramratnam B (2004) Enhanced gene silencing of HIV-1 specific siRNA using microRNA designed hairpins. *Nuclei Acid Research.* **32 (3)**: 1154-1158

Bok D, Yasumura D, Matthes M. T, Ruiz A, Duncan J. L, Chappelow A. V, Zolutukhin S, Hauswirth W. W, LaVail M. M (2002) Effects of AAV-vector CNTF on retinal structure and function in mice with P216L rds/peripherin mutation. *Exp. Eye. Res.* **74**: 719-735

Bonnafous P, Vernhes M, Teissie J, Gabriel B (1999) The generation of reactive-oxygen species associated with long-lasting pulse-induced electropermeabilization of mammalian cells is based on a non-destructive alteration of the plasma membrane. *Biochim Biophys Acta.* **1461**: 123–134

Bosch A, Perret E, Desmaris N, Heard J. M (2000) Long-term and significant correction of brain lesions in adult mucopolysaccharidosis type VII mice using recombinant AAV vectors. *Mol Ther.* **1**: 63-70

Boussif O, Lezoualc'h F, Zanta M. A, Mergny M. D, Scherman D, Demeneix B, Behr J. P (1995) A versatile vector for gene and oligonucleotide transfer into cells in culture and in vivo: polyethylenimine. *Proc Natl Acad Sci U S A.* **92(16)**: 7297-301

Bowes Rickman C, Ebright J. N, Zavodni Z. J, Yu L, Wang T, Daiger S. P, Wistow G, Boon K, Hauser M. A (2006) Defining the human macula transcriptome and candidate retinal disease genes using EyeSAGE. *Invest Ophthalmol Vis Sci.* **47**: 2305–2316

Bowne S. J, Sullivan L. S, Ding L, Traer E, Prescott S. M, Birch D. G, Kennan A, Humphries P, Daiger S. P (2000) Evaluation of human diacylglycerol kinase iota, a homolog of Drosophila rdgA, in inherited retinopathy mapping to 7q. *Mol. Vis.* **6**: 6–9

Bowne S. J, Sullivan L. S, Blanton S. H, Cepko C. L, Blackshaw S, Birch D. G, Hughbanks-Wheaton D, Heckenlively J. R, Daiger S. P (2002) Mutations in the inosine monophosphate dehydrogenase 1 gene (IMPDH1) cause the RP10 form of autosomal dominant retinitis pigmentosa. *Human Molecular Genetics.* **11 (5)**: 559-568

Bowne S. J, Liu Q, Sullivan L. S, Zhu J, Spellicy C. J, Rickman C. B, Pierce E. A, Daiger P (2006a) Why do mutations in the ubiquitously expressed housekeeping gene IMPDH1 cause retina-specific photoreceptor degeneration? *Invest Ophthalmol Vis Sci.***47 (9)**: 3754-3765

Bowne S. J, Sullivan L. S, Mortimer S. E, Hedstrom L, Zhu J, Spellicy C. J, Gire A. I, Hughbanks-Wheaton D, Birch D. G, Lewis R. A, Heckenlively J. R, Daiger S. P (2006b) Spectrum and Frequency of Mutations in IMPDH1 Associated with Autosomal Dominant Retinitis Pigmentosa and Leber Congenital Amaurosis. *Investigative Ophthalmology and Visual Science*. **47**: 34-42

Braasch D. A, Jensen S, Liu Y, Kaur K, Arar K, White M. A, Corey D. R (2003) RNA interference in mammalian cells by chemically-modified RNA. *Biochemistry*. **42**: 7967-7975

Brady H. J and Gil-Gomez G (1998) The pro-apoptotic Bcl-2 family member, Bax. *Int J Biochem Cell Biol*. **30**: 647-650

Brelen M. E, Duret F, Gerard B, Delbeke J, Veraart C (2005) Creating a meaningful visual perception in blind volunteers by optic nerve stimulation. *J Neural Eng*. **2**: 22–28

Brengues M, Teixeira D, Paerker R (2005) Movement of eukaryotic mRNAs between polysomes and cytoplasmic processing bodies. *Science*. **310**: 486-489

Brennecke J, Hipfner D. R, Stark A, Russell R. B, Cohen S. M. (2003) Bantam encodes a developmentally regulated microRNA that controls cell proliferation and regulates the proapototic gene hid in Drosophilia. *Cell*. **113**: 25-36

Bridge A. J., Pebernard S., Ducraux A., Nicoulaz A. L., Iggo R (2003) Induction of an interferon response by RNAi vectors in mammalian cells. *Nature Genet*. **34**: 263–264

Bron A. J, Tripathi R. C, Tripathi B. J. Wolff's Anatomy of the eye and orbit, 8th edition. *Chapman and Hall Medical* (1997)

Bronson R. T, Donahue L. R, Johnson K. R, Tanner A, Lane P. W, Faust J. R (1998) Neuronal ceriod lipofuscinosis (nclf), a new disorder of the mouse linked to chromosome 9. *Am J Med Genet*. **77**: 289-297

Brummelkamp T. R, Bernards R, Agami R (2002) A system for stable expression of short interfering RNAs in mammalian cells. *Science (Wash DC)*. **296**: 550–553

Bucciantini M, Calloni G, Chiti F, Formigli L, Nosi D, Dobson C. M, Stefani M (2004) Prefibrillar amyloid protein aggregates share common features of cytotoxicity. *J Biol Chem*. **279**: 31374-31382

Bulletin, B.R. Bio Rad Bulletin. 2084 (www.bio-rad.com/genetransfer)

Bullingham R. E. S, Nicholls A. J Kamm B. R (1998) Clinical pharmacokinetics of mycophenolate mofetil. *Clin. Pharmacokinet*. **34**: 429–455

Bunker C. H, Berson E. L, Bromley W. C, Hayes R.P, Roderick T. H (1984) Prevalence of retinitis pigmentosa in Maine, *Am J Ophthalmol*. **97**: 357–365

Bunt-Milam A. H, Kalina R. E, Pagon R. A (1983) Clinical-ultrastructural study of a retinal dystrophy. *Invest Ophthalmol Vis Sci*. **24**: 458-469

Burmeister P. E, Lewis S. D, Silva R. F, Preiss J. R, Horwitz L. R, Pendergrast P. S (2005) Direct in vitro selection of a 2'-O-methyl aptamer to VEGF. *Chem Biol*. **12**: 25-33

Campochiaro P. A (1997) Pathogenic mechanisms in proliferative vitreoretinopathy. *Arch Ophthamol.* **115**: 237-241

Campochiaro P. A (2000) Retinal and choroidal neovascularization. *J. Cell Physiol.* **184**: 301–310

Campochiaro P. A (2006) Potential applications for RNAi to probe pathogenesis and develop new treatments of ocular disorders. *Gene Therapy.* **13**: 559-562

Caplen N. J, Parrish S, Imani F, Fire A, Morgan R. A (2001) Specific inhibition of gene expression by small double-stranded RNAs in invertebrate and vertebrate systems. *Proc Natl Acad Sci USA.* **98**: 9742-9747

Carr S. F, Papp E, Wu J. C, Natsumeda Y (1993) Characterisation of human type 1 and type II IMP dehydrogenase. *J Biol Chem.* **268**: 27286-27290

Carter-Dawson L. D, Kuwabara T, O'Brien P. J, Bieri J. G (1979) Structural and biochemical changesin vitamin A-deficient rat retinas. *Invest. Ophthalmol. Vis. Sci.* **18**: 437-446

Cashman S. E, Binkley E. A, Kumar-Singh R (2005) Towards mutation-independent silencing of genes involved in retinal degeneration by RNA interference. *Gene Therapy.* **12**: 1223-1228

Cashman S. M, Bowman L, Christofferson J, Kumar-Singh R (2006) Inhibition of choroidal neovascularization by adenovirus-mediated delivery of short hairpin RNAs targeting VEGF as a potential therapy for AMD. *Invest Ophthalmol Vis Sci.* **47(8)**: 3496-504

Castanotto A, Li H, Rossi J.J (2002) Functional siRNA expression from transfected PCR products. *RNA.* **8**: 1454-1460

Castanotto D, Sakurai K, Lingeman R, Li H, Shively L, Aagaard L, Soifer H, Gatignol A, Riggs A, Rossi J. J (2007) Combinatorial delivery of small interfering RNAs reduces RNAi efficacy by selective incorporation into RISC. *Nuclei Acids Research.* **35(15)**: 5154-5164

Cech T. R, Zaug A. J, Grabowski P. J (1981) *In-vitro* splicing of the ribosomal RNA precurosor of Tetrahymena: involvement of a guanosine nucleotide in the excision of the intervening sequence. *Cell.* **27**: 487-496

Chakarova C. F, Hims M. M, Bolz H, Abu-Safieh L, Patel R. J, Papaioannou M. G, Inglehearn C. F, Keen T. J, Willis C, Moore A. T, Rosenberg T, Webster A. R, Bird A. C, Gal A, Hunt D, Vithana E. N, Bhattacharya S. S (2002) Mutations in HPRP3, a third member of pre-mRNA splicing factor genes, implicated in autosomal dominant retinitis pigmentosa. *Hum Mol Genet.* **11**: 87-92

Chalk A. M, Wahlestedt C, Sonnhammer E. L (2004) Improved and automated prediction of effective siRNA. *Biochem Biophys Res Commun.* **319**: 264-274

Challa P, Luna C, Liton P. B, Chamblin B, Wakefield J, Ramabhadran R, Epstein D. L, Gonzalez P (2005) Lentiviral mediated gene delivery to the anterior chamber of rodent eyes. *Mol Vis.* **11**: 425–430

Chang B, Hawes N. L, Hurd R. E, Wang J, Howell D, Davisson M. T, Roderick T. H, Nusinowitz S, Heckenlively J. R (2005) Mouse models of ocular diseases. *Visual Neuroscience*. **22**: 587-593

Chang K, Elledge S. J, Hannon G. J (2006) Lessons from Nature; microRNA based shRNA libraries. *Nature Methods*. **3**: 707-714

Chao H, Liu Y, Rabinowitz J, Li C, Samulski R. J, Walsh C. E (2000) Several log increase in therapeutic transgene delivery by distinct adeno-associated viral serotype vectors. *Mol. Ther.* **2**: 619–623

Chapple J. P and Cheetham M. E (2003) The chaperone environment at the cytoplasmic face of the endoplastic reticulum can modulate rhodopsin processing and inclusion formation. *J Biol Chem*. **278**: 19087-19094

Chemin I, Moradpour D, Wieland S, Offensperger W. B, Walter E, Behr J. P, Blum H. E (1998) Liver-directed gene transfer: a linear polyethlenimine derivative mediates highly efficient DNA delivery to primary hepatocytes in vitro and in vivo. *J Viral Hepat*. **5(6)**: 369-75

Chen P, Hao W, Rife L, Wang X. P, Shen D, Chen J, Ogden T, Van Boemel G. B, Wu L, Yang M, Fong H. K (2001) A photic visual cycle of rhodopsin regeneration is dependent on Rgr. *Nat Genet*. **28**: 256–260

Chen S, Peng G. H, Wang X, Smith AC, Grote S. K, Sopher B. L, La Spada A. R (2004a) Interference of Crx-dependent transcription by ataxin-7 involves interaction between the glutamine regions and requires the ataxin-7 carboxyl terminal region for nuclear localization. *Hum Mol Genet*. **13**:53-67

Chen CZ, Li L, Lodish H. F, Bartel D. P (2004b) MicroRNAs modulate hematopoietic lineage differentiation. *Science*. **303**: 83-86

Chen M, Zhang L, Zhang H. Y, Xiong X, Wang B, Du Q, Lu B, Wahlesedt C, Liang Z (2005) A universal plasmid library encoding all permutations of small interfering RNA. *Proc. Natl. Acad. Sci. USA*. **102 (7)**:2356-2361

Chen J. F, Mandel E. M, Thomson J. M, Wu Q, Callis T. E, Hammond S. M, Conlon F. L, Wang D. Z (2006) The role of microRNA-1 and microRNA-133 in skeletal muscle proliferation and differentiation. *Nat. Genet*. **38**: 228-233

Cheng L, Ziegelhoffer P. R, Yang, N. S (1993) *In-vivo* promoter activity and transgene expression in mammalian somatic tissues evaluated by using particle bombardment. *Proc Natl Acad Sci USA*. **90**: 4455-4459

Cheng H, Khanna H, Oh E. C, Hicks D, Mitton K. P, Swaroop A (2004) Photoreceptor-specific nuclear receptor NR2E3 functions as a transcriptional activator in rod photoreceptors. *Hum Mol Genet*. **13**: 1563-1575

Cheng L, Toyoguchi M, Looney D. J, Lee J, Davidson M. C, Freeman W. R (2005) Efficient gene transfer to retinal pigment epithelium cells with long-term expression. *Retina*. **25**: 193–201

Chiorini J. A, Yang L, Liu Y, Safer B, Kotin R. M (1997) Cloning of adeno-associated virus type 4 (AAV4) and generation of recombinant AAV4 particles. *J Virol.* **71**: 6823-6833

Chiorini J. A, F. Kim F, L. Yang L, R.M. Kotin R. M (1999) Cloning and characterization of adeno-associated virus type 5. *J. Virol.* **73**: 1309–1319

Chiu Y. L and Rana T. M (2002) RNAi in human cells: basic structural and functional features of small interfering RNA. *Mol Cell.* **10**: 549–561

Chiu Y. L and Rana T. M (2003) siRNAs function in RNAi: a chemical modification analysis. *RNA.* **9**: 1034-1048

Chook Y. M and Blobel G (2001) Karyopherins and nuclear import. *Curr. Opin. Struct. Biol.* **11:** 703–715

Choudhary S, De B. P, Banerjee A. K (2000) Specific phosphorylated forms of glyceraldehyde-3-phosphate dehydrogenase associate with human parainfluenza virus type 3 and inhibit viral transcription in vitro. *J. Virol.* **74**: 3634–3641

Chow R. L, Volgyi B, Szilard R. K, Ng D, McKerlie C, Bloomfield S. A, Birch D. G, McInnes R. R (2004) Control of late off-center cone bipolar cell differentiation and visual signaling by the homeobox gene Vsx1. *Proc Natl Acad Sci USA.* **101**: 1754-1759

Chu C. Y and Rana, T. M (2006) Translation repression in human cells by microRNA-induced gene silencing requires RCK/p54. *PLoS Biol.* **4(7)**: e210

Chuang J. Z, Vega C, Jun W, Sung C. H (2004) Structural and functional impairment of endocytic pathways by retinitis pigmentosa mutant rhodopsin arrestin complexes. *J Clin Invest.* **114**: 131-140

Cideciyan A. V, Hood D. C, Huang Y, Banin E, Li Z. Y, Stone E. M (1998) Disease sequence form mutant rhodopsin allele to rod and cone photoreceptor degeneration in man. *Proc Natl Acad Sci USA.* **95**: 7103-7108

Cingolani C, Rogers B, Shen J, Lu L, Campochiaro P. A (2005) Intraocular injection of paraquat: a new model of oxidative damage-induced retinal degeneration. *Invest Ophthamol Vis Sci.* **46**: 1599

Cohen M. B and Sadee W (1983) Contributions of the depletions of guanine and adenine nucleotides to the toxicity of purine starvation in the mouse T lymphoma cell line. *Cancer Res.* **43**: 1587-1591

Cokol M, Nair R, Rost B (2000) Finding nuclear localization signals. *EMBO Rep.* **1**: 411–415

Collart F and Huberman E (1988) Cloning and sequence analysis of the human and Chinese Hamster Inosine-5'-monophosphate dehygrogenase cDNAs. *The Journal of Biological Chemistry.* **263 (30)**: 15769-15772

Collart F. R, Chubb C. B, Mirkin B. L, Huberman, E (1992) Increased inosine-5'-phosphate dehydrogenase gene expression in solid tumor tissues and tumor cell lines. *Cancer Res.* **52**: 5826-5828

Coller J and Parker R (2005) General translational repression by activators of mRNA decapping. *Cell.* **122**: 875-886

Conrad C. K, Allen S. S, Afione S. A, Reynolds T. C, Beck S. E, Fee-Maki M, Barrazza-Ortiz X, Adams R, Askin F. B, Carter B. J, Guggino W. B, Flotte T. R (1996) Safety of single-dose administration of an adeno-associated virus (AAV)-CFTR vector in the primate lung. *Gene Therapy.* **3**: 658-668

Cooney D. A, Jayaram H. N, Gebeyehu G, Betts C. R, Kelley J. A, Marquez V. E, Johns D. G (1982) The conversion of 2-β- -ribofuranosylthiazole-4-carboxamide to an analogue of NAD+ with potent IMP dehydrogenase-inhibitory properties. *Biochem. Pharmacol.* **31**: 2133–31236

Cougot N, Babajko S, Seraphin B (2004) Cytoplasmic foci are sites of mRNA decay in human cells. *J. Cell. Biol.* **165**: 31-40

Cremers F. P, van den Hurk J. A, den Hollander A. I (2002) Molecular genetics of Leber congenital amaurosis. *Hum. Mol. Genet.* **11**: 1169–1176

Crocker S. J, Lamba W. R, Smith P. D, Callaghan S. M, Slack R. S, Anisman H (2001) c-Jun mediates axotomy-induced dopamine neuron death *in-vivo*. *Proc Natl Acad Sci USA.* **98**: 13385-13390

Crooke S. T (1999) Molecular mechanisms of action of antisense drugs. *Biochim. Biophys. Acta.* **1489**: 31-44

Cullen B. R (2004) Transcription and processing of human microRNA precurosors. *Mol Cell.* **16**: 861-865

Czauderna F, Fechtner M, Dames S, Aygün H, Klippel A, Pronk GJ, Giese K, Kaufmann J (2003) Structural variations and stabilizing modifications of synthetic siRNAs in mammalian cells. *Nucleic Acids Res.* **31**: 2705-2716

Dalke C and Graw J (2005) Mouse mutants as models for congenital retinal disorders. *Exp. Eye Res.* **81**: 503-512

Daly T. M, Vogler C, Levy B, Haskins M. E, Sands M. S (1999) Neonatal gene transfer leads to widespread correction of pathology in a murine model of lysosomal storage disease. *Proc. Natl. Acad. Sci. USA.* **96**: 2296–2300

Davidson B. L, Stein C. S, Heth J. A, Martins I, Kotin R M, Derksen T. A, Zabner J, Ghodsi A, Chiorini J.A (2000) Recombinant adeno-associated type 2, 4 and 5 vectors: Transduction of variant cell types and regions in the mammalian CNS. *Proc. Natl, Acad. Sci. USA.* **97 (7)**: 3428–3432

Davis G. L, Esteban-Mur R, Rustgi V, Hoefs J, Gordon S. C, Trepo C, Shiffman M. L, Zeuzem S, Craxi A, Ling M. H, Albrecht, J (1998) Interferon alfa-2b alone or in combination with ribavirin for the treatment of relapse of chronic hepatitis C. *N. Engl. J. Med.* **339**: 1493–1499

Dayton J. S, Lindsten T, Thompson C. B, Mitchell B. S (1994) Effects of human T lymphocyte activation on inosine monophosphate dehydrogenase expression. *J. Immunol.* **152**: 984-991

Dean D. A, Machado-Aranda D, Blair-Parks K, Yeldandi A. V, Young J. L (2003) Electroporation as a method for high-level nonviral gene transfer to the lung. *Gene Ther.* **10**: 1608-1615

DeClerq E (1993) Antiviral agents: characteristic activity target depending on the molecular target with which they interact. *Adv. Virus Res.* **42**: 1–55

Dejneka N.S and Bennett J. (2001) Gene therapy and RP: advances and future challenges. *Bioessays.* **2**: 662-8

Dejneka N. S, Auricchio A, Maguire A. M, Ye X, Gao G. P, Wilson J. M, Bennett J (2001) Pharmacologically regulated gene expression in the retina following transduction with viral vectors. *Gene Ther.* **8**: 442–446

Dejneka N. S, Surace E. M, Aleman T. S, Cideciyan A. V, Lyubarsky A, Savchenko A, Redmond T. M, Tang W, Wei Z, Rex T. S, Glover E, Maguire AM, Pugh E. N. Jr, Jacobson S. G, Bennett J (2004) *In-utero* gene therapy rescues vision in a murine model of congenital blindness. *Mol Ther.* **9**: 182–188

Deo M, Yu J. Y, Chung K. H, Tippens M, Turner D. L (2006) Detection of mammalian microRNA expression by *in-situ* hybridization with RNA oligonucleotides. *Dev. Dyn.* **235**: 2538-2548

Der S. D, Yang Y. L, Weissman C, Williams A (1997) A ds-RNA activated protein kinase dependent pathway mediating stress induced apoptosis. *Proc Natl Acad Sci USA.* **94**: 3279-3283

Devroe E and Silver P. A (2002) Retrovirus-delivered siRNA. *BMC Biotechnol.* **2**: 15
Dezawa M, Takano M, Negishi H, Mo X, Oshitari T, Sawada H (2002) Gene transfer into retinal ganglion cells by *in-vivo* electroporation: a new approach. *Micron* **33**: 1–6

Dhallan R. S, Macke J. P, Eddy R. L, Shows T. B, Reed R. R, Yau K. W, Nathans J (1992) Human rod photoreceptor cGMP-gated channel: amino acid sequence, gene structure, and functional expression, *J Neurosci.* **12**: 3248–3256

Doench J. G and Sharp P. A (2004) Specificity of microRNA target selection translational repression. *Genes Dev.* **18**: 504-511

Dorn G, Patel S, Wotherspoon G, Hemmings-Mieszczak M, Barclay J, Natt F. J, Martin P, Bevan S, Fox A, Ganju P, Wishart W, Hall J (2004) siRNA relieves chronic neuropathic pain. *Nucleic Acids Res.* **32**: 49

Dryja T.P and Li T. (1995). Molecular genetics of retinitis pigmentosa. *Human Mol. Genet.* **4**:1739-43

Dryja T. P, Berson E. L, Rao V. R, Oprian D. D (1993) Heterozygous missense mutation in the rhodopsin gene as a cause of congenital stationary night blindness. *Nat Genet.* **4**: 280-283

Dryja T. P, Hahn L. B, Reboul T, Arnaud B (1996) Missens mutation in the gene encoding the alpha subunit of rod transducin in the Nougaret form of congential stationary night blindness. *Nat. Genet.* **13**: 358-360

Dryja T. P, Hahn L. B, Kajiwara K, Berson E. L (1997) Dominant and digenic mutations in the peripherin/*rds* and ROM1 gene in retinitis pigmentosa. *Invest. Ophthalmol. Vis. Sci.* **38**: 1972-1982

Dryja T. P, McEvoy J.A , McGee T.L , Berson E. L (2000) Novel rhodopsin mutations Gly114Val and Gln184Pro in dominant retinitis pigmentosa. *Invest Ophthalmol Vis Sci.* **41**: 3124-7

Du Q, Thonberg H, Wang J, Wahlestedt C, Liang Z (2005) A systematic analysis of the silencing effects of an active siRNA at all single-nucleotide mismatched target sites. *Nucleic Acids Research.* **33 (5)**: 1671-1677

Duan D. S and Sadee W (1987) Distinct effects of adenine and guanine starvation on DNA synthesis associated with different pool sizes of nucleotide precursors. *Cancer Res.* **47**: 4047-4051

Duan D, Fisher K, Burda J, Engelhardt J. F (1997) Structural and functional heterogeneity of integrated recombinant AAV genomes. *Virus Res.* **48**: 41–56

Duan D, Yue Y, Engelhardt J. F (2001) Expanding AAV packaging capacity with trans-splicing or overlapping vectors: a quantitative comparison. *Mol. Ther.* **4**: 383–391

Dudus L, Anand V, Acland G. M, Chen S. J, Wilson J. M, Fisher K. J, Maguire A. M, Bennett J (1999) Persistent transgene product in retina, optic nerve and brain after intraocular injection of rAAV. *Vision Res.* **39**: 2545–2553

Durieux A. C, Bonnefoy R, Busso T, Freyssenet D (2004) *In-vivo* gene electrotransfer into skeletal muscle: effects of plasmid DNA on the occurrence and extent of muscle damage. *J Gene Med.* **6**: 809-816

Duxbury M. S, Matros E, Ito H, Zinner M, Ashley S. W, Whang E. E (2004) Systemic siRNA-mediated gene silencing: a new approach to targeted therapy of cancer. *Ann Surg.* **240**: 667-674

Dyer M. A, Donovan S. L, Zhang J, Gray J, Oritz A, Tenney R, Kong J, Allikmets R, Sohocki M. M (2004) Retinal degeneration in Aip11-deficient mice: a new genetic model of Leber congenital amaurosis. *Brain Res Mol Brain Res.* **132**: 208-220

Editorial (2003) Whither RNAi? *Nature Cell Biology.* **5:** 489-90

Ehrengruber M. U, Hennou S, Bueler H, Naim H. Y, Deglon N, Lundstrom K (2001) Gene transfer into neurons from hippocampal slices: comparison of recombinant Semliki Forest Virus, adenovirus, adeno-associated virus, lentivirus, and measles virus. *Mol Cell Neurosci* **17**: 855–871

Elbashir S. M, Harborth J, Lendeckel W, Yalcin A, Weber K, Tuschl T (2001a) Duplexes of 21-nucleotide RNAs mediate RNA interference in cultured mammalians cells. *Nature.* **411**: 494-498

Elbashir S.M, Lendeckel W, Tuschl T (2001b) RNA interference is mediated by 21- and 22-nucleotide RNAs. *Genes Dev.* **15**: 188–200

Elbashir S. M, Martinez J, Patkaniowska A, Lendeckel W, Tuschl T (2001c) Functional anatomy of siRNAs for mediateing efficienct RNAi in Drosophila melanogaster embryo lysate. *EMBO J.* **20**: 6877-6888

Elliger S. S, Elliger C. A, Aguilar C. P, Raju N. R, Watson G. L (1999) Elimination of lysosomal storage in brains of MPS VII mice treated by intrathecal administration of an adeno-associated virus vector. *Gene Therapy*. **6**: 1175-1178

Ellington A. D and Szostak J. W (1990) In vitro selection of RNA molecules that bind specific ligands. *Nature*. **346**: 818-822

Elmen J, Thonberg H, Ljungberg K, Frieden M, Westergaard M, Xu Y, Wahren B, Liang Z, Orum H, Koch T, Wahlestedt C (2005) Locked nucleic acid (LNA) mediated improvements in siRNA stability and functionality. *Nucleic Acids Res*. **33**: 439-447

Epstein A. L, Marconi P, Argnani R, Manservigi R (2005) HSV-1 derived recombinant and amplicon vectors for gene transfer and gene therapy. *Curr Gene Ther*. **5**: 445-448

Erbacher P, Zou S, Bettinger T, Steffan A. M, Remy J. S (1998) Chitosan-based vector/DNA complexes for gene delivery: biophysical characteristics and transfection ability. *Pharm Res*. **15(9)**: 1332-9

Eulalio A, Behm-Ansmant I, Izaurralde E (2007) P bodies: at the crossroads of post-transcriptional pathways. *Nat. Rev. Mol. Cell Biol*. **8**: 9-22

Evguenieva-Hackenberg E, Schlitz E, Klug G (2002) Dehydrogenases from all three domains of life cleave RNA. *J. Biol. Chem*. **277**: 46145–46150

Eystathioy T, Chan E. K, Tenenbaum S.A, Keene J. D, Griffith K, Fritzler M. J (2002) A phosphorylated cytoplasmic autoantigen, GW 182, associates with a unique population of human mRNAs within novel cytoplasmic speckles. *Mol. Biol. Cell*. **13**. 1338-1351

Fain G. L and Lisman J. E (1993) Photoreceptor degeneration in vitamin A deprivation and retinitis pigmentosa: the equivalent light hypothesis. *Exp Eye Res*. **57**: 335-340

Far R. K and Sczakiel G (2003) The activity of siRNA in mammalian cells is related to structural target accessibility: a comparison with antisense oligonucleotides. *Nucleic Acids Res*. **31 (15)**: 4417-4424

Farrar G. J, Kenna P, Redmond R, McWilliam P, Bradley D. G, Humphries M. M, Sharp E. M, Inglehearn C. F, Bashir R, Jay M, Watty A, Ludwig, M, Schinzel A, Samanns C, Gal A, Battacharya S, Humphries P (1990) Autosomal dominant retinitis pigmentosa: Absence of the rhodopsin proline→histidine substitution (codon 23) in pedigrees from Europe. *Am. J. Hum. Genet*. **47:** 941–945

Farrar G. J, Kenna P. F, Humphries P (2002) On the genetics of retinitis pigmentosa and on mutation-independent approaches to therapeutic intervention. *EMBO J*. **21**: 857-864

Favre D, Provost N, Blouin V, Blancho G, Cherel Y, Salvetti A, Moullier P (2001) Immediate and long-term safety of recombinant adeno-associated virus injection into the nonhuman primate muscle. *Mol Ther*. **4**: 559-566

Fechheimer M, Boylan J. F, Parker S, Sisken J. E, Patel G. L, Zimmer S. G (1987) Transfection of mammalian cells with plasmid DNA by scrape loading and sonication loading. *Proc Natl Acad Sci USA*. **84**: 8463-8467

Felgner P. L, Gadek T. R, Holm M, Roman R, Chan H. W, Wenz M, Northrop J. P, Ringold G. M, Danielsen M (1987) Lipofection: a highly efficient, lipid-mediated DNA-transfection procedure. *Proc Natl Acad Sci USA*. **84(21)**: 7413-7

Fernandes-Alnemri T, Litwack G, Alnemri E. S (1994) CPP32, a novel human apoptotic protein with homology to Caenorhabditis elegans cell death protein Ced-3 and mammalian interleukin-1 beta-converting enzyme. *J. Biol. Chem.* **269**: 30761-30764

Fernandez-Gonzalez A, La Spada A. R, Treadaway J, Higdon J. C, Harris B. S, Sidman R. L, Morgan J. I, Zuo J (2002) Purkinje cell degeneration (pcd) phenotypes caused by mutations in the axotomy induced gene, Nna1. *Science.* **295**: 1904-1906

Ferraiuolo M. A, Basak S, Dostie J, Murray E.L, Schoenberg D. R, Sonenberg N (2005) A role for the eIF4E-binding protein 4E-T in P body formation and mRNA decay. *J. Cell. Biol.* **170**: 913-924

Feskanich D, V Singh, WC Willett and GA Colditz (2002) Vitamin A intake and hip fractures among postmenopausal women. *JAMA.* **287**: 47–54

Filipowicz W, Jaskiewicz L, Kolb F. A, Pillai R. S (2005) Post-transcriptional gene silencing by siRNAs and miRNAs. *Current Opinion in Structural Biology.* **15**: 331-341

Fire A, Xu S, Montgomery M. K, Kostas S. A, Driver S. E, Mello C. C (1998) Potent and specific genetic interference by double-stranded RNA in *Caenorhabditis elegans. Nature.* **391**: 806-811

Flannery J. G, Zolotukhin S, Vaquero M. I, LaVail M. M, Muzyczka N, Hauswirth W. W (1997) Efficient photoreceptor-targeted gene expression *in vivo* by recombinant adeno-associated virus. *Proc Natl Acad Sci USA.* **94**: 6916-6921

Fletcher E. L and Kalloniatis M (1997) Neurochemical development of the degenerating rat retina. *J. Comp. Neurol.* **388**: 1-22

Fliesler S. J, Anderson R. E (1983) Chemistry and metabolism of lipids in the vertebrate retina. *Prog Lipid Res.* **22**: 79–131

Forman MS, Trojanowski JQ, Lee VM (2004) Neurodegenerative diseases: a decade of discoveries paves the way for therapeutic breakthroughs. *Nat Med.* **10**: 1055-1063

Franchetti P and Grifantini M (1999) Nucleoside and non-nucleoside IMP dehydrogenase inhibitors as antitumor and antiviral agents. *Curr. Med. Chem.* **6**: 599–614

Frasson M, Sahel J. A, Fabre M, Simonutti M, Dreyfus H, Picaud S (1999) RP: rod photoreceptor rescue by a calcium channel blocker in rd1 mouse. *Nat. Med.* **5**: 1183-1187

Frederick J. M, Krasnoperova N. V, Hoffmann K, Church-Kopish J, Rüther K, Howes K, Lem J, Baehr W (2001) Mutant rhodopsin transgene expression on a null background. *Invest Ophthalmol Vis Sci.* **42**: 826-833

Fuchs S, Nakazawa M, Maw M, Tamai M, Oguchi Y, Gal A (1995) A homozygous 1-base pair deletion in the arestin gene is a frequent cause of Oguchi disease in Japanese. *Nat. Gen.* **10**: 360-362

Fukuhara N, Ebert J, Unterholzner L, Lindner D, Izaurralde E, Conti E (2005) SMG7 is a 14-3-3-like adaptor in the nonsense-mediated mRNA decay pathway. *Mol. Cell.* **17**: 537-547

Furukawa T, Morrow E. M, Li T, Davis F. C, Cepko C. L (1999) Retinopathy and attenuated circadian entrainment in CRX deficient mice. *Nat. Genet.* **23**: 466-470

Gal A, Li Y, Thompson DA, Weir J, Orth U, Jacobson S. G, Apfelstedt-Sylla E, Vollrath D (2000) Mutations in MERTK, the human orthologue of the RCS rat retinal dystrophy gene, cause retinitis pigmentosa. *Nat Genet.* **26**: 270-271

Gao G. P, Lu F, Sanmiguel J. C, Tran P. T, Abbas Z, Lynd K. S, Marsh J, Spinner N. B, Wilson J. M. (2002a) Rep/Cap gene amplification and high-yield production of AAV in an A549 cell line expressing Rep/Cap. *Mol Ther.* **5**: 644-649

Gao G. P, Alvira M. R, Wang L, Calcedo R, Johnston J, Wilson J. M (2002b) Novel adeno-associated viruses from rhesus monkeys as vectors for human gene therapy. *Proc. Natl. Acad. Sci. USA.* **99**: 11854–11859

Gao X, Kim K. S, Liu D (2007) Non-viral Gene Delivery: What we know and what is next. *AAPS Journal.* **1**: 92-104

Garriga P, Liu X, Khorana H. G (1996) Structure and function in rhodopsin: Correct folding and misfolding in point mutants at and in proximity to the site of the retinitis pigmentosa mutation Leu-125 → Arg in the transmembrane helix C. *Proc. Natl. Acad. Sci. USA.* **93**: 4560–4564

Gehl J, Sorensen T. H, Nielsen K, Raskmark P, Nielsen S. L, Skovsgaard T, Mir L. M (1999). *In vivo* electroporation of skeletal muscle: threshold, efficacy and relation to electric field distribution. *Biochim Biophys Acta.* **1428**: 233–240

Gehl J, Skovsgaard T, Mir L. M (2002) Vascular reactions to *in vivo* electroporation: characterization and consequences for drug and gene delivery. *Biochim Biophys Acta.* **1569**: 51–58

Gehlbach P, Demetriades A. M, Yamamoto S, Deering T, Duh E. J, Yang H. S, Cingolani C, Lai H, Wei L, Campochiaro P. A (2003) Periocular injection of an adenoviral vector encoding pigment epithelium-derived factor inhibits choroidal neovascularization. *Gene Ther.* **10**: 637–646

Ghartey-Tagoe E. B, Babin B. A, Nusrat A, Neish A. S, Prausnitz M. R (2006) Plasmid DNA and siRNA transfection of intestinal epithelia monolayers by electroporation. *Int J Pharm.* **315(1-2):** 122-33

Ghazizadeh S, Carroll J. M, Taichman L. B (1997) Repression of retrovirus mediated transgene expression by interferon implications for gene therapy. *J. Virol.* **71 (12)**: 9163-9169

Giladi H, Ketzinel-Gilad M, Rivkin L, Felig Y, Nussbaum O, Galun E (2003) Small interfering RNA inhibits hepatitis B virus replication in mice. *Mol Ther.* **8**: 769-776

Gissel H and Clausen T (2001) Excitation induced Ca^{2+} influx and skeletal muscle cell damage. *Acta Physiol Scand.* **171**: 327-334

Glesne D, Collart F, Varkony T, Drabkin H, Huberman E (1993) Chromosomal localization and structure of the human type II IMP dehydrogenase gene (IMPDH2). *Genomics.* **16**: 274-277

Golzio M, Mazzolini L, Moller P, Rols MP, Teissié J (2005) Inhibition of gene expression in mice muscle by *in vivo* electrically mediated siRNA delivery. *Gene Ther.* **12**: 246-251

Gorbatyuk M. S, Pang J. J, Thomas Jr. J, Hauswirth W. W, Lewin A. S (2005) Knockdown of wild-type mouse rhodopsin using an AAV vectored ribozyme as part of an RNA replacement approach. *Mol Vis.* **11**: 648–656

Gorbatyuk M, Justilien V, Liu J, Hauswirth W. W, Lewin A. S (2007) Suppression of mouse rhodopsin expression in vivo by AAV mediated siRNA delivery. *Vision Res.* **47(9)**: 1202-8

Gossen M, Freundlieb S, Bender G, Müller G, Hillen W, Bujard H (1995) Transcriptional activation by tetracyclines in mammalian cells. *Science.* **268**: 1766-1769

Gothelf A, Mir L. M, Gehl J (2003) Electrochemotherapy: results of cancer treatment using enhanced delivery of bleomycin by electroporation. *Cancer Treat Rev.* **29**: 371–387

Goula D, Remy J. S, Erbacher P, Wasowicz M, Levi G, Abdallah B, Demeneix B. A (1998) Size, diffusibility and transfection performance of linear PEI/DNA complexes in the mouse central nervous system. *Gene Ther.* **5(5)**: 712-7

Gouras P, Carr R. E, Gunkel R. D (1971) Retinitis pigmentosa in abetalipoproteinemia: effects of vitamin A. *Invest Ophthalmol.* **10**: 784–793

Graessmann M, Michaels G, Berg B, Graessmann A (1991) Inhibition of SV40 gene expression by microinjected small antisense RNA and DNA molecules. *Nucleic Acids Res.* **19**: 53-58

Grant C. A, Ponnazhagans S, Wang X. S, Srivastava A, Li T (1997) Evaluation of recombinant adeno-associated virus as a gene ransfer vector for the retina. *Curr Eye Res.* **16**: 949-956

Green ES, Menz MD, LaVail MM, Flannery JG (2000) Characterisation of rhodopsin mis-sorting and constitutive activation in a transgenic rat model of retinitis pigmentosa. *Invest Ophthalmol Vis Sci.* **41**: 1546-1553

Green E. S, Rendahl K. G, Zhou S, Ladner M, Coyne M, Srivastava R, Manning W. C, Flannery J. G (2001) Two animal models of retinal degeneration are rescued by recombinant adeno-associated virus-mediated production of fgf-5 and fgf-18. *Mol Ther.* **3**: 507-515

Griffiths-Jones S (2004) The microRNA registry. *Nucleic Acids Res.* **32**: D109-D111

Grimm D (2002) Production methods for gene transfer vectors based on adeno-associated virus serotypes. *Methods.* **28**: 146–157

Grimm D, Pandey K, Kay M. A (2005) Adeno-associated virus vectors for short hairpin RNA expression. *Methods Enzymol.* **392**: 381-405

Grimm D, Streetz K. L, Jopling C. L, Storm T. A, Pandey K, Davies C. R, Marion P, Salazar F, Kay M. A (2006) Fatality in mice due to oversaturation of cellular microRNA/ short hairpin RNA pathways. *Nature.* **441**: 537-541

Grondahl J (1987) Estimation of prognosis and prevalence of retinitis pigmentosa and Usher syndrome in Norway. *Clin Genet.* **31**, 255–264

Grover S, Fishman G. A, Anderson R. J, Tozatti M. S, Heckenlively J. R, Weleber R. G, Edwards A. O, Brown J. Jr (1999) Visual acuity impairment in patients with retinitis pigmentosa at age 45 years or older. *Ophthalmology.* **106**: 1780–1785

Grover S, Fishman G. A, Stone E. M (2004) A novel IMPDH1 mutation (Arg231Pro) in a family with a severe form of autosomal dominant retinitis pigmetosa. *Ophthalmology.* **111 (10)**; 1910-1916

Grummt I (1999) Regulation of mammalian ribosomal gene transcription by RNA polymerase I. *Prog. Nucleic Acid Res. Mol. Biol.* **62**: 109–154

Grunweller A, Wyszko E, Bieber B, Jahnel R, Erdmann V. A, Kurreck J (2003) Comparison of different antisense strategies in mammalian cells using locked nucleic acids, 2'-O-methyl RNA, phosphorothioates and small interfering RNA. *Nucleic Acids Res.* **31**: 3185-3193

Gu J. J, Kaiser-Rogers K, Rao, K, Mitchell B. S (1994) Assignment of the human type I IMP dehydrogenase gene (IMPDH1) to chromosome 7q31.3-q32). *Genomics.* **24**: 179-181

Gu J. J, Spychala J, Mitchell B. S (1997) Regulation of the human inosine monophosphate dehydrogenase type I gene. *The Journal of Biological Chemistry.* **272 (7)**: 4458-4466

Gu, J. J., S. Stegmann, K. Gathy, R. Murray, J. Laliberte, L. Ayscue, and B. S. Mitchell (2000) Inhibition of T lymphocyte activation in mice heterozygous for loss of the IMPDH II gene. *J. Clin. Investig.* **106**: 599-606

Gu J. J, Tolin A. K, Jain J, Huang H, Santiago L, Mitchell B. S (2003) Targeted disruption of the inosine 5'-monophosphate dehydrogenase type I gene in mice. *Molecular and cellular biology.* **23 (18)**: 6702-6712

Guarneri R, Russo D, Cascio C, D'Agostino S, Galizzi G, Bigini P, Mennini T, Guarneri P (2004) Retinal oxidation, apoptosis and ade and sex-differences in the mnd mutant mouse, a model of neuronal ceroid lipofuscinosis. *Brain Res.* **1014**: 209-220
Gupta S, Schoer R.A, Egan J.E, Hannon G.J, Mittal V. (2004) Inducible, reversible, and stable RNA interference in mammalian cells. *PNAS.* **101 (7)**: 1927-1932

Guy J, Qi X, Hauswirth W. W (1998) Adeno-associated viral-mediated catalase expression suppresses optic neuritis in experimental allergic encephalomyelitis. *Proc. Natl. Acad. Sci. USA.* **95**: 13847–13852

Guy J, Qi X, Muzyczka N, Hauswirth W. W (1999) Reporter expression persists 1 year after adeno-associated virus-mediated gene transfer to the optic nerve. *Arch. Ophthalmol.* **117**: 929–937

Gwizdek C, Ossareh-Nazari B, Brownawell A. M, Doglio A, Bertrand E, Macara I. G, Dargemont C (2003) Exportin-5 mediates nuclear export of minihelix-containing RNAs. *J Biol Chem.* **278(8)**: 5505-8

Hager, P. W., Collart, F. R., Huberman, E., and Mitchell, B. S. (1995) Recombinant human inosine monophosphate dehydrogenase type I and type II proteins. Purification and characterization of inhibitor binding. *Biochem. Pharmacol.* **49**: 1323-1329

Hagstrom J. E, Hegge J, Zhang G, Noble M, Budker V, Lewis D. L, Herweijer H, Wolff J. A (2004) A facile nonviral method for delivering genes and siRNAs to skeletal muscle of mammalian limbs. *Mol Ther.* **10**: 386-398

Haley B and Zamore P. D (2004) Kinetic analysis of the RNAi enzyme complex. *Nat. Struct Mol Biol.* **11**: 599-606

Hall A. H, Wan J, Shaughnessy E. E, Ramsay Shaw B, Alexander K. A (2004) RNA interference using boranophosphate siRNAs: structure-activity relationships. *Nucleic Acids Res.* **32**: 5991-6000

Hamel C. P, Tsilou E, Pfeffer B. A, Hooks J. J, Detrick B, Redmond T. M (1993) Molecular cloning and expression of RPE65, a nocel retinal pigment epithelium-specific microsomal protein that is post-transcriptionally regulated *in-vitro*. *J. Biol. Chem.* **268**: 15751-15757

Hamm H. E (2001) How activated receptors couple to G proteins. *Proc. Natl. Acad. Sci. USA*. **98**: 4819–4821

Hammond S. M, Bernstein E, Beach D, Hannon G. J (2000) An RNA-directed nuclease mediates post-transcriptional gene silencing in Drosophila cells. *Nature*. **404**: 293-296

Hammond S. M, Boettcher S, Caudy A. A, Kobayashi R, Hannon G. J (2001) Argonaute2, a link between genetic and biochemical analyses of RNAi. *Science*. **293**: 1146-1150

Hanein S, Perrault I, Gerber S, Tanguy G, Barbet F, Ducroq D et al (2004) Leber congential amaurosis: comprehensive survey of the genetic heterogeneity, refinement of the clinical defincition, and genotype-phenotype correlations as a strategy for molecular diagnosis. *Hum Mutat*. **23**:306-317

Hannon G. J (2002) RNA interference. *Nature*. **418:** 244–251

Harborth J, Elbashir S. M, Vandenburgh K, Manninga H, Scaringe S. A, Weber K, Tuschl T (2003) Sequence, chemical, and structural variation of small interfering RNAs and short hairpin RNAs and the effect on mammalian gene silencing. *Antisense Nucleic Acid Drug Dev.* **13**: 83-105

Hargrave P. A (2001) Rhodopsin structure, function, and topography: The Friedenwald lecture. *Invest Ophthalmol Vis Sci*. **42**: 3-9

Harper S. Q, Staber P. D, He X, Eliason S. L, Martins I. H, Mao Q, Yang L, Kotin R. M, Paulson H. L, Davidson B. L (2005) RNA interference improves motor and neuropathological abnormalities in a Huntington's disease mouse model. *PNAS*. **102 (16)**: 5820-5825

Hartong D. T, Berson E. L, Dryja T (2006) Retinitis Pigmentosa. *Lancet*. **368**: 1795-1809

Haseloff J and Gerlach W. L (1998) Simple RNA enzymes with new and highly specific endoribonuclease activities. *Nature*. **334**: 585-591

Hasson E, Slovatizky Y, Shimoni Y, Falk H, Panet A, Mitrani E (2005) Solid tissues can be manipulated *ex-vivo* and used as vehicles for gene therapy. *J Gene Med.* **7**: 926-935

He L and Hannon G. J (2004) MicroRNAs: small RNAs with a big role in gene regulation. *Nat Rev Genet.* **5**: 533-531

Hebb M. O and Robertson H. A (1997) End-capped antisense oligodeoxynucleotides effectively inhibit gene expression *in vivo* and offer a low-toxicity alternative to fully modified phosphorothioate oligodeoxynucleotides. *Brain Res Mol Brain Res.* **47**: 223-228

Heckel A, Buff M. C, Raddatz M. S, Muller J, Potzsch B, Mayer G (2006) An anticoagulatant with light-triggered antidote activity. *Angew Cem Int Ed Engl*; **45**: 6748-6750

Heckenlively J. R, Rodriquez J. A, Daiger S. P (1991) Autsomal dominant sectoral retinitis pigmentosa: two families with transversion mutation in codon 23 of rhodopsin. *Arch Ophthalmol*: **109**: 84-91

Heckenlively J. R, Chang B, Erway L. C, Peng C, Hawes N. L, Hageman G. S, Roderick T. H (1995) Mouse Model for Usher syndrome: linkage mapping suggests homology to Usher type I reported at human chromosome 11p15. *Proc Natl Acad Sci U S A.* **92 (24)**:11100-4

Heiser W. C (1994) Gene transfer into mammalian cells by particle bombardment. *Anal Biochem.* **217**: 185-196

Heix J and Grummt I (1995) Species specificity of transcription by RNA polymerase I. *Curr. Opin. Genet. Dev.* **5**: 652–656

Heller L. C, Ugen K, Heller R (2005) Electroporation for targeted gene transfer. *Expert Opin Drug Deliv.* **2**: 255-268

Hennig A. K, Ogilvie J. M, Ohlemiller K. K, Timmers A. M, Hauswirth W. W, Sands M. S (2004) AAV-mediated intravitreal gene therapy reduces lysosomal storage in the retinal pigmented epithelium and improves retinal function in adult MPS VII mice. *Mol Ther.* **10**: 106–116

Henschel A, Buchholz F, B. Habermann B (2004) DEQOR: a web-based tool for the design and quality control of siRNAs. *Nucleic Acids Res.* **32**: 113–120

Hewitt A. T, Lindsey J. D, Carbott D, Adler R (1990) Photoreceptor survival-promoting activity in interphotoreceptor matrix preparations: characterization and partial purification. *Exp. Eye Res.* **50**: 79-88

Hildinger M, Auricchio A, Gao G, Wang L, Chirmule N, Wilson J. M (2001) Hybrid vectors based on adeno-associated virus serotypes 2 and 5 for muscle-directed gene transfer. *J Virol.* **75**: 6199–6203

Ho S. P and Hartig P. R (1999) Antisense oligonucleotides for target validation in the CNS. *Curr Opin Mol Ther.* **1**: 336-343

Ho T. T, Maguire A. M, Aguirre G. D, Surace E. M, Anand V, Zeng Y, Salvetti A, Hopwood J. J, Haskins M. E, Bennett J (2002) Phenotypic rescue after adeno-associated virus-mediated delivery of 4-sulfatase to the retinal pigment epithelium of feline mucopolysaccharidosis VI. *J. Gene Med.* **4**: 613–621

Hobert O (2004) Common logic of transcription factor and microRNA action. *Trends Biochem Sci.* **29**: 462-468

Hoffman D. R, Locke K. G, Wheaton D. H, Fish G. E, Spencer R, Birch D. G (2004) A randomized, placebo-controlled clinical trial of docosahexaenoic acid supplementation for X-linked retinitis pigmentosa. *Am J Ophthalmol.* **137**: 704–718

Holen T, Amarzguioui M, Wiiger M. T, Babaie E, Prydz H (2002) Positional effects of short interfering RNAs targeting the human coagulation trigger Tissue Factor. *Nucleic Acids Res.* **30**: 1757-1766

Holen T, Moe S. M, Sorbo J. G, Meza T. J, Ottersen O. P, Klungland A (2005) Tolerated wobble mutationsin siRNAs decrease specificity, but can enhance activity *in-vivo*. *Nucleic Acids Research.* **33 (15)**: 4704-4710

Holopigian K, Greenstein V, Seiple W, Carr R. E (1996) Rates of change differ among measures of visual function in patients with retinitis pigmentosa. *Ophthalmology.* **103**: 398–405

Hommel J. D, Sears R. M, Georgescu D, Simmons D. L, DiLeone R. J (2003) Local gene knockdown in the brain using viral-mediated RNA interference. *Nat Med.* **9(12)**: 1539-44

Hong J, Qian Z, Shen S, Min T, Tan C, Xu J, Zhao Y, Huang W (2005) High doses of siRNAs induce eri-1 and adar-1 gene expression and reduce the efficiency of RNA interference in the mouse. *Biochem J.* **390**: 675-679

Horwitz M. S (1990) Adenoviruses. In: Fields, B.N. and Knipe, D.M., Editors. "Fields Virology". **Vol. 2**, Raven Press, New York: 1723–1740

Hosseinkhani H, Azzam T, Tabata Y, Domb A. J (2004) Dextran-spermine polycation: an efficient nonviral vector for in vitro and in vivo gene transfection. *Gene Ther.* **11(2)**: 194-203

Huang Z. J, Kirkwood A, Pizzorusso T, Porciatti V, Morales B, Bear M. F, Maffei L, Tonegawa S (1999) BDNF regulates the maturation of inhibition and the critical period of plasticity in mouse visual cortex. *Cell.* **98**: 739–755

Huber P. E, Jenne J, Debus J, Wannenmacher M. F, Pfisterer P. (1999) A comparison of shock wave and sinusoidal-focused ultrasound-induced localized transfection of HeLa cells. *Ultrasound Med Biol.* **25**: 1451-1457

Huesken D, Lange J, Mickanin C, Weiler J, Asselbergs F, Warner J, Meloon B, Engel S, Rosenberg A, Cohen D, Labow M, Reinhardt M, Natt F, Hall J (2005) Design of a genome-wide siRNA library using an artificial neural network. *Nat. Biotechnol.* **23**: 995–1001

Hughes L and Maurice D. M (1984) A fresh look at iontophoresis. *Arch Ophthalmol.* **102**: 1825–1829

Humphries M. M, Rancourt D, Farrar G. J, Kenna P, Hazel M, Bush R. A, Sieving P.A, Sheils D. M, McNally N, Creighton P, Erven A, Boros A, Gulya K, Capecchi M. R, Humphries P (1997) Retinopathy induced in mice by targeted disruption of the rhodopsin gene. *Nat. Genet.* **15**: 216-219

Humphries M. M, Kiang A. S, McNally N, Donovan M. A, Sieving P. A, Bush R. A, Machida S, Cotter T, Hobson A, Farrar J, Humphries P, Kenna P (2001) Comparative structural and functional analysis of photoreceptor neurons of Rho-/- reveal increase survival on C57BL/6J incomparison to 129Sv genetic background. *Vis. Neurosic.* **18**: 437-443

Hungerbuhler J. P, Meier C, Rousselle L, Quadri P, Bogousslavsky J (1985) Refsum's disease: management by diet and plasmapheresis. *Eur Neurol.* **24**: 153–159

Hurwitz R. L (2001) Experiences with a human ocular gene therapy trial. *Invest Ophthalmol Vis Sci.* **42**: 302

Hutvágner G and Zamore P. D (2002) A microRNA in a multiple-turnover RNAi enzyme complex. *Science.* **297**: 2056–2060

Hutvágner G, McLachlan J, Pasquinelli A. E, Bálint E, Tuschl T, Zamore P. D (2001) A cellular function for the RNA interference enzyme Dicer in the maturation of the let-7 small temporal RNA. *Science.* **293**: 834-838

Illing M. E, Rajan R. S, Bence N. F, Kopito R. R (2002) A rhodopsin mutant linked to autosomal dominant retinitis pigmentosa is prone to aggregate and interacts with the ubiquitin proteasome system. *J Biol Chem.* **277**: 34150-34160

Isenmann S, Wahl C, Krajewski S, Reed J. C, Bahr M (1999) Up-regulation of Bax protein in degenerating retinal ganglion cells precedes apoptotic cell death after optic nerve lesion in the rat. *Eur J Neurosic.* **9**: 1763-1772

Ishitani R, Tanaka M, Sunaga K, Katsube N, Chuang D-M (1998) Nuclear localization of overexpressed glyceraldehyde-3-phosphate dehydrogenase in cultured cerebellar neurons undergoing apoptosis. *Mol. Pharmacol.* **53**: 701–707

Ishizuka T, Iizasa T, Taira M, Ishijima S, Sonoda T, Shimada H, Nagatake N, Tatibana M (1992) Promoter regions of the human X-linked housekeeping genes PRPS1 and PRPS2 encoding phosphoribosylpyrophosphate synthetase subunit I and II isoforms *Biochim. Biophys. Acta.* **1130**: 139-148

Itasaki N, Bel-Vialar S, Krumlauf R (1999) "Shocking" developments in chick embryology: electroporation and *in-ovo* gene expression. *Nat Cell Biol.* **1**: 203–207

Jackson A. L, Bartz S. R, Schelter J, Kobayashi S. V, Burchard J, Mao M, Li B, Cavet G, Linsley P. S (2003) Expression profiling reveals off target gene regulation by RNAi. *Nat Biotechnol.* **21**: 635-637

Jackson A. L, Burchard J, Leake D, Reynolds A, Schelter J, Guo J, Johnson J. M, Lim L, Karpilow J, Nicholas K, Marshall W, Khvorova A, Linsley P. S (2006) Position specific chemical modification of siRNAs reduces off target transcript silencing. *RNA.* **12**: 1179-1187

Jacobson M. D, Weil M, Raff M. C (1997) Programmed cell death in animal development. *Cell.* **88**: 347-354

Jakymiw A, Lian S, Eystathioy T, Li S, Satoh M, Hamel J.C, Fritzler M.J, Chan E.K (2005) Disruption of GW bodies impairs mammalian RNA interference. *Nat. Cell. Biol.* 7. 1267-1274

Jakymiw A, Pauley K. M, Li S, Ikeda K, Lian S, Eystathioy T, Satoh M, Fritzler M. J, Chan E. K (2007) The role of GW/P-bodies in RNA processing and silencing. *J Cell Sci.* **120**: 1317-23

Janas J, Skowronski J, Van Aelst L (2006) Lentiviral delivery of RNAi in hippocampal neurons. *Methods Enzymol.* **406**: 593-605

Janson C. G, McPhee S. W, Leone P, Freese A, During M. J (2001) Viral-based gene transfer to the mammalian CNS for functional genomic studies. *Trends Neurosci* **24**: 706–712

Ji T. H, Grossmann M, Ji I (1998) G protein-coupled receptors I. Diversity of receptor-ligand interactions. *J. Biol Chem.* **273**: 17299-17302

Ji J, Wernli M, Klimkait T, Erb P (2003) Enhanced gene silencing by the application of multiple specific small interfering RNAs. *FEBS Letters.* **552**: 247-252

Jiang L. Q, Jorquera M, Streilein J. W (1993) Subretinal space and vitreous cavity as immunologically privileged sites for retinal allografts. *Invest. Ophthalmol. Vis. Sci.* **34**: 3347–3354

Jiang J, Yamato E, Miyazaki J (2001) Intravenous delivery of naked plasmid DNA for *in-vivo* cytokine expression. *Biochem Biophys Res Commun.* **289**: 1088-1092

Jiao S, Williams P, Berg R. K, Hodgeman B. A, Liu L, Repetto G, Wolff J. A(1992) Direct gene transfer into nonhuman primate myofibers *in-vivo*. *Hum Gene Ther* **3**: 21-33

Johnston R. J and Hobert O (2003) A microRNA controlling left/right neuronal asymmetry in Caenorhabditis elegans. *Nature.* **426**: 845-849

Johnston R. J. Jr, Chang S, Etchberger J. F, Ortiz C. O, Hobert O (2005) MicroRNAs acting in a double-negative feedback loop to control a neuronal cell fate decision. *Proc. Natl. Acad. Sci. U.S.A.* 102: 12449-12454

Jordan S. A, Farrar G. J, Kenna P, Humphries M. M, Sheils D. M, Kumar-Singh R, Sharp E. M, Ayuso C, Benitez J, Humphries P (1993) Localization of an autosomal dominant retinitis pigmentosa gene to chromosome 7q. *Nat Genet.* **4**: 54–58

Juliano R. L (2005) Peptide-oligonucleotide conjugates for the delivery of antisense and siRNA. *Curr. Opin. Mol. Ther.* **7**: 132-136

Jung S. C, Han I. P, Limaye A, Xu R, Gelderman M. P, Zerfas P, Tirumalai K, Murray G. J, During M. J, Brady R. O, Qasba P (2001) Adeno-associated viral vector-mediated gene transfer results in long-term enzymatic and functional correction in multiple organs of Fabry mice. *Proc Natl Acad Sci USA.* **98**: 2676-2681

Junger H and Junger W. G (1998) CNTF and GDNF, but not NT-4, support corticospinal motor neuron growth via direct mechanisms. *Neuroreport.* **9**: 3749–3754

Kajiwara K, Berson E. L, Dryja T. P (1994) Digenic retinitis pigmentosa due to mutations at the unlinked peripherin/RDS and ROM1 loci. *Science.* **264**: 1604–1608

Kamei M, Fujikado T, Kanda H *et al.* (2006) Suprachoroidal-transretinal stimulation (STS) artificial vision system for patients with retinitis pigmentosa. *Invest Ophthalmol Vis Sci.* **47**: 1537

Karali M, Peluso I, Marigo V, Banfi S (2007) Identification and characterization of microRNAs expressed in the mouse eye. Investigative Opthalmology and Visual *Science.* **48(2)**: 509-515

Karan G, Lillo C, Yang Z, Cameron D. J, Locke K. G, Zhao Y, Thirumalaichary S, Li C, Birch D. G Vollmer-Snarr H. R, Williams D. S, Zhang K (2005) Lipofuscin accumulation, abnormal electrophysiology, and photoreceptor degeneration mutant ELOVL4 transgenic mice: a model for macular degeneration. *Proc Natl Acad Sci USA.* **102**: 4164-4169

Katsanis N, Ansley S. J, Badano J. L, Eichers E. R, Lewis R. A, Hoskins B. E, Scambler P. J, Davidson W. S, Beales P. L, Lupski J. R (2001) Triallelic inheritance in Bardet-Biedl syndrome, a Mendelian recessive disorder. *Science.* **293(5538)**: 2256-9

Kaushal S and Khorana H. G (1994) Structure and function in rhodopsin. 7 Point mutations associated with autosomal dominant retinitis pigmentosa. *Biochemistry.* **33**: 6121-6128

Kawasaki H and Taira K (2003) Short hairpin type of dsRNAs that are controlled by tRNA(Val) promoter significantly induce RNAi-mediated gene silencing in the cytoplasm of human cells. *Nucleic Acids Res* **31:** 700–707

Kay M. A, Manno C. S, Ragni M. V, Larson P. J, Couto L. B, McClelland A, Glader B, Chew A. J, Tai S. J, Herzog R. W, Arruda V, Johnson F, Scallan C, Skarsgard E, Flake A. W, High K. A (2000) Evidence for gene transfer and expression of factor IX in haemophilia B patients treated with an AAV vector. *Nat. Genet.* **24**: 257–261

Keats B, J and Corey D. P (1999) The usher syndromes. *Am J Med Genet.* **89(3)**: 158-166

Kedersha N, Stoecklin G, Ayodele M, Yacono P, Lykke-Andersen J, Fritzler M. J, Scheuner D, Kaufman R. J, Golan D.E, Anderson P (2005) Stress granules and processing bodies are dynamically linked sites of mRNP remodeling. *J. Cell. Biol.* **169**: 871-884

Kennan A, Aherne A, Palfi A, Humphries M, McKee A, Stitt A, Simpson D. A, Demtroder K, Orntoft T, Ayuso C, Kenna P. F, Farrar G. J, Humphries P (2002) Identification of an IMPDH1 mutation in autosomal dominant retinitis pigmentosa (RP10) revealed following comparative microarray analysis of transcripts derived from retinas of wild-type and Rho-/- mice. *Human Molecular Genetics.* **11 (5):** 547-557

Kermer P, Klocker N, Weishaupt J. H, Bahr M (2001) Transection of the optic nerve in rats: studying neuronal death and survival *in vivo. Brain Res. Protocol.* **7**: 255-260

Khvorova A, Reynolds A, Jayasena S. D (2003) Functional siRNAs and miRNAs exhibit strand bias. *Cell.* **115**: 209-216

Kiang A.S, Palfi A, Ader M, Kenna P.F, Millington-Ward S, Clark G, Kennan A, O'Reilly M, Tam L.C.S, Aherne A, McNally N, Humphries P, Farrar G.J. (2005) Toward a Gene Therapy for Dominant Disease: Validation of an RNA Interference-Based Mutation-Independent Approach. *Molecular Therapy.* **12 (3)**: 555-561

Kiguchi K, Collart F. R, Henning-Chubb C, Huberman E (1990a) Cell differentiation and altered IMP dehydrogenase expression induced in human T-lymphoblastoid leukemia cells by mycophenolic acid and tiazofurin. *Exp. Cell Res.* **187**: 47-53

Kiguchi, K., Collart, F. R., Henning-Chubb, C., and Huberman, E. (1990b) Induction of cell differentiation in melanoma cells by inhibitors of IMP dehydrogenase: altered patterns of IMP dehydrogenase expression and activity. *Cell Growth & Differ.* **1**: 259-270

Kim V. N (2005) MicroRNA biogenesis: coordinated cropping and dicing. Nat Rev *Mol Cell Biol.* **6**: 376-385

Kim V. N (2006) Small RNAs just got bigger: Piwi-interacting RNAs (piRNAs) in mammalian testes. *Genes Dev.* **20**: 1993-1997

Kim H. J, Greenleaf J. F, Kinnick R. R, Bronk J. T, Bolander M. E (1996) Ultrasound-mediated transfection of mammalian cells. *Hum Gene Ther.* **7(11)**: 1339-46

Kim S, Nollen E. A, Kitagawa K, Bindokas V. P, Morimoto R. I (2002) Polyglutamine protein aggregates are dynamic. *Natl Cell Biol.* **4**: 826-831

Kim B, Tang Q, Biswas P. S, Xu J, Schiffelers R. M, Xie F. Y, Ansari A. M, Scaria P. V, Woodle M. C, Lu P, Rouse B. T (2004) Inhibition of ocular angiogenesis by siRNA targeting vascular endothelial growth factor pathway genes: therapeutic strategy for herpetic stromal keratitis. *Am J Pathol.* **165**: 2177-2185

Kim D. H, Behlke M. A, Rose S. D, Chang M. S, Choi S, Rossi J. J (2005) Synthetic dsRNA Dicer substrates enhance RNAi potency and efficacy. *Nat. Biotechnol.* **23(2):** 222-226

Kim H. K, Lee Y. S, Sivaprasad U, Malhotra A, Dutta A (2006) Muscle-specific microRNA miR-206 promotes muscle differentiation. *J. Cell Biol.* **174**: 677-687

Klein D (2002) Quantification using real-time PCR technology: applications and limitations. *Trends Mol Med.* **8**: 257-260

Klein R and Klein B. E. K (1993) The Beaver Dam Eye study: the relation of age-related maculopathy to smoking. *Am J Epidermiol.* **137**: 190-200

Klein R, Klein B. E. K, Moss S. E, Davis M. D, DeMets D. L (1984) The Wisconsin Epidemilogical Study of Diabetic Retinopathy II. Prevalence and risk of diabetic retinopathy when age at diagnosis is less than 30 years. *Arch Ophthamol.* **102**: 520-526

Klein R. M, Wolf E. D, Wu R, Sanford J. C (1987) High velocity microprojectiles delivering nucleic acids into living cells. *Nature.* **327**: 70-73

Kloosterman W. P, Wienholds E, de Brujin E, Kauppmen S, Plasterk R. H (2006) *In-situ* detection of miRNAs in animal embryos using LNA modified oligonucleotide probes. *Nat. Methods.* **3**: 27-29

Ko K, Furukawa K, Takahashi T, Urano T, Sanai Y, Nagino M, Nimura Y, Furukawa K (2006) Fundamental study of small interfering RNAs for ganglioside GD3 synthase gene as a therapeutic target of lung cancers. *Oncogene.* **25**: 6924-6935

Kobashigawa J, Miller L, Renlund D, Mentzer R, Alderman E, Bourge R, Costanzo M, Eisen H, Dureau G, Ratkovec R, Hummel M, Ipe D, Johnson J, Keogh A, Mamelok R,

Mancini D, Smart F, Valantine H (1998) A randomized active-controlled trial of mycophenolate mofetil in heart transplant recipients. *Transplantation.* **66**: 507–515

Koch S, Pohl P, Cobet U, Rainov N. G (2000) Ultrasound enhancement of liposome-mediated cell transfection is caused by cavitation effects. *Ultrasound Med Biol.* **26(5):** 897-903

Koenekoop R. K (2004) An overview of Leber congenital amaurosis: a model to understand human retinal development. *Surv Ophthamol.* **49**: 379-398

Kopito R. R (2000) Aggresomes, inclusion bodies and protein aggregation. *Trends Cell Biol.* **10**: 524-530

Kornberg A. and Baker T.A (1992) DNA Replication. Freeman, New York

Kotin R. M, Linden R. M, Berns K. I (1992) Characterization of a preferred site on human chromosome 19q for integration of adeno-associated virus DNA by non-homologous recombination. *EMBO J.* **11**: 5071–5078

Kralinger M. T, Voigt M, Kieselbach G. F, Hamasaki D, Hayden B. C, Parel J. M (2003) Ocular delivery of acetylsalicylic acid by repetitive coulomb-controlled iontophoresis, *Ophthalmic Res.* **35**: 102–110

Krieg A. M and Stein C. A (1995) Phosphorothioate oligodeoxynucleotides: antisense or anti-protein? *Antisense Res. Dev.* **5**: 241

Kruger K, Grabowski P. J, Zaug A. J, Sands J, Gottschling D. E, Cech T. R (1982) Self splicing RNA: autoexcision and autocyclization of the ribosomal RNA intervening sequence of Tetrahymena. *Cell.* **31**: 147-157

Kusumi T, Tsuda M, Katsunuma T, Yamamura M (1988) Dual inhibitory effect of bredinin. *Cell Biochem. Funct.* **7**: 201–204

Kwak N, Okamoo N, Wood J. M, Campochiaro P. A (2000) VEGF is an important stimulaotr in a model of choroidal neovascularization. *Invest Ophthamol Vis Sci.* **41**: 3158-3164

Lagos-Quintana M, Rauhut R, Yalcin A, Meyer J, Lendeckel W, Tuschl T (2002) Identification of tissue-specific microRNAs from mouse. *Curr. Biol.* **12**: 735-739

Lagos-Quintana M, Rauhut R, Meyer J, Borkhardt A, Tuschl T (2003) New microRNAs from mouse and human. *RNA.* **9**: 175-179

Lai E. C (2002) Micro RNAs are complementary to 3'UTR sequence motifs that mediate negative post-transcriptional regulation. *Nature Genet.* **30**: 363-364

Lai Y. K, Shen W. Y, Brankov M, Lai C. M, Constable I. J, Rakoczy P. E (2002) Potential long-term inhibition of ocular neovascularisation by recombinant adeno-associated virus-mediated secretion gene therapy. *Gene Ther.* **9**: 804–813

Lammer E. J, Chen D. T, Hoar R. M, Agnish N. D, Benke P. J, Braun J. T, Curry C. J, Fernhoff P. M, Grix A. W Jr, Lott I. T *et al* (1985) Retinoic acid embryopathy. *N Engl J Med.* **313**: 837–841

Lassus P, Opitz-Araya X, Lazebnik Y (2002) Requirement for caspase-2 in stress induced apoptosis before permeablization. *Science*. **297**: 1352-1354

Lau D, McGee L. H, Zhou S, Rendahl K. G, Manning W. C, Escobedo J. A, Flannery J. G (2000) Retinal degeneration is slowed in transgenic rats by AAV-mediated delivery of FGF-2. *Invest Ophthalmol Vis Sci*. **41**: 3622-3633

LaVail M. M, Yasumura D, Matthes M. T, Drenser K. A, Flannery J. G, Lewin A. S, Hauswirth W. W. (2000) Ribozyme rescue of photoreceptor cells in P23H transgenic rats, long term survival and late-stage therapy. *Proc. Natl. Aca. Sci. USA*. **97**: 11488-93

Lawrie A, Brisken A. F, Francis S. E, Tayler D. I, Chamberlain J, Crossman D. C, Cumberland D. C, Newman C. M (1999) Ultrasound enhances reporter gene expression after transfection of vascular cells in vitro. *Circulation*. **99**: 2617-2620

Le Meur G, Stieger K, Smith A. J, Weber M, Deschamps J. Y, Nivard D, Mendes-Madeira A, Provost N, Péréon Y, Cherel Y, Ali R. R, Hamel C, Moullier P, Rolling F (2007) Restoration of vision in RPE65-deficient Briard dogs using an AAV serotype 4 vector that specifically targets the retinal pigmented epithelium. *Gene Ther*. **14(4)**: 292-303

Lebherz C, Auricchio A, Maguire A. M, Rivera V. M, Tang W, Grant R. L, Clackson T, Bennett J, Wilson J. M (2005) Long-term inducible gene expression in the eye via adeno-associated virus gene transfer in nonhuman primates. *Hum Gene Ther*. **16**: 178–186

Lee R. C, Feinbaum R. L, Ambros V (1993) The C. elegans heterochronic gene lin-4. *Cell*. **75**: 843-854

Lee Y, Jeon K, Lee J. T, Kim S, Kim V. N (2002a) MicroRNA maturation: stepwise processing and subcellular localization. *EMBO J*. **21**: 4663–4670

Lee N. S, Dohjima T, Bauer G, Li H, Li M. J, Ehsani A, Salvaterra P, Rossi J (2002b) Expression of small interfering RNAs targeted against HIV-1 rev transcripts in human cells. *Nat. Biotechnol*. **20**: 500-505

Lee J. H, Canny M. D, De Erkenez A, Krilleke D, Ng Y. S, Shima D. T, Pardi A, Jucker F (2005) A therapeutic aptamer inhibits angiogenesis by specifically targeting the heparin binding domain of VEGF165. *PNAS*. **102(52)**: 18902-18907

Lem J and Fain G. L (2004) Constitutive opsin signaling: night blindness or retinal degeneration? *Trends Mol Med*. **10**: 150-157

Lem J, Krasnoperova N. V, Calvert P. D, Kosaras B, Cameron D. A, Nicolò M, Makino C. L, Sidman R. L (1999) Morphological, physiological and biochemical changes in rhodopsin knockout mice. *Proc Natl Acad Sci USA*. **96**: 736-741

Leng Q and Mixson A. J (2005) Small interfering RNA targeting Raf-1 inhibits tumour growth *in vitro* and *in vivo*. *Cancer Gene Ther*. **12**: 682-690

Lestienne P and G Ponsot (1988) Kearns-Sayre syndrome with muscle mitochondrial DNA deletion. *Lancet*. **1**: 885

Leung A. K, Calabrese J. M, Sharp P. A (2006) Quantitative analysis of Argonaute protein reveals microRNA-dependent localization to stress granules. *Proc. Natl. Acad. Sci. U.S.A*. **103**: 18125-18130

Lewin A. S, Drenser K. A, Hauswirth W. W, Nishikawa S, Yasumura D, Flannery J. G, LaVail M. M (1998) Ribozyme rescue of photoreceptor cells in a transgenic rat model of autosomal dominant retinitis pigmentosa. *Nat. Med.* **4**: 967–971

Lewis DL, Hagstrom JE, Loomis AG, Wolff JA, Herweijer H (2002) Efficienct delivery of siRNA for inhibition of gene expression in postnatal mice. *Nat Genet.* **32**: 107-108

Lewis B. P, Shih I. H, Jones-Rhoades M. W, Bartel D. P, Burge C. B (2003) Prediction of mammalian microRNA targets. *Cell.* **115**: 787-798

Lewis B. P, Burge C. B, Bartel D. P (2005) Conserved seed pairing, often flanked by adenosines, indicates that thousands of human genes are mircoRNA targets. *Cell.* **120**: 15-20

Li Z. Y, Jacobson S. G, Milam A. H (1994) Autosomal dominant retinitis pigmentosa caused by the threonine-17-methionine rhodopsin mutation: retinal histopathy and immunocytochemistry. *Exp Eye Res.* **58**: 397-408

Li T, Snyder W. R, Olsson J. E, Dryja T. P (1996) Transgenic mice carrying dominant rhodopsin mutation P347S: evidence for defective vectorial transport of rhodopsin to the outer segments. *Proc. Natl. Acad. Sci. USA.* **93**: 14176-14181

Li Z. Y, Wong F, Chang J. H, Possin D. E, Hao Y, Petters R. M, Milam A. H (1998a) Rhodopsin transgenic pigs as a model for a human retinitis pigmentosa. *Invest Ophthalmol Vis Sci.* **39**: 808-819

Li T, Sandberg M. A, Pawlyk B. S, Rosner B, Hayes K. C, Dryja T. P, Berson E.L. (1998b) Effect of vitamin A supplementation on rhodopsin mutants threonine-17 → methionine and proline-347 --> serine in transgenic mice and in cell cultures. *Proc. Natl. Acad. Sci. U S A.* **95 (20)**: 11933-8

Li M. J, Kim J, Li S, Zaia J, Yee J. K, Anderson J, Akkina R, Rossi J. J (2005) Long-term inhibition of HIV-1 infection in primary hematopoietic cells by lentiviral vector delivery of a triple combination of anti-HIV shRNA, anti-CCR5 ribozyme, and a nucleolar-localising TAR decoy. *Mol Ther.* **12**: 900-909

Li Y, Li H, Yao G, Li W, Wang F, Jiang Z, Li M (2007) Inhibition of telomerase RNA (hTR) in cervical cancer by adenovirus-delivered siRNA. Cancer Gene Therapy. **14(8)**: 748-55.

Liang F. Q, Aleman T. S, Dejneka N. S, Dudus L, Fisher K. J, Maguire A. M, Jacobson S. G, Bennett J (2001) Long-term protection of retinal structure but not function using RAAV.CNTF in animal models of retinitis pigmentosa. *Mol Ther.* **4**: 461–472

Liao H and Wang J. H (2005) Biomembrane-permeable and ribonuclease-resistant siRNA with enhanced activity. *Oligonucleotides.* **15**: 196-205

Lim L. P, Lau N. C, Garrett-Engele P, Grimson A, Schelter J. M, Castle J, Bartel D. P, Linsley P. S, Johnson J. M (2005) Microarray analysis shows that some microRNAs downregulate large numbers of target mRNAs. *Nature.* **433**: 769-773

Lin M. T, Pulkkinen L, Uitto J, Yoon K (2000) The gene gun: current applications in cutaneous gene therapy. *Int J Dermatol.* **39**: 161-170

Lin X, Ruan X, Anderson M. G, McDowell J. A, Kroeger P. E, Fesik S. W, Shen Y (2005) siRNA-mediated off target gene silencing triggered by a 7 nucleotide complementation. *Nucleic Acids Res.* **33**: 4527-4535
Lindberg C. R, Fishman G. A, Anderson R. J, Vasquez V (1981) Contrast sensitivity in retinitis pigmentosa. *Br J Ophthalmol.* **65**: 855–858

Linden R. M, Ward P, Giraud C, Winocour E, Berns K. I (1996) Site-specific integration by adeno-associated virus. *Proc. Natl. Acad. Sci. USA.* **93**: 11288–11294

Lingor P, Koeberle P, Kugler S, Bahr M (2005) Downregulation of apoptosis mediators by RNAi inhibits axtomy-induced retinal ganglion cell death in vivo. *Brain.* **128**. 550-558

Liu X, Garriga P, Khorana H. G (1996) Structure and function in rhodopsin: Correct folding and misfolding in two point mutants in the intradiscal domain of rhodopsin identified in retinitis pigmentosa. *Proc. Natl. Acad. Sci. USA.* **93:** 4554–4559

Liu C, Li Y, Peng M, Laties A. M, Wen R. (1999a) Activation of caspase 3 in retina of transgenic rats with rhodopsin mutation s334ter during photoreceptor degeneration. *J. Neirosci.* **19**: 4778-4785

Liu F, Song Y, Liu D (1999b) Hydrodynamic-based transfection in animals by systematic administration of plasmid DNA. *Gene. Ther.* **6**: 1258-1266

Liu Q, Rand T. A, Kalidas S, Du F, Kim H-E, Smith D. P, Wang X (2003a) R2D2, a bridge between the initiation and effector steps of the Drosophila RNAi pathway. *Science.* **301**: 1921-1925

Liu D, Ren T, Gao X (2003b) Cationic transfection lipids. *Curr Med Chem.* **10(14)**: 1307-15

Liu J, Carmell M. A, Rivas F. V, Marsden C. G, Thomson J. M, Song J. J, Hammond S. M, Joshua-Tor L, Hannon G. J (2004a) Argonaute2 is the catalytic engine of mammalian RNAi. *Science.* **305**: 1437-1441

Liu X. D, Ma S. M, Liu Y, Liu S. Z, Sehon A (2004b) Short hairpin RNA and retroviral vector-mediated silencing of p53 in mammalian cells, *Biochem. Biophys. Res. Commun.* 324 (4): 1173–1178

Liu J, Rivas F. V, Wohlschlegel J, Yates J. R, III, Parker R, Hannon G. J (2005a) A role for the P body component GW182 in microRNA function. *Nat. Cell. Biol.* **7**. 1261-1266

Liu J, Valencia-Sanchez, M.A, Hannon G.J, Parker R (2005b) MicroRNA-dependent localization of targeted mRNAs to mammalian P-bodies. *Nat. Cell. Biol.* **7**: 719-723

Lorenz B, Gyürüs P, Preising M, Bremser D, Gu S, Andrassi M, Gerth C, Gal A (2000) Early-onset severe rod-cone dystrophy in young children with RPE65 mutations. *Invest Ophthalmol Vis Sci.* **41**: 2735-2742

Lorenz C, Hadwiger P, John M, Vornlocher H. P, and Unverzagt C (2004) Steroid and lipid conjugates of siRNAs to enhance cellular uptake and gene silencing in liver cells. *Bioorg. Med. Chem. Lett.* **14**: 4975-4977

Lotery A. J, Yang G. S, Mullins R. F, Russell S. R, Schmidt M, Edwin E. M, Lindbloom J. D, Chiorini J. A, Kotin R. M, Davidson B. L (2003) Adeno-associated virus type 5:

Transduction efficiency and cell type specificity in the primate retina. *Humna Gene Therapy*. **14**: 1663-1671

Lu P. Y and Woodle M. C (2005) Delivery siRNA *in vivo* for functional genomics and novel therapeutics. In RNA Interference Technology (K. Appasanied), Cambridge University Press
Lund E, Guttinger S, Calado A, Dahlberg J. E, Kutay U (2004) Nuclear export of microRNA precursors. *Science*. **303**: 95-98

Lyubarsky A. L, Falsini B, Pennesi M. E, Valentini P, Pugh Jr E. N (1999) UV- and midwave sensitive cone-driven retinal responses of the mouse: a possible phenotype for coexpression of cone photopigments. *J Neurosci*. **19**: 442-455

Ma H. T, On K. F, Tsang Y. H, Poon R. Y (2007) An inducible system for expression and validation of the specificity of short hairpin RNA in mammalian cells. *Nucleic Acids Research*. **35(4)**: e22

Machida S, Kondo M, Jamison J. A, Khan N. W, Kononen L. T, Sugawara T, Bush R. A, Sieving P. A (2000). P23H rhodopsin transgenic rat: correlation of retinal function with histopathology. *Invest. Ophthalmol. Visual Sci*. **41**: 3200–3209

Machida Y, Okada T, Kurosawa M, Oyama F, Ozawa K, Nukina N (2006) rAAV-mediated shRNA ameliorated neuropathy in Huntington disease model mouse. *Biochem Biophys Res Commun*. **343(1)**: 190-197

Mackey D. A, Heon E, Webster A. R (2003) Predicitive DNA testing in ophthalmology. *Br J Ophthamol*. **87**: 633-638

MacLaren R. E, Pearson R. A, MacNeil A, Douglas R. H, Salt T. E, Akimoto M, Swaroop A, Sowden J. C, Ali R. R (2006) Retinal repair by transplantation of photoreceptor precursors. *Nature*. **444**: 203-207

Maguire M, Fine S. L, Ying G. S (2005) Intravitreal injection of VEGF siRNA. *Retina*. **25**: 101-102

Mahnke-Zizelman D. K, Eddy R, Shows T. B, Sabina R. L (1996) Characterization of the human AMPD3 gene reveals that 5' exon useage is subject to transcriptional control by three tandem promoters and alternative splicing. *Biochim. Biophys. Acta*. **1306**: 75-92

Maita H, Kitaura H, Keen T. J, Inglehearn C. F, Ariga H, Iguchi-Ariga S. M (2004) PAP-1, the mutated gene underlying the RP9 form of dominant retinitis pigmentosa, is a splicing factor. *Exp Cell Res*. **300**: 283-96

Mamiya K, Ohguro H, Ohguro I, Metoki T, Ishikawa F, Yamazaki H, Takano Y, Ito T, Nakazawa M (2004) Effects of matrix metalloproteinase-3 gene transfer by electroporation in glaucoma filter surgery. *Exp Eye Res*. **79**: 405–410

Manno C. S, Chew A. J, Hutchison S, Larson P. J, Herzog R. W, Arruda V. R, Tai S. J, Ragni M. V, Thompson A, Ozelo M, Couto L. B, Leonard D. G, Johnson F. A, McClelland A, Scallan C, Skarsgard E, Flake A. W, Kay M. A, High K. A, Glader B (2002) AAV-mediated factor IX gene transfer to skeletal muscle in patients with severe hemophilia B. *Blood* **101**: 2963–2972

Mansergh F.C, Millington-Ward S, Kennan A, Kiang A. S, Humphries M, Farrar G. J, Humphries P, Kenna P. F. (1999) Retinitis pigmentosa and progressive sensorineural

hearing loss caused by a C12258A mutation in the mitochondrial MTTS2 gene, *Am J Hum Genet.* **64**: 971–985

Marmor M. F and Hock P. A (1982) A practical method for c-wave recording in man. *Doc. Ophthalmol. Proc. Ser.* **31**: 67-72

Martin K. R, Klein R. L, Quigley H. A (2002) Gene delivery to the eye using adeno-associated viral vectors. *Methods* **28**: 267–275

Martinez J, Patkaniowska A, Urlaub H, Luhrmann R, Tuschl T (2002) Single-stranded antisense siRNAs guide target RNA cleavage in RNAi. *Cell.* **110**: 563-574

Maruyama H, Higuichi N, Kameda S, Miyyazaki J, Gejyo F (2004) Rat liver targeted naked plasmid DNA transfer by tail vein injection. *Mol Biotechnol.* **26**: 165-172

Mathiesen I (1999) Electropermeabilization of skeletal muscle enhances gene transfer *in-vivo*. *Gene Ther.* **6:** 508-514

Matsuda T and Cepko C. L (2004) Electroporation and RNA interference in the rodent retina *in-vivo* and *in-vitro*. *Proc Natl Acad Sci U S A.* **101(1):** 16-22

Matsuda T and Cepko C. L (2007) Controlled expression of transgenes introduced by *in vivo* electroporation. *Proc Natl Acad Sci U S A.* **104(3)**: 1027-32

Mattaj I. W, Dathan N. A, Parry H. D, Carbon P, Krol A (1988) Changing the RNA polymerase specificity of U snRNA gene promoters. *Cell.* **55(3)**: 435–444

Matveeva O, Nechipurenko Y, Rossi L, Moore B, Saetrom P, Ogurtsoc A. Y, Atkins J. F, Shabalina S. A (2007) Comparison of approaches for rational siRNA design leading to a new efficient and transparent method. *Nucleic Acids Res.* **35(8):** 63

McCaffrey A. P, Meuse L, Pham T. T, Conklin D. S, Hannon G. J, Kay M. A (2002) RNA interference in adult mice. *Nature.* **418**: 38-39

McGee Sanftner L. H, Rendahl K. G, Quiroz D, Coyne M, Ladner M, Manning W. C, Flannery J. G (2001a) Recombinant AAV-mediated delivery of a tet-inducible reporter gene to the rat retina. *Mol. Ther.* **3**: 688–696

McGee Sanftner L. H, Abel H, Hauswirth W. W, Flannery J. G (2001b) Glial cell line derived neurotrophic factor delays photoreceptor degeneration in a transgenic rat model of retinitis pigmentosa. *Mol Ther.* **4**: 622-629

McGuire R. E, Gannon A. M, Sullivan L. S, Rodriguez J. A, Daiger S. P (1995) Evidence for a major gene (RP10) for autosomal dominant retinitis pigmentosa on chromosome 7q linkage mapping in a second, unrelated family. *Hum Genet.* **95:** 71–74

McGuire R. E, Jordan S. A, Braden V. V., Bouffard G. G, Humphries P, Green E. D, Daiger S. P (1996) Mapping the RP10 locus for autosomal dominant retinitis pigmentosa on 7q: refined genetic positioning and localization within a well-defined YAC contig. *Genome Res.* **6**: 255–266

McGuire R. E, Daiger S. P, Green E. D (1997) Localization and characterization of the human ADP-ribosylation factor 5 (ARF5) gene. *Genomics.* **41**: 481–484

McIlwain J. T. An introduction to the biology of vision. *Cambridge University Press* (1996)

McKie A. B, McHale J. C, Keen T. J, Tarttelin E. E, Goliath R, van Lith-Verhoeven J. J, Greenberg J, Ramesar R. S, Hoyng C. B, Cremers F. P, Mackey D. A, Bhattacharya S. S, Bird A. C, Markham A. F, Inglehearn C. F (2001) Mutations in the pre-mRNA splicing factor gene PRPF8 in autosomal dominant retinitis pigmentosa (RP13). *Hum Mol Genet.* **10**: 1555-62

McKinnon S. J, Lehman D. M, Tahzib N. G, Ransom N. L, Reitsamer H. A, Liston P, LaCasse E, Li Q, Korneluk R. G, Hauswirth W. W (2002) Baculoviral IAP repeat-containing-4 protects optic nerve axons in a rat glaucoma model. *Mol. Ther.* **5**: 780–787
McKusick V. A (1998) Mendelian Inheritance in Man. Baltimore, Maryland: The Johns Hopkins University Press

McLaren F. H, Svendsen C. N, Van der Meide P, Joly E (2001) Analysis of neural stem cells by flow cytometry: cellular differentiation modifies patterns of MHC expression. *J. Neuroimmunol.* **112**: 35–46

McLaughlin M. E, Sandberg M. A, Berson E. L, Dryja T. P (1993) Recessive mutations in the gene encoding the alpha-subunit of rod phosphodiesterase in patients with retinitis pigmentosa. *Nat. Gen.***4**: 130-134

McLean J. E, Hamaguchi N, Belenky P, Mortimer S. E, Stanton M, Hedstrom L (2004) Inosine 5′-monophosphate dehydrogenase binds nucleic acids in vitro and in vivo. *Biochem. J.* **379**: 243–251

McManus M. T, Petersen C. P, Haines B. B, Chen J, Sharp P. A (2002) Gene silencing using micro-RNA designed hairpins. *RNA.* **8**: 842-850

McNally N, Kenna P. F, Rancourt D, Ahmed T, Stitt A, Colledge W. H, Lloyd D. G, Palfi A, O'Neill B, Humphries M. M, Humphries P, Farrar G. J (2002) Murine model of autosomal dominant retinitis pigmentosa generated by targeted deletion at codon 307 of the rds-peripherin gene. *Hum Mol Genet.* **11**: 1005-1016

McWilliam P, Farrar G. J, Kenna P, Bradley D. G, Humphries M. M, Sharp E. M, McConnell D. J, Lawler M, Sheils D, Ryan C, Stevens K, Daiger S. P, Humphries P (1989) Autosomal dominant retinitis pigmentosa (ADRP): localization of an ADRP gene to the long arm of chromosome 3. *Genomics.* **5**: 619-22

Mears A. J, Kondo M, Swain P. K, Takada Y, Bush R. A, Saunders T. L, Sieving P. A, Swaroop A (2001) Nrl is required for rod photoreceptor development. *Nat Genet.* **29**. 447-452

Mehalow A. K, Kameya S, Smith R. S, Hawes N. L, Denegre J. M, Young J. A, Bechtold L, Haider N. B, Tepass U, Heckenlively J. R, Chang B, Naggert J. K, Nishina P. M (2003) CRB1 is essential for external limiting membrane integrity and photoreceptor morphogenesis in the mammalian retina. *Hum Mol Genet.* **12**: 2179-2189

Mehier-Humbert S and Guy R. H (2005) Physical methods for gene transfer: improving the kinetics of gene delivery into cells, *Adv Drug Deliv Rev.* **57**: 733–753

Meister G, Landthaler M, Patkaniowska A, Dorsett Y, Teng G, Tuschl T (2004) Human Argonaute2 mediates RNA cleavage targeted by miRNAs and siRNAs. *Mol. Cell.* **15**: 185–197

Melton D. A (1985) Injected anti-sense RNAs specifically block messenger RNA translation in vivo. *Proc. Natl. Acad. Sci. USA.* **82**: 144-148

Mendes H. F, Van Der Spuy J, Chapple J. P, Cheetham M. E (2005) Mechanisms of cell death in rhodopsin retinitis pigmentosa: implications for therapy. *Trends Mol Med.* **11 (4)**: 177-185

Meng E.C and Bourne H.R (2001) Receptor activation: What does the rhodopsin structure tell us? *Trends Pharmacol. Sci.* **22**: 587–593

Meyer J. S, Katz M. L, Maruniak J. A, Kirk M. D (2006) Embryonic stem cell-derived neural progenitors incorporate into degenerating retina and enhance survival of host photoreceptors. *Stem Cells.* **24**: 274–283

Meyer-Siegler K, Mauro D. J, Seal G, Wurzer J, deRiel J. K, Sirover M. A (1991) A human nuclear uracil DNA glycosylase is the 37 kDa subunit of glyceraldehyde-3-phosphate dehydrogenase. *Proc. Natl. Acad. Sci. U.S.A.* **88**: 8460–8464

Millán J. M., Martínez F, Vilela C, Beneyto M, Prieto F, Nájera,C. (1995) An autosomal dominant retinitis pigmentosa family with close linkage to D7S480 on 7q. Hum. Genet., 96, 216–218

Miller R. F and Dowling J. E (1970) Intracellular responses of the Muller (glial) cells of mudpuppy retina: their relation to the b-wave of the electroretinogram. *J. Neurophysiol.* **33**: 323-341

Miller TM, Kaspar BK, Kops GJ, Yamanaka K, Christian LJ, Gage FH, Cleveland DW (2005) Virus-delivered small RNA silencing sustains strength in amyotrophic lateral sclerosis. *Ann Neurol.* **57(5)**: 773-6

Millington-Ward S, O'Neill B, Tuoghy G, Al-Jandal N, Kiang A.S, Kenna P.F, Palfi A, Hayden P, Mansergh F, Kennan A, Humphries P, Farrar G.J. (1997) Strategems *in-vitro* for gene therapies directed to dominant mutations. *Human Mole. Genetics.* **6 (9):** 1415-26

Miyagishi M and Taira K (2002a) U6 promoter-driven siRNAs with four uridine 3' overhangs efficiently suppress targeted gene expression in mammalian cells. *Nat Biotechnol.* **20**: 497–500

Miyagishi M and Taira K. (2002b) Development and application of siRNA expression vector. *Nucleic Acid Research Suppl.* **2**: 113-114

Mohamed Z, Bell C, Hammer H. M, Converse C. A, Esakowitz L, Haites N, E (1996) Linkage of a medium sized Scottish autosomal dominant retinitis pigmentosa family to chromosome 7q. *J. Med. Genet.* **33**: 714–715

Moiseyev G, Chen Y, Takahashi Y, Wu B. X, Ma J. X. (2005) RPE65 is the isomerohydrolase in the retinoid visual cycle. *Proc Natl Acad Sci USA.* 102: 12413–12418

Molina R. P, Ye H. Q, Brady J, Zhang J, Zimmerman H, Kaleko M, Luo T (2004) A synthetic Rev-independent bovine immunodeficiency virus-based packaging construct. *Hum Gene Ther.* **15**: 865–877

Monahan P. E and Samulski R. J (2000) AAV vectors: is clinical success on the horizon? *Gene Therapy.* **7**: 24-30

Moore M. D, McGarvey M. J, Russell R. A, Cullen B. R, McClure M. O (2005) Stable inhibition of hepatitis B virus proteins by small interfering RNA expressed from viral vectors. *J Gene Med.* **7(7)**: 918-25

Mordes D, Luo X, Kar A, Kuo D, Xu L, Fushimi K, Yu G, Sternberg Jr. P, Wu J. Y (2006) Pre-mRNA splicing and retinitis pigmentosa. *Molecular Vision.* **12**: 1259-1271

Morenegg G, Winkler G. C, Hubscher U, Heizmann C. W, Mous J, Kuenzle C. C (1986) Glyceraldehyde-3-phosphate dehydrogenase is a non-histone protein and a possible activator of transcription in neurons. *J. Neurochem.* **47**: 54–62
Mori K, Gehlbach P, Yamamoto S, Duh E, Zack DJ, Li Q, Berns KI, Raisler BJ, Hauswirth WW, Campochiaro PA (2002) AAV-mediated gene transfer of pigment epithelium-derived factor inhibits choroidal neovascularization. *Invest. Ophthalmol. Vis. Sci.* **43**: 1994–2000

Morris K. V and Rossi J. J (2006) Lentivirus-mediated RNA interference therapy for Human immunodeficiency virus type 1 infection. *Hum. Gene. Ther.* **17 (5)**: 479-486

Morrissey D. V, Lockridge J. A, Shaw L, Blanchard K, Jensen K, Breen W, Hartsough K, Machemer L, Radka S, Jadhav V, Vaish N, Zinnen S, Vargeese C, Bowman K, Shaffer C. S, Jeffs L. B, Judge A, MacLachlan I, Polisky B (2005a) Potent and persistent in vivo anti-HBV activity of chemically modified siRNAs. *Nat. Biotechnol.* **23**: 1002-1007

Morrissey D. V, Blanchard K, Shaw L, Jensen K, Lockridge J. A, Dickinson B, McSwiggen J. A, Vargeese C, Bowman K, Shaffer C. S, Polisky B. A, Zinnen S (2005b) Activity of stabilized short interfering RNA in a mouse model of hepatitis B virus replication. *Hepatology.* **41**: 1349-1356

Morrow E. M, Furukawa T, Raviola E, Cepko C. L (2005) Synaptogenesis and outer segment formation are perturbed in the neural retina of Crx mutant mice. *BMC neurosci.* **6 (1)**: 5

Mortimer S. E and Hedstrom L (2005) Autosomal dominant retinitis pigmentosa mutations in inosine 5′-monophosphate dehydrogenase type I disrupt nucleic acid binding. *Biochem. J.* **390**: 41–47

Mount J. D, Herzog R. W, Tillson D. M, Goodman S. A, Robinson N, McCleland M. L, Bellinger D, Nichols T. C, Arruda V. R, Lothrop Jr. C. D, High, K.A (2002) Sustained phenotypic correction of hemophilia B dogs with a factor IX null mutation by liver-directed gene therapy. *Blood.* **99**: 2670–2676

Muramatsu S, Mizukami H, Young N. S, Brown K. E (1996) Nucleotide sequencing and generation of an infectious clone of adeno-associated virus 3. *Virology.* **221**: 208-217

Murata M, Takanami T, Shimizu S, Horiuchi S, Habano W, Ma J-X, Sate-Sanai (2006) Inhibition of ocular angiogenesis by Diced siRNAs specific to vascular endothelial growth factor (VEGF). *Current Eye Research.* **31**: 171-180

Mykytyn K, Mullins R. F, Andrews M, Chiang A. P, Swiderski R. E, Yang B, Braun T, Casavant T, Stone E. M, Sheffield V. C (2004) Bardet-Biedl syndrome type 4 (BBS4) null mice implicate Bbs4 in flagella formation but not global cilia assembly. *Proc Natl Acad Sci USA.* **101**: 8664-8669

Naash M. I, Hollyfield J. G, al-Ubaidi M. R, Baehr W (1993). Simulation of human autosomal dominant retinitis pigmentosa in transgenic mice expressing a mutated murine opsin gene. *Proc. Natl. Acad. Sci. USA* . **90**: 5499–5503

Nagai, M., Natsumeda, Y., Konno, Y., Hoffman, R., Irino, S., and Weber, G. (1991) Selective up-regulation of type II inosine 5'-monophosphate dehydrogenase messenger RNA expression in human leukemias. *Cancer Res.* **51**: 3886-3890

Nagai M, Natsumeda Y, Weber G (1992) Proliferation-linked regulation of type II IMP dehydrogenase gene in human normal lymphocytes and HL-60 leukemic cells. *Cancer Res.* **52**: 258-261

Naito Y, Yamada T, Matsumiya T, Ui-Tei K, Saigo K (2004) siDirect, highly effective target specific siRNA design software for mammalian RNAi. *Nucleic acid research.* **32**: 124-129

Naito Y, Yamada T, Matsumiya T, Ui-Tei K, Saigo K, Morishita S (2005) dsCheck: highly sensitive off target search soft ware for double-stranded RNA-mediated RNA interference. *Nucleic acid Research.* **33**: 589-591

Nakamura A, Amikura R, Hanyu K, Kobayashi S (2001a) Me31B silences translation of oocyte-localizing RNAs through the formation of cytoplasmic RNP complex during Drosophila oogenesis. *Development.* **128**: 3233-3242

Nakamura K, Jeong S. Y, Uchihara T, Anno M, Nagashima K, Nagashima T, Ikeda S, Tsuji S, Kanazawa I. (2001b) SCA17, a novel autosomal dominant cerebellar ataxia caused by an expanded polyglutamine in TATA-binding protein. *Hum Mol Genet.* **10**: 1441-8

Nakamura H, Siddiqui S. S, Shen X, Malik A. B, Pulido J. S, Kumar N. M et al (2004) RNA interference targeting transforming growth factor-beta type II receptor suppresses ocular inflammation and fibrosis. *Mol Vis.* **10**: 703-711

Napoli C, Lemieux C, Jorgensen R (1990) Introduction of a chimeric chalcone synthase gene into petunia results in reversible co-suppression of homologous genes in trans. *Plant Cell.* **2 (4)**: 279–289

Narfström K, Katz M. L, Bragadottir R, Seeliger M, Boulanger A, Redmond T. M, Caro L, Lai C. M, Rakoczy P. E (2003a) Functional and structural recovery of the retina after gene therapy in the RPE65 null mutation dog. *Invest Ophthalmol Vis Sci.* **44**: 1663-1672

Narfström K, Katz M. L, Ford M, Redmond T. M, Rakoczy E, Bragadottir R (2003b) *In vivo* gene therapy in young and adult RPE65-/- dogs produces long-term visual improvement. *J Hered.* **94**: 31–37

Nathans J and Hogness D. S (1984) Isolation and nucleotide sequence of the gene encoding human rhodopsin. *Proc Natl Acad Sci USA.* **81**: 4851-4855

Natsumeda Y. and Carr S.F (1993) Human type I and type II IMP dehydrogenases as drug targets. Ann. N. Y. Acad. Sci. 696, pp. 88–93

Natsumeda Y, Ohno S, Kawaski H, Konno Y, Weber G, Susuki K (1990) Two distinct cDNAs for human IMP dehydrogenase. *J. Biol. Chem.* **265**: 5292-5295

Nelson P. T, Baldwin D. A, Kloosterman W. P, Kauppmen S, Plasterk R. H, Mourelatos Z (2006) RAKE and LNA-ISH reveal microRNA expression and localization in archival human brain. *RNA*. **12**: 187-191

Neumann E, Schaefer-Ridder M, Wang Y, Hofschneider P. H (1982) Gene transfer into mouse lyoma cells by electroporation in high electric fields, *EMBO J.* **1**: 841–845

Neumann E, Sowers A. E, Jordan C. A (1989) Electroporation and Electrofusion in Cell Biology, Plenum Press, New York

Neumann E, Kakorin S, Toensing K (1999) Fundamentals of electroporative delivery of drugs and genes. *Bioelectrochem Bioenerg*. **48**: 3–16

Nicholson D. W, Ali A, Thornberry N. A, Vaillancourt J. P, Ding C. K, Gallant M, Gareau Y, Griffin P. R, Labelle M, Lazebnik Y. A (1995) Identification and inhibition of the ICE/CED-3 protease necessary for mammalian apoptosis. *Nature*. **376**: 37-43

Nilsen T. W (2007) Mechanisms of microRNA-mediated gene regulation in animal cells. *Trends in Genetics*. **23**(5): 243-9

Nir I, Kedzierski W, Chen J, Travis G.H (2000) Expression of Bcl-2 protects against photoreceptor degeneration in retinal degeneration slows rds mice. *J. Neurosci*. **20**: 2150-2154

No D, Yao T. P, Evans R. M (1996) Ecdysone-inducible gene expression in mammalian cells and transgenic mice. *Proc Natl Acad Sci USA*. **93**: 3346-3351

Novak-Lauš K, Suzana Kukulj S, Zoric-Geber M, Bastaic O (2002), Primary tapetoretinal dystrophies as the cause of blindness and impaired vision in the republic of Croatia, *Acta Clin Croat*. **41**: 23–27

Nykanen A, Haley B, Zamore P. D (2001) ATP requirements and small interfering RNA structure in the RNA interference pathway. *Cell*. **107**: 309-321

O'Neill B, Millington-Ward S, O'Reilly M, Tuohy G, Kiang A. S, Kenna P. F, Humphries P, Farrar G. J (2000) Ribozyme-based therapeutic approaches for autosomal dominant retinitis pigmentosa. *Invest Ophthalmol Vis Sci*. **41**: 2863-2869

Obernosterer G, Meister G, Poy M. N, Kuras A (2007) The impact of small RNAs. *EMBO Reports*. **8(1)**: 23-27

O'Brien J and Lummis SC (2002) An improved method of preparing microcarriers for biolistic transfection. *Brain Res Brain Res Protoc*. **10**(1): 12-15

Ogilvie J. M., Speck, J. D, Lett J. M, Fleming T. T (1999) A reliable method for organ culture of neonatal mouse retina with long-term survival. *J. Neurosci. Methods*. **87**: 57–65

Olah E, Natsumeda Y, Ikegami T, Kote Z, Horanyi M, Szelenyi J, Paulik E, Kremmer, Hollan S. R, Sugar J, Weber G (1988) Induction of erythroid differentiation and modulation of gene expression by tiazofurin in K-562 leukemia cells. *Proc. Natl. Acad. Sci. U. S. A*. **85**: 6533-6537

Olsen P. H and Ambros V (1999) The lin-4 regulatory RNA controls developmental timing in Caenorhabditis elegans by blocking LIN-14 protein synthesis after the initiation of translation. *Dev. Biol.* **216**: 671-680

Olsson J. E, Gordon J. W, Pawlyk B. S, Roof D, Hayes A, Molday R. S, Mukai S, Cowley G. S, Berson E. L, Dryja T. P (1992) Transgenic mice with rhodopsin mutation (Pro23His): A mouse model of autosomal dominant retinitis pigmentosa. *Neuron.* **9**: 815-830

O'Reilly M, Palfi A, Chadderton N, Millington-Ward S, Ader M, Cronin T, Tuohy T, Auricchio A, Hildinger M, Tivnan A, McNally N, Humphries M. M, Kiang A. S, Humphries P, Kenna P. F, Farrar G. J (2007) RNA interference-mediated suppression and replacement of human rhodopsin *in vivo*. *Am J Hum Genet.* **81**(1): 127-35

Oshima Y, Sakamoto T, Yamanaka I, Nishi T, Ishibashi T, Inomata H (1998) Targeted gene transfer to corneal endothelium *in-vivo* by electric pulse. *Gene Ther.* **5**: 1347–1354

Otteson D.C and Hitchcock P.F (2003) Stem cells in the teleost retina: persistent neurogenesis and injury –induced regeneration. *Vision. Res.* **43**: 927-936

Ozaki H, Seo M. S, Ozaki K (2000) Blockade of vascular endothelial cell growth factor receptor signaling is sufficient to completely prevent retinal neovascularization. *Am J Pathol.* **156**: 697-707

Paddison P. J, Caudy A. A, Bernstein E, Hannon G. J, Conklin D. S (2002a) Short hairpin RNAs (shRNAs) induce sequence-specific silencing in mammalian cells. *Genes Dev.* **16**: 948–958

Paddison P. J, Caudy A. A, Hannon G. J (2002b) Stable suppression of gene expression by RNAi in mammalian cells. Proc. Natl. Acad. Sci. USA. **99**: 1443-1448

Paddison P. J, Silva J. M, Conklin D. S, Schlabach M, Li M, Aruleba S, Balija V, O'Shaughnessy A, Gnoj L, Scobie K, Chang K, Westbrook T, Cleary M, Sachidanandam R, McCombie W. R, Elledge S. J, Hannon G. J (2004a) A resource for large scale RNA interference based screens in mammals. *Nature.* **428 (6981)**: 427-431

Paddison P. J, Cleary M, Silva J. M, Chang K, Sheth N, Sachidanandam R, Hannon G. J (2004b) Cloning of short hairpin RNAs for gene knockdown in mammalian cells. *Nat Methods.* **1**:163–167

Palczewski K, Kumasaka T, Hori T, Behnke CA, Motoshima H, Fox BA, Le Trong I, Teller DC, Okada T, Stenkamp RE, Yamamoto M, Miyano M (2000) Crystal structure of rhodopsin. A G-protein coupled receptor. *Science.* **289**: 739-745

Palfi A, Arder M, Kiang A-S, Millington-Ward- S, Clark G, O'Reilly M, McMahon H. P, Kenna P. F, Humphries P, Farrar G. J (2006) RNAi-based suppression and replacement of rds-peripherin in retinal organotypic culture. *Human Mutation.* **27 (3)**: 260-268

Pang J. J, Chang B, Hawes N. L, Hurd R. E, Davission M. T, Li J, Noorwez S. M, Malhotra R, McDowell J. H, Kaushal S, Hauswirth W. W, Nusinowitz S, Thompson D. A, Heckenlively J. R (2005) Retinal degeneration 12 (rd12): a new, spontaneously arising mouse model for human Leber congenital amaurosis (LCA). *Mol Vis.* **11**: 152-162

Pardue M. T, Phillips M. J, Yin H, Fernandes A, Cheng Y, Chow A. Y, Ball S. L (2005) Possible sources of neuroprotection following subretinal silicon chip implantation in RCS rats. *J Neural Eng.* **2**: S39–S47

Park Y. J, Liang J. F, Ko K. S, Kim S. W, Yang V. C (2003) Low molecular weight protamine as an efficient and nontoxic gene carrier: in vitro study. *J Gene Med.* **5**(8): 700-711

Parker R and Sheth U (2007) P Bodies and the Control of mRNA translation and degradation. *Molecular Cell.* **25**: 635-646

Parker A. L, Newman C, Briggs S, Seymour L, Sheridan P. J (2003) Nonviral gene delivery: techniques and implications for molecular medicine. *Expert Reviews in Molecular Medicine.* **5**: 1-15

Pasquinelli A. E, Reinhart B. J, Slack F, Martindale M. Q, Kuroda M. I, Maller B, Hayward D. C, Ball E. E, Degnan B, Müller P, Spring J, Srinivasan A, Fishman M, Finnerty J, Corbo J, Levine M, Leahy P, Davidson E, Ruvkun G (2000) Conservation of the sequence and temporal expression of let-7 heterochronic regulatory RNA. *Nature.* **408**: 86-89

Pauley K. M, Eystathioy T, Jakymiw A, Hamel J. C, Fritzler M. J, Chan E.K (2006) Formation of GW bodies is a consequence of microRNA genesis. *EMBO Rep.* **7**: 904-910

Pawlyk B. S, Smith A. J, Buch P. K, Adamian M, Hong D. H, Sandberg M. A, Ali R. R, Li T (2005) Gene replacement therapy rescues photoreceptor degeneration in a murine model of Leber congenital amaurosis lacking RPGRIP. *Invest Ophthalmol Vis Sci.* **46**: 3039–3045

Pelli D. G, Robson J. G, Wilkins A. J (1988) The design of a new letter chart for measuring contrast sensitivity. *Clin Vis Sci.* **2**: 187–199

Pennings R. J, Fields R. R, Huygen P. L, Deutman A. F, Kimberling W. J, Cremers C. W (2003) Usher syndrome type III can mimic other types of Usher syndrome, *Ann Otol Rhinol Laryngol.* **112**: 525–530

Pepe I. M (2001) Recent advances in our understanding of rhodopsin and phototransduction. *Progress Retinal and Eye Research.* **20**: 733-759

Perez-Castillo A, Pipaon C, Garcia I, Alemany S (1993) NGFI-A gene expression is necessary for T lymphocyte proliferation. *J. Biol. Chem.* **268**: 19445-19450

Perrault I, Rozet J. M, Clavas P., Gerber S, Camuzat A, Dollfus H, Chatelin S, Souied E, Ghazi I, Leowski C, Bonnemaison M, Le Paslier D, Frezal J, Dufier J-L, Pittler S, Munnich A, Kaplan J (1996) Retinal-specific guanylate cyclase gene mutations in Leber's congenital amaurosis. *Nat. Gen.* **14**: 461-464

Perrault I, Hanein S, Gerber S, Barbet F, Ducroq D, Dollfus H et al (2004) Retinal dehydrogenase 12 (RDH12) mutations in Leber congenital amaurosis. *Am J. Hum. Genet.* **75**: 639-646

Persengiev S. P, Zhu X, Green M. R (2004) Nonspecific, concentration-dependent stimulation and repression of mammalian gene expression by small interfering RNAs (siRNAs). *RNA.* **10**: 12-18

Petters R. M, Alexander C. A, Wells K. D, Collins E. B, Sommer J. R, Blanton M. R, Rojas G, Hao Y, Flowers W. L, Banin E, Cideciyan A. V, Jacobson S. G, Wong F. (1997) Genetically engineered large animal model for studying cone photoreceptor survival and degeneration in retinitis pigmentosa. *Nat. Biotechnol.* **15**: 965–970

Phillips M. I (2001) Gene therapy for hypertension: the preclinical data. *Hypertension.* **38:** 543–549

Phillips M. I, Tang Y, Schmidt-Ott K, Qian K, Kagiyama S (2002) Vigilant vector: heart-specific promoter in an adeno-associated virus vector for cardioprotection. *Hypertension.* **39**: 651–655

Pignatelli V, Cepko C. L, Strettoi E (2004) Inner retinal abnormalities in a mouse model of Leber's congential amaurosis. *J Comp Neurol.* **469**: 351-359

Pikal M. J (2001) The role of electroosmotic flow in transdermal iontophoresis. *Adv Drug Deliv Rev.* **46**(1-3): 281-305

Pillai R. S, Bhattacharyya S. N, Artus C. G, Zoller T, Cougot N, Basyuk E, Bertrand E, Filipowicz W (2005) Inhibition of translational initiation by let-7 microRNA in human cells. *Science.* **309**: 1573-1576

Poeschla E. M (2003) Non-primate lentiviral vectors. *Curr Opin Mol Ther.* **5**: 529–540

Ponjavic V, Abrahamson M, Andréasson S, Ehinger B, Fex G (1997) Autosomal dominant retinitis pigmentosa with a rhodopsin mutation (Arg-135-Trp). Disease phenotype in a Swedish family. *Acta Ophthlmol Scand.* **75**: 218-223

Ponting, C. (1997) CBS domains in ClC chloride channels implicated in myotonia and nephrolithiasis (kidney stones). *J. Mol. Med.* **75**: 160–163

Porello K, Bhat J. P, Bok D (1991) Detection of interphotoreceptor retinoif binding protein (IRBP) mRNA in human and cone-dominant squirrel retinas by in-situ hybridization. *J Histochem Cytochem.* **39**. 171-176

Prawitt D, Brixel L, Spangenberg C, Eshkind L, Heck R, Oesch F, Zabel B, Bockamp E (2004) RNAi knockdown mice: an emerging technology for post-genomic functional genetics, Cytogenet. *Genome Res.* **105**: 412-421

Provost P, Dishart D, Doucet J, Frendewey D, Samuelsson B, Radmark O (2002) Ribonuclease activity and RNA binding of recombinant human Dicer. *EMBO J.* **21**: 5864–5874

Qing K, Mah C, Hansen J, Zhou S, Dwarki V, Srivastava A (1999) Human fibroblast growth factor receptor 1 is a co-receptor for infection by adeno-associated virus 2. *Nat. Med.* **5**: 71–77

Que-Gewirth N. S and Sullenger B. A (2007) Gene therapy progress and prospects: RNA aptamers. *Gene Therapy.* **14**: 283-291

Rabinowitz J. E and Samulski R. J (2002) The adeno-associated virus crystal: impact inversely proportional to size. *Mol. Ther.* **6**: 443–445

Rabinowitz J. E, Rolling F, Li C, Conrath H, Xiao W, Xiao X, Samulski R. J (2002) Cross-packaging of a single adeno-associated virus (AAV) type 2 vector genome into multiple AAV serotypes enables transduction with broad specificity. *J Virol.* **76**: 791-801

Rabussay D, Dev N. B, Fewell J (2003) Enhancement of therapeutic drug and DNA delivery into cells by electroporation. *J Phys D: Appl Phys.* **36**: 348–363.

Radu R. A, Mata N. L, Bagla A, Travis G. H (2004) Light exposure stimulates formation of A2E oxiranes in a mouse model of Stargardt's macular degeneration. *Proc Natl Acad Sci USA.* **101**: 5928-5933

Raisler B. J, Berns K. I, Grant M. B, Beliaev D, Hauswirth W. W (2002) Adeno-associated virus type 2 expression of pigmented epithelium-derived factor or Kringles 1-3 of angiostatin reduce retinal neovascularization. *Proc. Natl. Acad. Sci. USA.* **99:** 8909–8914

Rajan R. S and Kopito R. R (2005) Retinopathy induced in mice by targeted disruption of the rhodopsin gene. *Nat Genet.* **15**: 216-219

Rand T, Petersen S, Du F, Wang X (2005) Argonaute2 cleaves the anti-guide strand of siRNA during RISC activation. *Cell.* **123**: 621-629

Rao M and Sockanathan S (2005) Molecular mechanisms of RNAi: implications for development and disease. *Birth Defects Res C Embryo Today.* **75**: 28-42

Rao M, Baraban J. H, Rajaii F, Sockanathan S (2004) *In-vivo* comparative study of RNAi methodologies by in ovo electroporationin the chick embryo. *Dev Dyn.* **231(3)**: 592-600
Rebello G, Ramesar R, Vorster A, Roberts L, Ehrenreich L, Oppon E, Gama D, Bardien S, Greenberg J, Bonpapace, Waheed A, Shah G. N, Sly W. S (2004) Apoptosis inducing signal sequence mutation in carbonic anhydrase IV indentified in patients with the RP17 form of retinitis pigmentosa. *PNAS.* **101 (17)**: 6617-6622

Reed S. E, Staley E. M, Mayginnes J. P, Pintel D. J, Tullis G. E (2006) Transfection of mammalian cells using linear polyethylenimine is a simple and effective means of producing recombinant adeno-associated virus vectors. *J Virol Methods.* **138**: 85–98

Reich S. J, Fosnot J, Kuroki A, Tang W, Yang X, Maguire A. M, Bennett J, Tolentino M. J (2003) Small interfering RNA (siRNA) targeting VEGF effectively inhibits ocular neovascularization in a mouse model. *Mol Vision.* **9**: 210-216

Remington L. A. Clinical anatomy of the visual system. *Butterworth Heinemann* (1998)

Reynolds A, Leake D, Boese Q, Scaringe S, Marshall W. S, Khovorova A (2004) Rational siRNA design for RNA interference. *Nat. Biotechnol.* **22**: 326-330

Reynolds A, Danciger M, Farrar G. J, Humphries P, Kenna P. F (2008) A quantitative trait locus on chromosome 19 controls variation in the murine light-adpated electroretinogram. *Invest. Ophthal. Vis. Sci.* doi:10.1167/iovs.07-1620

Ridge K, Abdulaev N. G, Sousa M, Palczewski K (2003) Phototransduction: crystal clear. *Trends Biochem Sci.* **28**: 479-487

Rivera V. M, Clackson T, Natesan S, Pollock R, Amara J. F, Keenan T, Magari S. R, Phillips T, Courage N. L, Cerasoli F Jr, Holt D. A, Gilman M (1996) A humanized system for pharmacologic control of gene expression. *Nat Med.* **2**: 1028-1032

Robinson P. R, Cohen G. B, Zhukovsky E. A, Oprian D. D (1992) Constitutively active mutants of rhodopsin. *Neuron.* **9**: 719-725

Robson A. G, Saihan Z, Jenkins S. A, Fitzke F. W, Bird A. C, Webster A. R, Holder G. E (2006) Functional characterisation and serial imaging of abnormal fundus autofluorescence in patients with retinitis pigmentosa and normal visual acuity. *Br J Ophthalmol.* **90**: 472–479

Rodriguez A, Griffiths-Jones S, Ashurst J. L, Bradley A (2004) Identification of mammalian microRNA host genes and transcription units. *Genome Res.* **14**: 1902-1910

Rohr U. P, Wulf M. A, Stahn S, Steidl U, Haas R, Kronenwett R (2002) Fast and reliable titration of recombinant adeno-associated virus type-2 using quantitative real-time PCR. *J Virol Methods.* **106**: 81–88

Rolling F (2004) Recombinant AAV-mediated gene transfer to the retina: gene therapy perspectives. *Gene Ther.* **1**: S26–S32.

Rosenberg M. I, Georges S. A, Asawachaicharn A, Analau E, Tapscott S. J (2006) MyoD inhibits Fstl1 and Utrn expression by inducing transcription of miR-206. *J. Cell Biol.* **175**: 77-85

Roth J. A, Nguyen D, Lawrence D, Kemp B. L, Carrasco C. H, Ferson D. Z, Hong W. K, Komaki R, Lee J. J, Nesbitt J. C, Psiters K. M, Puinam J. B, Schen R, Shin D. M, Walsh G. L, Dolormente M. M, Han C. T, Martin F. D, Yen N, Xu K, Stephens F. C, McDonnell T. J, Mukhopadhyay T, Car D (1996) Retrovirus mediated wild-type p53 gene transfer to tumours of patients with lung cancer. *Nat Med.* **2 (9)**: 985-999

Rother P. R, Fodor W. L, Springhorn J. P, Birks C. W, Setter E, Sandrin M. S, Squinto S. P, Rollins S. A (1995) A novel mechanism of retrovirus inactivation in human serum mediated by an anti-alpha-galactosyl natural antibody. *J. Exp. Med.* **182**: 1345-1353
Rowan S, Chen C. M, Young T. L, Fisher D. E, Cepko C. L (2004) Transdifferentiation of the retina into pigmented cells in ocular retardation mice defines a new function of the homeodomain gene CHx10. *Development.* **131**: 5139-51352

Rubinson D. A, Dillon C. P, Kwiatkowski A. V, Sievers C, Yang L, Kopinja J, Rooney D. L, Ihrig M. M, McManus M. T, Gertler F. B, Scott M. L, Van Parijs L. (2003) A lentivirus-based system to functionally silence genes in primary mammalian cells, stem cells and transgenic mice by RNA interference. *Nat. Genet.* **33 (3)**: 401-406

Rudolph C, Lausier J, Naundorf S, Müller R. H, Rosenecker J (2000) *In-vivo* gene delivery to the lung using polyethylenimine and fractured polyamidoamine dendrimers. *J Gene Med.* **2(4):** 269-78

Rusconi C. P, Roberts J. D, Pitoc G. A, Nimjee S. M, White R. R, Quick G. Jr, Scardino E, Fay W. P, Sullenger B. A (2004) Antidote mediated control of an anti-coagulant aptamer in vivo. *Nat. Biotechnology*; **22**: 1423-1428

Rutherford A. D, Dhomen N, Smith H. K, Sowden J. C (2004) Delayed expression of the Crx gene and photoreceptor development in the CHx 10-deficient retina. *Invest Ophthalmol Vis Sci.* **45**: 375-384
Rutkowski D. T and Kaufman R. J (2004) A trip to the ER: coping with stress. *Trends Cell Biol.* **14**: 20-28

Rutledge E. A, Halbert C. L, Russell D. W (1998) Infectious clones and vectors derived from adeno-associated virus (AAV) serotypes other than AAV type 2. *J Virol.* **72**: 309-319

Saari J. C (1990) Enzymes and proteins of the mammalian visual cycle. In: Osborn, N. N and Chader G. J. Editors. *Progress in Regional Research.* **9**. Pergamon Press, Oxford: 363-381

Saari J. C, Nawrot M, Kennedy B. N, Garwin G. G, Hurley J. B, Huang J, Possin D. E, Crabb J. W (2001) Visual cycle impairment in cellular retinaldehyde binding protein (CRALBP) knockout mice results in delayed dark adaptation. *Neuron*I. **29**: 739–748

Sabbioni S, Callegari E, Spizzo R, Veronese A, Altavilla G, Corallini A, Negrini M (2007a) Anticancer activity of an adenoviral vector expressing short hairpin RNA against BK virus T-ag. *Cancer Gene Therapy.* **14(3)**: 297-305

Sabbioni S, Callegari E, Manservigi M, Argnani R, Corallini A, Negrini M, Manservigi R (2007b) Use of herpes simplex virus type 1-based amplicon vector for delivery of small interfering RNA. *Gene Therapy.* **14**: 459-464

Sabina R. L and Holmes E. W (1995) The Metabolic and Molecular Bases of Inherited Disease. **2**: 1769-1780, McGraw-Hill, Inc., New York

Saenz D. T, Loewen N, Peretz M, Whitwam T, Barraza R, Howell K. G, Holmes J. M, Good M, Poeschla E. M (2004) Unintegrated lentivirus DNA persistence and accessibility to expression in nondividing cells: analysis with class I integrase mutants. *J Virol.* **78**: 2906–2920

Sætrom P, Snove O. Jr (2004) A comparison of siRNA efficacy predictors. *Biochem. Biophys. Res. Commun.* **321**:2 47–253

Saishin Y, Silva R. L, Saishin Y, Kachi S, Aslam S, Gong Y. Y, Lai H, Carrion M, Harris B, Hamilton M, Wei L, Campochiaro P. A (2005) Periocular gene transfer of pigment epithelium-derived factor inhibits choroidal neovascularization in a human-sized eye. *Hum Gene Ther.* **16**: 473–478

Sakamoto T, Oshima Y, Nakagawa K, Ishibashi T, Inomata H, Sueishi K (1999) Target gene transfer of tissue plasminogen activator to cornea by electric pulse inhibits intracameral fibrin formation and corneal cloudiness. *Hum Gene Ther.* **10**: 2551–2557

Saliba R. S, Munro P. M, Luthert P. J, Cheetham M. E (2002) The cellular fate of mutant rhodopsin: quality control, degradation and aggresome formation. *J Cell Sci.* **115**: 2907-2981

Sandberg M. A, Brockhurst R. J, Gaudio A. R, Berson E. L (2005) The association between visual acuity and central retinal thickness in retinitis pigmentosa. *Invest Ophthalmol Vis Sci.* **46**: 3349–3354

Sanyal S, De Ruiter A, Hawkins R. K (1980) Development and degeneration of retina in rds mutant mice: light microscopy. *J. Comp. Neurol.* **194**: 193-207

Sarra G. M, Stephens C, de Alwis M, Bainbridge J. W, Smith A. J, Thrasher A. J, Ali R. R (2001) Gene replacement therapy in the retinal degeneration slow (rds) mouse: the

effect on retinal degeneration following partial transduction of the retina. *Hum. Mol. Genet.* **10**: 2353–2361

Saunders P, Chen R-W, Chuang D-P (1999) Nuclear translocation of glyceraldehyde-3-phosphate dehydrogenase isoforms during neuronal apoptosis. *J. Neurochem.* **72**: 925–932

Sawa A, Khan A. A, Hester L. D, Snyder S. H (1997) Glyceraldhyde-3-phosphate dehydrogenase: nuclear translocation participates in neuronal and nonneuronal cell death. *Proc. Natl. Acad. Sci. U.S.A.* **94**: 11669–11674

Saxena S, Jonsson Z. O, Dutta A (2003) Small RNAs with imperfect match to endogenous mRNA repress translation. Implications for off target activity of small inhibitory RNA in mammalian cells. *J. Biol Chem.* **278**: 44312-44319

Saydam O, Glauser D. L, Heid I, Turkeri G, Hilbe M, Jacobs A. H (2005) Herpes simplex virus 1 amplicon vector-mediated siRNA targeting epidermal growth factor receptor inhibits grwoth of human glioma cells in vivo. *Mol Ther.* **12**: 803-812

Scacheri P. C, Rozenblatt-Rosen O, Caplen N. J, WOlfsberg T. G, Umayam L, Lee J. C, Hughes C. M, Shanmugam K. S, Bhattacharjee A, Meryerson M et al (2004) Short interfering RNAs can induce unexpected and divergent changes in the levels of untargeted proteins in mammalian cells. *Proc Natl Acad Sci. USA.* **101**: 1892-1897

Schatzlein A. G, Zinselmeyer B. H, Elouzi A, Dufes C, Chim Y. T, Roberts C. J, Davies M. C, Munro A, Gray A. I, Uchegbu I. F (2005) Preferential liver gene expression with polypropylenimine dendrimers. *J Control Release.* **101(1-3):** 247-58

Schlichtenbrede F. C, da Cruz L, Stephens C, Smith A. J, Georgiadis A, Thrasher A. J, Bainbridge J. W, Seeliger M. W, Ali R. R (2003) Long-term evaluation of retinal function in Prph2Rd2/Rd2 mice following AAV-mediated gene replacement therapy. *J Gene Med.* **5**: 757-764

Schlichtenbrede F. C, Smith A. J, Bainbridge J. W, Thrasher A. J, Salt TE, Ali R. R (2004) Improvement of neuronal visual responses in the superior colliculus in Prph2(Rd2/Rd2) mice following gene therapy. *Mol Cell Neurosci.* **25**: 103-110

Schratt G. M, Tuebing F, Nigh E. A, Kane C. G, Sabatini M. E, Kiebler M, Greenberg ME (2006) A brain-specific microRNA regulates dendritic spine development. *Nature.* **439**: 283-289

Schratzberger P., *et al* (1999) Ultrasound enhances gene expression following transfection of skeletal myocytes in vivo. *Circulation.* 100: 154

Schwarz D. S, Hutvagner G, Du T, Xu Z, Aronin N, Zamore P. D (2003) Assymetry in the assembly of the RNAi enzyme complex. *Cell.* **115**: 199-208

Scott J. W, Hawley S. A, Green K. A, Anis M, Stewart G, Scullion G. A, Norman D. G, Hardie D. G (2004) CBS domains form energy-sensing modules whose binding of adenosine ligands is disrupted by disease mutations. *J. Clin. Invest.* **113**: 274–284

Seeliger M. W, Grimm C, Stahlberg F, Friedburg C, Jaissle G, Zrenner E, Guo H, Reme C. E, Humphries P, Hofmann F, Biel M, Fariss R. N, Redmond T. M, Wenzel A (2001) New views on RPE65 deficiency: the rod system is the source of vision in a mouse model of Leber congential amaurosis. *Nat Genet.* **29**: 70-74

Seiving P. A (2004) Retinitis pigmentosa and related disorders. In: Yanoff M, Duker JS, editors. *Ophthalmology.* 2nd ed. St. Louis; Mosby: 813-824

Semizarov D, Frost L, Sarthy A, Kroeger P, Halbert D. N, Fesik S. W (2003) Specificity of short interfering RNA determined through gene expression signatures. *Proc Natl Acad Sci. USA.* **100**: 6347-6352

Semizarov D, Kroeger P, Fesik S (2004) siRNA-mediated gene silencing: a global genome view. *Nucleic Acids Res.* **32**: 3838-3845

Sen G. L and Blau H. M (2005) Argonate 2/RISC resides in sites of mammalian mRNA decay known as cytoplasmic bodies. *Nat. Cell. Biol.* **7**. 633-636

Senda M and Natsumeda Y (1994) Tissue-differential expression of two distinct genes for human IMP dehydrogenase. *Life Sci.* **54**: 1917-1926

Sergent-Tanguy S, Chagneau C, Neveu I, Naveilhan P (2003) Fluorescent activated cell sorting (FACS): a rapid and reliable method to estimate the number of neurons in a mixed population. *J Neurosci Methods.* **129(1)**: 73-9

Serguera C, Bohl D, Rolland E, Prevost P, Heard J. M (1999) Control of erythropoietin secretion by doxycycline or mifepristone in mice bearing polymer-encapsulated engineered cells. *Hum Gene Ther.* **10**: 375-383

Shen J (2006) Suppression of ocular neovascularization with siRNA targeting VEGF receptor 1. *Gene Ther.* **13**: 225-234

Shen W. Y, Yu M. J, Barry C. J, Constable I. J, Rakoczy P. E (1998) Expression of cell adhesion molecules and vascular endothelial growth factor in experimental choroidal neovascularisation in the rat. *Br J Opthalmol.* **82**: 1063-1071

Shen C, Buck A. K, Liu X, Winkler M, Reske S. N (2003) Gene silencing by adenovirus delivered siRNA. *FEBS Lett.* **539 (1-3)**: 111-114
Shen J, Yan X, Dong A, Petters R. M, Peng Y-W, Wong F (2005) Oxidative damage is a potential cause of cone cell death in retinitis pigmentosa. *J Cell Physiol.* **203**: 457-464

Sherman M. Y and Goldberg A. L (2001) Cellular defenses against unfolded proteins: a cell biologist thinks about neurodegenerative diseases. *Neuron.* **29**: 15-32

Sheth U and Parker R (2006) Targeting of aberrant mRNAs to cytoplasmic processing bodies. *Cell.* **125**: 1095-1109

Sheth U, Parker R (2003) Decapping and decay of messenger RNA occur in cytoplasmic processing bodies. *Science.* **300**: 805-808

Shi W, Sports C. D, Raman D, Shirakawa S, Osawa S, Weiss E. R (1998) Rhodopsin arginine-135 mutatns are phosphorylated by rhodopsin kinase and bind arrestin in the absence of 11-cis-retina. *Biochemistry.* **37**: 4869-4874

Silva JM, Li MZ, Chang K, Ge W, Golding MC, Rickles RJ, Siolas D, Hu G, Paddison PJ, Schlabach MR, Sheth N, Bradshaw J, Burchard J, Kulkarni A, Cavet G, Sachidanandam R, McCombie WR, Cleary MA, Elledge SJ, Hannon GJ (2006). Second-generation shRNA libraries covering the mouse and human genomes. *Nature Genetics.* **37**: 1281-1284.

Sinctak M. D and Nimersgern E (2000) The structure of inosine 5'-monophosphate dehydrogenase and the design of novel inhibitors. *Immunopharmacology.* **47**: 163-184

Singh R and Green M (1993) Sequence specific binding of transfer RNA by glyceraldehyde-3-phosphate dehydrogenase. *Science.* **259**: 365–368

Sintchak M. D and Nimmesgern E (2000) The structure of inosine 5'-monophosphate dehydrogenase and the design of novel inhibitors. *Immunopharmacology.* **47 (3)**: 163-184

Siolas D, Lerner C, Burchard J, Ge W, Linsley P.S, Paddison P.J, Hannon G.J, Cleary M.A. (2005) Synthetic shRNA as potent RNAi triggers. *Nature. Biotech.*, **23 (2)**: 227-231

Sioud M and Jesperen L (1996) Enhancement of hammerhead ribozyme catalysis by glyceraldehyde-3-phosphate dehydrogenase. *J. Mol. Biol.* **257**: 775–789

Skarnes W. C, von Melchner H, Wurst W, Hicks G, Nord A. S, Cox T, Young S. G, Ruiz P, Soriano P, Tessier-Lavigne M, Conklin B. R, Stanford W. L, Rossant J (2004) A public gene trap resource for mouse functional genomics. *Nat Genet.* **36**: 534-544

Sledz C. A, Holko M, de Veer M. J, Silverman R. H, Williams B. R (2003) Activation of the interferon system by short interfering RNAs. *Nature Cell Biol.* **5**: 834-839

Sliva K, Schnierle B. S (2006) Stable integration of a functional shRNA expression cassette into the murine leukemia virus genome. *Virology.* **351 (1)**: 218-225

Smirnova L, Grafe A, Seiler A, Schumacher S, Nitsch R, Wulczyn F. G (2005) Regulation of miRNA expression during neural cell specification. *Eur J Neurocil.* **21**: 1469-1477

Smith A. E (1995) Viral vectors in gene therapy. *Annu Rev Microbiol.* **49**: 807-838

Smith A. J, Schlichtenbrede F. C, Tschernutter M, Bainbridge J. W, Thrasher AJ, Ali R. R (2003) AAV-Mediated gene transfer slows photoreceptor loss in the RCS rat model of retinitis pigmentosa. *Mol Ther.* **8**: 188–195

Snyder R. O (1999) Adeno-associated virus-mediated gene delivery. *J Gene Med.* **1**: 166-175

Snyder R. O, Miao C, Meuse L, Tubb J, Donahue B. A, Lin H. F, Stafford D. W, Patel S, Thompson A. R, Nichols T, Read M. S, Bellinger D. A, Brinkhous K. M, Kay M. A (1999) Correction of hemophilia B in canine and murine models using recombinant adeno-associated viral vectors. *Nat. Med.* **5**: 64–70

Sollinger H. W (1995) Mycophenolate mofetil for the prevention of acute rejection in primary cadaveric renal allograftrecipients. *Transplantation.* **60**: 225–232

Somiari S, Glasspool-Malone J, Drabick J. J, Gilbert R. A, Heller R, Jaroszeski M. J, Malone R. W (2000) Theory and *in vivo* application of electroporative gene delivery, *Mol Ther.* **2**: 178–187

Song E, Lee S. K, Wang J, Ince N, Ouyang N, Min J, Chen J, Shankar P, Lieberman J. (2003) RNA interference targeting Fas protects mice from fulminant hepatitis. *Nat Med.* **9**: 347-351

Sorensen D. R, Leirdal M, Sioud M (2003) Gene silencing by systemic delivery of synthetic siRNAs in adult mice. J Mol Biol. 327: 761-766

Souied E, Soubrane G, Benlian P, Coscas GJ, Gerber S, Munnich A, Kaplan J (1996) Retinitis punctata albescens associated with the Arg135Trp mutation in the rhodopsin gene. *Am J Ophthalmol.* **121**: 19-25

Soutschek J, Akinc A, Bramlage B, Charisse K, Constien R, Donoghue M, Elbashir S, Geick A, Hadwiger P, Harborth J, John M, Kesavan V, Lavine G, Pandey RK, Racie T, Rajeev KG, Röhl I, Toudjarska I, Wang G, Wuschko S, Bumcrot D, Koteliansky V, Limmer S, Manoharan M, Vornlocher HP (2004) Therapeutic silencing of an endogenous gene by systemic administration of modified siRNAs. *Nature.* **432**: 173-178

Spilsbury K, Garrett K. L, Shen W. Y, Constable I. J, Rakoczy P. E (2000) Overexpression of vascular endothelial growth factor (VEGF) in the retinal pigment epithelium leads to the development of choroidal neovascularization. *Am J Pathol.* **157**: 135–144

Srivastava D (2006) Making or breaking the heart: from lineage determination to morphogenesis. *Cell.* **126**: 1037-1048

Stark G. R, Kerr I. M, Williams B. R. G, Silverman R. H, Schreiber R. D (1998) How cells respond to interferons. *Annu. Rev. Biochem.* **67**: 264–277

Stark A, Brennecke J, Russell R. B, Cohen S. M (2003) Identification of Drosophila: MicroRNA targets. *PLoS Biol.* **1(3)**: E60

Steinberg R. *et al.* (1996). Transgenic rat models of inherited retinal degeneration caused by mutant opsin genes. Invest. *Ophthalmol. Visual Sci.* **37**: S698

Stephenson M. L and Zamecnik P. C (1978) Inhibition of Rous sarcoma viral RNA translation by a specific oliogodeoxyribonucleotide. *Proc. Natl. Acad. Sci. USA.* **75**: 285-288

Stilwell J. L and Samulski R. J (2003) Adeno-associated virus vectors for therapeutic gene transfer. *Biotechniques.* **34(1)**:148-50, 152, 154
Stilwell J. L and Samulski R.J (2004) Role of viral vectors and virion shells in cellular gene expression. *Mol. Ther.* **9**: 337–346

Stoecklin G, Mayo T, Anderson P (2006) Are-mRNA degradation requires the 5'-3' decay pathway. *EMBO Rep.* **7**: 72-77

Streeter D. G, Witkowski J. T, Khare G. P, Sidwell R. W, Bauer R. J, Robins R. K, Simon L. N (1973) Mechanism of action of 1-β- -ribofuranosyl-1,2,4-triazole-3-carboxamide (virazole), a new broad-spectrum antiviral agent. *Proc. Natl. Acad. Sci. U. S. A.* **70**: 1174–1178

Sui G, Soohoo C, Affar el B, Gay F, Shi Y, Forrester W. C (2002) A DNA vector-based RNAi technology to suppress gene expression in mammalian cells. *Proc. Natl. Acad. Sci. USA*, **99**: 5515-5520

Sukharev S. I, Klenchin V. A, Serov S. M, Chernomordik L. V, Chizmadzhev Yu. A. (1992) Electroporation and electrophoretic DNA transfer into cells. The effect of DNA interaction with electropores. *Biophys J.* **63**: 1320–1327

Summerford C and Samulski R. J (1998) Membrane-associated heparan sulfate proteoglycan is a receptor for adeno-associated virus type 2 virions. *J. Virol.* **72**: 1438–1445

Summerford C, Bartlett J. S, Samulski R. J (1999) AlphaVbeta5 integrin: a co-receptor for adeno-associated virus type 2 infection. *Nat. Med.* **5**: 78–82

Sun G, Asami M, Ohta H, Kosaka J, Kosaka M (2006) Retinal stem/progenitor properties of iris pigment epithelial cells. *Dev Biol.* **289**: 243–252

Sung C. H, Schneider B. G, Agarwal N, Papermaster D. S, Nathans J (1993a) Functional heterogeneity of mutant rhodopsins responsible for adRP. *Proc Natl Acad Sci USA.* 88: 8840-8844

Sung C. H, Davenport C. M, Nathans J. (1993b) Rhodopsin mutations responsible for autosomal dominant retinitis pigmentosa. Clustering of functional classes along the polypeptide chain. *J. Biol Chem.* **268**: 26645-26649

Surace E. M and Auricchio A (2003) Adeno-associated viral vectors for retinal gene transfer. *Prog Retin Eye Res.* **22(6)**:705-19

Swaroop A, Xu J. Z, Pawar H, Jackson A, Skolnick C, Agarwal N (1992) A conserved retina-specific gene encodes a basic motif/leucine zipper domain. *Proc Natl Acad Sci USA.* **89**: 266–270

Swarup G (2004) How to design a highly effective siRNA. *J Biosci.* **29 (2)**: 129-3132

Szekeres T, Fritzer M, Pillwein K, Felzmann T, Chiba P (1992) Cell cycle dependent regulation of IMP dehydrogenase activity and effect of tiazofurin. *Life Sci.* **51**: 1309-1315

Taira M, Kudoh J, Minoshima S, Iizasa T, Shimada H., Shimizu, Y., Tatibana, M, Shimizu, N. (1989a) Localization of human phosphoribosylpyrophosphate synthetase subunit I and II genes (PRPS1 and PRPS2) to different regions of the X chromosome and assignment of two PRPS1-related genes to autosomes. *Somatic Cell Mol. Genet.* **15**: 29-37

Taira M, Iizasa T, Yamada K, Shimada H, Tatibana M (1989b) Tissue-differential expression of two distinct genes for phosphoribosyl pyrophosphate synthetase and existence of the testis-specific transcript. *Biochim. Biophys. Acta.* **1007**: 203-208
Taira M, Iizasa T, Shimada H, Kudoh J, Shimizu N, Tatibana M (1990) A human testis-specific mRNA for phosphoribosylpyrophosphate synthetase that initiates from a non-AUG codon. *J. Biol. Chem.* **265**: 16491-16497

Tan E, Wang Q, Quiambao AB, Xu X, Qtaishat N. M, Peachey N. S, Lem J, Fliesler S. J, Pepperberg D. R, Naash M. I, Al-Ubaidi M. R (2001) The relationship between opsin overexpression and photoreceptor degeneration, *Investigative and Ophthalmology Visual Science.* **42**: 589–600

Tang G (2005) siRNA and miRNA: an insight into RISCs. *Trends in Biochemical Science.* **30**: 106-114

Taniyama Y, Tachibana K, Hiraoka K, Aoki M, Yamamoto S, Matsumoto K, Nakamura T, Ogihara T, Kaneda Y, Morishita R (2002) Development of safe and efficient novel nonviral gene transfer using ultrasound: enhancement of transfection efficiency of naked plasmid DNA in skeletal muscle. *Gene Ther.* **9**: 372-380

Taxman D. J, Livingstone L. R, Zhang J, Conti B. J, Iocca H. A, Williams K. L, Lich J. D, Ting J. P, Reed W (2006) Criteria for effective design construction and gene knockdown by shRNA vectors. *BMC Biotechnol.* **24**: 6-7

Teissie J, Golzio M, Rols M. P (2005) Mechanisms of cell membrane electropermeabilization: a minireview of our present (lack of ?) knowledge. *Biochim Biophys Acta.* **1724(3)**: 270-80

Teixeira D, Sheth U, Valencia-Sanchez M. A, Brengues M, Parker R (2005) Processing bodies require RNA for assembly and contain non-translating mRNAs. *RNA.* **11**: 371-382

Tessitore A, Parisi F, Denti M. A, Allocca M, Di Vicino U, Domenici L, Bozzoni I, Auricchio A (2006) Preferential silencing of a common dominant rhodopsin mutation does not inhibit retinal degeneration in a transgenic model. *Molecular Therapy.* **14 (5)**: 692-699

Teupe C, Richter S, Fisslthaler B, Randriamboavonjy V, Ihling C, Fleming I, Busse R, Zeiher AM, Dimmeler S (2002) Vascular gene transfer of phosphomimetic endothelial nitric oxide synthase (S1177D) using ultrasound-enhanced destruction of plasmid-loaded microbubbles improves vasoreactivity. *Circulation.* **105**: 1104-1109

Thakker D. R, Natt F, Hüsken D, Maier R, Müller M, van der Putten H, Hoyer D, Cryan J. F (2004) Neurochemical and behavioural consequences of widespread gene knockdown in the adult mouse brain by using nonviral RNA interference. *Proc Natl Acad Sci USA.* **101**: 17270-17275

The age-related eye disease study research group (2001) A randomised, placebo-controlled, clinical trail of high dose supplementation with vitamins C and E, beta carotene, and zince for age-related macular degeneration and vision loss. *Arch Ophthamol.* **119**: 1417-1436

Thomas, C.E., Schiedner, G., Kochanek, S., Castro, M.G. and Lowenstein, P.R., (2000) Peripheral infection with adenovirus causes unexpected long-term brain inflammation in animals injected intracranially with first-generation, but not with high-capacity, adenovirus vectors: Toward realistic long-term neurological gene therapy for chronic diseases. *Proc. Natl. Acad. Sci. USA.* **97 (13)**: 7482–7487

Thompson D. A and Gal A (2003) Vitamin A metabolism in the retinal pigment epithelium: genes, mutations, and diseases. *Prog Retin Eye Res.* **22**: 683-703
Thompson D. A, Gyürüs P, Fleischer L. L, Bingham E. L, McHenry C. L, Apfelstedt-Sylla E, Zrenner E, Lorenz B, Richards J. E, Jacobson S. G, Sieving P. A, Gal A (2000) Genetics and phenotypes of RPE65 mutations in inherited retinal degeneration. *Invest Ophthalmol Vis Sci.* **41**: 4293–4299

Tieder M, Levy M, Gubler M. C, Gagnadoux M. F, Broyer M (1982) Renal abnormalities in the Bardet-Biedl syndrome. *Int J Pediatr Nephrol.* **3**: 199–203

Tobe T, Ortega S, Luna J. D, Ozaki H, Okamoto N, Derevjanik N (1998) Targeted disruption of the FGF2 gene does not prevent choroidal neovascularization in a murine model. *Am J Pathol.* **153**: 1641-1646

Tolentino M. J, Brucker A. J, Fosnot J, Ying G. S, Wu I. H, Malik G (2004a) Intravitreal injection of vascular endothelial growth factor small interfering RNA inhibits growth and

leakage in a nonhuman primate, laser-induced model of choroidal neovascularization. *Retina.* **24**: 51-56

Tolentino M. J, Brucker A, Wan S, Reich S. J, Gordon J, Duh Y. J (2004b) Intravitreal injection of vascular endothelial growth factor small interfering RNA inhibits growth and leakage in a nonhuman primate, laser-induced model of choroidal neovascularization. *Letter to the Editor Retina.* **24(4)**: 661

Tomar R. S, Matta H, Chaudhary P. M (2003) Use of adeno-associated viral vector for delivery of small interfering RNA. *Oncogene.* **22(36)**: 5712-5

Tomari Y, Matranga C, Haley B, Martinez N, Zamore P. D (2004) A protein sensor for siRA asymmetry. *Science.* **306**: 1377-1380

Tosi M. F (2005) Innate immune responses to infection. *J. Allergy Clin. Immunol.* **116**: 241-249

Toumi H, Hegge J, Subbotin V, Noble M, Herweijer H, Best TM, Hagstrom JE (2006) Rapid intravascular injection into limb skeletal muscle: a damage assessment study. *Mol Ther.* **13**: 229-236

Trezise A. E (2002) *In-vivo* DNA electrotransfer. *DNA Cell Biol.* **21:** 869–877

Tschaharganeh D, Ehemann V, Nussbaum T, Schirmacher P, Breuhahn K (2007) Non-specific effects of siRNAs on tumor cells with implications on therapeutic applicability using RNA interference. *Pathology Oncology Research.* **13 (2)**: 84-90

Tschernutter M, Schlichtenbrede F. C, Howe S, Balaggan K. S, Munro P. M, Bainbridge J. W, Thrasher A. J, Smith A. J, Ali R. R (2005) Long-term preservation of retinal function in the RCS rat model of retinitis pigmentosa following lentivirus-mediated gene therapy. *Gene Ther.* **12**: 694–701

Tubb B. E, Bardien-Kruger S, Kashork C. D, Shaffer L. G, Ramagli L. S, Xu J, Siciliano M. J, Bryan J (2000) Characterisation of human retinal fascin gene (FSCN2) at 17q25: close physical linkage of fascin and cytoplasmic actin genes. *Genomics.* **65**: 146–156

Tuschl T, Zamore, P. D., Lehmann R, Bartel, D. P, Sharp, P.A (1999) Targeted mRNA degradation by double-stranded RNA in vitro. *Genes & Dev.* **13**: 3191-3197

Urtti A, Polansky J, Lui GM, Szoka FC (2000) Gene delivery and expression in human retinal pigment epithelial cells: effects of synthetic carriers, serum, extracellular matrix and viral promoters. *J Drug Target.* **7**: 413-421

Valencia-Sanchez M. A, Liu J, Hannon G. J, Parker R (2006) Control of translation and mRNA degradation by miRNAs and siRNAs. *Genes Dev.* **20**: 515-524

van Adel B. A, Kostic C, Deglon N, Ball A. K, Arsenijevic Y (2003) Delivery of ciliary neurotrophic factor via lentiviral-mediated transfer protects axotomized retinal ganglion cells for an extended period of time. *Hum Gene Ther.* **14**: 103–115

van de Pavert S. A, Kantardzhieva A, Malysheva A, Meuleman J, Versteeg I, Levelt C, Klooster J, Geiger S, Seeliger M. W, Rashbass P, Le Bivic A, Wijnholds J (2004) Crumbs homologue 1 is required for maintenance of photoreceptor cell polarization and adhesions during light exposure. *J Cell Sci.* **117**: 4169-4177

van de Watering M, Oving I, Muncan V, Fong M. T. P, Brantjes H, Van Leenen D, Holstege F. C. P, Brummelkamp T. R, Agami R, Clevers H (2003) Specific inhibiton of gene expression using a stably integrated, inducible small interfering RNA vector. *EMBO reports*. **4 (6)**: 609-615

van Den Bergh F and Sabina R. L (1995) Characterization of human AMP deaminase 2 (AMPD2) gene expression reveals alternative transcripts encoding variable N-terminal extensions of isoform L. *Biochem. J.* **312**: 401-410

van der Krol A. R, Mur L. A, Beld M, Mol J. N, Stuitje A. R (1990) Flavonoid genes in petunia: addition of a limited number of gene copies may lead to a suppression of gene expression. *Plant Cell*. **2 (4)**: 291–299

van Hooser J. P, Aleman T. S, He Y. G, Cideciyan A. V, Kuksa V, Pittler S. J, Stone E. M, Jacobson S. G, Palczewski K (2000) Rapid restoration of visual pigment and function with oral retinoid in a mouse model of childhood blindness. *Proc Natl Acad Sci USA*. **97**: 8623–8628

van Lith-Verhoeven J. J, van der Velde-Visser S. D, Sohocki M. M, Deutman A. F, Brink H. M, Cremers F. P, Hoyng C. B (2002) Clinical characterization, linkage analysis, and PRPC8 mutation analysis of a family with autosomal dominant retinitis pigmentosa type 13 (RP13). *Ophthalmic Genet*. **23**: 1-12

Venkatesh S and Smith T. J (1997) Chitosan-mediated transfection of HeLa cells. *Pharm Dev Technol*. **2(4)**: 417-8

Ventura A, Meissner A, Dillon CP, McManus M, Sharp PA, Van Parijs L, Jaenisch R, Jacks T (2004) Cre-lox regulated conditional RNA interference from transgenes. *Proc. Natl. Sci. USA*. **101**: 10380-10385

Verma J. M and Somia N (1997) Gene therapy promises problems and prospects. *Nature*. **389 (6648)**: 239-242

Vithana E. N, Abu-Safieh L, Allen M. J, Carey A, Papaioannou M, Chakarova C, Al-Maghtheh M, Ebenezer N. D, Willis C, Moore A. T, Bird A. C, Hunt D. M, Bhattacharya S. S (2001) A human homolog of yeast pre-mRNA splicing gene, PRP31, underlies autosomal dominant retinitis pigmentosa on chromosome 19q13.4 (RP11). *Mol Cell*. **8**: 375-81

Voigt M, Kralinger M, Kieselbach G, Chapon P, Anagnoste S, Hayden B, Parel J. M (2002a) Ocular aspirin distribution: a comparison of intravenous, topical, and coulomb-controlled iontophoresis administration. *Invest Ophthalmol Vis Sci*. **43**: 3299–3306

Voigt M, de Kozak Y, Halhal M, Courtois Y, Behar-Cohen F (2002b) Down-regulation of NOSII gene expression by iontophoresis of anti-sense oligonucleotide in endotoxin-induced uveitis. *Biochem Biophys Res Commun*. **295**: 336–341

Vollrath D, Feng W, Duncan J. L, Yasumura D, D'Cruz P. M, Chappelow A, Matthes M. T, Kay M. A, LaVail M. M (2001) Correction of the retinal dystrophy phenotype of the RCS rat by viral gene transfer of Mertk. *Proc Natl Acad Sci USA*. **98**: 12584-12589

Wada Y and Tamai M (2003) Molecular genetic analysis for Japanese patients with autosomal dominant retinitis pigmentosa. *Nippon Ganka Gakkai Zasshi*. **1072**: 687-694

Wada Y, Sandberg M. A, McGee T. L, Stillberger M. A, Berson E. L, Dryja T. P (2005a) Screen of the IMPDH1 gene among patients with dominant retinitis pigmentosa and clinical features associated with the most common mutation, Asp226Asn. *Invest Ophthalmol Vis Sci.* **46**: 1735–1741

Wada Y, Tada A, Itabashi T, Kawamura M, Sato H, Tamai M (2005b) Screening for Mutations in the IMPDH1 Gene in Japanese Patients With Autosomal Dominant Retinitis Pigmentosa. *American Journal of Ophthalmology.* 140(1): 163-165

Wadhwa R, Kaul SC, Miyagishi M, Taira K (2004) Know how of RNA interference and its applications in research and therapy. *Mutation Research.* **567**: 71-84

Walters R. W, Yi S. M, Keshavjee S, Brown K. E, Welsh M. J, Chiorini J. A, Zabner J (2001) Binding of adeno-associated virus type 5 to 2,3-linked sialic acid is required for gene transfer. *J. Biol. Chem.* **276(23)**: 20610-6

Wang X. S, Ponnazhagan S, Srivastava A (1995), "Rescue and replication signals of the adeno-associated virus 2 genome" *Journal of Molecular Biology.* **250(5)**: 573-80

Wang S, Roy N. S, Benraiss A, Goldman S. A (2000) Promoter-based isolation and fluorescence-activated sorting of mitotic neuronal progenitor cells from the adult mammalian ependymal/subependymal zone. *Dev. Neurosci.* **22**: 167–176

Wang D. Y, Chan W. M, Tam P. O. S, Baum L, Lam D. S. C, Chong K. K. L, Fan B. J, Pang C. P (2005a) Gene mutations in retinitis pigmentosa and their clinical implications. *Clinica Chimica Acta.* **351**: 5-16

Wang Z, Zhu T, Qiao C, Zhou L, Wang B, Zhang J, Chen C, Li J, Xiao X (2005b) Adeno-associated virus serotype 8 efficiently delivers genes to muscle and heart. *Nat. Biotechnol.* **23**: 321–328

Watanabe T, Sudoh M, Miyagishi M, Akashi H, Arai M, Inoue K, Taira K, Yoshiba M, Kohara M. (2006) Intracellular-diced dsRNA has enhanced efficicacy for silencing HCV RNA and overcomes variation in the viral genotype. *Gene Ther.* **13**: 883-892

Weber G (1983) Biochemical strategy of cancer cells and the design of chemotherapy: G. H. A. Clowes Memorial Lecture. *Cancer Res.* **43**: 3466–3492

Weber G, Nakamura H, Natsumeda Y, Szekeres T, Nagai M (1992) Regulation of GTP biosynthesis. Adv. Enzyme Regul. **32**: 57–69

Weber B. H, Schrewe H, Molday L. L, Gehrig A, White K. L, Seeliger M. W, Jaissle G. B, Friedburg C, Tamm E, Molday R. S (2002) Inactivation of the murine X-linked juvenile retinoshcisis gene. Rs1h, suggests a role of retinoschisis in retinal cell layer organization and synaptic structure. *Proc Natl Acad Sci USA.* **99**: 6222-6227

Weber M, Rabinowitz J, Provost N, Conrath H, Folliot S, Briot D, Cherel Y, Chenuaud P, Samulski J, Moullier P, Rolling F (2003) Recombinant adeno-associated virus serotype 4 mediates unique and exclusive long-term transduction of retinal pigmented epithelium in rat, dog, and nonhuman primate after subretinal delivery. *Mol Ther.* **7**: 774-781

Weindler F. W and Heilbronn R (1991) A subset of herpes simplex virus replication genes provides helper functions for productive adeno-associated virus replication. *J. Virol.* **65**: 2476–2483

Weitzman M. D, Kyöstiö S. R, Kotin R. M, Owens R. A (1994) Adeno-associated virus (AAV) Rep proteins mediate complex formation between AAV DNA and its integration site in human DNA. *Proc Natl Acad Sci U S A.* **91(13)**: 5808-12

Wells D. J (2004) Gene therapy progress and prospects: electroporation and other physical methods. *Gene Ther.* **11**: 1363–1369

Wickens M, Bernstein D. S, Kimble J, Parker R (2002) A PUF family portrait 3UTR regulation as a way of life. *Trends Genet.* **18**: 150-157

Wienholds E, Kloosterman W. P, Miska E, Alvarez-Saavedra E, Berezikov E, de Bruijn E, Horvitz H. R, Kauppinen S, Plasterk R. H (2005) MicroRNA expression in zebrafish embryonic development. *Science.* **309**: 310-311

Wightman B, Ha I, Ruvkun G (1993) Posttranscriptional regulation of the heterochronic gene lin-14 by lin-4 mediates temporal pattern formation in C. elegans. *Cell.* **75**: 855-862

Wilson J. H and Wensel T. G (2003) The nature of dominant mutations of rhodopsins and implications for gene therapy. *Mol Neurobiol.* **28**: 149-158

Woodruff M. L, Wang Z, Chung H. Y, Redmond T. M, Fain G. L, Lem J (2003) Spontaneous activity of opsin apoprotein is a cause of Leber congenital amaurosis. *Nat Genet.* **35**: 158-164

Wrigstad A, Nilsson SE, Narfström K (1992) Ultrastructural changes of the retina and the retinal pigment epithelium in Briard dogs with hereditary congenital night blindness and partial day blindness. *Exp Eye Res.* **55**: 805–818

Wu G. Y and Wu C. H (1988) Receptor-mediated gene delivery and expression *in-vivo. J Biol Chem.* **263(29)**: 14621-4

Wu T. H, Ting T. D, Okajima T. I, Pepperberg D. R, Ho Y. K, Ripps H, Naash M. I (1998a) Opsin localization and rhodopsin photochemistry in a transgenic mouse model of retinitis pigmentosa. *Neuroscience.* **87**: 709-717

Wu P, Phillips M. I, Bui J, Terwilliger E. F (1998b) Adeno-associated virus vector-mediated transgene integration into neurons and other nondividing cell targets. *J. Virol.* **72 (7)**: 5919–5926

Wu H, Xu H, Miraglia L. J, Crooke S. T (2000) Human RNase III is a 160-kDa protein involved in preribosomal RNA processing. *J Biol Chem.* **275**: 36957-36965
Wu Z, Hackett S. F, Kachi S, Rogers B, Campochiaro P. A (2005) p66shc regulates redox-sensitive NF-κB activation and oxidative stress-induced apoptosis in human RPE cells. *Invest Ophthamol Vis Sci.* **46**: 1615

Xia H, Mao Q, Paulson H. L, Davidson B. L (2002) siRNA-mediated gene silencing *in-vitro* and *in-vivo. Nat Biotechnol.* **20**: 1006–1010

Xia H, Mao Q, Eliason S. L, Harper S. Q, Martins I. H, Orr H. T, Paulson H. L, Yang, L, Kotin R. M, Davidson B. L (2004) RNAi suppresses polyglutamine-induced neurodegeneration in a model of spinocerebellar ataxia. *Nat. Med.* **10(8)**: 816–820

Xia X, Zhou H, Huang Y, Xu Z (2006) Allele-specific RNAi selectively silences mutant SOD1 and achieves significant therapeutic benefit in vivo. *Neurobiol Dis.* **23**: 578-586

Xiao X, Li J, Samulski R. J (1998) Production of high-titer recombinant adeno-associated virus vectors in the absence of helper adenovirus. *J. of Virology*. **72**: 2224-32

Xiao W, Chirmule N, Berta S. C, McCullough B, Gao G, Wilson J. M (1999) Gene therapy vectors based on adeno-associated virus type 1. *J Virol*. **73**: 3994-4003

Xiao X, Li J, Tsao Y. P, Dressman D, Hoffman E. P, Watchko J. F (2000) Full functional rescue of a complete muscle (TA) in dystrophic hamsters by adeno-associated virus vector-directed gene therapy. *J Virol*. **74**: 1436-1442

Xie F. Y, Woodle M. C, Lu P. Y (2006) Harnessing *in vivo* siRNA delivery for drug discovery and therapeutic development. *Drug Discovery Today*.**11**: 67-73

Xie Q, W. Bu, S. Bhatia, J. Hare, T. Somasundaram, A. Azzi and M.S. Chapman (2002) The atomic structure of adeno-associated virus (AAV-2), a vector for human gene therapy. *Proc. Natl. Acad. Sci. USA*. **99**: 10405–10410

Xue L, Gollapalli D. R, Maiti P, Jahng W. J, Rando R. R (2004) A palmitoylation switch mechanism in the regulation of the visual cycle. *Cell*. **117**:761–771

Yalowitz J and Hiremagalur J (2000) Molecular targets of guanine nucleotides in differentiation proliferation and apoptosis. *Anticancer Res*. **20**: 2329–2338

Yang J, Chen S, Huang L, Michalopoulos G. K, Liu Y (2001) Sustained expression of naked plasmid DNA encoding hepatocytes growth factors in mice promotes liver and overall body growth. *Hepatology*. **33**: 848-859

Yang G. S, Schmidt M, Yan Z, Lindbloom J. D, Harding T. C, Donahue B. A, Engelhardt J. F, Kotin R, Davidson B. L (2002) Virus-mediated transduction of murine retina with adeno-associated virus: effects of viral capsid and genome size. *J Virol*. **76**: 7651-7660

Yang Z, Jakymiw A, Wood M. R, Eystathioy T, Rubin R. L, Fritzler M. J, Chan E. K (2004) GW182 is critical for the stability of GW bodies expressed during the cell cycle and cell proliferation. *J. Cell Sci*. **117**: 567-5578

Yasukawa T, Ogura Y, Tabata Y, Kimura H, Wiedemann P, Honda Y (2004) Drug delivery systems for vitreoretinal diseases. *Prog Retin Eye Res*. **23**: 253–281

Ye X, Rivera V. M, Zoltick P, Cerasoli F Jr, Schnell M. A, Gao G, Hughes J. V, Gilman M, Wilson J. M (1999) Regulated delivery of therapeutic proteins after *in-vivo* somatic cell gene transfer. *Science*. **283**: 88-91
Yi R, Qin Y, Macara I. G, Cullen B. R (2003) Exportin-5 mediates the nuclear export of pre-microRNAs and short hairpin RNAs. *Genes and Dev*. **17**: 3011-3016

Yi R, Doehle B. P, Macara I. G, Cullen B. R (2005) Overexpression of exportin 5 enhances RNA interference mediated by short hairpin RNAs and microRNAs. *RNA*. **11**: 220-226

Yokota T, Shiojiri T, Gotoda T, Arita M, Arai H, Ohga T, Kanda T, Suzuki J, Imai T, Matsumoto H, Harino S, Kiyosawa M, Mizusawa H, Inoue K (1997) Friedreich-like ataxia with retinitis pigmentosa caused by the His101Gln mutation of the alpha-tocopherol transfer protein gene. *Ann Neurol*. **41**: 826–832

Young M. J, Ray J, Whiteley S. J, Klassen H, Gage F.H (2000) Neuronal differentiation and morphological integration of hippocampal progenitor cells transplanted to the retina of immature and mature dystrophic rats. *Mol. Cell. Neurosci.* **16**: 197-205

Yu J. Y, DeRuiter S. L, Turner D. L (2002) RNA interference by expression of short-interfering RNAs and hairpin RNAs in mammalian cells. *Proc Natl Acad Sci USA.* **99**: 6047–6052

Zabner J, Seiler M, Walters R, Kotin R. M, Fulgeras W, Davidson B. L, Chiorini J. A (2000) Adeno-associated virus type 5 (AAV2) but not AAV2 binds to the apical surfaces of airway epithelia and facilitates gene transfer. *J. Virol.* **74**: 3852–3858

Zack D. J (1999) Birth and death in the retina: more related than we thought? *Neuron* **23**: 411–412

Zack D. J, Bennett J, Wang Y, Davenport C, Klaunberg B, Gearhart J, Nathans J. (1991) Unusual topography of bovine rhodopsin promoter-lacZ fusion gene expression in transgenic mouse retinas. *Neuron.* **6**: 187–199

Zamecnik P. C and Stephenson M. L (1978) Inhibition of Rous sarcoma virus replication and cell transformation by a specific oligodeoxynucleotide. *Proc. Natl. Acad. Sci. USA.* **75**: 280-284

Zamore P. D (2002) Ancient pathways programmed by small RNAs. *Science.* **296**: 1265–1269

Zampaglione I, Arcuri M, Cappelletti M, Ciliberto G, Perretta G, Nicosia A, La Monica N, Fattori E (2005) *In vivo* DNA gene electro-transfer: a systematic analysis of different electrical parameters. *J Gene Med.* **7**: 1475–1481

Zang W-Q, Fieno A. M, Grant R. A, Yen T. S. B (1998) Identification of glyceraldehyde-3-phosphate dehydrogenase as a cellular protein that binds to hepatitis B virus posttranscriptional regulatory element. *Virology.* **248**: 46–52

Zelenin A. V, Alimov A. A, Titomirov A. V, Kazansky A. V, Gorodetsky S. I, Kolesnikov V. A (1991) High-velocity mechanical DNA transfer of the chloramphenicolacetyl transferase gene into rodent liver, kidney and mammary gland cells in organ explants and *in-vivo*. *FEBS Lett.* **280**: 94-96

Zender L, Hutker S, Liedtke C, Tillmann HL, Zender S, Mundt B, Waltemathe M, Gosling T, Flemming P, Malek NP, Trautwein C, Manns MP, Kuhnel F, Kubicka S (2003) Caspase 8 small interfering RNA prevents acute liver failure in mice. *Proc Natl Acad Sci USA.* **100:** 7797-7802

Zeng Y and Cullen B. R (2002) RNA interference in human cells is restricted to the cytoplasm. *RNA.* **8**: 855–860

Zeng Y, Wagner E. J, Cullen B. R (2002) Both natural and designed micro RNAs can inhibit the expression of cognate mRNAs when expressed in human cells. *Mol Cell.* **9**: 1327-1333

Zeng Y, Yi R, Cullen B. R (2003) MicroRNAs and small interfering RNAs can inhibit mRNA expression by similar mechanisms. *Proc Natl Acad Sci. USA.* **100**: 9779-9784

Zeng Y and Cullen B. R (2004) Structural requirements for pre-microRNA binding and nuclear export by Exportin 5. *Nucleic Acids Res.* **32**(16): 4776–4785

Zeviani M, Moraes C. T, DiMauro S, Nakase H, Bonilla E, Schon E. A, Rowland L. P. (1988) Deletions of mitochondrial DNA in Kearns-Sayre syndrome. *Neurology*. **51**: 1525

Zhang G, Budker V, Wolff J. A (1999) High levels of foreign gene expression in hepatocytes after tail vein injections of naked plasmid DNA. *Hum Gene Ther*. **10**: 1735-1737

Zhang G, Song Y. K, Liu D (2000) Long term expression of human alpha1-antitrypsin gene in mouse liver achieved intravenous administration of plasmid DNA using a hydrodynamics-based procedure. *Gene Ther*. **7**: 1344-1349

Zhang G, Gao X, Song Y. K, Vollmer R, Stolz D. B, Gasiorowski J. Z, Dean D. A, Liu D (2004) Hydroporation as the mechanism of hydrodynamic delivery. *Gene Ther*. **11**: 675-682

Zhao Y and Srivastava D (2007) A developmental view of microRNA function. *Trends Biochem Sci*. **32(4)**: 189-97

Zhao Y, Samal E, Srivastava D (2005) Serum response factor regulates a muscle-specific microRNA that targets Hand2 during cardiogenesis. *Nature*. **436**: 214-220

Zhou X and Muzyczka N (1998) *In vitro* packaging of adeno-associated virus DNA. *Journal of Virology*. **72(4)**: 3241-7

Zhu L, Jang G. F, Jastrzebska B, Filipek S, Pearce-Kelling S. E, Aguirre G. D, Stenkamp R. E, Acland G. M, Palczewski K (2004) A naturally occurring mutation in the opsin gene (T4R) in dogs affects glycosylation and stability of the G-protein coupled receptor. *J Biol Chem*. **279**: 53828-53839

Zimmerman A. G, Spychala J, Mitchell B. S (1995) Characterisation of the Human Inosine-5'-monophosphate dehydrogenase type II gene. *J Biol Chem*. **270**: 6808-6814

Zimmermann A. G, Gu J. J, Laliberte J, Mitchell B. S (1998) Inosine-5'-monophosphate dehydrogenase: regulation of expression and role in cellular proliferation and T lymphocyte activation. *Prog. Nucleic Acid Res. Mol. Biol*. **61**: 181-209

Zoghbi H. Y and Orr H. T (2000) Glutamine repeats and neurodegeneration. *Annu Rev Neurosci*. **23**: 217-47

Zou H, Li Y, Wang X (1999) An apaf-1 cytochrome c multimeric complex is a functional apoptosome that activates procaspase-9. *J Biol Chem*. **274**: 11549-11556